canadian acoustics
acoustique canadienne

PROCEEDINGS

ACOUSTICS WEEK IN CANADA

SEMAINE CANADIENNE D'ACOUSTIQUE

2000

CAHIERS DES ACTES

canadian acoustics

acoustique canadienne

EDITOR-IN-CHIEF / RÉDACTEUR EN CHEF

Ramani Ramakrishnan
Aiolos Engineering Inc.
51 Constellation Court
Suite 200
Toronto, Ontario M9W 1K4
Tel: (416) 674-3017
Fax: (416) 674-7055
E-mail: ramani@aiolos.com

EDITOR / RÉDACTEUR

Chantai Laroche
Dépt. d'orthophonie et d'audiologie
Université d'Ottawa
545 King Edward
Ottawa, Ontario K1N 6N5
Tél: (613) 562-5800 extn/poste 3066
Fax: (613) 562-5256
E-mail: claroche@uottawa.ca

ASSOCIATE EDITORS / REDACTEURS ASSOCIES

Advertising / Publicité
Chris Hugh
Hatch Associates Ltd.
2800 Speakman Drive
Mississauga, Ontario L5K 2R7
Tel: (905) 403-3908
Fax: (905) 824-4615
E-mail: chugh@hatch.ca

News / Informations
Francine Desharnais
DREA - Ocean Acoustics
P. O. Box 1012
Dartmouth, NS B2Y 3Z7
Tel: (902) 426-3100
Fax: (902) 426-9654
E-mail: desharnais@drea.dnd.ca

EDITORIAL / ÉDITORIAL

Welcome to the 2000 Proceedings Issue of Canadian Acoustics. It contains details of the final programme and two page summaries of the Technical Symposium of Acoustics Week in Canada 2000 to be held in pristine Sherbrooke in October. Keeping with the usual trend, the Sherbrooke conference also is promising to contain an impressive collection of papers in acoustics with emphasis on noise and vibration control and with over 90 registered papers. The meeting will clearly be very interesting. See you there!

The final format of the journal is slowly shaping up and we envisage each journal (other than the Proceedings Issue) to contain the following: two refereed technical/research type articles, one case study, at least one book review, thesis abstracts, regular news items and update on Canadian Standards (once a year). We were attempting to include brief descriptions on Canadian facilities that conduct basic acoustics, noise and vibration research. We are yet to succeed, but I am sure that in course of time such descriptions would become a staple in the journal. Please write back to me with your critical comments, suggestions and of course ideas.

Bienvenue à l'édition 2000 de l'acte du colloque de l'Acoustique Canadienne. Cette édition contient des détails du programme final et deux pages sommaire du colloque technique de la semaine d'acoustique au Canada 2000 qui se tiendra à Pristine, Sherbrooke en Septembre. Conservant la tendance habituelle, la conférence de Sherbrooke est très prometteuse et contient une collection impressionnante d'articles en acoustiques avec un accent spécial pour le contrôle de bruits et vibrations avec plus 90 articles enregistrés. Il est clair que ce colloque sera très intéressant. Rendez-vous là-bas!

Le format final du journal prend forme lentement et nous envisageons d'inclure dans chaque édition du journal (autre que l'édition spéciale colloque) les thèmes suivants: deux articles de type technique/recherche, une étude de cas, au moins une revue de livre, des synthèses de thèse, des nouvelles régulières et une actualisation sur les normes canadiennes (une fois par an). Nous essayions d'inclure de courtes descriptions sur les moyens canadiens conduisant des recherches fondamentales en acoustique et sur les bruits et vibrations. Nous devons réussir! je suis sûr qu'avec le temps de telles descriptions deviendraient courantes. Envoyez-moi, s'il vous plaît, vos commentaires, suggestions et naturellement vos idées critiques.

WHAT'S NEW ?? QUOI DE NEUF ?

Promotions	Retirements	Promotions	Retraites
Deaths	Degrees awarded	Décès	Obtention de diplômes
New jobs	Distinctions	Offre d'emploi	Distinctions
Moves	Other news	Déménagements	Autres nouvelles

Do you have any news that you would like to share with Canadian Acoustics readers? If so, send it to:

Avez-vous des nouvelles que vous aimeriez partager avec les lecteurs de l'Acoustique Canadienne? Si oui, écrivez-les et envoyer à:

Francine Desharnais, DREA Ocean Acoustics, P.O. Box 1012, Dartmouth NS, Email: desharnais@drea.dnd.ca
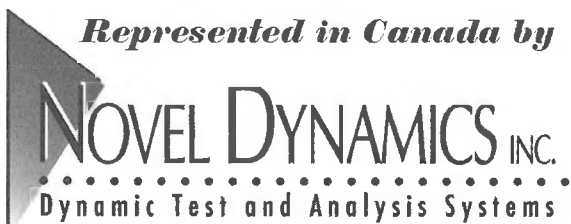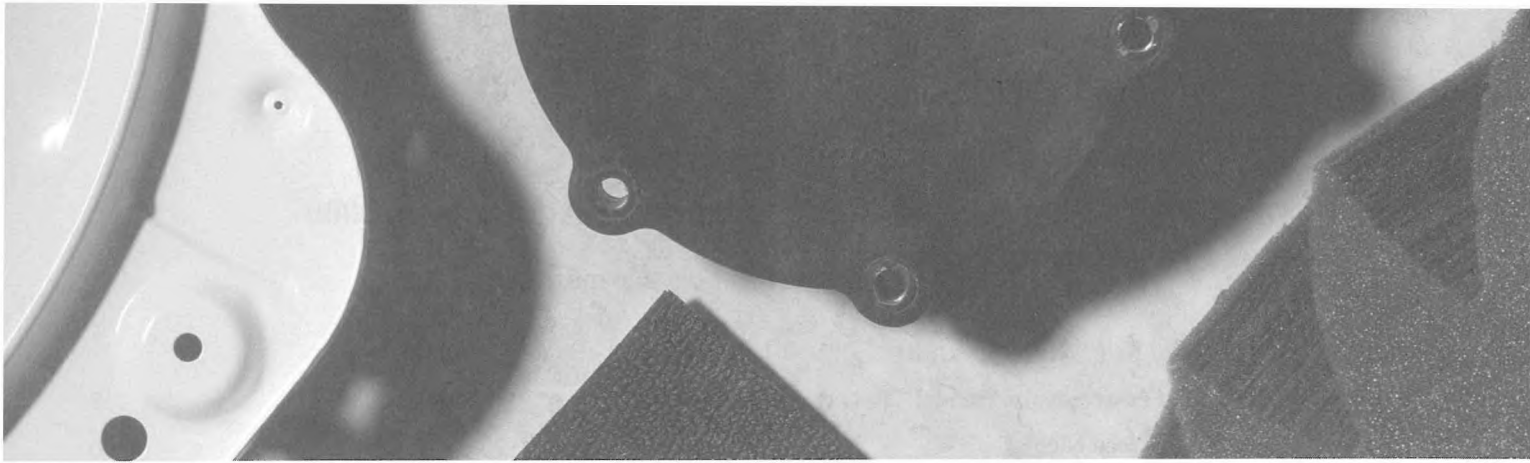
The ABC's of Noise Control
Comprehensive Noise Control Solutions

H.L. Blachford Ltd.'s Comprehensive Material Choices Noise treatments can be categorized into three basic elements: Vibration Dampers, Sound Absorbers and Sound Barriers.

Vibration Dampers

It is well known that noise is emitted from vibrating structures or substrates. The amount of noise can be drastically reduced by the application of a layer of a vibration damping compound to the surface. The damping compound causes the vibrational energy to be converted into heat energy. Blachford's superior damping material is called ANTIVIBE and is available in either a liquid or a sheet form.

Antivibe® DL is a liquid damping material that can be applied with conventional spray equipment or troweled for smaller or thicker applications.

It is water-based, non-toxic, and provides economical and highly effective noise reduction from vibration.

Antivibe DS is an effective form of damping material provided in sheet form with a pressure sensitive adhesive for direct application to your product.

Sound Barriers

Sound barriers are uniquely designed for insulating and blocking airborne noise. The reduction in the transmission of sound (transmission loss or "TL") is accomplished by the use of a material possessing such characteristics as high mass, limpness, and impermeability to air flow. Sound barrier can be a very effective and economical method of noise reduction.

Barymat® is a sound barrier that is limp, has high specific gravity, and comes in plastic sheets or die cut parts. It can be layered with other materials such as acoustical foam, protective and decorative facings or pressure sensitive adhesives to achieve the desired TL for individual applications.

Sound Absorbers

Blachford's **Conasorb®** materials provide a maximum reduction of airborne noise through absorption in the frequency ranges associated with most products that produce objectionable noise. Examples: Engine compartments, computer and printer casings, construction, forestry and agriculture equipment, buses and locomotives.

Available with a wide variety of surface treatments for protection or esthetics. Materials are available in sheets, rolls and die-cut parts – designed to meet your specific application.

Suggest Specific Materials or Design
Working with data supplied by you, H.L. Blachford Ltd. will recommend treatment methods which may include specific material proposals, design ideas, or modifications to components.

ISO 9001 A Quality Supplier
REGISTERED The complete integration of:
- Experience of over forty years
- Quality-oriented manufacturing
- Extensive research and development
- Problem solving approach to noise control

Proceedings of Acoustics Week In Canada 2000
Actes DE LA Semaine Canadienne D'Acoustique 2000

Table of Contents / Tables des matières

ACTIVE NOISE AND VIBRATION CONTROL I / CONTRÔLE ACTIF DE BRUIT ET VIBRATION I

ACTIVE NOISE AND VIBRATION CONTROL II / CONTRÔLE ACTIF DE BRUIT ET VIBRATION II

ACOUSTIC MATERIALS I / MATERIAUX ACOUSTIQUES I

ACOUSTIC MATERIALS II / MATERIAUX ACOUSTIQUES II

STRUCTURAL ACOUSTICS AND VIBRATION / ACOUSTIQUE STRUCTURALE ET VIBRATIONS

MID-FREQUENCY ACOUSTICS AND VIBRATION / ACOUSTIQUE ET VIBRATIONS EN MOYENNES FRÉQUENCES

AUDITORY AGING AND HEARING / AUDITION ET VIEILLISSEMENT

INDUSTRIAL NOISE AND VIBRATION CONTROL II / CONTRÔLE DU BRUIT ET DES VIBRATIONS INDUSTRIELLES II

HEARING AND SPEECH / AUDITION ET PAROLE

COMPUTATIONAL VIBROACOUSTICS II - TOOLS / VIBROACOUSTIQUE NUMÉRIQUE II: OUTILS

LIST OF NON-AVAILABLE SUMMARIES / LISTE DES SOMMAIRES NON-DISPONIBLES   176

EXHIBITORS / DÉMONSTRATEURS

- DALIMAR INSTRUMENTS INC.
- H. L. BLATCHFORD LTD.
- BRUEL & KJAER
- POLYTECH PL INC.
- NOVEL DYNAMICS INC.
- LMS NORTH AMERICA
- VIBRO ACOUSTICS SCIENCES
- STRACO

SPONSORS / COMMANDITAIRE

Strategies for Active and Passive Noise Control

Robert J. Bernhard

Ray W. Herrick Laboratories, School of Mechanical Engineering, Purdue University, West Lafayette, IN 47907-1077, USA

1.0 Introduction

The solution of noise control problems tends to involve three steps, the diagnosis of the problem, the analysis and design of various elements of the problem, and the application of the appropriate solution. Good practice in each of these areas tends to involve a thoughtful and careful approach. In this paper, observations of good practice in each of these areas will be discussed.

2.0 Problem Diagnosis

Favorite success stories of practicing engineers in the noise control engineering field often lead to the same conclusion, the key to resolving a particularly difficult problem is understanding it. To paraphrase these engineers, "*95% of solving the problem was understanding it, after that the solution was simple.*"

Getting to the root of a particular problem seems to be particularly difficult for noise control engineering applications. Typical noise control problems have the following characteristics repetitive and synchronous sources which are indistinguishable using traditional signal processing, reverberation and reflection which make the spatial location of the source hard to identify, and operational characteristics which make disconnect and wrapping studies difficult to apply while keeping the machinery operating under normal conditions. The key to successful diagnostics is having the correct tools and making a thoughtful and comprehensive effort to understand the problem.

The tools for diagnostics are numerous. Their presentation to the community is a bit disjointed and an attempt will be made here to put these methods in some perspective. Diagnostic approaches tend to use either signal characteristics or spatial characteristics.

Digital signal processing methods permit the study of signals measured during operation for characteristics that might indicate the source and/or path. The most straightforward signal characteristics to observe are coherence and transfer functions. However, for traditional signal processing the signal must be broadband, independent, and random signals. Repetitive sources are not random or broadband, synchronous sources are not independent, and reverberant environments mask any random characteristics that do exist with coherent reflections. Thus, traditional signal processing techniques have limited value for noise control applications when applied in a traditional manner.

More advanced signal processing and better application can overcome some of these limitations. As an example, Kompella investigated using multiple operating conditions where different sources would reveal themselves [1,2]. Roggenkamp investigated the application of inverse methods to forces at locations where measurements can not be made directly [3]. Both approaches adapt existing signal processing techniques to the particular features of noise control applications for better diagnostic information.

Acoustical intensity measurements allow the identification of net sound energy flux. Intensity measurement is helpful for identifying source locations under conditions where sound energy flow is reasonably simple and reverberation is low. Often acoustical inten- sity can be used instead of disconnect studies to identify a source. Acoustical intensity measurement methods should be available in the noise control engineer's toolbox of diagnostic methods.

Disconnect and wrapping studies are laborious and must be done with great care to keep machinery noise characteristics unchanged. In many cases this is the only option for diagnostics studies. Proper laboratory facilities and hardware are very important.

The diagnostic phase of a project is critically important. As experienced engineers have found, once the problem is well understood, the solution is often straightforward.

3.0 Analysis and Design

In his defense of research studies and analytical models, a colleague, Werner Soedel, says, "*There is nothing as practical as a good theory*" [4]. A model that is simple to exercise and explains the essential behavior of the machine saves trial and error design iteration and helps all participants of a design team understand the behavior of the system. Thus, simple models such as the mass law and room acoustics equations give the designer great intuition about design compromises and a good understanding of the behavior of the system.

However, not all systems are amenable to analytical models. Numerical methods, such as the finite element (FEM) or boundary element (BEM) methods, have made it possible to build very complete models of the behavior of machines. However, complex models conceal the essential behavior of a system. Simple numerical methods can be constructed to model just the essential behavior of the system. Such models are often very useful at the concept design phase of the design process. If simple models are constructed such that they can be exercised to give design insight, they can be used when analytical theories are unavailable for the same type of "good theory" understanding of a particular application. Parametric model definition techniques, improved postprocessing, and faster computers make it increasingly possible to implement a process where the behavior of systems and design trade-offs can be determined using numerical models.

Statistical energy analysis (SEA) is a more conceptually simple analysis procedure than the finite or boundary element methods. For many high frequency applications where the assumptions of SEA capture the essential behavior of the system, SEA models can be exercised to create "good theory". In some cases however SEA is not able to capture the essential dominant behavior of a system. For these cases, a more sophisticated but efficient prediction scheme is needed.

Along with capturing the essential behavior of the system, "good theory" for noise control applications must also represent the inherent variability of these applications. At frequencies of interest, typical systems are highly sensitive to normal environmental and manufacturing variations. Typical examples of the variation of manufactured products for a sport utility vehicle and light truck were reported by Kompella and Bernhard [5]. Particularly for harmonic sources, the response variation can be very significant from

day-to-day or from vehicle-to-vehicle. At high frequencies with broad band sources, the sensitivity does not cause significant variation since all of the important modes tend to be excited. These characteristics of machinery must be accounted for in design. Efficient methods for predicting this behavior are not readily available yet for all applications.

4.0 Noise Control Solutions

For noise control applications it is important to have a full "toolbox" of potential solutions. A "hammer" is not a solution to every problem. Potential noise control solutions include active and passive alternatives and range from acoustical materials to ear defenders to electronic devices. Different solutions fit different problems and the best solution is often determined by performance requirements unrelated to noise or cost constraints.

At times, active control methods have seemed to be the answer to a large percentage of problems because of the potential flexibility of the approach. However, as with most solutions, a particular active control solution is cost effective and performs well only for certain applications.

For example, most active control solutions presented in the literature are adaptive, feedforward configurations. For feedforward approaches, a reference sensor is placed near the source. The adaptation process is achieved using a signal from an "error" transducer placed in the region where control is desired. The signal from the reference sensor is filtered using the digital filter and is input to the control actuator. This type of controller tends to operate in either a "system identification" mode or a "signal identification" mode.

In the system identification mode, the reference signal and the error transducer signal are used to generate a model of the system between these transducers [6]. This approach is particularly efficient when the system that is to be identified is simple. In an acoustical duct application, the system can be modeled as a simple time delay. Feedforward, adaptive active control systems have been very effective for such applications regardless of the complexity of the excitation source.

For signal identification applications, the adaptive filter uses the error transducer signal to adjust the amplitude and phase of the reference signal to generate a signal that drives the control actuator. This type of controller is particularly effective for stationary, harmonic signals where only a relatively few digital filter coefficients are needed to model the signal. Many of the original active controllers were based on this principle.

For some applications, feedback control is more desirable than feedforward control. Feedback control is particular efficient in a collocated regulator configuration. The delay time that occurs when a feedback sensor and the control actuator are not collocated tends to be significant in most noise and vibration control applications and limits the bandwidth of feedback control. This type of control was used recently for effective control of the radiating modes of a panel driven by turbulent boundary layer excitation, an application where it is impossible to locate an appropriate reference transducer for a feedforward application [7].

There is also promise of better control solutions based on combining active and passive control principles. These might be classified as "smart" passive devices that adapt to the environment and operating conditions and maintain a high level of performance despite being primarily passive systems. One example is the adaptive tuned vibration absorber (ATVA) [8]. For this device, a variable spring is constructed from shape memory alloy wire. The natural frequency of the tuned absorber can be made to track the excitation frequency of the system by controlling the current through the wire. This is a very simple and efficient device that can be made very effective for certain applications.

The potential of active and hybrid active-passive solutions has not yet been fully realized. With the development of MEM's devices and continued improvement of electronics and "smart materials", more novel solutions can be expected that span the range of simple to complex and passive to active.

5.0 Conclusions

In a world where noise is increasingly important as a competitive feature of machines and where environmental concerns are becoming more important, it is crucial to have available the correct tools and resources to;

diagnose and understand a noise or vibration problem,

predict the behavior of a system and pick an optimal design, and

apply the best technology possible.

To accomplish this, noise control must be a primary issue for design and construction and the proper tools must be available. To improve the "toolbox" practicing engineers and researchers need to form partnerships to bring all of the technology available to bear on the correct problem. The industrialist and consultant are needed to define the need for technology and the constraints. Researchers are needed to unlock the technology required to address these problems. In a small community, this should be possible.

6.0   References

Murty S. Kompella, "Improved Multiple-Input, Multiple-Output Modeling Procedures with Consideration of Statistical Information", Ph.D. Thesis, Purdue University, August 1992.

R.J. Bernhard, "The Characterization of Vibration Sources and Measurement of Forces Using Multiple Operating Conditions and Matrix Decomposition Methods," *Proceedings of Internoise 2000*, August 2000.

T.J. Roggenkamp, "An Investigation of the Indirect Measurement of Broadband Force Spectra", Ph.D. Thesis, Purdue University, August 1992.

Werner Soedel, "Personal Communication," Purdue University, date unknown.

Murty S. Kompella and Robert J. Bernhard, "Measurement of the Statistical Variation of Structural-Acoustic Characteristics of Automotive Vehicles", *NCEJ*, Vol. 44(2) (1996), 93-99.

L.J. Eriksson, "Active Sound Attenuation using Adaptive Digital Signal Processing Techniques," Ph.D. Thesis, U. Wisconsin, 1985.

C.M. Heatwole, M.A. Franchek, and R.J. Bernhard, "Robust Feedback Control of Flow Induced Structural Radiation of Sound," *IEEE Trans Control Systems Tech.*, Vol. 8(2) 228-235.

K. Williams, G. Chiu, and R. Bernhard, "Passive-adaptive vibration absorbers using shape memory alloys," Proceedings of SPIE Vol. 3668 (1999).

INNOVATION AND ACOUSTIC

Jean Nicolas

G.A.U.S., Département de génie mécanique, Faculté de génie, Université de Sherbrooke, Sherbrooke (Québec) J1K 2R1 Canada

1. INTRODUCTION

In the last decade, at the dawn of a new millennium, a new key word has appeared in the field of R&D: "innovation". Buzz word? Momentary fashion? New word for the old terminology "development"? In fact, number of journals, reviews, papers, books and conferences about innovation are so great that they show that innovation is undoubtedly there for at least the next decade.

To better understand this wave, it is interesting to learn about its origin, its way of propagation, its impacts on the receiver. We will define innovation, innovation system, innovation process and describe briefly the mechanisms that encourage innovation. We will demonstrate that innovation is on going, as well as in industries, education and in the society in general. After describing this new type of wave, we will analyse the challenges that are proposed / prescribed to acousticians.

2. INNOVATION WAVE: SOURCE, PROPAGATION, AND TRANSMISSION

2.1 Definition

Various authors and working groups have tried to bring their own definition of innovation. The clearest and most concise is probably the one found in the Oslo Manual (OCDE): *"Innovation consists in managing knowledge in a creative way in order to respond to requests coming from the market and to other social needs." (Free translation)* [1]

Innovation relies on three key words : knowledge + creative + market; that is to say : learning + originality + needs.

Still referring to Oslo Manual, authors say: *"An innovation is accomplished when introduce on the market (product innovation) or used in a production process (process) or services"* and they add: *"Innovations interfere with all kinds of activities: scientific, technologic, organisational, financial and commercial".* So, innovation calls on a group of multisectorial resources and conditions. If creativity is the heart of innovation, innovation can take place only with team working, only with the interaction of many actors. Then, we talk about innovation system based principally upon four pillars: scientific research, human resources (education), legal and administrative environment, scientific and technical culture. Innovation depends strongly in research, but innovation by itself is not research. You have to go from the new knowledge / idea to the results (commercialisation) to realise an innovation. Patents are not innovation until they are not on the market. Development is optimization around a product, a process. If there is no originality in it: it is not innovation.

Key sequences of innovation process
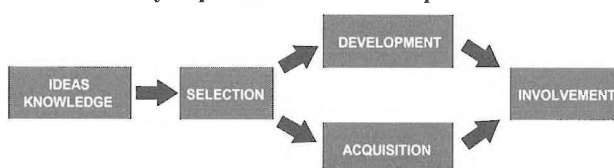
2.2 Innovation: from the source to the receiver

Speaking of innovation, it is important to go from the transmitter to the receiver and still, the receiver (client) has to get the power and spectrum he did want (market needs). So, the source has to be created in that regard and its propagation/transmission has to give the receiver the signal, rapidly and at low cost. It results from these conditions that to reach an innovation, you have to have interaction: innovation is a body contact sport. *"Technology transfer is a person-to-person activity or a body-contact-sport. Inventions and new technologies spring from and reside in the human kind".* [2]

Research about innovation revealed an important point: *"Most of the essential knowledge, in particular technological knowledge, does not exist under a written form. Therefore, transferring certain type of information can be done efficiently only between two experimented persons – by transmission to a receptive person expert enough to fully understand the information or by physical transfer from the persons having the knowledge".* [1]

Innovation depends on the flow of knowledge and this flow should be systematically encouraged and facilitated. *"The main way to increase academia's contribution to innovation is to increase the number of communication channels (knowledge flows) between Academia and industry".* [3]

"The motors of every efficient innovation system are communication and interaction, namely direct and open links between individuals in industries and universities, in languages that will speed the flow of human creativity". [4]

"Innovation is a continuous chain – innovation systems are as solid as their weakling mail". [4]

"But as good as basic knowledge or research quality could be, it does contribute to innovation only when its conversion to the industry and society is open and dynamic". [4]

The innovation wave: the author is strongly convinced that it relies on knowledge creation and diffusion through open interaction. This is also the opinion of other scientists: *"By far the greatest contribution of Academia to innovation takes the form of indirect and intangible flows of knowledge, and the bulk of these knowledge flows occurs through the literature and informal interaction. The main way to increase academia's contribution to innovation is to increase the number to communication channels (and thus knowledge flows) between Academia and industry".* [5]

"While the transfer of intellectual property is often though as the essence of technology transfer, such a view is misleading. Signing of licence agreements, payment of royalties, and transfer of intellectual property are among the few elements of technology transfer. But unpatented know-how, ideas and suggestions often constitute information of considerable value, however difficult to measure and evaluate". [6]

Basic innovation system, as proposed by the C.S.T. [7]
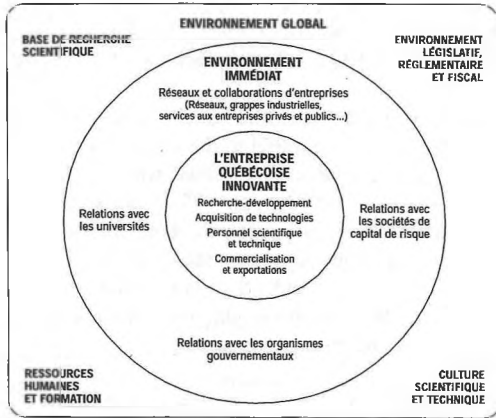
Wheel of Innovation proposed by the author [8]
(in French in the paper)
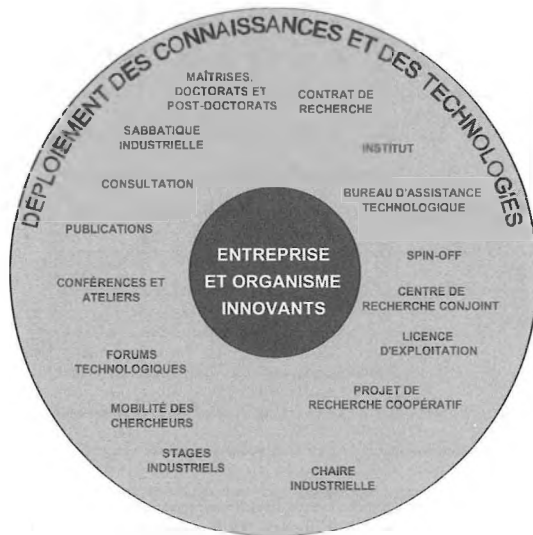
3. ACOUSTIC AND INNOVATION

What will or will not be the contribution of the acoustic field to innovation? Based on the main characteristics of the innovation wave, the author will approach the following subjects during the oral presentation:

What are the new promising fields in order to bring innovation in acoustic? The author will give some examples, especially regarding the medical field, which is very promising.

What are the mechanisms of interaction that should be put in place in order to increase the interactions between universities and industries, also in order to increase noteworthy the number of innovations driven by manufacture industries. The weakness of this link is the weak mail of innovation in acoustic.

"Technology Transfer from Higher Education Institutions. The primary missions of universities are education and research directed at the advancement of knowledge. However, engineering schools and engineering depart-

ments in both countries have long performed a considerable amount of applied as well as basic engineering research. The principal contribution of universities to the technical needs of industry is human capital, that is, well-educated, learning-skilled science and engineering graduates. Thus, movement of science and engineering graduates to other sectors of a nation's innovation system must be considered the most important technology transfer channel of universities. The primary research output of academic research remains nonproprietary new knowledge that is disseminated widely through publications and conferences. Because of the nonproprietary, or "public goods" nature, of much of its output, academic research is funded primarily by the public sector in both countries".[9]

What are the new approaches in education for young researchers in graduate studies? Do professors should train clones of themselves?

4. CONCLUSION

The innovation is there is stay. It takes its source in the original knowledge, which is put in human interaction and is diffused efficiently in regards of the signal emitted by the receiver (buyer). This brings challenges for the acousticians from all horizons, in enterprises, universities and public surroundings. The future of acoustic depends mostly on how acousticians will succeed in taking up this challenge.

5. REFERENCES

[1] *Manuel d'Oslo, Principes directeurs proposés pour le recueil et l'interprétation des données sur l'innovation technologique,* OCDE, 1997, 142 p.
[2] National Academy press, *Technology and transfer systems in the United States and Germany, lessons and perspectives,* 1997.
[3] Etzkowitz, M. *Capitalizing Knowledge,* 1998.
[4] Innovation et transfert technologique, *Innovation et créativité,* édition spéciale, juin 2000.
[5] J. Senker et al., dans *Capitalizing Knowledge – New Intersections of Industry and Academia.*
[6] National Academy Press, *Systems in the United States and Germany : Lessons and Perspectives,* 1997, 448 p.
[7] *L'entreprise innovante au Québec : les clés du succès,* Conseil de la science et de la technologie, 1998, 90 p.
[8] J. Nicolas, *L'innovation industrielle,* ADRIQ, 21 juin 2000.
[9] Lee, Yong S., *University-Industry Collaboration on Technology Transfer : Views from the Ivory Tower,* Policy Studies Journal, Vol. 26, No. 1, 1998, p. 69-84.

POWER BALANCE METHODS TO ESTIMATE JUNCTION ATTENUATION IN LIGHTWEIGHT CONSTRUCTIONS

Trevor RT Nightingale and Ivan Bosman
Institute for Research in Construction, National Research Council, Ottawa, Ontario, Canada K1A OR6

INTRODUCTION

In-situ junction attenuation is an important factor in determining the relative importance of structure borne flanking paths in buildings. Unfortunately, junction attenuation can not be measured directly and must be measured indirectly. Traditionally, this has been done using power balance methods, such as SEA, where measures of velocity level difference, VLD, between the two connected surfaces are related to the attenuation of the junction connecting them. For surfaces that are homogeneous, isotropic and lightly damped, such as cast-in-place concrete, this method has proven to be very effective.

This summary paper will assess the suitability the power balance method to estimate junction attenuation in a lightweight-framed construction by investigating the sensitivity of the measured VLD to the choice of measurement positions and by relating the variance in these measures to attenuation with distance in the surfaces.

THEORY – RELATING VLD TO JUNCTION ATTENUATION

The junction attenuation, in decibels, between two coupled plates can be expressed in terms of measurable properties, namely the VLD (term in first brackets) and the total loss factor η,

$$R_{12} = 10\log\left[\frac{\langle v_1^2 \rangle_{surface\,1}}{\langle v_2^2 \rangle_{surface\,2}}\right] + 10\log\left[\frac{m_1}{m_2}\frac{C_{g1}L}{\eta_2\omega\pi S_1}\right] \quad (1)$$

where m is the mass of the surface, v is the measured mean surface velocity, Cg is the group speed for bending waves, S is the plate area and L is the length of the junction. Theoretically, Eqn. 1 is valid only when the following conditions [1] are satisfied:

1.) The source plate must be sufficiently large to support many modes in each third octave band and should be moderately damped. These two requirements can be expressed by a single expression: the modal overlap factor which should exceed unity;

2.) The reverberation radius should be very small, i.e., the plate is lightly or moderately damped. This ensures that accelerometer positions located even a short distance from the source will be sampling the reverberant field. A highly damped plate has a large reverberation radius which is characterised by strong attenuation with distance from the source;

3.) Each of the surfaces must be homogeneous and isotropic thereby assuring that each surface is a single subsystem and that the energy will be sampled only in that subsystem. Also, the coupling must be sufficiently weak, and the damping of the receive system sufficiently great, that there will be a difference in the modal energies of the two surfaces.

Eqn. 1 may be considered to be approximate for surfaces that are orthotropic since it is assumed that the group speed is independent of the direction of propagation. This difficulty does not effect the linear dependence of junction attenuation on the VLD. For the cases and frequencies presented here, the modal overlap factor exceeded unity.

MEASURED VELOCITY LEVEL DIFFERENCE

The measurement method proposed by Craik [2] was used to estimate the VLD between the gypsum board wall and the subfloor surface of the wood-framed floor assembly shown in Figure 1. It is important to note the orientation of the framing members in the two surfaces as this determines the orientation of the butt joints between the

sheathing panels. In the floor, the 38x235 mm solid wood joists, spaced 400 mm o.c., are parallel to the wall/floor junction so the 1.2x2.4 m sheathing panels are oriented with the short axis and butt joints parallel to the junction. The long side of the panel joins to adjacent panels using interlocking tongue and groove joints. The 1.2x2.4 m gypsum board panels do not have a profile on the edges and the butt joints are oriented perpendicular to the wall/floor junction. Heavy dashed lines indicate the butt joints between panels.
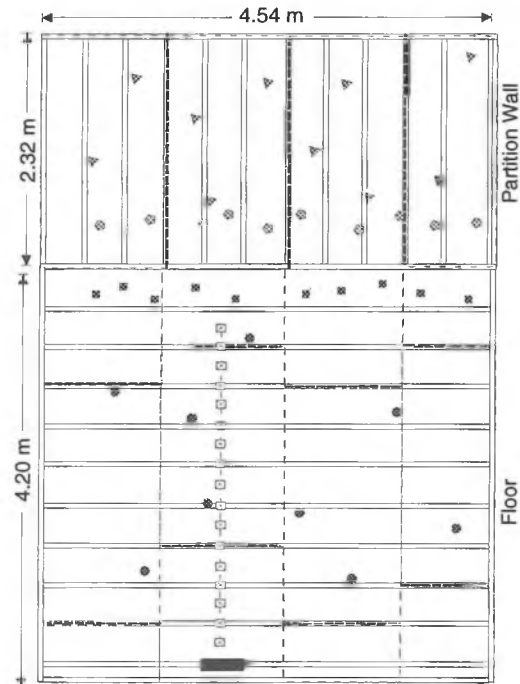
Figure 1: Accelerometer locations for VLD measurements the between the wall and the subfloor are shown by solid symbols. Positions used for the draw-away measurements are shown by the open symbols, while the source is indicated by the solid rectangle.

If, on average, Conditions 1, 2 and 3 are satisfied then the measured VLD should be reasonably insensitive to the location of the accelerometer positions with the largest change occurring in the low frequencies where there are fewer modes. Position sensitivity was investigated by measuring the wall/floor junction using three sets of accelerometer positions. In Set 1 the accelerometers were randomly located on both the wall and subfloor (shown in Figure 1 by the triangles on the wall and the circles on the subfloor). In Set 2 the accelerometers on the subfloor were moved toward the wall and located 0.25±0.07 m from the junction (and are shown by the squares). The wall positions were unchanged. In Set 3 both the wall and subfloor accelerometers were located 0.25±0.07 m from the junction. (Pentagonal symbols show the positions on the wall).

Comparing Set 1 and Set 2 data of Figure 2 it can be seen that the measured VLD is very sensitive to the measurement location on the subfloor. The change in VLD was greater than 10 dB for frequencies above 200 Hz. However, comparing Sets 2 and 3, it

can be seen that there was virtually no change in the measured VLD as a result of moving the wall accelerometers close to the junction. The marked drop in the measured VLD caused by moving the positions on the floor closer to the junction suggests that the vibration field is highly attenuated as it propagates in the subfloor. This suggests that Conditions 2 and/or 3 have not been satisfied and is the subject of the next section.
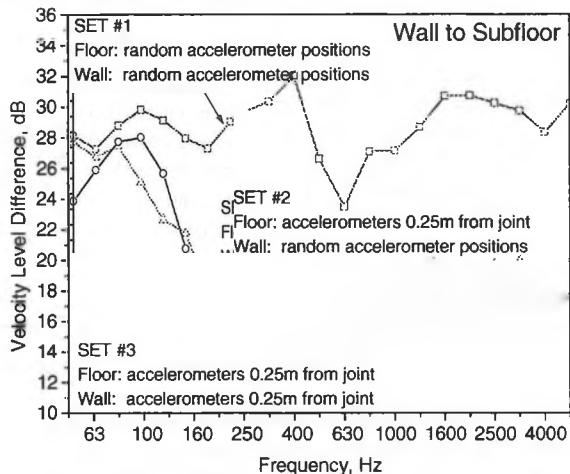
Figure 2: Measured VLD between the wall and subfloor for three different sets of accelerometer positions as shown in Figure 1.

VIBRATION RESPONSE OF THE SUBFLOOR SURFACE

Measurements of surface acceleration were made along a line perpendicular to the joint to see if Conditions 2 and 3 were satisfied.

From examination of the acceleration levels with distance shown in Figure 3 for the bare OSB subfloor of floor/ceiling assembly, it is evident that the vibration response is not uniform. There are two distinct regimes. One close to the source where there is strong localisation of energy and one further away where the level decreases with distance (a violation of Condition 2). This is particularly evident when compared to the very gradual change in response observed for single OSB sheet without attachments. The transition between the two regions in the floor/ceiling assembly with the bare subfloor occurs 1.2 m from the source where there is a butt joint in the OSB sheathing (as shown in Figure 1). Obviously the discontinuity in the vibration levels at a butt joint between the subfloor panels precludes treating the OSB subfloor surface as a single subsystem (a violation of Condition 3). These observations indicate that the presence of butt joints, joists and increased in-situ damping prevent a diffuse field in a framed floor [3].

Figure 3, which also shows the vibration response of the same floor when covered by a 38 mm layer of 2000 kg/m^3 concrete, indicates that a topping may reduce localisation of energy near the source. At 4 kHz the vibration response is quite uniform across the floor while at 500 and 1000 Hz there is still considerable localisation of energy near the source. Localisation increases with decreasing frequency.

It is interesting to note that at 4 kHz the rate of attenuation in the OSB subfloor after the butt joint is comparable to those observed for a single OSB sheet without attachments. At this frequency the coupling between the OSB and the joists is quite weak since the fasteners appear as individual points (rather than line-connected) and the dominant attenuation mechanism may be internal losses in the OSB. With the concrete topping the bending wavelength will increase and so too will the frequency at which the joists appear point-connected and one might expect greater localisation. However,

this is not the case and can be explained by recognising that the effect of rotary inertia of the joists will diminish as the stiffness and mass of the floor surface increases. Also, the topping will act as a bridge across the butt joint. Thus, with the topping the joists might be line-connected but their effect is greatly reduced compared to the case with the bare floor. The rate of attenuation with or without the topping is similar for distances after the butt joint (i.e., greater than 1.6 m) indicating that the loss mechanism is likely the same for both situations.
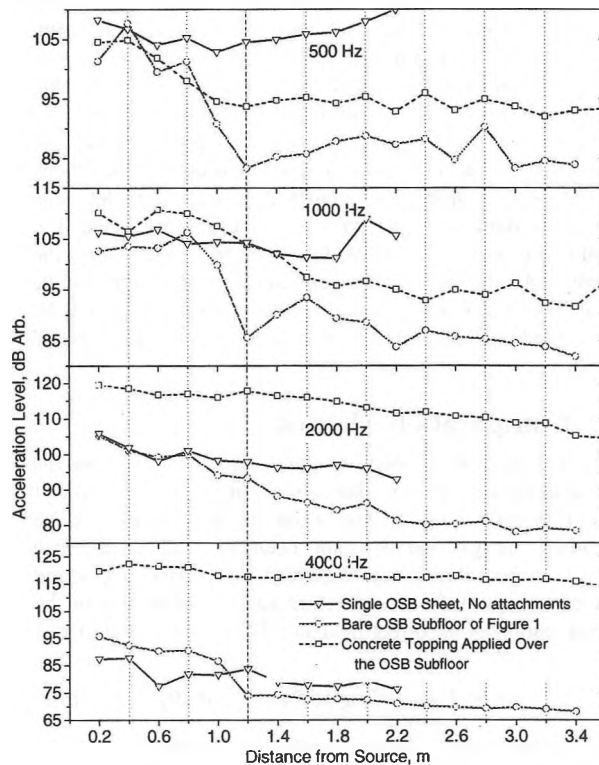
Figure 3: Measured third-octave band vibration response of the floor surface in a direction perpendicular to the joists. The dashed line at 1.2m from the source indicates the location of the butt joint between the OSB sheets. Shown for comparison is the response of a sheet of OSB without any attachments.

CONCLUSIONS

The measured VLD's shown in Figure 2 are the result of two attenuation mechanisms: the wall/floor junction and losses in the measurement surfaces. Additional attenuation in the surfaces, which is a complex function of the damping, size and spacing of the joists, presence of joints in the sheathing, will tend to increase the measured VLD and make the measurements very sensitive to accelerometer location. The most important factor appears to be the butt joints in the OSB subfloor. The effect of which is greatly reduced if the surface is covered by concrete. Further work is needed to determine a suitable in-situ test method for lightweight framed constructions.

REFERENCES

1.) T.R.T. Nightingale, Ivan Bosmans, "Estimating Junction Attenuation in Lightweight Constructions," Proceedings of INTERNOISE 2000, Nice France, August 28-30, 2000.
2.) R.J.M. Craik, Applied Acoustics, Vol. 15, pp. 355-361, 1981.
3.) T.R.T. Nightingale, Ivan Bosmans, Building Acoustics, Vol. 6, No.3/4, pp. 269-288, 1999.

HYBRID IMAGE/ENERGY APPROACH FOR ACOUSTICAL PREDICTIONS OF INDUSTRIAL ROOMS

André L'Espérance, ing.

Soft dB inc, Québec *(www.softdb.com*) and research associate at the G.A.U.S.

INTRODUCTION

Several approaches may be used for acoustical prediction computations, among which is Sabine method, ray-tracing method, images method, or empirical methods. However, these methods are either too approximate or too complex to be easily implemented by hygienists, engineers, and other persons who work in the field of industrial noise. To compensate for this gap, a hybrid approach based on geometry acoustics and on energy acoustics has been developed. To make this acoustical prediction model easy-to-use, a Windows graphical interface has been created. The following article presents the acoustic model and the graphical interface which facilitates its use. Some results that have been obtained with the proposed model will be presented and compared to results obtained with standard methods.

1. Computation Method

The new method is based on Sabine method. It first consists in determining the contributions of the direct field and of the first reflections on the walls. It then distributes the residual energy that has not been considered in those contributions. According to Sabine's approach, the sound field at an point in a reverberant room corresponds to the combination of the direct field and the reflected field, that is :

$$Lp = Lw + 10Log\ [1/(4\pi r^2) + 4/R] \qquad (1)$$

where the term $4/R$ represents the contribution of the diffuse field, R is equal to $S\overline{\alpha}/(1-\overline{\alpha})$, where $\overline{\alpha}$ is the average absorption coefficient of the room. The contribution of the reflected field is based on the hypothesis that, in diffuse filed and steady state, the energy after the first reflection, that is $Wa = W(1-\overline{\alpha})$, must be in balance with the energy absorbed by all the walls, which, in diffuse field, is equivalent to [1] :

$$Wa = W(1-\overline{\alpha}) = <P^2>S\overline{\alpha}/(4\rho c) \qquad (2)$$

where $<P^2>$ is the sound field, S is the total surface of the room wall, and ρc is the air density and sound speed.

- Sabine's method of order n

If one determines not only the contribution of the direct field but also the contributions of the paths that have been subjected to a first reflection on each wall of the room, equation (1) becomes :

$$Lp = Lw + 10Log\ [1/(4\pi r^2) + C_1 + 4/R_1] \qquad (3)$$

or $\qquad C_1 = \Sigma(Q_i/4\pi r_i^2) \qquad (4)$

where C_1 represents the contribution of order 1, that is the sum of the contributions associated to i paths (r_i) that have been subjected to a first reflection on each m wall of the

room. Those paths are balanced according to the absorption coefficient Q_i associated to the reflection on each wall.

The last term of eq. (3) corresponds to the contribution of the residual field, excluding the first reflection. Similarly to eq.(2), the residual field R may be evaluated from the balance between residual energy after the second reflection and the energy absorbed by all the walls, that is $Wa' = W(1-\overline{\alpha})(1-\overline{\alpha})$. By extension, knowing the contributions of the paths that have been subjected to 1, 2 or N reflections on each wall of the room, the sound level at a given j receiver may be evaluated with :

$$Lp(j) = Lw + 10Log\ [1/(4\pi r_j^2) + C_1(j) + ... + C_n(j) + 4/Rn\ ] \quad (5)$$

where $\qquad Rn = S\overline{\alpha}/(1-\overline{\alpha})^{n+1} \qquad (6)$

- **Determination of the contribution of order n, C_n**

The algorithm that was developed to determine the reflected paths on each wall and for each computation order uses the Borish[2] approach. This algorithm consists in determining the position of an image source through a wall using the normal of the wall and the position of the original source. When this computation is done for the m walls of the room, the process must be repeated using the position of the image sources as the original source, and so on. The number of potential Nbi image sources created for each order n becomes high :

$$Nbi = m^{(n-1)} \qquad (7)$$

The analysis of the contributions in relation to the computation order for different j receivers shows that the $Cn(j)$ contributions become relatively independent of the receiver's position as the order n increases. (figure 1).
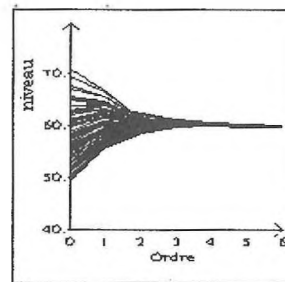
Figure 1 Contributions *Cnj* in relation to order n.

This result is explained by the fact that, for high reflection orders, the distances of the paths and their associated absorption coefficients $Qn(j)$ become relatively independent of the receiver's position. Combined with the fact that there are many reflected paths for each order and each position of receiver, the result is that the Cnj become independent of the receiver's position near order 5. This result corresponds to the fact that the reflected field is diffuse, and thus the Rn residual field becomes identical for all the receivers.

For rooms of complex shape, or when barriers are considered, some receivers will have different Cn contributions, even for higher orders, due to the fact that they are in a shadow zone in relation to walls or barriers. To take this phenomenon into account, residual energy at a (j) receiver is evaluated from the relation between the contribution received at order n at this $Cn(j)$ receiver and the average contribution received at the other Np receivers :

$$Rn(j)= Cn(j) / CMn *4 S/(1-\overline{\alpha})^{n+1} \qquad (8)$$

$$CMn=\Sigma Cn(j)/Np \qquad (9)$$

2. Graphical Interface

A user-friendly graphical interface under Windows environment allows to define or modify at any time the data that is necessary for modeling. The functionalities are grouped under 7 main menus, among which is *Room Construction*, a menu that offers tools to define the geometry and the acoustic parameters of the room.
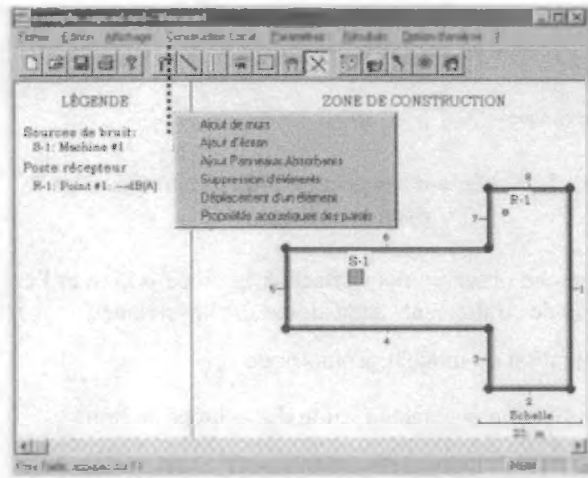
Figure 2 Main menu of the graphical interface

Furthermore, the user may, with the mouse, draw the lines to define the plan of the studied room. Some action buttons are also available to facilitate this construction and the definition of the acoustical parameters. For example, by clicking on a line that represents a wall of the room, the dialog box that allows to modify the acoustical parameters related to this wall will appear. Moreover, the user may put acoustic barriers or absorbing panels at certain specific points of the room.

3. Results

Besides the computation of the sound levels at specific points of the room, the model allows to obtain the noise map (isophone) of the room. Figure 3 compares, for an irregular shape room, the isophones obtained with the proposed model and the isophones obtained with the ray-tracing method[3]. Figure 3 gives 8 of the 64 paths that have been considered to calculate the sound level at R-1 point. Figures 3a and 3b show that the predictions are similar for both models, and that the absolute levels as well as the repartition of the sound field are respected everywhere in

the room. However, with the proposed model, it takes less than one minute to obtain the noise map.
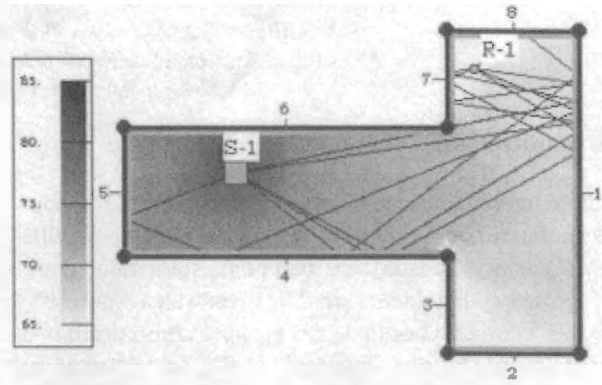
Figure 3a Isophone obtained with the proposed model
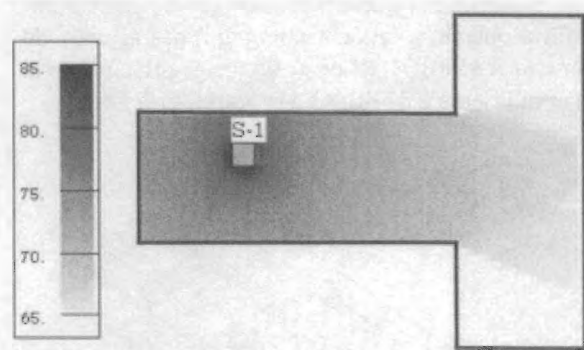
Figure 3b Isophone obtained with the ray-tracing method

4. Conclusion

A hybrid approach based on the image method and statistical energy has been developed. This approach, also called Sabine of higher orders, allows to consider the geometry and acoustical properties of each wall of irregular shape rooms. A user-friendly interface has been developed under Windows environment to facilitate the use of the model. The results obtained with the proposed model are similar to the ones obtained with other accurate methods, but the implementation of the proposed model is easier, and the computation time is shorter.

References

[1] Fundamentals of Acoustics, John Wiles & Sons.

[2] J.Borish. Expansion of the image model to arbitrary polyhedra, JASA 75,(6) p.1827-1836 (1984).

[3] Acoustique Prévisionnelle : Logiciel Rayscat, Les notes scientifiques et techniques de l'INRS, no 67 (1987).

Simulation et traitement acoustique de la centrale hydroélectrique Chute-des-Passes

André L'Espérance*, Alex Boudreau** et Gilles Pagé***

* *Soft dB inc,* Québec *(www.softdb.com*) et chercheur associé au G.A.U.S.
** G.A.U.S. Université de Sherbrooke, Sherbrooke (Québec) J1K 2R1, Canada
*** *Alcan* métal primaire, Alma, gilles.pag@alcan.com

1.0 Introduction

La centrale hydroélectrique Chute-des-Passes de la compagnie Alcan est située à environ 200 km au nord de la ville d'Alma (Québec, Canada). Le bâtiment, souterrain, comporte 5 groupes alternateurs de 250 mégawatt (Figure #1) répartis sur 5 étages, chacun de ces groupes comprenant une turbine et une génératrice (Figure #2 et #3). Le bâtiment est d'une grande complexité géométrique et les sources de bruit sont multiples et réparties sur tous les étages. L'objectif du projet est de déterminer quels traitements il convient d'implanter afin d'obtenir, à un coût minimum, des niveaux de bruit inférieurs à 85 dB(A) à l'étage #5 (étage principal de la centrale) et inférieurs à 87 dB(A) aux étages #1 à #4.
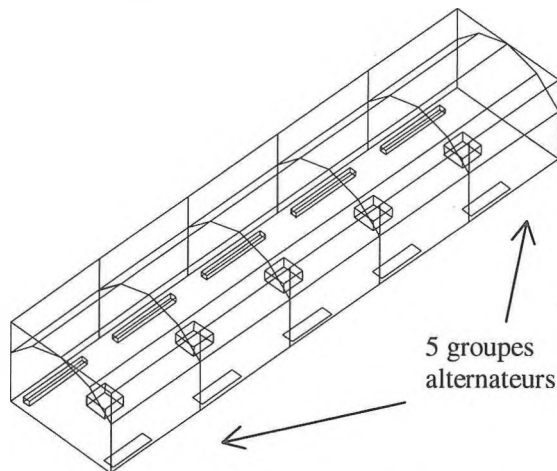
Figure 1. Schéma global de l'étage #5
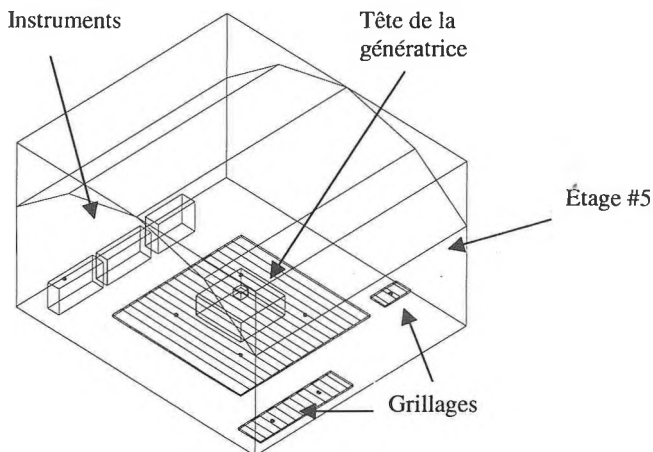
Figure 2. Schéma d'un groupe alternateur pour l'étage5
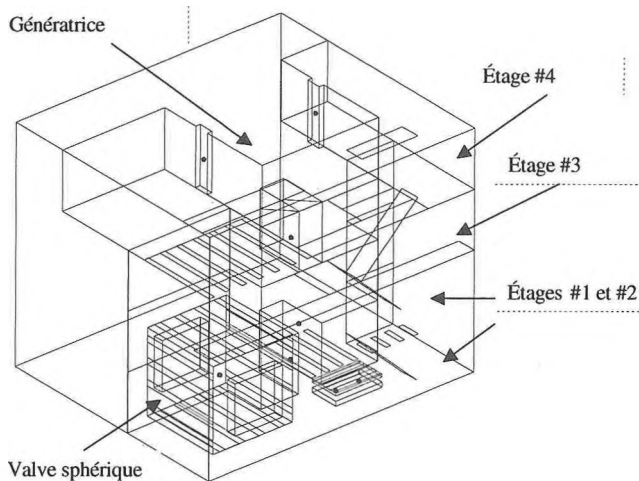
Figure 3. Schéma d'un groupe alternateur pour les 4 premiers étages.

La démarche observée pour effectuer la modélisation et l'évaluation des traitements acoustiques est la suivante :

1) Élaboration du modèle géométrique

2) Identification et caractérisation des sources de bruit

3) Évaluation de traitements acoustiques

2.0 Élaboration du modèle

La complexité de la centrale nécessite l'utilisation d'un modèle permettant la représentation d'une géométrie complexe et tenant compte des caractéristiques fréquentielles des sources de bruit et des matériaux du local. Le tir de rayon constitue un type de modèle répondant à ces exigences [1]. Cette technique se retrouve à la base du logiciel utilisé pour construire le modèle présenté dans ce texte (RAYSCAT) [2].

2.1 Modélisation des sources non ponctuelles

Pour modéliser une source non ponctuelle, une technique basée sur une représentation de la géométrie de la source à l'aide de plans espacés a été utilisée. Par exemple, les valves sphériques, une des sources importantes de la centrale, sont modélisées comme illustré à la Figure #4.
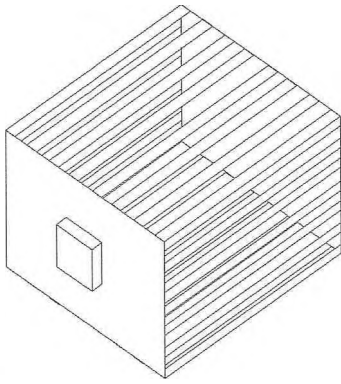
Figure 4. La représentation d'une source non ponctuelle

2.2 *Hypothèse simplificatrice pour réduire les temps de calculs*

La symétrie de la centrale a été utilisée afin de diminuer le nombre de plans. Les cinq postes sont identiques et disposés suivant le sens de la longueur (voir Figure #1). Les modèles des Figure #2 et #3 représentent le poste #3, au centre de la centrale. La présence des deux autres postes, situés de part et d'autre du poste #3, est simulée à l'aide de murs réfléchissants (virtuels).

3.0 Identification et caractérisation des sources de bruit

Une méthodologie structurée permettant d'évaluer de façon efficace les sources de bruit et leur puissance acoustique a été utilisée. Cette méthode consiste à effectuer :

1) une validation du modèle acoustique à l'aide d'une source de référence;

2) une série de mesures des niveaux de bruit à plusieurs endroits dans le bâtiment;

3) une localisation des sources et une mesure de leur puissance acoustique;

4) un calcul des niveaux de bruit générés par les sources du local à l'aide du modèle acoustique;

5) un retour à l'étape #3, s'il y a des écarts non négligeables entre les niveaux mesurés et ceux calculés par le modèle.

Cette technique a permis d'identifier 13 sources et d'obtenir un modèle où les différences par rapport aux mesures (point #2 de la méthodologie) ont été inférieures à 0.5 dB.

4.0 Évaluation de traitements acoustiques

Pour évaluer efficacement les traitements acoustiques, il est avantageux d'utiliser une technique d'évaluation basée sur les fonctions de transfert entre les différentes sources du modèle et des groupes de récepteurs. Pour une source donnée, les fonctions de transfert sont obtenues simplement par la différence entre les puissances des sources et les niveaux obtenus aux récepteurs. Ces fonctions de transfert sont ensuite utilisées dans un tableur pour recalculer les niveaux de bruit moyens globaux à chaque groupe de récepteurs à l'aide de l'expression suivante :

$$Niv_{globaux_i} = 10 * \log_{10}(\sum_{S=1}^{n}\sum_{f=1}^{m} 10^{\frac{\bar{P}_{sf} - \bar{H}_{sf_i}}{10}})$$

où H_{sf} représente la fonction de transfert entre la source s à la fréquence f pour un groupe de récepteurs i donné, et P_{sf} la puissance acoustique en dB mesurée de la source s à la fréquence f. À l'aide de cette technique, plusieurs traitements ont été évalués. La combinaison de traitements optimums donnant le meilleur rapport réduction/dollars investis a été implantée. Les réductions associées à ce traitement optimum ont été les suivantes :

Étage	Niveau (av.)	Niveau (ap.)	Réduc.
#1	101.4 dB(A)	87.5 dB(A)	**13.9 dB**
#2	102.4 dB(A)	87.5 dB(A)	**14.9 dB**
#3	100.1 dB(A)	88.0 dB(A)	**12.1 dB**
#4	97.2 dB(A)	88.0 dB(A)	**9.2 dB**
#5	92.4 dB(A)	83.0 dB(A)	**9.4 dB**

5.0 Conclusion

À l'aide de techniques originales de modélisation, un modèle acoustique fidèle de la centrale Chute-des-Passes a été construit. À partir de ce modèle et d'une technique efficace d'évaluation des traitements acoustiques, un traitement optimum a pu être élaboré et validé avec succès.

6.0 Références

[1] **Ondet A. M. and Barbry J. L.,** *Modeling of sound propagation in fitted worshops using ray tracing,* J. Acoust. Soc. Am. **85** (2), February 1989, p 787-796.

[2] **A.-M. Ondet et J.-L. Barbry,** *Modélisation de la propagation dans les locaux industriels encombrés à partir de la technique des rayons – logiciel Rayscat,* Les notes scientifiques et techniques de l'INRS **67**, Septembre 1987, (130 pages).

RECENT MEASUREMENTS OF TOTAL ENERGY DENSITY USING A UNIQUE TRANSDUCER ARRAY

Brandon Tinianov
Johns Manville Technical Center, 10100 West Ute Avenue, Littleton, Colorado, USA 80127

1.0 INTRODUCTION

Contemporary laboratory test methods determine the sound power of a noise source by sampling the sound pressure in a reverberant field. While these tests allow for a convenient assessment, they falsely assume that either the sound field is ideally diffuse, or that the sampled data adequately represent the average sound pressure in the room. The research of Budhiantho [1], developed theoretical probability density functions for the potential, kinetic, and total energy densities were modeled in a reverberant sound field. These models suggest that the variance of the total energy density is one half that of the potential energy density approximated by the sound pressure in current test methods and such measurements could yield more accurate results. Experiments were conducted to verify these theories and determine the practicality of the technique.

2.0 MODEL

Based o the earlier work of Waterhouse [2], Cooke and Schaede [3] and Lubman [4], Budhiantho derived a statistical model for the potential, kinetic, and total energy distributions in such a reverberant field.

The model states that a component of the velocity vector can be determined from the integral of the pressure gradient in a given direction.

$$v_x = \frac{1}{\rho d} \int (P_x - P_r) dt \qquad (1)$$

With the assumption that the in the case of a diffuse field, pressure magnitudes are Gaussian and performing only linear mathematical operations, the velocity component amplitude is Gaussian as well.

$$|V| = \left(v_x^2 + v_{y}^2 + v_z^2 \right)^{1/2} \qquad (2)$$

The vector velocity is the square root of the sum of the components squared. The result is a Maxwell distribution.

The kinetic energy density is proportional to the sum of the squares of the velocity components. The kinetic energy then becomes a Γ-distribution with three degrees of freedom.

Likewise, the potential energy is proportional to the acoustic pressure squared. This yields an exponential distribution, which is a Γ-distribution with one degree of freedom.

The total energy density is then a Γ-distribution with 4-degrees of freedom

3.0 EXPERIMENT

Several generations of total energy density sensors have been constructed, developing from one-dimensional probes to three-dimen-

sional arrays [5,6], but all were limited in their measurement frequency range. In the present study, there were two major modifications to earlier designs to allow implementation in a commercial laboratory setting: capability of broad band response and integration with a typical rotating microphone boom.

This latest array construction is composed of two nested microphone tetrahedrons with a common reference microphone, for a total of seven microphones. The microphone spacing for the smaller tetrahedron is 15 mm while the microphones of the larger array are separated by a 55 mm gap (see Figure 1).
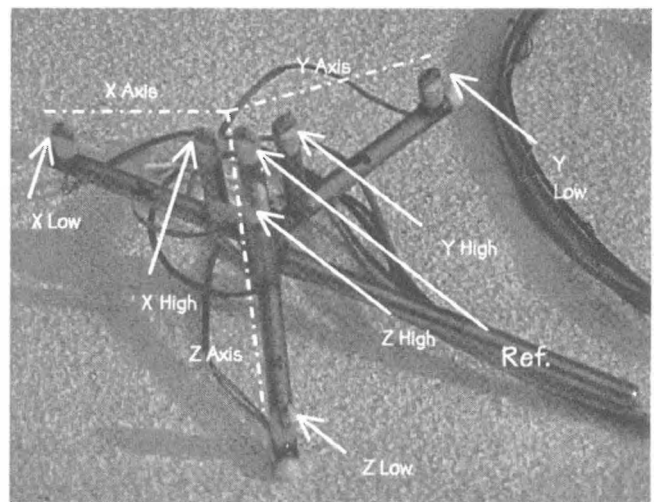
Figure 1: A seven-microphone array for total energy density measurements from 100 to 5000 Hz.

Responses of the arrays are combined in a signal conditioning/amplification module at a crossover frequency of 1000 Hz. This configuration allows the probe to be sensitive in three dimensions with flat response from 100 to 5000 Hz. A second signal conditioning module was added with a third order active low-pass filter to prevent signal aliasing.

Acquisition and processing were executed via LabVIEW processing software on a desktop computer. The processing algorithm sums the pressures to produce an average, then squares it to produce potential energy density. Pressure differences between microphone pairs are integrated to get velocity components, then squared and summed to yield kinetic energy density. Kinetic and potential energy densities are summed to yield total energy density.

Two sound sources were used for the experiments. For pure tones and dual tones, a JBL two-way dynamic driver was excited by a Hewlett Packard function generator. An ILG Industries squirrel cage fan was used as the broad band source.

For each measurement, the sensor was mounted to a 1.6 meter boom and sampled at various fractions of wavelengths along the 10

meter circular traverse. All measurements were conducted in a 319 m3 reverberation chamber qualified to 100 Hz by both ISO and ASTM test methods.

4.0 RESULTS

Experimental results were collected and processed for 26 unique source conditions with signals ranging from 100 to 5000 Hz. The measured standard deviations for 4 representative source configurations are compared to the theoretical standard deviations and are presented in Tables 1 through 3. In addition to tabular results, data was processed as bar chart histograms and showed excellent agreement to theoretical curves. Such graphical comparisons are presented elsewhere.

	Potential Energy Density Norm. Std. Deviation	
Source Configuration	Theory	Measured
Pure tone @ (500 Hz)	1.00	1.02
Pure tone @ (3500 Hz)	1.00	0.99
Dual tone @ (2000 & 2050 Hz)	1.00	1.06
Broad Band Noise	1.00	1.01

Table 1: Standard Deviations of the Potential Energy Density $[E_p]$ for selected measurement conditions

	Kinetic Energy Density Norm. Std. Deviation	
Source Configuration	Theory	Measured
Pure tone @ (500 Hz)	0.57	0.58
Pure tone @ (3500 Hz)	0.57	0.53
Dual tone @ (2000 & 2050 Hz)	0.57	0.60
Broad Band Noise	0.57	0.58

Table 2: Standard Deviations of the Kinetic Energy Density $[E_k]$ for selected measurement conditions

	Total Energy Density Norm. Std. Deviation	
Source Configuration	Theory	Measured
Pure tone @ (500 Hz)	0.50	0.51
Pure tone @ (3500 Hz)	0.50	0.56
Dual tone @ (2000 & 2050 Hz)	0.50	0.56
Broad Band Noise	0.50	0.52

Table 3: Standard Deviations of the Total Energy Density $[E_t]$ for selected measurement conditions

5.0 CONCLUSIONS

Experiments showed that the expanded sensor accurately measured the potential, kinetic, and total energy densities with distributions similar to those predicted by statistical models. In every case, sound power determination using total energy density offered greater accuracy over traditional measurements using potential energy density alone.

Modification allowing continued use of traditional commercial laboratory equipment did not adversely affect the experimental agreement with theory and offered an alternate method for more accurately determining the sound power of sources in reverberation chambers.

REFERENCES

[1] M.H.W. Budhiantho, "Acoustic Velocity Related Distributions," Dissertation, Univ. of Texas at Austin, ECE. Dept., Austin, Texas, August 1997.

[2] R.V. Waterhouse, "Statistical Properties of Reverberant Sound Fields," *J. Acoust. Soc. Am.* vol. 43, no. 6, pp.1436-1444, 1968.

[3] R.K. Cook and P.A. Schade, "New Method for Measurement of the Total Energy Density of Sound Waves," *Proc. Inter-noise 74*, pp.101-106, 1974.

[4] D. Lubman, "Precision of Reverberent sound power measurements," *J. Acoust. Soc. Am* .vol. 56, no. 2, pp. 522-533, 1974.

[5] B. Morton and E.L. Hixson, "System for the Measurement of Acoustic Energy Density," *J. Acoust. Soc. Am.* vol. 60, Suppl. 1, p. S59, Fall 1976.

[6] M. Schumacher and E.L. Hixson, "A Transducer and Processing System to Measure Total Acoustic Energy Density," *J. Acoust. Soc. Am.* vol. 74, Suppl. 1, p. S62, 1983.

TRACEABILITY FOR CANADIAN ACOUSTICAL STANDARDS

George S. K. Wong

Institute for National Measurement Standards, National Research Council, Ottawa, Ontario, Canada, KIA 0R6

ABSTRACT

Acoustical measurements in Canada are traceable to the primary acoustical standards maintained at INMS, NRC. In reality this may not be true since most of the users of acoustical measuring instruments in Canada may not realise the importance and understand the process of establishing traceability of a laboratory. There are two paths to establish traceability. A direct path, that is, a national metrology institute (NMI), calibrates an artefact that is used as a reference for measurement. The NMI may be a laboratory that has mutual recognition agreement with NRC. An indirect path may be traceable via laboratories that are accredited under the Calibration Laboratory Assessment Service (CLAS) program jointly administered by the Standards Council of Canada (SCC) and INMS. The latter provides technical support for the program.

SOMMAIRE

Les mesures acoustiques faites au Canada sont traçables aux étalons acoustiques primaires maintenus par l'IÉNM du CNRC. En réalité, il se peut que cela ne soit pas toujours le cas, parce qu'il est possible que la plupart des utilisateurs d'instruments de mesure acoustiques ne se rendent pas compte de l'importance d'établir la traçabilité des mesures et ne comprennent pas les méthodes utilisées pour l'établir. Il y a deux façons d'établir la traçabilité. Dans la méthode directe, un institut national de métrologie (INM) étalonne un objet qui sert de référence pour la mesure. L'INM peut être un laboratoire ayant conclu une entente de reconnaissance mutuelle avec le CNRC. Dans la méthode indirecte, on établit la traçabilité des mesures par l'entremise de laboratoires accrédités par le Service d'évaluation des laboratoires d'étalonnage (CLAS), un programme administré conjointement par le Conseil canadien des normes (CCN) et l'IÉNM. Ce dernier établissement assure le soutien technique du programme.

INTRODUCTION

When an acoustical measurement is made, it is reasonable to assume that the information obtained is reliable. Even with the purchase of a new instrument, during the transit of the instrument from its manufacturer, there may be unexpected vibration that can affect the performance of the instrument. In the case of a sound level meter (SLM), the usual quick check is to use a sound calibrator that generates a known sound pressure level to verify the reading provided by the SLM. However, other instrument functions, such as, the A-weighting circuits, microphone performance etc. may have been affected. Traceability of a measurement is usually related to the uncertainty of the sound pressure level measured. When an instrument is certified to be traceable to a National Metrology Institute (NMI), that means the instrument has been calibrated by that institute or certified by a laboratory that has been accredited under the Calibration Laboratory Assessment Service (CLAS) program jointly administered by the Standards Council of Canada (SCC) and INMS.

TRACEABILITY

There are two paths to establish traceability. A direct path, that is, a NMI, calibrates an artefact that is used as a reference for measurement. The NMI may be a laboratory that has mutual recognition agreement with NRC. An indirect path may be traceable via laboratories that are accredited under the Calibration Laboratory Assessment Service (CLAS) program jointly administered by the Standards Council of Canada (SCC) and INMS. The latter provides technical support for the program. It is a misconception to assume that after the calibration of an artefact, such as a pistonphone sound source, the certified artefact can then be used to "certify" another pistonphone, and then the latter is used to further "certify" others etc. One can see that as the chain of calibration is elongated, the uncertainty of the calibration increases.

INTERNATIONAL TRACEABILITY

For international trade, it is necessary to have mutual recognition agreements on physical measurements between countries. Currently, INMS (Canada) has mutual recognition of the equivalence of national standards with the National Institute of Standards and Technology (NIST, USA), the National Physical Laboratory (NPL, UK), and the Commonwealth Scientific and Industrial Research Organisation (CSIRO, Australia). Under the umbrella of the Bureau International des Poids et Mesures (BIPM), the Consultative Committee on Acoustics, Ultrasound and Vibration (CCAUV) has arranged international calibration

comparisons, involving over 15 countries. INMS currently participates in the above calibration comparisons on microphones, ultrasound power measurements and accelerometers. In the American states, INMS has completed microphone and accelerometer calibration comparisons with five countries under SIM (Sistema Interamericano de Metrologia): Canada, United States, Mexico, Brazil and Argentina.

BENEFICIARY OF TRACEABILITY

The above comparisons require a lot of effort from each participating country. One may ask the question: Who is the beneficiary of international comparisons? The answer is rather complex. The results of International Comparisons will provide confidence on the measurement capabilities of the participants. With mutual recognition, the need to have the manufacturer of a product to duplicate acoustical measurements in different countries vanishes. For example: It is mandatory for machinery sold in the EC countries to have a declared noise label (sound power or sound pressure level generated by the machine at a certain distance). With mutual recognition, if the measurements were to be conducted in Canada based on an approved method and with certified acoustical instruments, it is unnecessary to duplicate the measurements in the United Kingdom. This helps to eliminate the possibility of any country from using standardisation as a barrier to trade. In short, the consumer is the ultimate beneficiary.

There are other benefits such as research and development by each country to improve their primary standards. As an example, in a recent International Inter-comparison on microphone calibration, and base on precise measurements in an environmental control chamber, INMS developed an empirical equation[1] that enables other laboratory that do not have environmental controls to arrive at calibration of laboratory standard microphones with less uncertainty. The above equation makes it possible to correct for microphone sensitivity changes with barometric pressure at various frequencies. This information is important in precision freefield measurements.

CONCLUSIONS

It is important to consider traceability when a measurement is made. Legal consideration is usually the main incentive to seek traceability to ensure reliable acoustical measurements. The ability to demonstrate that the instruments are traceable is as important as the measurement made.

REFERENCE

[1] G. S. K. Wong and L. Wu, "Controlled environment for reciprocity calibration of laboratory standard microphone and measurement of sensitivity pressure correction, *Metrologia*, **36**(4), 275-280, (1999).

STATISTICAL FACTORS AFFECTING MACHINERY NOISE EMISSION DECLARATIONS

Stephen E. Keith and Stephen H.P. Bly

Health Canada, Radiation Protection Bureau, 775 Brookfield Rd. 6301B, Ottawa, ON, K1A 1C1

1.0 Introduction

Occupational noise-induced hearing loss is a significant public health problem in Canada. To help reduce workplace noise, purchasers of machinery need to be able to make meaningful comparisons of machinery noise emissions with: (i)emissions from other machines,
(ii)purchase specifications and (iii)occupational noise limits. This can be achieved if technical specifications and instruction manuals for machinery contain noise emission declarations; realistic, but conservative, estimates of the sound pressure levels and sound power levels emitted by machine(s) under standard conditions.

Guidelines for machinery noise emission declarations in Canada are being prepared by the Canadian Standards Association (CSA). They are based, in part, on ISO 4871[1], one of a series of international standards that can be used as an efficient way to either meet European regulatory requirements for noise emission declarations or to verify declarations.

The purpose of this study was to examine the implications of using ISO 4871 for the declaration and verification of the noise emission values of machinery manufactured in batches. For measurement of noise emission values to be feasible, the values must be based on measurements of a relatively small sample of machines from the batch. From health and safety considerations, it is important that there be a reasonably high probability that the noise emission value of machinery purchased for a workplace will not exceed the declared value. For the benefit of the manufacturer, there should also be a relatively high probability that a noise emission declaration for a batch will be verified, either by a purchaser or a regulatory authority. Therefore, this study examined the dependence of these probabilities on three factors: (i) the number of machines used to determine a noise emission declaration, (ii) reproducibility of the measurements and (iii) the difference between the total standard deviation and the reference standard deviation of the measurements.

2.0 Calculation details

The statistics of the declaration were calculated based on the following model for the measured noise emission value L_i, for the ith machine in a sample from a batch:

$$L_i = \mu + \sigma_P X_i + \sigma_R Y \tag{1}$$

where μ, was the true mean noise emission value for the entire batch the X_i, and Y values were normally distributed random numbers with mean 0 and standard deviation 1, and σ_P was the true standard deviation of production for the entire batch. The value σ_P characterized the variation in the noise emission values due to production differences between machines. The remaining quantity σ_R,

was the standard deviation of reproducibility. This quantity, normally obtained from a standard or test code, characterized the variation in the L_i due to random differences between the results of measurements of the same machine carried out under changed conditions of measurement. The value of σ_R normally includes repeatability differences but they were assumed negligible in these calculations. Except for the X_i, and Y all quantities in equation 1 are in decibels (dB). A new set of X_i and a new Y was generated for each trial.

The estimated mean noise emission value L_{avg} for the entire batch was calculated using[1]:

$$L_{avg} = \sum_{i=1}^{N} L_i \Big/ N \approx \mu \tag{2}$$

where $i=1$ to N, and N was the number of machines measured.

The estimated standard deviation of production s_P was calculated from the sample measurements and given by

$$s_P = \sqrt{\sum_{i=1}^{N} (L_i - L_{avg})^2 \Big/ (N-1)} \approx \sigma_P \tag{3}$$

The estimated total standard deviation s_t, for the batch was given by

$$s_t = \sqrt{s_P^2 + \sigma_R^2} \approx \sigma_t \tag{4}$$

where σ_t was the true total standard deviation for the batch. Note that σ_R would be obtained from the test code, or standard used to make the measurement, and was assumed to be the true value.

For each trial, the declared value for the batch , L_d, was obtained according to informative Annex A of ISO 4871from the equation

$$L_d = L_{avg} + 0.94\, s_t + 0.56\, \sigma_M \tag{5}$$

where σ_M was the reference standard deviation, a total standard deviation (as in equation 4) specified for a type of machine and considered to be typical for batches. A fixed value of $_M$ of 2.5 dB was chosen, as recommended in ISO 4871.

One of the quantities to be calculated was the probability that a noise emission declaration for a batch would be verified. This was obtained as the average, over 8000 trials, of the fraction of machines in a sample of three, that met the following criterion from ISO 4871

$$L_d - L_{avgV} > 0.56\, \sigma_M \tag{6}$$

where L_{avgV} was the estimated mean noise emission value measured by the verifier from a sample of 3 machines using equation 2. The values of L_i needed for L_{avgV} were obtained from equation 1. However, in each trial, the X_i and Y constants used to obtain L_{avgV} were uncorrelated with the constants used in the determination of L_d.

The other quantity of interest was the probability that the true noise emission value of a purchased machine was less than the declared value for the batch, L_d. This was obtained as the average, over 8000 trials, of the fraction of machines that met the criterion

$$\mu + \sigma_P X_i < L_d \tag{7}$$

where the true mean noise emission value from the ith machine was modeled as $\mu + \sigma_P X_i$. In each trial, the comparisons in equation 6 and 7 use the same three machines. This means that for each trial, the X_i constants used in equation 7 were the same as used to obtain the L_{avgV} in equation 6.

For a given L_d, the probability of verification was also calculated using the Student-t distribution[2]. The Welch-Satterthwaite formula[2] was used to determine the effective number of degrees of freedom. Typically, this calculation and the simulation gave results that agreed to within 1%.

3.0 Results

The results are given in Table 1. The first line of Table 1 shows that the probability of verification was 95% and the proportion of machines with noise emission values less than the declared value was 93% if three conditions were fulfilled[3]: (i) there were a large number of machines in the sample used to obtain the noise emission declaration, (ii) there were no reproducibility differences between the manufacturer and verifier and (iii) the total standard deviation, σ_t, was approximately equal to the reference standard deviation, σ_M.

A realistic example using a survey grade measurement is given in the last line of Table 1. None of the three conditions were met, which resulted in reductions in both the probability of verification and the number of machines with noise emission values below the declared value. The effect of each condition is illustrated below.

If conditions (i) and (ii) were fulfilled but the total standard deviation exceeded the reference standard deviation of 2.5 dB, the percentage of machines with noise emission values below the declared value decreased. However, the probability of acceptance remained unchanged. This is shown by comparison of the second row of Table 1 with the first row. Here, exaggerated production variations ($\sigma_P=10$dB) make the total standard deviation much larger than 2.5dB, and the percentage of machines below the declared value dropped to 86%.

For the third row of Table 1, the measurement reproducibility condition (ii) was violated. This reduced the probability of verification, even though the total standard deviation,σ_t, was the same as

in the first row. However, because σ_t was unchanged, the percentage of machines below the declared value remained the same. The likelihood of verification would increase if the manufacturer and verifier made measurements under identical conditions.

If conditions (ii) and (iii) were fulfilled but only 3 machines were used to calculate the declaration, the probability of verification was reduced and the proportion of machines with noise emission values below the declared value was also diminished. This is indicated by comparison of the first and fourth rows of Table 1. This resulted from the fact that, over the 8000 trials, the small sample size caused significant variations in the estimates of the mean and total standard deviation. This is shown by the wide range of differences between the declared and measured values in the fourth row of Table 1.

If, in each trial, the difference between the measured and declared values was doubled, the probability of verification would typically exceed 95%. The proportion of machines with noise emission values less than the declared value would also increase to over 93%.

4.0 Conclusions

To produce consistent declared values that allow simple comparisons between machinery, the CSA guidelines recommend the use of ISO 4871 and its informative Annex A. Declarations according to this standard are conservative estimates of the noise produced by the machines. To avoid difficulties when using declarations, manufacturers should be conservative in the estimation of errors. Purchasers should be aware that the declaration is a statistical upper limit, and some machines are expected to exceed the declared value.

References

[1] ISO 4871 (1996), "Acoustics - Declaration and verification of noise emission values of machinery and equipment"

[2] ISO GUM (1995), "Guide to the expression of uncertainty in measurement"

[3] ISO 7574 (1985), Part 4, "Acoustics - Statistical methods for determining and verifying stated noise emission values of machinery and equipment"

Integration of Acoustic Absorbing Porous Components in Vehicle Environment Using a Novel Finite Element Solver

M.A HAMDI, L. MEBAREK, A. OMRANI
STRACO, SA 20, Rue du Fonds Pernant, 60471 Compiegne cedex, France

N. ATALLA
GAUS, Department of Mechanical Engineering of the University of Sherbrooke, Canada

Abstract

A new mixed finite element formulation very well adapted to analyze the propagation of elastic and acoustic waves in porous absorbing media is presented. The proposed new formulation is based on modified Biot's equations [1,2,3] written in terms of the skeleton displacement and the acoustic pressure in the interstitial fluid. It generalizes the previous formulation proposed by Professor Atalla & Co-authors[11], and has the great advantage over existing formulations [5 to 13]of automatically satisfying all boundary conditions without having to compute surface coupling integrals at porous sub-domain interfaces. When elastic forces in the skeleton are neglected, the formulation automatically degenerates to an equivalent fluid model taking into account inertial coupling with the skeleton. This generalized mixed formulation and associated equivalent fluid model has been implemented by STRACO (France) in RAYON-PEM Solver. It is shown in this paper, that the numerical results predicted with RAYON-PEM agrees very well with experimental results using impedance tube tests and vibration measurements on multi-layered plates [14].

1. INTRODUCTION

The production at minimum cost of safety and high quality vehicles characterised by very low environmental noise and outstanding interior comfort becomes a very challenging objective for car manufacturers and for transportation industry in general. Therefore customers are becoming very sensitive to interior comfort and governmental authorities are imposing more and more severe regulations to reduce the external noise. To optimise at low cost the performances of vehicles by reducing vibration and noise levels, it is necessary to develop computer aided engineering analysis tools capable of predicting the vehicle performances at an early stage of the design cycle. During the last two decades a lot of research efforts has been devoted to the development of experimental techniques dedicated to the measurement of the local absorbing characteristics of Poro-Elastic Materials (PEM) and associated constitutive laws[15,16,17]. In parallel several analytical [1 to 4] and numerical models [5 to 13] have been proposed to solve the classical linear system of Biot's equations which governs the propagation of acoustic and elastic waves in porous media [1,2,3].

Section 2 of the paper presents the system of modified Biot's equations written in terms of the skeleton displacement and of the acoustic pressure in the interstitial fluid. It is shown that this system has the advantage of explicitly involving the total stress tensor in the porous media and the inertial force induced by the interstitial acoustic wave. Section 3 and 4 derives the variational formulations associated to modified Biot's equations, which

generalises the previous mixed formulation proposed by Professor Atalla and Co-authors [11]. It has the great advantage of automatically satisfying all boundary conditions without having to compute surface coupling integrals at sub-domain interfaces. Section 5 presents the numerical results predicted by the present formulation which has been implemented in STRACO's RAYON-PEM Solver. The numerical results compares very well with experimental results obtained using impedance tube and treated plates. The last section corresponds to the conclusion of the paper where the authors indicates the features of the new mixed formulation to solve vibro-acoustic problems encountered in transportation industries where the vehicle structure interacts with the passengers compartment through poro-elastic barriers.

2. MODIFIED BIOT'S EQUATIONS

Propagation of elastic and acoustic waves in porous media are governed by the system of Biot's equations [1], which could be written for time harmonic waves with a time dependence in $exp(-i\omega t))$:

$$\frac{\partial(\sigma_{kl}^s)}{\partial x_l} = -\omega^2(\tilde{\rho}_{11}U_k^s + \tilde{\rho}_{12}U_k^f) \qquad (1.1)$$

$$\frac{\partial(-\phi\, p\delta_{kl})}{\partial x_l} = -\omega^2(\tilde{\rho}_{12}U_k^s + \tilde{\rho}_{22}U_k^f) \qquad (1.2)$$

where, ω is the circular frequency, U_k^s and U_k^f represents respectively the skeleton and fluid displacement components.

The mass density coefficients appearing in equations (1.1) and (1.2) are given by:

$$\widetilde{\rho}_{11} = (1-\phi)\rho_s - (1-\tau)\phi\rho_f - \phi\,b\,/\,j\omega \quad (2.1)$$

$$\widetilde{\rho}_{22} = \tau\phi\rho_f - \phi\,b\,/\,j\omega \quad (2.2)$$

$$\widetilde{\rho}_{12} = (1-\tau)\phi\rho_f + \phi\,b\,/\,j\omega \quad (2.3)$$

where ϕ is the porosity, τ is the turtuosity, ρ_s and ρ_f are the mass densities of the skeleton material and of the interstitial fluid. The coefficient b represents the viscous coupling between solid and fluid phases given by [1],

$$b = \phi\sigma\sqrt{1 - 4j\omega\eta\rho_f(\frac{\tau}{\Lambda\phi\sigma})^2} \quad (3)$$

where σ is the flow resistivity, η is the viscosity of the interstitial fluid and Λ is the viscous characteristic length of the media. σ_{kl}^s and $\sigma_{kl}^f = -\phi\,p\delta_{kl}$ represent the components of the stress tensors respectively in the skeleton and in the interstitial fluid where p is the pressure.

The stress tensor components are related to the strain tensor components by the constitutive laws of the porous media,

$$\sigma_{kl}^s = (Adiv(U^s) + Qdiv(U^f))\delta_{kl} + G(\frac{\partial U_k^s}{\partial x_l} + \frac{\partial U_l^s}{\partial x_k}) \quad (4.1)$$

$$-\phi\,p = Qdiv(U^s) + Rdiv(U^f) \quad (4.2)$$

where, G is the skeleton shear modulus, Q is the coupling modulus, A and R are the first Lamé coefficient and the bulk modulus of the porous media. Coefficient A, Q and R are related to the bulk modulus K_s of the skeleton material, the bulk modulus K_b of the skeleton in vacuum and to the bulk modulus K_f of the interstitial fluid by the following formulas [1]:

$$A = \frac{(1-\phi)((1-\phi)K_s - K_b) + \phi K_s K_b / K_f}{1 - \phi - K_b / K_s + \phi K_s / K_f} - \frac{2G}{3} \quad (4.3)$$

$$Q = \frac{((1-\phi)K_s - K_b)\phi}{1 - \phi - K_b / K_s + \phi K_s / K_f} \quad (4.4)$$

$$R = \frac{K_s\phi^2}{1 - \phi - K_b / K_s + \phi K_s / K_f} \quad (4.5)$$

The relative displacement vector $(U^f - U^s)$ is given from equation (1.2) by,

$$U^f - U^s = \frac{1}{\omega^2\widetilde{\rho}_f} grad(\phi\,p) - \widetilde{\beta}\,U^s \quad (5)$$

where $\widetilde{\beta} = (1 + \widetilde{\rho}_{12} / \widetilde{\rho}_{22})$ is the inertial coupling factor.

Modified Biot's equations are derived by substituting constitutive laws (4.1) and (4.2) into equation (1.1) and into the divergence of equation (5). This leads to the following system of Modified Biot's equations:

$$\widetilde{\rho}_s\omega^2 U^s + div(\widetilde{\sigma}_{kl}^s(U^s)) - \widetilde{\alpha}\phi\,p\delta_{kl} + \beta\widetilde{g}rad(\phi p) = 0 \quad (6.1)$$

$$div(\frac{1}{\omega^2\widetilde{\rho}_f} grad(\phi p) - \widetilde{\beta}\,U^s) + \frac{\phi p}{R} + \widetilde{\alpha}\,div(U^s) = 0 \quad (6.2)$$

where $\widetilde{\alpha} = (1 + Q / R)$ is the stiffness coupling factor between the skeleton and the fluid.

The equivalent masses $\widetilde{\rho}_f$ and $\widetilde{\rho}_s$ appearing in modified Biot's equations (6.1) and (6.2) are given by:

$$\widetilde{\rho}_f = \phi\rho_e \quad (7.1)$$

$$\widetilde{\rho}_s = (1-\phi)\rho_s + \phi\rho_f(1 - \frac{\rho_f}{\rho_e}) \quad (7.2)$$

where $\rho_e = \rho_f\tau - b / j\omega$, is the effective mass of the interstitial fluid which includes the viscous coupling factor b with the skeleton.

Modified Biot's equations (6.1) and (6.2) have the great advantage of involving explicitly the total stress tensor, $\sigma_{kl}^{tot} = \widetilde{\sigma}_{kl}^s - \widetilde{\alpha}\phi\,p\delta_{kl}$ where,

$$\widetilde{\sigma}_{kl}^s = (K_b - \frac{2G}{3})div(U^s)\delta_{kl} + G(\frac{\partial U_k^s}{\partial x_l} + \frac{\partial U_l^s}{\partial x_k})$$

is the stress tensor of the skeleton with vacuum inside.

3. MIXED VARIATIONAL FORMULATION OF MODIFIED BIOT'S EQUATIONS

The mixed variational formulation associated to modified Biot's equations is simply derived by multiplying equation (6.1) by a virtual displacement vector V^s and equation (6.2) by a virtual pressure ϕq, and by integrating over the domain Ω occupied by the porous media,

$$Z(U^s, V^s) + A(p, q) - \hat{C}(p, V^s) - \hat{C}(q, U^s) = \widetilde{C}_S(T, V^s) + C_S(q, W_n - U_n^s) \quad (8)$$

for admissible $V^s(\Omega)$ and $q(\Omega)$ satisfying prescribed boundary conditions.

$$Z(U^s, V^s) = K(U^s, V^s) - \omega^2 M(U^s, V^s) \quad (9)$$

is the mechanical impedance operator of the skeleton where K and M are the stiffness and mass operators given by,

$$K(U^s, V^s) = \int_\Omega (\widetilde{\sigma}_{kl}^s(U^s)\widetilde{\varepsilon}_{kl}^s(V^s\,d\Omega \quad (9.1)$$

$$M(U^s, V^s) = \int_\Omega \widetilde{\rho}_s(U^s, V^s)d\Omega \quad (9.2)$$

$A(p,q) = H(p,q)-Q(p,q)/\omega^2$ is the acoustic admittance operator of the interstitial fluid where H and Q are the inertial and stiffness operators given by,

$$H(p,q) = \int_\Omega \frac{1}{\tilde{\rho}_f}((grad(\phi p), grad(\phi q))d\Omega \quad (10.1)$$

$$Q(p,q) = \int_\Omega \frac{\phi^2 pq}{R}d\Omega \quad (10.2)$$

$$\hat{C}(p,V^s) = \int_\Omega \left\{\tilde{\alpha}\phi p div(V^s) + (\tilde{\beta} V^s, grad(\phi\ p))\right\}d\Omega \quad (11)$$

is the volume coupling operator.
The coupling operator given by equation (11) is composed by the sum of the volume stiffness coupling operator proportional to $\tilde{\alpha}$ and of the volume inertial coupling operator proportional to $\tilde{\beta}$.

$$\tilde{C}_S(T,V^s) = \int_S (T,V^s)dS \quad (12)$$

is the surface loading operator, where $T_k = \sigma^{tot}_{kl} n_l$ represents the component on the coordinate axis x_k of the total surface stress vector T. Finally,

$$C_S(q,W_n - U^s_n) = \int_S q(W_n - U^s_n)dS \quad (13)$$

is the surface cinematic coupling operator, where n is the outgoing unitary vector normal to the boundary S of the porous domain Ω.
As shown in figure 1, for practical applications the porous media is attached on a part S_I of its boundary to an impervious master structure and is coupled on another part S_0 to an acoustic cavity.
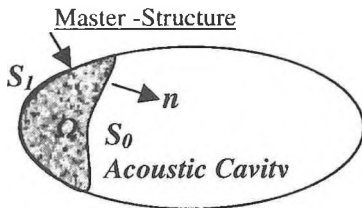
Figure 1: Porous Component attached to the Master-Structure and coupled with an acoustic cavity

The master structure S_I communicates to the porous media a total displacement vector $W = U^s$. Reciprocally the porous component applies to the master structure a surface loading T. At the interface S_0 with the acoustic cavity the normal component W_n of the total acoustic displacement and the normal components U^s_n and U^f_n of the skeleton and of the fluid are related by the equation,

$$W_n - U^s_n = \phi(U^f_n - U^s_n) \quad (14)$$

For impervious surfaces the relative displacement is null, and for perforated surfaces there exist a relative displacement

between the skeleton and the fluid. At the interface S_0 the acoustic cavity applies to the porous component a surface pressure loading $T_k = -pn_k$, and reciprocally the porous media communicates to the cavity a relative displacement $W_n - U^s_n$.

In summary the master structure communicates to the porous component a cinematic displacement and the acoustic cavity apply on it an acoustic surface loading. The porous component reacts by applying a surface loading on the master structure, and by communicating a relative displacement flux to the cavity.

In the configuration of figure 1, equation (8) could be rewritten in the following form,

$$Z(U,V) + A(p,q) - \overline{C}(p,V) - \overline{C}(q,U) = \tilde{C}_1(T,V) + C_0(q,W_n) \quad (15)$$

where,

$$\overline{C}(p,V) = C_0(p,V) - \hat{C}(p,V) \quad (16)$$

In order to avoid the assemblage of the complex porous component to the acoustic cavity, the continuity of the pressure at the interface S_0 could be relaxed and imposed in a weak form by a Lagrange multiplier X_n:

$$C_0(X_n,(p - p^c)) = \int_{S_0}(p - p^c)X_n dS_0 = 0 \quad (17)$$

where p^c is the pressure applied by the cavity. This technique allows the use of incompatible finite element meshes at the interfaces between the porous component and the surrounding environment.
Finally, the addition of equations (15) and (17) leads to the mixed variational equation,

$$Z(U,V) + A(p,q) - \overline{C}(p,V) - \overline{C}(q,U) - C_0(q,W_n) - C_0(p,X_n) = \tilde{C}_1(T,V) - C_0(p^c,X_n) \quad (18)$$

The right hand side of equation (18) is exactly proportional to the total energy exchanged between the porous media and its surrounding environment. The mechanical energy absorbed by the porous component from the Master-Structure corresponds to the first term, and the acoustic energy absorbed from the acoustic cavity corresponds to the second term.

4. EQUIVALENT FLUID- MODEL

For very soft porous media, elastic internal forces in the skeleton could be neglected. In this particular case the system of modified Biot's equations reduces to :

$$\tilde{\rho}_s\omega^2 U^s + div(-\tilde{\alpha}\phi\ p\delta_{kl}) + \tilde{\beta}grad(\phi p) = 0 \quad (19.1a)$$

$$div(\frac{1}{\omega^2 \tilde{\rho}_f} grad(\phi p) - \tilde{\beta} U^s) + \frac{\phi p}{R}$$

$$\quad (19.2)$$

$$+ \tilde{\alpha} \, div(U^s) = 0$$

Multiplying equation (19.2) by the trial function ϕq and integrating over the porous media domain Ω leads to the following variational equation,

$$A(p,q) - \omega^2 M(U^s, V^s) =$$
$$C_S(q, W_n - (1 - \phi\tilde{\alpha})U_n^s) \quad (20)$$

where the displacement vector V^s satisfies the equation,

$$\tilde{\rho}_s \omega^2 V^s + div(-\tilde{\alpha}\phi \, q\delta_{kl})$$
$$+ \tilde{\beta} grad(\phi q) = 0 \quad (19.1b)$$

which is equivalent to equation (19.1a) where the pressure p is replaced by the trial pressure q.

The coupling operator appearing in the right side of equation (20) is given by the integral,

$$C_S(q, W_n - (1 - \phi\tilde{\alpha})U_n^s) = \int_S q(W_n - (1 - \phi\tilde{\alpha})U_n^s)dS$$

$$\quad (21)$$

It is very easy to demonstrate by using equations (4.4) and (4.5) that,

$$1 - \phi\tilde{\alpha} = \frac{K_b}{K_s} \quad (22)$$

for soft porous material $K_b \ll K_s$, so the second surface integral relative to the term ($1 - \phi\tilde{\alpha}$) can be neglected. Finally by neglecting this second surface integral and by substituting U^s and V^s from equations (19.1a) and (19.1b) the variational equation (20) could be written in the following form,

$$A(p,q) + \tilde{H}(p,q)/\omega^2 = C_S(q, W_n) \quad (23)$$

where,

$$\tilde{H}(p,q) =$$
$$\int_\Omega \{(grad\tilde{\alpha}\phi p - \tilde{\beta}grad\phi p)(grad\tilde{\alpha}\phi q - \tilde{\beta}grad\phi q) / \tilde{\rho}_s \}d\Omega$$

$$\quad (24)$$

The variational equation (23) expressed in term of the acoustic pressure corresponds to the fluid equivalent model of the porous media, where the inertia of the skeleton is taken into account by the additional term given by equation (24).

5. FINITE ELEMENT RESULTS

Discretisation by the Finite Element Method (FEM) of equations (18) and (23) allows the computation of the mixed impedance matrix of the porous component Ω by eliminating all internal degrees of freedom (dof) of the porous component except those dof's attached to the master structure and to the acoustic cavity. *This has the great advantage of not increasing the size of the global vehicle model and of allowing suppliers to compute separately the impedance matrices of their components and deliver these matrices to vehicle manufacturers.* FEM results predicted by RAYON-PEM Solver developed by

STRACO (France) in cooperation with the University of Sherbrooke (Canada) are presented. Figure 2.a shows an excellent agreement between simulation and measurement for the case of homogeneous limp wool sample, protected by a thin perforated screen and placed at the end termination of an impedance tube. Figure 2.b compares with very good agreement the real and imaginary parts of the surface impedance predicted by the proposed model and impedance tube measurements for a multi-layers simple including a septum [4].
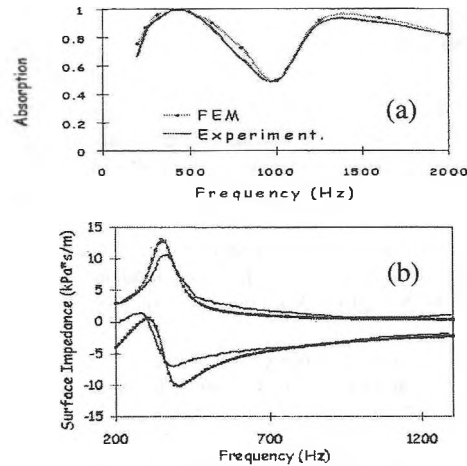
Figure 2: Impedance Tube Simulations
(a) homogeneous simple
(b) multi-layer simple with septum

Finally Figure 3 shows the results obtained for a system made up from two clamped rectangular plates separated by an unbounded foam. One plate is excited by a shaker and the normal quadratic velocity is measured on the facing plate. Good agreements are again achieved using both poro-elastic and equivalent fluid finite element models.
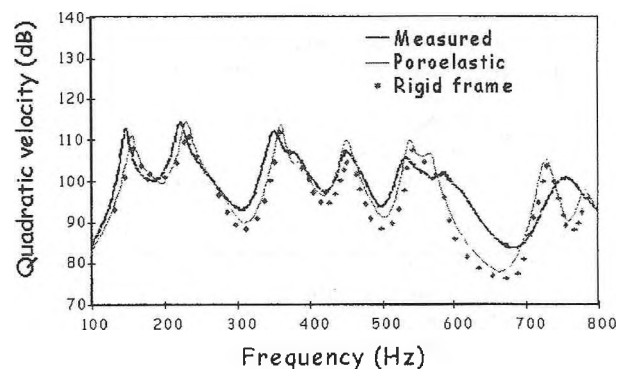
Figure 3: Finite Element Results for two rectangular plates coupled with foam

6. CONCLUSION AND PERSPECTIVES

The proposed mixed formulation based on modified Biot's equations has the advantage over existing formulations of automatically satisfying all interior and exterior boundary conditions at sub-domain interfaces. In addition it reduces at minimum the number of degrees of freedoms and considerably simplify the modelling effort by allowing the direct computation

of the impedance matrix added by a complex porous component to the vibro-acoustic impedance matrix of the bare vehicle body. This new approach also simplifies the co-operative work between vehicle suppliers and manufacturers. The resulting RAYON-PEM Solver developed by STRACO and commercially available in the environment of I-DEAS Vibro-acoustics software constitutes a very promising and powerful analysis tool, which could be advantageously used to optimize the acoustic treatment of industrial vehicles.

7. REFERENCES

[1] J.F. ALLARD, *"Propagation of sound in porous media, Modelling of sound absorption,* Charpman" & Hall, North Way Andover, Hampshire, SP105BE, England , (1993).

[2] M.A BIOT, *Theory of propagation of elastic waves in a fluid-saturated porous solid. I. Low frequency range,* Journal of the Acoustical Society of America 28, 168-178 (1956);

[3] M.A BIOT, *Theory of propagation of elastic waves in a fluid-saturated porous solid. II. Higher frequency range,* Journal of the Acoustical Society of America 28, 179-191 (1956);

[4] P.M Morse, "Vibration and Sound", New York, McGraw-Hill, republished by the Acoustical Society of America (1981).

[5] J.P. COYETTE, H. BLOEMHOF, *A generalized procedure for modelling multi-layer insulation systems,* Proceeding of ISMA19, Katholic Universiteit Leuven, Leuven Belgium, (1996);

[6] V. EASWAREN, W. LAURIKS and J.P. COYETTE, *"Displacement-Based Finite Element Method for Guded Wave Propagation Problems: Application to Poroelastic Media",* Journal of Acoustical Society of America, 100, 2989-3002, 1996.

[7] Y.J KANG and J.S BOLTON, *"Finite Element Modeling of Isotropic Elastic Porous Materials Coupled with Acoustical Finite Elements"* Journal of the Acoustical Society of America 98, 635-643, (1995).

[8] J.S BOLTON, N.M SHIAU, Y.J KANG, *Sound transmission through multi-panel structures lined with elastic porous materials,* Journal of Sound and Vibration 191(3), 317-347, (1996)

[9] R. PANNETON, N. ATALLA, *Numerical prediction of sound transmission through finite multi-layer systems with poro-elastic materials,* Journal of Acoustical Society of America 100(1), 346-354 (1996);

[10] R. PANNETON, N. ·ATALLA, *An efficient sheme for solving the three-dimensional pro-elasticity problem in acoustics,* Journal of Acoustical Society of America 101(6), 3287-3298 (1997);

[11] N. Atalla, R. Panneton and P. Debergue, *" A mixed pressure-displacement formulation for poroelastic materials "* J. Acoust. Soc. Amer., 104(3), 1444-1452, (1998).

[12] P. GORENSON, *A 3D Symmetric finite element formulation of the Biot Equations for a fluid saturated linear elastic porous medium,* international Journal for Numerical Methods in Engineering, 41, 167-192, (1998)

[13] P.GORENSON, *Numerical modelling of dynamics of light porous materials,* PHD, Lund University (1998)

[14] B. BROUARD & al. *Measurement and prediction of the surface impedance of a resonant sound absorbing structure,* Acta Acoustica, Vol. 2, 301-306, (1994).

[15]A. F SYBERT, D.F ROSS, *Experimental determination of acoustic properties using a two microphones random excitation technique,* Journal of Acoustical Society of America, 61, 1362-1370, (1977).

[16] D.A. BIES, "Acoustical Properties of Porous Materials",Noise and Vibration Control, Capter 10, Edition L.L. BERANEK (1988).

[17] M.E. DELANEY and E.N BAZLEY, "Acoustical characteristics of fibrous absorbent materials", National Physical Laboratory, Aerodynamics Division Report AC37, (1969).

SYSTEM 824
SLM/RTA
Five sophisticated acoustical instruments in One!

1 **Integrating Sound Level Meter** meeting Type 1 Standards with simultaneous measurement of sound pressure levels using fast, slow, and impulse detector, and simultaneous A, C, and flat weighting. It measures 48 sound pressure parameters at once! All this with a 105 dB linearity range!

Simple Sound Analyzer with simultaneous sound pressure level measurement and real-time 1/3 octave frequency analysis.

Logging Sound Level Meter permits data gathering of broadband sound pressure levels and frequency spectra over user-defined time intervals.

Real Time Frequency Analyzer with 1/1 and 1/3 octave analysis over a 20kHz frequency range and optimized for characterizing steady-state or high speed transient events.

Fast Fourier Transform Analyzer with 100, 200, and
5 400 lines resolution and 20kHz range for specific frequency investigations.

Listen 〰 with Larson•Davis

For use in a wide variety of applications

Research and Development

- Building Acoustics
- Sound Power Determination
- Vibration measurements
- Statistics
- Simple Point Shoot
- Transient Capture

Environmental

- Aircraft Noise
- Industrial Noise
- General Surveys
- Transportation Noise
- Community Noise

Worker Safety

- Noise Exposure Measurements
- Work Place Surveys
- Machinery Noise
- Audiometric Calibration
- Simultaneous C minus   A Measurements

Dalimar Instruments Inc.

At your service since 1986

193, Joseph Carrier, Vaudreuil-Dorion, Quebec, Canada J7V 5V5 Tel.: (450) 424-0033 Fax: (450) 424-0030
1234 Reid Street, Suite 8, Richmond Hill, Ontario, Canada L4B 1C1 Tel.: (905) 707-9000 Fax: (905) 707-5333
E-mail: info@dalimar.ca   Website: www.dalimar.ca

PROGRAMMATION ORIENTÉE OBJET DE LA MÉTHODE DES ELÉMENTS FINIS APPLIQUÉE À L'ÉTUDE DE MULTICOUCHES POROÉLASTIQUES

Pierre Lamary (*) (**) - Imad Tawfiq (**) - Jean-Baptiste Casimir (**) - Yvon Chevalier (**)

* DASSAULT AVIATION, Département des Etudes Scientifiques Amonts, 78 quai Marcel Dassault, 92214 Saint-Cloud, France
** ISMCM-CESTI, Ministère de l'Enseignement Supérieur et de la Recherche, Laboratoire d'Ingénierie des Systèmes Mécaniques et des Matériaux, 3 rue Fernand Hainaut, 93407 Saint-Ouen Cedex, France

1.0 INTRODUCTION

Nous présentons dans cet article les points les plus intéressants rencontrés lors de la réalisation d'un logiciel spécifique de vibro-acoustique basé sur une approche objet. Le code que nous avons appelé CAVOK (Calculs Acoustiques et Vibro-acoustiques OK) s'applique au domaine du transport (avion, voiture, train). Il est utilisé à la fois pour l'étude de problèmes spécifiques comme l'isolation des avions et pour l'enseignement.

L'aspect original de ce travail provient de l'implémentation de la Méthode des Eléments Finis (MEF) que nous proposons. L'approche classique, en Orienté Objet (OO), s'appuie sur l'héritage de classe pour spécialiser les éléments finis à l'acoustique ou à la structure. Dans notre cas, nous avons développé une programmation objet qui résout de manière formelle les équations aux dérivées partielles.

2.0 ORGANISATION DU LOGICIEL

L'ensemble du logiciel est programmé en C++ et fonctionne comme une application autonome sous Windows. Le C++ est particulièrement bien adapté à la programmation de la MEF puisqu'il permet de manipuler des abstractions de haut niveau, comme les Eléments Finis, tout en autorisant des implémentations bas niveau nécessaires à l'efficacité des calculs. De plus amples informations concernant les gains (temps de développement, maintenance, modularité, réutilisabilité,...) que l'on peut attendre d'une programmation objet comparée aux langages classiques (Fortran 77, C) peuvent être trouvées en [1,2,3].

Selon notre expérience deux niveaux de conception doivent être séparés, l'organisation générale du logiciel et la programmation de la MEF proprement dite. L'architecture générale du logiciel suit le schéma de conception MVC (Modèle-Vue-Contrôleur). Le modèle maintient des listes d'entités pertinentes du domaine (matériaux, éléments finis, calculs), les vues permettent de manipuler les données et le contrôleur assure la cohérence des informations . La programmation de la MEF, quant à elle, s'appuie sur deux classes fondamentales, la classe *Degrés-de-Liberté* et la classe *Elément-Fini-de-Référence*. L'aspect formel de notre implémentation provient du fait que ni les degrés de liberté , ni les

éléments finis ont une nature physique prédéfinie.

3.0 Application aux poroélastiques

Le problème final que nous cherchons à résoudre est celui de l'isolation acoustique des avions. Le sous-système à étudier est un empilement composé de la peau de l'avion, d'une couche viscoélastique, de plusieurs couches de laine de verre (poroélastique), d'une cavité d'air et du revêtement composite qui habille l'intérieur du fuselage.

Pour ce problème, nous avons utilisé notre logiciel pour créer des éléments finis de plaque basés sur la théorie de Love-Kirchhoff et sur la théorie de Reissner-Mindlin, des éléments finis poroélastiques selon la formulation (u,W) détaillée en [4] et [5] et des éléments finis d'acoustique en pression.

Glass wool measured characteristics :

Length : 25.4 (mm)
Porosity : 0.98
Tortuosity : 1
Resistivity : 35 E+3 (N s m-4)
Viscous dimension : 60 E-6 (m)
Thermal dimension : 150 E-6 (m)
Frame density : 9.6 (kg m-3)
Frame Young modulus (estimated) : Ys=10 E+3 (Pa)
Frame damping : Ns = 0.05 so that Y =Ys(1+jNs)
Poisson coefficient : 0.0

Figure 1 : Material characteristics

Les éléments finis poroélastiques créés par CAVOK ont tout d'abord été validés grâce aux travaux de [5] et [6]. Des exemples complets de validation de simplecouches et de multicouches peuvent être trouvés dans ces références. Par la suite, le code a été utilisé pour simuler une série d'expériences menée par l'Université du Maine pour le compte de Dassault Aviation. Les résultats présentés (fig. 2) sont extraits de cette étude où nous comparons essais et calculs d'un échantillon de laine de verre (fig. 1) placé dans un tube à impédance. Les résultats obtenus (fig. 2) sont satisfaisants.

4.0 CONCLUSION

L'orienté objet permet une nouvelle approche de la programmation de la méthode des éléments finis. Selon notre expérience, une implémentation formelle de la méthode peut naturellement être développée. Ceci permet d'aborder les problèmes couplés de vibro-acoustique où plusieurs domaines physiques interviennent. En particulier, nous montrons l'acquitté de notre approche et du logiciel CAVOK en traitant du problème de la poroélasticité.

5.0 RÉFÉRENCES

Bruce W. R. Forde, Ricardo O. Foschi and Siegfried F. Stiemer, « Object-Oriented Finite Element Analysis », Computers and Structures Vol. 34, No 3, 355-374 (1990)

Jean-Claude Gelin, Pascal Paquier, Luc Walterthum, « Application de la POO pour la conception d'un logiciel de simulation par éléments finis en mise en forme de matériaux », European Journal of Finite Elements, Vol 7, No 5, 505-533 (1998)

Jacques Besson, Ronald Foerch, « Object-Oriented Programming Apllied to the Finite Element Method », European Journal of Finite Elements, Vol 7, No 5, 535-566 (1998)

Pierre Lamary, Imad Tawfiq, Yvon Chevalier « Design of an Object-Oriented Finite Element Software for Vibro-acoustic problems - Formal FEM », IDMME'2000, Montreal, (may 2000)

T. F. Johansen, J. F. Allard, B. Brouard, « Finite element method for predicting the acoustical properties of porous samples », Acta Acustica, 3, 487-491 (1995)

R. Panneton, N. Atalla, « An efficient finite element scheme for solving the three-dimensional poroelasticity problem in acoustics », J.A.S.A., Vol 101, No 6, 3287-3298 (1997)

Figure 2: Absorption coefficient (alpha) from three tests (light curves) and FE calculation (bold curve)
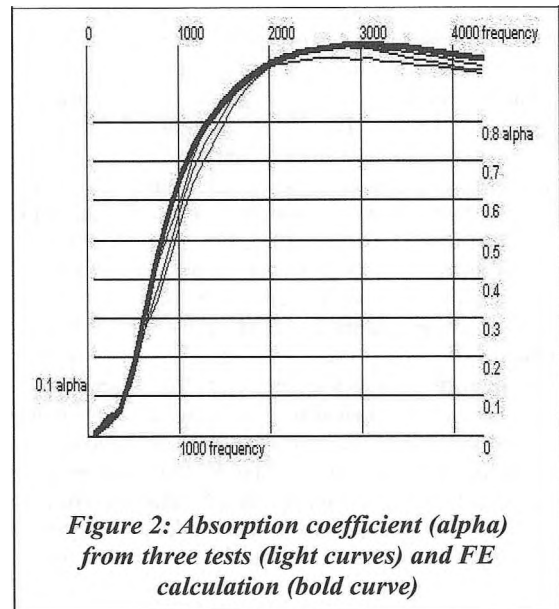
Modeling of multilayered structures including porous materials using hierarchical elements and non coincident meshes

S. Rigobert[1], F. Sgard[1], N. Atalla[2]

Laboratoire des sciences de l'habitat, DGCB URA CNRS 1652, ENTPE, rue Maurice Audin, 69518 Vaulx-en-Velin Cedex, France

G.A.U.S., Université de Sherbrooke, Sherbrooke, Québec, J1K2R1, Canada

1. INTRODUCTION

The finite element modeling of 3D poroelastic materials often leads to an important number of unknowns. The use of a mixed displacement-pressure {u,P} formulation [1] allows for an accurate description of porous media using only 4 degrees of freedom per node. Yet, 3D linear poroelastic elements based on this formulation have a slow convergence rate and are subject to numerical locking. An important refinement of the mesh is hence needed to get satisfactory results. As a result, the modeling of multilayered structures including porous materials and using coincident meshes implies the design of a refined mesh for the whole structure. Recently, the implementation of the {u,P} formulation using hierarchical elements has been presented [2]. The so called hierarchical poroelastic elements have proved to solve the problems of numerical locking related to the classical finite element implementation of the considered formulation, to increase its convergence rate in a significant way, and leads to a reduced number of degrees of freedom required for an accurate modeling of the porous medium. In this paper, the coupling of hierarchical elements with an elastic domain is considered. The enforcement of continuity equations between the two subdomains using continuous Lagrange multiplyiers is presented. Incompatible meshes are assumed. The present approach is then compared to the classical finite element representation of the multilayered structure using coincident meshes. Validation results are showed for the configuration of a porous material backed by an elastic plate and subjected to an acoustical excitation. The performance of the proposed approach is then underlined regarding the number of degrees of freedom required for the correct modeling the multilayered structure.

2. Theory

In the following, a 3D system composed of an elastic plate and a porous material is considered. The coupling between the two sub-domains consist in insuring the continuity of the solid displacement vector and the continuity of the normal stresses at the interface. Also, the normal component of the relative flow along the interface has to be set to zero. These two conditions can actually be directly taken into account in the weak formulation of the multilayered system. Yet, the continuity of displacement has to be enforced. In the present approach, the theory of continuous Lagrange multipliers is used to construct a two field hybrid formulation [3] for the multi-layer. This formulation is given in equation (1) where Ω_{el} (resp. Ω_p) and $\partial\Omega_{el}$ (resp. $\partial\Omega_p$) represent the elastic (resp. porous) sub-domain and its boundary. σ^{el}, ε^{el} and $\underline{u}^{el}$ are the stress and strain tensor related to the elastic domain and its displacement vector, ρ^{el} is its mass density. and are the strain and stress tensor related to the solid phase of the porous material *in vacuo*. is the total strain tensor in the porous material. $\underline{u}^S$ and p stand for the displacement vector of the solid phase and the pressure in the pores, and are the complex dynamic mass density of the solid and fluid phase respectively. h denotes porosity, γ, and are complex poroelastic coefficients [1]. Vector $\underline{\lambda}$ in equation (1) stands for the continuous Lagrange multiplier and can be physically interpreted as the force vector applying at the interface between the two subdomains and which allows for the continuity of displacement. In the present approach, each component of $\underline{\lambda}$ is then interpolated on an orthogonal basis of polynomials, namely Legendre polynomials, defined globally on the interface. The structure considered here has a planar geometry. Any point on the interface between the elastic plate and the porous material is located by its x and y coordinate. Component i of $\underline{\lambda}$ is interpolated in directions x and y using the following formula:

$$\lambda_i(x,y) = \sum_{m,n} \lambda^i_{mn} \cdot P_m(x) \cdot P_n(y) \qquad (2)$$

where P_m is the Lengendre polynomial of order m. Integrals I_1 and I_2 (as well as I'_1 and I'_2) are discretized on the mesh of the elastic plate and the porous domain respectively. The global definition of $\underline{\lambda}$ allow for an easy computation of the discretized form these integrals, because all the shape functions have a global definition on one element of the considered mesh. In the result section, the present approach is applied to the study of a baffled porous coated plate and subjected to an imposed pressure condition on the porous material. Two indicators are considered.

First, the mean quadratic velocity of the plate is computed using the approximated formula:

$$\int_{\Omega_{el}} \underline{\underline{\sigma}}^{el}\left(\underline{u}^{el}\right):\underline{\underline{\varepsilon}}^{el}\left(\delta\underline{u}^{el}\right)d\Omega - \rho_{el}.\omega^2 \int_{\Omega_{el}} \underline{u}^{el} \cdot \delta\underline{u}^{el}d\Omega + \int_{\Omega_p} \underline{\underline{\tilde{\sigma}}}^{S}\left(\underline{u}^S\right):\underline{\underline{\tilde{\varepsilon}}}^{S}\left(\delta\underline{u}^S\right)d\Omega - \tilde{\rho}.\omega^2 \int_{\Omega_p} \underline{u}^S \cdot \delta\underline{u}^S d\Omega$$

$$\int_{\Omega_p}\left[\frac{h}{\omega^2\widetilde{\rho}_{22}}\underline{\nabla}p \cdot \underline{\nabla}\delta p - \frac{h^2}{\widetilde{R}}p \cdot \delta p\right]d\Omega + \left[\gamma + h\left(1+\frac{\widetilde{Q}}{\widetilde{R}}\right)\right]\int_{\Omega_p}\left(\underline{\nabla}p \cdot \delta\underline{u}^S + \underline{\nabla}\delta p \cdot \underline{u}^S\right)d\Omega \qquad (1)$$

$$-h\left(1+\frac{\widetilde{Q}}{\widetilde{R}}\right)\int_{\Omega_p}\left(p \cdot \mathrm{div}(\delta\underline{u}^S) + \delta p \cdot \mathrm{div}(\underline{u}^S)\right)d\Omega - \iint_{\partial\Omega_{el}\backslash\partial\Omega_p}\left[\underline{\underline{\sigma}}^{el} \cdot \underline{n}^1\right]dS - \iint_{\partial\Omega_p\backslash\partial\Omega_{el}}\left[\underline{\underline{\tilde{\sigma}}}^t \cdot \underline{n}^2\right]dS$$

$$- \int_{\partial\Omega_p\backslash\partial\Omega_{el}}h(u_n - U_n)dS + \underbrace{\int_{\partial\Omega_p\cap\partial\Omega_{el}}\delta\lambda \cdot \underline{u}^{el}dS}_{I'_1} - \underbrace{\int_{\partial\Omega_p\cap\partial\Omega_{el}}\delta\lambda \cdot \underline{u}^S dS}_{I'_2} + \underbrace{\int_{\partial\Omega_p\cap\partial\Omega_{el}}\lambda \cdot \delta\underline{u}^{el}dS}_{I_1} - \underbrace{\int_{\partial\Omega_p\cap\partial\Omega_{el}}\lambda \cdot \delta\underline{u}^S dS}_{I_2} = 0$$

$$\langle v_z \rangle^2 = \frac{\omega^2}{2N} \sum_{i=1}^{N} \left| u_z^i \right|^2 \qquad (3)$$

where N is the number of nodes for the plate and u_n^i the displacement component along thickness for node i. Also the transmission loss (TL) is chosen as a power indicator. One defines:

$$TL = 10 * \log_{10}\left(\frac{P_{tr}}{P_{inc}} \right) \qquad (4)$$

where P_{inc} is the incident power and P_{tr} is the transmitted power. Given the amplitude P_0 of the imposed pressure, the incident power is given by:

$$P_{inc} = \frac{P_0^2}{2\rho_0 c} \qquad (5)$$

where ρ_0 and c are the density and celerity of air. Since the multi-layered structure is baffled, the transmitted power is given by :

$$P_{tr} = \frac{1}{2} \Re\left(\int_S p \cdot u^* dS \right) \qquad (6)$$

where * means complex conjugate. This integral is discretized on the F.E. mesh of the plate and computed using the values of the normal displacement and the pressure at the nodes of the mesh. The pressure is obtained from the normal displacements by the use of Rayleigh formula.

3. RESULTS

The porous coated plate has dimensions 0.35m*0.22m*0.005m is studied here. The plate is made up of aluminium and has simply supported edges constraints. The porous material is a foam with bonded lateral faces. The properties of the materials are given in tables 1 and 2. The excitation is an imposed pressure condition of amplitude 1Pa applied on the porous material front face. The computed indicators, either the mean square velocity or the transmission loss are compared to the results given by a FE code developed at the GAUS. This latter code, referred to as the classical approach in the following, is based on classical linear poroelastic elements for the porous medium and uses coincident meshes for the two sub-domains. The mesh for each approach is chosen in order to insure the convergence of the solution. The classical approach uses a 16*11 nodes mesh in the lateral dimensions for the plate and the
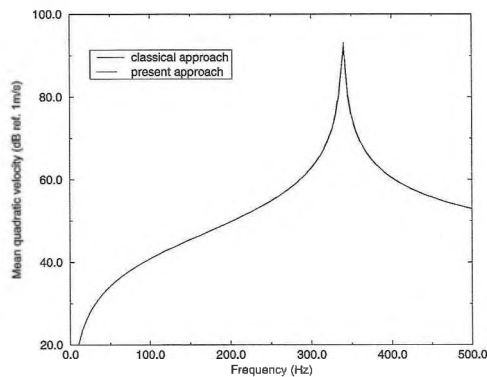
porous medium, and 2 elements along thickness for the porous sub-domain. The present approach uses the same mesh for the plate but only a 3*2 brick element mesh in the lateral dimensions of the porous medium and a single element along thickness. The interpolation order for the solid and the fluid phase are 3 and 2 respectively. The results are represented on figure 1 and 2 for a frequency ranging from 10Hz to 500Hz. These figures show an excellent agreement between the two approaches for the mean quadratic velocity of the plate as well as for the transmission loss. Besides, the present approach allows for an important reduction of the number of degrees of freedom required for the accurate description of the multilayer. Actually, 1095 degrees of freedom are sufficient to insure convergence instead of 2190 for the classical approach.

E (kPa)	ν	η	ρ (kg/m^3)
$6.9*10^7$	0.33	0.007	2742

Table 1 : Properties of the plate

h	σ (kN.s/m^4)	α_∞	Λ (μm)	Λ' (μm)
0.98	13.5	1.7	80	160
N (kPa)	ν	η	ρ_s (kg/m^3)	
200	0.35	0.1	1500	

Table 2 : Properties of the foam

4. CONCLUSION

This paper presented the coupling of the {u,P} formulation using hierarchical elements with a classical finite element plate modeling of an elastic domain assuming non coincident meshes. This approach has been used to predict the mean quadratic velocity and the transmission loss of a plate coated by a porous material. It gives accurate results with a reduced number of unknowns in comparison with a classical finite element modeling of the structure with coincident meshes.

5. REFERENCES

[1] Atalla N., Panneton R., Debergues P. "A mixed displacement-pressure formulation for poroelastic materials", J.A.S.A. 104(3), 1444-1452 (1998)

[2] Rigobert S., Sgard F., Atalla N. "Investigation of the convergence of the mixed displacement-pressure formulation for 3D poroelastic materials using hierarchical elements", submitted for publication.

[3] Farhat C., Géradin M. "On a component mode synthesis method and its application to incompatible substructures", Computers and Structures 51(5), 459-473 (1994).

Figure 1: Mean quadratic velocity for the plate
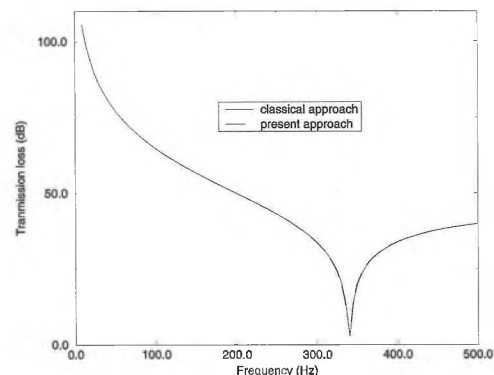
Figure 2: Transmission Loss for the multilayer

Non-linear Analysis of Electrostrictive Materials by the Finite Element Method

Jean Claude Debus, Jocelyne Coutte, Bertrand Dubus

Institut Supérieur d'Electronique du Nord, Dept Acoustique 41 Bvd Vauban 59046 Lille CEDEX France

1. INTRODUCTION

New electrostrictive lead magnesium niobate ceramics (PMN) are promising materials for realizing actuators or high power transducers for macrosonics or underwater acoustics. Because of their large dielectric permittivity, PMN materials have strains roughly an order of magnitude larger than those of lead titanate zirconate (PZT) ceramics. However, the use of PMN as active material in actuators or transducers presents some difficulties : highly non-linear properties (Fig.1), temperature and frequency dependence of dielectric permittivity, DC bias field needed. To help in the design of PMN-based transducers, a numerical modeling capability is needed.

2. CONSTITUTIVE EQUATIONS OF PMN ELECTROSTRICTIVE CERAMICS

PMN electrostrictive materials are relatively new and complicated in behavior [1]. Non-linear constitutive models for electrostrictors are not as mature as models for piezoelectrics [2]. The model used in this paper is Hom's model [2,3]. Choosing the electric displacement and the stress as the independent state variables, the constitutive equations can be written at constant temperature:

$$S_{ij} = S^D_{ijkl} T_{kl} + Q_{ijmn} D_m D_n$$

$$E_m = -2Q_{ijmn} D_n T_{ij} + \frac{\delta_{mn}}{k|D|} atanh(\frac{|D|}{P_s}) D_n$$

where S_{ijkl} is the elastic compliance at constant electric displacement, T_{kl} is the stress, D_m is the electric displacement, E_m is the electric field, S_{ij} is the strain, Q_{ijmn} is the electrostrictive coefficient, δ_{mn} is the Kronecker symbol, P_s is the spontaneous polarization and k is a new material constant.
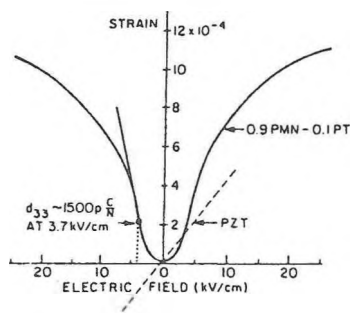
Fig. 1. Typical strain-electric field for electrostrictive and piezoelectric ceramics [4]

3. FINITE ELEMENT FORMULATION

The electrostrictive finite element is developed in the ATILA code [5,6]. Starting with Newton's law, Gauss's law and the equation of electrostriction in the electrostrictive material, Helmholtz's equation in the fluid and the Sommerfeld's radiation condition, the method of weighted residuals is used for the static and transient analyses to get the finite element formulation [7]. For transient analysis, the set of equations for the electrostrictive structure in a fluid domain is written:

$$
\begin{vmatrix} [M] & [0] & [0] \\ [0] & [0] & [0] \\ \rho_f^2 c_f^2[L]^T & [0] & [M_1] \end{vmatrix}
\begin{Bmatrix} \ddot{U} \\ \ddot{\phi} \\ \ddot{P} \end{Bmatrix}
+
\begin{vmatrix} [0] & [0] & [0] \\ [0] & [0] & [0] \\ [0] & [0] & [D_1] \end{vmatrix}
\begin{Bmatrix} \dot{U} \\ \dot{\phi} \\ \dot{P} \end{Bmatrix}
$$

$$
\begin{vmatrix} [K_{UU}] & [K_{U\phi}] & [L_U] \\ 2[K_{U\phi}]^T & [K_{\phi\phi}] & [0] \\ [0] & [0] & [H]+[D_0] \end{vmatrix}
\begin{Bmatrix} U \\ \phi \\ P \end{Bmatrix}
=
\begin{Bmatrix} F \\ -Q \\ Q \end{Bmatrix}
$$

where U, ϕ, P, F and Q are the vectors of the nodal values of the displacement, the electric potential, the pressure, the external force and the electric charge respectively. $[K_{uu}]$, $[K_{up}]$, $[K_{pp}]$ and $[M]$ are the classical stiffness, piezoelectric, dielectric and consistent mass matrices of a piezoelectric finite element model. $[0]$ is the zero matrix. For the fluid:

$$[D_0] = \frac{\rho_f c_f^2}{R}[D]$$

$$[D_1] = \rho_f c_f [D]$$

where $[H]$, $[M_1]$, $[D]$ are the stiffness, consistent mass and damping matrices, ρ_f and c_f are the density and the velocity of the fluid and R is the radius of the spherical boundary which limits the fluid mesh.

4. VALIDATION

4.1. STATIC ANALYSIS OF A PMN BAR

To validate the previous development, a long electrostrictive bar with electrodes located at both ends is analyzed at ambient temperature. A static mechanical force is applied at both ends and a quasi-static (1 Hz) electric field parallel to the length is prescribed. Numerical results are compared to measurements made on a PMN-PT-La (0.90/0.10/1%) bar at NUWC New London [8]. The finite element mesh of the bar consists of two axisymmetrical electrostrictive elements. These elements are eight-noded isoparametric quadrilaterals.

Figure 2 presents the quasi-static strain versus quasi-static applied electric field for various prestresses. The static strain is not measured. In both figures, good agreement is obtained between computed results and measurements in a broad range of applied electric fields and prestresses.

4.2. DYNAMIC ANALYSIS OF A PMN BAR

We study the dynamic response of the same PMN bar. Two types of excitations are considered:

- a step in voltage which generates a vibration of the bar at constant
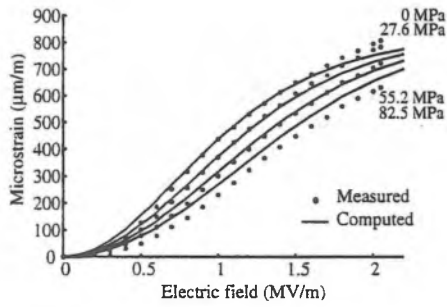
Fig. 2. Strain versus electric field at various prestresses

electric field E. The corresponding natural frequency is noted f_E.

• a step in charge which generates a vibration of the bar at constant electric displacement D. The corresponding natural frequency is noted f_D.

Knowing these two frequencies, the coupling coefficient of the bar is calculated from the expression:

$$k^2 = \frac{f_D^2 - f_E^2}{f_D^2}$$

This expression is similar to Ikeda's coupling coefficient definition from elastic constant c^D and c^E [9].

Figure 3 displays the displacement at the end of the bar versus time for an initial voltage of 2000 volts. The mesh of the bar is unchanged. The thin line represents the vibration at constant E and the bold line the vibration at constant D. The corresponding frequencies are obtained using Discrete Fourier Transform. In figure 4, the coupling coefficient is represented for various initial voltages and voltage steps. Saturation is observed around 45% at high electric field. The observed electrostrictive coupling coefficients are smaller than usual piezoelectric coupling coefficient of PZT8 ceramics (k_{33} around 60%).
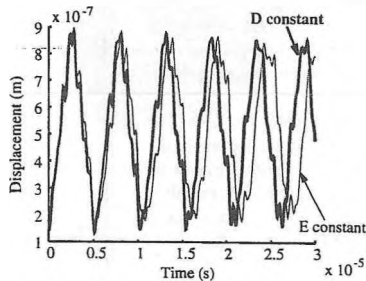
Fig. 3. Displacement at the end of a PMN bar submitted to a voltage (2000 V) or charge (23.8 nC) step versus time (initial voltage of 2000 V)

4.3. TRANSIENT RADIATION OF AN ELECTROSTRICTIVE PMN SPHERE

In this section, we study the response of a PMN spherical shell to a step in voltage. The finite element mesh consists of 6 axisymmetri-
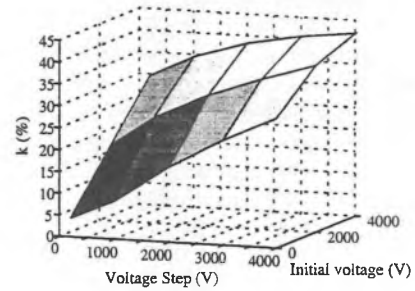
Fig. 4. coupling coefficients of a PMN bar for various initial voltages and steps

cal electrostrictive (eight node quadrilateral) elements. Figure 5 displays the displacement in the middle of the PMN shell versus time for LC (Lumped Constant model) and FE (Finite Element) models for an initial voltage of 4000 V and a voltage step of 1000 V. The thick line correspond to the analytical model, the thin line correspond to the finite element model. A very good agreement is observed between the LC and FE models. Figure 6 displays the deformation of the sphere (full line) versus the structure at rest (dashed line) at time t = 8 10-5s. We notice that the PMN shell is always in compression.
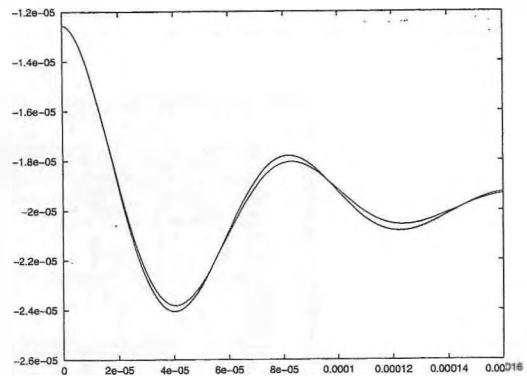
Fig. 5. Displacement of the PMN shell submitted to 1000 V step (initial voltage of 4000 V) versus time. Thick line: semi-analytical model (LC), thin line: finite element model (FE)
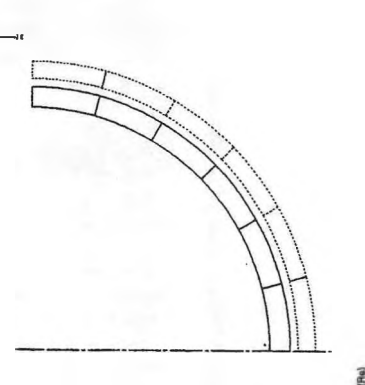
Fig. 6. Strained structure of the PMN spherical shell submitted to an initial voltage and a voltage step. Full line: strained structure, dashed line: initial structure

An Efficient Method Based On Multipole Expansion For Predicting The Sound Power Of Baffled Plane Plates

Stéphane Paquay

LTAS-Dynamique des Structures, Université de Liège au Sart Tilman, Chemin des Chevreuils 1 (B52), B-4000 Liège (Belgium)

1. INTRODUCTION

To evaluate the radiated power from a vibrating structure, the most popular approach consists in the integration of the active acoustic intensity normal to the structure surface. This method needs the evaluation of the pressure field on the surface of the structure. The latter can be calculated by classical discretization methods such as the boundary elements method (BEM). Nevertheless, this methodology suffers from the computational cost associated to forming and solving the frequency dependent linear system. If the system is large (complex structure or extended fre
uency range), the memory of the computer can be the limiting factor so that an out of core solver may be required which adds to the computational cost. To answer to this limitation, an iterative solver [2] can be used in order to avoid the construction of the discretized full matrix system in memory but the efficiency and stability of the algorithm can be disastrous.

To evaluate the acoustic power radiated by a collection of M sources (or a distributed volume source), the simple way consists in the integration of the far-field pressure over a sphere surrounding the M sources [6]. This operation is very expensive due to the need to calculate the field at numerous evaluation points on the sphere. Indeed, the operation cost is of order M at each evaluation point. Using a multipole expansion [4,7] for the set of source points, the field can be efficiently evaluated at points sufficiently far from a sphere enclosing the source points. This condition is always respected in the case of the evaluation of the radiated power since we need only to integrate the far-filed pressure over a sphere. A similar methodology has been already developed by Atalla and al [3]. However, the authors develop a multiple multipole expansion because they use only the first three terms for the expansion.

In the case of baffled plane plate, the pressure field is governed by the Rayleigh's integral [6]. Since this integral can be developed in a multipole expansion, it is shown in this paper that the radiated power can be found accurately and cheaply by integrating the far-field pressure over a hemisphere.

2. EQUATIONS

Consider a set of M punctual acoustic sources in a sphere S_a with centre **a**. Their positions are $(x_1, ..., x_M)$ and their intensities are given by $(q_1, ..., q_M)$. The acoustic pressure field caused by these sources at a point **r** can be written

$$p(\mathbf{r}) = \sum_{l=1}^{M} q_l \frac{\exp^{-ik|\mathbf{r}-\mathbf{x}_l|}}{4\pi|\mathbf{r}-\mathbf{x}_l|} = -\frac{ik}{4\pi} \sum_{l=1}^{M} q_l h_0(k|\mathbf{r}-\mathbf{x}_l|) \quad (1)$$

where

$$h_0(k|\mathbf{r}-\mathbf{x}_l|) = \frac{\exp^{-ik|\mathbf{r}-\mathbf{x}_l|}}{-ik|\mathbf{r}-\mathbf{x}_l|}$$

and k is the wave number. In this way, the cost of the evaluation at one point is of order M. If the evaluation point is outside the sphere S_a, the field can be expanded in an outer multipole expansion of the form

$$p(\mathbf{r}) = \sum_{n=0}^{\infty} \sum_{m=-n}^{n} C_n^m h_n(k|\mathbf{r}-\mathbf{a}|) Y_n^m(\frac{\mathbf{r}-\mathbf{a}}{|\mathbf{r}-\mathbf{a}|}) \quad (2)$$

with Y_n^m the spherical harmonics and h_n the spherical Bessel functions.

Using the Gegenbauer formula [1,4] which writes the spherical Bessel functions in terms of spherical harmonics, the multipole expansion coefficients, C_n^m, can be written after few algebraic manipulations,

$$C_n^m = \frac{-ik(2n+1)}{4\pi} \sum_{l=1}^{M} q_l j_n(k|\mathbf{x}_l-\mathbf{a}|) Y_n^{-m}(\frac{\mathbf{x}_l-\mathbf{a}}{|\mathbf{x}_l-\mathbf{a}|}) \quad (3)$$

The expansion (2) is exact for an infinite number of terms. Nevertheless, we always truncate the expansion to N so that each evaluation point has to be sufficiently far from the sphere S_a. Also, the terms $h_n(x)$ in the expansion (2) grow quickly with n for $n>x$. This fact can cause numerical instability. One more time, this difficulty vanishes if the point **r** is far from the centre of the expansion **a**. From equation (3), we can see that coefficients C_n^m do not depend on the observer position. Thus, once these coefficients are computed for a set of source points, the far-field at a large number of observer points can be cheaply evaluated using equation (2). This is the basic idea behind the efficiency of the approach for evaluation of the radiated power.

The acoustic power radiated by the collection of acoustic source points can be evaluated by integrating the far-field pressure over a sphere [6]

$$\Pi_{ac} = \int_{S_R} \frac{|p|^2}{2\rho_f c} dS_R = \int_0^{2\pi}\int_0^{\pi} \frac{|p(R,\vartheta,\varphi)|^2}{2\rho_f c} R^2 \sin\vartheta \, d\vartheta \, d\varphi$$

Introducing the multipole expansion (2) in the last expression, we obtain

$$\Pi_{ac} = \frac{1}{2\rho_f c} \int_0^{2\pi}\int_0^{\pi} |R \sum_{n=0}^{N} h_n(kR) \sum_{m=-n}^{n} C_n^m Y_n^m(\vartheta,\varphi)|^2 \sin\vartheta \, d\vartheta \, d\varphi$$

Posing and , the last equation becomes

$$\Pi_{ac} = \frac{1}{2\rho_f c} \int_0^{2\pi}\int_{-1}^{1} |R \sum_{n=0}^{N} h_n(kR) \sum_{m=-n}^{n} C_n^m Y_n^m(\arccos(x),\varphi)|^2 \, dx \, d\varphi$$

that we have to integrate in two directions. Along x, we need to use a Gaussian quadrature rule and for φ, we have to use trapezoidal quadrature rule. In the literature [5,7], it is suggested to use almost N points along x and almost 2 N points along φ. Finally, note that the terms $h_n(kR)$ have to be evaluated one time for the integration.

3. APPLICATION TO BAFFLED PLANE PLATES

Consider a baffled plane plate. The acoustic pressure in the surrounding fluid domain is governed by the Rayleigh's integral

$$p(\mathbf{r}) = -\rho_f \omega^2 \int_S w(\mathbf{r}') \frac{\exp^{-ik|\mathbf{r}-\mathbf{r}'|}}{2\pi |\mathbf{r}-\mathbf{r}'|} dS(\mathbf{r}') \qquad (4)$$

where w is the normal displacement on the plate.

If we evaluate the pressure on the plate (we have to compute the principal value of the last integral), we can compute the acoustic power by integrating the active acoustic intensity normal to the structure surface. Nevertheless, this methodology is time consuming and we prefer to use the following procedure. From the integral (4), we can construct an outer multipole expansion for the far-field pressure that we can integrate over an hemisphere to obtain the radiated acoustic power. Since we only integrate over an hemisphere ($x \in [0\ 1]$), the number of integration points can be reduced to in this direction.

4. NUMERICAL EXAMPLE

The algorithm will be demonstrated in the case of a simply-supported baffled rectangular steel plate vibrating in air. The dimensions of the plate are $a=1$m, $b=1$m and $h=0.01$m (it is the same plate Atalla [3] has tested with his method). The validity of the proposed method will be proved by the code ADNR. The efficiency of the proposed method for large values of ka, where a is the characteristic dimension of the plate, will be discussed. Finally, to demonstrate the applicability of the presented approach to problems with a high modal density, we consider the same plate 10 times thinner.

5. CONCLUSION AND GENERALISATION

In the general case, the Helmholtz integral equation can not be reduced to the Rayleigh's integral and the pressure on the structure have to be evaluated by a classical discretization method such as the boundary elements method (BEM). The multipole translation theory can be used with a fast algorithm (fast multipole method) to accelerate the computation of pressure on the surface in the boundary elements method [5]. Once the surface pressure is known, we can expand the integral equation in a multipole expansion for the sound field radiated by the structure. This expansion can be used to evaluate the source directivity and the radiated acoustic power. However, in this case it is still preferable to evaluate the acoustic power by integrating the active acoustic intensity normal to the structure surface.

In summary, the proposed technique is an efficient method to eval-

uate the sound field by vibrating structure. In the particular cases of baffled plane plates and distributed volume sources, the expansion can be directly used to efficiently predict the radiated sound power.

7. REFERENCES

1. M. Abramowitz and I. Stegun, "Handbook of mathematical Functions", Applied Math Series, National Bureau of Standards, Cambridge, MA, 1964

2. S. Amini, Chen Ke and P.J. Harris, "Iterative solution of boundary element equations for the exterior Helmoltz problem", ASME J. Vib. Acoust., 112:257-262, April 1990

3. Noureddine Atalla, Grégoire Winckelmans and Franck Sgard, "A multiple multipole expansion approach for predicting the sound power of vibrating structures", Acta Acustica, Vol. 84 (1998)

4. M.A. Epton and B. Dembart, "Multipole translation theory for the three-dimensional Laplace and Helmoltz equations", SIAM J. Sci. Comput., Vol.16, No.4, pp.865-897, July 1995

5. Mark F. Gyure and Mark A. Stalzer, "A prescription for the Multilevel Helmoltz FMM", IEEE Computational Science & Engineering, July-September 1998

6. Claude Lesueur, "Rayonnement acoustique des structures: vibroacoustique, interactions fluide-structure", Ed.Eyrolles, 1988

7. V. Rokhlin, "Diagonal forms of Translation Operators for the Helmholtz Equation in Three Dimensions", Applied and Computational Harmonic Analysis 1, pp.82-93, 1993.

BRUSHLESS DC MOTOR RINGING NOISE: A CASE STUDY

Sylvain Nadeau

Siemens Canada Limited, Automotive Systems, 1020 Adelaide Street South

1. INTRODUCTION

A brushless DC motor ringing noise case study is described in this paper. The motor analyzed is a 400 W brushless DC motor with 5 phases unipolar sensorless drive, 6 poles, 20 slots and external rotor configuration. It is used in the automotive industry to drive an engine cooling fan. The problem studied is a ringing noise that occurs at various speeds during wind up and wind down. This tone seriously affects the module's sound quality and has to be eliminated or significantly reduced.

2. EXPERIMENTAL INVESTIGATION

The SPL of the complete assembly (motor, fan and shroud), shown in Figure 1, has been recorded at 1 meter from the motor's side during a run up. This measurement shows that the module's SPL increase by more than 10 dB(A) at certain speeds. A colormap of the same measurement is presented in Figure 2 with the ringing noise highlighted. It clearly shows that the structure is excited at various orders, which tends to indicate that many forces are exciting it. One can also conclude from the colormap that the ringing noise is due to a resonance in the system because its frequency doesn't change with speed. This conclusion correlates very well with the subjective evaluations performed in conjunction with digital filtering that located the ringing noise around 1600 Hz.

3. MODAL ANALYSIS

A good understanding of the ringing mode's modal properties is necessary to eliminate the problem at a low cost. The analysis has been done with the motor mounted on a suspended shroud ring. A small shaker has been used to excited the motor while the input force was measured with a B&K 8200 force transducer and the response velocity with a Polytec scanning laser vibrometer. A natural frequency has been identified at 1592 Hz which is in the frequency range of interest. The associated damping was around 0.15% and the mode shape is shown in Figures 3 and 4.
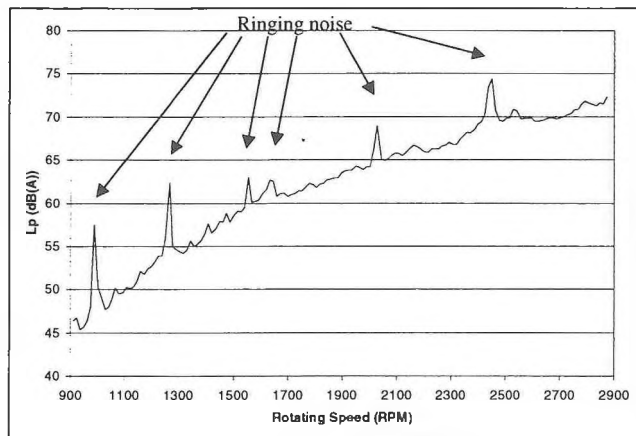
Figure 1 SPL vs speed

The mode shape is of the second order with a shape similar to a vibrating bell. As for a bell, it will create a quadrupole noise radiation [1]. The nodes are located near the end of 4 magnets and none is located between magnets or in the middle of a magnet. As shown in Figure 5, the rotor's side follows the same shape with larger amplitudes near the free extremity than near the front face.
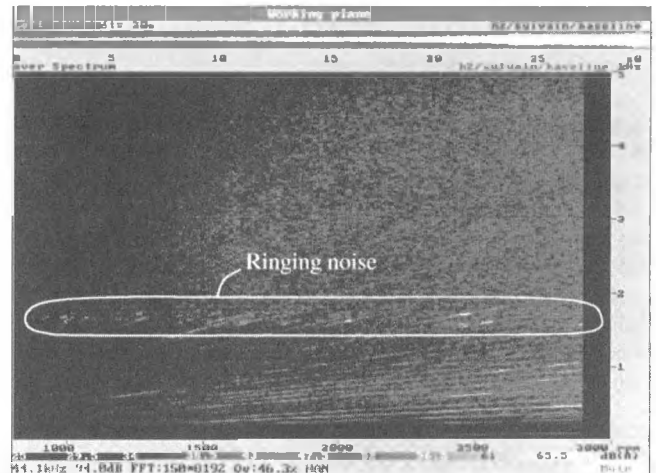
Figure 2 Colormap of a production module
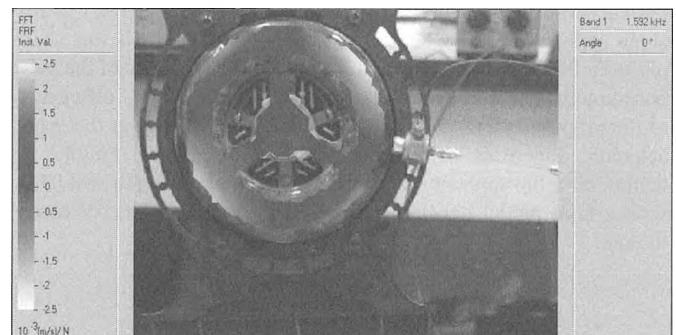
Figure 3 Front view of the 1592 Hz mode shape

Figure 4 Side view of the 1592 Hz mode shape

4. DESIGN MODIFICATION

It is obvious from the experimental investigation and the modal analysis that the ringing noise problem is due to the resonance of the 1592 Hz mode. It is useless to attempt changing the mode's frequency because the resonance would only occur at a different speed. A more appropriate modification is to increase the damping to reduce the noise radiated at that frequency.

Various strategies have been considered to increase the damping at minimum cost and without major modifications to the motor. Knowing that a viscoelastic material submitted to shear is much more effective than one submitted to tension/compression, it has been thought that the magnets could be used as a constraining layer for the damping material. An original design[1] has been developed by replacing a small portion of the magnet adhesive by a very thin layer of viscoelastic material. In the present prototypes, a 10 mm wide and 0.127 mm thick band of 3M ISD 110 viscoelastic material [2] was installed between the magnets and the rotor beside the free edge to take advantage of the maximum shear stress. The remaining magnet surface area was used to bond the magnets to the rotor with a standard adhesive. The Figure 5 illustrates the concept with one magnet removed for clarity. A damping level of 0.8% was achieved with this design and a ringing noise reduction of more than 10 dB(A) as shown in Figure 6 where a standard production sample is compared to 5 prototypes with viscoelastic material.

Figure 7 Colormap of a prototype module

A colormap of one of the prototypes is shown in Figure 7. As expected, the noise level around 1600 Hz has been significantly reduced without really reducing the noise level in the remainder of the spectrum.

5. CONCLUSION

A case study of a brushless motor ringing noise problem has been presented. It has been shown that a rotor's mode around 1600 Hz resonates at certain speeds due to various electromagnetic forces. A new design with viscoelastic material between part of the magnets and the rotor has been described. The experimental results have shown that the new design significantly increase the mode's damping and reduce the ringing noise by more than 10 dB(A). The addition of viscoelastic material between part of the magnets and the rotor offers a convenient way of reducing the ringing noise at a minimum cost and without any major modification to the motor itself.

6. ACKNOWLEDGMENTS

7. REFERENCES

[1]   Pierce, Allan D., "ACOUSTICS An Introduction to Its Physical Principles and Applications", Acoustical Society of America, Woodbury (1994).

[2]   "3M Viscoelastic Damping Polymers 110- 112- 130-", Technical Data (February 1999).

[1] Patent pending

Figure 5 Illustration of the design modification
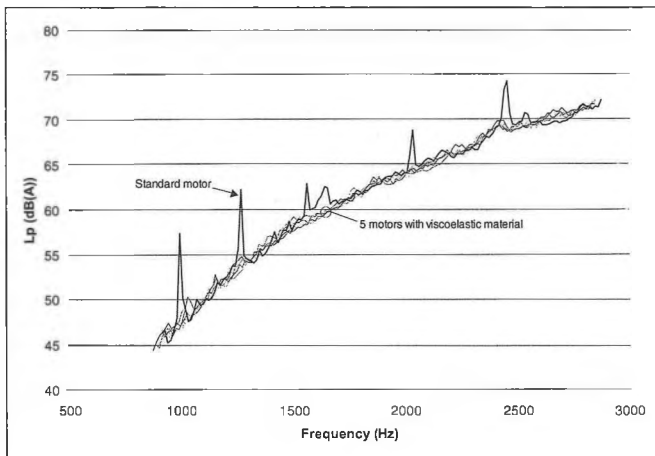
Figure 6 SPL comparison between production and prototypes

TRAITEMENT ACOUSTIQUE DES CABINETS DE REDRESSEURS DE COURANT, ALCAN-JONQUIÈRE

André L'Espérance, ing. *Soft dB inc*, Québec *(www.softdb.com)* et chercheur associé au G.A.U.S.
Marie-Louise Charbonneau, B.Sc., M.Env. Hygiéniste industrielle Alcan, Énergie Électrique, Jonquière, Québec
Alex Boudreau, étudiant gradués, Université de Sherbrooke

1. INTRODUCTION

Suite à la rénovation d'équipements appelés *redresseurs de courant*, le bruit dans la salle des redresseurs (36 redresseurs par salle) de l'usine d'Alcan à Jonquière a augmenté de 2 à 3 dB, faisant passer les niveaux de 90 à 92-93 dB(A). Des correctifs devaient donc être apportés pour diminuer ces niveaux sous le seuil de 90 dB(A). L'analyse des mécanismes de génération du bruit émis par ces redresseurs s'avérant toutefois complexe (phénomène électromagnétique), et les courants et voltages utilisés importants, des interventions et/ou modifications sur la conception des redresseurs mêmes étaient hasardeuses.

L'insonorisation de la salle paraissant à priori peu performante dû à la proximité des redresseurs des espaces de circulation et lieu de travail, l'insonorisation des cabinets de redresseur apparaissait la meilleure voix à explorer. Afin d'évaluer le potentiel de traitement acoustique à l'intérieur même des cabinets, une étude d'acoustique prévisionnelle incluant une modélisation détaillée de la source a donc été entreprise. Cet article décrit la démarche utilisée et les résultats obtenus.

2. MODÉLISATION

La salle de redresseur considérée est constituée de 6 cabinets, comprenant chacun 6 phases ou redresseurs. Un redresseur est principalement constitué d'une bobine électrique de forme cylindrique de 0,74 m de hauteur et 0,4m de diamètre. Chaque cabinet protégeant ces redresseurs fait environ 5m x 2m x 1,5 m, et est constitué de parois d'aluminium de 3mm sur chacun des côtés.
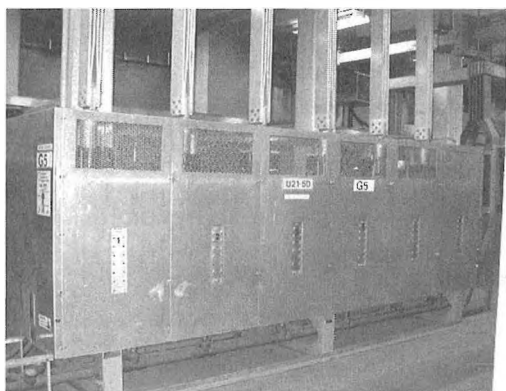
Figure 1 Photo d'un cabinet avant traitement

La capacité de refroidissement de ces équipements étant un facteur important pour leur bon fonctionnement et durée de vie, la partie supérieure des panneaux latéraux étaient constituée d'un grillage, tandis que le dessous du cabinet (situé à environ 0.3m du sol), et une portion de la surface du dessus (d'environ 0,1 m^2) étaient ouverts.

Afin de représenter le mieux possible la propagation sonore à l'in-

térieur de ces redresseurs et dans la salle, une modélisation par de tir-de-rayon a été utilisée[i]. Dans cette étude, pour obtenir des résultats significatifs de l'efficacité de traitement potentielle de l'intérieur des cabinets, la modélisation comportaient trois volets : 1) modélisation des redresseurs eux mêmes, 2) modélisation du cabinet et 3) modélisation du local .

Les redresseurs ont été modélisés par des sources ponctuelles entourées par un ensemble de plans disposés selon une forme cylindrique mais espacés par des ouvertures de sorte que les rayons puissent s'échapper.
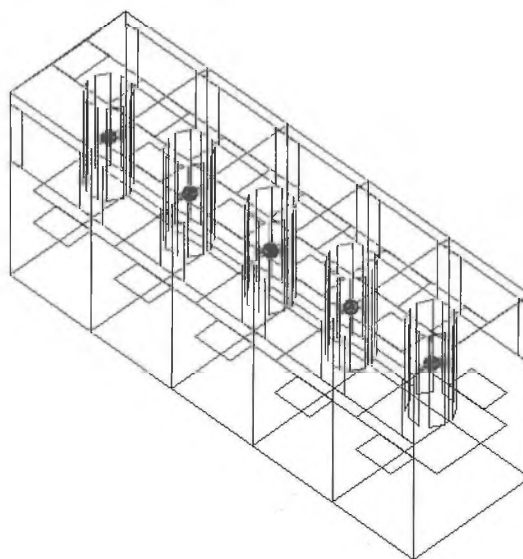
Figure 2 Modélisation des sources (redresseurs) avec le cabinet

Les cabinets sont pour leur part modélisés par un ensemble de plans représentant les différentes surfaces du cabinet, et en laissant des surfaces libres (i.e. sans plan) pour représenter les ouvertures du cabinet. Ainsi une section du haut des panneaux latéraux, une portion de la surface du dessus de même que le dessous du cabinet ont été laissé ouverts.

Comme plusieurs réflexions doivent généralement se produire avant que le rayon sorte du cabinet et se propage dans le local, on devait s'assurer que la majorité des rayons soient sortis des plans entourant la source d'émission et le cabinet. Aussi, le nombre maximal de réflexions qu'il est généralement suggéré d'utiliser, soit 30, a ici été augmenté à 40.

Finalement, le local lui-même doit être modélisé pour évaluer le champ sonore dans le local, et l'efficacité de traitement des parois du cabinet. Le nombre de plans nécessaires à la modélisation de la source et du cabinet, de même que le nombre de réflexions à considérer rendant la gestion du modèle, déjà relativement lourd et exigeant en temps de calcul, il était peu réaliste de modéliser l'ensemble des 36 redresseurs. Profitant de la symétrie du local de

la salle des redresseurs, seule une section de la salle a pu être mod-
élisée en utilisant des parois réfléchissantes de part et d'autres d'un
cabinet.
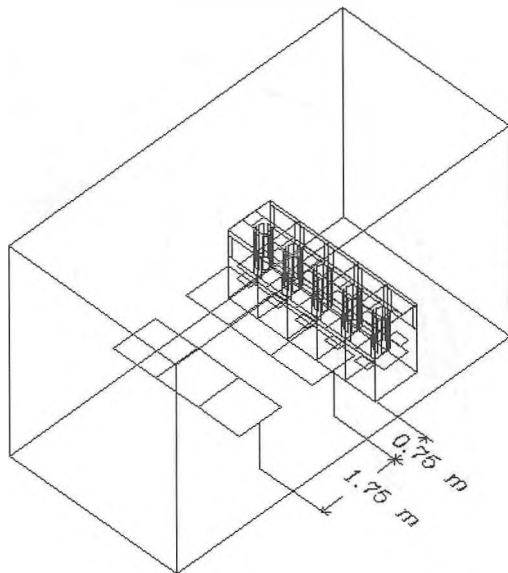
Figure 3. Modèle du local des cabinets

Les cellules de réception sont à 1.5 mètres du sol et elles sont
situées à 2.5 mètres et 0.75 mètre du cabinet. Le volume de ces cel-
lules de réception est important pour s'assurer d'avoir un nombre
représentatif de rayons qui les traversent.

La validité du modèle a par la suite été évaluée en introduisant une
source calibrée dans un cabinet réel hors fonction et en mesurant les
niveaux générés à l'extérieur. Finalement, la puissance acoustique
des sources ponctuelles représentant les redresseurs a été obtenue
en mesurant les niveaux dans le local réel et ajustant la puissance
de la source afin d'obtenir des résultats simulés comparables au
modèle.

3. RÉSULTATS

Utilisant ce modèle, diverses options de traitements acoustiques des
parois intérieures du cabinet ont été évaluées. Suite à cette évalua-
tion, un traitement consistant à boucher les ouvertures (grillages)
avant et arrière du cabinet et à placer un matériau absorbant sur ses
parois intérieures a été recommandé, ce traitement offrant en
théorie une réduction de 6 à 7 dB. Pour compenser la fermeture des
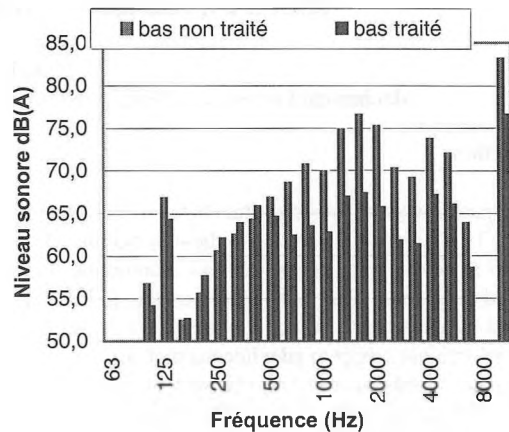
Figure 4 Atténuation moyenne après le traitement

grillages, l'ouverture sur le dessus du cabinet a toutefois été aug-
mentée de façon à compenser la perte d'ouverture sur les parois
latérales. De plus en procédant ainsi le refroidissement par con-
vection devait être augmenté dû à l'effet de cheminée que jouait
maintenant le cabinet.

Afin de valider ce traitement, le nouveau type de cabinet a été fab-
riqué et des mesures ont été réalisées à l'aide d'un haut-parleur
comme source. La figure 4 présente le spectre de bruit face au cab-
inet testé, avec et sans le traitement acoustique.

Ces résultats étant conformes aux prédictions, le traitement d'un
premier cabinet réel avec redresseur a été réalisé et un suivi des
températures a été effectués afin d'évaluer la viabilité thermique de
la solution. Ces évaluations ont été très positives, l'effet de chem-
inée anticipé ayant permis une réduction de 5°C de la température
d'opération.

Suite à ce résultat, le traitement de l'ensemble des 56 cabinets à été
entrepris. La réduction globale de bruit obtenue dans une salle de
redresseurs varie de 5 à 11 dB(A).

4. REFERENCES

1. A.M. Ondet, J.L. BarBry Acoustique Prévisionnelle,
    Modélisation de la propagation dans les locaux indus-
    riels à partir de la technique des rayons, Les Notes sci-
    entifiques et techniques de l'INRS, vol 67 (1987).

RIDER INFLUENCE ON MODAL PROPERTIES OF BICYCLE FRAMES

J. Thibault, Y Champoux

Mechanical Engineering Department, Université de Sherbrooke, Sherbrooke (Québec) Canada J1K 2R1

Introduction

Over the past few years, bicycles frames have evolved at an important rate. This is in major part due to the introduction of new materials used in frame composition such as aluminium, titanium and reinforced polymers. The use of these materials has been highly motivated by the need to reduce the weight of bicycles. There is also the vibrational aspect to take into account since the majority of the materials used possess low damping values. Particularly, manoeuvrability and comfort should be strongly influenced by the dynamic behaviour of the bicycle.

This work intends to be a first step towards the use of modal analysis to understand the dynamic behaviour of bicycles, and to investigate the influence of the rider and boundary conditions on the modal parameters of road bikes. Two approaches were used to identify the modes of the bicycle. We first looked at the out-of-plane motion using a lateral excitation. Then we studied the in-plane motion using a vertically mounted shaker recreating with more fidelity the road induced excitation. For each approach, modal analysis was performed in the "free-free" condition and with the bicycle standing stationary on the floor with a rider (see figure 1).

Out-of-Plane Motion Analysis

Out-of-plane motion is responsible in preponderance for the manoeuvrability issues since this kind of motion permits the rotation and translation of the two wheels.

Modal analysis was performed using "free-free" boundary condition. All moving components were removed from the bicycle to eliminate potential rattles. A 50-lbs. shaker was linked laterally to the top tube. The structure response was measured by a piezoelectric accelerometer displaced over 63 points on the bicycle. The frequency resolution used on the analyser was 0.5 Hz with a frequency span of 400 Hz.
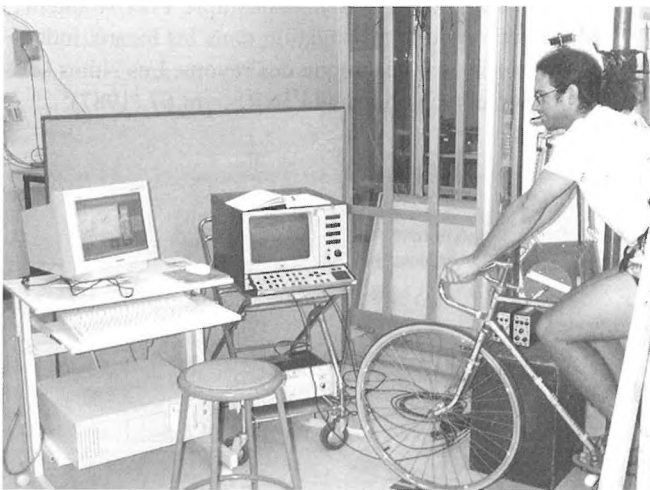
Figure 1 - Modal testing using lateral excitation with the bicycle standing stationary on the floor.
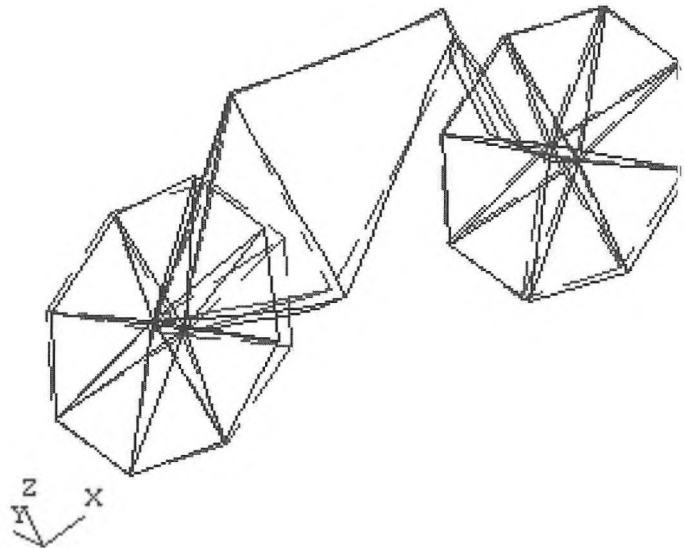
Figure 2 - Critical mode for manoeuvrability in "free-free" condition at 70 Hz. The rear wheel is rotating about the vertical axis.

Clean deformation shapes showing very little damping were obtained. Specific modes were identified as being critical to manoeuvrability since the rear wheel is rotating from left to right (see figure 2). The fundamental frequencies of the identified modes are contained between 26 Hz and 285 Hz.

Afterwards, we conducted the modal analysis with a rider on the bicycle. The curve-fitting process was laborious considering the mode coupling and highly damped peak of the measured FRFs. However, suitable deformation shapes were obtained. Only one mode has proved to be significantly correlated with one of the "free-free" analysis modes found. It is a local mode affecting only the seatstays and probably having a negligible effect on manoeuvrability. The fundamental frequency of this mode went from 175 Hz to 188 Hz when the rider was added.

In-Plane Motion Analysis

The in-plane motion has negligible effect on the manoeuvrability since wheels remain in line when the bicycle is deformed. On the other hand, the vertically oriented road-induced loads tend to animate the in-plane modes, which could be held responsible for the problems of discomfort.

The interaction between the rider and the bicycle has been observed at three different points: the feet, the posterior and the hands. The feet are probably the least significant element because the posterior and the hands mostly support the rider's weight. Moreover, the load applied to the wheels must go through the entire frame to get to the pedals. Conversely, the load applied to the front wheel is transmitted directly to the handlebars by the fork and the load applied to the rear wheel is transmitted directly to the saddle through the seatposts. Only the hands-handlebars interface will be considered in this work since a lot of damping is provided by the saddle, the racing shorts and the buttocks.
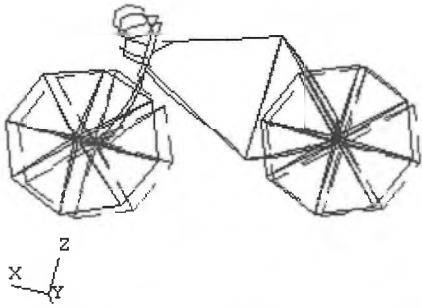
Figure 3 - Critical mode for comfort present respectively at 26 Hz and 22 Hz in "free-free" and "with rider" conditions.

This time, the modal analysis was performed using a vertical excitation on the stem. The frequency span of interest has been reduced to 200 Hz with a frequency resolution of 0.25 Hz. We increased to 82 the number of points on the bicycle to include the stem and the handlebars in the study. The FRFs measurement in the "free-free" condition led us to several interesting deformation shapes, particularly those implicating both the handlebars and the fork at the same time, resulting in more violent modes. We observed that the majority of the recognised modes were affecting locally the handlebars.

Afterwards, modal analysis with a rider on the bicycle was conducted. Most of the modes that were present in the "free-free" condition disappeared. It is mainly the case for the local modes implicating only the handlebars and leaving the fork and the frame static. One mode showed to be highly correlated with one of the modes identified in the "free-free" condition. This mode implicating mostly the fork and the handlebars was found at 26 Hz for the "free-free" condition and at 22 Hz with a rider (see figure 3).

Road Excitation

Since the modal analysis demonstrated that natural modes could be found to a frequency up to 200 Hz, it was interesting to have an idea of the excitation spectrum provided by the road. To do so, an accelerometer was mounted under the handlebars near the stem of a road bicycle. The bicycle was ridded through a typical "moderately rough" road for 10 seconds at a speed of 20 km/h. The experimentation was repeated several times on the same road section and repeatability has been proven.
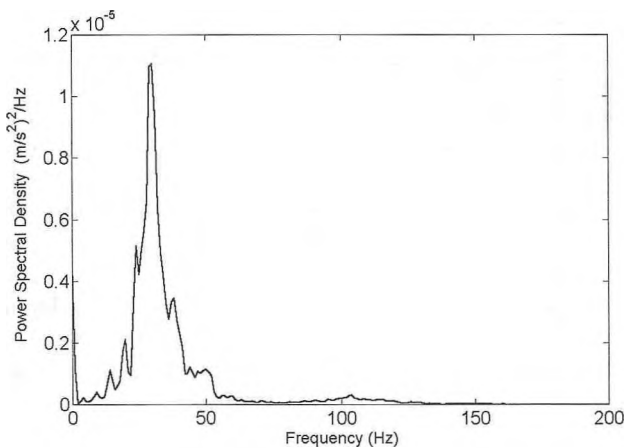
Figure 4 – Power spectral density measured on the handlebars of a road bicycle using a sampling rate of 800 Hz during a 10 s. ride on a moderately damaged surface.
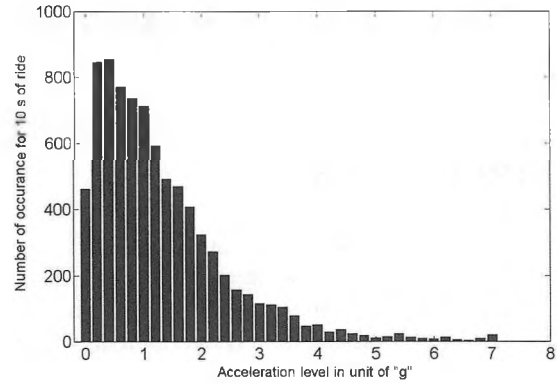
Figure 5 - Number of occurrence of acceleration levels during the 10 s. ride test for each of the 8192 measurement point.

We found a spectral density mostly concentrated in the range of 0-50 Hz (see figure 4). In terms of amplitude, we found that 7g of acceleration was obtained on a moderately damage surface with a speed of 20 km/h. Thus, it would be easily possible that acceleration in excess of 10g would be obtained on a different road or at a different speed. The histogram of figure 5 presents the number of occurrences of specific g levels attained in the 10 second ride test.

Discussion of Results

The out-of-plane analysis showed that the dynamic behaviour of a road bicycle is greatly modified with the interaction of the rider. This is confirming the need to take in consideration the rider interaction during the design process.

Since the road-induced vibrations are mostly contained between 0 Hz and 50 Hz, the modes having fundamental frequency above that level should not be held responsible for problems inherent to manoeuvrability or comfort.

Finally, the in-plane mode implicating the fork and the handlebars found in both "free-free" and "with rider" conditions, at respectively 26 Hz and 22 Hz, should be looked further because the power spectral density recorded in the 10 second ride test is very important in this range of frequency. The concerned mode could play an important role in the comfort of the bicycle.

References

[1]   Ferraresi, C., Garibaldi, L., Perocchio, D. and Piombo, B.A.D., "Dynamic Behaviour and Optimisation of Frames for Road and Mountain Bikes", IMAC Proceedings of the 16th International Modal Analysis Conference, Santa Barbara, CA, USA, vol. 1, pp. 387-393 (1998)

[2]   Okubo, N. and Ishida, N., "Application of CAE to Vibration and Strain Analysis of a Bicycle", IMAC Proceedings of the 9th International Modal Analysis Conference, Florence, Italy, vol. 2, pp. 860-865 (1991)

[3]   Gribb, Tye T., Worzala, F.J. and Gribb, G.W., "Modelling Bicycle-Rider Vibrations : Implications for Materials Selection", MRS Bulletin, vol.23, n.3, pp. 56-58 (1998)

NOISE FROM RAILWAY OPERATIONS IN CANADA

Bill Aird
Canadian Transportation Agency, 15 Eddy Street, Hull Quebec, K1A 0N9

1. INTRODUCTION

Railway operations by their very nature generate sounds. Those sounds are caused by the engines in the locomotives, the wheel/rail contact, coupling collisions, and whistles or bells. The sound of a passing train is intermittent while bell ringing and shunting collisions are impulsive. The intermittent rail sounds may vary from 73 to 96 dBA in intensity at 30 m while impulsive ones may vary from 75 to 90 dBAI at 30 m.

Noise is the human reaction to sound and reflects the level of human annoyance generated by the unwantedness of sound. Loudness alone is not an accurate measure of the degree of annoyance that a sound generates. A dripping tap can be very annoying while 110 dBA symphony or rock music can be very pleasing to the listener. Location is also an important factor. A train whistle in an industrial park can be accepted as a way of life while a whistle even many kilometres away, in a wilderness park, can be very annoying to wilderness campers.

When evaluating noise in residential areas, the universally accepted levels are 55 dBA during the day and 50 dBA at night. The latter level has been adopted to ensure an indoor level of 35 dBA which is the level for undisturbed sleep. The major Canadian railways support those residential levels. The Canadian National Guidelines for Environmental Noise Control call for a reception point limit of 50 dBAI for stationary impulsive sounds. Shunting collisions are considered stationary sources.

Source of Railway Noise	Noise Level (dBA at 30 m)	Setback (to achieve 50 dBA)
idling locomotive	70 -73 (summer)	420 m
idling locomotive	90 - 96 (winter)	5980 m
moving locomotive	90- 96	5980 m
coupling cars	80 - 90 dBAI (at 100 m)	10,000 m

Table 1: Sample Rail Noise Levels (Based on EPA levels)

Table 1 indicates the loudness of the sound emanating from four typical rail operations. It also shows that, in order to achieve a night-time residential level of 50 dBA across open ground, significant setbacks (assuming a 6 dB attenuation of sound per doubling of distance) may be involved.

2. EFFECTS OF NOISE

Noise has both physiological (hearing loss, increased blood pressure) and psychological (sleep disturbance, annoyance or emotional stress and violence) effects on people. Rail noise, as a form of community noise, leads to the interruption of rest, relaxation and sleep as well as speech interference. Annoyance is increased when people feel they have no control over the noise source.

People cope with noise by turning their emotions inward, changing their environment, complaining or taking legal action. Only a very small per centage of a population will actually complain or take legal action. Thus these two actions are very poor indicators of annoyance. There is no such thing as acclimatization to noise. Rather the human brain reduces an individual's conscious awareness of noise while the body continues to suffer the physiological and psychological effects (i.e. the body still experiences the fight or flight response.

Complainants indicate that rail noise affects the use of their outdoor spaces, interferes with conversation and disturbs their sleep. Some complainants report not being able to get a good night's sleep for months at a time ie. They are suffering from sleep depravation. Shunting noise is especially disturbing as it is unpredictable and usually involves loud impulses which can bring people bolt upright in their beds.

3. NOISE CONTROL

Environmental guidelines attempt to define exposure limits beyond which the impacts of a stressor are intolerable or unacceptable. Noise guidelines can be imperfect as it is difficult to establish the dose/effect relationship of noise due to the wide variability of individual responses to noise.

At present, there are no rail noise guidelines in Canada. The United States Environmental Protection Agency has issued source guideline lines for railway equipment. The major Canadian railways have expressed an interest in developing Canadian rail noise guidelines. The European Community is ahead of North America in that it has undertaken noise mapping and thus can identify areas of concern.

Rail noise can be controlled at source by installing mufflers on equipment, lubricating rails to reduce wheel squeal or making changes in railway operations . Noise barriers and

berms have been effective for abating road noise. However, due to the low frequency of diesel noise, the drumming of multiple diesels and impulsive nature of coupling noise, barriers and berms have often not been effective in controlling rail noise.

In urban areas, incompatible land use development has led to conflict e.g. where airports or railways and residential housing are adjacent to each other. Separation of source and receptor can be an effective approach at the project planning and design stages. However, this is not always possible when existing railways and homes are adjacent to each other. Many rail yards and airports alike were built at some distance from residential areas but subsequent residential development has occurred which has brought houses into close proximity of the yards or airports. Other presentations in this session deal more specifically with this land-use conflict.

4. RAIL COMPLAINTS

In the case of rail noise complaints, the source (railway) and receptors (residents) fall under different jurisdictions. Railways, which cross provincial or international boundaries, are under federal jurisdiction ie. the Canadian Transportation Agency (Agency). Under the *Canada Transportation Act* (Act), the Agency is responsible for regulating rail construction and operations including noise. Housing falls under provincial jurisdiction. The public is often confused because the provincial or municipal regulatory requirements, with which they are familiar don't apply to federal railways.

The Agency, in consultation with the Railway Association of Canada, has developed a process for investigating rail noise complaints under the Act. Complainants are urged to initially deal directly with the railway and to attempt to resolve the complaint at that level. If the parties cannot resolve the complaint, one of them can request the Agency to either mediate the dispute or formally investigate the complaint under the Act. The Agency's goal for mediation is to help parties to resolve their disputes as an alternative to the formal adjudicative process.

Agency investigations determine whether a railway company has done as little damage as possible in its construction and operation. The Agency then renders a decision and may order a railway to take corrective action. The wording of the Act does not anticipate either the incompatibility of rail operations with residential land use or the issue of which land use occurred first.

As stated above, there are no federal rail noise standards in Canada. Thus each complaint is dealt with on its own merit. Investigations centre on what steps a railway has or can take

to minimize the noise from its construction or operation.

5. CASE STUDIES

The Agency has dealt with a variety of noise complaints involving various rail operations:

- pass-by trains,
- idling diesels,
- shunting, and
- bells and whistling.

The presentation will outline examples of each type of operation and the Agency's decision in such cases case.

6. FUTURE OUTLOOK

Many rail noise complaints have arisen because of the incompatibility of rail and residential land-uses. This is because residential development has been permitted in close proximity to rail yards. Conversely with the improved Canadian economy, railways are using more yards than before and formerly idle rail lines or yards are being put into service again. The result is more rail traffic near homes. It is estimated that over 600,000 Canadians are exposed to excessive rail noise. To ultimately resolve the issue of rail noise, one must address both:

- new home construction near existing railways, and
- the increase or relocation of rail traffic near existing homes.

Canadian rail noise guidelines would be helpful to more objectively assess the impact of noise from rail operations and to evaluate the effectiveness of abatement measures.

8. REFERENCES

- Berglung, Birgitta, & Thomas Lindvall (eds). 1996. Community Noise. Stockholm: Centre for Sensory Research for the World Health Organisation.
- Federal/Provincial Working Group on Environmental Noise of Federal/Provincial Advisory Committee on Environmental and Occupational Health. 1989. National Guidelines for Environmental Noise Control (Procedures and concepts for the drafting of environmental noise regulations/by laws in Canada) Ottawa: National Health and Welfare Canada.
- Office of Noise Abatement and Control. 1974. Information Levels of Environmental Noise Requisite to Protect Public Health and Welfare with a Margin of Safety. Washington: U.S. Environmental Protection Agency.
- U.S. Environmental Protection Agency. 1998. Rail Noise Compliance Regulations. Washington: Title 40, Chapter I of the U.S. Code of Federal Regulations.

MINIMIZING THE INCOMPATIBILITY BETWEEN RAILWAY OPERATIONS AND NEW RESIDENTIAL DEVELOPMENT

Karen Fraser

Canadian National Railway, 8th Floor, 277 Front Street West, Toronto, Ontario, M5V 2X7

ABSTRACT

Rail noise and vibration becomes an environmental concern when residential development is approved by Municipalities adjacent to railways without regard for the impacts of existing and future railway operations. Canadian National Railway and Canadian Pacific Railway have developed a set of guidelines which includes standards to reduce the incompatibility between new residential developments and existing railway corridors and yard facilities. Adherence to the guidelines ensures that appropriate measures are implemented to mitigate the impacts of rail noise and vibration, as well as minimizing the potential effects of a derailment, collision or spillage. This paper will discuss the objectives of the railway's guidelines, CN's experience with adjacent development issues and the potential impact of new complaints in older neighbourhoods.

1.0 INTRODUCTION

As development continued to be approved adjacent to railway rights-of-way without regard for the impacts of rail operations, and as complaints about noise and vibration and concerns with regards to safety and security continued to increase, the Railways took action. CN and CP, with the aid of planning and engineering consultants, developed a guideline that established a set of criteria to address these concerns and reduce the incompatibility between new residential developments and the existing railway corridors.

The Railways' guideline was first introduced in February 1983. The document outlines measures to be incorporated into residential developments that are designed to mitigate the impact of rail noise and vibration and to enhance public safety. The guideline has subsequently been revised over the years to include measures to address non-residential development adjacent to the railway corridors and all proposed development in the vicinity of railway yard facilities.

2.0 ADJACENT DEVELOPMENT GUIDELINES

The guidelines set out standard procedures to be observed by the developer and municipalities in determining appropriate measures to mitigate the impact of rail noise, vibration and to minimize the effects of a derailment, collision or spill. The requirements were developed as a practical means of addressing rail noise, vibration and safety concerns and resulted from a review of railway operations, derailment

records, groundborne vibration data and existing noise guidelines. The purpose of the guideline is to provide land use decision makers with the measures necessary to ensure that new residential development is approved with provisions to: provide a suitable noise environment; minimize effects of vibration; provide appropriate protective buffers, berms, setbacks; prevent pedestrian trespass on active railway lines; and, ensure alterations to existing drainage patterns do not adversely affect Railway property. Noise sensitive areas generally include lands lying within 300 metres of a rail corridor and 1000 metres of a rail yard.

TABLE 1: Standards to be Met

Noise	Day*	Night*
sleeping quarters	35 Leq (dBA)	35 Leq (dBA)
living room	40 Leq (dBA)	40 Leq (dBA)
outdoor	55 Leq (dBA)	50 Leq (dBA)
Vibration	0.14mm/sec	
Safety	Restrain derailed train clear of occupied buildings Contain spillage Prevent trespassing	

*Day 0700 to 2300, Night 2300 to 0700

Vibration sensitive areas generally include lands lying within 75 metres. For residential development near a rail corridor, mitigation measures are required to achieve the minimum standards listed in Table 1. The measures to achieve these standards include building setbacks, earthen berms, acoustical barriers, vibration isolation, and security fencing. These measures are mutually supportive and all the measures must be provided to achieve the minimum required protection.

Canadian National Railway has been involved in reviewing and commenting on proposed adjacent development applications in Ontario since the early 1980's. When the guideline was developed, the Railways had hoped the provincial and municipal governments would ensure enforcement of the standards without Railway involvement however it was quickly determined that the Railways had to take an active role in the land use planning process to ensure the standards were being met. Through extensive commenting and many

appeals and successful Ontario Municipal Board hearings, CN's policies have become accepted by municipalities and developers in Ontario as standard constraints and conditions of development. CN is now involved in the planning process of municipalities across Canada by reviewing and commenting on submitted planning applications.

Within the last few years CN has experienced some extreme pressure from developers and municipalities to allow residential uses in traditionally heavy industrial areas, which includes railway yards. CN has responded to the pressure to locate new residential uses adjacent to rail yards through the use of objections and face an uphill battle in convincing developers and municipalities that railway yards and their operations are not compatible with residential or other sensitive land uses. The viability of a railway yard will be compromised if new residential development is permitted adjacent to such facility.

The nature of rail operations and the impulse noise generated from a rail yard make it impossible to permit residential development near a yard. As a result, CN has taken the position that no new residential development should be permitted within a minimum of 300 metres of a railway yard.

3.0 COMPLAINTS

Complaints from residents along a rail corridor or next to a rail yard generally arise as a result of the level of train activity and the noise at night. Many residents are not aware that railways operate 24 hours a day, 7 days a week and in some cases are not aware, prior to purchase, of the existence of the corridor or yard or are misinformed as to its use. In addition, fluctuation in rail activity is largely unpredictable as it is determined by the requirements of an existing or new rail customer and the economy. An increase in gasoline prices, as an example, could change the focus on transportation choices and could increase the demand on rail transportation.

CN has received complaints from residents unhappy with their living environment where residential development has been approved next to rail operations without appropriate mitigation measures. Unfortunately, CN is forced to fight municipalities and developers to prevent new residential uses from being developed next to rail yards and to prevent new residential uses from being developed next to rail corridors without measures to address noise, vibration and safety. In some cases, complaints have been in the form of petitions signed by the residential community and formal complaint filed with the Canadian Transportation Agency.

Municipalities, however, continue to disregard the concerns expressed by CN and approve new development adjacent to railway corridors and yards while sending letters to the Railway and passing Council resolutions on behalf of existing residents next to rail corridors and yards attempting to restrict operations. In some cases, municipalities have provided funding to help the residents groups fight against the Railway.

CN has rationalized most of its surplus facilities, those remaining will be optimized for use by CN. Rail service is a desirable and often essential option to many industries. The economic significance of rail transportation in the movement of goods is important to local, national and international economies. Municipalities and developers should ensure that an acceptable environment is created when developing communities near rail facilities.

APPLICATION OF THE RAILWAY NOISE MODEL FOR DETAILED NOISE ANALYSES FOR THE EAST SIDE ACCESS (ESA) PROJECT

Weixiong Wu and Stephen Rosen

Allee King Rosen & Fleming, Inc., 117 East 29th Street, New York, NY 10016

1. INTRODUCTION

This study presents the use of the Railway Noise Model (RWNM), developed by the University of Central Florida, for prediction of noise impacts at several sensitive receptor locations in the New York Metropolitan region that could be affected by the Long Island Rail Road's (LIRR) East Side Access (ESA) Project. During preparation of the East Side Access Environmental Impact Statement, a detailed noise analysis was made and implemented using the Federal Transit Administration (FTA) noise impact criteria. This study compares the modeling RWNM's sound levels with the FTA model's results. The RWNM simulates a 24-hour period of rail traffic and computes day/night sound pressure level (L_{dn}), maximum sound pressure level (L_{max}), sound exposure level (SEL), and equivalent sound pressure level (L_{eq}). The comparison indicates that the RWNM model is able to model typical railway projects, and is therefore applicable to projects subject to FTA review and/or funding.

2. OVERVIEW

The ESA project would provide direct access for LIRR passengers to Grand Central Terminal in Manhattan by the year 2020. ESA would use the lower level of the existing 63rd Street tunnel under the East River, which was built for LIRR trains (see Figure 1). It would increase LIRR's capacity into Manhattan by 45 percent; relieve crowding in Penn Station; strengthen ties between Manhattan and growing Nassau and Suffolk business centers; support regional employment growth; and reduce trip time by up to 30 minutes per day for 53 percent of LIRR riders. However, the new service network would increase train passbys along most branches, creating a potential for adverse noise impacts at sensitive locations along the right-of-way in Queens, Nassau, and Suffolk counties that many branches already have high noise levels due to existing rail service. This study compares the FTA results with the results from modeling done with the RWNM and examines the implications of relatively modest increases in rail service at sensitive locations.

The RWNM was developed at the University of Central Florida and is used to predict sound levels at receptors near railway operations for analysis in environmental noise assessments. It is a simulation model, and trains are modeled as moving point sources of sound. Using a mouse, the user can easily create model objects, tracks, barriers, and receptors. The RWNM can model light rail vehicles and some heavy freight vehicles, as specified by the FTA. The point sources supported by the RWNM are equivalent to those of the FTA manual, *Transit Noise and Vibration Impact Assessment* [1], and use the same maximum sound pressure level equations. However, the RWNM provides some features and capabilities not available in the current FTA model, such as noise modeling at locations where there are curves, multiple tracks, and barrier attenuation, and where trains sound their warning horns as they approach a crossing, etc.

The RWNM was applied to determine existing and project-generat-ed noise levels at a variety of sensitive receptor locations, such as at a very dense urban area; at two-level tracks; at locations where warning horns are sounded at at-grade crossings; and at locations where houses shield the receptor sites. Geographical Information Systems (GIS), aerial photographs, and field studies were used to select these noise-sensitive receptor sites. Existing noise levels were established by noise measurements and compared to the RWNM's calculated noise levels. Project-generated noise levels were calculated using both the FTA model and the RWNM. Using the FTA noise criteria, noise levels that would result in impacts or severe impacts were determined, and project RWNM and FTA noise level results were compared. At locations where impacts or severe impacts were predicted to occur, the feasibility and effectiveness of implementing mitigation measures was explored.
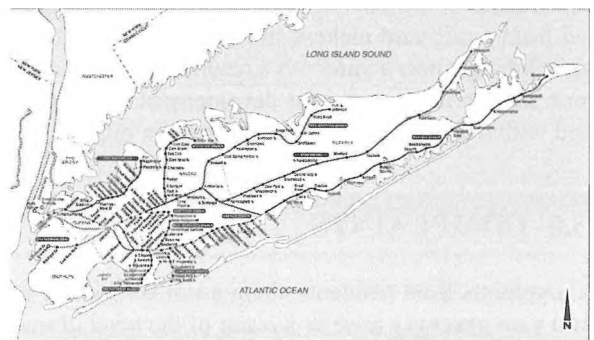
Figure 1: East Side Access Project–Long Island Rail Road Map

3. METHODOLOGY

Selection of Receptor Sites. Table 1 lists the locations of the five receptor sites selected for noise analysis. Noise measurements were made on public streets rather than on private residential property, and adjusted based upon distance from the track to reflect the noise levels at the closest appropriate receptor site to the railroad right-of-way. The receptor locations were selected based on an examination of GIS data for the rail segments that were previously identified as having the potential for project impacts. Field studies were then performed to confirm that each site had a sensitive land use (i.e., residences), that rail noise was the dominant noise source, and that each site was generally the closest sensitive receptor location to the rail tracks. In addition, the five sites were selected to provide geographic coverage of the areas that may potentially be affected

Site	Location	Land Condition	Track Condition
1	Woodside to Forest Hills	High-density residential	Ground-level
2	Jamaica to Floral Park	High-density residential	Two-level
3	Floral Park to Mineola	Mid-density residential	At grade
4	Mineola to Hicksville	Mid-density residential	At-grade crossing. warning horns
5	Huntington to Port Jefferson	Low-density residential	Ground-level. housing shielding

Table 1: Noise Receptor Sites and Locations

by the proposed project (i.e., they were spread over the various segments of the rail line potentially affected by the proposed project).

Noise Monitoring. At each of receptor sites, noise levels were measured to determine existing L_{dn} noise levels. Full 24-hour measurements were made during a typical weekday, between 12:00 Noon Monday and 12:00 Noon Friday. Noise monitoring was conducted using a Brüel & Kjær Noise Level Analyzer Type 4427, a Brüel & Kjær Sound Level Calibrator Type 4231, a Brüel & Kjær ½-inch microphone Type 4189, and a Brüel & Kjær microphone preamplifier Type 2669. Measurements were made on the A-scale (dBA) for a sampling period of 1 hour throughout a 24-hour measurement period. The analyzer was calibrated before and after each 24-hour reading., and a windscreen was used during all sound measurements, except for calibration. All measurement procedures conformed with the requirements of ANSI Standard S1.13-1971 (R1976). Measured quantities included L_{eq}, L_1, L_{10}, L_{50}, L_{90}, and L_{max}.

FTA Model. The noise analysis for the ESA project was performed using the procedures and modeling approach described in the FTA manual. This FTA guidance document provides a three-step process for analysis: a noise screening procedure, used to determine whether any receptors are within distances where impacts are likely to occur; a general noise assessment, used to determine locations where there is the potential for impacts; and a detailed noise analysis, used to predict the impact level and assess the effectiveness of mitigation with greater precision than can be achieved with the general noise assessment. Using FTA methodology, L_{dn} noise levels for free field acoustic conditions (no reflections above ground) from fixed-rail sources were determined based on a variety of factors, including the number of rail cars, train speed, distance to receptors, the surrounding terrain, and in the case of diesel trains, the number of locomotives [2].

Railway Noise Model. The RWNM simulates all daily train operations, followed by night operations. Night operations receive a 10-dB penalty, which is required for L_{dn} determination [3]. Train positions on the tracks are updated at a 1-second time period. This is constant speed simulation. Sound levels and energies from all sources are calculated at each receptor during each time period. The sound level calculation procedure follows the method of the following equation.

$$SPL = L_0 - A_s - A_g - A_e$$

SPL = sound pressure level, dBA,

L_0 = reference level at 15 meters (r_0),

A_s = attenuation as a result of the geometric spreading, $20\log(r_1/r_0)$,

r_1 = distance from source to receiver,

A_g = attenuation due to ground adsorption, and

A_e = diffraction effects due to barriers.

4. RESULTS

Existing noise levels at each location were monitored and calculated using measurements taken in the field and the RWNM model, respectively. Impacts and severe impacts were calculated based on measured levels. Project-generated noise levels were calculated using the RWNM and FTA model at each receptor location. Table 2 shows the existing calculated project-generated increment noise levels.

Based upon the noise impact analysis results, at all receptor locations the project-generated noise would result in noise impacts. The difference in the existing L_{dn} values when comparing measured and RWNM noise levels would be 0.4 dBA at Site 1, 1.5 dBA at Site 2, 0.9 dBA at Site 3, 5.2 dBA at Site 4, and 0.6 dBA at Site 5. The difference between the FTA and RWNM project-generated L_{dn} values would be 0.7 dBA at Site 1, 1.4 dBA at Site 2, 0.6 dBA at Site 3, and 1.8 dBA at Site 5. There would be no difference between the FTA and RWNM project-generated L_{dn} values at Site 4.

Site	Method	Existing Noise level	Allowable Project-generated Noise level		Method	Project Increment Noise level	Result
			Impact	Severe Impact			
1	Measured	69.6	64.1	69.2	FTA	67.6	Impact
	RWNM	70.0			RWNM	66.9	Impact
2	Measured	76.7	65.0	74.5	FTA	70.6	Impact
	RWNM	78.2			RWNM	72.0	Impact
3	Measured	77.2	65.0	75.0	FTA	71.6	Impact
	RWNM	78.1			RWNM	72.2	Impact
4	Measured	75.6	65.0	73.7	FTA	71.4	Impact
	RWNM	80.8			RWNM	71.4	Impact
5	Measured	63.7	60.0	65.4	FTA	62.6	Impact
	RWNM	63.1			RWNM	60.8	Impact

Note: Noise impact analysis values calculated based on measured Existing noise levels.

Table 2: Impact Evaluation of Rail Noise in Ldn dB(A)

5. CONCLUSIONS

Based upon the results, the RWNM provides the capacity for detailed noise analysis of typical railroad projects, and it can meet the FTA model's sound level prediction needs. The evaluations have led to the following conclusions:

With the exception of conditions in which the warning horn is sounded, the existing RWNM values are very close to measured values;
At all sites, there is a maximum difference of 1.8 dBA between RWNM and FTA model project-generated noise levels;
RWNM is user friendly in the creation of sources, receiver, barriers, etc.;
In general, RWNM provides accurate sound level values at typical railway situations;
RWNM provides the ability to assess practical railway projects; and
Train horn results need additional validation with measured noise levels.

At Site 4, where warning horns are sounded at an at-grade crossing, the monitoring noise level is 5.2 dBA higher than RWNM's noise level. Based upon field observations, it is concluded that this difference is because the train engineer tends to blow the warning horn for a longer time period during the daytime than during the nighttime. Therefore, situations with warning horn noise levels need additional validation with measured sound levels.

[1] *Transit Noise and Vibration Impact Assessment*. Report DOT-T-95-16. FTA, U.S. Department of Transportation, April 1995.
[2] *MTA Long Island Rail Road East Side Access*. United States Department of Transportation, Federal Transit Administration, Prepared by Allee King Rosen & Fleming Inc, May 2000.
[3] John M. MacDonald and Roger L. Wayson. *Railway Noise Model*. Journal of the Transportation Research Board, No. 1670, 1999, pp. 76-80.

COMPARISON OF LABORATORY AND FIELD MEASUREMENTS OF SOUND TRANSMISSION LOSS FOR AIRCRAFT NOISE

J.S. Bradley, J.A. Birta and K. Lay

Institute for Research in Construction, National Research Council, Montreal Rd. Ottawa, K1A 0R6

Introduction

The sound insulation of building façade components is most accurately measured in laboratory tests involving pairs of reverberation chambers. This paper reports on the problems of converting from laboratory to field measurements of sound insulation, and is part of a larger project to develop new data and procedures for predicting the sound insulation of buildings against aircraft noise.

Laboratory and Field Measurements

Laboratory sound transmission loss measurements were obtained following the standard ASTM E90 procedure with some extensions, that included increasing the frequency range to extend from 50 to 5k Hz.

Field measurements of sound insulation were obtained in a small wood frame test house located close to Ottawa Airport. The construction was based on 38 mm by 140 mm wood studs with glass fibre insulation in the wall cavity. Interior surfaces were gypsum board and the external surfaces were vinyl siding on OSB sheathing. The house had a sloping roof with 264 mm thick glass fibre insulation in the attic space. For the current results, the ceiling was two 13 mm layers of gypsum board mounted on resilient channels. The details of the construction were changed between tests so that various constructions could be evaluated. Temporary masking walls could be added making it possible to simplify comparisons to single walls having one particular orientation to passing aircraft.

Field measurements were obtained simultaneously from 8 microphones: an outdoor microphone on a mast 10 m high, an external façade microphone, and 3 microphones in each room. Some measurements included an outdoor microphone mounted 2 m away from the building façade.

Differences between Laboratory and Field Conditions

(a) **Effect of angle of incidence.** The transmission loss of a limp panel varies with $\cos^2(\theta)$, where θ is the angle of incidence. In random-incidence lab tests, sound is incident approximately equally from all directions. In the field, the sound is incident from specific angles.

(b) **Directionality of noise from aircraft.** The directionality of noise from aircraft affects the variation of incident sound levels with time. Data obtained by the Swiss lab, EMPA, shows large variations of directionality with both frequency and aircraft type. There is a trend for more modem aircraft to be less directional. Fig. 1 shows the horizontal directionality of a B737 aircraft.

(c) **Effect of aircraft speed and distance.** The incident intensity also varies with time and this depends on the speed of the aircraft and on the distance to the flight track. Fig. 2 compares the variation with time for an omnidirectional source with the calculated effect for a B737 aircraft. Time zero corresponds to the aircraft being closest to the receiver. Sound levels peak after the aircraft has passed the house and the time and amplitude of the delayed peaks vary considerably with frequency. Thus we cannot determine the position of the aircraft, and angles of incidence of the sound from only recorded sound levels.

(d) **Orientation of the building façade.** The total incident sound energy on a particular façade element also depends
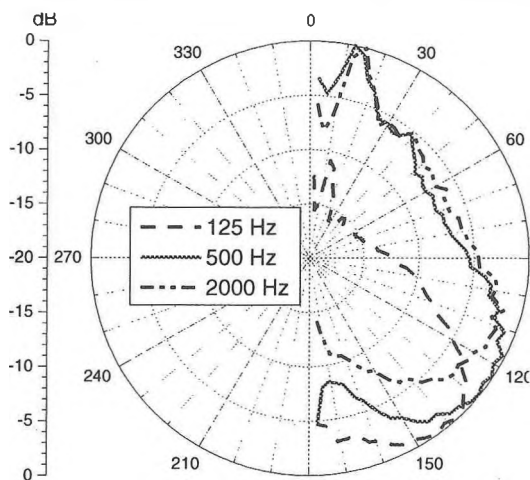
Fig. 1. B737 aircraft directionality at 3 frequencies.
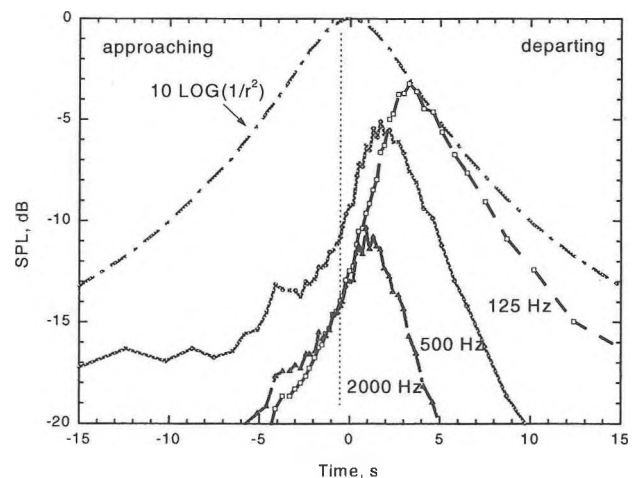
Fig. 2. Calculated pass-bys for B737 and point source.
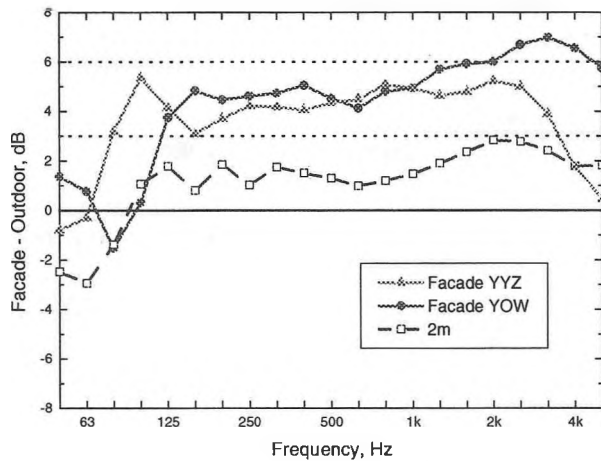
Fig. 3. Average level increases due to the building

the orientation of the façade relative to the aircraft flight path. This is partly a question of the portion of the complete flyby that is visible to the façade, but there is an interaction with the directionality of the aircraft noise. This is further complicated by the diffraction of sound around the corners of the building.

Measurement of Incident Sound Levels

Standards recommend 3 options for measuring the level of the incident sound. It can be measured in the free field, (far from reflecting surfaces), at the façade, or 2 m from the façade. Measurements at the façade are said to lead to 6 dB (pressure doubling) increases and at the 2 m position to 3 dB (energy doubling) increases relative to the free field.

Fig. 3 shows average results at the test house (YOW) and at new homes near Toronto airport (YYZ). Increases at façade microphone locations vary with frequency and rarely reach +6 dB. Measurements at a position 2 m from the façade provide less than 3 dB increases at all frequencies.

Level increases at a façade microphone location for varied angles of incidence are in qualitative agreement with

diffraction theory and demonstrate that a simple 6 dB increase is an over-simplification of what actually occurs.

Comparisons with Measured Noise Reductions

Laboratory TL results and reverberation times measured in the test house were used to calculate expected noise reductions (NR). In Fig. 4 these are compared with NR values measured in the field. Masking walls were positioned in front of the end walls so that only the facing walls transmitted significant sound energy. The results for both rooms A and B are quite similar because both walls are exposed in the same way to the complete aircraft flyby.

The figure shows systematic differences between lab and field results around 125 Hz and 1600 Hz. The 125 Hz dip is found in lab tests of walls with the same 406 mm stud spacing, but does not occur where normally incident sound energy is minimal as in these field tests. The high frequency difference may be due to leaks or different edge conditions.

Fig. 5 compares NR values for the end walls of each room. Here the differences between the two rooms are larger. For room B, the aircraft are approaching and the incident sound will be lower than for the other end of the building (room A) where the aircraft are departing. This leads to higher apparent NR values for room B than room A as was expected.

Conclusions

Although it is important to understand the differences between lab and field situations, practical considerations suggest that it is not possible to explicitly include all of the details in conversions from lab to field results.

Acknowledgements
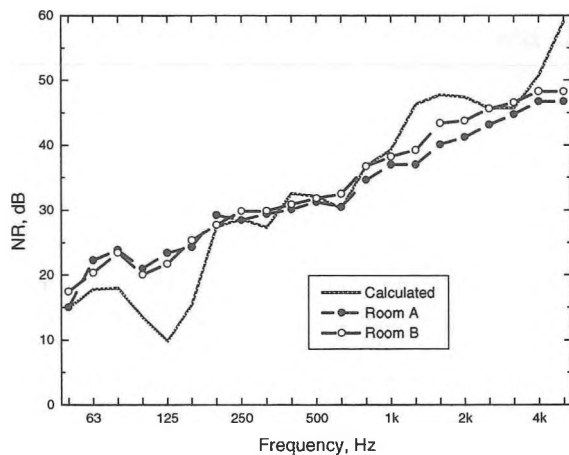
Fig. 4. NR values for walls facing the flight track.
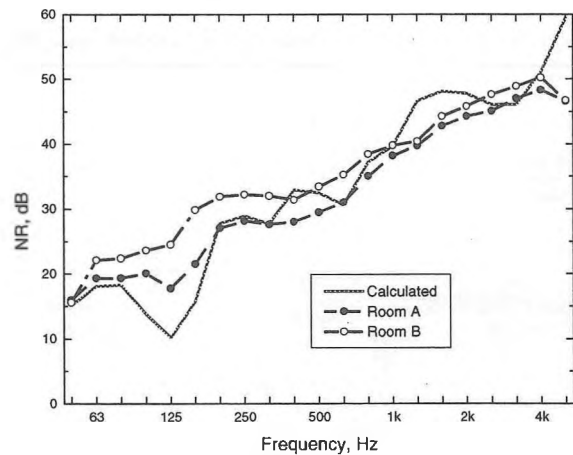
Fig. 5. NR values for walls perpendicular to flight track.

Ibana-Calc: New Software To Calculate The Effect Of Sound Insulation Against Aircraft Noise

J.S. Bradley and J.A. Birta

Institute for Research in Construction, National Research Council, Montreal Rd. Ottawa, K1A 0R6

Introduction

As part of the IBANA project (Insulating Buildings Against Noise from Aircraft), new software has been developed for calculating the effect of sound insulation against aircraft noise. The software is intended to be both more accurate and more convenient than previous approaches that have used look-up tables and single number ratings of sound insulation[1]. The program includes a large database of new sound transmission loss data of building façade components as well as aircraft noise spectra. While the included database is quite extensive, the user can add new data themselves. Users simply select the construction type of each façade element and enter its area. The total sound reduction or the expected indoor sound levels are calculated and displayed graphically. Multiple scenarios can be calculated and compared to evaluate their relative effectiveness either in terms of graphical results or audible simulations. The program is written in Visual Basic and is intended to run on a standard PC type computer.

Calculations

The user first enters the outdoor aircraft noise level either as an NEF or an Leq24 value. NEF values are assumed to be those calculated by Transport Canada's NEF_1.7 noise contour prediction software. The relationship between these NEF and Leq24 values is[2],

$$Leq24 = NEF + 32, dBA$$

The aircraft noise source type is then selected (See Fig. 1). Users can select one of several standard sources or create a mix of several types of aircraft. The overall level of the selected source is adjusted to equal the chosen NEF value. The user also has the option of entering their own source

Fig. 1 Source selector screen.

spectrum for other source types. The selected outdoor sound level and source spectrum are assumed to be the free field outdoor sound levels.

The indoor sound level is calculated for each 1/3 octave band from 50 to 5k Hz as,

$$L_2(i) = L_1(i) - TL(i) + 10 \log[S/A(i)] + 3, dB$$

Here, $L_1(i)$ is the outdoor sound level, $L_2(i)$ is the indoor sound level, $TL(i)$ is the transmission loss measured in the laboratory, $A(i)$ is the sound absorption in the receiving room and S is the area of the particular façade element. Sound absorption is entered as a fraction of the floor area.

Where a particular façade is made up of several components such as a wall section, a window and a door, the total transmission loss is calculated from the area-weighted transmission coefficients of each element.

Fig. 2. Façade element selection screen.

Data Bases

The program includes databases of source spectra and of laboratory transmission loss measurements of façade elements. The program currently includes aircraft noise spectra for: Chapter 2 and Chapter 3 jet aircraft as well as spectra for propeller aircraft and helicopters. It also includes several standard spectra such as previously used in the CMHC Guide[1], the spectrum in the ASTM OITC standard [3] and a new standard aircraft spectrum based on measurements at Ottawa, Vancouver and Toronto airports. These spectra can also be corrected for the effects of air absorption at different distances. The user can also add their own source spectra. Further corrections are being developed to account for the orientation of the façade relative to the flight track of the aircraft.
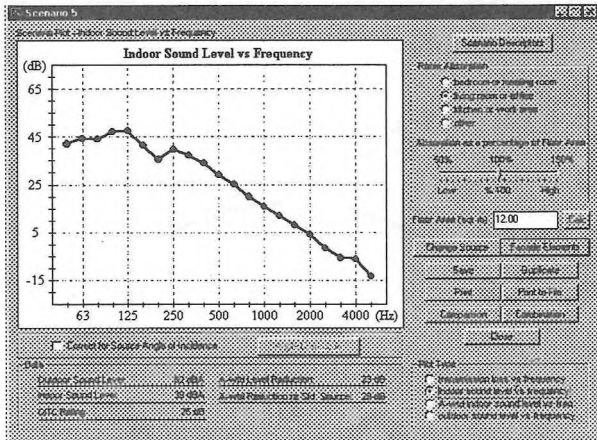
Fig. 3. Scenario results screen.

There is also a database of laboratory transmission loss measurements for various building façade elements. These were mostly obtained in tests for the current project and include 50 exterior walls, 50 roof-ceilings, 40 windows and glazing units and a few doors. Again the user is able to add their own new transmission loss results to the database using the screen shown in Fig. 4.

Scenarios

Each calculation is referred to as a *scenario*. The user can calculate and display multiple scenarios. For example, one could try various combinations of wall and window constructions to determine which combination gives the desired result. For each scenario, either the total transmission loss or the indoor sound levels can be displayed as shown in Fig. 3.

Scenario Comparisons

Multiple scenarios can be compared in terms of either indoor sound levels or sound transmission loss values (see Fig. 5).

Reports

The results of a particular scenario or the comparisons of several scenarios can be printed out as complete reports. The associated results can also be printed to a file for
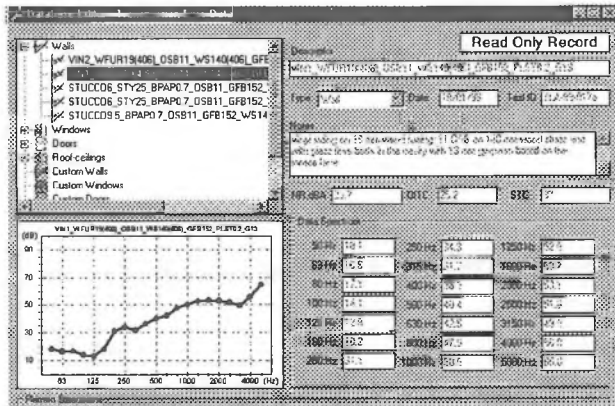
Fig 4. Transmission loss database screen.

importing into a spreadsheet or other software.

Scenario Combinations

The results of several scenarios can be combined. For example, a room at the corner of a building might have exterior walls exposed to quite different incident sound. The sound transmitted through each could first be calculated in separate scenarios and the results combined to give the total indoor sound levels.

Audible Simulations

The program can also produce audible simulations of several scenarios. The sound of an aircraft fly-over is modified according to the calculated sound attenuations of each scenario and played back using a standard sound card. For each audible simulation, up to four scenarios can be compared. Of course, the quality of the playback is improved with an external amplifier and reasonable quality loudspeakers.
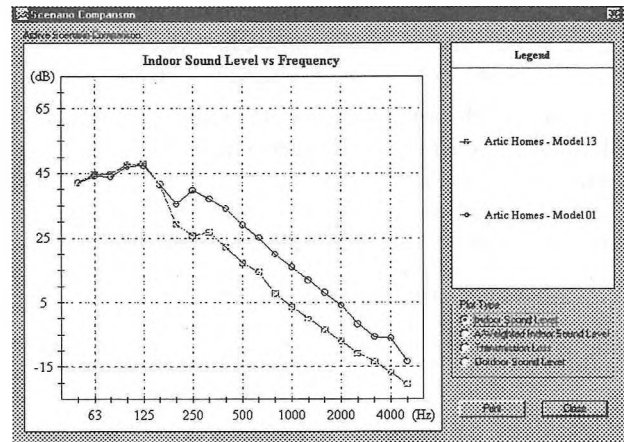
Fig. 5. Scenario comparison screen.

Acknowledgements

References

1. Anon, "New Housing and Airport Noise", Canada Mortgage and Housing (1981).

2. Bradley, J.S., "NEF Validation Study: (3) Final Report", IRC Contract Report A-1505.3, 1996.

3. ASTM 1332, "Standard Classification for Determination of Outdoor-Indoor Transmission Class", Am. Soc. for Testing and Materials, Philadelphia.

PIEZOELECTRIC ACTUATOR OPTIMIZATION FOR SIMULTANEOUS AIRCRAFT CABIN NOISE AND VIBRATION CONTROL

Daniel Tse and Anant Grewal

Institute for Aerospace Research, National Research Council Canada, Ottawa, Ontario, Canada

1. INTRODUCTION

In turboprop aircraft such as the de Havilland Dash 8, the unsteady pressure field generated by the propellers introduces high levels of fuselage vibration and cabin noise. The use of piezoelectric (PZT) elements as control actuators has been demonstrated to be effective in reducing both noise and vibration. The present study aims at exploring a strategy in which the PZT elements are divided into different control groups as a means to simplify the control system while increasing the control authority. The optimal grouping, placement and actuation of the piezoelectric elements constitute a large-scale combinatorial optimization problem that can be solved by applying computational intelligence methodologies such as genetic algorithms (GAs). A genetic algorithm, with a novel coding scheme for the design parameters, was developed[1] to address the optimization of noise and vibration separately and independently. By applying a Pareto cooperative optimization approach, the present work extends that application to consider the simultaneous maximization of both noise and vibration reduction performance.

2. PARETO GA OPTIMIZATION

Both the noise and vibration suppression problems can be cast into the same general form:

$$e_i = G_i u + d_i \quad i = n \text{ (noise)} \text{ or } i = v \text{ (vibration)}$$

The quantities in the above equation are complex-valued: u is the control force vector, d_i the primary forcing vector, G_i the matrix of transfer function coefficients, and e_i is the overall response at the sensors. The elements of d_i and G_i are determined experimentally as discussed in Grewal and Tse.[1] Altogether 6 microphones and 8 accelerometers are used to monitor the noise and vibration response. Their positions, together with those for the 31 pairs of PZT elements used in the experiment, are illustrated in Figures 1 and 2.

Given an actuator configuration, the optimal control force vector $\hat{u}$ is determined by applying a complex least squares procedure to minimize the Hermitian inner product $e_i^H e_i$, where e_i^H denotes the complex conjugate of e_i. A non-dimensional fitness function F_i is then defined for GA operation as follows:

$$F_i = 10 \cdot \log \left[d_i^H d_i / e_i^H e_i \right] \quad i = n \text{ (noise)} \text{ or } i = v \text{ (vibration)}$$

F_i represents the dB reduction due to an actuator set-up.
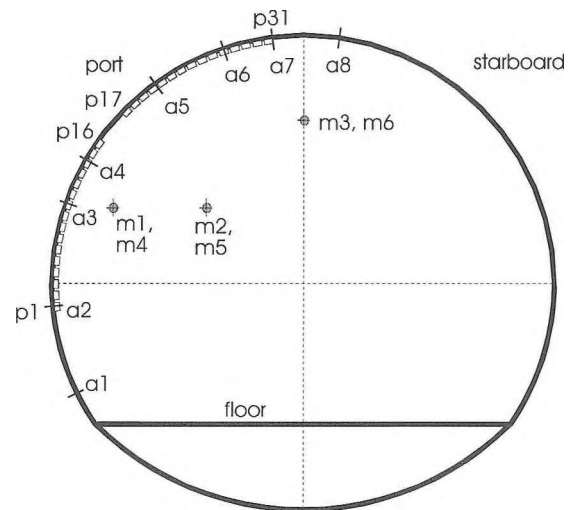
Figure 1: Sectional view of fuselage showing locations of piezoelectric pairs (p1 to p31), accelerometers (a1 to a8) and microphones (m1 to m6).
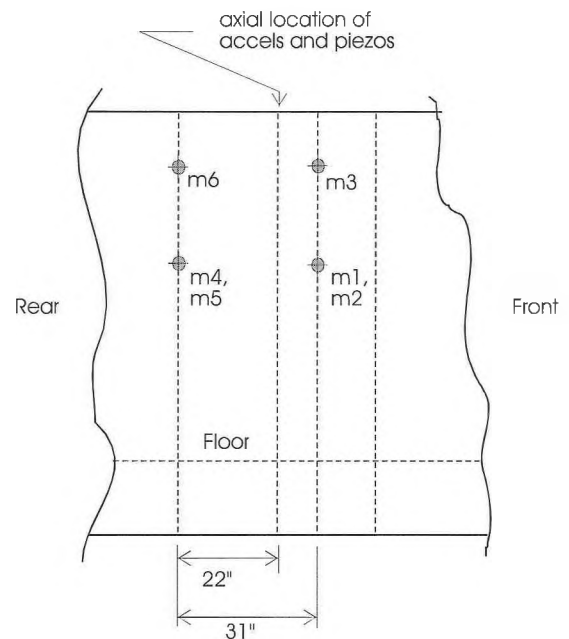
Figure 2: Side view of fuselage showing locations of microphones.

Pareto GA is a technique for the simultaneous optimization of problems with multiple objectives. For the present problem of maximizing the reduction in both noise and vibration, the ordered pair (F_n, F_v) are ranked according to a domina-

tion principle explained in Goldberg.[2] The goal is to generate a Pareto front which is a set of non-dominated solutions. The construction of such a front allows for an evaluation of solutions that represent the best compromises between the objectives.

With a particular actuator configuration, the optimal control force $\hat{u}$ for maximizing the noise reduction will in general be different from that for maximizing the vibration reduction. The simultaneous optimization of the two objectives thus requires a sequential approach. Three possibilities are examined – Method I: optimization is done with respect to the noise objective only with the vibration reduction obtained solely as a direct result of the former. Method II: optimization is done with respect to the vibration objective only with the resulting noise reduction being a direct result of the former. Method III: an alternating procedure is proposed – in one generation of GA operation, $\hat{u}$ is determined by maximizing the noise reduction objective, and in the next generation $\hat{u}$ is determined by maximizing the vibration reduction objective.

3. RESULTS AND DISCUSSIONS

The results to be discussed all use the same GA parameters: 100 population members, 100 generations, probability of crossover = 1.0, and probability of mutation = 0.1. Details of the GA procedure are given in Grewal and Tse.[1]

Figures 3 and 4 show the evolution of Pareto fronts for Methods I and II, respectively. The results of using 1 group of control actuators are contrasted to those of using 4 groups. When more control groups are used, there is a significant improvement in the simultaneous maximization of the noise and vibration reduction. As a consequence of the solution procedures, the Pareto fronts in Figure 3 are biased towards the noise objective while those in Figure 4 are biased towards the vibration objective.

Figure 5 shows the evolution of Pareto fronts for Method III. In contrast to the previous results, the fronts span evenly between the two objectives. While the approaches used in Methods I and II can give better performance for a particular objective, Method III produces more solutions that represent the best compromises in the medium range in either objective.

4. REFERENCES

[1]Grewal, A. and Tse, D., "Optimization of Piezoelectric Actuator Grouping for Aircraft Cabin Noise Control," AIAA Paper 2000-1558.

[2]Goldberg, D.E., *Genetic Algorithms in Search, Optimization, and Machine Learning*, Addison-Wesley, 1989, pp.197-201.
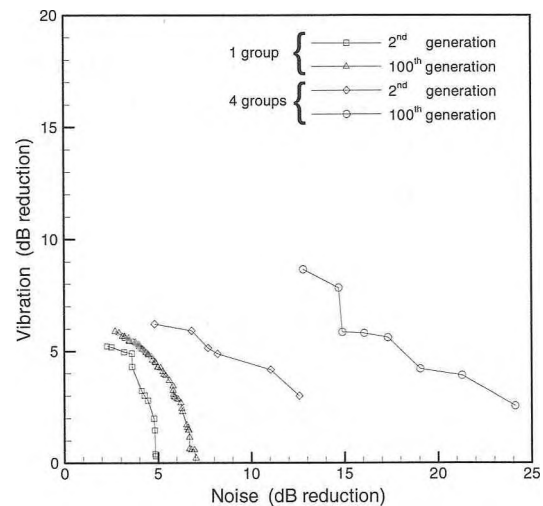
Figure 3: **Pareto fronts obtained by Method I.**
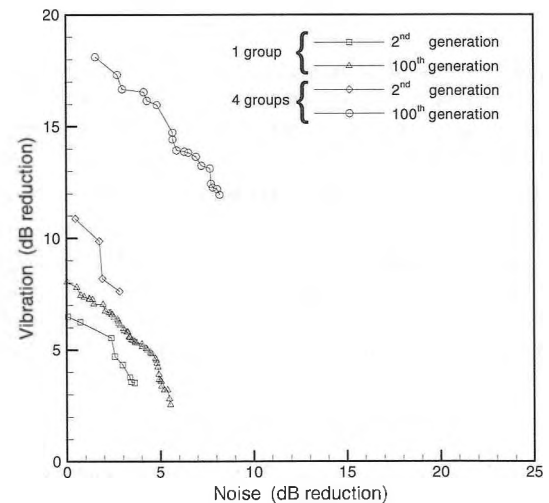
Figure 4: **Pareto fronts obtained by Method II.**
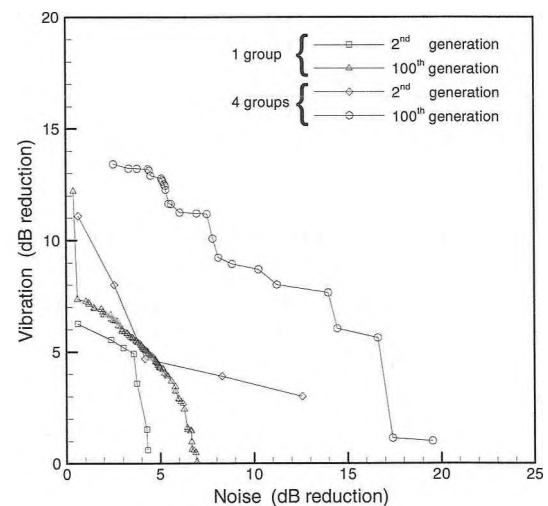
Figure 5: **Pareto fronts obtained by Method III.**

Passenger Cabin Noise Comfort Evolution of the Dash-8Q

D. Couture[1], W.R. Buckley[1], G. Burns[1] and J. Petzke[2]

Acoustics and Vibration Group, Bombardier Aerospace, Downsview, Ontario M3K 1Y5
Engineering and Product Development, Bombardier Aerospace, Downsview, Ontario M3K 1Y5

1.0 INTRODUCTION

The Dash-8 Q Series are considered today the quietest turbo-prop aircraft in their category. This success is mainly attributed to the increased passenger comfort, provided by the reduction of the low frequency noise and vibration tones generated in the passenger cabin by the propellers.

This achievement is the result of more than a decade of development work on this field by Bombardier Aerospace deHavilland with specialised partners and consulting experts.

The purpose of this paper is to present the different development activities, including the design and implementation of the Active Noise and Vibration Suppression™ (ANVS) system with ULTRA Electronics N&V System division, which is being installed today on all new Dash-8 models, Q100/Q200/Q300 and Q400.

In parallel, a series of improvements introduced in the interior design of the aircraft has contributed to the enhancement of the passenger cabin noise and vibration environment. A brief overview of those changes is also presented in the paper.

2.0 NOISE AND VIBRATION SOURCES IN THE CABIN

The major sources of noise and vibration in the passenger cabin of the cabin are listed below. It is important to note that while some of those sources do not contribute directly to the overall cabin noise and vibration levels, they can be significantly annoying to passengers, and need to be addressed in the design of the cabin environment.

a. Boundary layer noise.
b. Systems noise from the air distribution system, the cooling fans, the hydraulic pumps, and the galley and lavatory drains.
c. Propeller induced tones: which arise at the blade pass frequency (RPM x No. of blades), and its harmonics.
d. Propeller imbalance, which generates vibration at the propeller rotating frequency.
e. Buzz and rattles, and interior component resonance.
f. Propeller modulation noise and vibration caused by a slight difference in RPM between the two propellers.

In order to provide a "jet-like" quiet environment in a turbo-prop aircraft, sources "c", "d", "e" and "f" needed to be addressed specifically. Baseline surveys on the aircraft showed that the propeller induced tones were required to be reduced significantly to increase comfort.

3.0 PASSIVE TUNED VIBRATION ABSORBERS (TVAS)

The first step in cabin comfort improvement was launched in the early 90's, with the introduction of Passive TVAs of the production Dash-8 Series 100 and 300. An exhaustive test program, utilising a Series 300, was conducted with Anatrol Corp. to design the units and to determine their locations.

The in-flight measurements of the operating deflection shapes at the blade pass frequency (BPF) and harmonics were used to define the optimum positioning of the Passive TVAs.

The program lead to the definition of production kits that were to be installed on five frames of the fuselage in the propeller plane

area. Two sets of TVAs were required, one to attenuate the BPF and the other to attenuate its first harmonic, 2BPF. Figure 1.0 shows the in-flight operating deflection shape of the frames at the BPF with and without the Passive TVAs.

The advantages of such a system was a reduction of 4 dB(A) in the SPL at the worst seat, and a cabin average noise reduction of around 2 dB(A) in cruise condition. However, the residual propeller tones were still dominant in some area of the cabin, and the Passive TVAs were efficient only at the cruise RPM condition of 910 RPM, there was no real benefit at the take-off and climb RPMs of 1200 and 1050 RPM respectively.

4.0 ACTIVE NOISE CANCELLATION (ANC) SYSTEM

In parallel, the use of speaker based ANC system was considered by the company. In 1992, a technology demonstrator program was conducted on a Dash-8 Series 100. The trial system provided by Noise Cancellation Technologies consisted of one controller, 48 microphones and 23 speakers temporarily installed inside the passenger cabin.

The net advantages of such a system were its ability to reduce the BPF and its first 3 harmonics, and its capacity to operate at the different propeller RPMs. An overall noise reduction up to 6 dB(A) at the worst seat was measured in-flight, while the cabin average noise level was reduced by up to 5 dB(A) in the loudest cruise RPM condition. However, such a system provided no reduction in cabin vibration.

The main problem associated with the implementation of an ANC system on production aircraft is the installation of the speakers and their enclosures. These units interfere directly with the interior trim panels, the aircraft structure and system components. As a result, a number of favourable speaker locations for noise reduction could be eliminated, thus reducing the system performance.
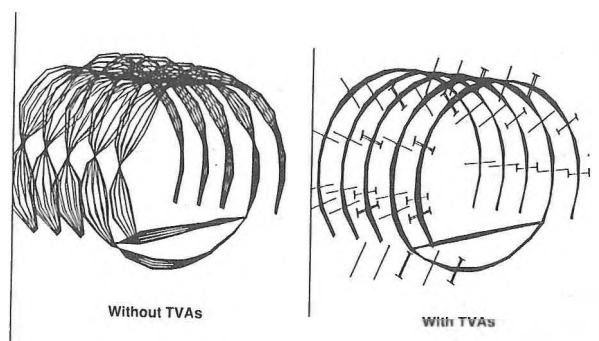

Without TVAs   With TVAs

Fig 1. Operation deflection shape at the BPF with and without passive TVAs.

5. ACTIVE NOISE AND VIBRATION SUPPRESSION (ANVS) SYSTEM

The advantages of both the Passive TVAs and the speaker based ANC system needed to be combined in order to achieve major noise

and vibration reductions in the cabin. Between 1994 and 1996, an intense development program was jointly conducted by Bombardier Aerospace and Ultra Electronics N&V System division.

The actuators designed for this system are Active Tuned Vibration Absorbers (ATVAs), which are installed with their power amplifier directly on the fuselage frames to control the vibration field of the fuselage.

In addition to the ATVAs, the system includes a central controller and a large set of microphones which are mounted behind the interior trim panels, leaving only a tiny hole seen from the inside for the cabin noise to be measured. The system on the Q400 Series also includes accelerometers as sensors to increase vibration reduction performance.

The system also utilises inputs from aircraft systems, such as tachometer signals to track the frequency, and the cabin differential pressure to account for the dynamic structural change of the fuselage with pressurisation.

The definition of the location of the sensors and actuators, and the system implementation were completed through specific development phases:

Identification of all possible sensor and actuator locations: this stage required drawing reviews and aircraft surveys.
Transfer Functions (FRF) measurements for all possible sensor and actuator locations with externally mounted ATVA on a furnished aircraft.
In-flight baseline cabin noise and vibration measurements at the various conditions throughout the whole cabin.
System layout definition: performance predictions and optimisation calculations.
Component design for light weight, high reliability, and stringent certification requirements.
Trial installation and system optimisation test flights.
System calibration and functional test procedures before entry into service.

6.0 RESULTS

The net result is a significant reduction of both noise and vibration in the passenger cabin. Both the BPF and the harmonics are reduced significantly throughout the cabin, for any of the operating propeller RPMs of the aircraft.

Figure 2.0 shows a typical noise spectra in the propeller plane area with the ANVS system both ON and OFF. On some seats, the combined induced tones are reduced by more than 12 dB(A). On cruise condition, the loudest seat is reduced by over 8 dB(A) in SPL, and the cabin average is improved by a reduction up to 5 dB(A) in SPL, which provides a cabin noise level equal or below the level of some commercial jets of same capacity.

The first production version of the ANVS system was incorporated on a production Dash-8 in 1996. Since then, the ANVS system is an integral part of the production aircraft built for all models, and over 125 Dash-8 aircraft have been delivered to date with the system installed.

7.0 INTERIOR DESIGN FEATURES

A series of additional improvement in the interior design was also introduced to enhance cabin comfort. Right at the design stage of the interior, specific guidelines were followed and passive treatment solutions were implemented, these includes :

The soft mounting of the trim panels and bins.
The sealing of joints and gaps between trim panels and bins.
The optimisation of the insulation package for noise absorption and maintainability.
The avoidance of the natural frequencies for interior components (panels, meal trays, seats, light lens, etc.) at the BPF and propeller shaft RPM.
The elimination of buzz and rattles.

8.0 SYNCHROPHASER AND PROPELLER BALANCING

Two other valuable systems are integrated in the aircraft for passenger comfort, the synchophaser and the propeller balance monitoring system.

The purpose of the synchrophaser is to maintain the two propellers at the exact same speed and with a constant relative angle between them. The main benefit of such a system is the elimination of the propeller modulation or beating noise. The programmable angle capability of the unit also allows to select the optimum angle to reduce the combined noise and vibration contribution of each propeller in the cabin.

The propeller balance monitoring system installed on the aircraft allows the continuous monitoring of the propeller balance condition. After a flight, the operator can read the balance status, calculate and install the required single plane mass balance solution to avoid any imbalance vibration. In case of imbalance, low frequency vibration at the propeller shaft RPM could be an annoyance to passengers due to the shaking of the seats, floors or interior components.

9.0 CONCLUSION

The Dash-8Q aircraft has achieved a new level in turbo-prop cabin comfort. The introduction of its ANVS system and additional features are providing comfortable cabin environment to both passengers and crew. The experimental approach and advance developments were the keys to this success. Through continuing test programs, new findings have also been made, which could lead to further advancements in cabin comfort in the near future of the Dash-8Q aircraft.
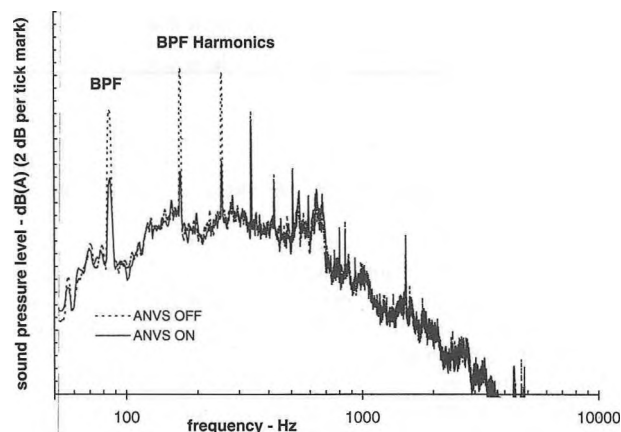
Fig 2. Typical Dash-8 noise spectra in the passenger cabin, propeller plane area.

A Index To Predict The Stability Of Decentralized Adaptive Feedback Active Noise Control System

Estelle Leboucher, Philippe Micheau and Alain Berry

GAUS, Mechanical Engineering Department, Université de Sherbrooke, Sherbrooke, J1K 2R1, Québec, Canada

1. Introduction

A large number of industrials applications like transformers or rotating machinery are concerned by radiation of unwanted periodic noise. Typically, centralized techniques are used to achieve the control of these systems. Nevertheless, the implementation of such a control requires a considerable processing power, rapidly growing with the number of actuators. One way to avoid this problem is to use a number of independently operating control systems in which, a subset of controllers drives a smaller number of secondary sources. However, such a control strategy does not take into account the different interactions between the actuators and error sensors, which possibly lead to instability and the degradation of the overall system performances.

This paper presents a decentralized adaptive feedback controller developed for the control of periodic disturbances. The study of the stability of the feedback loop and the the stability of the control is effectuated in the frequency domain. Simulations of the control are also presented to verify the accuracy of this analysis.

2. Description of the control system

In most of the practical applications, the only information available to implement a control is the knowledge of the physical plant of the system to be controlled h. In this case, the controller implemented for the control must have a feedback structure. Moreover, when the size of the system to be controlled is large, it is useful to achieve a decentralized control strategy, wich consists to employ independant operating controller. The equivalent controller of the system C (shown in figure 1) is thus a diagonal controller wich doesn't take into account all the interactions between the control units. If these interactions are too important to be neglected, the feedback loop will be unstable.
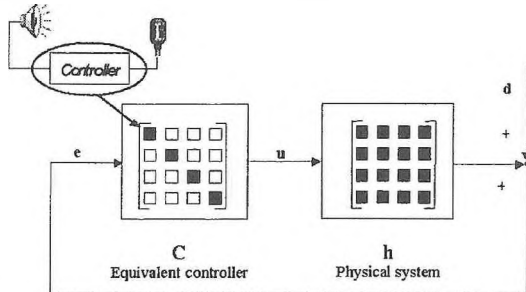
Figure 1: Representation of the decentralized control system.

The decentralized controller consider in this work is composed of M independant control unit. Each control unit, constituted of a loudspeaker and a error microphone, is a feedback loop with an internal model control architecture [1]. A filtered x-LMS algorithm is used to adapt the command signal of the loudspeaker to minimize the sound pressure at the microphone as represented in figure 2.

The LMS gradient descent algorithm implemented for the adaptation of each unit is defined in the frequency domain for the lth unit as:

$$\Gamma_l(k+1,\omega_0) = \Gamma_l(k,\omega_0) - 2\frac{\mu}{\left|\hat{d}_l(k,\omega_0)\right|^2} \hat{h}_{ll}^*(\omega_0)\, \hat{d}_l^*(k,\omega_0)\, e_l(k,\omega_0) \quad (1)$$

where ω_0 is the frequency of the primary disturbance, * denotes the complex conjugate and μ is step size parameter.
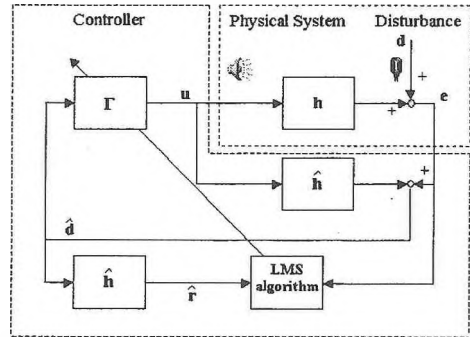
Figure 2: Bloc diagram of each control unit.

The study of the adaptation process realized in [2] has shown that, during the adaptation, each control filter converges in a quasi-straight line from its initial value (fixed to zero), to its steady state value $\Gamma_l^{opt}(\omega_0)$. This steady state value, which ensures an error signal equals to zero at the microphone is defined as:

$$\Gamma_l^{opt}(\omega_0) = \frac{-1}{\hat{h}_{ll}(\omega_0)} \quad (2)$$

Furthermore, the position of each control filter on its convergence path at any iteration k can be associated to a parameter β_k given by:

$$\beta_k = \frac{\Gamma_l(k,\omega_0)}{\Gamma_l^{opt}(\omega_0)} = 1 - e^{-2k\mu\left|\hat{h}_{ll}(\omega_0)\right|^2} \quad (3)$$

As the control performance depends on the value of the control filter, this parameter β_k is called performance index [2]. Indeed, the closer the control filter is of its steady state value, the better the attenuation measured at the microphone will be. If $k=0$ then $\beta_k = 0$, the control filter stays on its initial value and no control of the disturbance is accomplished. In the same way, if $k\to\infty$ then $\beta_\infty = 1$, the control filter has reached its optimal value and a perfect rejection of the perturbation is obtained with a large attenuation measured at the error microphone.

3. Stability of the feedback loop

The stability of the feedback loop of the decentralized control system presented in this section is realized by assuming the adaptation process "frozen" at an iteration k. The correponding values of the control filters at this iteration, are associated to a mean value of the index performance β calculated from equation 3. According to the classical Nyquist criterion, the closed loop system will be stable if and only if, the map of $L(s,\beta) = det\,(I + L_H(s)\,\overline{\mathbf{H}}\,(s,\beta))$ evaluated on the standard Nyquist D-contour doesn't encircle the origin point [2]:

$$N(0, L(s,\beta)) = 0 \quad (4)$$

With:

$$\overline{H}(s,\beta) = -\hat{h}(s)\ C(s,\beta)\ \left[I - \hat{h}(s)\ C(s,\beta)\ \right]^{-1} \qquad (5)$$

$$L_H(s) = [\ h(s) - \hat{h}(s)\ ]\ \hat{h}^{-1}(s) \qquad (6)$$

$$C(s,\beta) = [I + \Gamma(\beta)\ \hat{h}(s)]^{-1}\ \Gamma(\beta) \qquad (7)$$

$$\Gamma(\beta) = diag\left\{\frac{-\beta}{\hat{h}_{ll}(\omega_0)}\right\} \qquad (8)$$

3. Simulations of the control

Different results obtained from the simulation of the control in the time domain for a system composed of 7 coplanar control units at frequency 240 Hz are now presented. The geometrical configuration of the control units used for these simulations is illustrated in figure 3. The physical plant h, was obtained from the experimental values of the 128-order FIR filters that modelled the transfer function between each loudspeaker and each microphone.

Figure 3: Configuration of the control simulation.

During these simulations, the adaptation process is frozen at different iterations k. The corresponding values of the control filters Γ (modelled by 32-order FIR filter) are then used to calculate the mean values of the performance index β and $L(s,\beta)$.

Figure 4 shows the evolution of the map $L(s,\beta)$ obtained for these different values of the index performance. According to this figure, the stability of the system is affected by the values of β with a decrease of its stability margin when β increases. The control system is find to be stable while the map of $L(s,\beta)$ doesn't encircle the origin which correspond to values of $\beta \leq 0.30$. For $\beta=0.35$, the map of $L(s,\beta)$ encircles the origin and the control system is unstable in regard of the Nyquist criterion.

Figure 4: Map of L (s, β) on the Nyquist D-contour obtained for different values of β.

Figure 5: Sum of the temporal squared error signals measured at the
microphones for different values of the index performance β.

The sum of the squared error signals at the microphones for the same values of β are represented in figure 5. As observed on this figure, if $\beta \leq 0.30$, the control filters progress on their convergence path while the adaptation process is actuated. The error signal at the microphones decreases for increasing values of β. When the adaptation is frozen, the control filters stop their convergence on a specific value and the error signal at the microphone cease its decrease. For $\beta=0.35$, a decrease of the error signal is also noticed at the begining of the adaptation until a large increase of the error signal is observed. This one corresponds to the instability of the control system expected by the Nyquist criterion. This can be explain by the fact that during the adaptation, the control filters reached some values which cause the instability of the feedback loop.

4. Conclusions

This paper presents a decentralized adaptive feedback control system of periodic noise. A condition, derived from the Nyquist criterion, is given in order to predict the stability of the control. It has be shown, that the positions of the control filters on their convergence path play an important role on the stability and the performance of the control system. The control of the parameter β, called performance index wich was associated to these positions, appears thus a good alternative to make a compromise between performance and stability. The manner to control β presented in this paper, was to stop the adaptation of the control filters on the desired values. However, this technique is difficult to implement in practical cases. Others procedures of control of this parameter could be developped and implemented like introducing a leaky coefficient in the LMS algorithm, or reinjecting a proportional part of the estimate signal of the pertubation in the calcul of this same estimate signal of the perturbation realized by the internal model.

References

[1] B. Raphaely, S. J. Elliott, T. J. Sutton and M. Johnson, "Design of feedback controllers using a feedforward approach", Proceeding of Active 95, pp. 863-874, 1995.

[2] E. Leboucher, P. Micheau, A. Berry and A. L'Espérance, "A decentralised adaptive feedback active noise control system of periodic sound in free space", Proceeding of Active 99, pp. 973-984, 1999.

COMPARISON OF WAVE SENSING STRAGEGIES FOR ACTIVE STRUCTURAL ACOUSTIC CONTROL

P. Audrain, P. Masson and A. Berry
G.A.U.S., Université de Sherbrooke, Sherbrooke, Québec, J1K2R1, Canada

1 Introduction

Among the strategies available for the active control of energy transmission from one area of a structure to another area, the control of travelling waves, structural intensity or power flow can all be considered. The previous intensity or power flow control strategies usually assumed far field propagation and are based on an estimate of the exact structural energy flow [1, 2].

It is thererefore the purpose of this paper to present a strategy using strain sensing for the control of structural intensity associated with flexural motion in a coupled beam/plate mechanical system and compare it with a strategy based on the control of the acceleration at one point on the structure. The instantaneous intensity is completely taken into account in the control algorithm, *i.e.* all the terms are considered in the real-time control process and, in particular, the evanescent waves are considered in this approach. Previous work has shown the validity of this energy-based approach using acceleration sensing [3]. The approach is limited to cases where the geometry is such that the intensity at the error sensor will have the same sign for the control source and the primary disturbance.

2 Structural intensity measurement using strain sensing

2.1 Flexural structural intensity in a beam

The structural intensity is the instantaneous rate of vibrational energy transfer, or energy flow, per unit area in a given direction. The instantaneous energy flow in a beam, called the instantaneous structural intensity (subscript $_i$) in this paper, originating from a flexural displacement $w(x, t)$, can be expressed for an Euler-Bernoulli isotropic beam:

$$\vec{I}_i^f = \left(EI \frac{\partial^3 w}{\partial x^3} \right) \left(\frac{\partial w}{\partial t} \right) \vec{i} - \left(EI \frac{\partial^2 w}{\partial x^2} \right) \left(\frac{\partial^2 w}{\partial t \partial x} \right) \vec{i} \tag{1}$$

where E is the Young's modulus, I the area moment of inertia of the beam and $\vec{i}$ the unit vector in the x direction. The control algorithm will minimize the time average of the instantaneous intensity, called the active intensity.

2.2 Finite differences implementation

Since four discrete strain sensors are used to estimate the structural intensity, it is necessary to develop a

Figure 1: Experimental setup.

finite differences approximation based on strain sensing to measure structural intensity associated with flexural motion in beams. The flexural strain ε_z is related to the flexural displacement by $\varepsilon_z(x, t) = \dfrac{\partial^2 w(x, t)}{\partial x^2}$. The instantaneous intensity is evaluated at the center of the probe, x_e, with an error on the order of Δ, Δ being the spacing between two consecutive sensors. The time differentials of strain in equation (1) are estimated using a backward finite difference scheme with error on the order of τ^2, where τ is the time increment between samples.

3 Experimental validation

3.1 Experimental setup

The Fig. 1 shows the experimental setup used for the control. The structure is a plate ($0.48m \times 0.42m \times 0.003m$) connected to a beam ($3m \times 0.0254m \times 0.003m$) made of aluminium covered on one side by a *ISD 830* viscoelastic material combined with a constraining aluminium foil. The viscoelastic material is used to increase the structural damping such that the intensity signal can be measured.

The disturbance is generated by a *Bruel & Kjaer 4810* shaker connected to the beam by a stinger at one end of the beam. The control actuator consists of a PZT patch actuator (*PSI-5A-S2*). The coordinates of the edges of the patch are $0.2m$ and $0.27m$ from the shaker taken as the origin of coordinates. The coordinates of the four PVDF strain sensors are $x_1 = 0.22m$, $x_2 = 0.26m$, $x_3 = 0.3m$ and $x_4 = 0.34m$. The accelerometer used for acceleration control is located in the middle of the PVDF sensors array at $x_e = 26.5cm$. Two accelerometers located at $2.09m$ and $2.19m$ are used for monitoring the control and the mean RMS value of these signals is used as a performance indicator.

$$\overline{H}(s,\beta) = -\hat{h}(s) \ C(s,\beta) \ \left[I - \hat{h}(s) \ C(s,\beta) \right]^{-1} \qquad (5)$$

$$L_H(s) = [\ h(s) - \hat{h}(s) \ ] \ \hat{h}^{-1}(s) \qquad (6)$$

$$C(s,\beta) = [I + \Gamma(\beta) \ \hat{h}(s)]^{-1} \Gamma(\beta) \qquad (7)$$

$$\Gamma(\beta) = diag \left\{ \frac{-\beta}{\hat{h}_{ll}(\omega_0)} \right\} \qquad (8)$$

3. Simulations of the control

Different results obtained from the simulation of the control in the time domain for a system composed of 7 coplanar control units at frequency 240 Hz are now presented. The geometrical configuration of the control units used for these simulations is illustrated in figure 3. The physical plant h, was obtained from the experimental values of the 128-order FIR filters that modelled the transfer function between each loudspeaker and each microphone.

Figure 3: Configuration of the control simulation.

During these simulations, the adaptation process is frozen at different iterations k. The corresponding values of the control filters Γ (modelled by 32-order FIR filter) are then used to calculate the mean values of the performance index β and $L(s,\beta)$.

Figure 4 shows the evolution of the map $L(s,\beta)$ obtained for these different values of the index performance. According to this figure, the stability of the system is affected by the values of β with a decrease of its stability margin when β increases. The control system is find to be stable while the map of $L(s,\beta)$ doesn't encircle the origin which correspond to values of $\beta \leq 0.30$. For $\beta=0.35$, the map of $L(s,\beta)$ encircles the origin and the control system is unstable in regard of the Nyquist criterion.

Figure 4: Map of L (s, β) on the Nyquist D-contour obtained for different values of β.

Figure 5: Sum of the temporal squared error signals measured at the
microphones for different values of the index performance β.

The sum of the squared error signals at the microphones for the same values of β are represented in figure 5. As observed on this figure, if $\beta \leq 0.30$, the control filters progress on their convergence path while the adaptation process is actuated. The error signal at the microphones decreases for increasing values of β. When the adaptation is frozen, the control filters stop their convergence on a specific value and the error signal at the microphone cease its decrease. For $\beta=0.35$, a decrease of the error signal is also noticed at the begining of the adaptation until a large increase of the error signal is observed. This one corresponds to the instability of the control system expected by the Nyquist criterion. This can be explain by the fact that during the adaptation, the control filters reached some values which cause the instability of the feedback loop.

4. Conclusions

This paper presents a decentralized adaptive feedback control system of periodic noise. A condition, derived from the Nyquist criterion, is given in order to predict the stability of the control. It has be shown, that the positions of the control filters on their convergence path play an important role on the stability and the performance of the control system. The control of the parameter β, called performance index wich was associated to these positions, appears thus a good alternative to make a compromise between performance and stability. The manner to control β presented in this paper, was to stop the adaptation of the control filters on the desired values. However, this technique is difficult to implement in practical cases. Others procedures of control of this parameter could be developped and implemented like introducing a leaky coefficient in the LMS algorithm, or reinjecting a proportional part of the estimate signal of the pertubation in the calcul of this same estimate signal of the perturbation realized by the internal model.

References

[1] B. Raphaely, S. J. Elliott, T. J. Sutton and M. Johnson, "Design of feedback controllers using a feedforward approach", Proceeding of Active 95, pp. 863-874, 1995.

[2] E. Leboucher, P. Micheau, A. Berry and A. L'Espérance, "A decentralised adaptive feedback active noise control system of periodic sound in free space", Proceeding of Active 99, pp. 973-984, 1999.

Comparison of Wave Sensing Strategies for Active Structural Acoustic Control

P. Audrain, P. Masson and A. Berry

G.A.U.S., Université de Sherbrooke, Sherbrooke, Québec, J1K2R1, Canada

1 Introduction

Among the strategies available for the active control of energy transmission from one area of a structure to another area, the control of travelling waves, structural intensity or power flow can all be considered. The previous intensity or power flow control strategies usually assumed far field propagation and are based on an estimate of the exact structural energy flow [1, 2].

It is thererefore the purpose of this paper to present a strategy using strain sensing for the control of structural intensity associated with flexural motion in a coupled beam/plate mechanical system and compare it with a strategy based on the control of the acceleration at one point on the structure. The instantaneous intensity is completely taken into account in the control algorithm, *i.e.* all the terms are considered in the real-time control process and, in particular, the evanescent waves are considered in this approach. Previous work has shown the validity of this energy-based approach using acceleration sensing [3]. The approach is limited to cases where the geometry is such that the intensity at the error sensor will have the same sign for the control source and the primary disturbance.

2 Structural intensity measurement using strain sensing

2.1 Flexural structural intensity in a beam

The structural intensity is the instantaneous rate of vibrational energy transfer, or energy flow, per unit area in a given direction. The instantaneous energy flow in a beam, called the instantaneous structural intensity (subscript i) in this paper, originating from a flexural displacement $w(x,t)$, can be expressed for an Euler-Bernoulli isotropic beam:

$$\vec{I}_i^f = \left(EI \frac{\partial^3 w}{\partial x^3} \right) \left(\frac{\partial w}{\partial t} \right) \vec{i} - \left(EI \frac{\partial^2 w}{\partial x^2} \right) \left(\frac{\partial^2 w}{\partial t \partial x} \right) \vec{i} \tag{1}$$

where E is the Young's modulus, I the area moment of inertia of the beam and $\vec{i}$ the unit vector in the x direction. The control algorithm will minimize the time average of the instantaneous intensity, called the active intensity.

2.2 Finite differences implementation

Since four discrete strain sensors are used to estimate the structural intensity, it is necessary to develop a

Figure 1: Experimental setup.

finite differences approximation based on strain sensing to measure structural intensity associated with flexural motion in beams. The flexural strain ε_z is related to the flexural displacement by $\varepsilon_z(x,t) = \dfrac{\partial^2 w(x,t)}{\partial x^2}$. The instantaneous intensity is evaluated at the center of the probe, x_e, with an error on the order of Δ, Δ being the spacing between two consecutive sensors. The time differentials of strain in equation (1) are estimated using a backward finite difference scheme with error on the order of τ^2, where τ is the time increment between samples.

3 Experimental validation

3.1 Experimental setup

The Fig. 1 shows the experimental setup used for the control. The structure is a plate ($0.48m \times 0.42m \times 0.003m$) connected to a beam ($3m \times 0.0254m \times 0.003m$) made of aluminium covered on one side by a *ISD 830* viscoelastic material combined with a constraining aluminium foil. The viscoelastic material is used to increase the structural damping such that the intensity signal can be measured.

The disturbance is generated by a *Bruel & Kjaer 4810* shaker connected to the beam by a stinger at one end of the beam. The control actuator consists of a PZT patch actuator (*PSI-5A-S2*). The coordinates of the edges of the patch are $0.2m$ and $0.27m$ from the shaker taken as the origin of coordinates. The coordinates of the four PVDF strain sensors are $x_1 = 0.22m$, $x_2 = 0.26m$, $x_3 = 0.3m$ and $x_4 = 0.34m$. The accelerometer used for acceleration control is located in the middle of the PVDF sensors array at $x_e = 26.5cm$. Two accelerometers located at $2.09m$ and $2.19m$ are used for monitoring the control and the mean RMS value of these signals is used as a performance indicator.

The control of instantaneous intensity and of acceleration were experimentally performed using a feedforward filtered-X least mean square algorithm (FX-LMS) [2] adapted to this energy-based cost function. The output control signal $\mathbf{Y}(m)$ at the actuators is obtained by filtering the reference signal $\mathbf{X}(m)$ by the control filter $\mathbf{W}^T(m)$ which is updated using $\mathbf{W}(m+1) = \mathbf{W}(m) - \mu_0 \nabla_W I_i(m)$ where μ_o is a parameter taken to ensure convergence and $\nabla_{\mathbf{W}} I_i(m)$ is the gradient of the error surface with respect to the coefficients of the control filter given by $\nabla_{W_f} I_i = [\mathbf{R}_1 e_2 + \mathbf{R}_2 e_1 - \mathbf{R}_3 e_4 - \mathbf{R}_4 e_3]$ where the four error functions e_i corresponding to the four physical quantities involved in the instantaneous intensity (Eq. (1)) can be defined as:

$$e_1(m) = \frac{\partial \varepsilon_{zp}}{\partial x}(m) + \mathbf{W}^T(m)\mathbf{R}_1(m) \tag{2}$$

$$e_2(m) = \frac{1}{k^4}\frac{\partial^3 \varepsilon_{zp}}{\partial t \partial x^2}(m) + \mathbf{W}^T(m)\mathbf{R}_2(m) \tag{3}$$

$$e_3(m) = \varepsilon_{zp} + \mathbf{W}^T(m)\mathbf{R}_3(m) \tag{4}$$

$$e_4(m) = \frac{1}{k^4}\frac{\partial^3 \varepsilon_{zp}}{\partial t \partial x^3}(m) + \mathbf{W}^T(m)\mathbf{R}_4(m) \tag{5}$$

where $\mathbf{R}_i$ are the corresponding filtered reference signals and where the flexural wavenumber is $k = \left(\frac{\rho S}{EI}\omega^2\right)^{1/4}$, where ρ is the density, S is the section of the beam and ω is the angular frequency.

The algorithm was implemented on a *dSPACE* prototyping environment, equipped with three *DEC Alpha* processors. The reference input signal was taken as the signal from the generator that drives the disturbance shaker. The sampling rate was set at $3kHz$ in the experiments. A piezoelectric patch is used to inject the control signal in the structure, in the form of two moments along its two edges.

3.2 Experimental control results

The Fig. 2 presents some typical control results obtained using two different approaches. The mean RMS value measured at the two monitoring accelerometers is presented in this figure, using two different strategies. The first strategy aims at minimizing the acceleration level at the point x_e. The second strategy aims at minimizing the structural intensity with the sensor centered at x_e. These preliminary results indicate that the intensity suffers from convergence problems, indicated by points superimposed with the without control curve, while the acceleration control algorithm converges over the entire frequency band. Apart from these convergence problems, the control of intensity tends to perform adequately on the resonances below 350 Hz while intensity and acceleration control behave almost the same above this frequency. The location of the actuator explains the lost in the performance of both algorithms
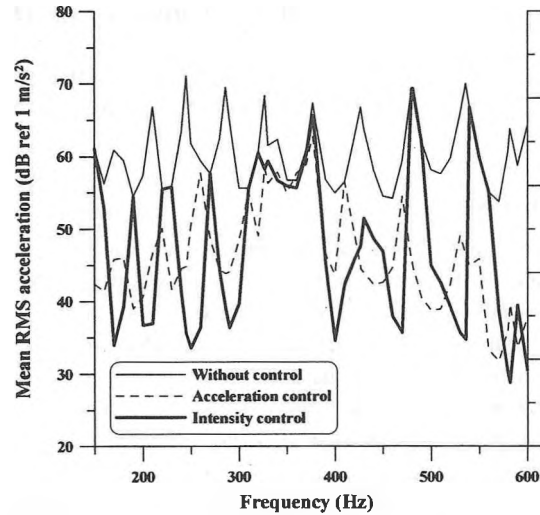
Figure 2: Two structural active control strategies.

around 350 Hz. Three reasons could explain the problems noticed with intensity algorithm: 1) the PVDF sensors signals were not filtered, which could lead to spurious energy in the frequency band of interest, 2) the extensional waves were not considered in the intensity algorithm, it is suspected that a coupling between the two types of waves leads to poor performance of the control algorithm and 3) low and high frequency limitations arise due to the limited accuracy of the measurement including the finite difference scheme.

4 Conclusions

The control of flexural intensity in complex structure originating from point force and using a piezoelectric patch actuator has been experimentally validated by comparison with a classical acceleration control. High attenuation of the mean RMS acceleration downstream of the error sensor location can be achieved when controlling harmonic disturbance with a piezoelectric patch. Some problems have been identified with the intensity control algorithm and reasons have been proposed to tentatively explain these problems. Work is in progress to alleviate these limitations.

References

[1] C.R. Fuller and G.P. Gibbs. Simultaneous active control of flexural and extensional waves in beams. *J. Intell. Mat. Syst. Struct.*, 1:235–247, April 1990.

[2] A.E. Schwenk, S.D. Sommerfeldt, and S.I. Hayek. Adaptive control of structural intensity associated with bending waves in a beam. *J. Acoust. Soc. Am.*, 96(5):2826–35, November 1994.

[3] P. Audrain, P. Masson, and A. Berry. Theoretical and experimental investigation of structural intensity control in a finite beam. *J. Acoust. Soc. Am.*, accepted, 2000.

Finite Element Modeling of Damping Using Piezoelectric Materials

A.-C. Hladky-Hennion and C. Granger

IEMN (UMR 8520 CNRS), département ISEN, 41 Boulevard Vauban, 59046 Lille Cedex, France

1.0 INTRODUCTION

Damping of mechanical vibrations has attracted a great deal of interest because it can reduce noise and peak vibration amplitudes in systems. Piezoelectric materials possess properties which make them useful as dampers or control elements for structures. Piezoelectric materials have the following properties : they strain when an electrical field is applied accross and they produce a voltage under strain. In general, piezoelectric materials have the ability to transform mechanical energy into electrical energy and reciprocally. Hagood *et al* [1] have presented a passive damping mechanism for structural systems in which piezoelectric materials bonded to the structures are used. They present the possibility of dissipating mechanical energy with piezoelectric materials shunted with passive electrical circuits. More recently, Law *et al* [2] have studied the damping behavior of a piezoelectric material, shunted by a resistance, described by a mechanical energy conversion and dissipation by the material, instead of a change in stiffness.

The use of the finite element method to tackle these problems can strongly broaden the designer's possibility, particularly because it allows the modeling of any structure geometry, any materials as well as any external electrical circuit. The paper presents the finite element modeling of damping using piezoelectric materials, with the help of the ATILA code [3], that has been adapted to take into account an external electrical circuit. After the presentation of the formalism, two applications are presented.

2.0 FORMALISM

In order to be able to model any type of piezolectric transducer, without any restriction on the shape and the materials, a model has been developed, in the ATILA code, based on a variational principle. Classically, for an in-air piezoelectric structure, the system of equations is :

$$
\begin{bmatrix}
[K_{uu}] - \omega^2 [M] & [K_{u\Phi}] \\
[K_{u\Phi}]^T & [K_{\Phi\Phi}]
\end{bmatrix}
\begin{bmatrix}
U \\
\Phi
\end{bmatrix}
=
\begin{bmatrix}
F \\
-Q_p
\end{bmatrix}
$$

where U and Φ are the vectors containing the nodal values of the displacement field and of the electrical potential, F and Q_p contain the nodal values of the applied forces and of the electrical charges. $[K_{uu}]$ and $[M]$ are the structure stiffness and mass matrices, $[K_{u\Phi}]$ and $[K_{\Phi\Phi}]$ are the piezoelectric and dielectric stiffness matrices. ω is the angular frequency.

In practical cases, the general system of equation has to be modified, depending upon the electrical boundary conditions and the type of applications [3]. First, the electrical potential vector Φ is partitioned into two parts, the applied electrical potential Φ_A,

which is the same for all the nodes of the hot electrode and the vector Φ_I which includes the electrical potential nodal values for all the inner nodes. The reference potential is assumed to be zero (grounded electrode). Similarly, Q_p can also be split into two parts. The nodal value associated with Φ_A is equal to $I/j\omega$, where I is the current entering the hot electrode. The nodal values associated with the inner nodes are all equal to zero. Then, the system is simplified, after summing the lines corresponding to the hot electrode nodes and deleting those corresponding to the ground electrode.

If the transducer is loaded by an external impedance, the applied voltage Φ_A is simply equal to IZ where Z is the complex electrical impedance to which each piezoelectric element is assumed to be coupled. Solving the simplified system of equations provides the displacement field and the electrical potential in all the structure. By varying the value of the external impedance Z, damping can be evaluated.

3.0 FIRST APPLICATION

The first application is a piezoelectric ring placed between two masses (Fig. 1). The piezoelectric ring is made of PZT4, inner radius of which is equal to 2 mm, its external radius is 5 mm and its length is 18 mm. The piezoelectric ring is placed between two masses, the weights of which are 2.272 kg each and is shunted by a passive resistance. A force is applied on one face of the system. This example is close to the example considered by Law *et al* [2]. With a view to having the value of the optimal resistance, an equivalent electrical circuit model [4] is used. The model describes the electrical behavior of piezoelectric material and determines the required optimal resistive load with a view to minimizing the acceleration on the opposite face.

Figure 2 presents the Frequency Response Function (*FRF*), which is the ratio between this acceleration and the applied force, calculated with the finite element method, as a function of the frequency. The *FRF* shows the damping capability of the system and is expressed in dB. Different values of the external resistance are considered. The lowest level is clearly obtained for $R = R_{opt}$, in the frequency band of interest.
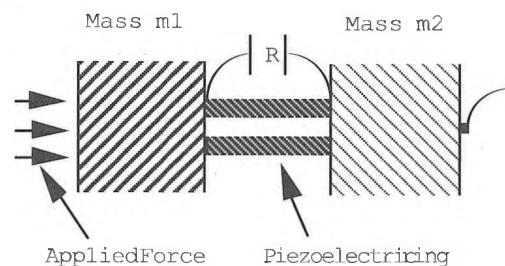
Fig. 1. Description of the system.

With a view to improving the model, it can be envisaged to shunt the piezoelectric material by a resistance and an inductance, the optimal values of which have to be determined. Experiments are under progress.

4.0 SECOND APPLICATION

The second application is a aluminum plate, clamped on a boundary and submitted to a force on the opposite side (Fig. 3). A piezoelectric plate is put on the plate. Its size and its position are determined with a view to maximizing the coupling factor. Then, the piezoelectric element is shunted by an external electrical circuit. In that case, with a view to finding the value of the optimal external impedance, the equivalent electrical circuit model is no more suitable but a numerical approach, using the modal decomposition, is used. Figure 4 presents the variations of the normalized displacement at the boundary of the plate as a function of the frequency, normalized to the first resonance frequency, with open circuit and with the external electrical circuit. It is clear that damping is observed, when the value of the external impedance is optimized. Experiments are under progress.

More generally, this approach could be used for any structure, containing a piezoelectric part, coupled to an external impedance [5]. Moreover, applications to sensor-actuator panels for underwater acoustic control could be foreseen [6].
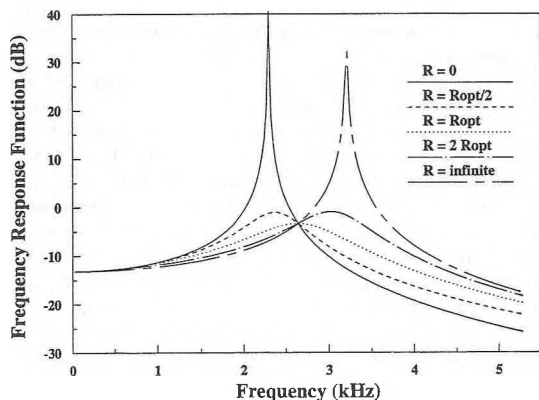
Fig. 2. Variations of the Frequency Response Function (*FRF*) in dB, as a function of frequency, for different values of the external resistance.
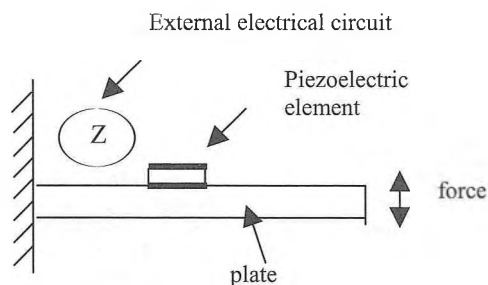
Fig. 3. Aluminum plate, with a piezoelectric element connected to an external electrical circuit.

5.0 REFERENCES

[1] N.W. Hagood, A. Von Flotow « Damping of structural vibrations with piezoelectric materials and passive electrical networks », Journal of Sound and Vibration, **146**, 243-268, (1991).

[2 H.H. Law, P.L. Rossiter, G.P. Simon, L.L. Koss, « Characterization of mechanical vibration damping by piezoelectric materials », Journal of Sound and Vibration **197**, 489-513, (1996).

[3] A.C. Hladky-Hennion, J.N. Decarpigny, « Finite element modeling of active periodic structures : application to 1-3 piezocomposites », Journal of the Acoustical Society of America, **94**, 621-635, (1993).

[4] O.B. Wilson, « Introduction to theory and design of sonar transducers », Peninsula Publishing Ed., Los Altos, USA, (1985).

[5] X.Q. Bao, V.K. Varadan, V.V. Varadan, « Additional damping in 1-3 piezoelectric composites due to electrical conductivity », Ceramic Transaction 8, (Ceramic Dielectric: Composition, Process and Properties) 366-374, (1990).

[6] R.D. Corsaro, B. Houston, J.A. Bucaro, « Sensor-actuator tile for underwater surface impedance control studies », Journal of the Acoustical Society of America, **102**, 1573-1581, (1997).
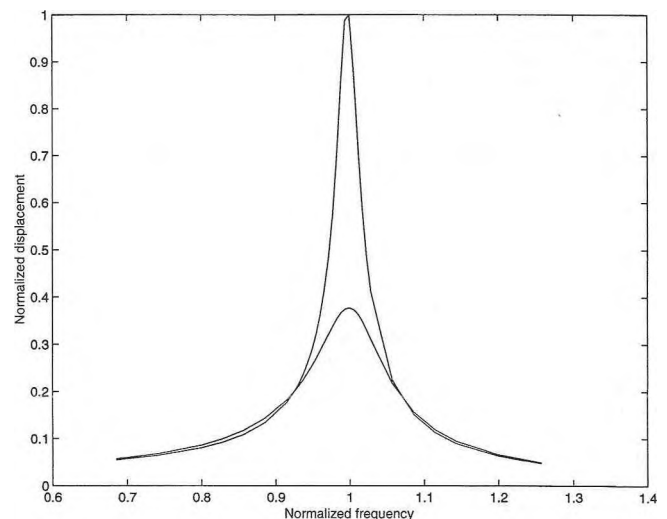
Fig. 4. Normalized displacement at the boundary of the aluminum plate, with open circuit and with the external electrical circuit, as a function of the normalized frequency.

Recursive Least-squares Algorithms with Improved Numerical Stability and Constrained Least-squares Algorithms for Multichannel Active Noise Control Systems

M. Bouchard

School of Information Technology and Engineering, University of Ottawa, Ottawa, Ontario, K1N 6N5

1.0 Introduction

This paper deals with the convergence of adaptive FIR filters used for multichannel active noise control (ANC) systems [1]. In a recent paper [2], recursive least-squares (RLS) algorithms and fast-transversal-filter (FTF) algorithms were introduced for multichannel ANC. It was reported that these algorithms can greatly improve the convergence speed of ANC systems, compared to algorithms using steepest descent algorithms or their variants, as expected. However, numerical instability of the algorithms was an issue that needed to be resolved. This paper summarizes some work that has recently been done to address this numerical instability problem. For the full detailed description of the new proposed algorithms, the reader should refer to [3].

In this paper, extensions of stable realizations of recursive least-squares algorithms such as the inverse QR-RLS [4], the QR decomposition least-squares-lattice (QRD-LSL) [4] and the symmetry-preserving RLS algorithms [4] are first discussed for the specific problem of multichannel ANC. Constrained adaptive least-squares algorithms for multichannel ANC are discussed next. The need for these constrained algorithms is mostly in undetermined ANC systems (systems with more actuators than error sensors), where even the typically numerically stable realizations of RLS algorithms will not produce stable convergence, unless some noise is added to the input signals of the algorithms. The algorithms to be discussed use either the structure of the filtered-x LMS algorithm for ANC [1] (i.e. the "filtered-x structure") or the structure of the modified filtered-x LMS algorithm for ANC [6] (i.e. the "modified filtered-x structure"). The main difference between the two structures is that the modified filtered-x structure computes an estimate of the primary field signals and removes the effect of the plant delay [6]. As a consequence, higher adaptation gains can be used in the algorithms using the modified filtered-x structure.

2.0 Inverse QR-RLS algorithms for multichannel ANC systems

The QR-RLS and the inverse QR-RLS algorithms (also called square-root RLS algorithms) are known to have very good numerical stability, because they make use of matrix rotations with good numerical properties [4]. However, the QR-RLS algorithm does not explicitly computes the coefficients of the adaptive FIR filters. For multichannel ANC systems, this is an important issue. It is not sufficient to have an algorithm that produces an estimate of a target signal for each iteration of an algorithm, it is also required to have the knowledge of the adaptive filter coefficients. To obtain those coefficients from the QR-RLS algorithm, an inversion of a square-root inverse correlation matrix is required. This adds many operations to the computational load, and may reduce the stability of the solution if the matrix is ill-conditioned. At the opposite, the inverse QR-RLS algorithm computes explicitly the adaptive filter coefficients [4]. This is why this algorithm was chosen as the algorithm to be extended for multichannel ANC systems. An inverse QR-RLS algorithm for multichannel ANC systems was thus developed in [3] for both the filtered-x and the modified filtered-x structures, and the numerical stability of the algorithm will be discussed later in this paper.

3.0 QRD-LSL algorithms for multichannel ANC systems

The inverse QR-RLS algorithm for multichannel ANC systems of the previous section has a computational load proportional to the square of the number of adaptive filter coefficients. For adaptive FIR filters with a lot of coefficients, this computational load can become too high for real-time implementations. This is the

motivation for developing "fast" RLS algorithms for multichannel ANC systems, where the computational load will increase linearly with the number of adaptive filter coefficients, not quadratically. A low computational realization is the fast-transversal-filters (FTF) algorithm, and a FTF algorithm for multichannel ANC was introduced in [2]. It is however well known that this algorithm suffers from numerical instability, and although it is possible to use a "rescue variable", it was found using simulations that for multichannel ANC systems this often lead to continuously re-initialized algorithms (and therefore a slower convergence). It is also not a trivial task to adjust the threshold for the "rescue variable", in particular for multichannel systems. There is thus a need for a numerically stable "fast" algorithm for multichannel ANC. The QR-decomposition least-squares-lattice (QRD-LSL) algorithm [4] is known to be a very numerically robust algorithm. It can be used to develop the least-squares-lattice (LSL) algorithms [4]. Some of those LSL algorithms also have a good numerical stability (in particular the versions with error feedback), but the stability of the QRD-LSL algorithm is typically better [4]. The QRD-LSL algorithm was thus extended for multichannel ANC systems in [3], and the numerical stability of the extended algorithm will be discussed later in this paper.

Since the QRD-LSL algorithm requires the knowledge of the "target" or "desired" signals, it can only be developed for ANC systems with the modified filtered-x structure. Also, the QRD-LSL provide auxiliary joint-process coefficients which are different from the time domain adaptive filter coefficients (i.e. the auxiliary coefficients are in a time-varying transformed basis). Therefore a time-varying inverse transformation from the auxiliary joint process coefficients to the time domain coefficients is required. Such an inverse transformation exists for the classical QRD-LSL algorithm [4], and it can be extended to the multichannel ANC case [3]. However, the inverse transform has a computational load proportional to the square of the number of adaptive filters coefficients, and the reason for developing the QRD-LSL for multichannel ANC systems was to avoid such a quadratic dependency. However, the inverse transform does not need to be computed on a sample by sample basis: it can be computed and applied at a reduced rate. The update of the multichannel joint-process auxiliary coefficients can still be done on a sample by sample basis, as in any recursive least-squares algorithm, it is just the update to the time-domain coefficients that occurs at a reduced rate. For example, if a forgetting factor of 0.999 is used in the algorithm (and therefore the "memory" of the algorithm has a time constant of 1000), then updating the coefficients every 10 or every 100 samples will not greatly affect the convergence performance or the tracking performance of the algorithm.

4.0 Symmetry-preserving recursive least-squares algorithm for multichannel ANC systems

Another approach to develop a numerically stable RLS algorithm for multichannel ANC is to use a simple symmetry-preserving approach [4]. This approach simply requires to compute the upper triangular part of the inverse time-averaged correlation matrix in the RLS algorithm, and then copy the values to the transposed positions in the lower triangular part. It is reported that this simple approach improves the numerical stability of the standard RLS algorithm [4]. It is straightforward to modify the RLS algorithm for multichannel ANC systems found in [2] to obtain a symmetry-preserving version. This is done in details in [3] for both the filtered-x and the modified filtered-x structures, and the numerical stability of the resulting algorithm will be discussed later in this paper.

5.0 Constrained least-squares algorithms for multichannel ANC systems

As mentioned in the introduction, in some cases multichannel ANC systems will be underdetermined, and in these cases unconstrained recursive least-squares algorithms may become numerically unstable unless some noise is added to the input signals of the algorithms. In [3], three constrained least-squares algorithms were developed for multichannel ANC systems. The different constraints were: the minimization of the frequency weighted actuator outputs power, the minimization of the adaptive filters coefficients squares, and a pseudo-inversion of the multichannel correlation matrix. Because of the constraint, the matrix inversion lemma is not directly applicable, and therefore these least-squares algorithms are not recursive like the algorithms of the previous sections. Also, the least-squares algorithms require the knowledge of the primary field signals, and therefore they are only applicable to the modified filtered-x structure. The reduce the high computational load required by the inversion of the multichannel correlation matrix, an option is to compute the inversion offline every 10, 100, or 1000 iterations (with preferably less iterations between updates than the time constant caused by the forgetting factor). The numerical stability of the constrained least-squares algorithms will be discussed in the next section.

6.0 Simulation results

In order to evaluate the numerical stability of the different algorithms, simulations were performed in [3] using a C program implementation, with a single precision floating point representation. The code from [7] was used for matrix inversions with LU decompositions and, in the case of the constrained least-squares algorithm with pseudo-inversion, for matrix pseudo-inversions with SVD decompositions. The simulations were performed for multichannel ANC systems with the modified filtered-x structure. Time domain and frequency domain characteristics of some of the transfer functions from which the simulations were performed can be found in [2]. Adaptive filters with 100 coefficients each were used in the simulations.

The first set of simulations was performed for a system with one reference sensor, two actuators and two error sensors (a 1-2-2 system). The algorithms tested for this first set of simulations were the RLS and FTF algorithms found in [2], and the new inverse QR-RLS, QRD-LSL and symmetry-preserving RLS algorithms. Table 1 compares the numerical stability of the different algorithms for multichannel ANC systems. From Table 1, it is clear that the RLS and FTF algorithms developed for multichannel ANC systems are numerically unstable, as previously reported in [2]. Although it is obtained from a slight modification to the numerically unstable RLS algorithm, the symmetry-preserving RLS algorithm was found to be stable (unless a very low value of forgetting factor such as 0.9 was used). The QRD-LSL algorithm was always stable and always produced a good performance in the transformed domain, but the simulations have shown that the inverse transformation required to compute the time-domain adaptive filters coefficients only produces a good convergence performance in the time-domain when the value of the forgetting factor was sufficiently high (such as 0.999 shown in Table 1). Finally, the inverse QR-RLS produced the best performance of all algorithms: it was always stable and always produced a good attenuation.

A second set of simulations was performed in [3], this time for an underdetermined 1-3-2 system. In this second set of simulations, the algorithms that were simulated were the recursive least-squares algorithms used in the first set of simulations and the constrained least-squares algorithms of Section 5. Table 2 summarizes the results of this second set of simulations. First of all, since the simulated system is underdetermined, the (unconstrained) recursive least-squares algorithms all suffered from numerical instability. At the opposite, all the constrained least-squares algorithms were numerically stable if a sufficient constraint was used (a good attenuation could still be achieved

with the constraint). The update of the coefficients in these constrained least-squares algorithms was computed once for every 100 iterations, but this did not reduce much the convergence speed.

7.0 Conclusion

This paper discussed recursive least-squares algorithms with improved numerical properties and constrained least-squares algorithms for multichannel ANC systems. The choice of the most suitable algorithm for ANC will depend on the specific application. If the ANC system is underdetermined, then the constrained least-squares algorithms of Section 5 may be used. If the ANC system is not underdetermined, then the algorithms of Sections 2-4 may be used. In that case, the inverse QR-RLS algorithm has the best numerical properties, but it also has the highest computational load. The QRD-LSL algorithm has the lowest computational load [3], but it requires the use of a forgetting factor with a fairly high value (typically 0.999 or higher). At last, the symmetry-preserving RLS has the simplest software implementation (but not the lowest computational load). This may be a factor is some implementations.

References

[1] S.M. Kuo and D.R. Morgan, "Active noise control: a tutorial review", *Proc. of the IEEE*, vol. 87, pp.943-973, June 1999

[2] M. Bouchard and S. Quednau, "Multichannel recursive least-squares algorithms and fast-transversal-filter algorithms for active noise control and sound reproduction systems," *IEEE Trans. Speech Audio Processing*, vol. 8, n.5, Sept. 2000.

[3] M. Bouchard "Recursive least-squares algorithms with good numerical stability and constrained least-squares algorithms for multichannel active noise control or transaural sound reproduction systems," submitted for publication in *IEEE Trans. Speech Audio Processing*

[4] S. Haykin, *Adaptive filter theory*, 3rd edition, Englewood Cliffs (NJ), Prentice Hall, 989 p., 1996

[5] M. Miyoshi and Y. Kaneda, "Active control of broadband random noise in a reverberant three dimensional space," *Noise Control Engineering*, vol. 36, pp.85-90, Mar.-Apr. 1991

[6] S. Douglas, "Fast, exact filtered-x LMS and LMS algorithms for multichannel active noise control", *Proc. ICASSP-97*, Munich, Germany, 1997, pp.399-402

[7] W.H. Press, S.A. Teukolsky, W.T. Vetterling and B.P. Flannery, *Numerical Recipes in C : The Art of Scientific Computing*, 2nd edition, Cambridge Univ. Press, 994 p., 1993

Multichannel ANC algorithm (forgetting factor 0.999)	Numerical stability/instability for the 1-2-2 system
RLS	unstable, 200 iterations
FTF (no rescue variable)	unstable, 27000 iterations
inverse QR-RLS	stable, 23 dB average attenuation
QRD-LSL	stable, 22 dB average attenuation
symmetry-preserving RLS	stable, 23 dB average attenuation

Table 1 Numerical behavior of the algorithms for the 1-2-2 system

Multichannel ANC algorithm (forgetting factor 0.999)	Numerical stability/instability for the 1-3-2 system
RLS	unstable, 200 iterations
FTF (no rescue variable)	unstable, 1300 iterations
inverse QR-RLS	unstable, 50000 iterations
QRD-LSL	unstable, 3000 iterations
symmetry-preserving RLS	unstable, 9000 iterations
least-squares constrained with actuators power	stable, >35 dB attenuation
least-squares constrained with coefficient squares	stable, >35 dB attenuation
least-squares using SVD pseudo-inverse	stable, >60 dB attenuation

Table 2 Numerical behavior of the algorithms for the 1-3-2 system

Multichannel Active Noise Control Algorithms Using Inverse Filters

M. Bouchard and Yu F.

School of Information Technology and Engineering, University of Ottawa, Ottawa, Ontario, K1N 6N5

1.0 Introduction

For active noise control (ANC) systems, a common approach is to use adaptive FIR filters trained with the filtered-x LMS algorithm [1], for both feedforward systems and Internal Model Control (IMC) feedback systems, in monochannel or multichannel systems. Variations of the algorithm sometimes called the modified filtered-x LMS algorithm have been published [2], which can achieve a faster convergence speed by using a larger step size in the algorithm. Fast exact realizations of the filtered-x LMS and the modified filtered-x LMS algorithms have also been published [2]. In most cases, these fast realizations can reduce the computational complexity of the filtered-x LMS and modified filtered-x LMS algorithms for multichannel systems.

Many algorithms that can achieve a faster convergence than the multichannel filtered-x LMS or the modified filtered-x LMS algorithms for ANC systems have also been published over the years. However, these algorithms can only provide increased convergence speed at the cost of increased computational load, compared to the multichannel filtered-x LMS algorithm or its fast exact realizations. In this paper, a simple multichannel algorithm that can both reduce the computational load and increase the convergence speed compared to the multichannel filtered-x LMS algorithm or its fast exact realizations is introduced, using an inverse structure and filtered-x LMS-based algorithms.

In the proposed approach, the standard FIR controller is split into two parts: multichannel predictors and multichannel delayed non-causal models of the inverse plant between some error sensors (typically microphones in ANC systems) and some actuators (typically loudspeakers). Figure 1 shows the structure of the proposed approach for a simplified monochannel case, using the delayed non-causal filter.

With the proposed inverse structure that uses adaptive FIR filters, there are two benefits of using delayed non-causal filters modeling the inverse plant of an ANC system. One benefit is that the combination of the delayed non-causal models and the models of the direct plant becomes approximately pure delays (approximately because models are never perfect). Using these pure delay operations can eliminate some costly convolutions. The second benefit of using the delayed non-causal filters is due to the fact that the convergence speed of filtered-x LMS-based algorithms is related to the eigenvalue spread in the correlation matrix of the filtered reference signals in the algorithms. This eigenvalue spread can be typically reduced using the proposed structure, because the resulting combination of the delayed non-causal models and the models of the direct plant will have flat, uniform frequency responses, thus eliminating the eigenvalue spread caused by filtering reference signals with the models of the direct plant in the standard filtered-x LMS structure [1].

Reference signal

Disturbance
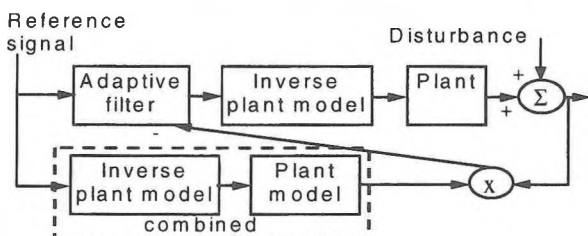
Figure 1 : structure using the delayed non-causal inverse filter

2.0 Description of the inverse algorithms

To describe explicitly the proposed the multichannel inverse filtered-x LMS (IFX) and inverse modified filtered-x LMS (IMFX) algorithms, the following notation is defined:

I, J, K number of reference sensors, actuators and error sensors in a feedforward ANC system

$e_k(n)$ value at time n of the signal measured by the k th error sensor

$x_i(n)$ value at time n of the i th reference signal in a feedforward ANC system (measured with a reference sensor)

$t_k(n)$ estimated value of the disturbance signal $d_k(n + D)$ at time n, where D is the delay required to make the FIR filter modeling the inverse plant causal. $t_k(n)$ is obtained by filtering the reference signals $x_i(n)$ with the adaptive FIR filters.

$y_j(n)$ value at time n of the j th actuator signal

$z_{i,j,k}(n)$ value at time n of the signal obtained by filtering the reference signal $x_i(n)$ with the FIR filter modeling the inverse plant between $e_k(n)$ and $y_j(n)$

$v_{i,k',k}(n)$ value at time n of the filtered reference signal, i.e. the signal obtained by filtering the $z_{i,j,k'}(n)$ signal with the FIR filter modeling the direct plant between $y_j(n)$ and $e_k(n)$

$d'_k(n)$ value at time n of the estimated primary sound field at the k th error sensor (for the modified structure only [2])

$e'_k(n)$ value at time n of the alternative error computed in the modified structure [2]

$w_{i,k,l}(n)$ value at time n of the l th coefficient in the adaptive FIR filter linking $x_i(n)$ and $t_k(n)$

$h_{j,k,m}$ value of the m th coefficient in the non-adaptive FIR filter model of the direct plant between $y_j(n)$ and $e_k(n)$.

$g_{j,k,p}$ value of the p th coefficient in the non-adaptive FIR filter modeling the inverse plant between $e_k(n)$ and $y_j(n)$.

$h_{j,k}$, $g_{j,k}$, $w_{i,k}(n)$ column vectors containing the $h_{j,k,m}$, $g_{j,k,p}$, and $w_{i,k,l}(n)$ coefficients, respectively

$x_i(n)$, $t_k(n)$, $y_j(n)$, $z_{i,j,k}(n)$, $v_{i,k',k}(n)$ column vectors containing the current and previous values of $x_i(n)$, $t_k(n)$, $y_j(n)$, $z_{i,j,k}(n)$ and $v_{i,k',k}(n)$, respectively.

The inverse filtered-x LMS (IFX) algorithm is first described, using equations (1)-(5). In these equations, k and k' are both used as an index for the error sensor signals or their prediction:

$$t_k(n) = \sum_{i=1}^{I} w_{i,k}(n)^T x_i(n) \qquad (1)$$

$$y_j(n) = \sum_{k=1}^{K} g_{j,k}{}^T t_k(n) \tag{2}$$

$$z_{i,j,k}(n) = g_{j,k}{}^T x'_i(n) \tag{3}$$

$$v_{i,k',k}(n) = \sum_{j=1}^{J} h_{j,k}{}^T z_{i,j,k'}(n) \tag{4}$$

$$w_{i,k'}(n+1) = w_{i,k'}(n) - \mu \sum_{k=1}^{K} v_{i,k',k}(n) e_k(n) \tag{5},$$

where μ is a scalar convergence gain. Note that the $g_{j,k}$ filters in (3) can be convoluted with the $h_{j,k}$ filters in (4), and these convolutions only need to be computed once. Therefore, equations (3),(4) can be combined in a single equation, which will significantly reduce the number of computations of the algorithm:

$$v_{i,k',k}(n) = \left(\sum_{j=1}^{J} g_{j,k'} * h_{j,k} \right)^T x_i(n) \tag{6},$$

where " $*$ " is the convolution operator and $\sum_{j=1}^{J} g_{j,k'} * h_{j,k}$ is only computed once, offline. Since $h_{j,k}$ and $g_{j,k}$ are models of the direct and inverse plant, their combination can also be estimated by pure delays (the same delay required to make $g_{j,k}$ causal). Therefore, it is possible to further simplify equations (3)-(5) and use (7) instead, to have a simplified IFX algorithm:

$$w_{i,k}(n+1) = w_{i,k}(n) - \mu x_i(n-D) e_k(n) \tag{7}$$

where D is the delay required to make $g_{j,k}$ causal.

The inverse modified filtered-x LMS (IMFX) algorithm is described next. It combines the modified filtered-x LMS algorithm [2] with the inverse structure that uses the models of the inverse plant. The algorithm can be described by equations (1),(2),(6) and (8)-(10):

$$d'_k(n) = e_k(n) - \sum_{j=1}^{J} h_{j,k}{}^T y_j(n) \tag{8}$$

$$e'_k(n) = d'_k(n) + \sum_{i=1}^{I} \sum_{k'=1}^{K} w_{i,k'}(n)^T v_{i,k',k}(n) \tag{9}$$

$$w_{i,k'}(n+1) = w_{i,k'}(n) - \mu \sum_{k=1}^{K} v_{i,k',k}(n) e'_k(n) \tag{10}.$$

Again, since the combination of $h_{j,k}$ and $g_{j,k}$ results in pure delays, a simplified IMFX algorithm can be described by equations (1),(2) and by (11)-(13):

$$d'_k(n) = e_k(n) - t_k(n-D) \tag{11}.$$

$$e'_k(n) = d'_k(n) + \sum_{i=1}^{I} w_{i,k}(n)^T x_i(n-D) \tag{12}$$

$$w_{i,k}(n+1) = w_{i,k}(n) - \mu x_i(n-D) e'_k(n) \tag{13}.$$

3.0 Computational load of the algorithms
The computational load of the simplified IFX and simplified IMFX algorithms was compared with the computational load of the fast exact versions of the filtered-x LMS and the modified

filtered-x LMS found in [2]. Detailed results can be found in [3],[4]. For a system with $I=1$, $J=4$, $K=4$, 300 coefficients for the adaptive filters, 256 coefficients for the direct plant models and 256 coefficients for the inverse plant models, the fast exact realizations of the standard filtered-x LMS and modified filtered-x algorithm require 8 030 and 32 606 multiplies per iteration, respectively. For the same system, the simplified IFX and IMFX algorithms require only 6 100 and 7 100 multiplies per iteration, respectively. There is thus a potential for a significant reduction of the computational load using the proposed inverse algorithm, in particular for algorithms using the modified structure [2].

4.0 Simulation results
To evaluate the potential gain in convergence speed, simulations were performed using an acoustic plant measured on a headphone. The plant and its inverse are described in [3],[4]. The inverse impulse response of the plant required a delay of 15 samples to become approximately causal [3],[4]. The convergence speed of the filtered-x LMS algorithm, the modified filtered-x LMS algorithm, the IFX/IMFX algorithms and their simplified versions appears in Fig. 2, for a 20 dB SNR on the plant direct and inverse models. All the algorithms using the inverse filter produced a better convergence performance, as expected, and the simplification using a pure delay did not affect much the performance of the inverse algorithms for this system. With a SNR of more than 10 dB on the plant direct and inverse models, the algorithms using the inverse filter produced a faster convergence speed. However in the SNR was less or equal to 10 dB, then the classical algorithms performed better.

5.0 Conclusion
In this paper, an inverse structure was introduced for the use of adaptive FIR filters in ANC systems. Multichannel adaptive FIR filter learning algorithms based on the filtered-x LMS algorithm were introduced for this inverse structure. It was shown with simulations using a realistic acoustical plant that some versions of the introduced algorithms can achieve both a reduction of the computational load and an increase of the convergence speed, compared to standard algorithms for ANC such as the multichannel filtered-x LMS algorithm, the modified filtered-x LMS algorithm or their fast exact realizations. Some theoretical work on the effect of plant model and inverse plant model errors would be of interest.

References
[1] S.M. Kuo and D.R. Morgan, *Active noise control systems : algorithms and DSP implementations*, New-York : J. Wiley & Sons, 1996
[2] S. Douglas, "Fast, exact filtered-x LMS and LMS algorithms for multichannel active noise control", *Proc. ICASSP-97*, Munich, Germany, 1997, pp.399-402
[3] Bouchard, M., and Yu, F. Inverse structure for active noise control and combined active noise control/sound reproduction systems, accepted for publication in IEEE Trans. on Speech and Audio Processing (scheduled for September 2000)
[4] Yu, F. and Bouchard, M. Multichannel active noise control algorithms using inverse filters, ICASSP 2000, Vol. II, 825-828 (Istanbul, Turkey, June 2000)
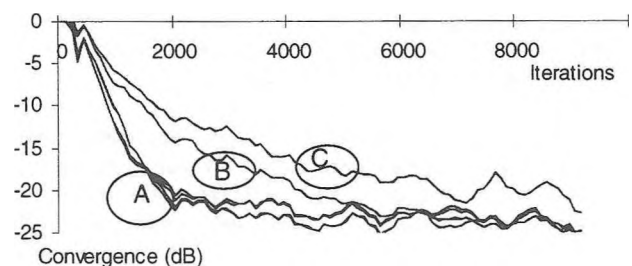
Figure 2: convergence curves of A) IFX/IMFX algorithms B) modified filtered-x LMS algorithm C) filtered-x LMS algorithm

COMPARAISON ENTRE RÉSEAU DE NEURONES ET LMS À RÉFÉRENCE FILTRÉE APPLIQUÉS AU CONTRÔLE ACTIF DE BRUIT

Yvan Pelletier, Stéphane Renault, Alain Berry

GAUS, Université de Sherbrooke, J1H 2R1, Québec, e-mail : yvan.pelletier@gaus.gme.usherb.ca

INTRODUCTION

L'algorithme généralement utilisé pour des problèmes de contrôle actif de bruit est du type LMS [Ne92]. Celui-ci est bien connu, facile à implanter et converge rapidement vers la solution optimale. Cependant, le LMS est sensible aux perturbations externes. Les réseaux de neurones sont, pour leur part, bien adaptés aux systèmes non-linéaires [Ha94]. En effet, la sortie d'un neurone est modulée par une fonction sigmoïde, dans le cas présent, une tangente hyperbolique. Cela implique qu'une modélisation par un réseau de neurones intègre la saturation qui intervient sur le signal de commande à la sortie du processeur.

La présente étude compare le comportement d'un algorithme FX-LMS (LMS normalisé à référence filtrée) à celui d'un réseau de neurones à référence filtrée face à une perturbation externe.
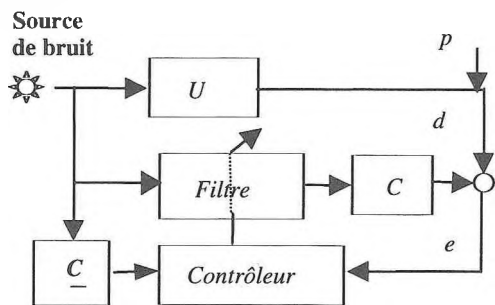
MÉTHODE EXPÉRIMENTALE

Figure 1 : Schéma bloc de l'expérience.

La figure 1 présente le schéma bloc général de l'expérience. U représente la fonction de transfert entre le signal au capteur de référence et le signal au capteur d'erreur. C représente la fonction de transfert entre la commande donnée au secondaire et le signal au capteur d'erreur.

Dans le cas où l'algorithme FX-LMS est utilisé, le filtre est un FIR et le contrôleur est l'algorithme FX-LMS, de plus, le FIR possède 20 coefficients. Dans le cas où le réseau de neurones est utilisé, le filtre est le réseau de neurone, alors que le contrôleur est l'algorithme de rétropropagation. Chaque neurone a 20 coefficients. Outre les 20 coefficients d'entrés, il y a 4 neurones sur la couche cachée et un neurone sur la couche de sortie.

La source de bruit (p) est fournie par un haut-parleur alimenté avec un sinus à 80 Hz. La perturbation externe est fournie par un autre haut-parleur, alimenté avec un sinus à 50 Hz. L'identification du secondaire ($\underline{C}$) est faite avec un X-LMS dont le FIR a 500 coefficients.

La procédure pour étudier le comportement de chacune des méth-

odes face à une perturbation externe est en trois étapes. (1) On laisse converger le contrôleur, (2) on applique ensuite la perturbation externe et on la maintient pendant 15 secondes, (3) on coupe la perturbation. À chacune de ces étapes, on récupère le spectre de puissance du signal d'erreur. L'adaptation se poursuit tout le long de ces trois étapes.

RÉSULTATS EXPÉRIMENTAUX ET ANALYSE

La figure 2 montre l'atténuation de la raie à 80 Hz par chacun des algorithmes. Le FX-LMS a éliminé la raie, tandis que le réseau de neurone l'a atténuée de 15 dB. Les deux méthodes ont la capacité de réduire le bruit primaire. Les performances du réseau de neurones sont moins bonnes que le FX-LMS, mais le réseau de neurones n'a pas été optimisé en ce sens, alors que le FX-LMS l'était.
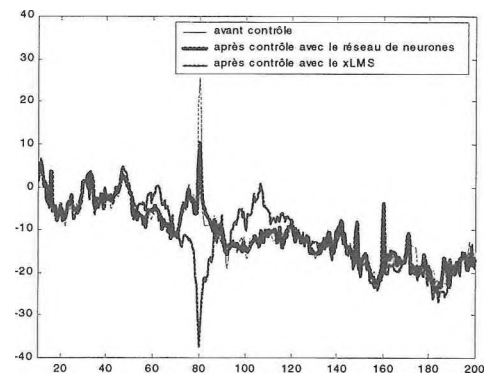
Figure 2 : Spectre de puissance du signal d'erreur avant et après contrôle avec l'algorithme FX-LMS et le réseau de neurones.

Les figures 3 et 4 présentent, respectivement, le comportement du FX-LMS et du réseau de neurones avant, pendant et après l'application de la perturbation externe à 50 Hz. Pour le FX-LMS, durant la perturbation, le niveau général du bruit est près de 15 dB plus élevé qu'avant la perturbation. Plusieurs raies sont apparues pendant la perturbation, elles ont persistés après la coupure de la perturbation. Dans le cas du réseau de neurones, plusieurs raies apparaissent durant la perturbation, mais elles disparaissent lorsque la perturbation est coupée. D'ailleurs, les courbes des spectres de puissance, à la figure 4, avant et après la perturbation sont pratiquement confondues. Le réseau de neurones retourne rapidement aux même performances qu'avant la perturbation. Les figures 5 et 6 montrent le comportement de la commande, pour chacune des méthodes, lors de l'application de la perturbation externe à 50 Hz. Le FX-LMS s'avère très sensible en comparaison du réseau de neurone. Dans le cas du FX-LMS, les amplitudes de commande, durant la perturbation, peuvent être dangereuses pour le haut-parleur secondaire. Pour le réseau de neurone, lors de l'application de la perturbation externe, la commande demeure sensiblement au même niveau qu'avant la perturbation.
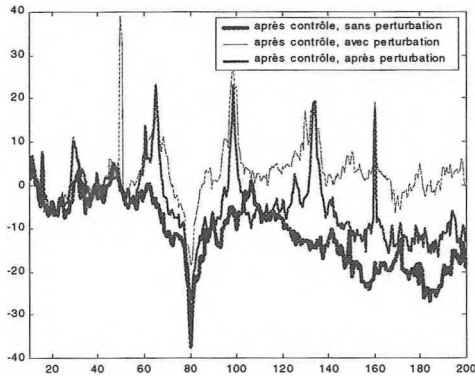
Figure 3 : Spectre de puissance du signal d'erreur avant, pendant et après la perturbation à 50 Hz. Le contrôleur FX-LMS est en fonction dans les trois cas.
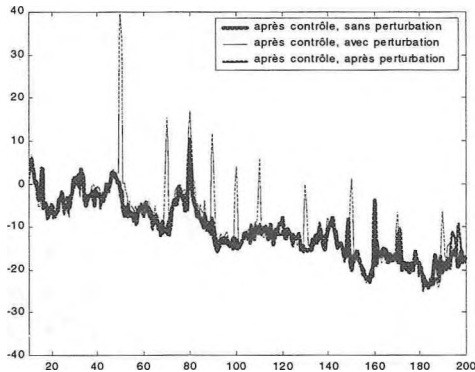
Figure 4 : Spectre de puissance du signal d'erreur avant, pendant et après la perturbation à 50 Hz. Le contrôleur réseau de neurones à référence filtrée est en fonction dans les trois cas.
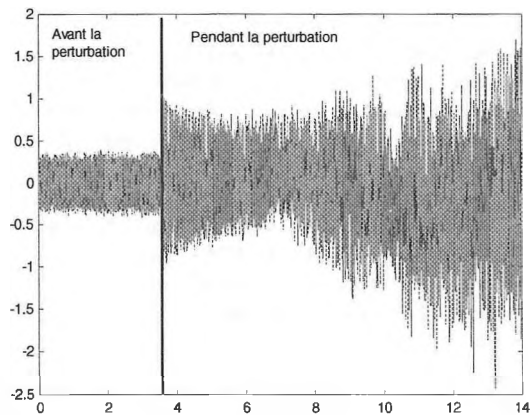
Figure 5 : Comportement de la commande du FX-LMS avant et pendant l'application de la perturbation externe à 50 Hz.
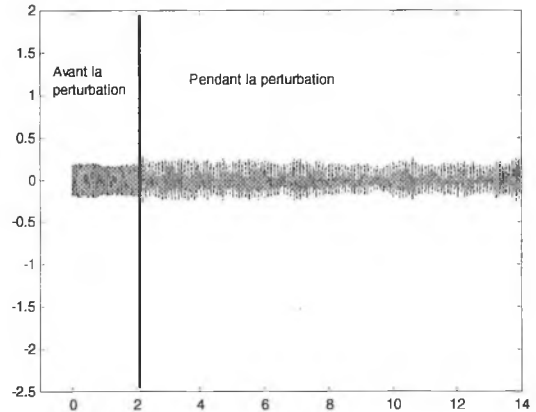
Figure 6 : Comportement de la commande du réseau de neurones à référence filtrée avant et pendant l'application de la perturbation externe à 50 Hz.

CONCLUSION

Les résultats préliminaires démontrent que la commande du réseau de neurone est moins sensible à une perturbation externe que le FX-LMS. Aussi, après la coupure de la perturbation externe, le spectre de puissance du signal d'erreur montre que le réseau de neurone redonne rapidement les même performances qu'avant la perturbation, tandis que le FX-LMS continue de générer d'autres raies.

Une étude plus approfondie pourrait permettre de déterminer la configuration du réseau de neurones pour avoir de meilleures atténuations.

RÉFÉRENCES

[Ne92] – P.A Nelson, S.J. Elliott, « Active control of sound », Academic Press, New York, 1992.

[Ha94] – S. Haykin, « Neural networks a comprehensive foundation », IEEE Press, 1994.

ACTIVE NOISE CONTROL IN ENCLOSURE WITH VIRTUAL MICROPHONE

Stéphane Renault, Franck Rymeyko, Alain Berry

GAUS, Université de Sherbrooke, J1H 2R1, Quebec, e-mail: Stephane.Renault@gaus.gme.usherb.ca

INTRODUCTION

This study concerns local active noise control (ANC) in confined spaces [Ne92]. In cases where an active zone of quiet is intended in an enclosure, it is not always practical to place error microphones in this zone. Error microphones placed on the enclosure walls would sometimes be a more convenient solution. This article discusses the concept of a "virtual" microphone, which consists to generate a quiet zone distant from the error microphone used during control. Two virtual microphone algorithms are presented and experimentally tested. Such a virtual microphone technique has been implemented in the past for essentially fixed primary sources with respect to the enclosure (e.g. active control of propeller-induced aircraft cabin noise). The virtual microphone technique is especially examined here in the context of a moving primary source with respect to the enclosure (such as road traffic noise).

VIRTUAL MICROPHONE CONCEPT

The principle is shown on figure 1. Because of the extreme difficulty to achieve global active noise control in enclosures, most successful applications of active noise control are based on a local approach. Indeed, in many cases (in automobile interiors for example), there is no need to reduce noise at all locations, but only around the passengers' head. Such systems use one or several microphones (called error microphones) located in the area where the noise must be reduced. The control algorithm minimizes the signals given by the error microphones to produce a "quiet zone" in the neighborhood of the microphones. The size of the quiet zone around one microphone is closely related to the frequency of the disturbance (it is approximately proportional to the wavelength).
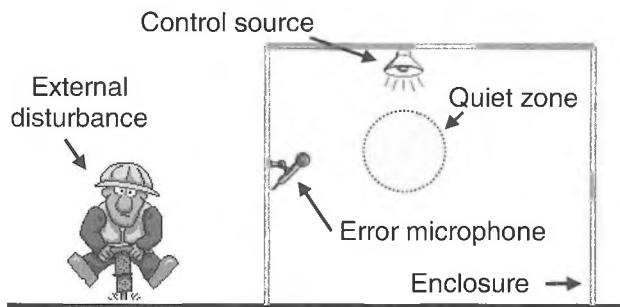

Figure 1 : The principle of virtual microphone

The dimension of the quiet zone can be from a few centimeters to approximately one meter for very low frequencies. However, in many cases, it is not practical to place microphones in the area where the noise must be controlled. Additionally, if the error microphones are located outside of the desired zone, the reduction should be acceptable for low frequency, because the quiet zone is rather large, but not for higher frequencies.

Several algorithms, called "virtual microphone arrangement (VMA)" [Ga97] or "remote microphone technique (RMT)" [Ro99], have been proposed to locate the error microphone outside of the intended zone of quiet. In both algorithms a preliminary identification step is required, with an extra microphone (the "virtual " microphone) located inside the zone of quiet. During this step, the RMT algorithm estimates three transfer functions : - first, between the control source and the virtual microphone (inside the zone of quiet), - second, between the control source and the error microphone (outside the zone of quiet), - and third, the difference between the disturbance signal at the error microphone and the disturbance signal at the virtual microphone. Consequently, if the frequency or the location of the disturbance source vary, this third transfer function may vary and the control performance is degraded. The RMT algorithm is thus based on the assumption that the disturbance source is stationary in space and time, or more strictly that the disturbance signals at the two microphone locations do not change in time. The VMA algorithm is a simplified version that additionally assumes that the disturbance signals at the two microphone locations are identical.

a) Side view   b) Top view
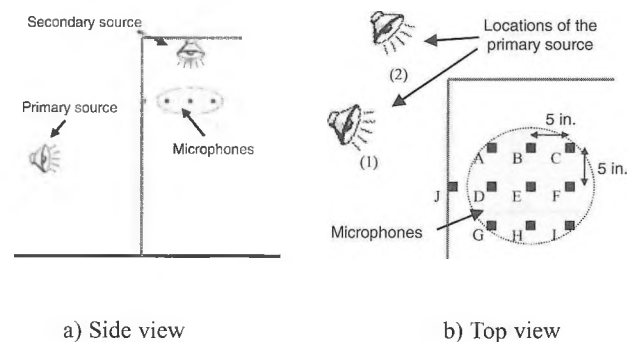
Figure 2 : Experimental setup

EXPERIMENTAL SETUP

The two virtual microphone algorithms (VMA and RMT) and the classical feedforward control approach (filtered-X LMS) have been experimentally compared. The primary source is a loudspeaker placed about 1 meter outside of the enclosure (figures 2a and 2b), that produced a white noise in the 50-300 Hz range. For the RMT algorithm, two different locations of the source (indexed (1) and (2) in figure 2b) were tested. The grey area on the figures depicts the intended quiet zone. Nine monitoring microphones (indexed A to I in figure 2b) were placed in this area to measure the sound attenuation obtained. For the RMT and VMA algorithms, the central microphone (E) is used during the identification stage as the virtual microphone. The error microphone used by the controllers is placed on the wall (J). The control source, also called secondary source, is fixed to the ceiling of the enclosure, and is about 50 cm from the microphones. The reference signal, which is necessary for these algorithms, is directly obtained from the white noise generator connected to the primary source.
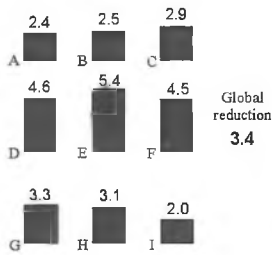
Figure 3 : LMS algorithm with the error microphone inside the control area (E) *
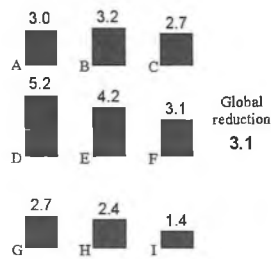
Figure 4 : LMS algorithm with the error microphone on the wall (J) *
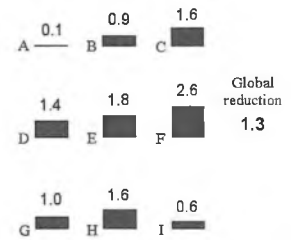
Figure 5 : VMA algorithm *
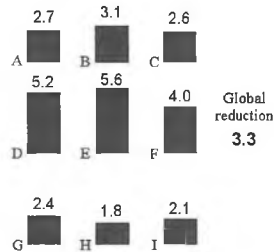
Figure 6 : RMT algorithm *
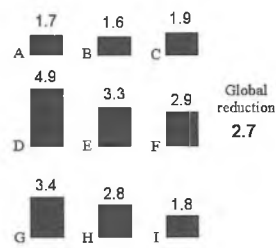
Figure 7 : RMT algorithm after displacement of the disturbance source *

* Each value corresponds to the noise reduction at each microphone in the quiet zone. The number on the top of each column is the value of the sound reduction in decibels. To the right of each figure is given the mean value of the reduction for the nine monitoring microphones.

RESULTS

A classical feedforward approach (filtered-X LMS) was first tested, with the error microphone (E) in the center of the desired quiet zone (figure 3). The classical filtered-X LMS corresponds to the case where the virtual microphone and error microphone are collocated. This first test experiment thus gives the achievable reduction if the error microphone is placed inside the quiet zone. The classical filtered-X LMS is then tested, but with the error microphone placed on the wall (J) (figure 4). The quiet zone is obviously shifted to the left, near the error microphone. Since the acoustic wavelength remains fairly large compared to the distance between microphones E and J (25cm), the average sound attenuation at the 9 monitoring microphones is almost the same. The VMA algorithm was the tested (figure 5), with microphone E as the virtual microphone in the identification step, and microphone J as error microphone during control. The reduction obtained with this algorithm (1.3 dB) is considerably less than the reduction obtained with the filtered-X LMS (3.4 and 3.1 dB). This is due to the fact that the primary disturbance at the physical (J) and at the virtual (E) microphone locations are not identical similar in this particular case. Finally, the RMT algorithm was tested, with microphone E as the virtual microphone in the identification step, and microphone J as error microphone during control. As expected, the reduction obtained with the RMT algorithm (3.3 dB) is close to the optimal reduction (3.4 dB). If this experiment is repeated after moving the primary disturbance source between the identification step and the control step (figure 7), a significant control degradation is observed (2.7 dB instead of 3.3 dB), as a result of the transfer function variation between the primary sources and the virtual and error microphones.

CONCLUSION

For low frequency sound in enclosures, it is possible to obtain a large quiet zone, with only one error microphone using a classical filtered-X LMS algorithm. It implies that if the error microphone cannot be placed inside the desired quiet zone, acceptable - if not optimal sound reduction can be obtained with the filtered-X LMS. However, a virtual microphone technique can provide a significant improvement of the control in this case. The VMA algorithm (that assumes no variation of the primary sound between virtual and error microphones), and the more general RMT algorithm were tested. While the VMA algorithm did not perform well in our case, the results obtained with the RMT algorithm are encouraging. Despite the predictable fact that when the primary disturbance source is not fixed in space, the control performance is degraded, this solution will certainly be interesting in the case of a disturbance source moving in a limited area. Further work is needed to more precisely quantify the effect of the displacement of the disturbance source during the experiment.

REFERENCES

[Ne92] P.A. Nelson, S.J. Elliott, "Active control of sound", Academic Press, New York, 1992.

[Ga97] J. Garcia_Bonito, S. J. Elliot, and C. C. Boucher, "Generation of zones of quiet using a virtual microphone arrangement", J. Acoust. Soc. Am., **101** (6), 3498-3516 (1997).

[Ro99] Alain Roure, Anne Albarrazin, "The remote microphone technique for active noise control", ACTIVE 99, pp1233-1244.

A Comparison of Software Tools for the Implementation of Spatial Sounds in Virtual Environments

Yu F. and M. Bouchard

School of Information Technology and Engineering, University of Ottawa, Ottawa, Ontario, K1N 6N5

1.0 Introduction

Since its earliest days, the human-computer interface has been almost entirely visual. Until fairly recently, audio was limited to some kind of altering "beep" for output. Then CD-quality stereo sound appeared in the multimedia-equipped computers. Conventional stereo can easily place a sound in any spot between left and right loudspeakers. However, with true 3-D sound using binaural technology, the source can be placed in any location - right or left, up or down, in the front or in the back [Blau97]. This can be useful when a listener is presented with multiple auditory streams, when information about the positions of events outside of the field of vision is required, or when a listener would benefit from increased immersion in an environment [Dura94]. Current applications of 3-D sound include computer games, videoconference systems, complex supervisory control systems, civil and military aircraft warning systems and computer-user interfaces. More and more, producing 3-D sound is essential to build a virtual environment. In this paper, we review some of the current software tools available for creating the illusion of three-dimensional sounds in virtual environments using binaural technology, and we attempt to evaluate their performance and compare their virtues and shortcomings.

2.0 C++ implementation using HRIRs available from the World Wide Web

To find the sound pressure that an arbitrary source x(t) produces at an ear drum, all that is required is the impulse response h(t) from the source to the ear drum. This is called the Head-Related Impulse Response (HRIR), and its Fourier transform H(f) is called the Head Related Transfer Function (HRTF). The HRTF captures many of the physical cues required for source localization [Bega94]. Once the HRTF is known for the left ear and the right ear, it is possible to synthesize accurate binaural signals from a monaural source. The HRTF is a surprisingly complicated function of four variables: the three space coordinates and the frequency. Systems based on HRTFs are able to produce elevation and range effects as well as azimuth effects [Ming98]. This means that, in principle, they can create the impression of a sound being at any desired 3-D location. In practice, because of person-to-person differences and computational limitations, it is much easier to control azimuth than elevation or range. Nevertheless, HRTF-based systems are fast becoming the standard for advanced 3-D audio interfaces.

A basic and effective spatial audio system is shown in Figure 1, which provides a conceptually simple way to use HRTFs for spatial audio. Basically, it consists of two "convolution engines", each of which can convolve the same audio input stream with a head-related impulse response (HRIR) retrieved from a table of measured values. The outputs of the convolvers go through amplifiers to headphones worn by the listener. The use of headphones eliminates the problem of cross-talk between loudspeakers [Sen97], [Gard98], however it has its own drawbacks such as user fatigue and sounds that sometimes seem to come from inside the head [Bega94]. The first implementation that was tested was thus a simple demo C++ program that convolves an input monaural file with HRIRs and produces a 3D sound stereo output file. The HRIRs that we used in our demo were downloaded from MIT Media Lab web site [Mit]. No attempt to compensate for the response of the headphones or the listener's ear canal was made.

As a whole, the 3D effect of the demo was found to be good. The sound source can be felt moving around the head instead of moving between the two ears. Since no appropriate HRTF transition mechanism (i.e. "crossfading") was added when a sound source was moving from one location to another, 'click' sounds could be heard in the demo.
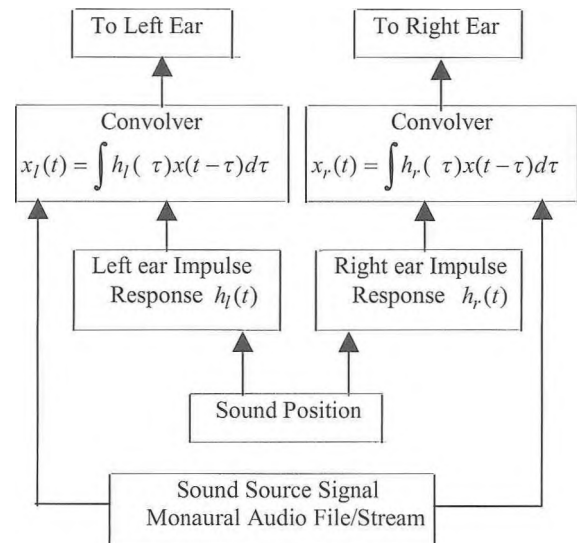
Fig 1. HRTF-Based System

3.0 Real-time Implementation using DirectSound3D™

DirectSound is the wave-audio component of Microsoft's DirectX API [Brad98]. Actually it serves as a middle layer between applications and device drivers, providing numerous sound management capabilities. DirectSound3D (DS3D) is a subset of the DirectSound API calls, that allows for the placement of sounds using a 3-D-coordinate system instead of a simple "left-right" pan. DS3D also automatically calculates things like attenuation due to distance and Doppler shift caused by the relative speed between the listener and the sound source. One demo was implemented to show the functionality of this API. Up to two sounds can be added into the demo, which are represented by two dots in a 2-D plane. The graphical interface of the demo is shown in Figure 2. For each sound source, parameters such as the position, velocity, minimum and maximum distance can be changed individually. The minimum distance is the distance where the volume stops to increase as a listener gets near a sound source, and the maximum distance for a sound source is the distance beyond which the sound does not get any quieter. The user can change the Doppler factor and rolloff factor (i.e. sound attenuation with distance). As in input, the demo uses a Wave monaural sound file. DirectSound3D also provides an additional feature: sound cones. A sound with an amplitude that is the same in all directions at a given distance is called a point source, but in DirectSound3D it is also possible to have sound sources that will only generate sound in a specific region with the shape of a cone.

The 3D sound effect of the DirectSound3D demo was found to be very good, even better than that of the HRTF-based system. Since appropriate crossfading between HRTFs is used by the DirectSound3D API, the 'click' effect which could be heard in the C++ demo of Section 2 was removed.

4.0 Real-time implementation using Java3D™ sound

Java3D is a high-level platform–independent 3-D graphics and sound programming API that can reduce application development time, simplifying all of 3-D graphics and sound programming. A Java3D program creates instances of Java3D objects, which is at least partially assembled from the Java3D class hierarchy, and places them into a scene graph data structure. The scene graph is an

arrangement of 3-D objects in a tree structure that completely specifies the content of a virtual universe, and how it is to be rendered. There are several sound leaf nodes that define the different sounds in a virtual universe [Kevi98]. A BackgroundSound node defines an unattenuated, nonspatialized sound source that has no position or direction. It is useful for playing a mono or stereo music or an ambient sound effect. A PointSound node defines a spatially located sound whose waves radiate uniformly in all directions from some point in space. A piecewise linear curve (defined in terms of pairs consisting of a distance and a gain scale factor) specifies the gain scale factor slope. A ConeSound node object defines a PointSound node whose sound source is directed along a specific vector in space. It is attenuated by gain scale factors and filters based on the angle between the vector from the source to the listener, and the ConeSound's direction vector. There is also a Soundscape node, which defines the attributes that characterize the listener's aural environment, such as gain scale factor, atmospheric rolloff, reverberation, distance frequency filtering and velocity-activated Doppler effect. Multiple Soundscape nodes can be included in a single scene graph.

A simple demo was built to show the functionality of a point sound node in the Java3D API. The point sound source (represented by a color cube), was moved around the listener in the frontal plane. The user could use the mouse or keyboard to navigate in the virtual universe. The 3D sound effect of this implementation was found to be almost as good as the demo of section 3, except that there was a bit more trouble distinguishing above from below.

5.0 Real-time implementation using a sound node in VRML

VRML stands for "Virtual Reality Modeling language". It allows specifying dynamic 3-D scenes through which users can navigate with the help of a VRML browser [Chri97], most of which are plug-ins for Netscape and Internet Explorer. A sound source model in VRML looks like two ellipsoids, one nested inside the other, with the inner ellipsoid sharing a foci with the outer one. The sound source emanates from the shared ellipsoid foci, and goes out in one direction toward the second foci of the outer ellipse. When a listener enters the outer ellipsoid, he/she hears the sound very quietly, and as he/she approaches the inner ellipsoid, the volume increases (the volume drops from the inner ellipsoid to the outside ellipsoid proportionally with the square of distance). Once the listener is inside the inner ellipsoid, the sound becomes ambient, which is to say the volume remains constant, and no 3D effect is computed. No sound is heard outside the outer ellipse.

To compare the sound functionality of VRML with those in Java3D and DirectSound3D, three sound nodes were programmed to move around the listener in horizontal, frontal and median planes, individually. The VRML browser that was used was Internet Explorer™ with the CosmoPlayer™ add-on. The 3D sound effect of the VRML demo was quite good, but the DirectSound3D implementation was slightly better.

6.0 Comparison of implementations and conclusion
Different ways to implement 3-D sounds in virtual environments have been studied through demo building. The 3D sound performance was only measured by a simple subjective listening evaluation, but the 3-D effect of all demos was quite impressive with or without visual cues. There are some obvious implementation differences between the different methods. It is quite complicated and time-consuming to build a HRIR-based system with the C language. But such a system has a high flexibility: extra acoustic characteristics such as echoes and diffraction could be added, and also different sets of HRIRs could be used for each individual to improve the performance. This cannot be done with other techniques. Also the exact spatialization algorithm that is used in the other techniques is unknown. The most interesting aspect of Microsoft DirectSound is that it provides a standard interface for the developers, which is supported by almost all the hardware manufacturers. This is important because software-emulated 3-D sounds are computationally expensive, and DirectSound can provide hardware acceleration. On PCs with audio cards supporting DirectSound acceleration, the host CPU consumption by the 3-D

sound system will thus not be a problem.
The DirectSound3D API can deal with all kinds of input sound files. On the other hand, Java platforms only support the following audio file formats: AIFF, AU and WAV, linear or u-law PCM encoded. But the most attractive aspect of Java3D is that it is an API of Java, which is a platform-independent language. Once it is compiled, it can be run anywhere. Java3D also provides more control on the attributes of the acoustic environment to be rendered, for example with the Soundscape nodes. This is unique among all the techniques tested. Since VRML is just a modeling language used to describe 3-D scenes, it is the easiest way to implement 3-D sounds into a virtual environment. But it has to pay for these advantages with low flexibility and less efficiency. Also the implementation of spatialization in a VRML sound model is browser dependent. So it will be very difficult to allow consistent, reliable, high-quality 3-D audio on all platforms, using VRML. This platform-dependency may be the most serious disadvantage of VRML sound nodes.

To conclude, the best language or implementation tool to integrate 3-D sounds into a virtual environment depends on the application itself. If the efficiency is crucial for your application, DirectSound3D is a good choice, just as many computer game developers did. If your application is required to be platform independent, Java3D may be used instead. But if it is required to reduce the development time to its minimum, VRML is an interesting alternative, since it is the easiest one to use. And do not forget the most important rule of all in 3-D sound implementation: the content is the king.

References

[Bega94] Begault, D. (1994). *3-D Sound for Virtual Reality and Multimedia* Academic Press, Boston, MA, 1994.
[Blau97] Blauert, J. (1997). *Spatial Hearing* 2nd edition MIT Press, Cambridge, MA.
[Brad98] Bargen, B. and Donnelly, T.P. (1998) *Inside DirectX (Microsoft Programming Series)*. Microsoft Press.
[Chri97] Marrin, C. and Campbell, B. (1997) *Teach Yourself VRML 2 in 21 Days*. SAMS Net.
[Dura94] Begault, D.R. and Erbe, T. (1994). "Multichannel Spatial Auditory Display for Speech Communications," *J. Audio Eng. Soc.*, Vol. 42, No. 10, pp. 819 – 826.
[Gard98] Gardner, W.G. (1998). *3-D Audio Using Loudspeakers*, Kluwer Academic, Norwell, MA.
[Kevi98] Sowizral, H., Rushforth, K. and Deering, M. (1998). *Java3D API Specification*. Addison Wesley Longman
[Ming98] Ming Z., Kah-Chye T. and Er M.H., (1998) "Three-dimensional Sound Synthesis Based on Head-Related Transfer Functions," *J. Audio Eng. Soc.*, Vol. 46, No. 10, pp. 836 –844.
[Mit] http://sound.media.mit.edu/KEMAR.html
[Sen97] Sen M.K. and Canfield, G.H. (1997) "Dual-Channel Audio Equalization and Cross-talk Cancellation for 3-D Sound Reproduction," *IEEE Trans.On Consumer Electrics*, Vol. 43, No. 4, pp. 1189 – 1196.
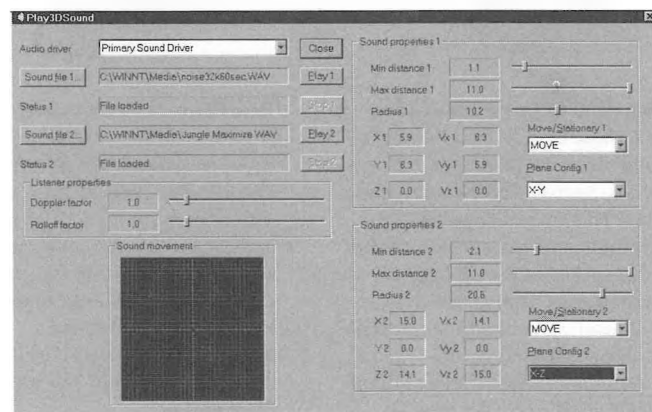
Fig. 2 Demo for the DirectSound API

West Caldwell
Calibration
Laboratories, Inc.
uncompromised calibration

Head Office: 1086 Bloomfield Avenue West Caldwell
New Jersey, 07006, U.S.A.
Phone: (973) 882-4900 Fax: (973) 808-9297

Branch Office: 5200 Dixle Road, Suite 118, Mississauga
Ontario, L4W 1E4, Canada
Phone: (905) 624-3919 Fax: (905) 624-3926

Web Site: www.wccl.com
E-Mail: info@wccl.com

A PRIMARY SOURCE LABORATORY
for Calibration and Repair of
Sound, Vibration, and Electronic Test Instrumentation

SPECIALIZING IN:
- ACCELEROMETERS
- MICROPHONES
- SOUND LEVEL METERS
- VIBRATION METERS

- FIELD CALIBRATORS
- AUDIOMETRIC EQUIPMENT
- VIBRATION TEST EQUIPMENT
- FREQUENCY ANALYZERS

Authorized Calibration and Repair Center for:
- Rion
- Ono-Sokki
- Scantek Inc.

We service equipment Manufactured by:
- ACO Pacific
- Brüel & Kjær
- Endevco
- Fluke
- Hewlett-Packard
- Larson Davis
- Simpson
- and others
(Contact for Details)

OUR AUTOMATED FACILITY ASSURES YOU OF:

CALIBRATION TRACEABLE TO N.I.S.T.
CERTIFICATION: ISO 9002
ACCREDITATION: ANSI/NCSL Z540-1-1994
ISO/IEC GUIDE 25 (1990)
COMPLIANCE MIL-STD-45662A
ISO 10012-0 1992 (E)

SUPER WORKMENSHIP
COMPLETE TEST DOCUMENTATION
QUICK TURNAROUND TIME:
- TWO WEEK TURNAROUND
- 48 HOUR CALIBRATION SERVICE
AVAILABLE FOR ADDITIONAL FEE.

OTHER SERVICES INCLUDE:
- CUSTOM SYSTEM INTEGRATION
- ON-SITE CALIBRATION

SAMPLE OF REPORT & CERTIFICATE:

Accelerometer calibration performed on the
system chosen by the U.S. Air Force [PMEL]

Détermination Expérimentale du Module de Rigidité en Flexion d'une Plaque de Poreux aux Basses Fréquences

B. Brouard, M. Etchessahar, S. Sahraoui

Laboratoire d'Acoustique de l'Université du Maine - UMR CNRS 6613, Av O. Messiaen - 72085 Le Mans Cedex 9 - France

1. INTRODUCTION

La connaissance des constantes viscoélastiques des matériaux poreux sont indispensables pour analyser les vibrations aux basses fréquences et décrire le comportement vibroacoustique des structures comportant des couches poreuses telles que les mousse polymères. Cette étude présente une méthode expérimentale de détermination du module de rigidité en flexion des plaques de ces matériaux qui sont souvent utilisés dans cette configuration. On montre que pour les faibles résistivités au passage de l'air la prise en compte de la nature diphasique de ces matériaux n'est pas nécessaire aux fréquences de résonances obtenues (10-100 Hz).

La propagation des ondes acoustiques dans fun matériau poreux saturé d'air tel que les mousses ou les laines de verres est décrite par la théorie du fluide équivalent où le squelette est supposé immobile (en hautes fréquences) et par le modèle de Biot-Johnson-Allard [1] quand la phase solide se déforme (en basses fréquences). L'étude des propriétés mécaniques de ces matériaux sur le plan expérimental pose de nombreuses difficultés liées à leur nature diphasique et à leur morphologie fibreuse ou cellulaire.

Un banc de mesure des constantes viscoelastiques a été mis en place au laboratoire pour analyser la dépendance fréquentielle [4] des mousses sur des échantillon cubiques. Ces travaux ont mis en évidence leur anisotropie transverse et ont pu dégager les possibilités d'atteindre les constantes élastiques [5].

Dans les applications industrielles (bâtiment et transports en particulier), les matériaux poreux utilisés se présentent sous forme de plaques plus ou moins épaisses travaillant en flexion. Notons que les travaux de Dauchez [2] ont montré le rôle important joué par ces matériaux dans l'amortissement des structures plaque-poreux. Pour ces raisons, la méthode de mesure proposée ici vise à atteindre directement le module de rigidité en flexion. Dans un premier temps on s'intéressera à des plaques suffisament peu résistives au passage de l'air pour négliger les effets de couplages entre les 2 phases. Cette hypothèse est vérifiée numériquement par éléments finis. Dans une deuxième étape, non présentée dans ce papier, nous aborderons le problème plus général incluant ces effets.

2. LES MATÉRIAUX ÉTUDIÉS

L'étude menée ici est concentrée sur les mousses polymères, matériaux souvent utilisés en acoustique. Les matériaux constituant leur structure présentent un comportement viscoélastique. Cela implique que les caractéristiques mécaniques de ces mousses sont complexes et dépendent de la fréquence d'excitation et de la température ambiante. Ainsi le module d'Young d'un matériau poroviscoélastique s'écrit :

$$E*(\omega) = E'(\omega) + jE''(\omega) = E'(\omega)\left[1 + j\eta(\omega)\right]$$

le coefficient de Poisson reste quant à lui réel et indépendant de la fréquence [6] [4]. Le module de rigidité en flexion dépend du module d'Young et du coefficient de Poisson, il s'écrit :

$$D*(\omega) = D'(\omega)\left[1 + j\eta(\omega)\right]$$

3. PROCÉDÉ EXPÉRIMENTAL

La procédure utilisée pour déterminer le module de rigidité en flexion est basée sur la méthode classique des résonances. Les expériences sont faites à température ambiante, celle ci étant constante au cours d'une expérience. Le dispositif expérimental est représenté par la figure de la page suivante

- L'échantillon :

L'échantillon est une plaque de poreux (mousse ou fibreux). Le système de fixation est simple et modulaire, de sorte que des plaques de différentes dimensions peuvent être testées, la taille maximum étant 50x50x6 cm3.

- les conditions aux limites :

L'une des conditions aux limites la plus simple à mettre en oeuvre avec un poreux est l'encastrement, elle peut être réalisée par simple collage avec une colle spéciale pour matériaux polymères. La configuration retenue est encastrée-libre-encastrée-libre.

- l'excitation :

Elle est de type mécanique, elle se fait via un pot vibrant B&K 4810. L'interface pot-échantillon est réalisée par une pastille plastique montée sur une rotule, ceci en gage d'adaptation d'impédance.

- le signal d'excitation :

Le signal envoyé est une séquence MLS de degré 14, échantillonnée à 3000 Hz et composée de 10 périodes ce qui assure un signal d'une durée de 54,61s. Cela permet donc de travailler sur une bande de fréquence 1Hz-1500Hz avec une résolution de 0.18Hz. La génération du signal MLS et son traitement sont contrôlés par un PC. Les séquences MLS ont été choisies pour leurs propriétés remarquables : elles peuvent être facilement traitées par la méthode des corrélations et permettent des mesures très rapides (environ 1 minute par point), répétables avec un excellent rapport Signal sur Bruit.

- les mesures :

Les vitesses sont mesurées à l'aide d'un vibromètre laser en différents points de la plaque, le déplacement bidimensionel de l'appareil étant assuré par un robot. La force est mesurée par une tête d'impédance B&K 8001. Ces deux signaux sont collectés par le PC, celui ci nous restituant les signaux temporels de force et de vitesse à chaque point de mesure.

Les vitesses sont mesurées suivant 15 points. Les modes de résonance sont mis en évidence par le calcul, en chaque point, de la Fonction de Réponse en Fréquence V(f)/F(f) où V(f) et F(f) sont les transformée de Fourier des signaux temporels v(t) et f(t).

4. L'INVERSION

L'inversion utilisée pour calculer le module de rigidité en flexion $D*(\omega)$ est basée sur la théorie des plaques minces monophasiques. Dans un premier temps, les effets inertiels et dissipatifs engendrés par la présence de l'air dans le matériau sont supposés négligeables. La plaque poreuse est alors assimilée à une plaque monophasique de masse volumique équivalente ρ_{equiv} définie par la relation : où ϕ est la porosité et ρ_0 et ρ_1 sont les masses volumiques de l'air et de la matrice constituant le squelette.

$$\rho_{equiv} = (1-\phi)\rho_1 + \phi\rho_0,$$

Dans le cas d'une plaque mince, homogène et isotrope, d'épaisseur h, de module d'Young E et de coefficient de Poisson υ, l'équation du mouvement pour le déplacement transverse w(x,y,t) s'écrit:

$$D*\nabla^4 w + \rho\frac{\partial^2 w}{\partial t^2} = F\delta(x-a)\delta(y-b)e^{j\omega t},$$

où a et b sont les coordonnées du point d'application de l'excitation et où

$$D* = \frac{E*h^3}{12(1-\upsilon^2)}$$

représente le module de rigidité en flexion de la plaque et ρ est sa densité surfacique. On montre que les fréquences propres sont données par [7]:

$$f_{mn} = \frac{\pi \lambda_{mn}}{2a^2} \sqrt{\frac{D'(\omega_{mn})}{\rho}},$$

où D' est la partie réelle de D*(ω) et où λ_{mn} dépend des conditions aux limites.

Le coefficient d'amortissement structural η(ω_{mn}) est calculé à partir de la méthode à -3db.

5. RÉSULTATS-COMMENTAIRES

La plaque de poreux étudiée ici à une épaisseur de 3 cm et des dimensions extérieures de 25 cm suivant l'encastrement et 23 cm suivant le bord libre.
Après inversion les résultats obtenus sont consignés dans le tableau suivant :

Mode	m	n	fmn	D'	η	E'
1	2	0	19.6	0.1106	0.05	44.73
2	2	1	25.2	0.1229	0.04	49.70
3	2	2	36.4	0.0825	0.06	33.36
4	3	0	53.4	0.1081	0.02	43.72
5	3	1	59.0	0.1064	0.04	43.30

Tableau : Résultats obtenus par l'inversion monophasique. fmn est la fréquence modale exprimée en Hz, D' est le module de rigidité en flexion exprimé en N.m, η est le coefficient d'amortissement structural, E' est le module d'Young équivalent calculé à partir de D' exprimé en kPa.

Malgré les hypothèses faites (plaque équivalente monophasique sans cisaillement) les résultats obtenus montrent une bonne tendance. Les modules d'Young équivalents sont groupés, le matériau présente donc une isotropie transverse dans le plan de la plaque. L'erreur commise sur la mesure est encore mal maîtrisée, cela empêche d'observer la croissance d'environ 5% prédite par Mariez [4] sur le module d'Young. L'ordre de grandeur du coefficient d'amortissement est bon mais ce résultat est à prendre avec précautions car les dissipations par effets visqueux et l'action de l'air environnant sur la plaque ne sont pas pris en compte. La résistivité au passage de l'air est un paramètre prépondérant aux basses fréquences. Ainsi, pour les matériaux à plus forte résistivité, l'air peut avoir une influence sur les vibrations de la plaque. A titre d'exemple, une simulation par éléments finis d'une plaque de poreux Encastrée-Libre-Encastrée-Libre a été réalisée.

La variation de la résistivité au passage de l'air a pour conséquence de décaler en fréquence les modes de résonance de la plaque de poreux. Ce décalage reste faible pour les deux premiers modes, mais croîtra avec la fréquence. La dissipation par effets visqueux (voir graphique) prend une part importante de la dissipation totale dès que la résistivité au passage de l'air est supérieure à 10000 Nm4.s. Elle est maximum à proximité des modes, là où la différence de vitesse entre la phase solide et la phase fluide est maximum.
Cette simulation montre que les résultats obtenus à partir de l'inversion monophasique sont justifiés pour les matériaux testés. Cependant, elle montre aussi la nécessité de créer une inversion tenant compte de la nature diphasique de la plaque pour des matériaux ayant une résistivité au passage de l'air supérieure à 10000 Nm4.s.

6. CONCLUSION.

Un processus de mesure des modules de rigidité en flexion D*(ω) d'une plaque de poreux a été développé. Dans un premier temps les résultats obtenus par l'inversion monophasique sont cohérents et

donnent une bonne information sur le module d'Young global de la plaque et sur l'isotropie du matériau. Ces résultats ne sont pour le moment exploitables que pour les matériaux peu résisiitfs. Une inversion plus générale dans laquelle la nature diphasique de la plaque est prise en compte ainsi que l'effet du milieu environnant est en cours de développement.

Références.

[1] ALLARD, J.F. *Propagation of sound in porous media : modeling sound absorbing materials.* Chapman et Hall, Londres, 1993
[2] DAUCHEZ, N. *Etude vibroacoustique des matériaux poreux par éléments finis,* PhD Thesis Université du Maine, Le Mans, 1999.
[3] FERRY, J.D. *Viscoelastic properties of polymers.* John Willey, N.Y. 1961.
[4] MARIEZ, M. AND SAHRAOUI, S. *Elastic constants of polyurethane foam's skeleton for Biot model.* Internoise 96 Liverpool, Royaume Uni 1996
[5] MARIEZ, M. AND SAHRAOUI, S. *Mesurement of mechanical anisotropic properties of acoustic foams* Internoise 96 Liverpool, Royaume Uni 1996
[6] SAHRAOUI, S. AND MARIEZ, M. *Anisotropic elasticity model for acoustic foams* Internoise 97 Budapest, Hongrie 1997
[7] WARBURTON, G.B. *The vibration of rectangular plates* Proc. Inst. Mech. Eng., ser. A, 168(12).371-384, 1954.
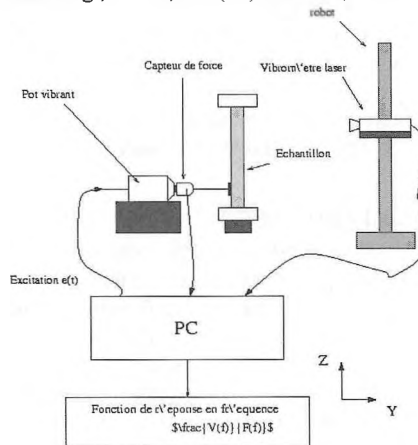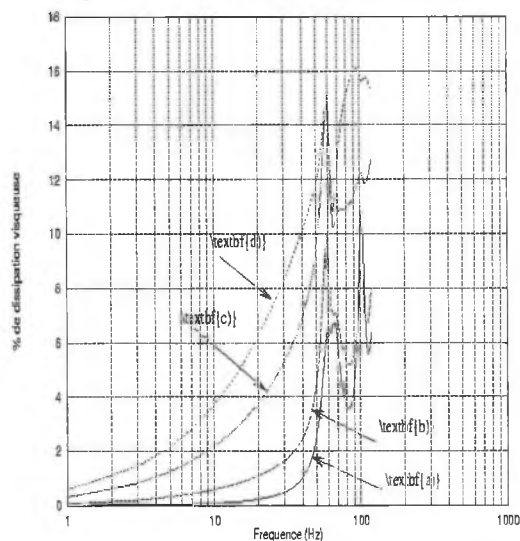
Figure : Vue d'ensemble du banc de mesure

Graphique :Etude numerique du pourcentage de dissipation visqueuse dans une plaque de poreux en fonction de la fréquence pour différentes résistivité au passage de l'air (a): 1000, (b): 10000 (c) : 50000 et (d) : 100000 Nm4.s

Inverse Characterization of the Geometrical Macroscopic Parameters of Porous Materials

Youssef Atalla and Raymond Panneton

GAUS, Mechanical engineering department, Université de Sherbrooke, Sherbrooke QC Canada J1K 2R1

1. Introduction

This paper considers the inverse problem of determining acoustically the geometrical macroscopic parameters (geometrical tortuosity α_∞, viscous Λ and thermal Λ' characteristic lengths) of an open celled porous specimen using a standing wave tube. The unknown parameters can be identified from simple measurements of the normal specific acoustic impedance of the specimen. The inverse characterization scheme is based on the equivalent fluid model in which the solid frame is assumed to be rigid, i.e. motionless. The identification of the parameters is performed over the frequency range [50-2000 Hz]. The test specimen is backed by the rigid impervious end of the tube and held tight on its contour. This set of boundary conditions, especially under acoustical excitations, tends the frame to be motionless.

In the following, a description of the equivalent fluid model is firstly presented. Secondly, the inverse problem strategy is briefly discussed. Thirdly, inverse characterization results on a real porous specimen are given. Finally, to confirm the validity of the approach, numerical predictions using the inversely identified parameters are compared to the measured sound absorption coefficient of the specimen for different thicknesses.

2. Equivalent fluid model

Allard [1] has shown that the acoustic behavior of open celled porous materials can be well described with the use of the Biot theory. When excited by acoustical waves, frames of these materials behave approximately as acoustically rigid (motionless) over a wide range of frequencies [1,2]. For such a case, the porous material can be replaced on a macroscopic scale by an equivalent fluid of effective density and effective bulk modulus occupying a proportion ϕ of the volume of the porous material. In the widely used equivalent fluid model of Johnson-Champoux-Allard[1], these effective quantities depend on five macroscopic parameters of the porous medium: the flow resistivity σ, the porosity ϕ, the tortuosity α_∞, and the viscous Λ and thermal Λ' characteristic lengths.

According to this model, expressions for the and have been suggested [3]:

$$\widetilde{\rho}(\omega) = \rho_0 \alpha_\infty \left(1 + \frac{\sigma\phi}{j\omega\alpha_\infty\rho_0} G_J(\omega) \right) \qquad (1)$$

$$\widetilde{K}(\omega) = \frac{\gamma P_0}{\gamma - (\gamma-1)\left(1 + \frac{H'}{j2\omega} G_{J'}(\omega)\right)^{-1}} \qquad (2)$$

where $G_J(\omega)$ and $G_{J'}(\omega)$ are respectively viscous and thermal correction factors defined as:

$$G_J(\omega) = \left(1 + j\frac{\omega}{H}\right)^{1/2} \qquad (3)$$

$$G_{J'}(\omega) = \left(1 + j\frac{\omega}{H'}\right)^{1/2} \qquad (4)$$

with

$$H = \frac{\sigma^2 \Lambda^2 \phi^2}{4\alpha_\infty^2 \eta \rho_0} \qquad \text{and} \qquad H' = \frac{16\eta}{B^2 \Lambda'^2 \rho_0} \qquad (5)$$

where ω is the angular frequency, ρ_0, η, γ, and B^2 are the density, the dynamic viscosity, the ratio of the specific heats and the Prandtl number of the air. The tilde ($\sim$) indicates that the associated variable is complex-valued and frequency dependent.

For a porous specimen of thickness d, backed by a rigid impervious wall, its specific acoustic surface impedance is:

$$Z_S = -j \frac{Z_c}{\rho_0 c_0} \cot(k\,d)/\phi \qquad (6)$$

where Z_c and k are the characteristic impedance and the complex wave number of the porous specimen, respectively. They are related to the effective properties of the porous medium by:

$$Z_c = (\widetilde{\rho}(\omega)\widetilde{K}(\omega))^{1/2} \qquad (7)$$

$$k = \omega\left(\frac{\widetilde{\rho}(\omega)}{\widetilde{K}(\omega)}\right)^{1/2} \qquad (8)$$

3. Inverse problem strategy

In this work is presented application of an acoustic inverse problem (i.e. acoustic experimental/numerical procedure), for the characterization of the three geometrical macroscopic parameters (α_∞, Λ, Λ') of a porous specimen. The proposed strategy is based on the standing wave tube measurement and on the acoustical model (using Eq. 6) of the specific surface impedance Z_s of the specimen. The presented inverse scheme can be interpreted as a nonlinear optimization problem wherein the cost function is defined as the difference between measured and predicted values of the specific acoustic impedance. Using the nonlinear least squares approach, the cost function to be minimized is defined as:

$$R(\mathbf{a}) = \frac{1}{2} \|F(\mathbf{a})\|_2^2 = \frac{1}{2} \sum_{i=1}^{N} (F_i(\mathbf{a}))^2 \qquad (9)$$

such that, $lb \leq \mathbf{a} \leq ub$ with,

$$F_i(\mathbf{a}) = |Z_{sR}(\dot{u}_i;\mathbf{a}) + j Z_{sI}(\dot{u}_i;\mathbf{a})| - |Z_{iR} + j Z_{iI}| \qquad (10)$$

where lb is the vector of lower bounds, and ub is the vector of upper bounds. Z_{iR} and Z_{iI} are respectively the measured real and imaginary parts of the specific surface impedance at the i-th angular frequency ω_i. $Z_{sR}(\omega_i,\mathbf{a})$ and $Z_{sR}(\omega_i,\mathbf{a})$ are the corresponding numerical prediction at the same angular frequency for the unknown adjusted parametric vector $\mathbf{a} = \{\alpha_\infty, \Lambda, \Lambda'\}^T$.

Eq.10 represents a set of N equations, where N is the number of measured data which is arbitrarily large and only depends on the sampling of the frequency domain.

A number of numerical tests have been performed and the results were used like a prior knowledge of how to set up an adequate statistical optimization algorithm [4] to solve such a difficult

problem in the shortest time. In the second step, the final set up parameters estimation algorithm was applied for evaluation of the geometrical parameters from real experimental data.

4. Application of the inverse strategy

To start the inverse characterization strategy, standing wave tube measurements of the specific surface impedance for three specimens taken from an elastic foam were performed. The specimens were 24.67, 24.70, and 24.73-mm thick, respectively, with a diameter of 99.8-mm. The diameter of the specimens is slightly greater than the diameter of the tube, so that the specimens were held tight to reduce frame motion. The measurements were done with a B&K 4206 impedance tube. Figure 1 reports the results. The results indicate that the foam from which the specimens were taken seems homogeneous in its material properties, at least at the scale of the specimens.

For the three specimens, a direct characterization of the flow resistivity, open porosity, foam density, and elastic properties were done using LCMA facilities [5]. The mean values of these properties are given in Table 1.

Using the inverse characterization strategy, discussed in the previous section, with the acoustical model (Eq. 6) and the measured specific surface impedance (Fig. 1), the three geometrical properties (α_∞, Λ, Λ') are estimated. Their numerical values are given in Table 2 [more details on the algorithm will be presented at the conference].

5. Numerical simulations

To partly verify the validity of the inverse strategy, numerical simulations using the parameters given in Tables 1 and 2 are compared to standing wave tube measurements of the sound absorption coefficient for three different thicknesses of the foam. The numerical simulations are done with MNS/Nova™[6] which is based on the Biot and Johnson-Champoux-Allard models. The rigid-frame limit of the Biot model was used.

Figure 2 presents these comparisons. It is noted that the numerical simulations are in very good agreement with the measured sound absorption coefficients. Since the estimated parameters, based only on the 24.70-mm test specimens (Fig. 1), leads to fine predictions for two other thicknesses, it may be concluded that they are not just "fudge factor" but physical.

Table 1 - Direct measurement of some foam parameters

ϕ	Porosity	0.96
σ	Flow resistivity (Ns/m^4)	4971
ρ_1	Bulk density (kg/m^3)	21.66
E	Young's or elastic modulus (Pa or N/m^2)	46 300
ν	Poisson's ratio	0.37
η	Damping loss factor	0.135

Table 2 - Inverse characterization of the geometrical parameters

α_∞	Geometrical tortuosity	1.25
Λ	Viscous characteristic lengths (10^{-6} m or μm)	105.8
Λ'	Thermal characteristic lengths (10^{-6} m or μm)	339.1
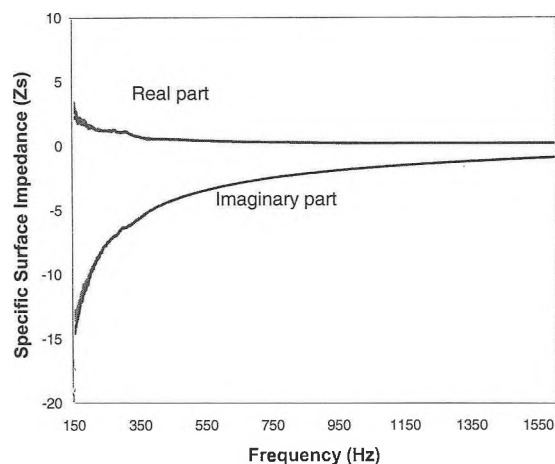
Figure 1 - Standing wave tube measurements of the specific surface impedance for three specimens of the same material. The specimens are 24.67, 24.70, and 24.7-mm thick.
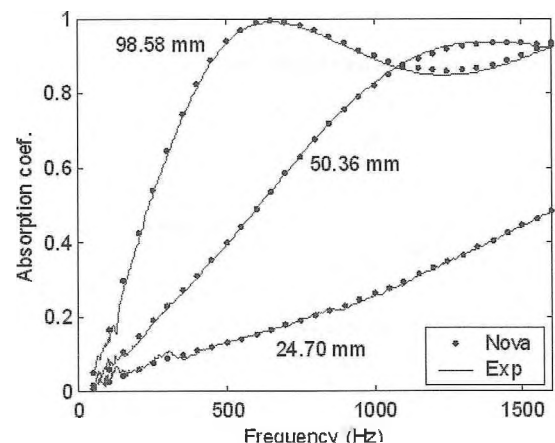
Figure 2 - Comparison between numerical predictions using properties given in Tables 1 and 2 and standing wave tube measurements in terms of sound absorption coefficient for three thicknesses of the tested foam.

6. References

[1] J. F. Allard., Propagation of Sound in Porous Media: Modeling Sound Absorbing Materials (Elsevier Applied Science, New York, 1994).

[2] Bardo. A., Brouard. B., & Allard. J. F., Frame decoupling at low frequencies in thin porous layers saturated by air., J. Apll. Phys. 79-11 (1996).

[3] Y. Champoux., Étude Expérimentale du Comportement Acoustique des Matériaux Poreux à Structure Rigide., Ph.D thesis, Univ. Carleton, Canada (1991).

[4] Bäck, T.,Evolutionary Algorithms in Theory and Practice, (University Press, Oxford, 1995), 314p.

[5] R. Panneton, Acoustic Materials Characterization Lab, SEA Tech-Club 2000, 2nd meeting, Troy, MI.

[6] MNS/Nova™, version 1.0. http://www.mecanum.com

A Method for the Mechanical Characterisation of Poroelastic Materials

Christian Langlois, Raymond Panneton, Noureddine Atalla

Groupe d'Acoustique et vibrations de l'Université de Sherbrooke, Université de Sherbrooke, Sherbrooke, QC Canada, J1K 2R1

1. Introduction

Following theoretical models based on the Biot theory, the solid phase of an isotropic elastic porous material is defined by three vacuum elastic properties: Young's modulus, Poisson's ratio and loss factor. However, under vacuum conditions, closed cells trapped in the materials may burst and change the properties of the material. To prevent this problem and for the sake of simplicity, current techniques based on static or dynamic measurements with compression, shear or torsion tests are performed in air to characterize the elastics properties.

In the classical compression test sketches in figure 1, frequency, boundary conditions, initial strain, and the air saturating the material may affect the transfer function measurement $(F(L)/x_0)$ uses to compute the elastic properties of an open-cell porous material. The objective of this paper is to analyse one of these effects, the boundaries conditions, and to derive by the way a measurement method for the three elastic parameters.

2. Influence of boundaries conditions

For the compression test sketches in figure 1, the shape factor of the porous test specimen is defined by the ratio of its cross-sectional area to the total area of the stress-free surfaces. For sample of large shape factor, the transfer function is strongly dependent on the shape factor if the ends of the sample are bonded. That is, under compression, the sample bulge out as shown in figure 2.

Because the shape factor is related to the geometry of the sample and to the Poisson's ratio, many works have been done with the goal of using it as a secondary effect methods, using two different geometry, to compute both the Poisson's ratio and the Young's modulus [1]. However, it generally led to the development of methods that requires at least one sample of negligible shape factor effect since the appropriate shape factor are not known exactly [2]. These samples are inconvenient since they are long, slim, and then subjected to buckling.

Our investigation with an axisymmetrical poroelastic FEM model showed us that the measured transfer function $(F(L)/x_0)$ may be correlated to the shape factor of the test specimen for different Poisson's coefficients as shown in figure 3. In figure 3, H, $H\infty$ and R are the static () transfer function with boundary conditions effects (N/m), the static transfer function with a zero shape factor (N/m), and the specimen radius (m). These results were obtained using an in-house axisymmetrical poroelastic FEM code.

3. Measurement method

The method proposed here is to first offset the dynamic transfer function measurement $(H(\omega))$ to a static value with an analytical relation. This yields the static transfer function H. Using figure 3, a relation between the transfer function H, the Poisson's ν, and the L/R ratio can be drawn:

$$\frac{H_i L_i}{EA_i} = G_i\left(\frac{L_i}{R_i}, \nu\right) \tag{1}$$
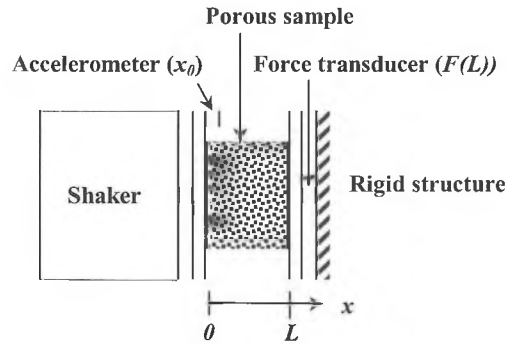
Fig. 1 - Sketch of the vibration transmissibility test

where i simply refers to a specific test specimen, G is a curve fit relation established from the FEM results (figure 3), and A is the surface area (m^2) of the sample. For two specimens of different L/R ratios taken from the same material, since both have the same Young's modulus, it is then possible to write the following relation:

$$\frac{H_1 L_1}{G_1\left(\frac{L_1}{R_1}, \nu\right) A_1} - \frac{H_2 L_2}{G_2\left(\frac{L_2}{R_2}, \nu\right) A_2} = 0 \tag{2}$$

Solving the latter equation for ν is a simple matter using any kind of minimisation algorithm. The solution for ν can then be used in relation (1) to compute the Young's modulus.

In applying this procedure, one then makes the assumption that boundary conditions and frequency have independent effects in the frequency range of measurements. This holds true if measurements are taken well above the first resonance. Another important assumption is that the saturating air does not influence the measurements. As stated by Mariez *et al* [4], this is true at relatively low frequencies. The same assumptions are also valid for the loss factor.

Because the Young's modulus was considered as a real algebraic value until this point, the damping factor is then simply the ratio of the imaginary part to the real part of any transfer function used for the computation.
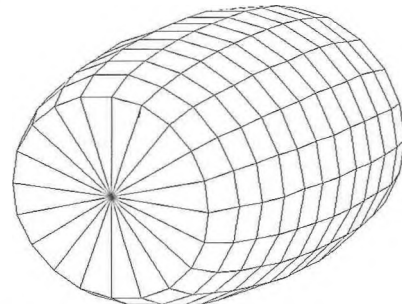
Fig. 2 - Representation of the bulge out effect of the specimen under compression test with bonded ends.
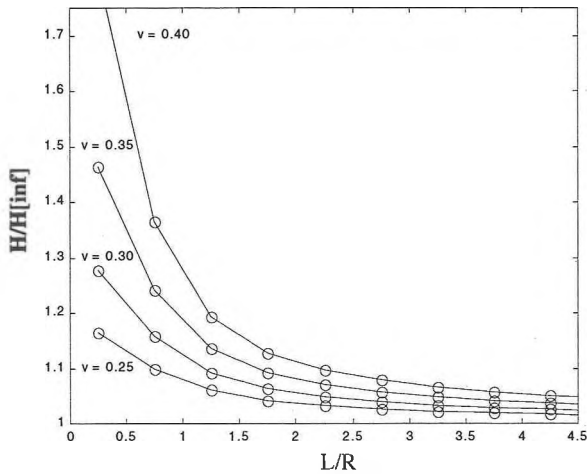
Fig. 3 - Correlation between the transfer function and the L/R ratio for a specimen under the compression test with bonded ends

4. Results

To partly verify the validity of the method, numerical simulations using the parameters given in Tables 1 and 2 are compared to standing wave tube measurements of the sound absorption coefficient for a 54.4-mm thick foam specimen. The numerical simulations are done with software MNS/Nova™ [5] which is based on the Biot and Johnson-Champoux-Allard models [3,6]. Both rigid-frame and elastic-frame models are used. For the elastic-frame model, sliding edge conditions are used.

Figure 4 presents the comparisons. It is noted that the numerical simulations are in good agreement with the measured sound absorption coefficients. The simulation using a rigid-frame approximation does not show the frame resonance of the foam backed on the rigid wall. In this case, the use of the elastic-frame model gives better predictions.

The discrepancies between the elastic-frame prediction and the measurement may be due to the additional friction loss between the specimen contour and the tube. Also, the numerical sliding edge boundary conditions are not a perfect representation of the experimental one. The experimental one is something between bonded edge and sliding edge.

Table 1 - Foam parameters measured with LCMA/GAUS facilities

ϕ	Porosity	0.960
σ	Flow resistivity (Ns/m^4)	49 541
α_∞	Geometrical tortuosity	3.82
Λ	Viscous characteristic lengths (10^{-6} m or μm)	65.4
Λ'	Thermal characteristic lengths (10^{-6} m or μm)	141.0
ρ_1	Bulk density (kg/m³)	47.45

Table 2 - Elastic properties measured with the proposed method

E	Young's or elastic modulus (Pa or N/m²)	337 300
ν	Poisson's ratio	0.15
η	Damping loss factor	0.135
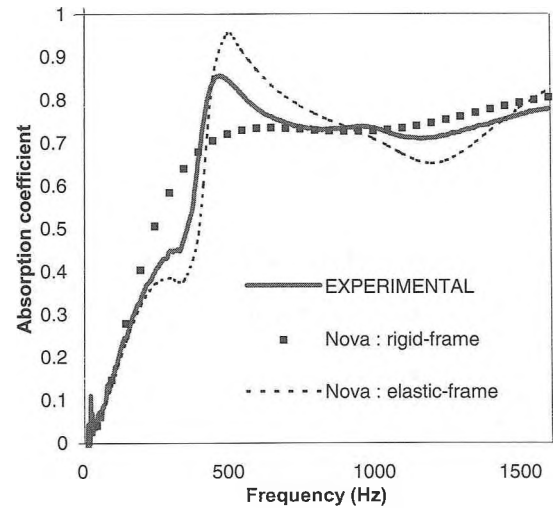
Fig. 4 - Experimental results used to explore the validity of the proposed method

5. Acknowledgments

6. References

[1] Pritz, T., Measurement methods of complex Poisson's ratio of viscoelastic materials, Applied Acoustics **60**, p. 279-292

[2] Sim, S. & Kim, K-J, A method to determine the complex modulus and Poisson's ratio of viscoelastic materials for FEM applications, Journal of Sound and Vibration (1990) **141**(1), p.71-82.

[3] N. Atalla and R. Panneton, A mixed displacement-pressure formulation for poroelastic materials, J. Acoust. Soc. Am. **104**, p. 1444-1452.

[4] Mariez *et al*, Elastic constants of polyurethane foam's skeleton for Biot model, Proceedings of Internoise 96, p.951.

[5] MNS/Nova™, version 1.0. http://www.mecanum.com

[6] R. Panneton, Modélisation numérique 3D par éléments finis des milieux poroélastiques, Ph.D. thesis, Univ. Sherbrooke, Qc Canada (1996).

CHARACTERIZATION OF MULTI-LAYERED PANELS MECHANICAL PROPERTIES

I. Sow, O. Beslin, and J. Nicolas

GAUS, Département de génie mécanique, Université de Sherbrooke, Sherbrooke, Québec, J1K 2R1

INTRODUCTION

With the advancement of science and technology, materials with high damping capabilities and high modulus of elasticity are increasingly popular as they reduce vibration and noise. However, most of the time, there is a lack of tools that allow quick and easy characterization of the effective materials properties when used in 2D structures. Usually, prediction is made using Finite Element Method (FEM) and in most cases, these FEM codes require input data that cannot be easily obtained. This is particularly true when the material is a "home made" composite sandwich material (glass fibers with polyester resin, etc.), in a procedure that cannot ensure a rigorous control on thickness, density, etc. This paper presents a method which uses a simple experimental setup (clamped at the corners) and a fast numerical code running on a personal computer. It allows extraction of equivalent properties of small rectangular composite panels in terms of "young modulus", "density" and "damping factor" versus frequency. A dedicated numerical code (based on hierarchical finite element method) is used to fit parameters in order to match measured and simulated data. It is shown that this method allows to quickly extract useful equivalent properties for composite materials.

1 - HIERARCHICAL FINITE ELEMENT FORMULATION

The simulation part of this hybrid method is based on the hierarchical finite element formulation [1,2] of a rectangular Love-Kirchoff plate. The normal displacement of the plate is given by:

$$w(\xi,\eta)=\sum_{r=1}^{p}\sum_{s=1}^{p}q_{rs}Q_r(\xi)Q_s(\eta),$$

where ξ and η are defined such that $x = \dfrac{(1+\xi)a}{2}$ and $y = \dfrac{(1+\eta)b}{2}$

a and b are the length and width of the plate.

The $\{Qr\}$ basis functions set is presented in fig.1.

Function order	Equation	Hybrid set $Q_r(\xi)$
r=1	$Q_1(\xi)=\frac{1}{2}-\frac{3}{4}\xi+\frac{1}{4}\xi^3$	
r=2	$Q_2(\xi)=\frac{1}{8}-\frac{1}{8}\xi-\frac{1}{8}\xi^2+\frac{1}{8}\xi^3$	
r=3	$Q_3(\xi)=\frac{1}{2}+\frac{3}{4}\xi-\frac{1}{4}\xi^3$	
r=4	$Q_4(\xi)=-\frac{1}{8}-\frac{1}{8}\xi+\frac{1}{8}\xi^2+\frac{1}{8}\xi^3$	
r>4 For example here r=10	$Q_{10}(\xi)=\sin(3\pi\xi+3\pi)\sin(5\pi\xi+5\pi)$	

Fig. 1 Hierarchical Hybrib Basis Functions Set

This basis functions set is built from polynomial functions [1] for the first four functions and from trigonometric functions [2] for the rest. This functions set allows to easily define cinematic boundary conditions (free, simply supported, clamped, rigid point) on each edge and on each corner of the plate, simply by removing appropriate functions from the complete set.

2 - VALIDATION OF THE FORMULATION

Validation of the formulation is obtained by comparing the developed code results to those of well known codes.
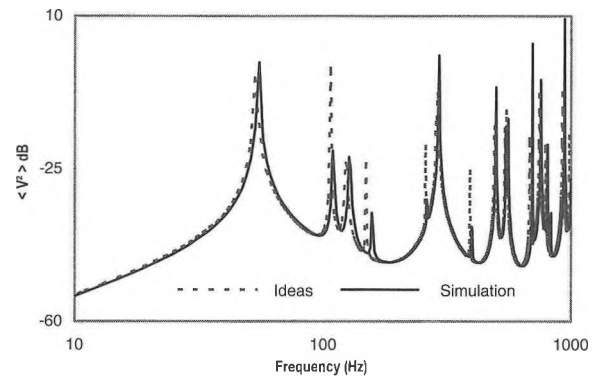
Fig. 2 $<V^2>$ of an Aluminum plate: Ideas versus Simulation

Figure 2 shows a comparison of the developed code and **SDRC-IDEAS Vibroacoustics** results (mean quadratic velocity of a plate excited by a shaker) in the case of a "Four corners pin clamped" case (see figure 4) for an Aluminum plate. This figure shows that the boundary conditions are well mastered by the developed code. Figure 3 shows a comparison of the developed code and **MNS/ADNR**[1] results in the case of a "simply supported plate" case for a viscoelastic plate (Young modulus and damping factor are frequency dependent). This figure shows that the developed code allows to efficiently simulate viscoelastic plates.
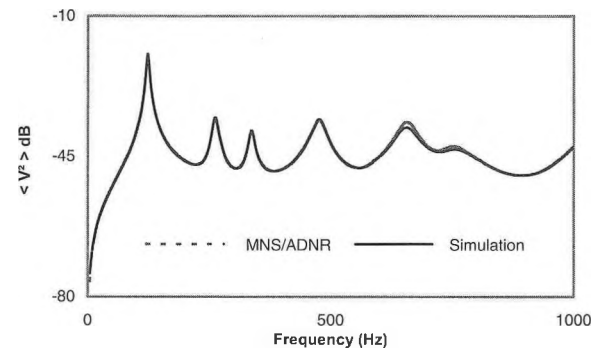
Fig. 3 $<V^2>$ of a Viscoelastic plate: ADNR versus Simulation

3 - EXPERIMENTAL SETUP

The measurement part of this hybrid method consist on a clamp fixture presented in figure 5 which allows to set "Four corners pin clamped" boundary conditions. This type of fixture has two advantages: (*i*) Easy mounting set-up (*ii*) Low vibration energy losses at the boundaries, allowing a better characterization of the intrinsic panel damping. The plate is excited by an electro-dynamic shaker and its mean quadratic velocity is measured using a scanning laser vibrometer coupled to a PC.
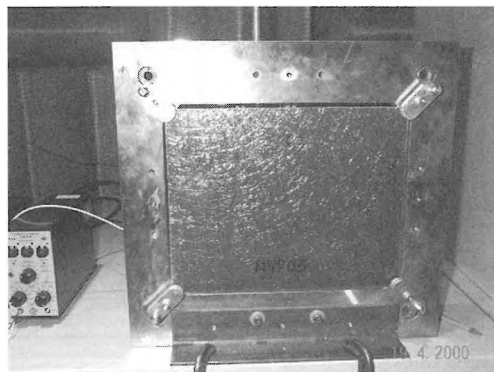
Fig. 5 Plate fixture with "Four corners clamped"

4 - VALIDATION OF THE EXPERIMENTAL SETUP
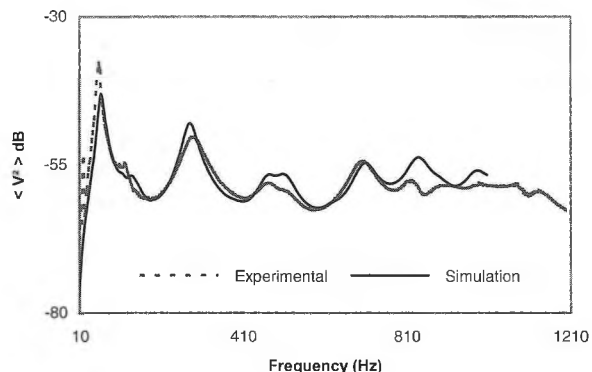
Fig. 6 $<V^2>$ of a Multi-layered Viscoelastic plate:
Experimental versus Simulation

Figure 6 shows the comparison of experimental measurements versus theoretical prediction using the developed code. Good agreement is found between experimental and numerical results for the Multi-layered Viscoelastic Panel. For the case shown, the Multi-layered Panel consists of a layer of 3M ISD112 between two steel panels.

5 - EXPLOITATION OF THE METHOD

As example of exploitation of this hybrid method, after extracting equivalent properties in terms of Young modulus and damping factor, an untreated Glass Fiber Reinforced Plastic (GFRP) composite panel is compared to a GFRP containing a layer of 3M ISD112 and to a panel of Glass Fibers embedded in viscoelastic resin (figure 7 panels 4 mm thick).
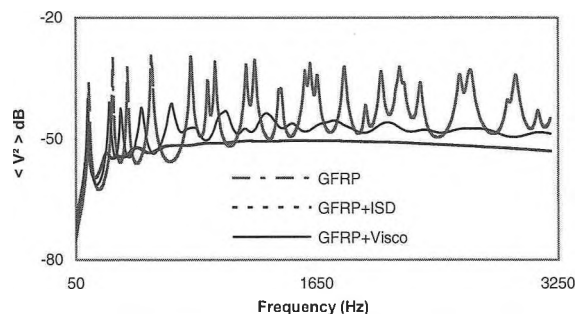
Fig. 7 Results for 4 mm Thick Composite Panels

Hence, the Hybrid method allows extraction of the properties of each 4 mm panel by fitting experimental results. The global attenuation with respect of the reference panel (GFRP) is 11.0 dB for the GFRP with 3M ISD112 panel and 6.8 dB for the GFRP with BF Goodrich VTBN panel. Although the constrained panel exhibits the highest damping level, the integrated viscoelastic panel should not be ruled out as it shows a good damping level with less manufacturing costs.

Parametric study can also be performed and figure 8 presents another exploitation of the hybrid method by implementing the extracted equivalent properties in the developed code while changing the thickness of the plate (panels 6 mm thick).
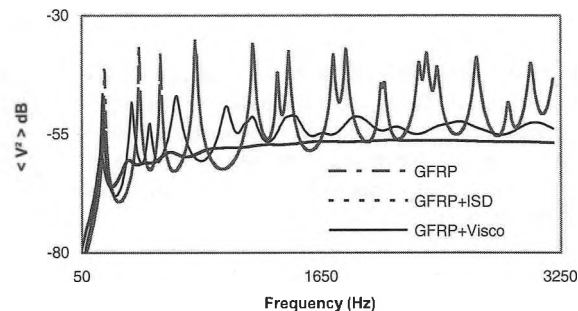
Fig. 8 Simulation Results for 6 mm Thick Composite Panels

Global attenuation is now respectively 9.6 dB and 6.4 dB for the constrained panel and the integrated viscoelastic panel.

6 - CONCLUSION & PERSPECTIVES

This proposed hybrid method allows to quickly extract equivalent properties of unknown materials in order to obtain input data for finite element code and to help design. The fitted results presented in this paper have been manually fitted. The authors are presently studying an automatic fitting procedure.

REFERENCES

[1] **N. S. Bardell**, Free vibration analysis of a flat plate using the hierarchical finite element method, Journal of sound and vibration, 151, 263-289, 1991

[2] **O. Beslin, J. Nicolas**, A hierarchical functions set for predicting very high order plate bending modes with any boundary conditions, Journal of sound and vibration, 202 (5), 633-655, 1997

ERRORS AND UNCERTAINTIES OF CLASSICAL STANDING WAVE TUBE METHODS: SWR, TMTC AND TMTM

Benoit **Lanctot**, Raymond **Panneton**, and Noureddine **Atalla**
GAUS, Mechanical engineering department, Université de Sherbrooke, Sherbrooke QC Canada J1K 2R1.

1. Introduction

For the past decades, several methods based on the standing wave tube have been developed to characterize the acoustical properties (surface impedance, reflection coefficient, sound absorption coefficient) of sound absorbing materials. Due to their respective sensitivity to measurement errors, results obtained by the methods may diverge from one to another. Moreover, during measurements, two basic types of error occur: (i) random error and (ii) systematic error. Usually, the precision of a method is characterized by the repeatability of the method, but doing so, only random errors are taken into account. Methods having low random errors will then be considered more precise than they really are. In view of comparing the precision and identifying the most sensitive parameters regarding the experimental procedure and set-up, a detailed analysis on three classical standing wave tube methods is presented. The studied methods are "Standard Wave Ratio" (SWR) [1], "Two Microphone Three Calibration Method" (TMTC) [2], and "Two-Microphone Transfer Method" (TMTM) [3].

2. Methodology

A differential formulation is used to evaluate the errors and uncertainties on each of the standing wave tube methods [4,5]. As input to the formulation, sound pressure measurements and uncertainties on the experimental setup are required. To operate, each method needs a dedicated experimental setup [1,2,3] and sound pressure measurements at specific locations.

For the sake of simplicity and to avoid going into heavy experimental setups and procedures, a numerical model for each of the 3 methods is used to simulate the required sound pressures. In the simulations, the porous test sample is modeled as an equivalent fluid using the Johnson-Champoux-Allard model [6]. Also, attenuation in the tube and variations of the atmospheric pressure and temperature are taken into account in the modeling.

The different parameters, for which measurement errors may affect the accuracy of the standing wave tube methods, are: the temperature, the atmospheric pressure, the tube diameter, the test sample thickness, the length(s) of the air cavity(ies), and the position and response of the microphones

3. Results

In order to see the influence of the measurement errors on the acoustical indicators computed by each method, a detailed investigation of parameters uncertainties is performed. Preliminary results are shown in figures 1 to 3. These results are obtained for the 25-mm thick polyamide foam described in Table 1, and for the uncertainties given in Table 2. For a better comparison between the three methods, their respective optimal tube lengths and microphone positions are used.

Table 1 - Properties of the porous used in the preliminary results

ϕ	σ Ns/m^4	α_∞	Λ (μm)	Λ' (μm)
0.99	19163	1.6	65	130

Table 2 - Uncertainties used in the preliminary results

Parameters	Uncertainties ($\pm$)
Temperature	0,3° C
Pressure	0,1 kPa
Tube diameter	0,1 mm
Test sample thickness	0,5 mm
Cavities lengths	0,1 mm
Microphones position	0,1 mm
Microphones position	SWR Max (1,5° wavelength, 0,1 mm)
Microphones amplitude responses	0,2%
Microphones phase responses	0,2°

In figures 1 to 3, three types of comparison are done. Figure 1 shows a comparison of the methods' error which is defined as the difference between the theoretical value [6] and the values obtained by the methods. Figure 2 shows a comparison of the methods' uncertainty which is due to measurement uncertainties (table 2). Figure 3 shows a comparison of methods' maximal error which take into account the both uncertainty and error on the methods.

4. References

[1] ANSI\ASTM C384-77 (1997). "Standard test method for impedance and absorption of acoustical material by the tube method", revised 1977.

[2] Gibait, V and Laoë, F. (1990). "Acoustical impedance measurements by the Two-Microphone-Three-Calibration (T.M.T.C.) method", J. Acoust. Soc. Am. 88, 2533-2545.

[3] Chung, J. Y. and Blaser D. A. (1980). "Transfer function method of measuring in-duct acoustic properties", J. Acoust. Soc. Am. 68, 907-921.

[4] Peng, C., Morrey, D., and Sanders, P. (1998). "The measurement of low frequency impedance using an impedance tube", J. of Low Frequency Noise Vibration and Active Control, 17(1), p.1.

[5] Beckwith, T.G and Marangoni, R.D. (1990). *Mechanical measurements* (Fourth edition, Addison-Wesley Publishing Company inc).

[6] Allard, J.-F. (1993). *Propagation of sound in porous media: modelling sound absorbing materials* (Elsevier Applied Science, London).

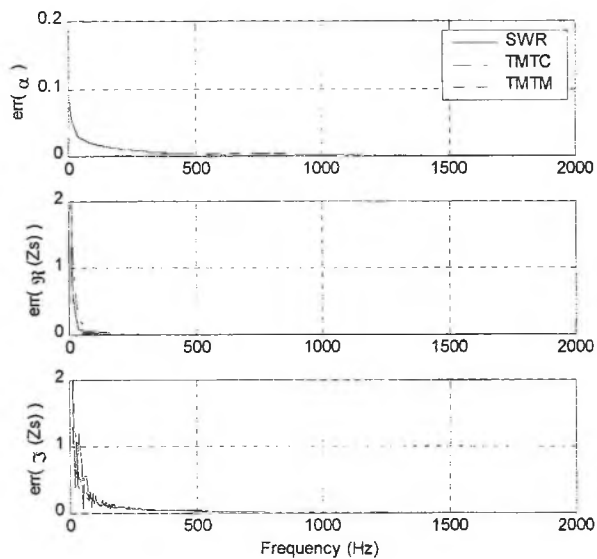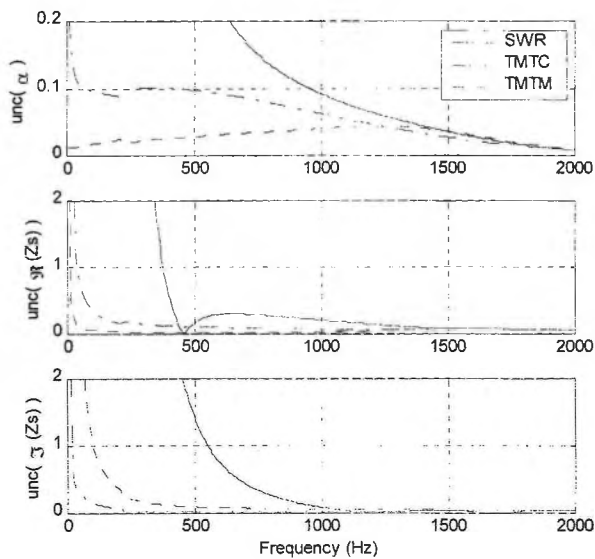*Figure 1 - Comparison of the methods' error.*
Preliminary results

Figure 2 - Comparison of the methods' uncertainty.
Preliminary results
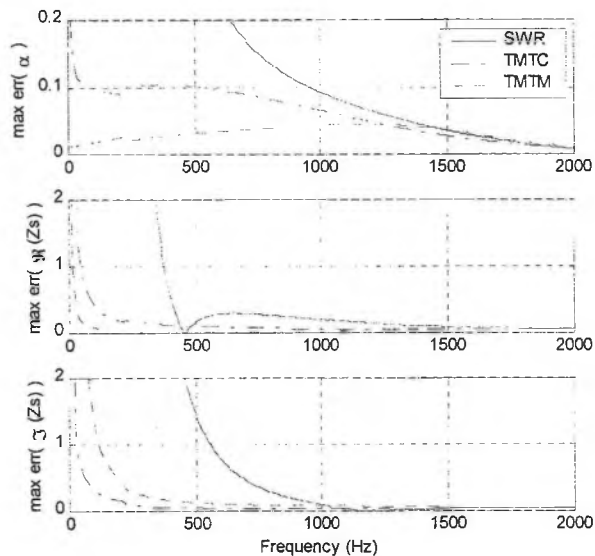
Figure 3 - Comparison of the methods' maximal error.
Preliminary results.

Dynamic Behaviors and Absorption of Double Porosity Media

X. Olny, C. Boutin

Ecole Nationale des Travaux Publics de L'Etat, Département Génie Civil et Bâtiment, URA CNRS 1652, VAULX-EN-VELIN, 69518
CEDEX

1. Introduction

Porous media, used as passive absorbers, are usually considered as single porosity material. Their macroscopic properties (dynamic permeability and compressibility) can be deduced from the knowledge of one elementary representative volume (ERV), defined at the microscopic scale.

Physics and absorption properties of double porosity media can be significantly different, because two interconnected networks of very different sizes, and then permeabilities coexist in the system.

In this paper we clarify the coupling effects that occurred in these systems according to the contrast of static permeability in the two fluid networks.

Two macroscopic descriptions are proposed and compared to experimental measurements performed on artificial double porosity media. Then, the advantages of such systems are underlined.

2. Theory

A double porosity medium can be seen as a porous medium with a micro-porous solid skeleton. Then, three scales are necessary to describe the material (Fig. 1): the **macroscale** for which the medium appears to be homogeneous. The wavelength in the material allow to estimate this scale. The **mesoscale** is defined from the pores and microporous domains, and is characterized by the size l_p. Last, the **microscale** is related to the micropores and the solid skeleton (assumed rigid), and is characterized by the size l_m.
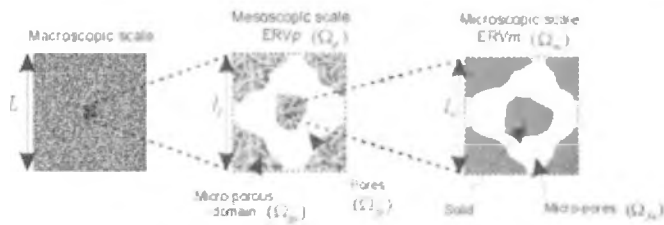
Fig.1   The three scales in double porosity media

The dynamic behaviors of such a system can be successfully worked out using the rigorous homogenization technique of multi-scales periodic media [1]. In that way, the first step consists in understanding the consequences of the double separation of scales and estimating parameters, and couplings, governing waves propagation in the medium.

Two main behaviors, depending on the contrast of static permeability between the pores and the micropores, can be identified [2][3], and are now briefly described.

Assuming that waves propagation in the pores is not strongly affected by the presence of the micropores, the wavelength (neglecting thermal effects) in the material can be estimated by the one in the pores. Using asymptotic developments at low and high frequencies, it comes :

$$|\lambda_p| = O(2\pi l_p \sqrt{P_0/\omega\eta}) \qquad \text{for } \omega << \omega_{vp} \qquad (1)$$

$$|\lambda_p| = O(2\pi\sqrt{P_0/\rho_0}/\omega) \qquad \text{for } \omega >> \omega_{vp} \qquad (2)$$

with ω_{vp} ($O(\eta/\rho_0 l_p^2)$), the viscous frequencies in the pores. P_0, η, and ρ_0 are respectively the static pressure, the viscosity and the density of air.

An analog estimation can be obtain for the wavelength in the micropores (subscript p replaced by m).

These estimations are very important in order to predict the variation range of the pressure in the fluid networks ($O(|\lambda|/2\pi)$), and the ratio between local velocities.

Case 1: low permeability contrast

In this case, the difference between l_p, and l_m is small enough so that ($|\lambda_p|/2\pi$), and ($|\lambda_m|/2\pi$) are always greater than l_p, the characteristic size of the "meso-heterogeneities". Then, it can be shown that the pressure is uniform in the double porosity system, meaning that it varies at the macroscopic scale (x space variable). It results a **total coupling** of the pores and the micropores in terms of compressibility, and permeability when the frequency is greater than ω_{vm}. General macroscopic equations obtained in this case are:

Compressibility : $$j\omega\left(\frac{1}{K_p(\omega)} + \frac{1-\phi_p}{K_m(\omega)}\right)p(x) + \vec{\nabla}_x.\vec{v}_{db} = 0 \qquad (3)$$

Dynamic flow : $$\vec{v}_{db} = -\frac{\Pi_{db}(\omega)}{\eta}\vec{\nabla}_x p(x) \qquad (4)$$

In these equations, acoustical variables are the first terms of the asymptotic developments used in the homogenization process. Eq. (3) shows clearly how the equivalent compressibility of the system can be simply expressed by means of K_p and K_m, respectively the equivalent bulk modulus of the porous medium (without micro-porosity), and of the microporous material. ϕ_p is the porosity of the network of pores.

Regarding the macroscopic dynamic flow (4), we showed that it can be written in the form of a "dynamic Darcy law". The equivalent permeability Π_{db} depends on the microporous medium dynamic equivalent permeability (Π_m), and on the meso-structure. Analytic expressions can be found for simple meso-structures.

Case 2: strong permeability contrast [4]

Now, it is supposed that the characteristic size l_m is small enough, so that the $|\lambda_m|/2\pi$ can be of the same order as l_p. $|\lambda_p|$

being large compared to $|\lambda_m|$. This situation can only be raised if waves are diffusive in the micropores (below ω_{vm}). This involves that pressure in the microporous domain varies at the mesoscale (space variable y) and we have:

$$\Delta_y p_m(x, y) - \frac{j}{\omega} \frac{\phi_m}{P_0} \frac{\Pi_m(0)}{\eta} p_m(x, y) = 0 \quad \text{in } \Omega_{xp} \tag{5}$$

$\Pi_m(0)$ is the intrinsic static permeability of the microporous medium. Equation (5) is bounded by the macroscopic pressure field in the pores $(p_p(x))$. The problem is analog to the thermal diffusion problem in porous media and show that p_m is linearly related to p_p. The phenomenon raises a new characteristic frequency $(\omega_d = P_0 \eta / \phi_m \Pi_m(0))$. Moreover, the average pressure in the microporous structure can be written in the form:

$$\langle p_m \rangle = F(\omega / \omega_d) p_p \tag{6}$$

where F, complex, denotes the **partial coupling** between pores and micropores. Its modulus varies between 1, and 0 from low to high frequencies. It only depends on the meso-geometry, and can be expressed with simple semi-phenomenological functions [3] for general descriptions.

Finally, the macroscopic mass equation giving the equivalent compressibility (with thermal effects) of the system is:

$$j\omega \left(\frac{1}{K_p(\omega)} + \frac{1 - \phi_p}{K_m(\omega)} F(\frac{\omega}{\omega_d} \frac{P_0}{\phi_m K_m}) \right) p(x) + \vec{\nabla}_x . \vec{v}_{db} = 0 \tag{7}$$

Regarding the macroscopic permeability, it is given, in this case, by the equivalent permeability of the porous medium (without microporosity), flow in the micropores being negligible at the first order.

3. Experimental results and discussion

Artificial double porosity materials have been built by perforating (pores network) microporous rock wool panels (5.75 cm thick.). The cylindrical holes are circular (radius R) and placed in square lattice, perpendicular to the panels' faces (Fig.2). This configuration allows to determine a maximum of parameters for the model and the material is easy to realize.
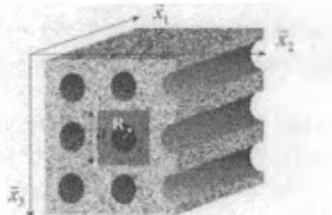
Fig.2   Perforated microporous panel

Measurements have been made using standing waves tubes, in the direction of perforations. The rock wool material have been chosen for is high resistivity ($\sigma = 135000 \, \text{Nm}^{-4}\text{s}^{-1}$) with the aim to observe pressure diffusion effects. First, results show that the "total coupling" model is not able to describe the absorption coefficient of the double porosity medium (Fig.3). However, a good agreement can be obtained with the "partial coupling" model, what demonstrates that pressure is not uniform in the system at the mesoscale. This phenomenon brings additional dissipation, and the absorption of the initial rock wool panels is greatly improved on a wide range of frequencies by creating a second network of pores. It is to be noticed, that for this low additional porosity (ϕ_p=13%), taking flow in the microporous medium into account improves the

agreement with measurements. In this case, a simple and exact expression can be found for the equivalent dynamic permeability in the perforations direction:

$$\Pi_{db}(\omega) = (1 - \phi_p) \Pi_m(\omega) + \phi_p \frac{\eta}{j\omega\rho_0} \tag{8}$$

In this last equation, viscous dissipation is neglected in the perforations, considering their size. A second series of measurements (Fig.4) have been performed on the same material, with smaller perforations, in order to modify ϕ_p. The results show how the performances of the material can be easily adjusted to obtain low frequencies efficient materials.
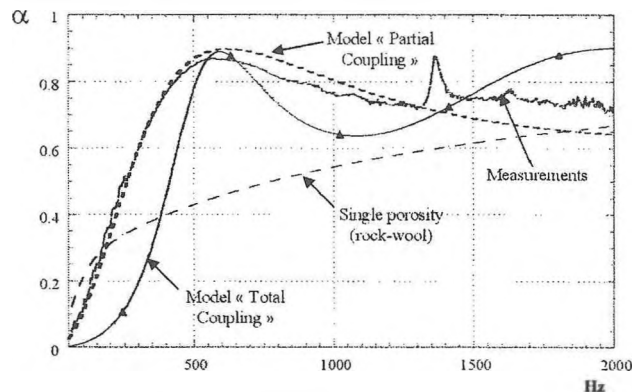
Fig.3   Absorption coefficient of perforated porous panel
(R=1.73cm, $\phi_p = 13\%$)
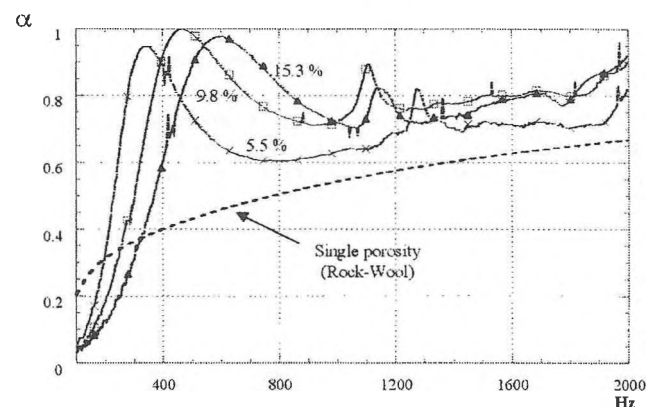
Fig.4   Absorption coefficients of perforated porous panel
(R=0.38cm) for different ϕ_p

4. References

[1] **Auriault, J. L. et Boutin, C.** Deformable porous media with double porosity III : Acoustics. *Transport in Porous Media*, 1994, vol. 14, p. 143-162.
[2] **Boutin, C. et Olny, X.** Diversity of interscale couplings. The case of acoustics of multiporosity media. In *Mechanics of Heterogeneous Materials, Grenoble, 1999*. vol p. 27-34
[3] **Olny, X.** Absorption acoustique des milieux poreux à simple et double porosité. Modélisation et validation expérimentale. PHD Thesis – INSA Lyon, 1999. 281p.
[4] **Boutin, C., Royer, P. et Auriault, J. L.** Acoustic absorption of porous surfacing with dual porosity. *Int. J. Solids Structures*, 1998, vol. 35, n° 34-35, p. 4709-4737.

Acoustic Absorption Of Non-Homogeneous Poro-Elastic Materials

Celse K. Amédin[1], Noureddine Atalla[1] et Franck Sgard[2]

1. GAUS, Département de Génie Mécanique, Université de Sherbrook, Sherbrooke, QC, Canada, J1K 2R1

2. Laboratoire des Sciences de l'Habitat, DGCB URA CNRS 1652, Ecole Nationale des Travaux Publics de l'Etat, 69518 Vaux-enVelin Cedex, France

1. Introduction

Porous materials offer a poor acoustic absorption performance at low frequencies. A way to improve the sound absorption of these materials is to investigate 3-D complex configurations with the finite elements method. The main objective of this paper is to propose an accurate model to evaluate the acoustic absorption performance of configurations consisting of a non-homogeneous porous material, made up from porous-elastic patches, bonded onto the hard termination of a semi-infinite rectangular wave-guide. Each patch is correctly described in the context of the Biot theory [1], and the coupling between the porous material and the wave-guide is accounted for explicitly using the modal behavior of the wave-guide. A power balance approach is then used to evaluate the performance of the porous material in terms of its absorption coefficient.

2. Theoretical background

The finite element model associated to the porous-elastic media is based on the mixed displacement-pressure (u, p) formulation of Biot's poro-elasticity equations [2]. A modified weak integral form of these equations has the advantage to depict the boundary terms in a suitable form for the application of the coupling conditions with other media [3]. In this weak integral form, the boundary conditions terms of the porous media are:

$$\int_{\delta\Omega_p} (\underline{\underline{\tilde{\sigma}}}'(\underline{u}) \cdot \underline{n}) \cdot \delta\underline{u}\, dS + \int_{\delta\Omega_p} h(U_n - u_n)\, \delta p\, dS$$

where $\delta\Omega_p$ refers to the boundary surface of the porous-elastic domain Ω_p, $\underline{u}$ and p are the solid phase displacement vector and the interstitial pressure of the porous-elastic medium, respectively; $\delta\underline{u}$ and δp refer to their admissible variation, respectively; $\underline{n}$ denotes the unit normal vector external to the bounding surface; $\underline{\underline{\tilde{\sigma}}}'$ is the total stress tensor of the material; U_n and u_n refer to the normal component of the solid and fluid macroscopic displacement vectors, respectively, and h stands for the porosity of the material.

Using the modal behavior of the wave-guide, these boundary coupling conditions between the porous-elastic material and the wave guide can be expressed in terms of a classic coupling matrix, a radiation admittance and a blocked-pressure loading [4].

With a particular choice of admissible functions, the weak integral form provides the following power balance equation:

$$\Pi_{elas}^s + \Pi_{iner}^s + \Pi_{elas}^f + \Pi_{iner}^f + \Pi_{coup}^{fs} + \Pi_{exc}^f = 0$$

where Π_{elas}^s, Π_{iner}^s represent the power developed by the internal and inertia forces in the solid-phase in vacuo, respectively; Π_{elas}^f, Π_{iner}^f represent the power developed by the internal and inertia forces in the interstitial fluid, respectively; Π_{coup}^{fs} represents the power exchanged between the two phases; and Π_{exc}^f represents the power developed by external loading.

The time-averaged power dissipated within the porous medium can be subdivided into contributions from powers dissipated through structural damping of the skeleton, viscous and thermal effects:

$$\Pi_{diss} = \Pi_{diss}^s + \Pi_{diss}^v + \Pi_{diss}^t$$

The power Π_{diss}^s dissipated through structural damping is obtained from Π_{elas}^s, the power Π_{diss}^v dissipated through viscous effects is obtained from $\Pi_{iner}^s + \Pi_{iner}^f + \Pi_{coup}^{fs}$, and the power Π_{diss}^t dissipated through viscous effects is obtained from Π_{elas}^f. So, the total dissipated power and its components can be calculated for each element at a post-processing stage.

To characterize the absorption performance of the 3D studied patchworks, one defines the power absorption coefficient:

$$\alpha = \frac{\Pi_{diss}}{\Pi_{inc}}$$

where Π_{inc} is the incident power. If the excitation in the wave guide is a plane wave of amplitude p_0, this incident power is given by:

$$\Pi_{inc} = \frac{S|p_0|}{2\rho_0}$$

where S is the cross-section of the wave guide, ρ_0 and c_0 refer to the density and the velocity of the air in the wave guide, respectively.

3. Results

An experimental validation has been performed in the case of a macro-perforated material, which consists in a mineral wool with periodic holes containing air (called macro-pores) [5]. Such a material is referred to as a *double porosity* material. It consists in a periodic lattice made up of several periods of a generic cell which is a square mineral wool sample with dimensions $L \times L$ with a center square hole with dimensions $a \times a$. The macro-porosity ϕ_p corresponding to this cell is defined by:

$$\phi_p = \frac{a^2}{L^2}$$

Figure 1 shows the comparison between simulation and measurement for a macro-perforated sample whose the macro-porosity is 0.11. Excellent agreement is found, the numerical model reproduces the two biggest peaks. It proves the validity and increases the confidence level of the proposed method.

Next, a numerical simulation is shown to depict the absorption performance of a non-homogeneous material. Two configurations are considered. The first is a double-layer material made up from a 5 cm thick layer of a rock-wool and a 1 cm thick layer of a rigid glass wool. The rock-wool is bonded onto the rigid termination of a wave-guide. The second configuration is a non-homogeneous layer made with 6 cm of the rock-wool material in which the rigid glass wool is randomly distributed in the form of cubic cells. The ratio of the volume occupied by the two materials is kept constants in the two configurations. Figure 2 shows that the absorption performance is better with the non-homogeneous configuration. This result confirms that the different patches do interact, and that a non-homogeneous configuration increases the acoustic absorption.

Conclusion

The absorption coefficient of non-homogeneous porous-elastic layers has been predicted from a 3D numerical model where each patch is modeled with the Biot theory. An experimental validation has been presented in the case of a macro-perforated material, and it proved the accuracy of the presented model. Also, it has been proved that non-homogeneous layer has a better sound absorption than a multi-layer made of homogeneous materials.

References

[1] Allard, J.-F. "Propagation of sound in porous media, Modelling sound absorbing materials", New York, London: Elseivier Application Science (1993).

[2] Atalla, N. Panneton, R. and Debergue, P. "A mixed displacement-pressure formulation for poro-elastic materials", J. Acoust. Soc. Am. 104, 1444--1452 (1998).

[3] Atalla, N., Hamdi, M.A., and Panneton, R. "Enhanced weak integral formulation for the mixed (u,p) poroelastic equations", submitted to J. Acoust. Soc. Am., 2000.

[4] Atalla, N., Sgard, F.C., Olny, X. and Panneton R., Acoustic absorption of macro-perforated porous materials, submitted to Journal of Sound and Vibration, 2000.

[5] Olny, X., Absorption acoustique des milieux poreux à simple et double porosité. Modélisation et validation expérimentale, PhD, Insa de Lyon, 1999, 281p.
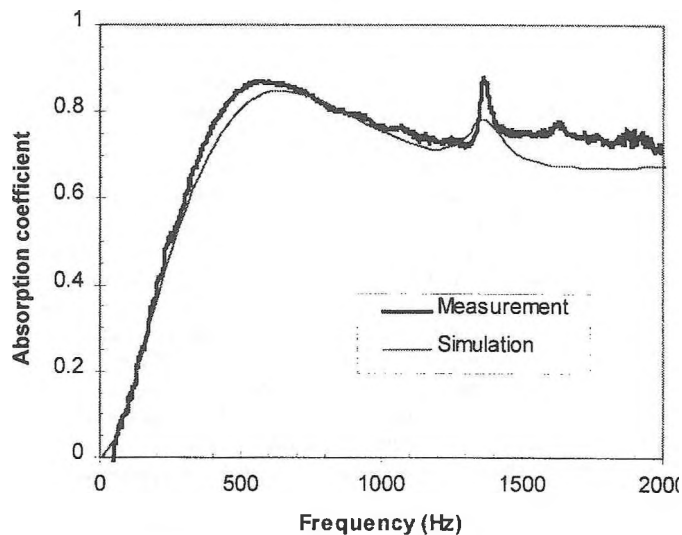
Figure 1. Comparison between prediction and measurements for a double porosity material.
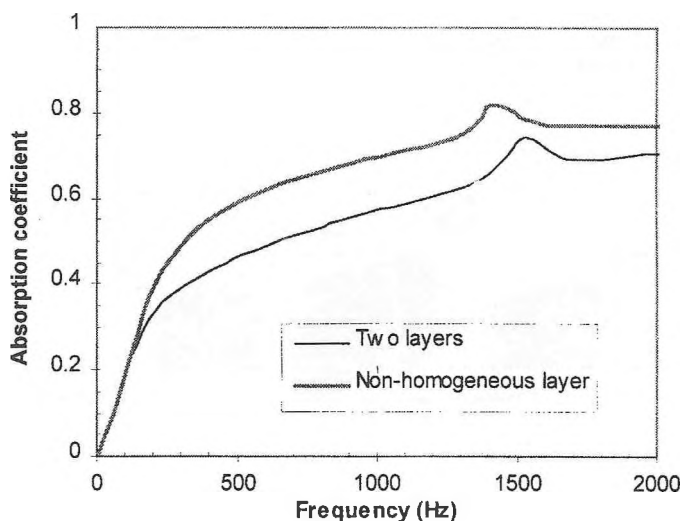

Figure 2. Comparison between a double layer and an equivalent non-homogeneous layer.

Transmission Loss Through Barriers Lined with Heterogeneous Porous Materials

F. C. Sgard[1], N. Atalla[2]

1. Laboratoire des Sciences de l'Habitat, DGCB URA CNRS 1652, Ecole Nationale des Travaux Publics de l'Etat, CEDEX, FRANCE.
2. Groupe d'Acoustique de l'Université de Sherbrooke, Univ. de Sherbrooke, Sherbrooke, QC,J1K2R1,Canada

1. Introduction

Recently, several studies have revealed the benefit of performing air holes in porous material to improve their absorption efficiency. Olny [1] showed both theoretically and experimentally that the absorption coefficient of porous materials could be significantly increased in a large frequency band in the case of properly designed macroperforated highly resistive porous materials. Atalla et al [2] used a finite element based numerical formulation to model such configurations. Transmission loss through heterogeneous materials is also a major issue in all industries. Indeed, it is important to predict how the isolation performance of systems involving porous materials is affected by the presence of air cavities (leaks) such as holes carrying electric wires or plumbing pipes for instance. In addition, one may wonder if the transmission loss of double wall barriers lined with porous material can be improved or at least not deteriorated by keeping constant or decreasing the weight of the system, if heterogeneities such as air cavities or solid inclusions are added in the porous material. This paper investigates how the normal incidence transmission loss of heterogeneous porous materials inserted in an infinite rectangular wave-guide is affected by solid heterogeneities and acoustic cavities. The proposed model is based on a finite element Biot-Allard's formulation for the porous patches and classical finite element formulation for the solid inclusions. The coupling between the porous material and the wave-guide is accounted for explicitly using the modal behavior of the wave-guide. In this paper, numerical results are presented regarding the effect of geometric and physical parameters on the transmission loss performance of single highly resistive plastic foam. Results regarding the performance of multilayered systems involving heterogeneous porous materials will be shown during the oral presentation.

2. Theory
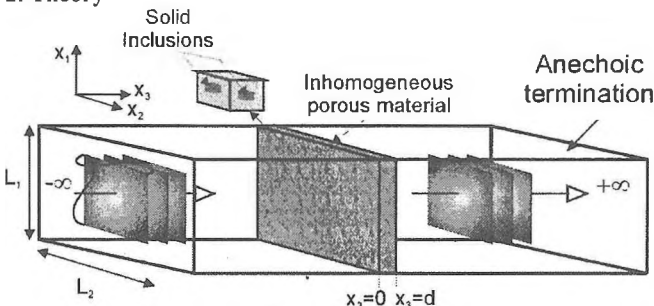
Fig.1: Configuration of the problem

The geometry of the problem is depicted in Fig.1. It consists of a three-dimensional patchwork inserted in a semi-infinite rectangular wave-guide. An incoming plane wave propagating in the wave-guide excites the system. Each 3-D patch is rectangular and either made from a homogeneous porous material modeled using Biot-Allard's theory or from a solid elastic material. The density and

sound speed in the wave-guide are noted ρ_0 and c_0, respectively. In the following, a temporal dependency $e^{j\omega t}$ for all the fields is assumed. It is also supposed that the solid patches are located within the porous material, that is the patches on the front and rear faces of the material are all porous.

The classical weak integral form associated to the porous material has been given in Atalla [2]. Here, a modified form which has been presented in Sgard [3] is used:

$$\int_{\Omega_p} \left[\widetilde{\underline{\underline{\sigma}}}^s(\underline{u}) : \underline{\underline{\varepsilon}}^s(\delta\underline{u}) - \omega^2\widetilde{\rho}\underline{u}.\delta\underline{u} \right]d\Omega + \int_{\Omega_p}\left[\frac{\phi^2}{\omega^2\widetilde{\rho}_{22}}\nabla p.\nabla\delta p - \frac{\phi^2}{\widetilde{R}}p\delta p \right]d\Omega$$

$$- \int_{\Omega_p}\frac{\phi^2\rho_0}{\widetilde{\rho}_{22}}\delta(\nabla p.\underline{u})d\Omega - \int_{\Omega_p}\phi\left(1+\frac{\widetilde{Q}}{\widetilde{R}}\right)\delta(p\underline{\nabla}.\underline{u})d\Omega \qquad (1)$$

$$- \int_{\partial\Omega_p}\phi\left[\underline{U}.\underline{n} - \underline{u}.\underline{n}\right]\delta p d\Gamma - \int_{\partial\Omega_p}\left[\underline{\underline{\sigma}}^t.\underline{n}\right]\delta\underline{u}d\Gamma = 0 \quad \forall(\delta\underline{u},\delta p)$$

Ω_p and $\partial\Omega_p$ refer to the porous-elastic domain and its bounding surface. $\underline{u}$ and p are the solid phase displacement vector and the interstitial pressure in the porous-elastic medium, respectively. $\underline{U}$ is the fluid macroscopic displacement vector. $\delta\underline{u}$ and δp refer to their admissible variation, respectively. $\underline{n}$ denotes the unit normal vector external to the bounding surface $\partial\Omega_p$. $\widetilde{\underline{\underline{\sigma}}}^s$ and $\underline{\underline{\varepsilon}}^s$ are the in-vacuo stress and strain tensors of the porous material. $\widetilde{\underline{\underline{\sigma}}}^t$ is the total stress tensor of the material given by: $\widetilde{\underline{\underline{\sigma}}}^s = \underline{\underline{\sigma}}^t + \phi\left[1+\frac{\widetilde{Q}}{\widetilde{R}}\right]p\underline{\underline{1}}$.

Note that $\widetilde{\underline{\underline{\sigma}}}^s$ accounts for structural damping in the skeleton through a complex Young's modulus $E(1+j\eta_s)$. ϕ stands for the porosity, $\widetilde{\rho}_{22}$ is the modified Biot's density of the fluid phase accounting for viscous dissipation, $\widetilde{\rho}$ is a modified density given by

$\widetilde{\rho} = \widetilde{\rho}_{11} - \frac{\widetilde{\rho}_{12}}{\widetilde{\rho}_{22}}$ where $\widetilde{\rho}_{11}$ is the modified Biot's density of the solid phase accounting for viscous dissipation. $\widetilde{\rho}_{12}$ is the modified Biot's density which accounts for the interaction between the inertia forces of the solid and fluid phase together with viscous dissipation. $\widetilde{Q}$ is an elastic coupling coefficient between the two phases, $\widetilde{R}$ may be interpreted as the bulk modulus of the air occupying a fraction ϕ of the unit volume aggregate.

This modified form is particularly suited for treating the coupling of porous-solid patches since it allows for the surface terms to vanish provided that one ensures the continuity of displacements. No calculation of coupling matrices is needed which saves considerable time during the assembly process.

For a porous material placed into a wave guide, the surface terms corresponding to the front $(\partial\Omega_p^1)$ and rear $(\partial\Omega_p^2)$ faces of the porous material lead to:

$$\int_{\partial\Omega_p^i} \delta(\underline{pu.n})d\Gamma - \int_{\partial\Omega_p^i} \frac{1}{\omega^2\rho_0}\frac{\partial p}{\partial n}\delta p d\Gamma \qquad (2)$$

This equation is the result of applying continuity conditions at the air-porous interface. The first term amounts to the calculation of a classical coupling matrix whereas the second term can be rewritten using the orthogonal modes of the rectangular wave-guide, as [2]:

$$\int_{\partial\Omega_p^i} \frac{1}{\omega^2\rho_0}\frac{\partial p}{\partial n}\delta p d\Gamma = \frac{1}{j\omega}\int_{\partial\Omega_p^i}\int_{\partial\Omega_p^i}\underline{\underline{A}}^i(\underline{x},\underline{y})p(\underline{y})\delta p(\underline{x})d\Gamma_y d\Gamma_x$$

$$-\frac{\varepsilon}{j\omega}\int_{\partial\Omega_p^i}\int_{\partial\Omega_p^i}\underline{\underline{A}}^i(\underline{x},\underline{y})p_b(\underline{y})\delta p(\underline{x})d\Gamma_y d\Gamma_x \quad i=1,2 \qquad (3)$$

where $\varepsilon=1$ if i=1 and 0 if i=2; $\underline{x}=(x_1,x_2)$ and $\underline{\underline{A}}^i$ is an admittance operator given by

$$\underline{\underline{A}}^i(\underline{x},\underline{y}) = \sum_{(m,n)}\frac{k_{mn}^i}{\rho_0\omega N_{mn}}\varphi_{mn}(\underline{x})\varphi_{mn}(\underline{y}) \qquad (4)$$

with:

$$\varphi_{mn}(\underline{x}) = \cos\left(\frac{m\pi}{L_1}\right)\cos\left(\frac{n\pi}{L_2}\right), \left(k_{mn}^i\right)^2 = \left(k^i\right)^2 - \left(\frac{m\pi}{L_1}\right)^2 - \left(\frac{n\pi}{L_2}\right)^2 \text{ and}$$

$$N_{mn} = \int_{\partial\Omega_p^i}\left|\varphi_{mn}(\underline{x})\right|^2 d\Gamma_x$$

p_b is the blocked pressure loading at the porous material interface $(x_3=0)$.
This form has the advantage of depicting the coupling with the wave guide in terms of radiation admittance in the emitter and receiver media together with a blocked-pressure loading. Note that at low frequencies (below the cut-off frequency of the wave-guide), higher modes lead to a purely imaginary admittance operator of an inertance type.

The transmission loss is defined as $TL = -10\log\tau$ where Π^t is the transmitted power given by

$$\Pi^t = -\frac{1}{2\omega}\Im\left[\int_{\partial\Omega_p^2} p^*(\underline{y})\underline{\underline{A}}^2(\underline{x},\underline{y})p(\underline{x})d\Gamma_x d\Gamma_y\right] \qquad (5)$$

and Π_{inc}, is the incident power which in the case of a plane wave excitation, of complex amplitude p_0, is given by $\Pi_{inc}=S|p_0|^2/(2\rho_0 c)$ where S is the cross-section of the wave guide.

3. Results

The normal incidence transmission loss through a 10cm wide and 3.75cm thick square heterogeneous plastic foam sample with characteristics given in Table 1 is considered. The influence on the transmission loss of the spatial distribution of very light elastic trapped heterogeneities (polystyrene $\rho_s=2kg/m^3$, $E=3E^{+9}Pa$) is studied. Figure 2 shows a cross section perpendicular to the x_3 axis inside the porous material together with the location of solid inclusions marked in light grey. Case (a) refers to the simple porosity (i.e without heterogeneities added); cases (b) to (d) represent respectively one single inclusion, 9 regularly spaced inclusions and 45 inclusions randomly distributed in 5 layers 0.53cm thick each, within the porous material (9 inclusion per layer). All inclusions are 2.68cm deep except for the random distribution. These configurations correspond to a percentage of 7.9% of the total volume of the porous material occupied by the trapped cavities. Figure 3 presents the normal incidence transmission loss for the different configurations interest. The transmission loss is not affected at low frequencies but small gains are found at high frequencies. The different distributions do not exhibit strong differences. Yet, case (b) is the most efficient at high

frequencies while case (c) provides the best overall improvement. Case (d) yields an improvement around 1000Hz but performs less compared to the 2 other configurations .

ϕ	σ (kNm^{-4}s)	α_∞	Λ (μm)	Λ' (μm)	ρ_1 (kgm^{-3})	E (kPa)	ν	η
0.97	87	2.52	37	121	31	143	0.3	0.055

Table 1: Characteristics of the studied plastic foam
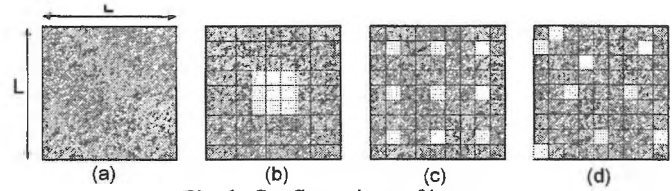
Fig. 2: Configurations of interest
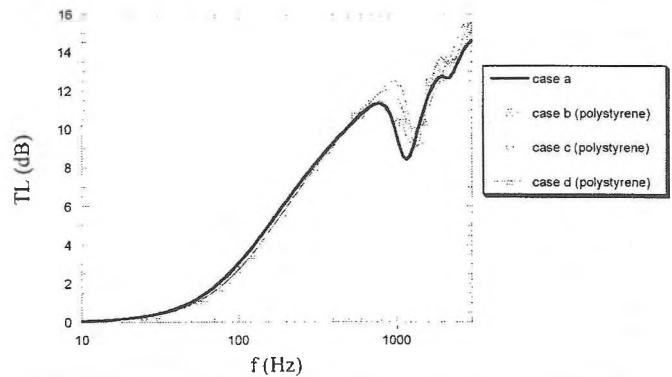
Fig. 3: Normal incidence transmission loss of a plastic foam for several distributions of solid trapped heterogeneities

4. Conclusion

The normal incidence transmission loss of porous media with added trapped solid heterogeneities has been predicted from a 3D numerical model wherein each porous patch is modeled using Biot-Allard poroelasticity equations. The coupling between the porous material and the wave-guide is accounted for explicitly using the modal behavior of the wave-guide. It has been shown that the normal incidence transmission loss of homogeneous materials could be slightly increased at sufficiently high frequencies by adding very light elastic solid inclusions like polystyrene ones. Further work involves studying the coupling of heterogeneous porous materials with elastic structures.

References

[1] Olny, X., Absorption acoustique des milieux poreux à simple et double porosité. Modélisation et validation expérimentale, PhD, Insa de Lyon, 1999, 281p.
[2] Atalla, N., Sgard, F.C., Olny, X. and Panneton R., Acoustic absorption of macro-perforated porous materials, submitted to Journal of Sound and Vibration, 2000.
[3] Sgard, F.C., Atalla, N., A numerical model for the low frequency diffuse field sound transmission loss of double wall barriers with elastic linings, submitted to Journal of the Acoustical Society of America, 1999.

VALIDATION OF 3-D POROELASTIC FINITE ELEMENT FROM THE IMPEDANCE MEASUREMENT OF A VIBRATING FOAM SAMPLE

N. Dauchez[1], S. Sahraoui[2], N. Atalla[3]
1. Centre de Transfert de Technologie du Mans, 72 000 Le Mans, France
2. Laboratoire d'Acoustique de l'Université du Maine, 72 000 Le Mans, France
3. Groupe d'Acoustique de l'Université de Sherbrooke, Sherbrooke (QC) J1K R21, Canada

1.0 Introduction

Porous materials like glass wool and plastic foam are widely used for noise control in different areas such as building construction, aeronautics and automotive industries. In order to investigate the effect of such materials in finite size structures, finite element codes including 3-D poroelastic elements based on Biot displacement theory [1] have been recently developed [2-5]. However validation of these formulations is incomplete for two reasons. The first is that comparaison is made with lateral extent multilayers excited by a normal incidence plane wave, reducing the validation in the case of 1-D motion. Secondly, preliminar mechanical characterisation of the porous material is not made. Only Vigran and al. [6] show satisfactory results for a sandwich plate with a foam core assumed isotropic.

The present paper deals with validation in comparison with a real 3-D motion of the porous material with skeleton motion and acoustic coupling : it concerns the impedance measurement of a resonant porous sample in a duct with lateral air gap. Because determination of specific porous parameters (porosity, air flow resistivity, tortuosity, viscous and thermal characteristic lenghts) has been widely presented [7-8], focus is first made on the determination of the skeleton mechanical properties.

2.0 Mechanical parameters determination

Anisotropy is currently observed on foams [9] and fibrous materials. In order to investigate both isotropic and axisymmetrical viscoelastic skeletons, a quasistatic measurement method has been developed [10]. It is based on a small amplitude sinusoidal compression of a cubic sample of 50 mm edge size between two planes for which applied force, longitudinal and lateral displacements are monitored (Figure 1). The ratio K of force over longitudinal displacement is homogeneous to a stiffness, and the ratios R, R' between the two lateral and the longitudinal displacements are homogeneous to a Poisson ratio. Positioning the sample succesively according to its three axes gives three triplets. If all triplets are equal and $R=R'$, then the material is isotropic : a numerical inversion is processed to determine the Young modulus E and the Poisson ratio v. If only two triplets are equal, the material is axisymmetrical. Then five independant complex components of stress-strain tensor are determined : moduli E_L, E_T, G_{LT} and ratios v_{LT}, $v_{TT'}$, where subscripts L and (T,T') are respectively related to longitudinal and transverse directions. The quasistatic frequency range is restricted to frequencies which are well below the resonance of the sample, typically from 0.1 Hz up to 100 Hz. In this low frequency range, inertial and viscous coupling with the air can usually be neglected.
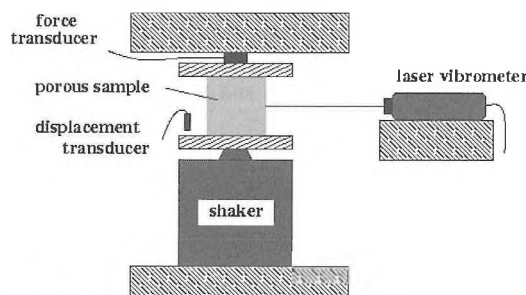
Fig. 1 : Mechanical parameters measurement set-up.

The material used for the validation experiment is a plastic foam. Measurement of triplets (K,R,R') shows that this material is not isotropic. However isotropic inversion can be made for each triplet : this gives three couples of pseudoYoung modulus and Poisson ratio according to each direction L, T and T'. These values do not characterise the viscoelastic tensor of the material. An axisymmetrical inversion has been also made, using direction L for symmetry. Table 1 gives the corresponding values. The other parameters are : ϕ=0.97, σ=165500 Nm^{-4}s, α_∞=1.8, Λ=60 μm, Λ'=180 μm, $\rho_{skeleton}$=39.5 kgm^{-3}, $\eta_{skeleton}$=0.11 .

3.0 Validation set-up

The validation experiment concerns the impedance measurement of a porous sample in a duct of section 10 cm × 10 cm. The porous sample and the boundary conditions have been chosen so that one resonance of the skeleton can be observed in the frequency range of 50 Hz to 500 Hz. Its thickness is 10 cm. The rear surface of the sample is bonded to the rigid end of the duct. Lateral surfaces are separated from the duct by an air gap of either 1.8 mm or 5 mm width (Figure 2). The measurement is achieved using Sybert ans Ross technique [11].

Simulations have been done with a 3-D finite element code, *Phenix*, coupling poroelastic, fluid and elastic elements [5]. One quarter of the geometry has been meshed by 5×5×10 linear hexaedric elements for the porous sample. A compatible mesh is used for the air domain, with only one element along the air gap width. The excitation is simulated by a flat piston at a distance from the sample. This ensures flatness of the acoustic field where pressure is taken for the calculation of the impedance. Both isotropic and axisymmetrical laws are used to model the skeleton motion. The values corresponding to the longitudinal direction are used for the isotropic model : this direction corresponds to the axis of the tube. A calculation using equivalent fluid element (= motionless skeleton) is also made for comparison purpose.

4.0 Results

Figure 3 presents the comparison between measured and simulated absorption coefficients. The general shape of both curves is well

	L	T	T'
E (kPa)	206	136	100
v		0.45	0.31	0.26

E_L	E_T	G_{LT}	v_{LT}	v_{TT}
200	100	80	0.5	0.15

Table 1 : Mechanical parameters of foam determined from (a) isotropic and (b) axisymmetrical inversions.
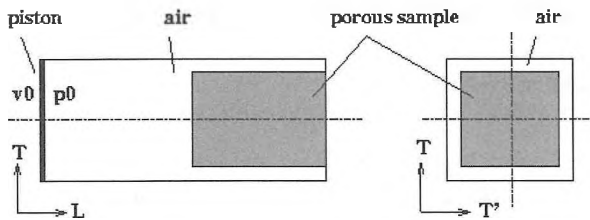
Fig. 2 : Model of the porous sample in the duct.

predicted by the equivalent fluid model. By comparison with the measured quantities, it emphasizes the skeleton resonance around 150 Hz (Fig. 2.a) and 200 Hz (Fig. 2.b). The agreement with Biot models is very good, specially when isotropic law is used : the resonance is well estimated and the influence of the skeleton motion is clearly noticeable.

However results are not so satisfactory when axisymmetrical law is used. This shows that axisymmetrical law is not applicable to this material. Two reasons can explain this fact. In the first instance, the stiffness in the two lateral directions are not strictly equal (Tab. 1.a), and that distorts the inversion. Secondly the symmetry axis may not coincide exactly with the longitudinal direction.

5.0 Conclusion

In conclusion, it appears that the determination of skeleton mechanical parameters for simulation purpose has to be made carefully because of anisotropy. The use of isotropic law is efficient when mechanical parameters are related to the kind of deformation undergone by the material. In these conditions, it is shown that the use of 3-D poroelastic elements based on Biot theory is a powerful way to model real structures including porous media.

Acknowledgement

References

Biot M. A., The theory of propagation of elastic waves in a fluid-saturated porous solid, J. Acoust. Soc. Am., 28, pp. 168-191, 1956

Coyette J.-P., Wynendaele H., A finite element model for predicting the acoustic transmission characteristics of layered structures, Internoise 1995, Newport Beach, pp. 1279-1282, 1995

Johansen T.F., Allard J.-F., Brouard B., Finite element method for predicting the acoustical properties of porous samples, Acta Acoustica, 3, pp. 487-491, 1995

Kang Y.J., Bolton J.S., Finite element modeling of isotropic elastic porous materials coupled with acoustical finite element, J. Acoust. Soc. Am., 98, pp. 635-643, 1995

Panneton R., Atalla N., An efficient finite element scheme for solving the three dimensional poroelasticity problem in acoustics, J. Acoust. Soc. Am., 101, pp. 3287-3298, 1997

Vigran T.E., Kelders L., Lauriks W., Dhainaut M., Johansen T.F., Force response of a sandwich plate with a flexible core described by a Biot-model, Acoustica, 83, pp. 1024-1031, 1997

Allard J.F., Propagation of sound in porous media : modeling sound absorbing materials, Chapman & Hall, Londres, 1993

Dauchez N., Mariez E., Sahraoui S., Bardot A., Determination of acoustic foam parameters for isotropic Biot model, Biot Conference on Poromechanics, Louvain-la-Neuve, pp. 557-560, 1998

Melon M., Mariez M., Ayrault C., Sahraoui S., Acoustical and mechanical characterisation of anisotropic open-cell foams, J. Acoust. Soc. Am., accepted paper

Mariez E., Sahraoui S., Measurement of mechanical anisotropic properties of acoustic foams for the Biot model, Internoise 1997, Budapest, pp. 1683-86, 1997

Seybert A.F., Ross D.F., Experimental determination of acoustic properties using a two microphones random excitation technique, J. Acoust. Soc. Am., 61, pp. 1362-1370, 1977

Fig. 3 : Comparison of simulated and measured absorption coefficients of a porous sample in a duct with lateral air gaps of width (a) 1.8 mm and (b) 5 mm.

TRANSMISSION LOSS OPTIMIZATION OF MULTI-LAYER NOISE CONTROL TREATMENTS

Sebastian Ghinet and Noureddine Atalla
Department of Mechanical Engineering, Université de Sherbrooke, Boul. Université, Sherbrooke, Quebec, Canada J1K 2R1

INTRODUCTION
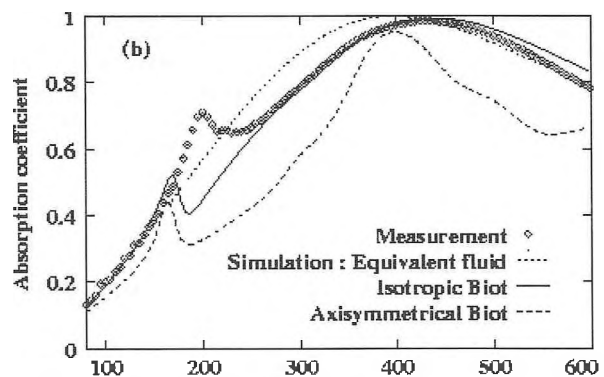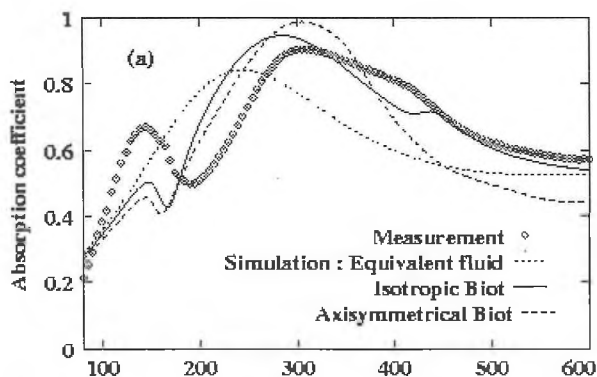
The design of sound barriers is of utmost importance in several industries including automotive, aerospace and buildings. These barriers are typically made up of a decoupling layer sandwiched between a thin skin and a limp massive impervious layer classically known as a septum. As such, they may be considered as a double wall system. The decoupling layer is usually made up from a porous-elastic material such as cellular (e.g. polyurethane foam) and fibrous (e.g. glass fibers) materials. In designing sound barriers for multiple engineering applications, the engineer must select the type and geometric configuration of the barrier and decoupler materials to be used. This task necessitates a thorough understanding of the mechanisms governing the transmission loss of such systems together with an accurate data bank of the mechanical and acoustical properties of these materials.

The paper discusses the optimization of the diffuse field transmission loss through double-wall sound barriers with porous linings. The studied sound barriers are made up from a porous decoupling material sandwiched between an elastic skin and a septum, figure 1. The wave approach is used to calculate the transmission loss of the system [1,2].
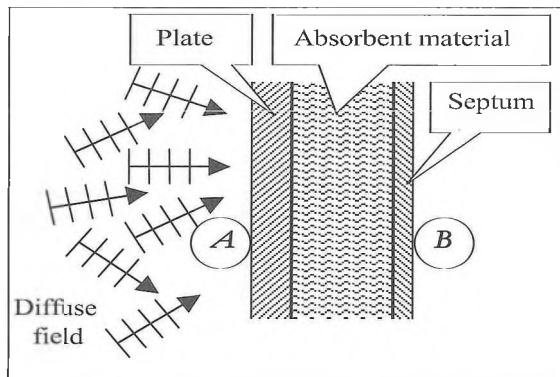
Fig.1. Plate – absorbent material – septum configuration.

OPTIMIZATION AND OBJECTIVE FUNCTION FORMULATION

This study aims at optimizing the frequency band averaged diffuse field transmission loss of the three layers system represented in figure 1 while imposing constraints on the weight and thickness of the system. Other variations on this objective include a combination minimum weight and transmission loss. However, in this latter case, both objectives are combined to form a single objective; no use of multi-objective algorithms is attempted. The band frequency averaged diffuse field transmission loss defined as:

$$TL = -10\log_{10}\left[\frac{\int_{f_{min}^i}^{f_{max}^i}\int_{\theta_{min}}^{\theta_{max}}|T(\theta,f)|^2\cos\theta\sin\theta\,d\theta\,df}{\int_{f_{min}^i}^{f_{max}^i}\int_{\theta_{min}}^{\theta_{max}}\cos\theta\sin\theta\,d\theta\,df}\right]$$

where f_{min} and f_{max} are the lower and upper limits of the frequency band and $T(\theta, f)$ is the transmission coefficient, at frequency f, for a plane wave of incidence angle θ. Constraints are imposed on the weight of the system, as well as upper and lower bounds on the design variables. The optimization problem reads:

Minimize:
$$TL(X)$$

Subject to:
$$\frac{W(X)}{W_{max}} - 1 \le 0$$
$$C_i(X) \le 0 \quad i=1,Nc$$

Where X represents the vector of design variables, W represents the surface mass of the system, W_{max} represents a maximum specified weight, C_i represents the lower and upper bounds constraints on the design variables and N_c represents the number of these constraints.

Two optimization algorithms are studied and compared. The first is based on the Matlab implementation of the Sequential quadratic Programming algorithm [3]. The second is based on an in-house implementation of evolutionary algorithms. The design of this latter algorithm is problem dependent and allows the search of the whole design space for the global minimum [4]. Also, a combination of both algorithms is investigated to combine the advantages of both algorithms: locating the desirable region of the search space using the evolutionary algorithm and rapid convergence using the SQP algorithm in the reduced search space.

IMPLEMENTATION

The above optimization problem is implemented by combining the optimization engine (MATLAB or in-house) to an acoustic-indicator engine for the transmission loss calculation. The high frequency module of MNS/Nova is used for this part [5]. It uses the wave approach, which is essentially based on the representation of plane wave propagation in different media in term of transfer matrices [1]. This approach allows easily for multi-layers made up from a combination of elastic, porous-elastic and fluid layers. In a given layer, sound propagation is represented by a transfer matrix [T] such that $V(M_1) = [T] V(M_2)$, where M_1 and M_2 are two points set close the forward and backward face of the layer, respectively, and where the components of the vector V(M) are the variables witch describe the acoustic field in a point M of the medium. The derivation of the transfer matrices for solid, poro-elastic and fluid layers are detailed in [1,2]. Using continuity equations at the different interfaces, and the impedance equations in the source and receiving domains (assumed semi-infinite), a global system of equation is formed and solved for the reflection and trans-

mission coefficients.

RESULTS AND DISCUSSION

In the first part of the paper the properties of the plate and septum are fixed and the optimization is limited to the properties of the porous layer. The aim is to tailor certain material properties of the porous layer (the flow resistivity) to achieve the desired minimum noise condition. However, contrary to previous work, constraints are imposed on the dependent variables of the porous layer (characteristic lengths) in order to keep the optimized solution realistic. Several types of problems are studied. Firstly, to test the used optimization approach, the porous layer is assumed to be fibrous and its flow resistivity is selected as the primary variable. Fibrous layers are classically modeled as a rigid frame porous layer and an empirical model is used to link the primary variable to the secondary variables used to define the porous layer within Biot-Allard theory [1]:

$$\sigma R^2 \rho_1^{-1.53} = 0.79*10^{-9}; \quad \alpha_\infty \approx 1;$$

$$\Lambda = \frac{1}{2\pi LR} \qquad \Lambda' = 2\Lambda \qquad L = \frac{\rho_1}{\pi R^2 \rho_m}$$

where σ enotes the porosity, α_∞ the tortuosity, Λ the viscous characteristic length, Λ' the thermal characteristic length, R denotes the radius of the fibber, ρ_m the density of glass and ρ_1 the density of the material.

Secondly, a foam layer is considered and once again the flow resistivity is used as the primary variable. To define the dependent variable, the viscous characteristic length is varied with the flow resistivity so that the form factor M is kept constant. The ratio between thermal and viscous characteristic lengths is fixed to 2.5. In such conditions, the intrinsic geometry of the skeleton is kept realistic. The other parameters are fixed and correspond to usual foam properties: porosity F = 0.98, a_∞ = 1.3 and skeleton density r_2 = 33 Kg/m^3. Finally, for a given prescribed maximum total thickness and weight, the thickness and properties of the foam and septum layers are used as the primary variables.

In all the above optimization problems, two frequency regions are considered in the objective function definition, a low frequency range B_1 that includes the double wall resonance frequency and a mid to high frequency range B_2.

We consider as an example the diffuse field transmission loss of a typical three-layer system made up from a foam layer sandwiched between a 0.92-mm thin steel plate and an EVA barrier with surface density 2.43 kg/m^2.

Figure 2 shows, in the case of the mid-to high frequency range, that there exists an optimal value of the flow resistivity for which the transmission loss is maximal. A detailed description, validation and interpretation of such results will be given at the oral presentation.

CONCLUSION

The paper investigates the transmission loss optimization of classical configuration in the automotive industry wherein a decoupling porous layer is sandwiched between the body sheet metal and a septum. Several optimization strategies and problems are studied and compared. The results discussed in this paper are preliminary. Detailed and more realistic results will be presented at the oral presentation.

REFERENCES

1. J.F. Allard, Propagation of Sound in Porous Media: Modeling Sound Absorbing Materials, Elsevier Science Publishers, New York, 1993.
2. B. Brouard, D. Lafarge and J.F. Allard, "A General Method of Modeling Sound Propagation In Layered Media", Journal of Sound and Vibration, 183(1), 129-142, 1995.
3. T. Coleman, M.A. Branch and A. Grace, "Matlab : Optimization Toolbox", The math Works Inc., (http://www.mathworks.com) 1999.
4. A. Ratle, N. Atalla, "Evolutionary optimization strategies for the combinatorial design of heteregeneous materials", Journal of Evolutionary Optimization, 1(1), 77-88, 1999.
5. Theoretical manual: MNS/ Nova: design of multi-layer structures in the both the low and high frequency range. MECANUM INC (http://www.mecanum.com). 1999.
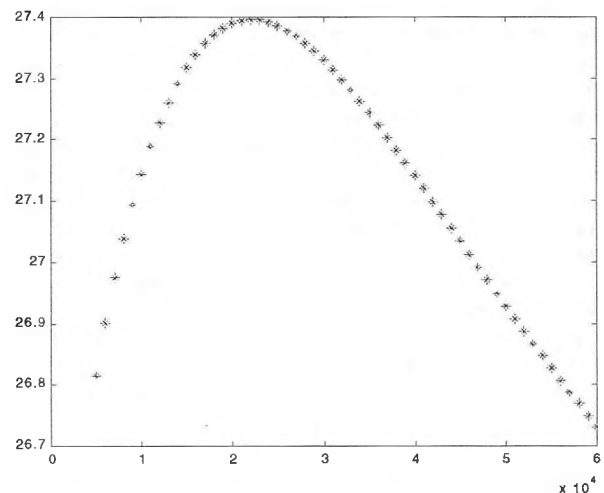
Fig.2. Optimization in middle to high frequency range for the foam material case.

MODELLING STRUCTURE-BORNE SOUND TRANSMISSION AT BOLTED JOINTS

Ivan Bosmans and Trevor R.T. Nightingale

National Research Council Canada, Institute for Research in Construction, Montreal Road, Ottawa, Ontario, K1A 0R6

1. INTRODUCTION

Structure-borne sound transmission at a bolted junction between a plate and a stiffening rib is modelled using an analytical calculation model. This model is based on the wave approach for semi-infinite plates and calculates coupling loss factors for Statistical Energy Analysis (SEA). Modelling vibration transmission in rib stiffened plate structures is very relevant when studying flanking transmission in wood frame buildings, where walls and floors are composed of plate elements (gypsum board and OSB sheets) which are supported by a series of beams (studs and joists). These plate and beam elements are connected using nominally equally spaced screws or nails.

A model for a bolted plate/rib joint must properly account for the rib as well as for the characteristics of the connection. The first problem has been studied in earlier work [1], where the stiffening rib was modelled as an infinite plate strip. The plate strip formulation allows for the deformation of the rib cross-section and includes the effects of standing waves. The second problem regarding the characteristics of a bolted junctions represents the topic of this paper.

Historically, junctions involving bolts, rivets or spot weldings have been modelled using the modal approach in SEA [2]. In this approach, the coupling loss factors are expressed in terms of point mobility functions. This method is implemented in most commercial SEA packages and its popularity is due to the simplicity of the formulation and the low cost of calculations. However, there are some drawbacks to this simplified method. Firstly, expressions for the point mobility are not available for all situations and often assume an infinitely small connection length. Secondly, the modal approach assumes that the point connections act independently, which implies that the energy flow at the junction is independent of the point spacing. This assumption is not justified at low frequencies, where the structural wavelength is considerably larger than the point spacing. In reality, a junction with multiple point connections behaves as a line junction at low frequencies, but changes into a point connection as the frequency increases. Therefore, the point mobility formulation in SEA represents only a high frequency solution and the frequency at which the transition occurs between line and point connection cannot be readily determined.

The solution to this problem has been reported as a modification of the wave approach for semi-infinite plates, where the junction is assumed to be periodic and the response of the plates is described as a scattered wave field [3,4]. The models discussed in Refs. 3 and 4 are very similar, and both approaches accurately predict the transition from line to point connection. The main difference is that Heron [3] assumed an infinitely small connection length as opposed to Ref. 4, where the connections may have an arbitrary contact length. This feature is desirable when the dimensions of the connector are not negligible with respect the structural wavelength.

In the absence of any spacers or isolators between the surfaces connected using bolts, a contact area can not be defined. In fact, the surfaces are nominally in direct contact of the entire length of the junction. However, experimental data have shown that these junctions still behave as a series of local connections [1]. The frequency at which the transition occurs from line to local connection was found to increase with decreasing spacing between the bolts. The data also suggested that bolted junctions could be modelled using an equivalent connection length for each fastener.

In this paper the concept of an effective connection length is evaluated for a bolted joint between a plate and a stiffening rib. The bolted plate/rib junction is modelled by combining the plate strip theory for the rib [1] and the point connection theory for the bolted junction [4]. The following paragraph discusses the experimental verification on a Plexiglas structure where spacers were inserted between the plate and the rib to create a well-defined connection length. In the following section, an equivalent connection length is determined by fitting numerical data to the experimental results obtained for the same structure without spacers.

2. EXPERIMENTAL VERIFICATION

The experimental verification was carried out on the Plexiglas structure shown in Fig. 1. A stiffening rib (1.23 x 0.05 x 0.0187 m) was attached to a sheet (2.46 x 1.23 x 0.0117 m) using equally spaced bolts. Three different cases were considered by using 4, 8 and 16 bolts. Thin metal spacers (0.0187 x 0.0187 x 0.0006 m) were inserted between the sheet and the rib. The velocity level difference (VLD) was measured between both plate subsystems on each side of the stiffening rib.

Measurement and prediction are compared in Fig. 2. The measured VLD for the case with 16 connections displays a pronounced peak at 1 kHz. At this frequency, an anti-resonance of the stiffening rib significantly reduces the rotation of the junction, leading to a reduction in bending wave transmission [1]. The predicted data also show a maximum in the VLD, but its location is shifted to a higher frequency. This discrepancy might be explained by uncertainties in the measured material properties or inaccuracies in the modelled boundary conditions of the plate strip. The measured results also show a less pronounced maximum at 315 Hz,
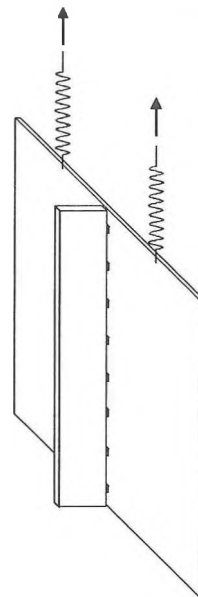

Figure 1. Experiments were carried out on a Plexiglas sheet suspended from the laboratory ceiling using two soft springs. The stiffening rib was attached using equally spaced bolts. Thin metal spacers were inserted between the plate and the rib at each bolt.
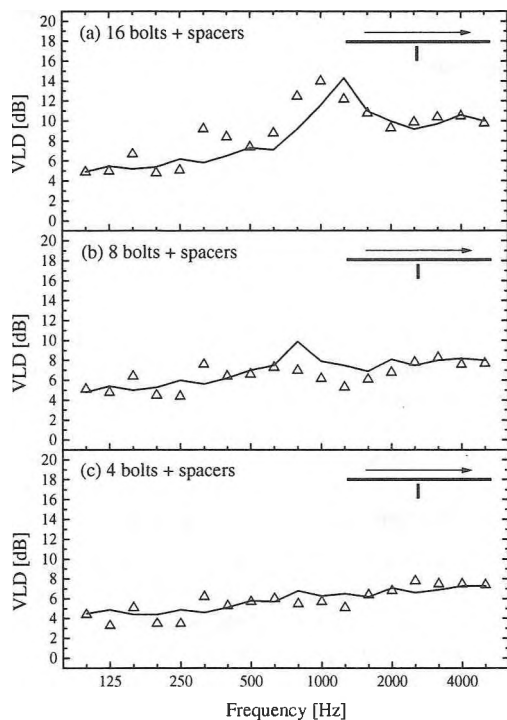
Figure 2. Comparison between measured and predicted VLD for the junction with spacers for three different numbers of bolts. Measurement (△), prediction (———).

Figure 3. Comparison between measured and predicted VLD for the junction without spacers for three different numbers of bolts. Measurement (△), calculation: equivalent connection length (———), line connection (— — —), point connection (·····).

which is not predicted by the model. Overall, the agreement between theoretical data and measured results is fair since both curves show a similar trend. Good agreement is achieved for the case with 8 connections in Fig. 2b, although the peak predicted at 800 Hz seems to be missing in the measured data. The 4 connection case in Fig. 2c clearly shows the best agreement between measurement and prediction.

3. EQUIVALENT CONNECTION LENGTH

To evaluate the concept of an equivalent connection length, a parametric calculation is carried out with varying width of the connections. The equivalent connection length is determined as the connection width which minimizes the frequency averaged rms prediction error. The measured data for the junction without spacers, together with the results calculated using the equivalent connection length are shown in Fig. 3. Also shown in Fig. 3 are the results for the extreme cases considered in the parametric calculations: idealized point connection (infinitely small connection length at each bolt) and continuous line connection. The point connection and the line connection correspond to the weakest and the strongest coupling, respectively, between the rib and the plate, and the difference between both cases increases with increasing bolt spacing.

In all three cases of bolt spacing, the best agreement between measurement and calculation is obtained when using the equivalent connection length. The measured data for the junction with 16 bolts approaches the results for a line connection, the main difference being a shift in the peak of the VLD. The junction with 8 bolts clearly represents an intermediate case between a line and a point connection. Fig. 3c demonstrates that the junction with 4 bolts can be modelled in first approximation by a point connection, although the latter approach leads to a systematic underestimation of the VLD.
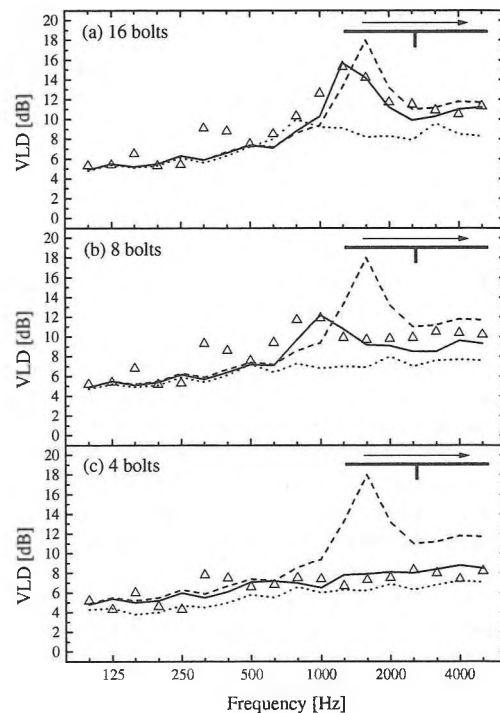
The results in Fig. 3 illustrate that an appropriate choice of the connection width yields calculated data which agree well with measured results. Although the equivalent connection length was assumed to be frequency independent, the calculated data matched the measured results in most of the frequency range. Consequently, it was demonstrated that a bolted plate/rib junction can be modelled by assigning an equivalent connection length to each fastener.

4. CONCLUSIONS

Structure-borne sound transmission at a bolted plate/rib joint has been studied theoretically and experimentally. By fitting numerical to experimental data, it was demonstrated that a bolted junction can be modelled using the concept of an equivalent connection length. It should be stressed that the equivalent connection length does not represent a physical parameter, since the detailed behaviour of the junction is, in reality, much more complex. The results of this paper merely show that a structure-borne sound transmission model, which incorporates the periodic boundary condition of a bolted junction, can be improved if a finite connection length is assigned to the fasteners.

REFERENCES

[1] Bosmans, I. and Nightingale, T.R.T. 1999 *Build. Acoust.* **6**(3&4), 289-308. Structure-borne sound transmission in rib-stiffened plate structures typical of wood frame buildings.

[2] Lyon, R.H. and DeJong, R.G. 1995 *Theory and Application of Statistical Energy Analysis.* Butterworth-Heinemann, Boston, second edition.

[3] Heron, K.H. 1998 *Proceedings NOISE-CON 98*, 579-584. The wave approach to predictive Statistical Energy Analysis and equally spaced point connections with isolators.

[4] Bosmans, I. and Vermeir, G. 1997 *J. Acoust. Soc. Am.* **101**(6), 3443-3456. Diffuse transmission of structure-borne sound at periodic junctions of semi-infinite plates.

SOUND RADIATION FROM A FLOW-EXCITED RECTANGULAR PLATE WITH VISCO-ELASTIC SUPPORTS

Junhong Park and Luc G. Mongeau

School of Mechanical Engineering, 1077 Herrick Laboratories, Purdue University, West Lafayette, IN47907-1077

1. Introduction

The prediction of the sound radiated by visco-elastically supported plates excited by turbulent flows is relevant to the problem of interior vehicle noise. This subject, which has been investigated previously [1], has recently gained much interest due to the fact that aero-dynamic noise sources become more significant as other vehicle noise sources (such as the engine, the transmissions, or the tires) have been significantly reduced. In this study, a model was developed to predict the vibration response of a rectangular plate mounted on visco-elastic supports. The plate was assumed to be excited by a distributed surface pressure field, described by a Corcos model. The radiated sound was calculated from the transverse velocity of the plates. Visco-elastically supported plates can be modeled as a rectangular plate with general boundary conditions along the edges. The boundary conditions are homogeneous. The assumed mode method was used to calculate the plate response at low frequencies. The results from the assumed mode method (frequency dependent damping ratio of the plate vibration) were fed into a Statistical Energy Analysis formulation for the prediction of the velocity spectrum at high frequencies.

2. Assumed Mode Method for Plates

Fig. 1 shows description of the visco-elastically supported rectangular plate. From the external loads from fluctuating wall pressure, the most significant contributor to noise generation is due to flexural waves inside the plate. The equation of motion for flexural displacement (normal to the plate) in the plate is

$$DV^4 w(x, y, t) + C\dot{w}(x, y, t) + \rho_s \ddot{w}(x, y, t) = -p(x, y, t) \quad (1)$$

where where, D is the plate bending stiffness($Eh^3/12(1-\nu^2)$) and C is the damping coefficients, ρ_s is mass per unit area of the plate. If we assume that the displacement of the plate can be described by using assumed mode analysis, the displacement of the plate is

$$w(x, y, t) = \sum_{m,n} \Psi_{m,n}(x, y) q_{m,n}(t) \quad (2)$$

where, $\Psi_{mn}(x,y,t)$ is the assumed modes of the plate and $q_{m,n}(x,y,t)$ is the generalized coordinate of the plate. For the choice of assumed modes, from the results of Allain Berry[2], Taylor expansions of displacement field are used.
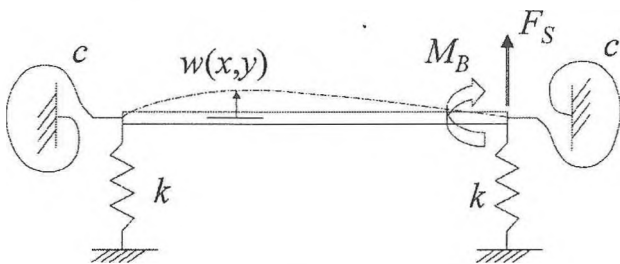

Fig. 1 description of the rectangular plate boundary conditions

The base function of assumed mode methods looks like,

$$\phi_m(x) = \left(\frac{2}{a}x\right)^m, \quad \varphi_n(y) = \left(\frac{2}{b}y\right)^n \quad (3)$$

where a and b are plate dimensions in x and y directions respectively. Boundaries of the plate are supported by the rotational and translational complex stiffness. Using this formulation, continuous plates problem is transformed to the m×n DOF discrete system. Mass matrix and stiffness matrix and general force matrix are calculated using the formula proposed in [2].

3. Turbulent Wall Pressre Modeling

The excitation from the low-Mach number turbulent flow was the topic for decades. An important contribution to the theoretical modeling of the wall pressure field was made by Corcos. Corcos postulated that the cross-power spectral density of the wall pressure can be represented as

$$S(\xi_x, \xi_y, \omega) = \Phi_{pp}(\omega) A(\omega\xi_x/U_c) B(\omega\xi_y/U_c) \exp(-j\omega\xi_x/U_c) \quad (6)$$

where U_c is the flow convection speed, A and B are two functions that are determined from experiments. The coherence is determined from the dimensionless parameter of $\omega\xi/U_c$. The advantage of this Corcos model is its simplicity. For the choice of functions $A(\varpi\xi_x/U_c)$ and $B(\varpi\xi_y/U_c)$, Strawderman found that, for a zero gradient flow, the functions A and B can be chosen to be simple exponentials.

$$A(\omega\xi_x/U_c) = e^{-\gamma_x|\omega\xi_x/U_c|}, \quad B(\omega\xi_y/U_c) = e^{-\gamma_y|\omega\xi_y/U_c|} \quad (7)$$

where γ_x and γ_y are constants related to the ordinary coherence in the streamwise and the spanwise directions, respectively. These constants are usually determined from measurements to yield the best agreements with the experiments. The wavenumber-frequency spectral density can be obtained by performing a Fourier transform of Corcos model. The wave number-frequency spectral density is

$$\Phi(k_x, k_y, \omega) = \Phi_{pp}(\omega)\left(\frac{U_c}{\omega}\right)^2 \frac{\gamma_x}{\pi\left[(k_x U_c/\omega - 1)^2 + \gamma_x^2\right]} \frac{\gamma_y}{\pi\left[(k_y U_c/\omega)^2 + \gamma_y^2\right]} \quad (8)$$

This model is widely used for its mathematical simplicity. Its disadvantage is that it over predicts the sub-convective range of wave number spectrum.

4. Experimental Apparatus

The experiment was done using a custom-built test fixture installed in a low speed quite wind tunnel as depicted in Fig. 2. A rectangular, flat panel supported on all four edges by a glass run sealing system was mounted on a rigid aluminum frame connected to a rectangular, acoustically treated enclosure. The frame is flush with the closed test section wind tunnel floor, and structurally isolated from the vibration of the wind tunnel walls using a primary bulb sealing systems, and silicone. The wind tunnel included many vibration isolation and muffling devices. These minimized the acoustic noise in the wind tunnel test section, the turbulence level of the inflow at the

wind tunnel section, the turbulence level of the inflow at the wind tunnel inlet, and the mechanical vibrations of the test section walls.

The test plate is made of aluminum and has the dimension of 0.446m×0.375m×0.003175m. For the simulation, the material property of aluminum was used. (Density: 2700kg/m³, E: 7.2Gpa, v: 0.34) The longitudinal wave speed in the plate is 5413m/sec and model density is 0.016542modes/Hz. The aluminum plate is supported by the glass run sealing system used for actual car window. The plate itself shows very little damping ratio. When it is supported by the sealing system, damping ratio gets much higher[3]. The experimental modal analysis was used to measure the damping factor and modal frequency value. This data was used in assumed mode methods to make an analytical model of the system.

Flat fence was used to increase the turbulence level over the plate. The pressure over the plate was measured using condenser microphone (EK3024, manufactured by Emkay Products.). The wall pressure auto spectrum variation over the plate shows very little variance over the plate when the plate is placed in the region of reattached flow. The parameters for Corcos model (decay rates) was measured by comparing Corcos model to measured coherence. Convection velocity was chosen to be $0.65 * U_0$ where U_0 is free stream velocity. γ_x and γ_y was chosen as 0.37 and 0.77 respectively. Fig. 3 shows the comparison between experimental results and model in coherence variation with frequency. These results were measured at the center of the plate. Three microphone spaced 12.7mm apart to each other was used for the comparison of coherence data (in stream wise direction). At the other position on the plate, it shows a little variation especially for stream wise direction.
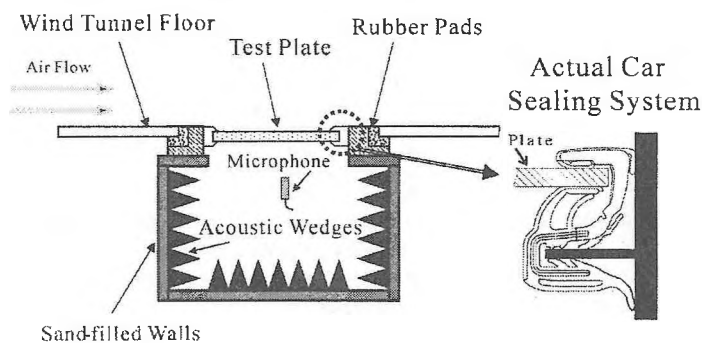
Fig. 2 Experimental apparatus
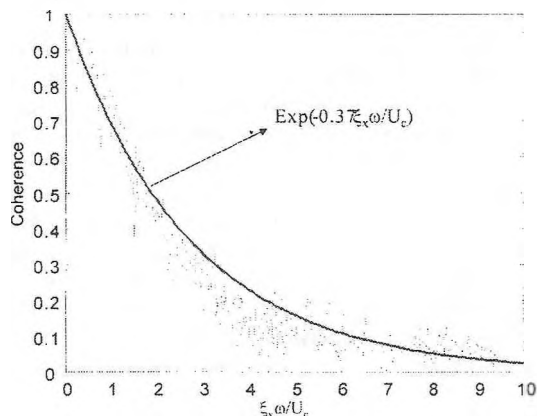
Fig. 3 Coherence variation in stream-wise direction

5. Results and Discussions

The response of the velocity spectrum was calculated using SEA. For the evaluation of the wave number spectrum integral of mode shape and wall pressure level, we used the assumption that all the vibration energy is constrained at the peak of mode shape wave number spectrum. [5]

The damping factor of the plate is calculated from the assumed mode method results. This damping factor is frequency dependent. For visco-elastically supported plates, the damping comes from boundary. The results from assumed mode methods shows peak value in damping ratio around 500Hz and shows decay with frequency. In the SEA simulation, Corcos model over predicts the velocity spectrum significantly due to the fact that plate wave number usually corresponds to sub-convective range of the wall pressure wave number spectrum (more than 20dB). It was necessary to use refined Corcos model (Smol'yakov and Tkachenko model). Fig 4 shows the measured velocity spectrum at the center of plate and the analytical results from SEA comparison. It shows general agreement in the frequency region between 200Hz and 1000Hz. But the error was great when it exceeds that frequency region.

REFERENCES

[1]   Han, F, Mongeau, L. G., and Bernard, R. J. 1998, "Energy flow analysis of beams and plates for random distributed loading.", Journal of Fluids and Structures, Vol. 12, pp315-333.

[2]   Allain Berry, Jean-Louis Guyader and Jean Nicolas. 1990, "A general formulation for the sound radiation from rectangular baffled plates with arbitrary boundary conditions." J. Acoust. Soc. Am. Vol 88 pp2792-2802.

[3]   Park, J. and Mongeau, L. G., 1999, "Effects of seal mechanical properties on sound radiation from road vehicle side-glass windows." Proceedings of Inter-noise 99, pp795-800.

[4]   Borisyuk, A.O. 1997, "Vibration and noise generation by elastic elements excited by a turbulent flow." Journal of Sound and Vibration, 204(2), 213-237.

[5]   W. K. Blake 1986 *Mechanics of Flow-induced Sound and Vibration*, New York: Academic Press.
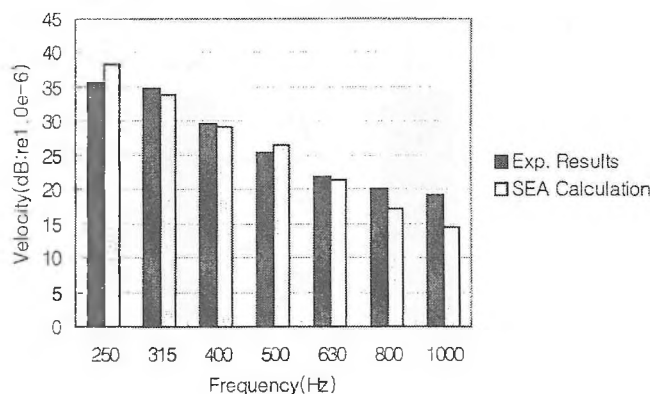
Fig. 4 Comparison between experimental result and sprediction.

Sound Transmision Characteristics Of Elastomeric Sealing Systems

Junhong Park, Luc G. Mongeau and Thomas Siegmund

School of Mechanical Engineering, 1077 Herrick Laboratories, Purdue University, West Lafayette, IN47907-1077

1. Introduction

Sound transmission through door and window sealing systems is one important contributor to interior aerodynamic noise in road vehicles [1]. Two primary noise generation mechanisms involve the aspiration through small leaks and structural sound transmission due to flow-induced mechanical vibrations of the seals. Aspiration noise when leaks are present is the most significant noise source. It is therefore critical to ensure the air-tightness of the sealing system at the design stage of new vehicles. A good understanding of the dynamic behavior of sealing systems excited by unsteady surface pressures caused by turbulent flow over the vehicle is also essential for the design of sealing systems that are quite. Experiments in actual vehicles on the road or in wind tunnels are costly, time consuming and complicated by the presence of multiple sources and flanking paths. Recent efforts have been towards the prediction of the sound transmission characteristics of the seals using detailed finite element model [2]. Experimental study to evaluate the acoustic barrier properties of different rubber seals and their effectiveness to prevent aspiration were measured in controlled laboratory conditions (Mongeau, [3]). In the present study, simple sound transmission model of the sealing system is presented. Both finite element method and transfer function matrix method is used as an analytical model. These results are compared with experimental data obtained from reverberation room test.

2. Sound Transmission Loss Calculation

Fig. 1 shows the simplified model of the bulb seal for sound transmission calculation. Each seal wall is modeled as an unbounded mass. Here $\hat{P}_{11}$ is incident pressure field to the seal. $\hat{P}_5$ is the transmitted sound wave. For this system, transmission loss is defined as (In an assumption of plate traveling wave on both sides.)

$$R = 10 \log(1/\tau), \quad \tau = |\hat{P}_5|^2 / |\hat{P}_{11}|^2 \tag{1}$$

where, R is transmission loss and τ is the transmission coefficient. Finite Element method(ABAQUS) is used to analyze this system. Structural and acoustic coupling elements are used for the interaction between air and seal boundary.
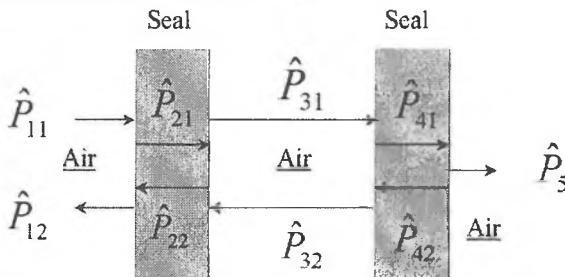

Fig. 1 Simplified model of vehicle door bulb seal

Boundary condition for the left and right ends of the model is non-reflecting to prevent the standing wave resonance at both sides. Boundary condition for top and bottom of the model is rigid wall boundary condition. Incident load can be applied at left side of the wall (acoustic loads) or directly to the left sides of the seal (distributed load to seal face). The loads from turbulent wall pressure fluctuation are more similar to direct loads on the seal surface. Boundary condition for seal edges can be free or fixed. Here, free boundary condition is used for comparison with transfer function matrix method.

Transfer function matrix method was developed and compared with finite element methods. In transfer matrix methods, continuity of the pressure and the velocity of traveling wave field were used. Then relationship between incident pressure and transmitted pressure fields is acquired. It has the form of 8×8 matrix.

$$
\begin{bmatrix}
-1 & 1 & 1 & 0 & 0 & 0 & 0 & 0 \\
\frac{r2}{r1} & 1 & -1 & 0 & 0 & 0 & 0 & 0 \\
0 & e^{-jk_2 d_1} & e^{jk_2 d_1} & -1 & -1 & 0 & 0 & 0 \\
0 & \frac{r3}{r2}e^{-jk_2 d_1} & -\frac{r3}{r2}e^{jk_2 d_1} & -1 & 1 & 0 & 0 & 0 \\
0 & 0 & 0 & e^{-jk_3 L} & e^{jk_3 L} & -1 & -1 & 0 & 0 \\
0 & 0 & 0 & \frac{r4}{r3}e^{-jk_3 L} & -\frac{r4}{r3}e^{jk_3 L} & -1 & 1 & 0 \\
0 & 0 & 0 & 0 & 0 & e^{-jk_4 d_2} & e^{jk_4 d_2} & -1 \\
0 & 0 & 0 & 0 & 0 & \frac{r5}{r4}e^{-jk_4 d_2} & -\frac{r5}{r4}e^{jk_4 d_2} & -1
\end{bmatrix}
\begin{bmatrix}
\hat{P}_{12} \\
\hat{P}_{21} \\
\hat{P}_{22} \\
\hat{P}_{31} \\
\hat{P}_{32} \\
\hat{P}_{41} \\
\hat{P}_{42} \\
\hat{P}_5
\end{bmatrix}
=
\begin{bmatrix}
1 \\
\frac{r2}{r1} \\
0 \\
0 \\
0 \\
0 \\
0 \\
0
\end{bmatrix}
\hat{P}_{11}
$$

This matrix is solved to get transmission loss as defined in Eq. (1). Here, r_1, r_2, r_3, r_4, r_5 are the acoustic impedances and k_2, k_3, k_4 are the wave numbers in the medium. d_1 and d_2 are seal thickness and L is the separation distance between seal walls.

3. Results and Discussions.

Dynamic mechanical properties of seal material (foamed rubber) were measured (TA Instruments 2970), and used as inputs to the material property for the simulation. The simulation was done for two bulb seals that have different density. One bulb seal has the density of 670kg/m³ and the other has the density of 370kg/m³. Measured elastic modulus were 8.0MPa and 2.0MPa respectively. This elastic modulus was measured at 20Hz, room temperature. These measured data were used as an input for simulation. d_1 and d_2 were measured as 2mm and L was 12mm for both seal. Fig. 2 shows the simulation results. Obviously there exist dip in the transmission loss due to mass-air-mass resonance frequency for two different seals. High density seal shows lower resonance frequency as expected. Another possible resonance is the half-wave length resonance inside the seal wall. The longitudinal wave speed in the seal is 126m/sec and 86m/sec respectively. So half-
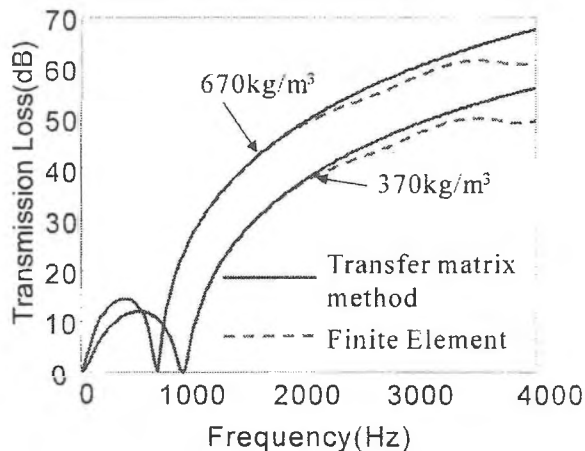
Fig. 2 Simulation results

Fig. 3 is the experimental setup for the measurement of the sound transmission loss of the seal. The fixture can host 25.4cm long samples. The effects of seal compression and material property of the bulb seal can be investigated. Efforts were given to minimize any sound transmission into the receiver side through franking paths by eliminating all leaks. For the generation of reverberant sound fields, two speakers were used as a sound source. At the other sides of the seal, intensity prove (B&K sound intensity probe) was used to measure the transmitted sound intensity. It is located inside the jig cavity. All sides of the cavity walls are treated with sound absorbing material to prevent the acoustic resonance inside cavity. The seal vibration at the receiver side was also measured using the laser vibrometer. The frequency range of interest is from 500Hz to 5kHz.

The bulb seals that were used in the experiment include 670kg/m³, 370kg/m³ and 430kg/m³ density seals. 430kg/m³ density seal is made from thermoplastic elastomer. The others are made from thermoset rubber compound. The transmission loss measurement results from experiments are shown in Fig. 4. For the calculation of the transmitted sound intensity, the plane wave propagation from the seal and small cavity resonance phenomena was assumed. The incident and transmitted intensity to seal was calculated from (3), (4). (In the assumption that the reverberation room is truly diffuse sound fields.)
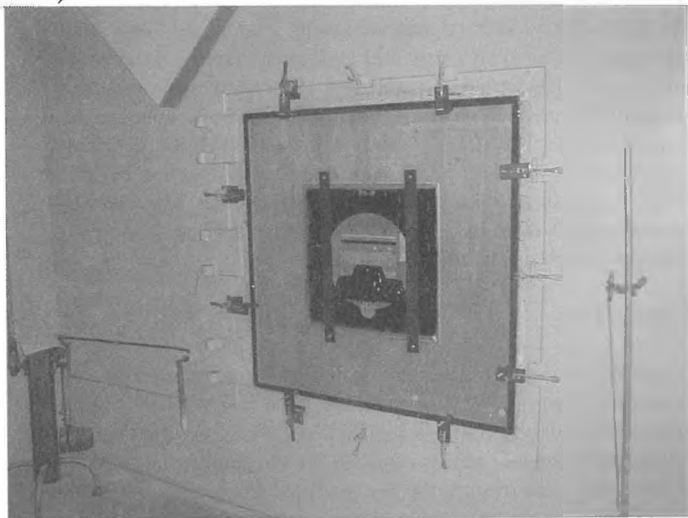
Fig. 3 Experimental setup for transmission loss measurements of bulb seal

$$I_i = \langle p^2 \rangle / (4\rho c) \tag{3}$$

$$I_t = \langle V^2 \rangle \cdot (\rho c) \tag{4}$$

where I_i is the effective intensity inside the reverberation room and p is the average sound pressure inside reverberation room. V is the velocity of the seal wall measured from laser vibrometer. I_t is transmitted intensity.

The comparison between simulation and experimental results does not show much similarity. The measured dip in transmission loss is located at much higher frequency than simulation results. Such phenomena are severe for high density sealing systems. Currently the analytical model for sound transmission calculation is too simple to account for actual seal shapes. Actual seal has round shape. Two walls of the seal are not separated. So, further investigations for the effects of actual seal shape and non-linear visco-elastic properties of the elastomer are necessary.

ACKNOWLEDGMENTS

REFERENCES

[1] George, A.R., and Callister, J.R., 1991, "Aerodynamic Noise of Ground Vehicles." SAE Paper No. 911027.

[2] Gur, Y., and Morman, K.N., 1999, "Sound Transmission Analysis of Vehicle Door Sealing System." Proceedings of the 1999 SAE Noise & Vibration Conference, Paper No. 1999-01-1804, pp1187-1196.

[3] Mongeau, L., and Danforth, R.J., 1997, "Sound Transmission through Primary Bulb Rubber Sealing Systems." 1997 SAE Transactions, Journal of Passenger Cars, Vol. 106, Sec. 6., pp2668-2674.
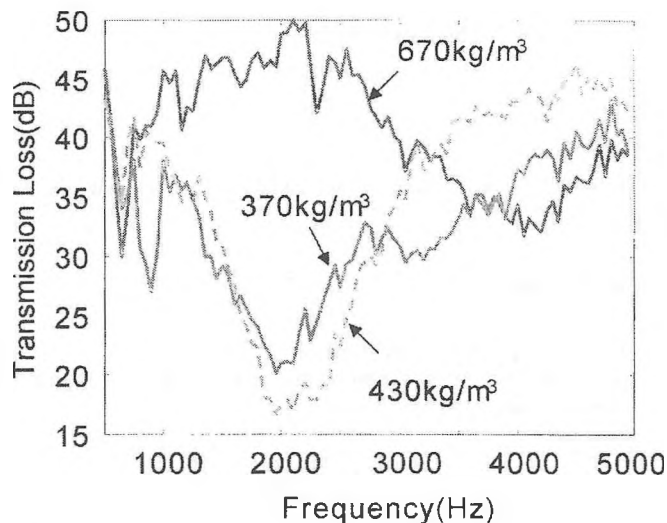
Fig. 4 Experimental results for sound transmission loss calculation from laser vibrometer velocity measurement.

NUMERICAL AND EXPERIMENTAL CHARACTERIZATION OF THE TRANSMISSION LOSS OF COMPLEX COMPOSITE PANELS

Maxime Bolduc, Raymond Panneton, Noureddine Atalla and Jean-Luc Wojtowicki

Groupe d'acoustique de l'Université de Sherbrooke, Université de Sherbrooke, Sherbrooke, Québec, J1K 2R1, Canada.

1. INTRODUCTION

The noise reduction in aircraft is now one of the top priorities for the aerospace industry, the passengers, and the crew members. Until now, many numerical studies (FEM/BEM) were conducted to predict the sound pressure levels inside the fuselage, but the size of the problem is so big that only the interior problem was taken into account.

Moreover, to be able to predict the acoustical behavior of an entire fuselage, it is a necessary to consider the exterior problem as well as the interior problem, without ignoring the fluid-structure interaction. A method to partly achieve this is to characterize the vibroacoustic behavior of the different panels from which the fuselage is made of. In order to do this, it is necessary to start with a fine validation of the numerical procedure on simpler structures such as plates and double plates systems.

In this paper, a numerical method is used and compared with experimental measurements to show its ability to finely predict the sound transmission loss of simple and complex composite panels. The studied configurations are: a simple plate, an air-filled double plate, and a double plate with cavity absorption. First, a review of the numerical modeling is presented. Second, the experimental setup is discussed. Finally, numerical and experimental results are compared.

2. NUMERICAL CALCULATIONS

The numerical calculations are achieved using both the finite element method (FEM) and the boundary element method (BEM). The calculations are done using an in-house software Nova. The transmission loss is obtained with [4]:

$$TL = 10 Log \frac{W_I}{W_T} \tag{1}$$

Where W_I is the incident power and W_T is the radiated transmitted power.

a) The simple plate

For the simple plate system, application of the coupled finite and boundary element discretization procedure yields the following matrix system [2,4] :

$$\left[[K] + j\varpi [Z] - \varpi^2 [M] \right] \{u\} = \{F\} \tag{2}$$

where [K] is the stiffness matrix, [Z] the radiation impedance matrix, and [M] the mass matrix. The vector {u} contains the nodal displacement of the meshed plate. Finally, the force vector {F} is essentially a pressure force generated by a diffuse sound field in the emission domain.

b) The double plate

For the double plate system, the fluid in the cavity is coupled to the plates. Hence, each plate, modeled using (2), is coupled to the finite element formulation of the air cavity through a coupling matrix $[C_i]$. The global FEM/BEM matrix system is then [2,4]:

$$\begin{bmatrix} \left[K_1 + j\varpi Z_1 - \varpi^2 M_1 \right] & -[C_1] & 0 \\ -[C_1]^T & \frac{H}{\varpi^2} - Q & [C_2] \\ 0 & [C_2]^T & \left[K_2 + j\varpi Z_2 - \varpi^2 M_2 \right] \end{bmatrix} \begin{Bmatrix} U_1 \\ P \\ U_2 \end{Bmatrix} = \begin{Bmatrix} F \\ 0 \\ 0 \end{Bmatrix} \tag{3}$$

c) The double plate system with porous material

The finite element model for the porous material is based on the Johnson-Champoux-Allard model [3,5]. The physical properties of the porous material were measured using GAUS facilities for poroelastic material characterization and are given in table 1.

Table 1 : Physical property for the equivalent fluid

Property	
Porosity	0.9479
Tortuosity	3.83
Resistivity	42097.89 Ns/m^4
Caracteristic thermal lenght	139.9^E-6 m.
Caracteristic viscous lenght	66.37^E-6 m.

3. EXPERIMENTAL SETUP

The experimental setup is a coupled anechoic-reverberant room. The diffuse sound field is generated using 2 sources. The studied structure is mounted on a very stiff and massive frame fixed on the middle wall. The boundary conditions of the plates are considered clamped. The incident power is measured with 4 microphones distributed in the reverberant room and the reverberation times are measured using a 2133 B&K analyzer. The transmitted radiated power is measured with a sound intensity probe. The intensity measurement is done by sweeping the entire surface of the plate facing the anechoic chamber.

4. RESULTS

The sound transmission loss results presented here are obtained for rectangular plates of 0.93-m x 0.5-m wide and 4.67-mm thick. Clamped boundary conditions are used. *Figure 1* shows the numerical and experimental results obtained for the simple plate. *Figure 2* shows the same results for the air-filled double plate system, while *figure 3* is for the double plate with porous material. *Figure 4* demonstrates the evolution of the transmission loss of the differ-

ent structures. It shows that the porous material increases considerably the sound transmission loss of the double plate system..

5. CONCLUSIONS

We found for all three systems good agreement between the simulations and the experiments in the range between 20 to 1000 Hz. The ability of the numerical method to predict correctly the low frequency acoustic behavior of finite size simple structures has been shown..

6. ACKNOWLEDGEMENTS

7. REFERENCES

[1]   ALLARD, J.F. *Propagation of sound in porous media : modeling sound absorbing materials.* Elsevier applied science, New York, 1994.

[2]   ATALLA, N. *Méthodes numériques en interaction fluide-structure.* Notes du cours GMC-722, Maîtrise en génie mécanique, été 1999.

[3]   Champoux, Y. *Étude expérimentale du comportement acoustique des matériaux poreux à structure rigide.* Ph.D. thesis, Univ. Carleton, Canada, 1991.

[4] : LESUEUR, C. *Rayonnement acoustique des structures.* Collection Département Etudes et Recherches EDF, Eyrolles, France 1988.

[5]   PANNETON, R. Modélisation numérique 3D par éléments finis des matériaux poroélastiques. Ph.D. thesis, Univ. Sherbrooke, Canada, 1996.
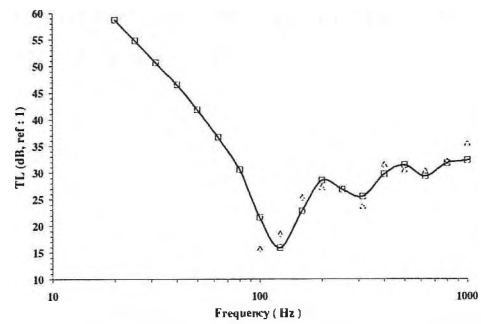
Figure 1 : Transmission loss of the simple plate. Numerical (?) and experimental (?)

Figure 2 : Transmission loss of the double plate system coupled with a 50 mm cavity filled with air. Numerical (?) and experimental (?)
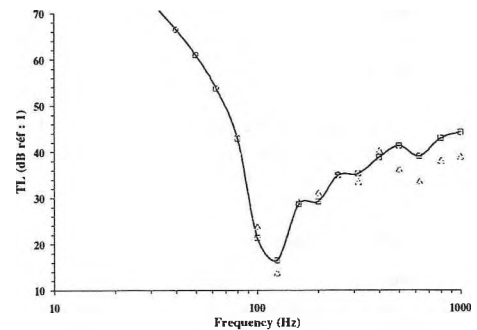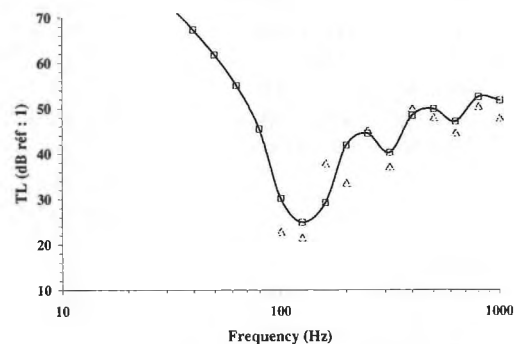

Figure 3 : Transmission loss of the double plate system coupled with a 50 mm cavity filled with a porous material. Numerical (?) and experimental (?)
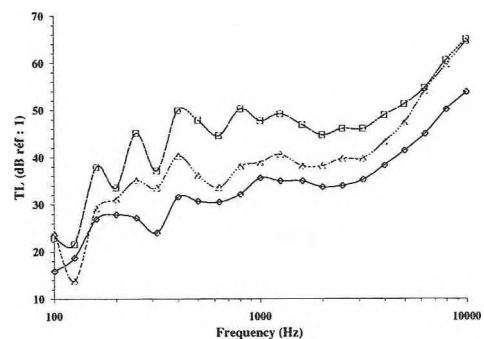

Figure 4 : Experimental results in the entire bandwidth. Simple plate (?), the double plate with air (?) and the double plate with the equivalent fluid (?)

RELATIONSHIPS BETWEEN QUANTITATIVE AND QUALITATIVE ASPECTS OF SOUNDS: CASE OF ACOUSTIC RADIATION FROM A PLATE

C. Marquis-Favre and J. Faure

LASH/DGCB URA CNRS 1652 ,ENTPE, Rue M. Audin, 69518 Vaulx-en-Velin, France, E-mail : Cathy.Marquis@entpe.fr

1. Introduction

Recent studies undertaken in car and household appliances industries [1] have underlined the importance of taking into account sound perception in the acoustic behaviour analysis of vibrating objects. These important results have led one to undertake a sound quality study applied to building structures. The starting point of this study is one particular component of a building wall: a single panel. The purpose of this work is to determine the influence of the mechanical parameters of a rectangular steel plate according to the relationships between a qualitative analysis and a quantitative analysis. This paper accounts for methods used to achieve the results obtained in the case of a radiating steel plate. The obtained results can also be applied to other industry trade such as car industry.

2. Method and experimentation

The general approach (fig.1) consists of two steps. First, the response of the structure is studied on the physical standpoint by varying various mechanical parameters. Then, the effect of these variations on sound perception is analyzed. This study makes it possible to evaluate the importance of the different parameters.

The studied structure is a homogeneous steel baffled and simply supported plate radiating in a semi-infinite field. The variation of three mechanical parameters is considered: the density, the Young's modulus and the plate thickness. The variation range of these parameters corresponds to the current values encountered for steel plate (fig.2). The vibroacoustic response of the plate, excited by a normal incidence plane wave, has been simulated for each value of parameter.

This computation has been undertaken from 0.5Hz up to 5kHz by 0.5Hz interval in two steps: first, the plate displacement has been analytically calculated by decomposition on the plate *in vacuo* eigenmodes basis [2]; secondly, the acoustic response of the baffled plate has been calculated at two receiver points corresponding to ears positions of a human who would have been placed in front of the plate. The influence of these different mechanical parameters on the vibroacoustic behaviour of the plate is succinctly presented in part 3.

At the same time, sounds have been synthesized from the calculat-

Density	Young modulus	Thickness
7700 Kg/m³	1.700 10¹¹ Pa	1.00 10⁻³ m
7800 Kg/m³	1.900 10¹¹ Pa	1.30 10⁻³ m
7870 Kg/m³	2.000 10¹¹ Pa	1.50 10⁻³ m
7900 Kg/m³	2.050 10¹¹ Pa	1.55 10⁻³ m
7950 Kg/m³	2.075 10¹¹ Pa	2.00 10⁻³ m
	2.100 10¹¹ Pa	3.00 10⁻³ m
	2.150 10¹¹ Pa	

Fig. 2. Variation of parameters

ed spectra by using inverse Fourier transform. For each parameter, the various sounds have been submitted to a jury of 15 persons (between 21 and 45 years old) using the pair comparison method [4]. For each pair of sounds, it was required of them to judge the similarity between sounds on a seven-point response scale with verbal end points, starting from 1 for "very different" up to 7 for "very similar". The subjects were also asked to choose which of the two sounds they preferred. The test was 20 minutes long and was carried out in a semi-anechoic room. The sounds listening and subjects responses were done with the help of a graphic interface. For sounds restitution, a sound card Sound Blaster (Sr. 44KHz) and an open headphone (SENNHEISER HD580) have been used. According to test results and data processing, an evaluation of the perceived distance between sounds as well as a note of preference have been obtained for each sound. These notes allow the preference to be represented versus different values of the considered parameter. Distances between stimuli have been evaluated using the Torgerson matrix and his factorial analysis [5]. This latter gives a graphical representation of sounds distances for each parameter.

3. Results and discussions

From a physical point of view, the density increase shifts down natural frequencies to low frequencies and leads to a decrease in the radiation efficiency [3]. When various sounds have been submitted to the jury, the subjects have found them all similar. This feeling is due mainly to the small percentage of the density variation (3.3 % of the minimum value). The range of this variation is however significant for a material such as steel. The sound radiation modification does not affect the perception of the distances in the present case. The density is thus not a very influential parameter on sound
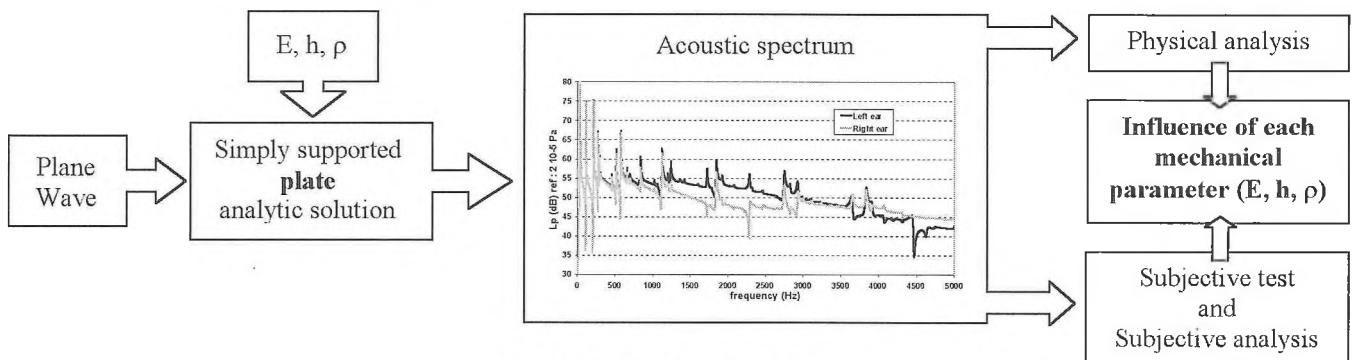

Fig. 1. Method and experimentation

perception in the case of a steel plate. The accurate knowledge (±100 kg/m^3) of this parameter as input of predictive computational tools or for the choice of a specific steel is thus not necessary.

Increasing Young's modulus shifts up natural frequencies to high frequencies and leads to an increase in the radiation efficiency [3]. Distances between sounds are in this case perceived as a linear function of Young's modulus (fig.3(a)). This linearity is expressed in a significant manner in terms of ratio of distances between sounds for the studied variation range and is given by the following relation:

$$\frac{\delta(i,j)}{\delta(i,k)} = \frac{|E_i - E_j|}{|E_i - E_k|}$$

with $\delta(i, j)$ denotes the perceived distance between the ith and jth sounds and E_i is the plate Young's modulus corresponding to the ith sound. The study of the preference has underlined that subjects have a slight tendency to prefer the weakest Young's modulus for the used variation range. This tendency is not very important as the variation percentage is not enough significant (27 % of the minimum value). In this case, the sound radiation modification does not have influence on the preference. It is nevertheless important to pay attention to the accuracy of the Young's modulus values as input to numerical softwares or in the choice of a specific steel since a Young's modulus variation of $0.1 \ 10^{11}$ Pa is perceived. However it has no influence on sounds preference. The operator will judge the necessity of this parameter accuracy according to the application context.
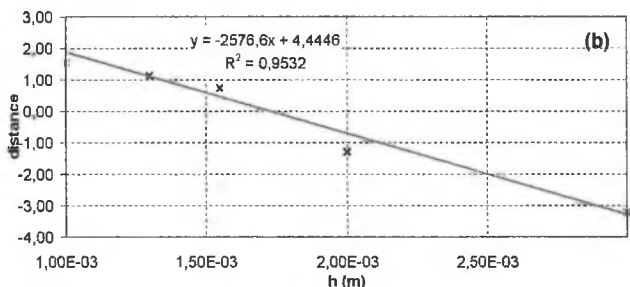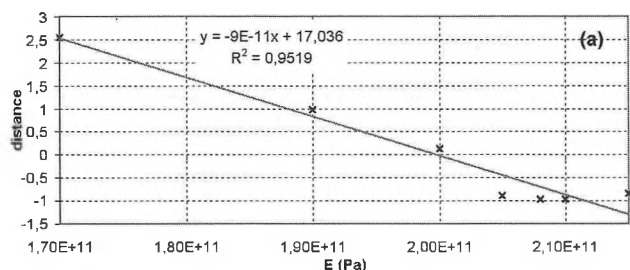
Fig. 3. (a) Perceived distance versus Youngs modulus and (b) Perceived distance versus thickness

The conclusions obtained for the thickness are similar to the Young's modulus ones. Namely, the thickness increase shifts up the natural frequencies to high frequencies and leads to an increase in radiation efficiency [3]. In addition, distances between sounds are perceived as a linear function of thickness (Fig.3(b)). One can establish for the studied variation range the following relation:

$$\frac{\delta(i,j)}{\delta(i,k)} = \frac{|h_i - h_j|}{|h_i - h_k|}$$

where $\delta(i, j)$ denotes the perceived distance between the ith and jth sounds, and h_i is the plate thickness corresponding to the ith sound. The preference study shows a more accentuated preference compared to the one observed in the case of Young's modulus variation. In the case of thickness variation, the preference grows as thickness increases (fig.4). The percentage of the thickness variation is more significant (300 % of the minimum value) than for the other studied parameters and thus, the subjects judgements are more accentuated for this parameter.
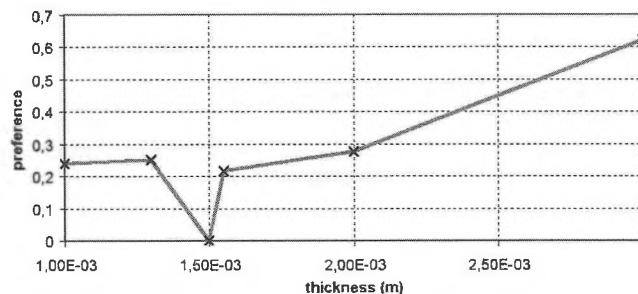
Fig. 4. Preference versus thickness

In the case of plate thickness, it is thus necessary to known with accuracy the thickness values as input of predictive numerical codes and in the design stage of structures since an absolute error of $0.05 \ 10^{-3}$ m is perceived for the studied thickness variation range and causes a different judgement of subjects preference.

Some investigations are carried out for other structural parameters such as boundaries conditions or structural damping of the plate in order to know whether the tendency given by a qualitative analysis confirms or not the one given by a classical physical study.

4. Acknowledgements

5. References

[1] BLAUERT, J. and JEKOSCH, U. - *Sound-Quality Evaluation - A Multi-Layered Problem* - Acta Acustica, 83, #5, 747-753 (1997).

[2] LESUEUR, C. - *Rayonnement acoustique des structures, vibroacoustique, interaction fluide-structure* - Eyrolles, Paris (1988).

[3] BERRY, A. - *Vibrations et rayonnement acoustique de structures planes complexes immergées dans un fluide léger ou dans un fluide lourd* - Rapport de Thèse, Université de Sherbrooke, Canada (1991).

[4] THURSTONE, L.L. - *Method of pair comparaison* - Journal of abnormal and social psychology, 21, 384-400 (1926).

[5] SAPORTA, G. - *Probabilités, analyse des données et statistique* - Editions Technip, Paris (1990).

NOISE GENERATION BY AGITATED INDUSTRIAL LIQUID MASSES

A. Warsame, I. Stuharu and R. B. Bhat

CONCAVE, Department of Mechanical Engineering, Concordia University

1. INTRODUCTION:

Quite often liquid masses are subjected to agitation in industrial processes such as in liquid baths used for cooling of parts heated during working them, centrifuges, turbulent fluid flow. Invariably, such agitated liquid masses generate noise. An analytical treatment of such noise is quite difficult in view of the various parameters involved, the shape of the containers, depth of the liquid mass, agitating mechanism, frequency of agitation etc.

When a mass of fluid flows past another fluid mass or a rigid or flexible solid with considerable relative velocity, the shear causes flow separation resulting in turbulence and pressure fluctuations. When these pressure fluctuations are transmitted through the surrounding air to the human ear, it gives the sensation of noise.

This phenomenon is quite common and can be seen in jet noise, wind noise in automobile and airplanes and when wind blows past our ears. The motivation for the present study came from the high noise levels from industrial liquid baths used to cool the drawn wires in the wire drawing industry. The noise from the drawing operation itself is muffled by the oil surrounding the drawing dies in a tank, however, the noise from the liquid baths were excessive and reached levels of 108 dB. The drawn wires passed through idler pulleys which agitated the cooling liquid in which they were submerged.

In the present study the noise generated in such agitated liquid masses is measured. A container filled with liquid is agitated using rotating blades. Noise measurements are carried out with the lid of the container open and closed at different speeds. Measured results are presented and discussed.

2. EXPERIMENTAL SET UP:

Preliminary studies are done using a simple kitchen blender shown in Fig. 1. The blender jar was filled with water and the noise was measured at a distance of 30 cm and a height of 50 cm from the base of the jar. Initially the background was measured and then the noise generated by the motor alone was measured without the jar. Subsequently, the noise generated by the agitated water was measured with and without the lid of the jar, at different speeds of rotation of the blades and for different levels of water.

3. RESULTS AND DISCUSSION:

The results are presented in Table 1. The motor noise is about 6 dB higher than the background noise. When the lid of the jar is closed the noise is not significant in comparison with the background noise. However, when the lid is removed, the noise from the agitated liquid is about 5 to 6 dB higher than the motor noise.

4. CONCLUSIONS:

Agitated liquids are capable of generating high noise levels. More investigations are needed with spectral decomposition of the noise and relating it to the motor speed, number of blades, density of the liquid, presence of vortices etc.

5. REFERENCE:

C.J. Hemond, Jr., "Engineering Acoustics and Noise Control", Prentice Hall, Inc., Englewood, New Jersey, 1983

L.B. Freund, S. Leibovitch and V. Tvergaard, "Acoustics of Fluid Structure Interactions" Cambridge University press, 1998.

Table 1. Measured Noise levels

Speed	jar 0.25 full Lid (dB)	No Lid (dB)	jar 0.5 full Lid (dB)	No Lid (dB)	jar full Lid (dB)	No Lid (dB)	motor only (dB)	room only 74 dB
1	82	86.8	81.2	86.6	80	87.2	79.2	range from
2	82.3	87.3	81.4	86.2	80.1	87	79.7	73.5
3	83.1	87.3	81.8	86.6	91	87.2	79.8	to
4	82	87.4	82.1	86.5	82	87.3	80	74.3
5	81.6	86.9	82.4	86.9	82.4	87.5	80	
6	81	86.9	82.5	87.1	83.1	87.5	80.2	
7	81.1	86.8	82.2	87.3	83.1	87.4	80.7	

Fig. 1 Experimental Setup

A Hybrid Methodology for the Identification of Incoherent Noise Sources

S. T. Raveendra and S. Sureshkumar
Automated Analysis Corporation, Ann Arbor, MI 48104, USA

1.0 Introduction

Modeling of noise sources is difficult when there are many potential noise sources and the interaction among them is complex. The measurement of sound field in these situations is laborious due to the need to make measurement at a large number of potential locations. A hybrid numerical/experimental approach based on Nearfield Acoustical Holography (NAH) alleviates some of the difficulties associated with the purely numerical or experimental technique. However, traditionally NAH has been applied mostly for the identification of coherent noise sources on planar structures using measurements taken on a planar grid [1-3]. The planar NAH was subsequently extended for the noise source identification on separable geometry such as cylindrical and spherical surfaces using measurements taken on conforming surfaces [4-10]. In the present development a generalized NAH that is applicable for the identification of multiple, incoherent noise sources on complex geometry is developed.

2.0 Mathematical Background

Numerical method such as boundary element method [11] can be used to generate transfer functions that relate the sound field in the acoustic domain to the surface velocity on an arbitrary source geometry. This relationship can be symbolically represented as

$$\{p\} = [T]\{V\} \qquad (1)$$

where p is the field acoustic pressure, V is the normal acoustic velocity on the surface and T is the transfer matrix. In principle, the above matrix equation can be solved to identify the noise sources (i.e. V) on any complex arbitrary surface.

In a typical analysis, $[T]$ is not a square matrix since the size of the matrix depends on the number of pressure measurement locations and the number of surface nodes. As result, equation (1) is solved by using a Singular Value Decomposition (SVD) technique. The application of SVD to the transfer matrix results in

$$[T] = [U][\sigma][V]^H, \qquad (8)$$

where superscript H indicates Hermitian (conjugate transpose) of a matrix, $[\sigma]$ is a diagonal matrix consisting of the singular values ranked from the highest to the lowest values and $[U]$, $[V]$ are unitary matrices containing the eigenfunctions of the SVD decomposition. The accuracy of the reconstruction process depends considerably on the SVD process [17]. A Tikhonov regularization scheme has been utilized in the present study.

The procedure described above is applicable for noise source identification of coherent sources. In situations where sources are generated by independent mechanisms, the number of independent sources are determined initially. This information together with a partial coherence technique is then used to separate the composite field into coherent partial fields. The noise sources corresponding to each partial coherent field are then identified using the NAH procedure described earlier in this section.

3.0 Results and Discussion

Interior noise in a propeller driven aircraft represents a non-stationary source that changes position with respect to time. Using a scanning microphone system, a pressure hologram of these kinds of sources can be acquired if measurements are taken at time increments which correspond to a fixed position in space of the rotating source.

For the aircraft this fixed position can be obtained from a synchro-phaser signal off of the propeller shaft, and data acquisition is synced to it. This simulates a stationary source and a coherent hologram can be acquired. One benefit of this is the ability to use signal averaging at each microphone position to increase the SNR of the pressure measurement. The analysis was done on a Beechcraft 1900D airplane [12].

The geometry of the fuselage and the hologram surface is depicted in figure 1. In the lower mosaic, the fuselage surface is cutout so that the hologram surface is visible. The hologram surface includes two closely spaced sets of pressure measurements at the ends, which are used to prescribe the velocity at the end caps using Euler's equation. The hologram consists of 30 axial rings with 43 microphones each in addition to the end caps.

The hologram pressure, looking aft, measured at 103.7 Hz using the outer 43 microphones of the array, acquired during the in-flight experiment is depicted in figure 2. One can see that the pressure is 180 degrees out of phase on either side of the aircraft. The quality of the data is outstanding. The smoothness of the pressure is proof that the synchro-phaser was an excellent time reference for the triggering of the data acquisition system.

We present the reconstruction of the normal velocity for the blade passage frequency (BPF) at 103.7 Hz. The reconstruction boundary is the exposed surface of the fuselage lining, located 8.59 cm from the hologram. The actual skin of the fuselage was 12.4 cm from the hologram surface. Figure 3 depicts the magnitude on a decibel scale of the reconstructed normal velocity looking aft. Only the top 20dB of data is shown as indicated by the color bar. The velocity is normalized by the velocity of an accelerometer located on a fuselage panel in the prop plane. The asymmetry of the panel vibrations is consistent with other measurements on this aircraft.
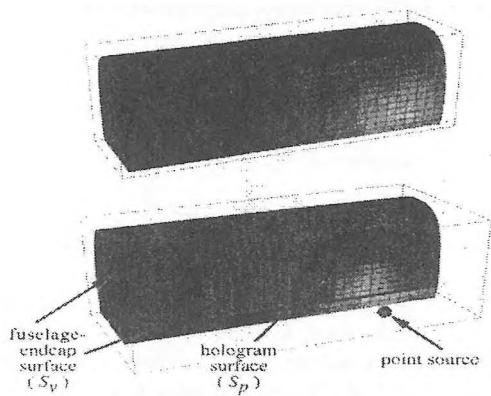
Fig. 1 Geometry of the Fuselage and Hologram
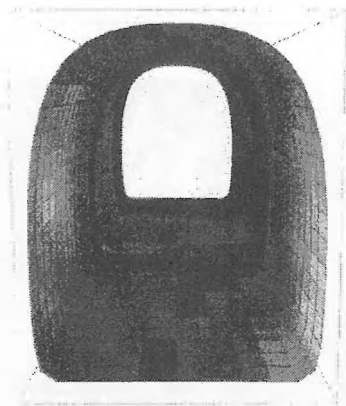
Fig. 6 Hologram Pressure Looking Aft
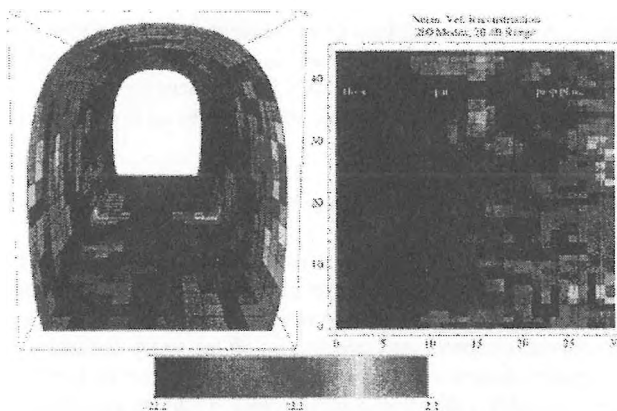
Fig. 3 Magnitude of the Reconstructed Normal Velocity

References

1. Williams, E. G., Fourier Acoustics: Sound Radiation and Nearfield Acoustical Holography, Academic Press, London, 1999.
2. Williams, E. G., Maynard, J. D. and Skudrzyk, E., Journal of the Acoustical Society of America, 68(1), pp. 340-344, 1980.
3. Maynard, J. D., Williams, E. G. and Lee, Y. Nearfield Acoustic Holography: I Theory of Generalized Holography and the Development of NAH, Journal of the Acoustical Society of America, 78(4), pp. 1395-1413, 1985.
4. Williams, E. G., Dardy, H. D. and Washburn, K. B., Generalized Nearfield Acoustical Holography for Cylindrical Geometry: Theory and Experiment, Journal of the Acoustical Society of America, 81(2), pp. 389-407, 1987.
5. Vernosi, W. A. and Maynard, J. D. Digital Holographic Reconstruction of Sources with Arbitrary Shaped Surfaces, Journal of the Acoustical Society of America, 85, pp. 588-598, 1989.
6. Borgiotti, G. Sarkissian, A. and Williams, E. G., Generalized Nearfield Acoustic Holography for Axisymmetric Geometries, Journal of the Acoustical Society of America, 88, pp. 199-209, 1990.
7. Sarkissian, A. Nearfield Acoustic Holography for Axisymmetric Geometry: A New Formulation, Journal of the Acoustical Society of America, 88, pp.961-966, 1990.
8. Kim, G. T. and Lee, B. H. 3-D Sound Source Reconstruction and Field Reproduction Using the Helmholtz Integral Equation, Journal of Sound and Vibration, 136, pp. 245-261, 1990.
9. Bai, M. R., Application of BEM (Boundary Element Method)-Based Acoustic Holography to Radiation Analysis of Sound Sources with Arbitrarily Shaped Geometries, Journal of the Acoustical Society of America, 92, pp. 533-549, 1992.
10. Kim, B. and Ih, J., On the Reconstruction of Vibro-Acoustic Field over the Surface Enclosing an Interior Space Using the Boundary Element Method, Journal of the Acoustical Society of America, 100, pp. 3003-3016, 1996.
11. Banerjee, P. K. Boundary Element Methods in Engineering, Mc-Graw Hill, 1993.
12. Williams, E. G., Houston, B. H., Herdic, P. C., Raveendra, S. T. and Gardner, B., Interior NAH in Flight, submitted to Journal of the Acoustical Society of America, 1999.
13. COMET/Acoustics: User's Manual, Version 5.0, Automated Analysis Corporation, Ann Arbor, Michigan, 2000.

VIBROACOUSTIQUE HAUTES FRÉQUENCES : MODÈLE ENERGÉTIQUE LOCAL POUR LE RAYONNEMENT

V. Cotoni, A. Le Bot, L. Jezequel

Laboratoire de Tribologie et Dynamique des Systèmes (UMR 5513 CNRS), Ecole Centrale de Lyon - France

INTRODUCTION

Ce papier décrit une nouvelle méthode de modélisation de problèmes vibroacoustiques dans le domaine des moyennes et hautes fréquences. En raison de l'augmentation du nombre de degrés de liberté, le spectre audible qui nous intéresse monte en effet au-delà des limites fréquentielles des codes classiques. Des méthodes alternatives dédiées aux hautes fréquences ont ainsi été développées. Notre approche s'inspire de la plus connue d'entre elles, la SEA [1]. Traitant de variables énergétiques également, elle s'attache cependant à donner une description locale des phénomènes. A cette fin, un formalisme intégral s'appuyant sur des noyaux énergétiques et sur les bilans de puissance locaux, est mis en œuvre.

Des exemples concernant des structures isolées et le rayonnement en milieu infini permettent d'illustrer la méthode à travers des comparaisons calculs / essais.

I- LA FORMULATION ÉNERGÉTIQUE INTÉGRALE

Les champs d'énergie et de flux de puissance dans les systèmes sont décrits de la façon suivante [2]:

- suivant le principe de Huygens, nous considérons que l'énergie en un point M du système W est due aux actions conjuguées des sources primaires de puissance r dans le système et des sources secondaires s correspondant aux puissances diffractées sur les frontières dW du système,
- postulant que les ondes propagatives dans le système sont décorrélées, nous appliquons le principe de superposition linéaire aux différentes contributions énergétiques.

Ainsi, partant des noyaux énergétiques G et H décrivant en coordonnée radiale les densités d'énergie et de flux de puissance du système infini excité ponctuellement,

$$G(r) = \frac{e^{-mr}}{c\gamma_0 r^{n-1}} \qquad et \qquad \vec{H}(r) = \frac{e^{-mr}}{\gamma_0 r^{n-1}} \vec{u}_r$$

nous écrivons les champs d'énergie et de flux de puissance,

$$W(M) = \int_\Omega \rho(S) G(S,M) dS + \int_{\delta\Omega} \sigma(P, \vec{u}_{PM}) G(P,M) dP$$

$$\vec{I}(M) = \int_\Omega \rho(S) \vec{H}(S,M) dS + \int_{\delta\Omega} \sigma(P, \vec{u}_{PM}) \vec{H}(P,M) dP$$

c représente la vitesse de groupe des ondes, l'angle solide de l'espace considéré, et m le coefficient d'atténuation. Cette formulation s'applique aux espaces monodimensionnels tels que les poutres [3], bidimensionnels tels que les plaques [4], et tridimensionnels tels que les milieux acoustiques [5].

Les sources de puissance de frontière s sont les inconnues du problème, qu'il convient de résoudre en exprimant les conditions limites énergétiques. A partir des formulations intégrales des variables énergétiques, nous écrivons donc les bilans de puissance locaux aux frontières. Ainsi, à l'image de la théorie géométrique de la diffraction [6], les amplitudes et directivités des sources de frontière font l'objet d'un calcul canonique préliminaire local. Exploitant ensuite le principe de localité valide en hautes fréquences, les expressions des sources secondaires sont introduites dans le système global. Nous développons maintenant deux exemples applicatifs que nous validons expérimentalement.

II- PLAQUE ISOLÉE, EXCITÉE PONCTUELLEMENT

Le cas d'une plaque isolée et excitée ponctuellement est résolu en écrivant que le flux de puissance à travers les bords de la plaque est nul. Afin de simplifier l'analyse, la directivité des sources de puissance structurale de frontière est postulée : la directivité diffuse de Lambert est utilisée. En introduisant cette expression dans la forme intégrale du flux de puissance, une équation de Fredholm de deuxième espèce est obtenue sur σ. La résolution de cette équation par collocation donne les amplitudes des sources de frontière.

Une validation expérimentale a été effectuée sur la plaque de la Figure 1, sur l'intervalle de fréquence [200,3200]Hz. Une tête d'impédance et un vélocimètre laser mesurent la puissance injectée et l'énergie structurale.
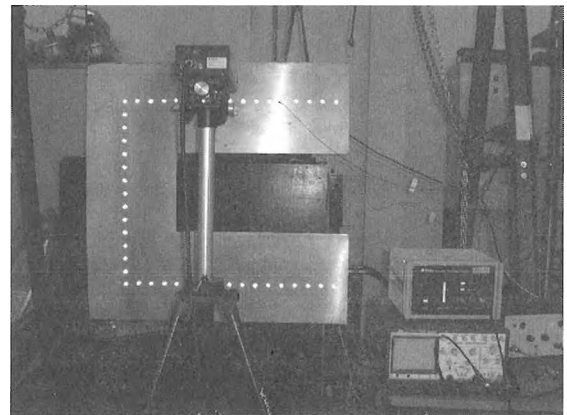
Fig. 1 : Dispositif expérimental.

Sur la Figure 2, le calcul (en gras) est comparé aux données expérimentales moyennées sur un tiers de bande d'octave. L'évolution spatiale de l'énergie autour de 1000 Hz est tracée à gauche. A droite sont représentées les évolutions fréquentielles en trois points de la structure.

III- RAYONNEMENT D'UNE PLAQUE EN MILIEU ACOUSTIQUE INFINI

Le problème d'une plaque couplée à un fluide acoustique est résolu de la même manière que précédemment en tenant compte des pertes de puissance par rayonnement. Les échanges ont lieu au niveau des discontinuités structurales où les ondes de flexion sont diffractées dans le milieu acoustique, et tout au long de la propagation des ondes si elles sont supersoniques (au dessus de la fréquence critique). Chaque type de discontinuité (le point d'injection de force et les bords de la structure pour le cas présent) donne donc lieu à un calcul canonique permettant de caractériser la directivité et l'amplitude des sources de puissance diffractée en fonction des flux de puissance structuraux.
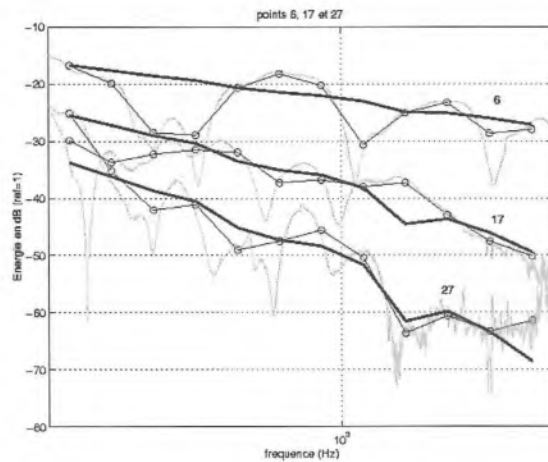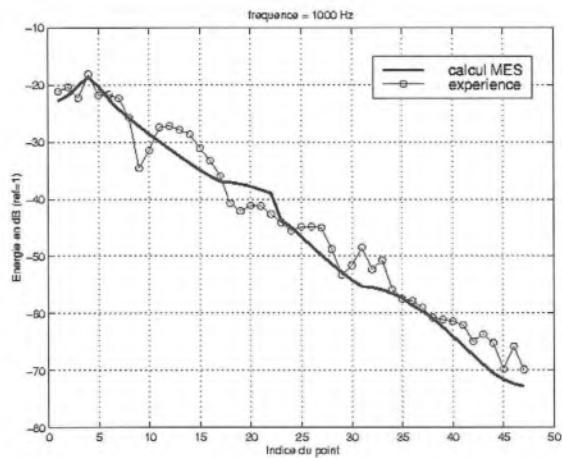
Fig. 2 : Evolutions spatiales et fréquentielles de l'énergie de flexion : comparaison calcul (en gras) / essai.
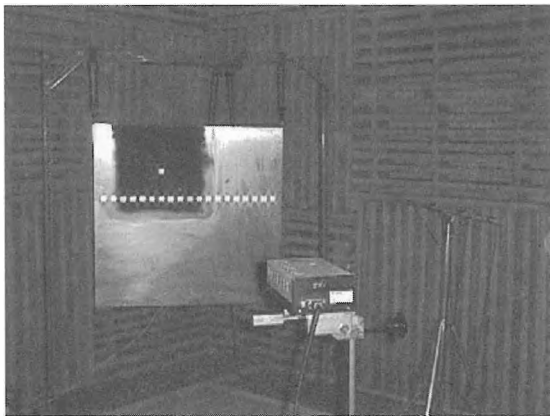
Fig. 3 : Dispositif expérimental pour le rayonnement.

Pour le calcul correspondant à l'expérience de la Figure 3, nous aurons donc des sources localisées sur les bords et au point d'excitation dans le domaine subsonique. Dans le domaine supersonique, nous rajouterons les sources de surface. L'énergie acoustique a été relevée en 6 points sur l'intervalle [3200,12800]Hz. Les comparaisons des calculs (-o-) aux essais moyennés par tiers de bande d'octave (-*-) sont présentées sur la Figure 4. Le graphique de gauche correspond à trois points sur une antenne orthogonale à la plaque, celui de droite sur une antenne parallèle. Les maxima correspondent au rayonnement supersonique très efficace de toute la surface.

Références

[1] Lyon and Dejong. *Theory and applications of statistical energy analysis*. Butterworth-Heinemann USA, 1995.

[2] Le Bot. *A vibroacoustic model for high frequency analysis*. JSV, 211(4), 1998.

[3] Bocquillet. *Méthode énergétique de caractérisation des réseaux complexes*. Thèse d'université. ECL 2000

[4] Bouthier and Bernhard. *Simple models of the energetics of transversely vibrating plates*. JSV, 182(1), 1995.

[5] Kuttruff. *Energetic sound propagation in rooms*. Acustica, 83, 1997.

[6] Keller. *Geometrical theory of diffraction*. JOSA, 52(2), 1962.
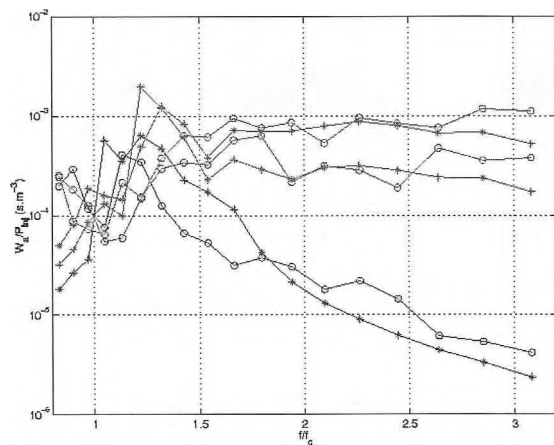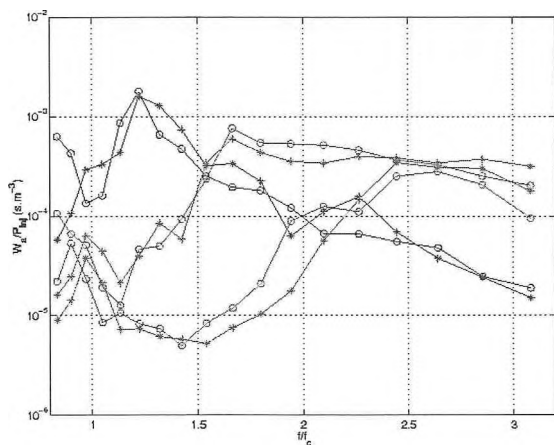
Fig. 4 : Evolutions fréquentielles de l'énergie acoustique en 6 points de l'espace.

FORMULATION OF AN EQUATION OF DIFFUSION FOR HETEROGENEOUS RODS

J.M. Mencik[1], A. Berry[1] and J.L. Guyader[2]

1. G.A.U.S., Mechanical Engineering Department, Université de Sherbrooke, Sherbrooke, Qc, J1K 2R1, CANADA
2. Laboratoire Vibrations Acoustique de l'INSA de Lyon, 20 Avenue Albert Einstein, 69621 Villeurbanne Cedex, FRANCE

1. Introduction

The present article is devoted to the characterization of the vibratory behavior of heterogeneous structures, i.e when material or geometrical discontinuities are considered. Usual displacement formulations are rapidly limited when heterogeneity density and high frequency are considered. Energetic methods seem to be well adapted in this case, because an energetic response of the system is spatially smoother and more frequency robust than a classical displacement response.

Statistical energy Analysis (SEA) [1] is successfully used to characterize mean energies of lightly coupled subsystems; however the method is valid at high frequency when each mode of a subsystem is assumed to be uniformly probable over a frequency band. The energy flow method is based on the derivation of an equation of diffusion for homogeneous structures, in analogy with heat transfer [2]. An approximate solution is derived when quantities are spatially averaged over half a structural wavelength [3-4];. Difficulties however occur when spatially averaged energetic boundary conditions have to be specified, meaning that the method is not well adapted when heterogeneities occur.

In this paper, a new formulation characterizing the energetic diffusion in a rod with cross-sectional area discontinuities is presented. At low frequency, it appears that the energy flow is governed by heterogeneities since an heterogeneous gradient exists. The theoretical result is validated by a numerical simulation for a clamped-free heterogeneous rod which is excited at the free end by a power source.

2. Theoretical analysis

The structure under study is shown on Figure 1: It is composed of N elements, element p has a length L_p and contains n_p homogeneous rod of random lengths $l_{p,i}$ and cross-sectional areas $S_{p,i}$, the index p,i meaning homogeneous rod i from element p. The mean potential energy density for element p is $<\overline{U}>_p$.
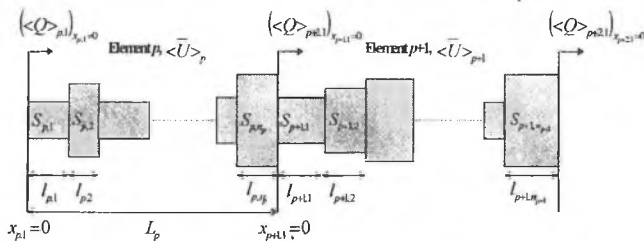
Figure 1. Description of two consecutive rod elements for random scheme.

The active power which is transmitted through an homogeneous rod p,i is expressed by

$$<Q>_{p,i}=\frac{1}{2}\mathrm{Re}\left\{j\omega ES_{p,i}\frac{\partial u_{p,i}}{\partial x}u_{p,i}^*\right\}, \qquad (1)$$

where E is the complex Young's modulus and $u_{p,i}$ is the longitudinal displacement which is solution of the equation of motion for homogeneous rod outside of the external force points [5].

Displacement and axial force continuity between homogeneous rods p,i and p,i-1 [5] enforces power continuity

$$\left(<Q>_{p,i}\right)_{x_{p,i}=0}=\left(<Q>_{p,i-1}\right)_{x_{p,i-1}=l_{p,i-1}}, \qquad (2)$$

as well as the continuity of the second derivative if one derives equation (1) twice.

$$\left(\frac{\partial^2}{\partial x^2}<Q>_{p,i}\right)_{x_{p,i}=0}=\left(\frac{\partial^2}{\partial x^2}<Q>_{p,i-1}\right)_{x_{p,i-1}=l_{p,i-1}}. \qquad (3)$$

Similarly, equation (1) yields the following discontinuity condition for the first derivative of the power

$$\left(\frac{\partial}{\partial x}<Q>_{p,i}\right)_{x_{p,i}=0}=\frac{S_{p,i-1}}{S_{p,i}}\left(\frac{\partial}{\partial x}<Q>_{p,i-1}\right)_{x_{p,i-1}=l_{p,i-1}}. \qquad (4)$$

Let us define the first semi-local derivative of the power evaluated at the junction between elements p-1 and p

$$\left(\overline{\frac{\partial}{\partial x}}<Q>_{p,1}\right)_{x_{p,1}=0}$$
$$=\frac{1}{L_p}\left[\left(<Q>_{p+1,1}\right)_{x_{p+1,1}=0}-\left(<Q>_{p,1}\right)_{x_{p,1}=0}\right], \qquad (5)$$

and the second semi-local derivative

$$\left(\overline{\frac{\partial^2}{\partial x^2}}<Q>_{p,1}\right)_{x_{p,1}=0}$$
$$=\frac{1}{L_p}\left[\left(\overline{\frac{\partial}{\partial x}}<Q>_{p+1,1}\right)_{x_{p+1,1}=0}-\left(\overline{\frac{\partial}{\partial x}}<Q>_{p,1}\right)_{x_{p,1}=0}\right]. \qquad (6)$$

Assuming that dimensions of elements are small, and that the power slowly varies over each element (i.e. the structural wavelength is large compared to element lengths), then Taylor series expansions result in

$$\left(\overline{\frac{\partial}{\partial x}}<Q>_{p,1}\right)_{x_{p,1}=0}=\frac{1}{L_p}\left(\sum_{r=1}^{n_p}l_{p,r}\frac{S_{p,1}}{S_{p,r}}\right)\left(\frac{\partial}{\partial x}<Q>_{p,1}\right)_{x_{p,1}=0}. \qquad (7)$$

and

$$\left(\overline{\frac{\partial^2}{\partial x^2}}<Q>_{p,1}\right)_{x_{p,1}=0}$$
$$=\frac{1}{L_p}\left[\frac{1}{L_{p+1}}\left(\sum_{r=1}^{n_{p+1}}\frac{l_{p+1,r}}{S_{p+1,r}}\right)\left(\sum_{r=1}^{n_p}l_{p,r}S_{p,r}\right)\left(\frac{\partial^2}{\partial x^2}<Q>_{p,1}\right)_{x_{p,1}=0}\right.$$
$$\left.-S_{p,1}G_p\left(\frac{\partial}{\partial x}<Q>_{p,1}\right)_{x_{p,1}=0}\right] \qquad (8)$$

where the heterogeneous gradient is defined by

$$G_p = \gamma_p - \gamma_{p+1} \qquad (9)$$

from the heterogeneous density of element p

$$\gamma_p = \frac{1}{L_p} \sum_{r=1}^{n_p} \frac{l_{p,r}}{S_{p,r}} . \qquad (10)$$

If one supposes that the heterogeneous gradient is different from zero, it is possible to neglect the first term in the right-hand side of equation (8) compared to the second term. This means that the second derivative of the power does no diverge in space. This argument is detailed below.

According to the local energy balance for steady state and outside of the input power points [4], the mean potential energy density of element p is defined by

$$< \overline{U} >_p = -\frac{1}{2\omega\eta} \left(\frac{\overline{\partial}}{\partial x} <Q>_{p,1} \right)_{x_{p,1}=0} \qquad (11)$$

and the semi-local energetic gradient by

$$\overline{\nabla}_x <\overline{U}>_p = \frac{1}{L_p} [<\overline{U}>_{p+1} - <\overline{U}>_p] . \qquad (12)$$

Using equation (7), it is then possible to formulate an equation of diffusion, expressing the energy flow from mean potential energy density

$$\overline{\nabla}_x <\overline{U}> + \alpha_r^{het} <\overline{U}> = 0 , \qquad (13)$$

where

$$\alpha_r^{het} = \frac{G_p}{L_p \gamma_p} \qquad (14)$$

is the heterogeneous coefficient of diffusion. Assuming a spatially-uniform coefficient, the solution of equation (13) is

$$< \overline{U} > = A \exp(-\alpha_r^{het} x) \qquad (15)$$

from constant A, identified from boundary conditions. Potential energy density increases as the heterogeneous density does. The solution given by equation (15) stays admissible, as we saw, if the second derivative of the power is not great compared to first derivative. That means that the energy flow provided by loss factor, that is the first term of equation (8), goes in the same direction than the energy flow expressed by equation (13).

3. Numerical results

Let us consider the clamped-free heterogeneous rod illustrated on Figure 2, excited by a known input power $\left(<Q>_{1,1} \right)_{x_{1,1}=0} = <Q>_{in}$.
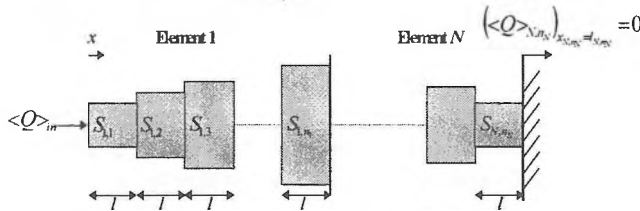
Figure 2. Free-clamped excited heterogeneous rod.

It is composed of N=400 elements, each of them containing n=4 homogeneous rods of random cross-sectional areas, and is excited at a frequency f=1000Hz. The Young's modulus is

E_R=2.1×10^{11}Pa, the loss factor η=0.01 and the density ρ=7800kg/m^3, the lengths of homogeneous rod are similar, $l = 10^{-2}$ m. In order to validate the equation (13), the energy flow due to heterogeneities must decay in the same way as the energy flow due to loss factor, therefore one fixes constant decrease of the heterogeneous density along the length of the rod. The value of the energetic gradient theoretically predicted by equation (13) is compared to the numerical value derived from the exact equations on Figure 3.
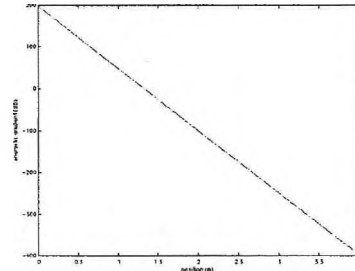
Figure 3. Semi-local energetic gradient :low frequency results, numerical value (——), theoretical solution (···).

The theoretical formulation is very well validated as the two curves fit perfectly.

4. Conclusion

In this work, a new formulation characterizing the energy flow in heterogeneous rod was derived when heterogeneities are modeled by cross-sectional area discontinuities. This method is semi-local when energetic diffusion is identified between elements containing a random scheme of heterogeneities. The energetic diffusion is governed at low frequency by cross-sectional area discontinuities as an heterogeneous gradient occurs. The theoretical results succeed in estimating the exact value provided by the numerical simulation when the energetic gradient is spatially plotted along the length of the rod.

A next important development in analyzing the energetic diffusion in heterogeneous structures is to study more complicated structures, such as beams with cross-sectional area discontinuities and plates with local masses. A long-term objective is to predict vibratory behavior of industrial structures such as car frames. It involves another important study when identifying energetic boundary conditions for heterogeneous coupled subsystems, that is local transmitted powers and energies.

5. References

[1] R.H. Lyon and R.G. DeJong, "Theory and application of Statistical Energy Analysis", second edition (Cambridge, Massachusetts: MIT Press, 1975).

[2] D.J. Nefske and S.H. Sung, "Power flow finite element analysis of dynamic systems: basic theory and applications to beams", Statistical Energy Analysis, NCA **3**, 47-54, (1987).

[3] Y. Lase, M.N. Ichchou and L. Jezequel, "Energy flow analysis of bars and beams: theoretical formulations", Journal of Sound and Vibration, **192**(1), 281-305, (1996).

[4] J.C. Wohlever and R.J. Bernhard, "Mechanical energy flow models of rods and beams", Journal of Sound and Vibration, **153**(1), 1-19, (1992).

[5] S. Timoshenko, G.H. Young and W. Weaver jr., "Vibration problems in engineering", 4th edition (New York, John Wiley, 1974).

Wave Compatibility Condition: An Alternative For Vibro-Acoustic Problems In Medium Frequency Range

Olivier BAREILLE, Louis JEZEQUEL

Laboratoire de Tribologie et Dynamique des Systèmes (UMR 5513 CNRS), Ecole Centrale de Lyon - France

Dealing with vibro-acoustic problems brings to the choice of a method to solve them. Those methods are usually classified in two categories: low and high frequency ranges. This is justified by the reachable or needed precision to achieve (versus the numerical cost).

If we want to keep the easiness of the FE-based or modal methods in writing the equations of the problem, we need to reduce the numerical size of the problem. For that purpose, we can see the boundary element methods and modal sampling ones as a great improvement.

In this paper, let's see how describing the primal and the dual fields on a very particular set of variables leads to straight-forwardly written equations along the boundaries. Moreover, on a rather simple generic vibro-acoustic problem, we will be able to derive the coupling equations in an easily understandable way.

Choice of the variables

Primal and dual local patterns are expanded on a basis of plane- or cylindrical-wavelike functions. These functions are selected among the solutions of the local equation of motion. The local variables are then the amplitudes $\{a_j\}_j$ of these functions.

In order to ensure the wave compatibility from one domain to an other when dealing with their coupling, we introduce two intermediate sets of boundary variables : $\{d_j\}_j$ and $\{F_j\}_j$. These variables are the trace of the local patterns projected, along the boundary on a Fourier series-like basis.

$$d_i = P_{1,ij} \, a_j$$

$$F_i = P_{2,ij} \, a_j$$

with P_1 and P_2, operators of projection.

The equation of coupling are then derived in term of boundary values; the Fourier-series decomposition allows us to write the coupling in a straight forward manner. The whole problem is then solved along the boundaries of the domains through the variables $\{d_i, F_i\}$ which are compatible with the description of wave propagation : the local primal and dual fields can be reconstructed thanks to their projections on these boundaries.

Therefore the modal behavior can be approached thanks to those boundary generalized values, whereas the propagative aspect is induced by the choice of the field variables. And the Wave Compatibility Condition (W.C.C.) ensures the connection between the two representations.

Vibro-acoustic example

Let's study the response to a point harmonic acoustic excitation of a rigid walled cavity, except on one side. This problem is considered as bi-dimensional, thus the flexible part will be described as a beam loaded with a continuous 2D field of pressure.
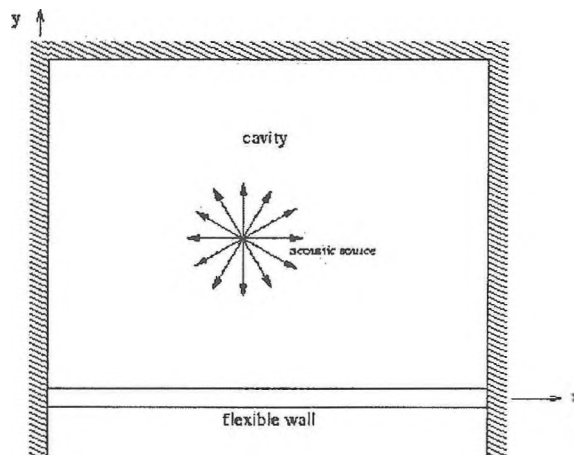
The number of generalized variables, N+1, for a portion (or face) of the boundary is given by the highest apparent number of wave lengths ,N , along that portion. Then, the total number of variables is limited to (N+1) x (element's number of faces).

We divide the domain in sub-elements so that the point exciting source can be located on the boundary of one of those elements. The excitation is then taken into account in the force continuity equations through this interface. In our case, if we divide the cavity in triangular elements, we have 3x(N+1) variables per element.

The boundary generalized values are the coefficients of a Fourier series which represent the projections of each wave onto the boundary of the sub-domain under scrutiny.

The fields of pressure p and the normal velocity v are described as introduced in the first part. The number of waves used in the basis is limited to 3N+3 per triangle sub-domain.

$$p(\vec{x}) = a_j \Phi_j(\vec{x})$$

$$v(\vec{x}) = i\rho\omega \, a_j \nabla\Phi_j(\vec{x}).\vec{n}$$

with $j = 1, \dots 3N+3$.

The boundary generalized values $\{d_i, F_i\}$ are the amplitudes of the waves' projections on this very boundary.

$$p(s) = F^a_j G^a_j(s)$$

$$v(s) = i\omega \, d^a_j D^a_j(s)$$

with s the curvilinear variable, G^a_j Fourier function (sinus, cosinus) or dirac function located at the corner between two faces, D^a_j Fourier function or linear interpolating function associated to one corner.

As to the beam, the transversal displacement w and the shear stress t are also expressed in the same way: the wave description

is used for the field patterns and the generalized-variable description is used along the boundaries:

$$t(s) = F^b{}_j G^b{}_j(s)$$

$$w(s) = d^b{}_j D^b{}_j(s)$$

Example of a loaded beam

In order to deal with the coupling of the flexible wall (the beam) and the cavity, we must first study the response of a clamped-clamped beam to an harmonic continuous loading.

The equation of motion gives the relation between the transverse displacement $w(x)$ and the continuous loading $f(x)$.

$$w^{(4)} - k^4 w = f(x) \qquad (1)$$

The clamped boundary conditions at the ends of the beam define a set of equations to be satisfied
by the integrative constants. According to the type coupling here, $f(x)$ takes the form :

$$f(x) = F_C \cos(\bar{k} x) \text{ or } F_S \sin(\bar{k} x) \qquad (2)$$

with $\bar{k} = \dfrac{2\pi m}{L}$, L the length of the beam and $(F_C, F_S) \in R^{*2}$

Actually, $\bar{k}$ is linked to k by a relation involving the hysteretic damping of the beam, named η :

$$k = \bar{k}(1 - i\eta)$$

Solving (1) with (2) we obtain the response in amplitude as drawn on the following figure.

For a continuous variation of $\bar{k}$, we have drawn the exact response of the beam to time and space harmonic loadings. Yet, the WCC response of the same beam is observed by using the following approximation :

$$k \approx \frac{2\pi m}{L}(1 - i\eta)$$

with m, an integer number and

$$\frac{2\pi m}{L} \le \Re(k) < \frac{2\pi(m+1)}{L}$$
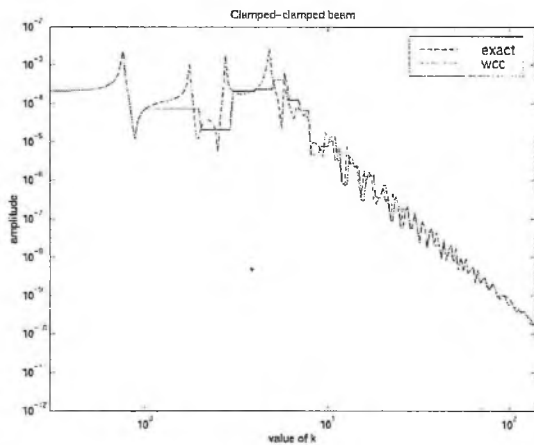
Finally, the WCC coupling with a bi-dimensional neighboring domain leads us to choose :

$$\bar{k} = \frac{2\pi m}{L} \text{ and } k = \frac{2\pi m}{L}(1 - i\eta)$$

By this mean, we are able to connect the solution of the loaded beam to the kind of coupling we use between the beam and the cavity (through Fourier functions).

The 3 different types of responses are compared on the figure at the bottom of this page. All the caracteristics of the beam are set equal to 1, the loading is in cosinus with 5 period along the length of the beam. The observation point is at 3/10 of the length from the end of the beam.

The step-like variations are due to the sharp variations of $\bar{k}$ when the frequency changes. Such effect becomes negligeable as the frequency rises up to medium and high ranges.

Coupling equations

We use this example to derive the coupling equations for the vibro-acoustic problem with $F_{C \text{ or } S} = F^b{}_m$. Each boundary variable is associated to a solution for the beam just like in the previous part. The final solution is obtained by adding all those single solutions.

The coupling between the flexible wall and the cavity, whatever dimension they might be is obtained by expressing their wave compatibility conditions through the set of Fourier variables defined at their interface $\{F^a{}_j, d^a{}_j\}$ and $\{F^b{}_j, d^b{}_j\}$.

Since we use the same kind of functions to describe the primal and the dual patterns along the interface (between the flexible wall and the cavity), the coupling equations are obtained by writing the continuity of the boundary variables from one domain to another. These equations represent the Wave Compatibility Condition.

Conclusion

The method presented in this paper allows us to solve vibro-acoustic problems in a straight-forward.

Once described on a local propagative basis, the primal and the dual fields are projected on the boundaries of each sub-domains where the coupling equations are derived thanks to a Fourier-like writing of the projected patterns.

This method keeps some advantages of so-called low frequencies ones and remains applicable to medium and high frequency ranges thanks to the condensed description of the primal and the dual fields.

References

L. Jezequel, H.D. Setio, Components Modal Synthesis Methods Based on Hybrid Models, part I : Theory of Hybrid Models and Modal Truncation Methods, J.Applied Mechanics, 61, pp.100-108, 1994.

L. Jezequel, H.D. Setio, Components Modal Synthesis Methods Based on Hybrid Models, part II : Numerical Tests and Experimental Identification of Hybrid Models, J.Applied Mechanics, 61, pp.109-116, 1994.

A Hybrid Approach to The Mid-Fferquency Problem

Phil Shorter

Vibro-Acoustic Sciences, 12555 High Bluff Drive, Suite 310 , San Diego, CA 92130, USA.

Overview

The response of a structural-acoustic system in the mid-frequency range typically consists of both long and short wavelength behavior. Modeling the short-wavelength behavior deterministically is usually computationally prohibitive and structural-acoustic techniques such as statistical energy analysis (SEA) are often adopted. However, SEA cannot adequately capture the long-wavelength global behavior of the system. Recent work aimed at addressing the mid-frequency problem has led to the development of a hybrid approach [1] based on a wavenumber partitioning scheme. This paper provides a brief overview of the approach.

1. Introduction

Consider the frame-plate structure illustrated in Figure 1. The structure consists of a stiff beam framework with two bays. A thin flexible plate has been inserted into one of the bays and the structure is excited by a point force applied to the framework as indicated.
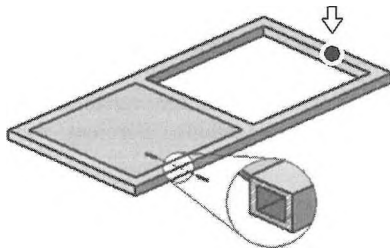
Figure 1. Frame structure typifying behavior of a system in the mid-frequency range.

The response of such a structure typically consists of a mix of both long and short-wavelength behavior over the frequency range of interest and is representative of a much wider class of mid-frequency problems. Such problems include the response of aerospace and automotive structures which contain stiffening frames, shells and enclosed acoustic cavities with disparate modal densities. The response of the framework in the previous example is dominated by long wavelength global behavior, while the response of the plate is dominated by short wavelength local behavior.

One approach to analyzing the dynamic behavior of the structure would be to model the interactions between the various beam and plate subsystems using an SEA model. However, the beam subsystems are typically strongly coupled and have relatively few interacting modes; their response therefore tends to be dominated by global rather than local dynamic behavior. In such circumstances SEA tends to overestimate the mean response due to coherence effects [2] and doesn't capture the resonant variations in the framework response.

One might therefore attempt to analyze the dynamic behavior of the structure using an FE model. However, the high modal density of the plate subsystem complicates such an analysis. Much of the computational effort involved in creating the FE model and solving the global eigenproblem is associated with capturing the short wavelength local behavior of the plate. Even if this computational expense is affordable one finds that the short wavelength behavior is also very sensitive to perturbations in the properties of the plate. One is then uncertain as to whether the predicted dynamic interactions between the plate and the framework are representative of those that occur in nominally identical structures.

It is therefore natural to question whether one can perform a hybrid analysis which combines FE and SEA in order to address the mid-frequency problem. This is the motivation behind the Resound method described in [1]. In Resound the subsystems in a system are partitioned into those that exhibit long wavelength global behavior (for example the framework in the previous example) and those that exhibit short wavelength local behavior (the plate). The latter are referred to as fuzzy subsystems. The long wavelength global behavior is then modeled deterministically using FE while the short wavelength local behavior is modeled statistically using SEA. There is clearly an interaction between the two partitions of the model and this interaction is fully accounted for with the calculation of various fuzzy coupling terms.

2. Local and global basis functions

The local and global partitioning described in the previous section is an important part of the Resound approach and merits further discussion. In general, a lumped-parameter model of a structural-acoustic system can always be obtained by expressing the response in terms of a finite number of basis functions. Equations of motion are then formulated using Lagrange's equations or Hamilton's principle. In Resound a distinction is made between short wavelength local basis functions (defined over the various fuzzy subsystems) and long wavelength global basis functions (defined over the whole system). The global basis functions are chosen so that they provide a good basis with which to describe the long wavelength global deformation of the system. Similarly, the local basis functions are chosen so that they provide a good basis with which to describe the local short wavelength behavior of the various fuzzy subsystems.

The global basis functions may be obtained by suppressing the local dynamic behavior in a (coarsely meshed) FE model. A convenient way to achieve this suppression is to apply Guyan reduction [3] to the interior degrees of freedom associated with each fuzzy subsystem. Additional techniques have also been developed to suppress individual wavefields within a FE model [5]. The local basis functions are then taken to be the local component modes associated with each fuzzy subsystem. The local component modes are never computed explicitly; instead, asymptotic estimates of the component modal properties are employed. There are clear similarities between the basis functions used in Resound and those used

in a component mode synthesis model [4]. Indeed, Resound may be viewed as a form of statistical component mode synthesis.

3. Reduction of the equations of motion

The partitioned equations of motion for a given system can be written as

$$
\begin{bmatrix} \mathbf{D}_{gg} & \mathbf{D}_{gl} \\ \mathbf{D}_{lg} & \mathbf{D}_{ll} \end{bmatrix} \begin{bmatrix} \mathbf{q}_g \\ \mathbf{q}_l \end{bmatrix} = \begin{bmatrix} \mathbf{f}_g \\ \mathbf{f}_l \end{bmatrix} \quad (1)
$$

where $\mathbf{D}$ is the dynamic stiffness matrix, $\mathbf{f}$ is the generalized force vector, $\mathbf{q}$ is a vector of displacements and the subscripts l and g represent the local and global degrees of freedom respectively. From the previous discussion it is apparent that there are likely to be far more local degrees of freedom than global degrees of freedom in the model. The large dimension of the local partitions typically renders a deterministic analysis of the system computationally impractical. It is therefore beneficial to reduce the local degrees of freedom from the above equation. It can be shown [6] that the perturbation to the mn'th entry of the global dynamic stiffness matrix is then given by

$$
\left(\Delta \mathbf{D}_{gg} \right)_{mn} = \sum_i \alpha_i \beta_{i,mn} \quad (2)
$$

where the summation i is over all local component modes in the various fuzzy subsystems and where

$$
\alpha_i = \frac{\omega^4}{\omega_i^2 (1 + i\eta_i) - \omega^2}
$$

$$
\beta_{i,mn} = \left(\int_{V'} \rho \phi_{g,m}^T \phi_{l,i} \, dx \right) \left(\int_{V'} \rho \phi_{g,n}^T \phi_{l,i} \, dx \right) \quad (3)
$$

The term α_i accounts for frequency effects and depends on the distribution of the local natural frequencies about the excitation frequency. The term β_i accounts for spatial effects and depends on the local and global mode shapes.

4. Asymptotic fuzzy coupling

In principle, the previous expression could be evaluated exactly for any given system. This would require the 'exact' local natural frequencies and modes shapes to be calculated in order to accurately determine α and β. There are a number of reasons why this approach is not beneficial. Firstly, there may be a significant number of local modes, which would render an exact deterministic calculation computationally impractical. Secondly, an exact deterministic calculation does not account for the effects of uncertainties in the local natural frequencies and mode shapes. The extra effort required to perform the deterministic calculation is therefore unlikely to result in an increase in the accuracy of the predictions.

One of the fundamental features of the Resound approach is that the summation in equation (2) is replaced by an integration over various regions of wavenumber space. The influence of the local modes on the global dynamic behavior can then be accounted for without having to explicitly calculate the mode shape and natural frequency associated with each local mode (resulting in a significant reduction in computational expense). Asymptotic expressions are derived for α and β as discussed in [1,6,7]. The overall approach remains computationally tractable yet captures the overall dynamic behavior of the system in a manner that is not possible using FE or SEA in isolation.

5. Acknowledgements

6. References

[1] R.Langley, P.Bremner, A hybrid method for the vibration analysis of complex structural-acoustic systems, Journal of the Acoustical Society of America, 105(3), pp.1657-1671, 1999.

[2] B.R.Mace, Wave coherence, coupling power and statistical energy analysis, Journal of Sound and Vibration, 199(3) pp. 369-380, 1997.

[3] R.D.Cook, Concepts and applications of finite element analysis, John Wiley and Sons, New York. 1989.

[4] R.Craig Substructure methods in vibration, Trans ASME 117, 207-213, 1995.

[5] P.J.Shorter, R.S.Langley, Wavefield suppression and its application to mid-frequency structural acoustics, Proc. of Internoise 2000.

[6] P.J.Shorter, Resound theory document, Vibro-Acoustic Sciences, Inc., Internal Report, March 2000.

[7] P.J.Shorter, R.S.Langley, The spatial correlation of vibrational wavefields and their application to mid-frequency structural-acoustics, Novem 2000.

Estimation Of Fuzzy Structure Parameters For Continuous Junctions

C. Soize[1] and K. Bjaoui[2]

[1]Structural Dynamics and Coupled Systems Department, ONERA, BP 72, 92322 Chatillon Cedex, France.

[2] GAUS, Département de Génie Mécanique, Sherbrooke (Qc), Canada, J1K 2R1.

1. Introduction

The fuzzy structure theory was introduced by Soize [1] 15 years ago in order to model structural complexity in the medium frequency range. This structural complexity plays a fundamental role in the response of a master structure coupled with complex substructures in the context of structural-acoustic systems. In 1993, a second fuzzy impedance law was proposed [2] to model the case of fuzzy substructures attached to the master structure through a continuous junction. Since 1993, much research has been conducted concerning the problem of a master structure coupled with a large number of simple linear oscillators but few concerning continuous cases. Two main problems had to be solved to be able to apply the fuzzy structure theory (described in details in Ref. [3]) to the case of continuous junctions. The first problem was related to the construction of a procedure for identifying the fuzzy structure parameters in order to solve complex problems and to allow experimental identifications to be performed. The second one, which requires solving the first, is related to validation of the fuzzy structure theory for continuous junctions. A general procedure has been developed to solve the first problem. In this paper, we present a first validation of the fuzzy structure theory for continuous junctions between the master structure and the complex substructures. We introduce a new cost function replacing the cost function previously introduced [4]. It allows an efficient estimation of the fuzzy structure parameters using a procedure based on the statistical energy approach (SEA).

2. Reference complex structure

The reference complex structure is made of a master structure coupled with four complex substructures (a), (b), (c) and (d) (see Figure 1). The master structure is made of two rectangular homogenous isotropic thin plates (1) and (2), in bending modes and simply supported, coupled along their common edge; the rotation around this edge is continuous. Each complex substructure is made of a rectangular homogenous isotropic thin plate on which many simple oscillators are attached. The plate of each complex substructure is in bending modes and simply supported, coupled to a plate of the master structure along their common edge; the rotation around this edge is continuous. Consequently, there is a continuous junction between the master structure and each complex substructure. Two plates belonging to different complex substructures are not coupled along their common edge. The method used to construct the model of the reference complex structure consists in constructing the generalized impedance matrix of an isolated plate belonging to the master structure and an isolated complex substructure. Then the coupling between the isolated subsystems is done using a Lagrange multiplier technique in order to express the continuity of the rotation on the junctions.

A dynamical response of the reference complex structure is calculated for a force excitation applied at a point of a master structure plate. It should be noted that at low frequency range the complex substructures do not significantly affect the response of the master structure. In medium frequency range, the complex substructures play an important role in the response of the master structure; complex substructures induce an apparent strong damping in the master structure due to the power flow from the master structure to structural complexity.

3. Reference complex structure modeling using the fuzzy structure theory

Using the fuzzy structure theory, the reference complex substructure is modeled by a fuzzy structure. The effects of each fuzzy substructure on its related master structure plate are taken into account using a random boundary impedance (on $\Gamma^{(a)}_{(1),fuz}$, $\Gamma^{(b)}_{(1),fuz}$ for plate (1) and on $\Gamma^{(c)}_{(2),fuz}$, $\Gamma^{(d)}_{(2),fuz}$ for plate (2)) whose expression can be found in Ref. [5-6]. For each fuzzy substructure, the impedance law related to each substructure depends on four mean coefficients (parameters) and their associated deviation coefficients. These mean parameters are the mean coefficient of the participating inertial moment, the mean rate of internal damping, the mean modal density and the mean equivalent coupling factor. The generalized impedance matrix of a master structure plate coupled with its fuzzy substructure is constructed using Ritz-Galerkin method. The coupling between the two plates of the master structure is written using Lagrange multipliers technique as done before. The construction of the random response of the fuzzy structure is based on the use of Neumann series expansion limited to order 2. Then, we obtain the mean response function of the fuzzy structure. And in order to get more information about the random response level in dB, we construct the confidence region defined by the upper and lower envelopes of the frequency-response-function modulus corresponding to a given probability level. The upper envelope is constructed using Chebychev's inequality.

4. Estimation of fuzzy structure mean parameters

It is assumed that a direct estimation of the mean rate of the internal damping and the mean modal density of the fuzzy substructures can be obtained. Since the junction between a plate of the master structure and one of its fuzzy substructures is continuous, the fuzzy structure theory yields a mean equivalent coupling factor much lower than 1. A sensitivity analysis was performed and showed that the frequency independent value 0.005 was a good approximation for this mean parameter.

Concerning the estimation of the mean coefficient of the participating inertial moment, we use the statistical energy approach introduced in [2], but using a new cost function [5-6]. The mean coefficient of the participating inertial moment is obtained minimizing this new function cost. But this cost function is not convex, then the optimization problem is not easy to solve. Consequently, we developed an algorithm with two main steps. In the first step, a neighborhood containing the solution of the optimization problem is constructed using a random research algorithm. In the second step, the optimization problem is solved in this neighborhood.

5. Validation

We consider the response of the reference complex structure and the mean response of the fuzzy structure with zero deviation coefficients. It was shown that the fuzzy structure mean response with zero deviation coefficients gives a good representation of the reference complex structure response.

We consider the response of the reference complex structure and the envelopes of the fuzzy structure response with nonzero deviation coefficients. The deviation coefficients associated with the participating inertial moments and the modal densities are nonzero whereas those associated with internal damping rates and equivalent coupling factors are taken equal to zero. It was shown that the response of the reference complex structure belong to the confidence region defined by the upper and lower envelopes predicted by the fuzzy structure theory and corresponding to a probability level equal to 0.95. Consequently, the prediction is satisfactory and this example validates the fuzzy structure theory for continuous junctions.

6. Conclusion

This paper constitutes a first validation of the fuzzy structure theory for continuous junctions between the master structure and the fuzzy substructures. The mean response function calculated by the fuzzy structure theory with zero deviation coefficients gives a good representation of the reference complex structure response. The calculation of the envelopes with nonzero deviation coefficients based on the use of a second-order Neumann series expansion and Chebychev's inequality is very efficient. In addition, a new function cost allowing estimation of fuzzy structure parameters has been introduced. Statistical energy approach has been proved very efficient This procedure for estimating the fuzzy structure parameters, validated by numerical simulation, opens the field to experimental identifications.

References

[1]   Soize, C., "Probabilistic structural modeling in linear dynamic analysis of complex mechanical systems. I-Theoretical elements", Rech. Aerosp. **5**, pp. 23-48, (1986). (English edition).

[2]   Soize, C.,"A model and numerical method in the medium frequency range for vibroacoustic predictions using the theory of structural fuzzy", J. Acoust. Soc. Am. **94**, pp. 849-865, (1993).

[3]   Ohayon, R. and Soize, C., "Structural Acoustics and Vibration", Academic, San Diego, (1998).

[4]   Soize, C., "Estimation of the fuzzy substructure model parameters using the mean power flow equation of the fuzzy structure", Proceeding of the ASME Noise Control and Acoustics Divisions, Vol. 1, ASME/WAM, 28-30, NCA-Vol. 22, pp. 23-30 (1996), also published in Journal of Vibration and Acoustic **120**, pp. 279-286 (1998).

[5]   Bjaoui, K., "Estimation des paramètres d'une structure floue pour des jonctions continues", Thèse du Conservatoire National des Arts et Métiers, Paris, (1999).

[6]   Soize, C. and Bjaoui, K., "Estimation of fuzzy structure parameters for continuous junctions", J. Acoust. Soc. Am. **107** (4), pp. 2011-2020, (2000).
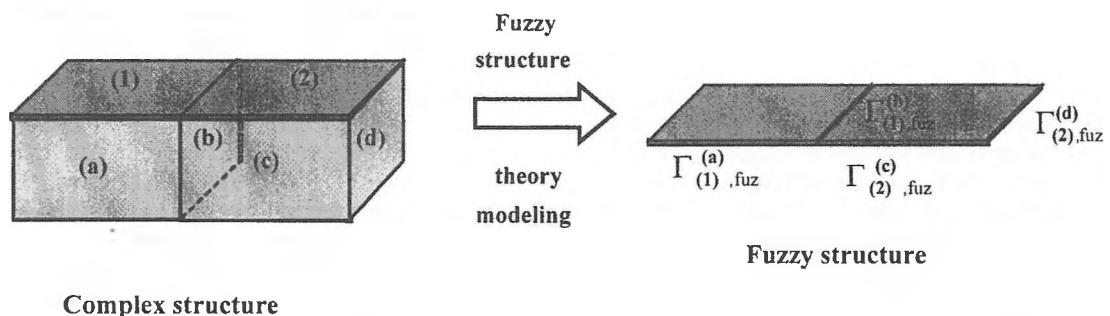
Fig. 1. Model of the reference complex structure by fuzzy structure theory

The Overshoot Effect In Older Versus Young Adults With Normal Hearing

E.F. Wong and M.F. Cheesman

National Centre for Audiology, School of Communication Sciences and Disorders, University of Western Ontario, London, ON N6G 1H1

INTRODUCTION

The detectability of a short-duration auditory signal improves as the onset of that signal is delayed relative to the onset of a longer-duration masker. This phenomenon has been termed the "overshoot" effect (Zwicker, 1965). The overshoot effect has been well-characterized with respect to its time course and frequency dependent nature (Bacon & Viemeister, 1985; Bacon & Moore, 1986; Bacon & Smith, 1991; Carlyon, 1987; McFadden, 1989), as well as the effect of varying qualities of the masker or signal (Bacon, 1990; Carlyon & White, 1992), in normal hearing young adults.

The magnitude and time course of the overshoot effect in listeners with normal hearing and those with high-frequency hearing loss have also been examined. A permanent, sensorineural hearing loss may disrupt the mechanisms responsible for a large overshoot effect in the frequency region of the hearing loss (Bacon & Takahashi, 1992). Conversely, however, Carlyon and Sloan (1987) have shown that the size of the overshoot effect is not influenced by sensorineural hearing loss. This discrepancy may be due to the fact that two-thirds of Carlyon and Sloan's subjects had a slight hearing loss in the control ears, or due to the use of different masker levels which affect the degree of overshoot. Furthermore, studies have also shown that the detection threshold for a signal near masker onset improved, and thereby reduced overall degree of overshoot, with temporary hearing loss using either intense sound exposure (Champlin & McFadden, 1989) or aspirin (McFadden & Champlin, 1990).

Several explanations for the underlying mechanism for the simultaneous masking phenomenon of overshoot have been proposed. The most common of these is the result of adaptation of auditory neurons tuned to the signal frequency, particularly those with primarily "onset"-like responses. This explanation has been supported by neurophysiological data, which show that primary auditory neurons give a second onset response to an additional short stimulus regardless of the time interval between the first and second stimuli (Smith, 1979; Smith & Zwislocki, 1975). However, by itself, neural adaptation can only partially account for the large overshoot effect observed in normal hearing young adults. Additional mechanistic contributions must therefore be considered to explain overshoot.

Studies by Bacon and Smith (1991) showed that larger overshoot effects are observed in the presence of broadband maskers than maskers of a single critical band width, suggesting the involvement of components remote from the signal frequency. This off-frequency processing may be susceptible to cochlear damage and therefore responsible for the reduced overshoot effect observed in hearing-impaired subjects (Bacon & Takahashi, 1992).

Another hypothesis is based on synchronous across-fiber firing (Champlin & McFadden, 1989; McFadden & Champlin, 1990; Bacon & Smith, 1991). Large overshoot values may be dependent on large pooled responses from groups of auditory fibers. A large pooled onset response would require that the individual onset responses be combined in a synchronous fashion. Desynchronized firing would lead to a reduced pooled onset response and conse-

quently reduced threshold near onset (and hence degree of overshoot).

Finally, more central processes such as neural inhibition may be involved in overshoot (Bacon & Moore, 1987; McFadden & Champlin, 1990).

Several studies have shown that age-related factors other than peripheral hearing loss account for losses in temporal resolving ability, which may contribute to the speech perception difficulties commonly experienced in the aging population, particularly under degraded listening conditions such as background noise and/or reverberation (Lutman, 1991; Snell, 1997; Strouse et al., 1998; Kricos & Lesner, 1995; Gordon-Salant & Fitzgibbons, 1993).

Physiological changes due to aging, particularly the demyelinization and desynchronous firing of auditory nerve fibers, may contribute to poorer temporal resolution. This change in temporal resolving abilities may reduce the degree of overshoot and/or increase the time-course of overshoot in older adult subjects.

This research compared the overshoot phenomenon in older versus young adults with normal hearing sensitivity. More specifically, this research determined what differences existed in the threshold and time-course characteristics of the overshoot effect between normal hearing older adults (55-70 years of age) and normal hearing young adults (20-30 years of age).

METHODS

Subjects

The subject pool consisted of 12 young adults (20-30 years), and 6 older adults (55-70 years) with normal hearing sensitivity (thresholds not worse than 25 dB HL at any of the octave frequencies from 250-8000 Hz), thus minimizing the possible confounding effect of hearing loss. Subjects did not have prior experience with overshoot experiments. Participation was strictly on a voluntary basis, and participants were not paid for their involvement.

Each subject was asked to complete a background information questionnaire relating to general health and other factors that may affect hearing performance. Then, each subject underwent a standard audiometric assessment of hearing sensitivity. Impedance measures were also administered to determine middle ear function.

Stimuli and Apparatus

Sinusoidal signals were 10 ms in duration, with 5-ms cosine rise/fall times. There was no steady state portion of the signals. Signal frequency was either 1000 Hz or 4000 Hz. The onset of the signal occurred near the beginning of the masker (1-ms delay) or near the temporal center of the masker (250-ms delay).

Noise maskers were 475 ms in duration, including 5-ms cosine rise and fall time. For the narrowband condition, white noise was bandpass filtered between 860-1160 Hz for the 1000 Hz condition, and 3440-4640 Hz for the 4000 Hz signal. For the wideband condition, the noise was highpass filtered with a cutoff frequency of 50 Hz. Masker spectrum level was 30 dB SPL, which has been shown to be the level that produces a maximum overshoot effect in most listeners (Bacon, 1990).

Procedure

Quiet thresholds (in the absence of the noise masker) were obtained at both signal frequencies to provide baseline measures of threshold. Subjects were then given a practice run to familiarize them with the stimuli and the task prior to data collection.

Thresholds were then measured using an adaptive two-interval, forced choice procedure that estimates a 70.7% on the psychometric function (Levitt, 1971). Both intervals contained the masker; one also included the signal. Overshoot was determined as the difference in masked thresholds between 250 and 1-ms signal delay conditions.

Four overshoot values were obtained in total: wideband 1000 Hz, wideband 4000 Hz, narrowband 1000 Hz, and narrowband 4000 Hz.

RESULTS

Mean overshoot values for both young and older adult subjects were larger in the wideband cases than the narrowband (Figure 1). This is consistent with results obtained previously in the literature (Bacon & Smith, 1991). Upon comparison of the mean young versus older adult subject results using a split-plot ANOVA (within-subjects and between-subjects design), there was no significant difference between the two groups for any measure.

	Wideband 1000Hz	Wideband 4000Hz	Narrowband 1000Hz	Narrowband 4000Hz
Younger	5.1 (sd=5.3)	6.1 (sd=7.9)	0.19 (sd=4.6)	0.3 (sd=7.8)
Older	8.7 (sd=7.0)	7.7 (sd=9.7)	2.3 (sd=4.7)	0.2 (sd=5.7)

Figure 1. Mean masking overshoot (in dB) for each masking condition.

DISCUSSION

There were considerable individual differences, regardless of age or audiometric threshold. Some normal-hearing young adult subjects showed little or no overshoot; some older adult subjects demonstrated large degrees of overshoot.

In a temporal resolution study of older adults by He *et al.* (1999), gap detection was better for the long-duration stimulus than for the shorter-duration stimulus. The researchers suggested that the detection of a gap in a noise burst in gap detection studies, and the detection of a signal in a masker in overshoot studies may share a common underlying mechanism. Further research by the current authors involved obtaining gap detection thresholds for the same young adult and older adult populations and comparing gap detection vs. overshoot thresholds on an individual basis.

REFERENCES

Bacon, S.P. (1990). Effect of masker level on overshoot. *J. Acoust. Soc. Am.* 88:698-702.

Bacon, S.P. and Moore, B.C.J. (1986). Temporal effects in simultaneous pure-tone masking: effects of signal frequency, masker/signal frequency ratio, and masker level. *Hear. Res.* 23:257-266.

Bacon, S.P. and Moore, B.C.J. (1987). Transient masking and the temporal course of simultaneous tone-on-tone masking. *J. Acoust. Soc. Am.* 81:1073-1077.

Bacon, S.P. and Smith, M.A. (1991). Spectral, intensive, and temporal factors influencing overshoot. *Quart. J. Exp. Psych.* 43A(3):373-399.

Bacon, S.P. and Takahashi, G.A. (1992). Overshoot in normal-hearing and hearing-impaired subjects a). *J. Acoust. Soc. Am.* 91:2865-2870.

Bacon, S.P. and Viemeister, N.F. (1985). The time course of simultaneous tone-on-tone masking. *J. Acoust. Soc. Am.* 78: 1231-1235.

Carlyon, R.P. (1987). A release from masking by continuous, random, notched noise. *J. Acoust. Soc. Am.* 81:418-426.

Carlyon, R.P. and Sloan, E.P. (1987). The 'overshoot' effect and sensory hearing impairment. *J. Acoust. Soc. Am.* 82:1078-1081.

Carlyon, R.P. and White, L.J. (1992). Effect of signal frequency and masker level on the frequency regions responsible for the overshoot effect. *J. Acoust. Soc. Am.* 91:1034-1041.

Champlin, C.A. and McFadden, D. (1989). Reductions in overshoot following intense sound exposures. *J. Acoust. Soc. Am.* 85: 2005-2011.

Gordon-Salant, S. and Fitzgibbons, P.J. (1993). Temporal factors and speech recognition performance in young and elderly listeners. *J. Sp. Hear. Res.* 36:1276-85.

He, N-J. Horwitz, A.R., Dubno, J.R. and Mills, J.H. (1999). Psychometric functions for gap detection in noise measured from young and aged subjects. *J. Acoust. Soc. Am.* 106:966-978.

Kricos, P. B. and Lesner, S.A. (1995). Hearing care for the older adult. Boston: Butterworth-Heinemann.

Levitt, H. (1971). Transformed up-down methods in psychoacoustics. *J. Acoust. Soc. Am.*, 49(2):467-477.

Lutman, M.E. (1991). Degradations in frequency and temporal resolution with age and their impact on speech identification. *Acta Otolaryngol. (Stockh.) Suppl.* 476:120-126.

McFadden, D. (1989). Spectral differences in the ability of temporal gaps to reset the mechanisms underlying overshoot. *J. Acoust. Soc. Am.* 42:143-153.

McFadden, D. and Champlin, C.A. (1990). Reductions in overshoot during aspirin use. *J. Acoust. Soc. Am.* 87:2634-2642.

Smith, R.L. (1979). Adaptation, saturation, and physiological masking in single auditory-nerve fibers. *J. Acoust. Soc. Am.* 65: 166-178.

Smith, R.L. and Zwislocki, J.J. (1975). Short-term adaptation and incremental responses of single auditory-nerve fibers. *Biol. Cybernetics* 17:169-182.

Snell, K.B. (1997). Age-related changes in temporal gap detection. *J. Acoust. Soc. Am.* 101: 2214-2220.

Strouse, A., Ashmead, D.H., Ohde, R.N. and Grantham, D.W. (1998). Temporal processing in the aging auditory system. *J. Acoust. Soc. Am.* 104: 2385-2399.

Zwicker, E. (1965). Temporal effects in simultaneous masking by white-noise bursts. *J. Acoust. Soc. Am.* 37:653-663.

DURATION DISCRIMINATION IN YOUNGER AND OLDER ADULTS

Tonya R. Bergeson, Bruce A. Schneider, and Stanley J. Hamstra

University of Toronto

1.0 INTRODUCTION

Older adults, even those with little or no hearing loss, often find it difficult to understand speech when the listening situation is less than ideal (e.g., a noisy or reverberant background) or when the rate of speech is high (e.g., Pichora-Fuller, 1997). Because the temporal modulation of the speech signal has been shown to contribute substantially to speech recognition in younger adults (e.g., Kingsbury, Morgan, & Greenberg, 1998), several researchers have posited that older adults' speech understanding difficulties might stem, in part, from diminished temporal resolution (e.g., Schneider, 1997), although the evidence for this has been mixed. For instance, older listeners who have poor gap duration discrimination abilities have been shown to have more trouble understanding temporally degraded speech (Gordon-Salant & Fitzgibbons, 1993). On the other hand, some studies have suggested that the contribution of age-related changes in temporal resolution to speech recognition are minimal (e.g., Humes, 1996). It is possible that some of the discrepancies across studies may be due to differences in how temporal resolution was measured.

There are several paradigms that measure temporal processing ability. For example, in gap detection studies, listeners try to detect a short period of silence between two sounds. Studies have shown that age-related losses in detecting a gap may only occur when the durations of the tones marking the gap are very short (e.g., Schneider & Hamstra, 1999). If so, we might expect older adults to be generally poorer at processing short-duration stimuli.

Another paradigm used to investigate temporal processing capacity is duration discrimination. In duration discrimination experiments, listeners are asked to detect a change in stimulus duration. Older adults generally have more difficulty discriminating the signal durations than younger adults (Abel, Krever, & Alberti, 1990; Fitzgibbons & Gordon-Salant, 1994; 1995). Moreover, hearing loss or degree of hearing loss does not influence older adults' performance.

Given that the duration of the stimuli that mark a gap has such drastic effects on younger and older listeners' gap-detection performance, perhaps the duration of the stimuli has similar effects on younger and older adults' duration discrimination abilities. In the present experiment, we examined the temporal resolution abilities of younger and older adults in a duration discrimination paradigm in which we systematically varied the standard tone duration from 1.5 ms to 1000 ms. Based on the duration discrimination literature presented previously and the results of Schneider and Hamstra (1999), we predicted that older adults would perform more poorly than younger adults, and that this age effect would be much more pronounced at short standard tone durations, independent of audiometric thresholds.

2.0 METHOD

Ten younger adults (mean age = 22.3 years; S.D. = 1.6 years) and ten older adults (mean age = 70.9 years; S.D. = 5.7 years) were paid participants in this experiment. The younger adults were students at University of Toronto at Mississauga; the older adults were recruited from a pool of seniors from the local community. All par-

ticipants had pure-tone, air-conduction thresholds $\leq$ 25 dB HL between .25 and 2 kHz.

Stimuli were generated digitally with a sampling rate of 20 kHz and converted to analog form using a 16-bit Tucker Davis Systems (TDS) digital-to-analog converter. The 2 kHz tone was gated on and off by multiplying it by an envelope constructed by summing a series of Gaussian functions (standard deviation ½ ms), spaced ½ ms apart. The duration of the stimulus was defined as the time between the centers of the first and last Gaussian envelopes comprising the sum. The standard tone durations ranged from 1.5 ms to 1000 ms. Stimuli were presented over the left ear over TDH-49 earphones in a single-wall sound-attenuating booth.

Duration discrimination thresholds were determined by presenting stimuli at each standard tone duration in a 2IFC paradigm. A staircase procedure was used to determine the 79.7% point on the psychometric function (Levitt, 1971). At the beginning of a block, a standard tone duration was chosen and the comparison tone duration was set to a previously established value. The standard and comparison tones were randomly assigned to the two intervals. After each trial was initiated by pressing a button, the two tones would occur, separated by a 100 ms silent period. Participants were asked to choose which interval they thought contained the longer tone by pressing one of two buttons that corresponded to the two intervals. Lights on the response box indicated the beginning of the trial and whether the participants' response had been correct. The duration of the comparison tone was adjusted trial-by-trial according to a 3 down, 1 up rule. That is, if participants successfully discriminated between the two tone durations 3 times in succession, the next comparison tone duration would be decreased (closer in duration to the standard tone). However, if the participant responded incorrectly the comparison tone duration would be increased. Each block was terminated after 12 reversals; duration discrimination thresholds were defined as the mean of the last 8 reversals.

The order of standard tone durations was randomly assigned to each participant. Although all participants completed this procedure four times (four 1- to 1.5-hour sessions were required per participant), the first runs at all standard tone durations were treated as practice sessions and were not included in subsequent analyses; only the last three runs were used for the final threshold estimate.

TIME IN MILLISECONDS
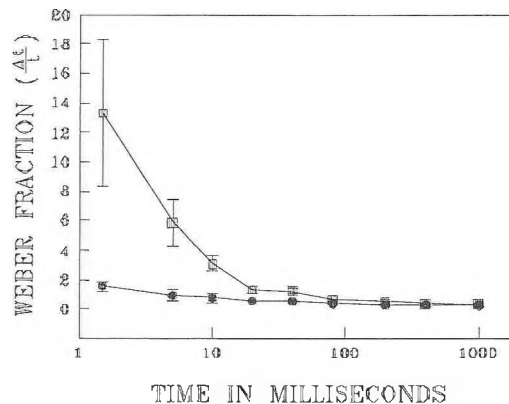
3.0 RESULTS

Figure 1 shows duration discrimination Weber fractions as a function of standard tone duration for younger and older listeners. It is clear that older listeners found duration discrimination much more difficult than younger listeners at the shortest durations tested, although there is considerable variability in the older listeners' performance. In fact, the Weber fractions for the older adults at the shortest duration (1.5 ms) were almost 7 times greater than the younger adults' Weber fractions, compared to just 2 times greater at the 20 ms standard tone duration. This larger difference between younger and older adults' duration discrimination abilities at the 1.5 ms standard tone duration is also much larger than those performance differences found in previous duration discrimination studies (e.g., Abel et al., 1990; Fitzgibbons & Gordon-Salant, 1994; 1995).

To ensure that the variability in the older adults' performance at the shortest duration could not be explained by their audiometric thresholds, we compared the older listeners' Weber fractions to their audiometric thresholds at 2 kHz. Younger and older adults' Weber fractions were not significantly correlated with audiometric threshold at 2 kHz at any of the standard tone durations

The size of the duration discrimination difference between older and younger listeners decreases with increasing standard tone duration, almost converging by 1000 ms.

4.0 DISCUSSION

Duration discrimination is much more difficult for older listeners than for younger listeners at very short standard tone durations, but becomes easier at longer standard tone durations, where the performance of older and younger listeners is nearly identical. Younger listeners' duration discrimination performance also improves with increasing standard tone duration, but the slope is not nearly as steep as that of older listeners. The differential results for older and younger listeners are independent of audiometric thresholds, as expected from similar results reported in most duration discrimination experiments. That is, age-related changes in hearing threshold level most likely have no systematic effect on duration discrimination for older adults with relatively good hearing. Moreover, the independence of duration discrimination and hearing thresholds suggests that older adults' duration discrimination deficits reflect central rather than peripheral auditory dysfunction, as other researchers have also proposed (e.g., Fitzgibbons & Gordon-Salant, 1996).

These results have implications for older listeners' understanding of speech, especially speeded speech or speech in noise. Considering that critical phonemic information in speech often occurs at durations much shorter than 20 ms, older adults would have a very difficult time utilizing such cues to decipher particular words in the speech stream, especially in noisy situations. In addition, Peterson and Lehiste (1960) have shown that, in English, the duration of a vowel is influenced by the preceding or following consonant. For example, the vowel duration in the word "rice" is much shorter than vowel duration in the word "right." Hence, vowel duration can serve as an additional cue to word identification in noisy situations where the consonants may be partially or completely masked. Older adults would be disadvantaged in such situations if they could not easily discriminate differences in vowel duration.

Some studies of older adults' temporal processing have supported this idea. For example, Lutman (1991) found that older adults with extremely poor gap detection thresholds also tended to

have diminished speech identification scores. Furthermore, Gordon-Salant and Fitzgibbons (1993) found that gap duration discrimination is related to older adults' ability to recognize reverberant speech, as mentioned earlier. However, they did not find strong correlations between duration discrimination and understanding of temporally distorted speech. Similarly, Abel et al. (1990) did not find that duration discrimination was a factor in the intelligibility of speech.

In conclusion, the present study demonstrates that older adults perform more poorly than younger adults at duration discrimination for short duration stimuli, but older and younger adults perform similarly at longer duration stimuli. This diminished temporal processing capability in older adults could make it more difficult for them to process speech in difficult listening situations where there is noise, reverberation, or when speech is speeded.

6.0 REFERENCES

- Abel, S. M., Krever, E. M., & Alberti, P. W. (1990). Auditory detection, discrimination and speech processing in ageing, noise-sensitive and hearing-impaired listeners. Scandinavian Audiology. 19, 43-54.
- Fitzgibbons, P. J., & Gordon-Salant, S. (1994). Age effects on measures of auditory duration discrimination. Journal of Speech and Hearing Research. 37, 662-670.
- Fitzgibbons, P. J., & Gordon-Salant, S. (1995). Age effects on duration discrimination with simple and complex stimuli. Journal of the Acoustical Society of America. 98, 3140-3145.
- Fitzgibbons, P. J., & Gordon-Salant, S. (1996). Auditory temporal processing in elderly listeners. Journal of the American Academy of Audiology. 7, 183-189.
- Gordon-Salant, S., & Fitzgibbons, P. J. (1993). Temporal factors and speech recognition performance in young and elderly listeners. Journal of Speech and Hearing Research. 36, 1276-1285.
- Humes, L. E. (1996). Speech understanding in the elderly. - Journal of the American Academy of Audiology. 7, 161-167.
- Kingsbury, B. E. D., Morgan, N., & Greenberg, S. (1998). Robust speech recognition using the modulation spectrogram. Speech Communication. 25, 117-132.
- Levitt, H. (1971). Transformed up-down methods in psychoacoustics. Journal of the Acoustical Society of America. 49, 467-477.
- Lutman, M. E. (1991). Degradations in frequency and temporal resolution with age and their impact on speech identification. Acta Otolaryngol. Supp. 476, 120-126.
- Peterson and Lehiste (1960
  Pichora-Fuller, M. K. (1997). Language comprehension in older listeners. Journal of Speech-Language Pathology and Audiology. 21, 125-142.
- Schneider, B. A. (1997). Psychoacoustics and aging: Implications for everyday listening. Journal of Speech-Language Pathology and Audiology. 21, 111-124.
- Schneider, B. A., & Hamstra, S. J. (1999). Gap detection thresholds as a function of tonal duration for younger and older listeners. Journal of the Acoustical Society of America. 106, 371-380.

TEMPORAL JITTER MIMICS THE EFFECTS OF AGING ON WORD IDENTIFICATION AND WORD RECALL IN NOISE

Sasha Brown & M. Kathy Pichora-Fuller

School of Audiology and Speech Sciences, University of British Columbia

Difficulty understanding speech spoken in noise is a particular problem for older adults, even when they have no clinically significant elevation in pure-tone audiometric thresholds (CHABA, 1988). Because spectral models of hearing loss are inadequate to account for their particular difficulties (for a review see Schneider & Pichora-Fuller, 2000), researchers have devoted increasing effort to the investigation of the nature of behavioural and physiological declines in auditory temporal processing with age and the effects this could have on speech perception.

Physiological studies have yielded converging evidence suggesting that there is age-related loss of neural temporal synchrony at various levels of the auditory system (for a review see Schneider, 1997). Such a loss of synchrony has been implicated in age-related changes on a number of perceptual measures relevant to the extraction of temporal fine structure speech cues. Monaurally, loss of synchrony could explain why age-related increases in frequency difference limens (DL) are greater for low frequencies than for high frequencies (Abel, Krever, & Alberti, 1990). Because frequency DL is thought to depend on phase-locking at low frequencies, a loss of synchrony would have more of an effect at these frequencies. Binaurally, age-related changes in masking-level differences have been observed for both non-speech and speech signals and have been attributed to an increase in temporal jitter or a loss of temporal synchrony (Pichora-Fuller & Schneider, 1992). Thus, loss of synchrony in aging auditory systems may have wide-reaching perceptual consequences, including disruption of the fine structure cues important for understanding language spoken in noise.

Furthermore, such an asynchrony may affect cognitive processing beyond the level of word recognition. If the fidelity of the auditory signal is compromised in transmission up the auditory pathway, more cognitive resources may be allocated to interpreting the signal. It has been found that older adults are better able to use contextual cues in order to compensate for declines in perceptual acuity (Pichora-Fuller, Schneider, & Daneman, 1995). Such an allocation of resources, however, leaves fewer cognitive resources for other processes necessary to the integration and retention of spoken language. Thus, a perceptual difficulty can potentially cascade into a reduction in working memory capacity, which can be manifest in problems recalling speech even if it is correctly perceived (Pichora-Fuller, et al., 1995).

The current studies attempt to simulate auditory aging by introducing an asynchrony to the speech signal and presenting it to young adults with normal hearing ability[1]. The results were then compared to those obtained in an earlier study (Pichora-Fuller et al., 1995) in which older adults with normal pure-tone thresholds listened to intact stimuli. The first experiment focused on word identification performance in four different S/Ns, while the second added a memory task in order to determine if the increased perceptual difficulties would impact working memory span.

EXPERIMENT 1.

Methods:

Participants. The participants were twelve young adult paid volunteers (mean age = 24.7 years, S.D. ± 3.2), with clinically normal hearing (pure-tone thresholds from 250 to 8,000 Hz ≤ 20 dB HL). All participants provided informed consent and their rights as participants were protected.

Stimuli and Apparatus. In this study the effects of temporally jittering the sentences of the Revised Speech Perception in Noise test (SPIN-R; Bilger, Neutzel, Rabinowitz, & Rzeczkowski, 1984) were investigated. The SPIN-R test consists of 8 lists of 50 sentences.

The listener's task is to report the last word of the sentence immediately following its presentation. In half of the sentences in each list, the last word is predictable from the sentence context (e.g. *The wedding banquet was a feast.*) and in the other half it is not predictable (e.g. *We could consider the feast.*). Performance with low-context sentences is thus meant to assess ability when only auditory cues are present, while an improvement in performance with contextual cues would indicate the participant's ability to deploy cognitive resources to rescue a degraded signal.

The SPIN-R sentences were presented both intact and jittered. Visualizing the speech signal as a graph portraying changes in amplitude over time, jitter can be seen to cause slight alterations in the timing of each point. The program used allowed the experimenter to determine both the range of changes and the rate at which these changes occur. Within these parameters, the alterations occur based on the Gaussian distribution of band-limited white-noise. For each sample in the sound file (20 kHz sampling rate), a delay value is selected by referring to the distribution of noise, determining the amplitude of the noise at the corresponding point in time and the using this amplitude as a delay value. The delay value then determines the position of the time sample in the original speech waveform whose amplitude value is to be substituted in for the value at the time position in question. The chosen bandwidtdh of the low-passed noise determines the rate at which the delay values will change and the standard deviation alters the amplitude of the noise signal thereby increasing the range of delay values that can be selected. To create the low-frequency jittered stimuli a Fast Fourier Transform was used to separate the speech signal into its component frequencies. The signal was then divided into two bands, one above and one below 1,200 Hz. Each band was converted back to the time domain using an Inverse Fast Fourier Transform. The lower band was jittered based on a LP noise with a 500-Hz bandwidth and .25 msec standard deviation; the upper band was not jittered. The two bands were then recombined.

The speech signal remained at 70dB HL, and the babble was adjusted to create the S/N conditions presented to each participant through TDH-39 10W earphones in a sound attenuating IAC booth. The experimenter controlled the SPIN-R form number, jitter condition, S/N and presentation level of the stimuli through an in-house computer program on an IBM-compatible personal computer. The digital signals were routed through the Tucker Davis Technologies DDI, FT5, PA4, SM3 and HB5 modules before reaching the listener's earphones.

Procedure. Participants were required to repeat the sentence-final word from each sentence. All participants completed the lists in a fixed order during two sessions each lasting about one hour. In session one, they heard intact sentences at +8 and then at +4 dB S/N, followed by jittered sentences at +8 and then at +4 dB S/N. In the second session, they heard intact sentences at 0 and –4 dB S/N, and then jittered sentences at 0 and –4 dB S/N. The order of SPIN-R lists differed for each subject; the first four SPIN-R lists were counter-balanced over the +8 and +4 dB S/N presentations, and the last four SPIN-R lists were counter-balanced over the 0 and –4 dB S/N presentations.

Results and Discussion:

Analyses of variance confirmed that, consistent with previous literature (e.g., Pichora-Fuller et al., 1995), the participants in the study were better able to correctly identify the sentence-final words when the S/N was higher ($F(3,33)=424.1$, $p<0.001$), and when the context of the sentences provided cues ($F(1,11)=416.8$, $p<0.001$). When jitter was introduced to the speech signal, performance was

Figure 1
Mean Percent-Correct Word-Identification Scores for Young Participants with Jittered Stimuli and Old Participants with Intact Stimuli with High- and Low-Context Sentences

Figure 2
Number of Words Correctly Recalled for Each Recall Set Size: Young Participants with Jittered Stimuli at S/N=4 dB, and Old Participants with Intact Stimuli at S/N=5 dB with High- and Low-Context Sentences
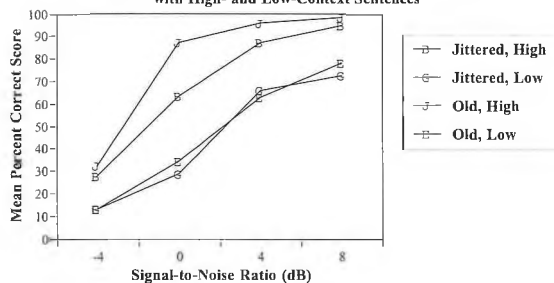
significantly effected ($F(1,11)=262.5$, $p<0.001$). There were also interaction effects between jitter and S/N ($F(3,33)=6.7$, $p<0.001$) and S/N and context ($F(3,33)=20.6$, $p<0.001$). No other interactions were found to be significant. It is thus apparent that the introduction of a temporal asynchrony does have a deleterious effect on word identification. The results are also remarkably similar to those obtained from old listeners with normal pure-tone thresholds in the Pichora-Fuller et al. (1995) study. Figure 1 displays the mean percent-correct sentence-final word-identification scores for jittered sentences in this experiment as well as for the elderly listeners in the 1995 study so that the results can be easily compared. For low context sentences (empty symbols), the resemblance is immediately striking. The young subjects in the current study were able to identify close to the same number of sentence-final words when presented with jittered sentences as were the older adults with intact sentences. The jitter manipulation thus appears to mimic the effect of age in word identification, at least when contextual cues are minimal.

Recall that performance on the low-context SPIN-R sentences is believed to represent auditory skill, whereas increased performance on high-context sentences represents the listener's ability to make use of contextual cues. Pichora-Fuller et al. (1995) found that older adults were better able to make use of context than were younger adults, especially as the listening conditions became less favourable. In Figure 1, it can be seen that a performance difference occurs when the S/N is moderately difficult (+4 dB and 0 dB). These listening conditions likely mimic the more difficult ones encountered in every-day life, in which the older adults have more experience relying on contextual cues to rescue degraded signals.
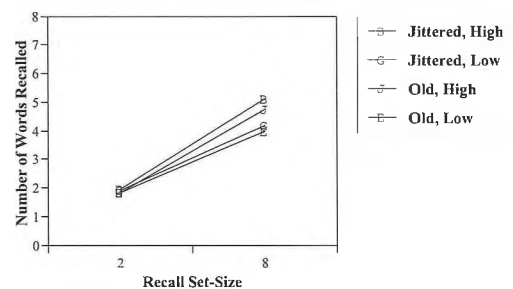
EXPERIMENT 2.

Methods:

Participants. The participants in this experiment were sixteen young adult paid volunteers (mean age = 26.8 years, S.D. $\pm$ 1.78), whose hearing was clinically normal (pure-tone thresholds from 250 to 8,000 Hz $\leq$ 20 dB HL). All participants provided informed consent and their rights as participants were protected.

Stimuli and Apparatus. As with Experiment 1 a temporal asynchrony was applied to the eight forms of the SPIN-R test, and the participants listened to both intact and jittered sets of each. Again, the jitter was applied only to the frequency components below 1200 Hz, but in this experiment the S/N conditions were restricted to +8 and +4 dB. The signal was presented in the same manner outlined for Experiment 1.

Procedure. Again listeners were required to repeat the sentence-final word. In this experiment, however, participants were also instructed to judge the predictability of the sentence final word in order to ensure that they attempted to comprehend the entire sentence rather than attending to only the sound of the last word. Participants were also required to recall as many words as possible from the just completed set of either two or eight sentences. The set sizes remained constant for a given SPIN-R form and the listener

was told ahead of time whether they would be required to remember words from a set of two or eight.

The first half of the experiment consisted of intact SPIN-R forms, at both S/Ns and both recall set sizes, progressing from most easy to most difficult condition. The second half consisted of the same order of conditions, but the sentences were jittered. The forms were balanced across conditions and participants.

Results and Discussion:

Performance on the word identification task was similar to that obtained in Experiment 1 for the same S/N conditions; when the sentence-final word-identification scores for Experiment 1 and Experiment 2 were compared, it was found that there was no significant difference between the participant groups ($F(1,26)=1.8$, $p>0.10$). Again analyses of variance confirmed that main effects were found for jitter ($F(1,15) = 86.4$, $p<0.001$), S/N ($F(1,15) = 70.2$, $p<0.001$), and context ($F(1,15) = 330.5$, $p<0.001$) in Experiment 2. Recall set-size had no main effect ($F(1,15)=0.16$, $p>0.1$), suggesting that an increased memory load does not effect perceptual processing. Significant interaction effects were found for jitter x context ($F(1,15)=7.1$, $p<0.05$), and S/N x context ($F(1,15)=24.3$, $p<0.001$). No other interactions were found to be significant.

Participants were also required to indicate whether they thought the sentence-final word was predictable from the context of the sentence. Mean scores on this task remained above 94%, suggesting that the listeners were comprehending the entire sentence rather than simply attending to the sentence-final word.

When the young listeners were required to recall the sentence final words, it was found that there were main effects for jitter ($F(1,15)=43.72$, $p<0.001$), recall set-size ($F(1,15)=286.7$, $p<0.001$) and context ($F(1,15)=53.6$, $p<0.001$). The young listeners in the current study performed very similarly to those in the study of Pichora-Fuller et al. (1995)[2], and when the sentences were jittered, the young subjects' performance was reminiscent to that of the elderly listeners when presented with intact stimuli. Figure 2 compares the number of words correctly recalled for the young people in the current study when presented with jittered stimuli in a S/N of 4 dB and those for elderly listeners with intact stimuli at a S/N of 5 dB.

It appears that the introduction of jitter decreased word-recall ability in young subjects in a manner similar to the decreased ability in older adults, thereby supporting the hypothesis that external jitter resembles the internal jitter inherent in the aged auditory system, and results in similar processing demands. Presumably for both older adults with intact stimuli and younger adults with jittered stimuli, fewer cognitive resources are left for remembering. The fact that a slight difference in recall performance is noted between elderly adults and young adults with jittered stimuli suggests that although the increased resources allocated to the perceptual channel may explain a large part of the word-recall deficits, something else further contributes to the noted recall difficulties. This is in keeping with a large body of research that proposes that the memory difficulties experienced by older adults have a cognitive com-

ponent and that an age difference is noted more often as task complexity increases (e.g., Obler, Fein, Nicholas, & Albert, 1991). The performance difference between young adults listening to jittered stimuli and older adults listening to intact stimuli occurred when the memory load was high (recall set-size of 8), and when the listening conditions were fairly difficult (S/N of 4 to 5 dB). It is thus not surprising that a slight difference occurred and indicates that perceptual and cognitive factors cannot be considered in isolation, particularly in the aged population.

Although it appears that both perceptual and cognitive deficiencies contribute to the noted word-recall difficulties in older adults, the findings of the current study and those of Pichora-Fuller et al. (1995) suggest that perceptual processing receives priority in resource allocation. In both of these experiments, word identification performance was not affected by an increased memory load, even though increased perceptual stress reduced recall. From the perspective of an information-processing model, it makes sense that priority is given to perceptual processing; preserving resources for memory and other cognitive processes would be of little benefit if the cost were a loss or reduction in quality of incoming information

General Discussion:

This simulation of the neural jitter that is thought to disrupt the ability to phase-lock to lower frequencies in the aging auditory system was successful. The applied jitter was determined to affect young adults' performance such that it resembles that of older adults in two different tasks. Such a finding helps explain why there tends to be an age-related decline in the ability to perceive speech, particularly in the presence of background noise, when no hearing loss is evidenced by standard clinical pure-tone audiometry. The findings also help explain some aspects of working-memory problems experienced when information is presented auditorily under challenging listening conditions

Furthermore, this series of experiment provides evidence for the inter-relationship between perceptual (bottom-up), and cognitive (top-down) channels. It was demonstrated that degraded perceptual processing affects processes, such as memory, which are traditionally believed to be cognitive. Cognitive processes, such as the use of available semantic cues to help one predict content, were also shown to be employed to rescue signals degraded at the perceptual level. It is thus evident that as people age numerous factors interact and affect the way speech is heard, interpreted and remembered.

Abel, S.M., Krever, E.M., & Alberti, P.W. (1990), *Scand. Aud, 19*, 43-54;
CHABA (1988), *JAAA, 7*, 190-202;
Obler, I.K., Fein, D., Nicholas, M., & Albert, M.L (1991), *Applied Psycholinguistics, 12*, 433-452;
Pass, H. (1998) M.Sc. Thesis, UBC;
Pichora-Fuller, M.K., & Schneider, B.A. (1992), *JASA, 91*, 2129-2135;
Pichora-Fuller, M.K., Schneider, B.A., & Daneman, M. (1995), *JASA, 97*, 593-607;
Schneider, B.A., (1997), *JSLPA, 21*, 111-124;
Schneider, B.A., Pichora-Fuller, M.K., (2000), In F.I.M Craik & T.A. Salthouse (Eds) Handbook of Aging and Cognition, pp 155-219.

[1] A previous study (Pass, 1998) has already applied jitter to the SPIN-R sentences, but the means of application resulted in spectral splatter that masked the high frequencies of the speech signal, making it difficult to determine the relative contributions of the jitter and the masking. The present study refined this jitter by applying it only to the frequencies below 1200 Hz.

[2] Because different S/N conditions and recall set sizes were used in the 1995 experiment, the findings cannot be directly compared, although it is still possible to discuss the trends.

YOUNGER AND OLDER ADULTS DEMONSTRATE SIMILAR ABILITY TO FOCUS ATTENTION WHEN LISTENING TO SIGNALS IN NOISE

Dana R. Murphy, Filippo Speranza, Giampaolo Moraglia, and Bruce Schneider

Department of Psychology, University of Toronto at Mississauga, Mississauga, ON L5L 1C6

A pure-tone signal embedded in a background noise is easier to detect when its frequency is known, indicating that listeners can narrow their attentional focus to a specific frequency region. Low-intensity signals falling within the attentional "window" or band are detected whereas equally-intense signals falling outside the window are not as easily detected (Dai, Scharf, & Buus, 1991; Greenberg & Larkin, 1968; Scharf Quigley, Aoki, Peachey, & Reeves, 1987). To get listeners to establish an attentional focus, listeners are typically presented with a prime tone immediately before each detection trial. On most of the trials, the tone to be detected is identical to the prime; on the remainder of trials, a probe tone differing in frequency but not in intensity is presented. The detection accuracy for the primary and for each of the probes is then compared with the detection accuracy for each of these stimuli when they are being presented alone.

Scharf and his colleagues (Dai et al. 1991; Scharf et al., 1987) have used this "probe-signal" methodology to demonstrate that younger adults can effectively focus their attention on a narrow range of frequencies (typically corresponding to the critical bandwidth centred at the primary frequency). When attention is focused in such a way, probe-tone detection accuracy is maximal when the probe tone is identical to the priming tone, and declines to change levels as the frequency separation between the probe and prime tone approaches the limits of the critical band.

While extensive testing has been conducted on younger adults, there has been little or no use of the probe-signal methodology to test the ability of older adults to effectively focus their attention when detecting signals in noise. Cognitive psychology research has indicated that younger and older adults differ in terms of their ability to selectively focus their attention in the auditory modality (Barr & Giambra, 1990; Panek, Barrett, Sterns, & Alexander, 1978) with cognitive aging theorist proposing that this is related to an inability to inhibit the processing of unwanted information (Hasher, Soltsfus, Zacks, & Rympa 1991; Hasher & Zacks, 1988; McDowd & Oseas-Kreger, 1991; Tipper, 1991). If older adults do indeed have such difficulties focusing their attention and inhibiting the processing of unwanted information, then the possibility exists that the older adults will not detect tones in the same fashion as younger adults in a probe-signal situation. In particular, older adults would not demonstrate a tight focus of attention and would instead detect all tones at the same level of accuracy.

A possible basis for expecting a broader attentional focus in older adults comes from the work of Scharf and his colleagues (Scharf, Magnun, & Chays, 1997; Scharf, Magnun, Collett, Ulmer, & Chays, 1994), who have shown that individuals who have had their olivocochlear bundle severed do not demonstrate attentional selectivity in the probe-signal methodology. The olivocochlear bundle is known to be an important part of the efferent auditory pathway leading from the cortex to the cochlea. This system is believed to be important in allowing for the top-down control of the micro-mechanical properties of the cochlea and may serve an important role in detecting signals in noise. The olivocochlear bundle synapses mostly with outer hair cells of the cochlea which are known to suffer widespread damage as a person ages. In addition, infants and very younger children (also known to have inhibitory problems) do not show the attentional selectivity of young adults

(Bargones & Werner, 1994). Thus, the possibility exists that older adults will also show a lack of attentional focus.

Method

Participants

Seven younger adults (mean age = 21.00 years) and 7 older adults (mean age = 69.71 years) participated in this research. All participants had what is considered to be "normal" hearing. That is, they all had pure tone thresholds 25 dB HL for all frequencies 3000 Hz (consideration was given such that one frequency could be 35 dB HL).

Apparatus and Material

In this experiment, we presented pure tones varying in frequency. We presented these tones over a Tucker Davis sound board and Tucker Davis equipment. These pure tones were then delivered to the right earphone of TDH 49 earphones.

We used 7 pure tones in this experiment. For the primary tone, we used a 350 ms 1-kHz tone. We used an additional 6 tones as probe frequencies. The specific frequencies of these probes were 800, 875, 950, 1050, 1125, and 1200 Hz. All tones were ramped on and off with a 10 ms ramp and were presented in a background of continuous noise presented at an overall level of approximately 60 dB SPL (approximately 25 dB/Hz).

Procedure

Individuals were tested in 3 phases in this experiment. In the first phase of the experiment, we used a method of constant stimuli to determine the level of the 1-kHz primary tone that would produce 85% accuracy when detected in noise in a standard 2IFC paradigm. To determine the level necessary for 85% accuracy, we found a level of presentation that produced accuracy above 85% over 100 trials and a level of presentation that produced accuracy below 85% (but above chance) over 100 trials and then calculated the 85% threshold by means of linear interpolation.

This 85% threshold was then used to set the level for all of the tones the individual listened to in the second phase of the experiment. Thus, all 6 of the probe frequencies as well as the primary frequency were presented at the same level which was the level producing 85% accuracy of detection for a 1-kHz tone as determined in phase 1.

In the second phase of the experiment, we used a variant of the probe-signal methodology similar to that used by Dai et al (1991). All individuals were required to detect the presence of a tone in a standard 2IFC paradigm with the tone presented in noise. To begin each trial, the participant pushed the middle button of a 3-button button-box. Five hundred milliseconds after the button press starting the trial, a "warning" tone (also a 1-kHz tone presented at 60 dB) was presented for 350 ms. This was followed by 400 ms of silence and then the noise began. This was followed 100 ms later by the first interval lasting for a total of 350 ms. This interval was signified by the presentation of a light above the left hand-button of the button box. Five-hundred ms after the end of the first interval, the second interval began which also lasted for 350 ms. This interval was marked by the presentation of a light above the right- hand button on the button box. The noise ceased 100 ms after the end of the second interval and there was silence until the participant indicated which interval contained the target stimulus by pressing the

appropriate button. There was no feedback provided following the participant's response. Instead, the light above the central button came on indicating that the system was ready for the next trial and the participant pushed the center button when ready to begin the next trial.

In this probe-signal phase of the experiment, all 7 tones were presented. The primary tone (1-kHz) was presented on 75% of the trials while one of the 6 probe tones was presented on the remaining 25% of the trials. In addition, a warning tone (a 1-kHz) tone was presented prior to the two intervals in the 2IFC paradigm. Participants were instructed to listen for a tone in one of the two intervals and indicate which interval contained the tone by pressing the appropriate button.

In the third and final phase of this experiment (the single frequency phase), individuals were tested for their detection accuracy for each frequency used in the experiment when only one single frequency was tested. Testing was completed with the same methodology used in the probe-signal phase of the experiment, except that only one tone was presented in a block of 100 trials. This tone was used as both the primary and the warning tone in the 2IFC paradigm described previously. Completion of the testing of the different frequencies was counterbalanced so that no two individuals within an age-group completed testing in exactly the same order.

Results

Figure 1 presents the mean detection accuracy for both younger and older adults at each frequency when multiple frequencies were presented in the Probe-Signal condition, and when only single frequencies were presented as both prime and probe. The top two lines represent data from Single Frequency testing (circles represent older adults, squares represent younger adults) while the lower two lines represent the data from the probe- signal phase of the experiment (labeled Prb-Sig, circles represent older adults, squares represent younger adults). It is easy to see from this figure that younger and older adults are performing very similarly in this task, with both groups demonstrating a very narrow focus of attention. In particular, tones with frequencies more than one critical band away from the primary stimulus are processed at a level of accuracy near chance, while the two frequencies that are within 1 critical band are detected with a greater than chance level of accuracy. Meanwhile, the primary frequency is detected with a very similar level of accuracy as when it was tested alone.

Discussion

Clearly, younger and older adults demonstrate a similar ability to focus attention in order to improve their ability to detect pure tones presented in noise. Both age groups demonstrate a very narrow band of attentional focus. Only the two tones within 1 critical band away from the expected primary frequency were detected with a greater than chance level of accuracy. Thus, when detecting tones in noise, younger and older adults seem to demonstrate a very similar ability to narrow their focus in order to improve detection. This indicates that the differences between the two age groups in terms of inhibitory functioning are either smaller than expected or that the inhibitory functioning of the older adults remains intact for such simple auditory stimuli. We do not know if the ability to narrowly focus attention will be the same in all situations and with all stimuli. Perhaps more complicated stimuli (such as words or spoken sentences) do not lend themselves to the same sort of selective analysis in noisy situations. This would mean that older adults, despite their ability to narrowly focus attention when processing very simple stimuli may find it difficult

to narrow their focus when more complex stimuli are employed and multiple frequency regions might have to be monitored. More research is needed in order to determine if older adults do indeed have difficulty narrowing their focus when trying to process more complex stimuli in noisy situations.

References

Bargones, J. Y. & Werner, L. A. (1994). Adults listen selectively; Infants do not. *Psychological Science, 5,* 170-174.

Barr, R. A., & Giambra, L. M. (1990). Age-related decrement in auditory selective attention. *Psychology and Aging, 5, 597-599.*

Dai, H., Scharf, B., & Buus, S. (1991). Effective attenuation of signals in noise under focused attention. *Journal of the Acoustical Society of America, 89,* 2837-2842.

Greenberg, G., & Larkin, W. (1968). Frequency-response characteristics of auditory observers detecting a single frequency in noise: The probe-signal method.. *Journal of the Acoustical Society of America, 44,* 1513-1523.

Hasher, L., Stoltsfus, E. R., Zacks, R. T. & Rympa, B. (1991). Age and inhibition. *Journal of Experimental Psychology: Learning, Memory, and Cognition, 17,* 163-169.

Hasher, L., & Zacks, R. T. (1988). Working memory, comprehension and aging: A review and a new view. *Psychology of Learning and Motivation, 22,* 193-225.

McDowd, J. M., & Oseas-Kreger, D. M. (1991). Aging, inhibitory processes, and negative priming. *Journal of Gerontology: Psychological Sciences, 46,* P340-P345.

Panek, P.E., Barrett, G. V., Sterns, H. L., & Alexander, R. A. (1978). Age-differences in perceptual style, selective attention, and perceptual-motor reaction time. *Experimental Aging Research, 4,* 377-387.

Scharf, B., Magnan, J., & Chays, A. (1997). On the role of the olivocochlear bundle in hearing: 16 case studies. *Hearing Research, 103,* 101-122.

Scharf, B., Magnan, J., Collett, L., Ulmer, E., & Chays, A. (1994). On the role of the olivocochlear bundle in hearing: A case study. *Hearing Research, 75,* 11-26.

Scharf, B., Quigley, S., Aoki, C., Peachey, N., & Reeves, A., (1987). Focused auditory attention and frequency selectivity. *Perception & Psychophysics, 42,* 215-223.

Tipper, S. P. (1991). Less attentional selectivity as a result of declining inhibition in older adults. *Bulletin of the Psychonomics Society, 29,* 45-47.
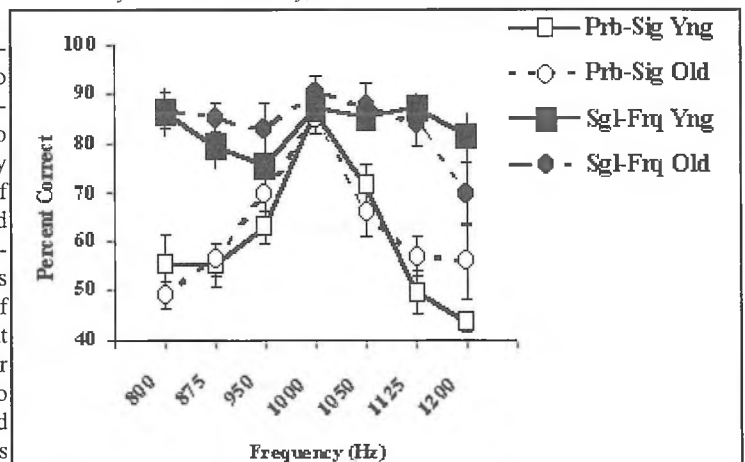
Figure 1. Mean detection accuracy of younger and older adults as a function of testing phase. Prb-Sig = Probe-Signal testing (Phase 2). Sgl-Frq = Single Frequency testing (Phase 3).

Modelling Of Outer Hair Cell Damage And Implications For Hearing Aid Signal Processing

Christian Giguère

Programme d`audiologie et d`orthophonie, Université d`Ottawa, Ottawa (ON), K1N 6N5

1.0 INTRODUCTION

Sensorineural hearing loss is associated with a variety of auditory disabilities such as elevated detection threshold, reduced frequency selectivity and temporal resolution, abnormal growth of loudness, and poor speech perception. Outer hair cell (OHC) damage is the underlying cause in many cases. Yet, despite rapid advances in hearing aid technology, the optimal solution to combat OHC damage is still a matter of debate and research. The success of future amplification strategies depends on our detailed knowledge of the effects of OHC loss, and on our understanding of what hearing aids can and cannot do to restore normal hearing.

2.0 GENERAL APPROACH

A mathematical model of the cochlea was used to assess the theoretical benefits of hearing aids to compensate for outer hair cell (OHC) damage (Giguère and Woodland, 1994; Giguère and Smoorenburg, 1999).
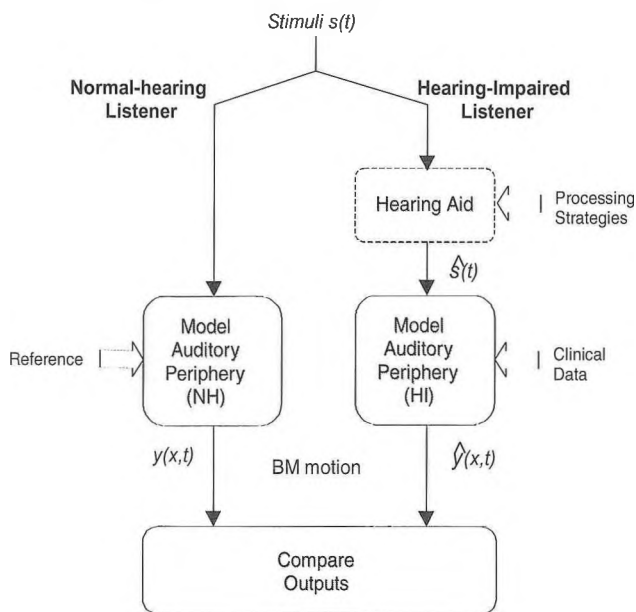

Figure 1: Modelling framework

Question — To which extent the BM response from a cochlea with damaged OHCs can be restored to that of a normal cochlea by processing the input signal as in a hearing aid?

Tool — A computational model of the auditory periphery (external ear, middle ear, cochlea) with OHC elements.

Stimuli — Pure tones, speech.

Method — Compare the BM excitation pattern of a normal-cochlea model against that of a model configured for different degrees of the OHC damage in conjunction with different hearing aid process-

ing strategies (see Figure 1).

Hearing aid processing — Multi-band amplitude compression, spectral sharpening.

3.0 SIMULATIONS

Figure 2a illustrates the basilar membrane excitation patterns at the output of the model with intact OHCs (N) and for different degrees of OHC damage (D) for a synthetic vowel /ae/. With increasing hearing loss: (1) the gain gradually decreases throughout the cochlea, (2) the spectral resolution decreases and the formants (F1 to F3) broaden, and (3) the basalward (upward) spread of masking increases (F2 on F3).
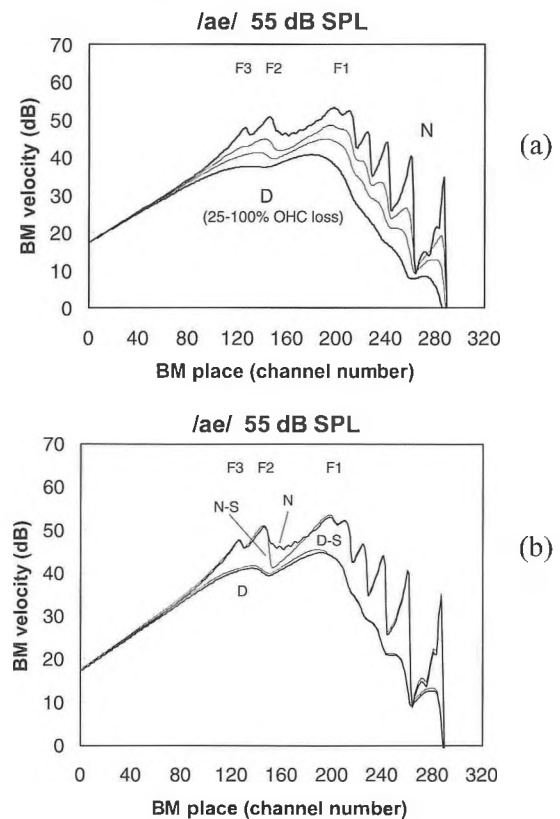

Figure 2: Basilar membrane excitation patterns at the output of the cochlea model from base (channel 0) to apex (channel 320). N = normal cochlea, D = damaged cochlea, N-S: normal cochlea with spectral sharpening, D-S: damaged cochlea with spectral sharpening, F1 to F3: vowel formants.

Figure 2b illustrates the effects of spectral sharpening (S) on the basilar membrane excitation patterns. The benefits of spectral sharpening is only evident in the case of the normal cochlea (N vs N-S), where there is an increase in the peak-to-valley ratio between formants F1 and F2. There are no benefits of spectral sharpening

when the basilar membrane excitation patterns have been degraded due to OHC damage (D vs D-S).

4.0 CONCLUSIONS

- The effects of OHC loss on BM vibration depend on both frequency and place:

- OHC loss leads to:
  (1) a basalward shift of the place of maximum vibration,
  (2) a decreased gain near the characteristic place,
  (3) a broadening of the tuning curves,
  (4) an altered summation of activity across frequency components, and
  (5) an altered temporal waveform.

- From a hearing aid point of view, only the frequency dimension is accessible, not the place dimension. The main consequence of this mismatch is that hearing aids cannot, in general, compensate for the exact damage caused by OHC loss;

- Hearing aids can compensate for the general loss of sensitivity and reduced dynamic range, but they cannot compensate completely for the reduced frequency selectivity associated with OHC damage.

- BM vibration cannot be completely restored for pure tones, complex tones, vowels, and in general for sounds where the BM excitation pattern is dominated by narrow-band energy.

- A broadening of the BM excitation curves by a factor 2 to 3 would severely limit the choice of signal processing strategies available.

REFERENCES

[1] Giguère C. and Woodland P.C. (1994). "A Computational model of the auditory periphery for speech and hearing research. I. Ascending path," J. Acoust. Soc. Am. 95: 331-342.

[2] Giguère, C. and Smoorenburg, G.F. (1999). "Computational modeling of outer hair cell damage: Implications for hearing aid signal processing," in: Psychoacoustics, Physiology and Models of Hearing, edited by T. Dau, V. Hohmann and B. Kollmeier (World Scientific, Singapore), pp. 155-164.

Identification of Tonic in Popular and Baroque Music in Young and Older Adults Using a Dual Keyboard Apparatus

Ian D. Toms, Annabel J. Cohen & M. J. Reina Lamothe

University of Prince Edward Island, Charlottetown, P.E C1A 4P3

INTRODUCTION

Tonality induction refers to the process of establishing a mental representation of the hierarchical relationship among tones in the Western European chromatic scale, during the unfolding of a musical selection. In the representation, one tone, known as the tonic, stands out as the most important tone. The key signature of notated music arbitrarily identifies the tonic but, in the first instance, tonality resides in the mind of the listener, not the musical notation. Key-finding algorithms (KFA) have been designed to predict the perceived tonic (e.g., Krumhansl, 1990; Temperley, 1999).

Using short excerpts from Bach's *Well-Tempered Clavier*, Cohen (1991) demonstrated high correspondence between Bach's designated key and the tonic selected by musically-trained listeners. The listeners identified the tonic by singing the first scale that came to mind that fit the excerpt. The KFA of Krumhansl also successfully identified the perceived tonic (1990, p. 84). The present study extends this investigation of tonality identification to listeners who lack musical training. Although such listeners may be able to abstract tonality as musicians do, they may have greater difficulty than musicians in singing a musical scale, hence they cannot be tested under Cohen's original vocalization procedures. To overcome this problem a method was developed by Ian Toms by which experimental subjects could explore possible tonic candidates on one keyboard and subsequently enter their choice on a second keyboard which recorded the data.

Using the dual keyboard apparatus, the present study also focussed on the role of experience in tonality induction by comparing younger and older adults on contemporary popular and classical music excerpts by Bach. While older adults would have many more years of exposure to Western-European music, their experience with recent popular music might be limited. If, as Cohen (2000) has argued, musical grammar, like language grammar, is acquired in one's youth, it is possible that the new styles represented by contemporary popular music would challenge the grammar of the older persons and make tonality induction of those pieces diffi-

cult. Specific music training of older persons might attenuate rigidity of the musical grammar representation (cf. Mainz, 2000) and enable older persons to perform equally well for classical and popular music. Conversely, young adults who would have more familiarity with popular music might be better able to induce tonality for the popular music as compared to the less familiar Baroque style.

METHOD

Subjects. There were 24 subjects representing four groups differing in age and musical training. For the younger group, mean age was 18.3 years (SD=1.3, range 16 to 20 years). For older adults, mean age was 62.8 years (SD=7.1, range 55 to 77 years). None of the untrained listeners reported any music training. Young trained listeners reported a mean of 9.7 years training (SD=2.5, range 6 to 13 years). Older trained listeners reported 31.8 mean years of training (SD. 24.2, range 3 to 68 years). The young untrained group reported listening to music 5.6 hours/week, the older untrained group reported 7.6 hours/week, the young trained group reported 19.6 hours/week and the older trained group reported 29 hours/week. All groups had equal male and female representation except for the older untrained group which had 2 males and 4 females. Several older persons reported some hearing problems but none wore a hearing aid. Audiometry for five tones (500 to 8000 Hz) was obtained for 9 older subjects and 3 young subjects and revealed poorer hearing in the older listeners especially at higher frequencies.

Music materials. There were 20 musical excerpts of approximately 10 sec in length (range 8 to 13 sec). One half of the excerpts were from the beginnings of the Preludes from the *Well-Tempered Clavier* of J. S. Bach, five from Book I and five from Book II. One half of the examples were in major keys and one half in minor. All selections achieved a score of at least .735 (mean score .88 major and .84 minor) when analysed with the KFA based on Krumhansl and Schmuckler. In all but one case (B minor, Bk II), the algorithm
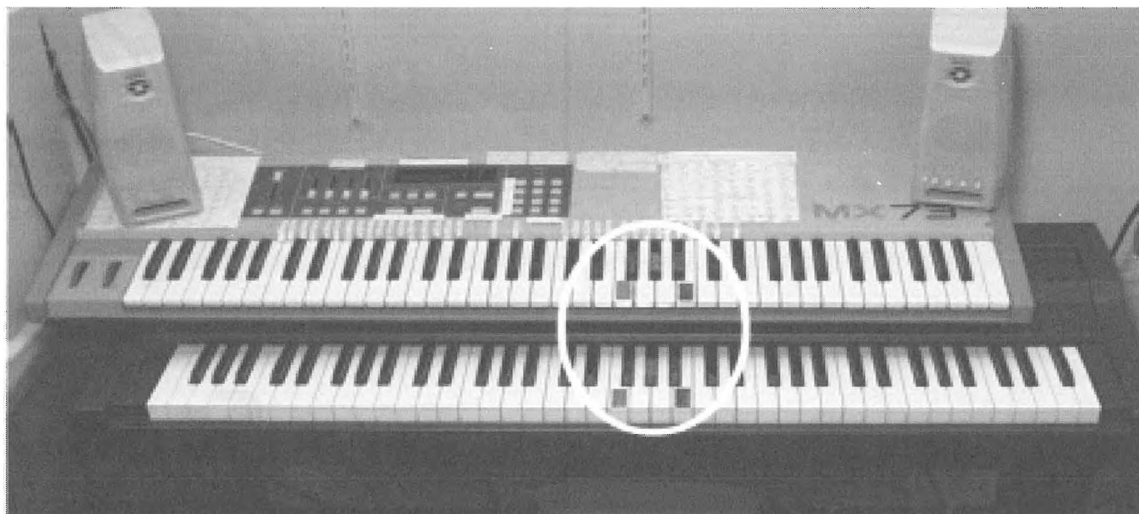
agreed with the key signature of the excerpt. The exception was the musically related dominant key. Similarly, 10 excerpts of music popular in the last 1 to 30 years (mean 13 years) were chosen in major and minor keys that achieved a score 0.63 by the KFA (mean score .89 for major, and .86 for minor). Files were downloaded as MIDI files from several WWW sites. Excerpts were musically transposed from their original keys to represent tonics of F, F#, G#, A#, and B, and were converted to .wav files for access by the computer program.

Procedure. Subjects were tested individually. The concept of tonality and tonic was explained and three practice trials were presented through Altec Lansing speakers to provide familiarity with the apparatus and task. Of the three tunes used in the practice trials, two were familiar nursery tunes and one had been created specifically to represent the key; two tunes were major and one was minor. The presentations and data entry were under computer control using the Music Experiment Development System (MEDS at http://www.ethnomusic.ucla.edu/systematic/Faculty/Kendall/meds. htm) developed by Roger Kendall. Experimental trials were presented in four blocks of five trials. Each block consisted of either Baroque or popular excerpts, with major and minor modes distributed roughly equally within the block. Within a block, excerpts were randomly presented. During presentation, the subject was allowed to play (and hear) any of five colour-coded keys (F, F#, G#, A#, B) on a lower keyboard (Kawai digital piano 135) as he/she searched for the best-fitting tone. The selection was presented three times in succession and, after the third presentation, the subject played his/her chosen colour-coded tonic key on an upper "dumb" keyboard (Akai MX-73 controller) connected to the Dell Pentium 300 computer for the purpose of data entry.

Theoretical identification of tonic. A key-finding algorithm was implemented by calculating the duration of each of the 12 chromatic notes in each excerpt using software created by Temperley & Sleator (Temperley, 1999). This vector was then correlated with the 12 values from the probe-tone task for each of the chromatic tones for both major and minor keys (see Krumhansl, 1990).

RESULTS

Because there were five choices of tonic, chance performance was 20 %. For both the untrained (45.8%) and trained (74.2%) listeners, mean per cent correct identification of tonic statistically exceeded chance, $t(11) = 3.7$, and 8.2 respectively, both p's < .005, respectively; however, training led to higher performance. Young persons (67.5%, $t = 6.2$) and older adults (52.5%, $t = 4.6$) also performed significantly better than chance (p <.005). The further breakdown also revealed better than chance performance for all four age variable (young/old) by training variable (untrained /trained) subgroups ($p < .05$). Mean performance was 86.7 % (SD = 17.4) for the young trained group, 48.3 % (17.6) for the young untrained group, 61.7 % (25.0) for the trained senior group, and 43.3 % (30.5) for the untrained senior group.

The per cent correct for each of the major and minor popular and classical categories for each subject was entered into an analysis of variance having two within-subjects factors of style (classical/contemporary popular) and musical mode (major/minor), and two between-groups factors of musical training (untrained, highly trained) and age (young/older). The main effect of musical training $F(1,20) = 13.2$; $p < .005$, was statistically significant. There were

no other statistically significant effects, however, this might have been attributable to the small sample size. We are in the process of increasing the sample size.

DISCUSSION

The dual-keyboard technique was successful in revealing the ability of young and older listeners to systematically induce tonality regardless of their musical or keyboard experience. Using this technique, identification of tonic was significantly above chance for all groups of listeners. There was no effect of musical style on the task. Finally, there was no significant effect of declining age on performance, although the task is associated with complex cognitive activity, and has sensory and memory components. The procedure, however, minimized memory and sensory constraints through repetition and provision of auditory feedback via the keyboard set-up.

REFERENCES

Cohen, A. J. (1991). Tonality and perception: Musical scales primed by excerpts from *The Well-Tempered Clavier* of J. S. Bach. *Psychological Research, 53*, 305-314.

Cohen, A. J. (2000). Development of tonality induction: Plasticity, exposure and training. *Music Perception, 17*, 437-459.

Krumhansl, C. (1990). *Cognitive foundations of musical pitch*. Toronto: Oxford.

Mainz, E. J. (2000). Experience-based attenuation of age-related differences in music cognition task. *Psychology and Aging, 15*, 297-312.

Temperley, D. (1999). What's key for key? The Krumhansl-Schmuckler key-finding algorithm reconsidered. *Music Perception, 17*, 65-100.

Comparison of Three Distortion Product Otoacoustic Emission Devices

Victoria Young*, Robert Harrison[++], Alf Dolan*, and Hans Kunov*

*Institute of Biomaterials & Biomedical Engineering, University of Toronto, Toronto, Ontario, M5S 3G9.

[++]Department of Otolaryngology, Hospital for Sick Children, Toronto, Ontario, M5G 1X8.

1.0 Introduction

Distortion Product Otoacoustic Emissions (DPOAEs) are low amplitude sounds generated from within a normal cochlea in response to simultaneous acoustic stimulation by two pure tones. In humans, this type of testing is used to assess the normalcy of cochlear function, specifically outer hair cell function. Current DPOAE devices are highly susceptible to noise, both physiological and environmental. In test conditions where there is a low signal to noise ratio artifacts may appear that negatively affect the repeatability and reliability of the measured DPOAEs. Secure probe placement and low noise conditions are thus necessary to accurately measure DPOAEs. Typical DPOAE devices use data averaging with artifact rejection to increase the signal to noise ratio in the recorded DPOAE signal [4]. A new type of DPOAE device that obtains signals in real-time and uses digital signal processing techniques to reduce background noise level could also minimize testing time and decrease data variability. A prototype DPOAE device with real-time ability was developed at the University of Toronto.

The goal of this study is to perform a comparison of noise susceptibility and DPOAE variability between the University DPOAE device prototype and two different DPOAE recording devices, on a small sample of adults, in quiet and noisy conditions. The results of this study are presented.

Apparatus and Method

DPOAE devices have a basic equipment design including the probe assembly (two speakers, low-noise microphone(s), ear tips); a digital signal processing (DSP) board; operational software; and an isolation transformer for patient safety [1,4].

The DPOAE device operation follows a basic pattern with different features associated with different machines. See Figure 1. The two DPOAE instruments used in the comparison study were the ILO 92, made by Otodynamics, and the GSI 60, made by Grason-Stadler. These instruments were available from the Hospital for Sick Children, in Toronto, Ontario. The ILO 92 is a "research tool" rather than a clinical tool, but the GSI 60 is used for clinical applications. Both the ILO 92 and the GSI 60 use a "check probe-fit" routine to test probe placement, use Fast Fourier Transforms (FFT) and data averaging to reduce noise, and possess an artifact rejection capability. The University prototype uses only signal modeling and digital signal filtering to process the acquired signal, remove noise and minimize artifacts [3].

Testing for this study was conducted inside an audiology booth in the Audiology Department at the Hospital for Sick Children. The background noise level of the audiology booth was measured at 57 dB SPL and the simulated noisy environment, generated by a HIFI Stereo system and a pink noise CD, was measured at 65 dB SPL. The high background noise level measured inside the quiet booth was a result of the hum from the printer and computers of the three instruments. The sound level was measured using a Brüel & Kjaer, BZ7110 sound level meter.

The typical DPOAE test begins by having the volunteer sit comfortably in a chair close to the test device. An ear probe is fitted into the volunteer's ear canal with a rubber probe tip or a foam piece used to seal and hold the probe in place. If a 'check probe fit' routine is available the position of the probe is checked before the DPOAE test is executed. Once the probe is positioned properly, two pure tones are simultaneously presented to the ear. The receiver portion of the ear probe receives and transmits the distortion product otoacoustic emission, if present, and the data is subsequently processed and analyzed by the computer for display.

Before subject testing could be conducted, it was necessary to calibrate the three DPOAE machines to ensure that the pure tones, F1 and F2, and sound levels, L1 and L2 were approximately the same for each machine. Previous studies have shown that the DPOAE amplitude is affected by the F1 and F2 frequencies as well as the L1 and L2 sound pressure levels [1,2]. The default setting on the ILO 92 was used as the parameter template since specific frequencies and sound level outputs could not be pre-set for this machine.

The sound level for the first pure-tone, F1, was set at L1 = 60 dB SPL, and the level for the second pure-tone, F2, was set at L2 = 50 dB SPL. The F1 and F2 ratio was kept constant at 1.22, and a total of nine frequencies groups were included in a test sweep: F1 values were at 818 Hz, 1038 Hz, 1306 Hz, 1636 Hz, 2063 Hz, 2600 Hz, 3284 Hz, 4126 Hz and 5200 Hz.

For each frequency, the L1 and L2 sound pressure levels were measured from the ILO 92 using a dead (dummy) ear and a sound level meter. These L1 and L2 values were recorded and used to configure both the GSI 60 and the University Prototype. The default clinical settings for sampling rate and bin number were also used for the GSI 60 and ILO 92. Each device had its own specific ear probe: the GSI 60 and the University prototype each had disposable ear tips of various sizes and the ILO 92 had disposable foam seals to place around the probe tip.

In total, nine adult ears (eight males and one female between

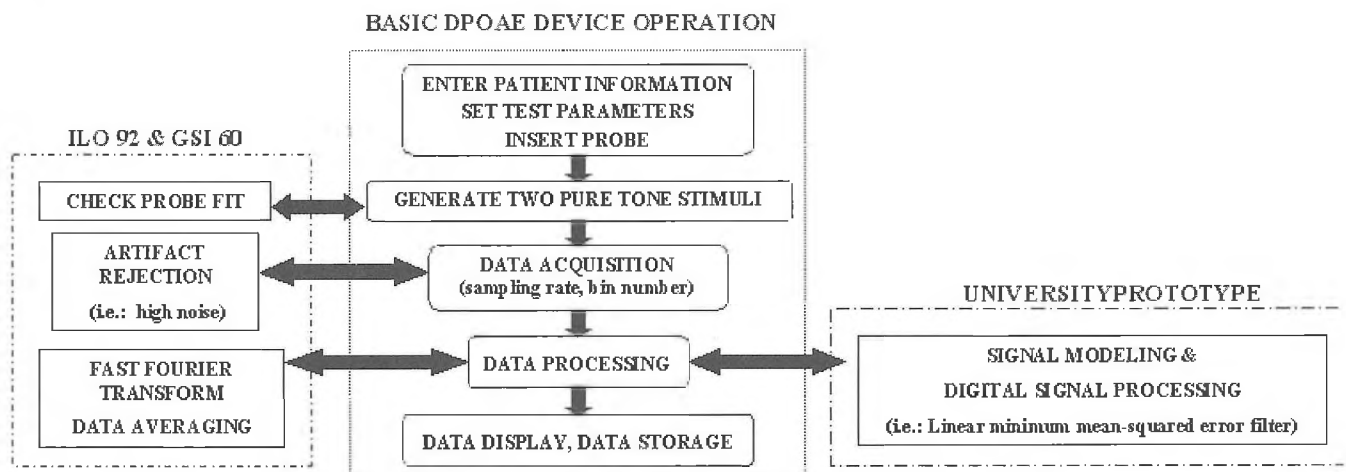## BASIC DPOAE DEVICE OPERATION

Figure 1: Basic DPOAE device operation with ILO 92, GSI 60 and University Prototype special features identified [1,2,3,4].

the ages of twenty and sixty years) were tested on each DPOAE device. Five tests in total were conducted per ear. Three test sweeps were conducted in the quiet environment. Two test sweeps were conducted in the noisy environment.

Results and Discussion

To compare machine susceptibility to noise the effect of background noise level on measured DPOAE values for each machine was examined. It was necessary to compare DPOAE data acquired in low noise conditions with DPOAE data acquired in high noise conditions.

For each of the nine subjects, the data was divided into 'low noise' and 'high noise' sections. In the low noise section, the tests were repeated three times, where one test was a sweep over nine frequencies, so the median DPOAE value at each tested frequency was selected as the final DPOAE value. The corresponding background noise value for the DPOAE value was also used. In the high noise section, the tests were repeated two times only, so the average DPOAE and background noise value was used for the comparison.

In analyzing the DPOAE data, it is important to note that DPOAEs are visually inspected at each test frequency and the presence of a DPOAE is determined qualitatively. Since the background noise conditions may change even during one sweep of a test (i.e. subject coughs or moves), the variance of the DPOAE amplitude may be quite a bit. The median DPOAE value will account for these odd variances in the data. For the high noise conditions, similar changes in background noise are less likely to affect the signal and since the test sweeps were repeated only two times, the average DPOAE value is sufficient for the study's purpose.

For each subject, the difference in DPOAE amplitude, measured in low noise and high noise conditions, was calculated and then the average difference over all subjects at each frequency was determined. The results indicate that the University prototype has the lowest difference value at 6/9 frequencies, followed by the GSI 60 at 3/9 frequencies. The ILO 92 has the highest difference values at all frequencies. See Figure 2. An average difference over all subjects across all test frequencies gives the same results. The University prototype has an average difference between low noise and high noise DPOAE amplitudes of 3.39 dB SPL, the GSI 60 has an average difference of 6.34 dB SPL, and the ILO 92 has an average difference of 10.75 dB SPL.

To compare data variability over repeated testing the standard deviations of the DPOAE amplitude values in the 'low noise' and 'high noise' sections were calculated. Three tests were used in the low noise section and two tests were used in the high noise section. The standard deviations were then averaged over all subjects at each frequency. For the low noise conditions (LN) and the high noise conditions (HN), the University prototype had the lowest data variability, LN: 6/9 frequencies, HN: 6/9 frequencies, followed by the GSI 60 with low variability at LN: 2/9 frequencies and HN: 4/9 frequencies. The ILO 92 had the lowest variability for LN: 1/9 frequencies and HN: 0/9 frequencies. See figure 3 and 4. In figure 4, values are missing for the ILO 92 at frequencies 818 Hz-1306 Hz because the noise was too loud for the device to obtain valid data.

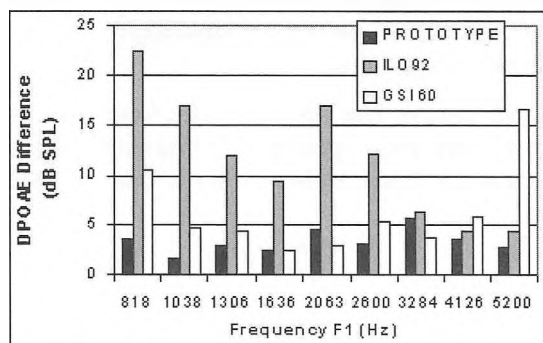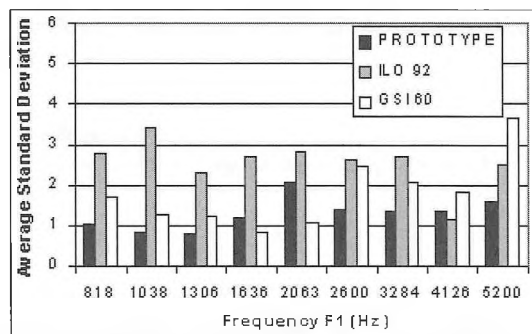In this study, the three DPOAE machines were compared by

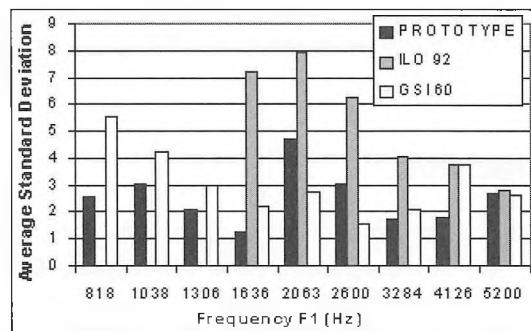Figure 3. Low Noise Tests – Data Variability

Figure 4. High Noise Tests – Data Variability

examining the affect of background noise level on the measured DPOAE values and the variability of the measured DPOAE values over repeated test trials. Overall, the University Prototype was the least susceptible to the pink noise than both the GSI 60 and the ILO 92. The GSI 60, in turn, was less susceptible than the ILO 92. The results of the study also suggest that the University Prototype provides more repeatable data than either the GSI 60 or the ILO 92. The GSI 60 provides more repeatable data than the ILO 92.

In general, the University Prototype acquired data faster than the GSI 60, which in turn acquired data faster than the ILO 92. Probe placement was more difficult with the ILO 92 than with either the GSI 60 or the University Prototype, however comfort level varied among subjects. The difficulty in probe placement for the ILO 92 may be a reason the measured data from this machine was more susceptible to noise and more variable than either the GSI 60 or the University Prototype.

Acknowledgements

References

Whitehead, M.L., B.B. Stagner, B.L. Lonsbury-Martin, and G.K. Martin (April/May 1994) Measurement of Otoacoustic Emissions For Hearing Assessment. IEEE Engineering in Medicine and Biology: 210-226.

Whitehead, M.L., B.L. Lonsbury-Martin, and G.K. Martin (October 1993) The Influence of Noise on the Measured Amplitude of Distortion-Product Otoacoustic Emissions. Journal of Speech and Hearing Research. 36:1097-1102.

X. Li, Y. Sokolov & H. Kunov. Method for Real-Time Recording of Distortion Product Otoacoustic Emissions, University of Toronto, 2000.

Otoacoustic Emissions : Clinical Applications, Eds., M. S. Robinette and T.J. Glattke, Thieme, New York, 1997.

Figure 2: Average DPOAE Amplitude Difference, Low Noise – High Noise (average over 9 subjects)

Validation d'une Méthode De Plans D'expérience Appliquée Aux Choix Des Modèles Acousticques

Joris Brun-Berthet, Frédéric Laville

Ecole de Technologie Supérieure, Génie Mécanique, 1100, rue Notre Dame Ouest, Montréal, Quebec, H3C 1K3

Cette communication fait suite à une précédente communication sur "L'utilisation des plans d'expérience afin de choisir la modélisation acoustique d'un téléphone mains-libres", présentée en octobre 1999 à Victoria, B.C. [6] et en novembre 1999 à Columbus, Ohio [5].

Introduction

Le développement de téléphones mains-libres « Full Duplex » où le haut-parleur et le microphone fonctionnent en même temps a posé des problèmes de couplage acoustique entre les deux transducteurs. Ces problèmes sont actuellement résolus en partie grâce au développement d'algorithmes de traitement du signal [3]. Pour compléter la résolution de ces problèmes, il est nécessaire d'améliorer la conception physique du boîtier téléphonique, ce qui implique de développer un outil de simulation informatique de l'acoustique de ce boîtier.

La réalisation d'une telle simulation est rendue difficile à cause des nombreux phénomènes à prendre en compte, de la complexité de la géométrie du téléphone et de la largeur de la bande de fréquence utilisée (300 Hz à 3400 Hz en téléphonie classique et 150 Hz à 7000 Hz en téléphonie large bande).

Un modèle par simulation numérique à l'aide du logiciel I-DEAS Vibro-Acoustics a déjà été fait, pour un téléphone existant, ainsi que pour un prototype de téléphone à géométrie simplifiée. La limite en ressource informatique nécessite des simplifications afin de couvrir toute la gamme de fréquence de la téléphonie large bande. Il est donc nécessaire de faire un choix quant aux simplifications envisagées dans le modèle afin de rester le plus proche possible de la réalité.

La technique utilisée pour faire ces choix est une technique de plan d'expérience. Celle-ci est fréquemment utilisé dans le domaine du génie industriel mais très peu en acoustique ou comme outil de choix de modèle.

1 Plan d'expérience

Le principe de la méthode des plans d'expérience a déjà été présenté auparavant [6] (voir aussi [4]). Elle permet une étude expérimentale d'un système de façon méthodique et ajoute un poids statistique aux analyses. Le plan d'expérience va permettre de déterminer l'importance des effets des facteurs du système.

1.1 Définition du système

Le but de ce projet est d'améliorer la conception physique du téléphone. Le travail expérimental se fait sur le boîtier. Pour réaliser un plan d'expérience, il faut définir un système, des facteurs susceptibles de modifier ce système, et une ou plusieurs variables de réponse à mesurer pour chaque expérience.

Le système étudié est le téléphone mains-libres sans son combiné. Les facteurs évalués sont aux nombres de 5 et pour chacun des facteurs 2 niveaux sont définis :

- Grille : présence ou non de la grille devant le haut-parleur du boîtier,
- Epaisseur : 2 épaisseurs différentes pour le boîtier,
- Mousse : présence ou non de matériaux absorbant à l'intérieur du boîtier,
- Plaque : avec ou sans obstacles à l'intérieur du boîtier,
- Trou : avec ou sans trou sur le boîtier.

La variable de réponse est la pression mesurée à une distance définis selon les normes [1] et [2], c'est à dire à une distance de 50 cm du téléphone dans un environnement semi-anéchoïque.

L'étude permet donc de dire si les facteurs sont influents et dans quelle gamme de fréquence ils le sont. Les facteurs influant seront pris en compte dans le modèle.

1.2 Représentation

Dans la méthode des plans d'expérience, la variable de réponse est habituellement une valeur discrète. La représentation et la comparaison sont directes. Dans le cas de spectre en fréquence, une nouvelle représentation a été proposée. Celle-ci permet de visualiser les effets de chaque facteur sur la variable de sortie en grandeur physique (décibel acoustique) en fonction de la fréquence.

1.3 Résultats

Les résultats de cette étude permettent de définir expérimentalement les effets de chacun des facteurs.

- Grille : son effet est important sur toute la gamme de fréquence. Autour de 300 Hz c'est à dire proche de la résonance du haut-parleur il y a un effet résistif. A plus haute fréquence, entre 2000 Hz et 5000 Hz, l'ensemble cavité devant la membrane du haut-parleur et grille se comporte comme un résonateur provoquant une augmentation de niveau,
- Epaisseur : l'importance de l'épaisseur de la boite est assez faible en dehors de la région autour de la résonance du haut-parleur,
- Mousse et Plaque : les effets de ces 2 facteurs sont assez semblables étant donné qu'ils agissent sur les modes de cavité, et principalement sur ceux dans la plus petite dimension du boîtier (apparaissant à 4000 Hz)
- Trou : les trous créent un phénomène basse-reflex. Il y a une effet de resonance du à ce phénomène qui apparait dans la réponse du téléphone. L'effet est peu important ailleurs.

Très peu d'interaction ont été constatée entre les facteurs. L'interaction la plus importante est celle entre le facteur Trou et le facteur Epaisseur. En effet le volume d'air eprisonné dans l'epaisseur du boitier est differente, donc l'effet du facteur Trou va etre dépendant du facteur Epaisseur.

2 Modélisation

Parallélement à cette étude expérimentale, une modélisation par éléments finis et éléments de frontière avec le logiciel I-DEAS Vibro-Acoustics a été faite.

Le premier modèle est celui d'un prototype à géométrie simplifiée. Le deuxième modèle est celui d'un téléphone mains-libres réel. Pour les 2 modèles numériques une comparaison entre les résultats provenant du modèle numérique et les résultats expérimentaux a été faite. Pour le prototype à géométrie simplifiés les résultats du modèle ont été validés jusqu'à 4000 Hz, par contre, dans le cas d'un téléphone réel où la géométrie est complexe les résultats de la modélisation ont été validé seulement jusqu'à 2500 Hz.

Le modèle actuel est un modèle de prototype dont certaines simplifications du plan d'expérience sont prises en compte. Une comparaison entre le modèle initial du prototype et un modèle où la structure est considérée comme rigide sera présenté. Dans ce cas, le calcul couplé se fera uniquement avec la surface de la membrane du haut-parleur.

Conclusion

L'étude expérimentale grâce à la méthode des plans d'expérience a permis de faire des simplifications sur le modèle numérique. Ces simplifications vont permettre d'élargir la validité du modèle sur une plus grande gamme de fréquence.

Remerciements

Références

[1] ITU-T Draft revised recommendation *Transmissions characteristics of hands-free telephones.* P.340, 1995.

[2] ITU-T Draft revised recommendation *Transmissions characteristics of wide band hands-free telephones.* P.341, 1995.

[3] Hänsler, Eberhard, 1994, *The hands-free telephone problem - An annotated bibliography update*, Ann. Télécommun., 49, nᵒ 7-8, pp 360-367.

[4] Montgomery, Douglas C., *Design and analysis of experiments Fourth edition*, John Wiley & Sons, 1996.

[5] Brun-Berthet J., Laville F., Dedieu S., *Using experimental design to choose an acoustical model for a hands-free telephone* 139th Meeting, Acoustical Society of America, 1-5 novembre 1999.

[6] Brun-Berthet J., Laville F., Dedieu S. *L'utilisation de plans d'expérience pour choisir la modélisation acoustique d'un téléphone mains-libres* Semaine Canadienne d'Acoustique 1999, 18-19 octobre 1999.

COMPARISON OF OBJECTIVE FUNCTIONS FOR ENGINE MOUNTS OPTIMIZATION

Denis Blanchet and Yvan Champoux

Department of Mechanical Engineering, Universite de Sherbrooke, Boul. Universite, Sherbrooke, Quebec,Canada J1K 2R1.

1 INTRODUCTION

Passenger's comfort is of prime importance in nowadays vehicule design. In order to improve this comfort, engine suspension design has to be based on comfort criteria describing passenger's perceptions. Acoustic pressure in vehicle cabin and vibration of components in contact with passengers are (seats, driving wheel, floor) typical examples. Using such an approach differs greatly from classical optimization techniques which only consider force injected into a rigid base structure. Considering only force functions limits the power of optimization techniques. In fact, passengers may not even feel the changes in perceptions between different configurations.

Futhermore, considering base structure as beeing rigid suppose that the mobility of the base is significantly different from that of engine mounts. However, in certains circumstances, mounts stiffness and structure impedance may coïncide and significantly alter engine's response to a determined excitation. In fact, at frame natural frequencies and for local mode, the mounts stiffness can even be higher than the attachment point frame stiffness.

On the other hand, transfer functions between force injected to the frame at engine mount locations and cabin vibration response or acoustic pressure often show high level peaks at specific frequencies. Cabin comfort can be compromise if there is energy transmitted at these frequencies from the powerplant. For all of these reasons, it is appropriate to adopt a design method which takes into account both structure flexibility and transfer path between engine attachment points and passenger's zone. The substructuring approach is well suited for these requirements.

Finally, classical optimization techniques usualy minimize a cost function for only one driving condition, typically idling. This can lead to undesired increase in noise and vibration levels at other driving conditions. This paper presents an optimization method which consider every steady state operating conditions of the engine.

2 GENERAL ASSUMPTIONS

This paper presents a straighforward method to model the behavior of an elastically supported engine attached to a rigid or a flexible structure. Model predicts sound pressure or vibration level that are directly linked with passenger's perception using a so called comfort criteria.. Each criteria is the sum in space and frequency of a cost function and optimization is based on these criterias. Cost functions studied are:

- Force injected into rigid structure
- Power injected into flexible structure
- Vibration in passenger's zone
- Acoustic pressure in passenger's zone

The engine is modeled as a rigid body. External force load acting on the engine's body is refered to as shaking forces, moments and torques [1]. This periodic load is due to the inertia of the moving parts. At first, Idling conditions are studied since external excitations frequencies and system's natural frequencies are much closer than in any other conditions. In a second step, a whole RPM range will be considered since higher order modes migth be ignored in the idle condition.

Mounts are made of rubber which dissipates energy and offers a wide range of possible stiffnesses. Structure is considered rigid or flexible depending on its stiffness relationship with mounts. All

calculations are made in steady state conditions using a frequency based analysis. Figure 1 presents a schematic view of the system to model. For clarity, structure is not show.
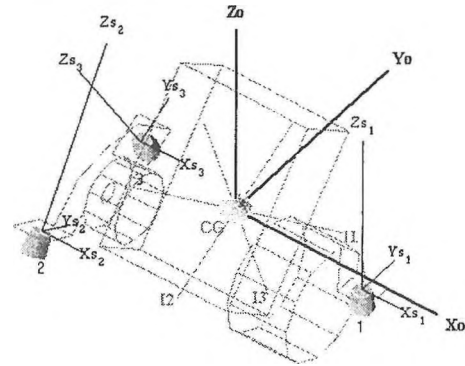

Figure 1 – Engine model with engine mounts principal axis of inertia.

3 EQUATIONS OF MOTION

The engine is modeled as a rigid body of mass m. Its center of gravity (CG), mass moments of inertia $(Ixx, Iyy...)$ and principal inertia axes are considered known properties. The engine sits on n mounts with position x,y,z and orientation γ, τ relative to global coordinate system (CG,Xo,Yo,Zo) as illustrated in Figure 1. Since mounts are generally made of elastomeric material, dynamic complex stiffness is used to model hysteresis damping properties. All mounts properties expressed in local coordinate system (n_i,Xs_i,Ys_i,Zs_i) must be transformed into global coordinates system. Once engine and suspension are defined, the magnitude of the force applied to either rigid or flexible base structure can be estimated. These forces are then used to estimate several comfort criterias using the appropriate measured FRF.

A simple way to implement this approach is to combine a substructuring model [2] which assembles all components into a global system and a rigid body modelisation model [3].

$$\{f_s\} = \left(\left[H_{ss}^A \right] + \left[H_{ss}^B \right] + \left[K \right]^{-1} \right)^{-1} \left[H_{sp}^A \right] \{f_p\} \qquad (1)$$

where

$\{f_s\}$ Reaction forces in the connection points between engine and structure

$\left[H_{ss}^A \right]$ Compliance FRF matrix of the engine in free-free conditions at connection points

$\left[H_{ss}^B \right]$ Compliance FRF matrix of the base structure in free-free conditions at connecting points

$\left[K \right]$ Stiffness matrix containing the stiffness characteristics of the isolation elements

$\left[H_{sp}^A \right]$ Compliance FRF matrix describing tranfer in free-free conditions from excitation points to interface points

$\{f_p\}$ Input forces and moments at excitation points

Most of the preceeding FRF can be measured. The only FRF that can't be measured easily is $[H_{sp}^A]$. This FRF can be derived from the rigid body relations between excitation forces and interface

points acceleration [6]. It is then possible to determine the force $\{f_s\}$ injected into rigid or flexible structure from eq (1). This force is used to evaluate all objective functions.

4 OBJECTIVES FUNCTION DEFINITION

4.1 Force injected in rigid structure

For a rigid structure, $\left| H_{ss}^{B} \right| \approx 0$, and eq (1) can be rewritten as :

$$\{ f_s \} = \left(\left[H_{ss}^{A} \right] + \left[K \right]^{-1} \right)^{-1} \left[H_{sp}^{A} \right] \{ f_p \} \qquad (2)$$

where $\{f_s\}$ corresponds to the objective function. In order to minimize this fonction, criteria φ_F is defined. This criteria corresponds to the total force injected into rigid base.

4.2 Power injected in structure

Power injected in a flexible structure is defined as [4]

$$P = \frac{1}{2} \text{Re} \left\{ f_s^{*} \cdot j\omega \left[H_{ss}^{B} \right] \cdot f_s \right\} \qquad (3)$$

where P corresponds to the objective function. In order to minimize this fonction, criteria φ_{Pw} is defined. This criteria corresponds to the total power injected into flexible base.

4.3 Acceleration at driver seat

Measured FRFs allow the computation of vibration levels in passenger's area. It is defined as :

$$\{ a \} = \left| H_{as}^{B} \right| \{ f_s \} \qquad (4)$$

where $\{a\}$ corresponds to the objective function. In order to minimize this fonction, criteria φ_{acc} is defined. This criteria corresponds to the total acceleration level of a specified region.

4.4 Acoustic pressure at driver's ears

Acoustic pressure may be computed using :

$$\{ P_r \} = \left[H_{ps}^{B} \right] \{ f_s \} \qquad (5)$$

where $\{Pr\}$ corresponds to the objective function. In order to minimize this fonction, criteria φ_{Pr} is defined. This criteria corresponds to the total pressure level over all locations considered as described in [5]

5 OPTIMIZATION

Let $\{X\}$ be a vector of mount properties such as position, orientation and stiffness. It is necessary to minimize φ with respect to variable $\{X\}$. Implementation of this optimisation is done with Matlab's Optimization Toolbox functions. In order to run the optimization, upper and lower limits on $\{X\}$ as well as constraints such as maximum engine displacement must be defined. Since the objective functions can be expressed in terms of single or multiple RPM values, the optimization Toolbox will solve for the specified RPM range of the objective function.

5.1 RESULTS

For simplicity and ease of interpretation, only positions of engine mounts are optimized. These mounts can move according to the geometry of the engine. In general, each mount may be moved up to 10 cm away from its original position.

In the next figures, results from optimization for a wide range of RPM are presented. These results suggest that from the starting configuration, each objective function taken separately can be well minimized. In fact, a significant gain of comfort can be experienced by changing the positions of the engine mounts.
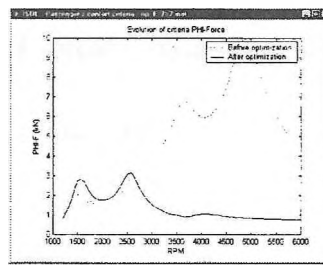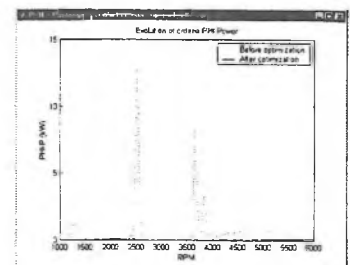

Figure 2 – Force criteria for force optimization

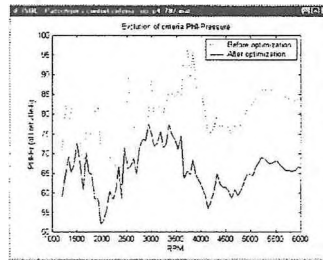Figure 3 - Power criteria for power optimization

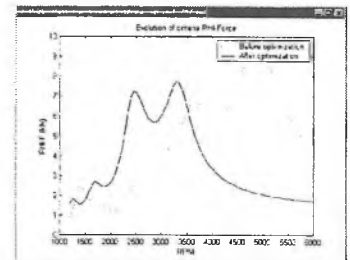Figure 4 – Pressure criteria for pressure optimisation

Figure 5 – Force criteria for power optimization

One should realise that optimization based on one criteria will not necessarily provide a good minimization of the other criterias. In other words, minimizing the power criteria will not necessarily minimize the force criteria. Figure 5 shows the level of minimization of the force applied to the rigid base when minimizing the power function. It is clear that minimizing for the power doesn't reduce injected force in the structure. These results can't be generalized since they greatly depend on vehicule FRFs, suspension availability and engine type. If the objective is to reduce vibroacoustic response at driver's location, it is useless to optimize with respect to the force injected into a rigid base.

Finally, in order to find the best suitable engine mount configuration, it is possible to combine certain criterias as defined before and to find the ideal position to minimize a weigthed sum of criteria according to the desired NVH vehicle quality.

6 CONCLUSION

A new approach in suspension optimization has been developped. It seeks to minimize passenger's perception of noise and vibration inside the vehicle. It allow designers to model structureborne noise generated by the engine. That is from the point of excitation on the engine chassis, throughout vehicle transfer path and up to the vehicle cabin. It was demonstrated that optimizing with flexible base structure, adequate structure FRFs and on a complete range of RPM is an efficient and promising approach. Optimization of the original position of the case study confirms that better positions can be found in order to enhance passengers comfort.

7 REFERENCES

[1] R.L. Norton, Design of Machinery. 2nded. McGraw-Hill. 1999

[2] K. Wyckaert, M.Brughmans, Hybrid substructuring for vibro-acoustical optimization : Application to suspension – car body interaction. SAE Paper 971944, pp 591-598.

[3] P.S.Heyns, An optimization approach to engine mounting design. IMAC XX, pp 1124-1129

[4] Jing-Lei Qu, Bei-Li Qian, On the vibrationnal power flow from engine to elastic structure through singlr and double resilient mounting systems. SAE Paper 911057. pp 149-153

[5] P.J.G.Van der Linden, Using mechanical-acoustic reciprocity for diagnosis of structure borne sound in vehicles. SAE Paper 931340. pp 625-630

[6] D. Blanchet, Champoux. Y. Comparison of objective functions for engine mounts optimization. IMAC 2000

ELIMINATION OF STRUCTURE-BORNE NOISE USING AN ELASTOMERIC INSULATING MATERIAL

P.Downey [1] , K.H.Guecker [2]

Dodge-Regupol Incorporated (DRI), Lancaster, PA 17601

Berleberger Shaumstoffwerk (BSW), Bad Berleburg, Germany, 57301

1.0 Introduction

New buildings are increasingly being constructed on sites subject to vibration. Often, the source of the noise is railway lines or industrial installations that are close by. In the building, the vibrations can cause excessive amplitudes or an increase in airborne noise level due to reflection from vibrating components, for example floors or ceilings. An acoustical consultant or engineer is faced with the task of constructing the building in such a way that the specifications of the client are maintained, but the permissible values are not exceeded.

Whether the vibrations in the foundation cause excessive disturbances in the finished building depends on the excitation strength and frequency, the foundation and the structure of the building. For an evaluation, the excitation must be measured as a function of the frequency whilst the connection of the building to the foundation as well as the structure of the building must be know. A computer model calculation of the vibration system can provide information about the expected vibrations in the building. An acoustical consultant must be present to measure the vibrations at several points near the site to maintain an accurate model. Where the vibration and consequently the secondary airborne noise exceed the specified limits, the excitation or transmission into the building must be reduced. For disturbances emanating from rail traffic and for the isolation of machine vibrations, there is a wide range of procedures available to reduce the emission. Even so, and in many cases, isolation at the source may not be possible for a variety of reasons. The designer must then reduce the vibration and ground-borne noise within the planned building. By means of bedding the building on an elastomeric material such as REGUPOL® or REGUFOAM®, this transmission can be effectively reduced.

2.0 Technical Information

2.1 Natural Frequency

There are only two parameters that effect the *natural frequency* of a system. There are mass (weight) and stiffness (spring rate).

Increasing the mass (weight) or reducing the spring rate will produce a lower natural frequency and conversely reducing the weight or increasing the spring weight will result in a higher natural frequency. With a REGUPOL® or REGUFOAM® material the above relates as follows: An increase or decrease in weight produces a corresponding stress change in the material, and an increase or decrease in thickness results in a spring rate change. That is a thinner material increases the spring rate while a thicker material decreases the spring rate.

The metric formula for natural frequency is [1]:

$$Nf = 0.159 \sqrt{\frac{k}{m}}$$

where :

Nf = Hertz, k = SpringRate(N/m), m = mass(kg)

If the weight referred to represented a machine, it would definitely have a natural frequency on its mounting. Furthermore it may generate disturbing vibrations of its own while in operation. These latter vibrations are caused by either unbalanced moving parts within the machine or an unbalanced condition arising from the work being performed. These vibrations are referred to as forcing vibrations, and their frequencies are called *forcing frequencies*. The major forcing (disturbing) frequency is generally the operating speed of the heaviest parts of the machine. However, higher secondary frequencies can sometimes create more of a disturbance than those created by the operating speed itself, thus requiring that these secondary frequencies also be isolated. Instrumentation used by an acoustical consultant is usually required to determine the disturbing secondary frequencies.

2.2 Frequency Ratio

The forcing frequency divided by the natural frequency is the ratio that indicates the effectiveness of a vibration insulation material [1].

$$\text{Frequency Ratio} = \frac{Ff}{Nf}$$

Where :

Ff = Forcing Frequency in Hertz; Nf = Natural Frequency in Hertz

2.3 Transmissibility

Transmissibility is the percentage of disturbance being transmitted through the insulation material. It is expressed by the ratio of the vibration amplitudes or forces. For example, if the purpose of an insulation material is to reduce the force transmitted to the support, then [1]:

$$T = \frac{Ft}{Fd} ;$$

Where : T = Transmissibility; Ft = Force Transmitted; Fd = Disturbing Force

Transmissibility can also be expressed as an insulation factor. An insulation factor is essentially (1-T) expressed as a percentage. Most insulation materials are designed so that the force transmitted to the foundation is only a small fraction of the unbalanced force or disturbing vibration being generated and acting on the system. As can be seen, the larger the difference between the disturbing frequency and the natural frequency of the insulating material, the more insulation is present. A transmissibility of zero is necessary for theoretically perfect insulation. However, for this to happen the frequency ratio would have to be infinitely large and thus is impossible to achieve. Realistically, insulation factors above 80% are usually adequate for the intended application, be it architectural or industrial.

3.0 Case Studies

Two case studies will be presented in brief, the first being an industrial application and the second an architectural one. These two examples show the extremes of loads that can be involved in a vibration problem and how to best find a solution to structure-borne noise and vibration problems using different insulation materials.

3.1 Industrial

In this case, a generator test cell at Siemens AG headquarters in Erfurt, Germany was insulated. This division of Siemens is a global manufacturer of generators, turbines and auxiliary equipment for the power generation industry. The problem involved a generator test pad where generators were being moved into place for quality control and other testing. These generators are quite heavy, weighing in at 627 kN. It was decided to isolate the generator on an inertia block or plinth. Siemens was looking for a solution to insulate this isolating inertia block against the transmission of vibration to other parts of the building, in order to reduce structure-borne noise in the nearby offices and protect surrounding equipment from damage due to vibration. The isolating plinth weighed in at an additional 863kN. The dimensions of the isolating plinth were a width of 4.3m and a length of 16.5m. The height of the plinth was 2.3m. The plinth was reinforced with steel rebar to bear the extreme weight of the generator.

The generators that were being tested were of two rotating speeds, 3000 rpm and 3600 rpm. This is equivalent to 50 and 60 Hz respectively. From this information a calculation can be done to determine the optimal dimensions of the insulating material supplied.

3.1.1 Calculations

Calculation of the Load :

$$Load = \frac{Weight(N)}{Area(mm^2)} := \frac{627kN + 863kN}{4.3m \times 16.5m} = 0.021 N/mm^2$$

The design was done with the lower frequency in mind since the lower frequencies are usually the more difficult to attenuate. Using A natural frequency versus load chart for the Regupol 6010SH supplied by DRI, it was found that at a load of 0.021 N/mm² would give a material natural frequency of 24Hz at 30 mm thickness [1]. This relates to a transmissibility or insulation factor of about 0.50, which was deemed to be sufficient for their application. Had a larger insulation factor have been required, a more compressible insulation material could have been chosen with a lower natural frequency down to 7Hz, or additional layers could have been added.

3.2 Architectural

In this case, a condominium/townhouse complex was being constructed in Toronto, Canada, situated between a freight railway line and a subway line. The subway passes about 20m west of the building and the rail line is about 40m to the south. No vibration reducing measures had been applied to the subway track, and the rails were directly connected to a slab. The rail line featured rail on tie configuration, with gravel ballast, but no insulation for the ballast. A quantitative forecast of vibration was required by an acoustical consultant before it could be determined if a form of vibration insu-

lation was required and to what extent. The structure-borne sound from the railways is determined by the condition of the rails, wheels, soil composition, etc. making it difficult to forecast. Measurements were taken of the vibration of the ground surface at the planned site and of the vibration of the ground surface and structures along the subway line. It is not possible to go into detail of the forecasting of vibration and any sound pressure levels at this point, however it was revealed that for both sites the vibration of the ground surface has a peak at 63Hz. There is almost no difference in the level between the two sites between the 63Hz and 125Hz bands, where structure-borne noise from the railway lines is generally a problem. [2]

The acoustical consultant specified a design frequency of 10Hz. For the porches facing the street, which were the last items to be insulated against vibration, different loads were calculated based on regular and snow loads. Short-term loads such as snow loads do not have to be taken into account with the REGUFOAM® material since brief peak loads of up to 4 times of the static constant loads can be absorbed. To insulate the porches, an area of 200mm x 200mm was specified. Forces were specified at 17N. The other constraint was on material thickness which could be no greater than 50mm.

3.2.1 Calculations

$$Area = \frac{Force}{Load} = \frac{17N}{0.012N/mm^2} = 1417 \ mm^2 = 38mm \ x \ 38mm$$

Using a load versus frequency chart for 50mm Regufoam 150, it was determined that the required static load was 0.012 N/mm² for insulation down to 9 Hz [1]. The dimensions of the insulating material required was calculated to be:
At these parameters, the deflection of the material is 7mm, and the building has an insulation factor of 85%. Unfortunately, no follow up readings have yet been taken on site.

References

[1] Regupol Vibration Insulation Handbook – Dodge-Regupol Inc., Lancaster, PA (2000).

[2] A. Minemura and T. Koga, "Measures to Insulate an Underground Lecture Hall from Structure-Borne Sound Caused by a Subway", Internoise '99 (1999).

Predicting The Movement Of An Engine Supported By An Elastic Suspension During A Transient Phenomenon

Christian Bissonnette and Yvan Champoux

Groupe d'acoustique de l'Université de Sherbrooke, Université de Sherbrooke, Sherbrooke, Québec, J1K 2R1, Canada

1.0 INTRODUCTION

In the quest for noise reduction, the purpose of the engine's suspension is the minimisation of vibration transmission between the motor and the structure. On the other hand, the engine's movement must be minimised to prevent failure in the propulsion system. At the conceptual stage of development, one must evaluate the dynamic behaviour of the suspension since it dictates the motor's movement. Suspension design is a delicate balance between adequate engine support and low vibration transmission to its structure.

This paper presents an experimental approach in determining engine behaviour when submitted to transient phenomenon. First, an experimental approach to determine the non-linear dynamic properties of a suspension is developed. Then, an equation of motion is elaborated, using the experimental properties of the suspension. This equation gives the maximal movement of the motor in regards to the transient phenomena measured on the vehicle.

2. SUSPENSION

The studied suspension has viscoelastic properties. This kind of material is associated with viscous damping. Based on a Voigt model [1], which consists of a dashpot in parallel with a spring, a non-linear equation of the force transmitted by the suspension is establish:

$$F = K(x)x + C(\dot{x})\dot{x} \qquad (1)$$

Where $K(x)$ is the spring function, which depends on the amplitude of the deformation, and $C(\dot{x})$ is the damper function, which depends on the velocity of the deformation.

The damper causes the energy dissipated by a mass-spring-damper system, since the spring doesn't produce any net work over a complete cycle or any integral number of cycles [3]. This energy is related to the area enclosed by the hysteresis loop [2], which is the transmitted force versus displacement (figure 1).
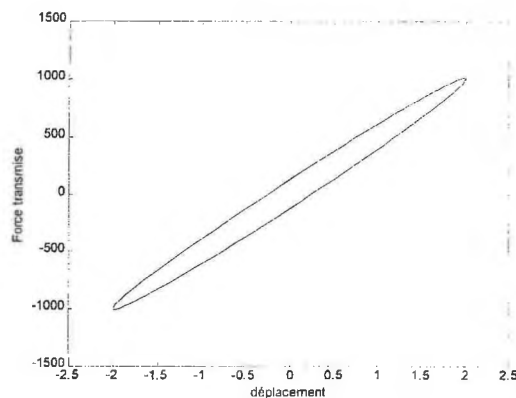

Figure 1: Hysteresis loop.

An experimental set-up produces a harmonic movement at one end of the suspension while the other extremity is fixed. Sensors read simultaneously the displacement, the velocity and the force transmitted by the suspension.

The area enclosed by the hysteresis loop leads to the damper force. The spring force is then the difference between the transmitted force and the damper force.

To approximate the spring function, a curve fitting on the spring force versus displacement is made (figure 2).

A similar process is followed for the damper function (figure 3).
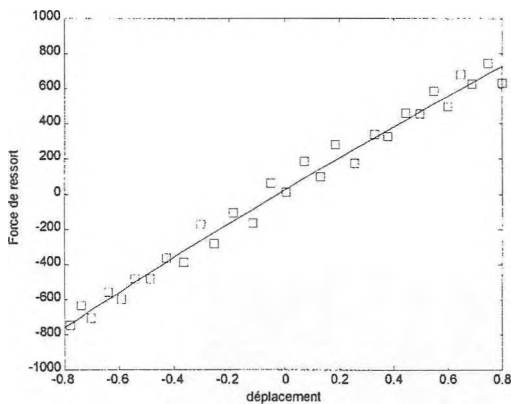
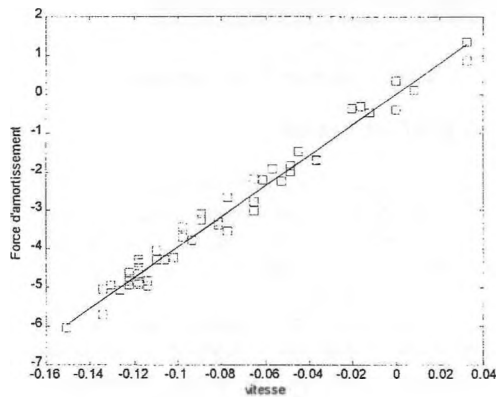Figure 2: Curve fitting on the spring force versus displacement curve.

Figure 3: Curve fitting on the damper force versus velocity curve.

3. EQUATION OF MOTION

The goal is to determine the behaviour of the motor when submitted to transient phenomena. Since it is only affect by the suspension, its equation of motion is:

$$M\ddot{x} = F \qquad (2)$$

Where M is the motor mass, $\ddot{x}$ is the motor absolute acceleration and F is the force transmitted by the suspension, found with equation 1. Otherwise, the motor's behaviour is associate with the relative movement between the motor and its structure.

If we assume the relative movement between the motor and its support to be:

$$z = x - y \qquad (3)$$

The equation of motion of the motor-suspension system becomes:

$$M\ddot{z} - C(\dot{z})\dot{z} - K(z)z = -M\ddot{y} \qquad (4)$$

Where $\ddot{y}$ is the absolute acceleration of the frame. This acceleration is measured experimentally.

Knowing the initial conditions of the motor-suspension system and an approximation of the rigidity and damper functions, a numerical method is used to determine the state of the system at each time interval. The computation is done in the time domain to find the behaviour of the motor.

4. CONCLUSION

The use of a Voigt model gives theoretical results that fit well with reality. The resolution of second order differential equations in the time domain is an easy way to include the non-linearity behaviour of the viscoelastic suspension.

5. ACKNOWLEDGEMENTS

6. REFERENCES

[1]   GALLAS, G. (1978) *Propriétés dynamiques des élastomères, application aux supports et butées*, Ingénieurs de l'automobile, 11-78.

[2]   THOMSON, W.T. (1998) *Theory of vibration with applications*, U.S.A., 5th ed., Prentice Hall, 524 p.

[3]   RAO, S.S. (1995) *Mechanical vibration*, U.S.A., 3rd ed., Addison-Wesley, 912 p.

THE SIDE BRANCH RESONATOR DESIGN METHOD FOR TWO-STROKE ENGINE EXHAUST SYSTEM

Gaétan Lecours ing.

RECREATIONAL PRODUCTS, Bombardier Inc. Valcourt, Québec, Canada, J0E 2L0

1.0 INTRODUCTION

The exhaust noise of a two-stroke engine is still a prior source of noise in recreational vehicle. Noise standard and consumers demand for noiseless vehicle require to find new solutions in exhaust noise attenuation. These solutions must be efficient in a large range of frequencies in order to reduce the noise at each engine RPM and load of the vehicle. Priorities like cost, weight, safety, reliability, packaging and performance need to be taken into account very seriously.

The purpose of this paper is to present an innovative approach to achieve the above target in term of noise and performance along the load line of the vehicle.

First, an experimental approach is developed to determine the exhaust noise along the load line. This approach allows the engineer to determine the problematic frequencies due to the exhaust system.

Then an analytical model developed by Bombardier is used in order to tune a set of side-branch resonators. This model, based on experimental data, allows to optimise the resonators design.

2. EXHAUST NOISE EVALUATION

First, the exhaust noise with typical muffler is measured from an engine running on a dynamometer. All the parameters representing the in field condition must be controlled, (engine rpm vs throttle opening following the load line, engine cooling flow and temp, exhaust temp., water injection (if applicable), etc ...) A schema of the apparatus is showed in figure 1.
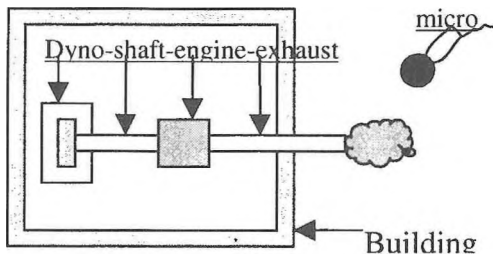

Figure 1.

Measurements are made at each RPM of the load line of the vehicle. Typically, it requires around 13 measurements at different engine speed. In order to pin-point all the different resonance in the exhaust noise, all the measurements are logarithmically averaged.

Typical exhaust noise spectra are showed in figure 2. The thick curve represents the averaged data. All the resonance can be clearly identified. It is important to work on each of these peaks in order to reach a good sound quality of the vehicle.
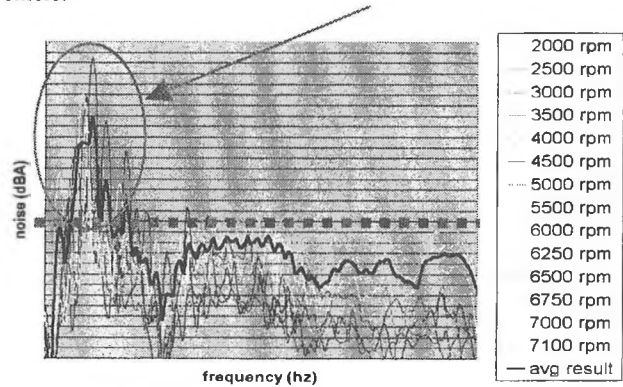

Figure 2: Exhaust noise without resonators

3. SIDE-BRANCH RESONATORS

As vehicles get smaller, there is less room for big expansion chamber. At the same time, expansion chambers create more restriction and back pressure in the exhaust line, which affect the engine efficiency. This lead to a new approach in order to control the exhaust noise.

The side branch resonator has no flow going through it. The principle of attenuation is that the reflective plane wave cancel the coming plane wave. The frequency efficiency of these resonators is selective. The length of the tube corresponding to the frequencies to be cut can be calculated by the following equation.

$$L = C.n/2f \quad n=0.5\text{-}1.5\text{-}2.5\text{-}3.5\text{-}4.5...$$
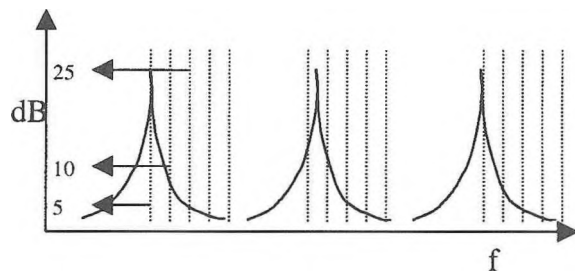
C=speed of sound
f=frequency to be cut

Figure 3 : transmission loss of a resonator

Note that the resonator acts not only at a single frequency but in a certain band. The graph presented figure 4 allows a

quick determination of the tube length for the frequency to be cut. Each set of curves in the figure 4 represent the 5 dot line showed in figure 3. The centred curve in the figure 4 being the highest point of attenuation zone and the 4 others curves showing the different range of attenuation. By example, a the efficiency of a 300 mm tube will more than be 5 dB between 250 and 400 Hz, and more than 10 dB between 275 and 310 Hz.
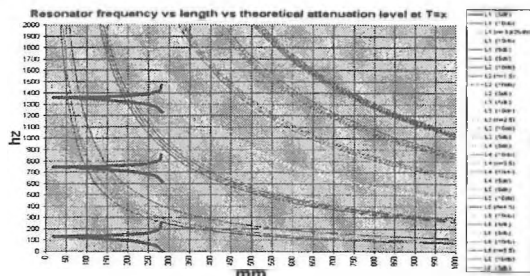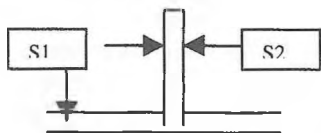

Figure 4: Efficiency of a resonator

The resonator efficiency is related to the expansion ratio m=S2/S1 (S1, S2 being area) [1]. Higher is the ratio, better is the transmission lost.

The figure 5 shows the measured exhaust noise with resonators. Note that the low frequencies peaks are removed from the spectra.
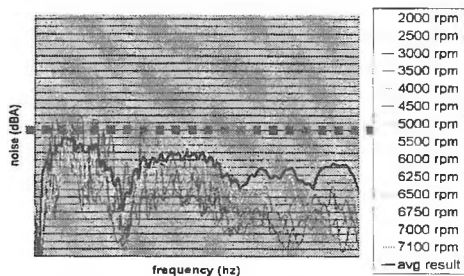

Figure 5: Exhaust noise with resonators

4. PREDICTIVE TOOL

We have seen how to design resonators tubes and their effect in an exhaust line.

If one wants to predict perfectly the sound attenuation along the exhaust line, there are a lot of parameter that need to be known; the speed of sound vary with temperature, the exhaust flow vary with the speed of the engine, the engine power vary with the load line, the exhaust noise vary with the load line, etc.... Because most of the parameters vary with the load line, the software uses an experimental database containing information related at each engine RPM.

First, we calculate the transfer function of the exhaust line corresponding to each rpm and then we sum up to predict the results. The software will calculate the attenuation that the resonator produce along the load line. The inputs are basically the tubes length and the noise spectra before adding the resonator:
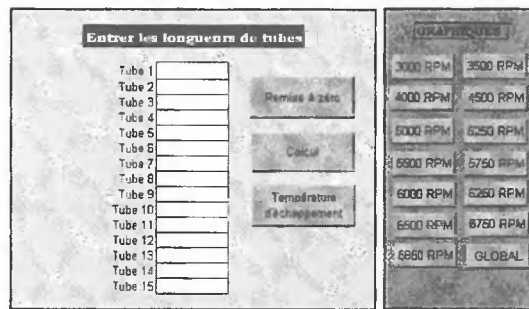

Figure 6: input panel of the software

With this tool we can vary manually the tube length in a way to optimise the attenuation with the target fixed earlier. The result can be printed at each rpm of the load line or only on the average result.

5. CONCLUSION

Both the experimental and the analytical approach allows to design very efficient exhaust system.

The use of side branch resonators, in conjunction with classical expansion chamber, give a very good attenuation of the exhaust noise in all the spectra, without compromise on the packaging of the system and on the back pressure of the exhaust. The use of these resonators in a PWC was patented in 1999.

6. ACKNOWLEDGEMENTS

7. REFERENCES

[1]   HARRIS. (1957) *Handbook of noise control*, McGRAW-HILL. Chapter 21.

[2]   Lecours & al. US patent 6.019.648, noise reducing system.

Participation In Noisy Leisure Activities In A Sample Of High School Students

L.G. Ciona and M.F. Cheesman

National Centre for Audiology, School of Communication Sciences and Disorders, University of Western Ontario, London, ON N6G 1H1

Introduction

Recent interest in the prevalence of noise-induced hearing loss in young people has shifted the focus from occupational noise levels to the noise levels of leisure activities. The recreational activities of youth, particularly those activities which use high fidelity, high intensity sound delivery systems (e.g. personal stereo systems, movie theatres), impulse noises (e.g. hunting, fireworks), and high powered motorized vehicles (e.g. motocross bikes, race cars) have been implicated as damaging to the human auditory system. An increased incidence of high-frequency hearing loss in young adults has been attributed to exposure of such leisure noises. Lees et al. (1985) conducted a study with 60 Canadian 16-25 year olds, and found that 40% of the subjects showed evidence of a 'notch' at the 6000 Hz frequency region [1]. These results showed a significant correlation of detectable hearing loss with the amount of reported leisure noise exposure. As a result, the investigators attributed the measured hearing loss to individual's leisure noise exposure. Some studies have shown, however, that leisure noise has little effect on the audiometric thresholds of adolescents. Axelsson et al. (1993) conducted a study with 52 Swedish children in grades one, four and six from a small, suburban community, who were provided with diaries in which they recorded the amount of time spent in various recreational activities [2]. When compared to the audiometric results, the investigators found that the children with higher thresholds did not have higher mean weighted noise exposures. These results seemed to suggest that the normal noise exposure experienced by children does not have a major impact on hearing sensitivity. Burén and colleagues (1992), when examining the audiometric thresholds of children and adolescents in Norway, concluded that children between the ages of 10 and 18 years were not exposed to any harmful noise [3].

There is little controversy in the assumption that some recreational activities have the *potential* to be hazardous to the human auditory system in that they exceed sound levels of 80 dBA. However, there is a lack of adequate research to determine the amount of risk that exposure to these leisure noises may impose. Damage risk to the human auditory system is dependent on the characteristics of the sound itself (i.e. sound level) and the temporal aspects of the sound exposure, including the duration and patterns of participation. Risk criteria cannot be established without adequate information regarding the sound intensity and temporal patterns of leisure noise exposure, which include the frequency and duration of exposure.

Noise hazard and risk criteria are often based upon occupational noise limits, such as those established in ISO 1999 [1990] [4]. These criteria demonstrate the relationship between hearing hazard and the intensity, frequency, and temporal pattern of the noise. As a result, the estimate of risk gathered from occupational noise exposures cannot be directly applied to the duration, type and exposure levels of leisure noises. For example, the occupational noise exposure limits are based upon a high intensity, continuous noise for an 8 hour workday, and a five day work week. While studies have primarily examined the A-weighted sound pressure levels of noisy recreational activities, the potential risk imposed by leisure noises has not been adequately investigated. It is essential to cal-

culate the accumulated duration of the individual's noise exposure as a component of establishing hazardous leisure noise levels, duration and frequencies. In order to determine the potential risk of damaging noise exposures arising from leisure activities, the noise immission levels, which include estimates of duration and temporal pattern of leisure noise must be described. A review conducted by MRC Institute of Hearing Research in Britain (1986) stresses the need for a participation survey to determine the rate of participation of young people in noisy leisure activities [5].

This research is an initial attempt to quantify the participation by Canadian teens and young adults in noisy leisure activities in terms of participation rates, hours per activity, and frequency of participation. This paper reports the preliminary results from the first phase of the study.

Method

A questionnaire was administered to a group of local, semi-urban high school students between the ages of 15 and 19 during the spring months of April and May. A total of 123 respondents participated (57 males, 66 females). Questionnaire administration was performed in a quiet school room. The questionnaire listed 32 recreational activities that have been previously implicated as potentially damaging to the auditory system, such as listening to the stereo through loud speakers, riding go carts, and hunting. Students indicated their participation in specific leisure activities during the previous one-week period. Given the limitations of self-report surveys, such as respondent bias, memory limitations and other uncontrolled factors, the questionnaire provided a cued-recall report, and restricted the responses that occurred over a one-week period, in order to minimize any memory constraints that might have an impact on the responses. The students were then asked to indicate the total duration of participation or exposure in the activities in which they participated. Responses to the questionnaire were analyzed for total participation time and number of activities reported.

3.0 Results

The responses to the questionnaires were analyzed cumulatively as a group and compared with sub-groups based on gender and age. The activities that were identified as the most popular sources of noise exposure were: listening to stereo through speakers (96.7%), listening to music through headphones (64.2%), vacuuming and attending sporting events (57.7%) and riding in a 'boom car'* (55.3%) [Table 1]. Of the students that listened to music through loudspeakers, 65.1% indicated that the music was 'loud', as did the 64.9% of those who listened to 'loud' music through headphones. Analysis by gender revealed that listening to the stereo through speakers remained the most popular activity for both males and females. The average number of noisy activities in which males participated was not significantly different than females (males: $\underline{M}$=7.91, $\underline{SD}$=4.20; females: $\underline{M}$=7.38, $\underline{SD}$=3.93). When the respondents were grouped according to year of birth (age), the mean number of activities decreased with increasing age, with exception to the youngest age group (see Table 2). Figure 1 shows the percentage of respondents and total number of noisy

recreational activities.

The activities which displayed the highest amount of exposure based on total duration of all respondents over a one week period included listening to the stereo ($\underline{M}$=4.66 hours, range=0.17–21); attending sporting events ($\underline{M}$=3.68 hours, range=0.25–12.5); listening to music through headphones ($\underline{M}$=2.45 hours, range=0.08–16); and using lawn mowers ($\underline{M}$=2.31 hours, range=0.33–15).

N.B. "Boom car" was interpreted by the students to mean a vehicle playing loud music.

Leisure Activity	Males (N=57)	Females (N=66)	TOTAL (N=123)
Stereo	96.5%	97.0%	96.7%
Headphones	68.4%	60.6%	64.8%
Sports event	59.6%	56.1%	58.2%
Vacuum	47.4%	66.7%	57.7%
Boom Car*	54.4%	56.1%	55.3%
Lawn mower	66.7%	43.9%	54.5%
Attend a movie	36.8%	43.9%	40.7%
Play in band	35.1%	34.8%	35.0%
Power tools	43.9%	15.2%	28.5%
Fitness class	8.8%	43.9%	27.6%
Restaurant	17.5%	31.8%	25.2%
ATV	35.1%	9.1%	21.1%
Club attendance	19.3%	21.2%	20.3%
Farm equipment	28.1%	13.6%	20.5%
Motor bikes	28.1%	9.1%	17.9%
Other activity	21.1%	13.6%	17.6%
Attend dance	10.5%	18.2%	14.6%
Firecrackers	14.0%	15.2%	14.6%
Arcade	10.5%	12.1%	11.4%
Drag race	12.3%	7.6%	9.8%
Rock concert	12.3%	7.6%	9.8%
Fireworks	7.0%	10.6%	9.1%
Leafblower	12.3%	6.1%	8.9%
Gocarts	8.8%	7.6%	8.1%
Hunting	10.5%	4.5%	7.4%
Carnival	7.0%	6.1%	6.5%
Orchestra	3.5%	6.1%	4.9%
Jet ski	0.0%	7.6%	4.1%
Models	3.5%	4.5%	4.1%
Airplane	3.5%	3.0%	3.3%
Snowmobile	5.3%	1.5%	3.3%
Rug shampooing	1.8%	3.0%	2.5%
Snowblower	1.8%	0.0%	0.8%

Table 1. Participation rates for males vs. females and total group

Age	N	Mean	Median	Mode	S.D.
19	20	5.90	4.50	3	3.85
18	20	6.80	6.50	5	2.53
17	13	8.38	8.00	3	4.72
16	37	8.95	8.00	6	4.50
15	33	7.39	6.00	5	3.76

Table 2. Average number of activities according to age

4.0 SUMMARY AND FUTURE DIRECTIONS

Limited numbers of studies have examined popular adolescent leisure activities. Those that have done so have generally focused on the sound levels produced by activities and not the amount of time spent in the activities or their frequency of occurrence. The results obtained from this study confirm that listening to stereos, either through loudspeakers or headphones are consistently popular among youth [6], followed by attendance at sporting events, vacu-
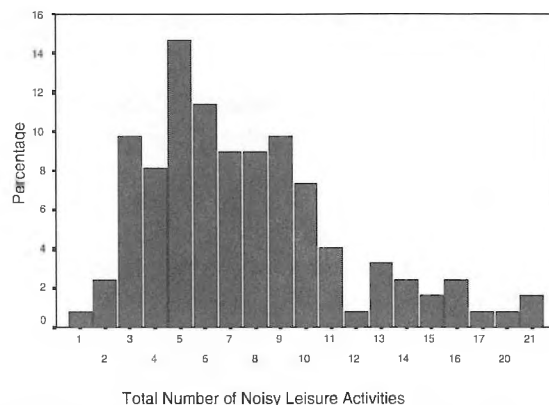

Figure 1. Percentage of respondents participating in number of leisure activities.

uming, and riding in cars playing loud music. Popularity in these activities suggest that further investigations are required to examine the duration and temporal characteristics of these leisure noise exposures, in order to accurately determine the risk of noise-induced hearing loss from participation in or exposure to these activities. In addition, in a country such as Canada, seasonal variations are a likely determinant of participation activities and patterns. Future goals include the administration of this survey during the summer and winter months to determine any seasonal variants or other participation patterns.

REFERENCES

[1]   Lees, R.E.M., Roberts, J.H., & Wald, Z. "Noise induced hearing loss and leisure activities of young people: A pilot study", Canadian Journal of Public Health, 76, pp. 171-173 (1985)

[2]   Axelsson, A., Dengerink, H., Hellstrom, P.A. and Mossberg, A.-M. "The sound world of the child:the relationship between daily activities and hearing acuity", Scandinavian Audiology, 22, pp. 117-124 (1993)

[3]   Buren,M., Solem, B.S., & Laukli, E. "Threshold of hearing (0.125-20 kHz) in children and youngsters", British Journal of Audiology, 26, pp. 23-31 (1992)

[4]   International Organization for Standards. "ISO 1999: Acoustics – determination of occupational noise exposure and estimation of noise-induced hearing impairment", (1990)

[5]   Medical Research Council Institute of Hearing Research, "Damage to hearing arising from leisure noise", British Journal of Audiology, 20, pp. 157-164 (1986).

[6]   Lankford, J.E., Mikrut, T.A., Jackson, P.L. "A noise-exposure profile of high school students", Hearing Instruments, 42 (12), pp. 19-24 (1991)

THE EFFECT ON SOUND ATTENUATION PROVIDED BY EARMUFFS OF OTHER SAFETY GEAR WORN IN COMBINATION

Sharon M. Abel*, Andrea Sass-Kortsak** and Shirliana Bruce*

Depts. of Otolaryngology* and Public Health Sciences**, University of Toronto, Toronto, ON M5S 1A1

1.0 Introduction

The purpose of this study in progress is to determine whether the sound attenuation afforded by hearing protective earmuffs is compromised, if the muffs are worn in combination with other safety gear. The safety equipment of interest are those devices which are worn in close proximity to the head. Combined usage of such devices has the potential of compromising the seal between the muff and the outer ear, resulting in noise leakage under the earcup. The objectives of the present research are to assess attenuation and speech understanding in subjects wearing a Class A muff[1] mounted on a hard hat, either worn alone or in combination with commonly used safety glasses and/or an air-purifying half-mask respirator, relative to unoccluded listening.

There is virtually no information in the literature on the effect on hearing protector attenuation of other safety equipment worn in combination.[2,3] The Canadian Standard on hearing protection[1] cautions, in an appendix, that "the type of protector that best suits a person will depend upon other equipment he must wear." However, there is no documentation of the possible outcomes. As well, the consequences, and possible interactive effects of other factors such as the gender of subjects, their hearing status, and age, have not been well researched. Subject factors have been shown to influence both the attenuation of hearing protectors (worn alone) and auditory performance measures in noise.[4-8]

2.0 METHODS AND MATERIALS

2.1 Experimental Design

Seventy-two working-aged adults (36 males and 36 females) are being tested. Each gender group comprises 12 normal-hearing subjects, 18-39 years of age, and 24 subjects, 40-65 years of age, half of whom will have normal hearing and half, moderate bilateral high-tone sensorineural hearing loss, characteristic of noise-induced hearing loss. Each subject is tested under five listening conditions: (1) with the ears unoccluded-UN, (2) with Class A muffs attached to a hard hat-M, (3) with the muffs and safety glasses-MG, (4) with the muffs and an air-purifying half-mask respirator-MR, and (5) with the muffs, safety glasses and respirator-MGR. All the devices are fit by a trained technician.

Within each condition, measurements are made of (1) free-field hearing thresholds in quiet for eight one-third octave noise bands centred at frequencies from 0.25 kHz to 8 kHz, and (2) consonant discrimination (75 dB SPL) in quiet and in a continuous background of 80 dB SPL speech spectrum noise. Attenuation is derived by subtracting the unoccluded

from the occluded hearing threshold for each frequency, within each of the protected conditions.

2.2 Subjects

The study is open to individuals who are fluent in English. Prospective candidates are screened for a history of head injury, systemic disease and neurological disorders. Those whose health status does not preclude participation are invited for a hearing screening test. Headset hearing thresholds are measured in each ear at two pure-tone frequencies, 0.5 kHz and 4 kHz. Those with thresholds in both ears equal to or less than 20 dB HL[9] are admitted to the normal-hearing groups. Those over the age of 40 years with thresholds of 25-50 dB HL at 4 kHz and normal hearing at 0.5 kHz in both ears are admitted to the groups with hearing loss.

2.3 Apparatus

The apparatus has been previously described in detail.[10] Subjects are tested individually within a semi-reverberant sound proof booth (3.5m by 2.7m by 2.3 m) that meets the requirements for hearing protector testing.[11] Pure-tone stimuli used for hearing screening are generated by a Hewlett Packard multifunction synthesizer (HP 8904A), and presented monaurally over a Telephonics TDH-49P headset. One-third octave noise bands for the experimental hearing threshold task are generated by a Bruel & Kjaer noise generator (B&K 1405) and band pass filter (B&K 1617). The speech test is commercially available on audio cassette and is played by a Yamaha twin cassette deck (KX-W900/U). The stimuli for the latter two tasks are presented free-field over a set of three loudspeakers (Celestion DL10) positioned to create a uniform sound field. Stimulus selection and fine adjustment of stimulus level, duration and envelope shaping are accom-plished by means of a Coulbourn Instruments modular system. The output will be fed to a pair of manual range attenuators (HP 350D) and Rotel mixer amplifier (RA 1412). For the measurement of hearing thresholds, subjects signify their responses by means of a hand held push-button switch. Paper and pencil are used for the consonant discrimination task. Devices are controlled from a personal computer (AST Premium 286) via IEEE-488 and Lablinc interfaces, and digital I/O lines.

2.4. Procedure

Hearing thresholds are measured once for each of eight one-third octave noise bands centred at frequencies ranging from

0.25 kHz to 8 kHz, using a variation of Bekesy tracking.[9] For each threshold determination, the stimulus is pulsed continuously at a rate of 2.5 per second. The pulse duration is 250 ms, including a rise/decay time of 50 ms. Subjects depress an on/off push-button switch whenever the pulses are audible, and release the switch when they can no longer be heard. The sound level of consecutive pulses is increased in steps of 1 dB until the switch is depressed and then decreased at the same rate of change until the switch is released. A trial is terminated after a minimum of eight alternating intensity excursions with a range of 4 to 20 dB. Hearing threshold is defined as the average sound level of the eight final peaks and valleys. The unoccluded condition is presented first, followed by the four protected conditions in random order.

Speech understanding is assessed using the Four Alternative Auditory Feature Test (FAAF) of consonant discrimination.[12] The subject is given a type-written list of 80 sets of four common monosyllabic words in the form of consonant-vowel-consonants. Half the sets contrast the initial, and half the final consonant (eg., wet, bet, get, yet OR bad, bag, bat, back). One word from each set is presented over the loud-speakers, and the subject circles the alternative heard. Five different lists are available on audio cassette. These are counter-balanced across the five ear conditions, in combination with the quiet and noisy backgrounds, and subjects within groups. The unoccluded condition is presented first, followed by the four protected conditions in random order.

3.0 Results and Discussion

To date, half the subjects have been tested. Nested analyses of variance (ANOVA) were applied to the attenuation and consonant discrimination data sets, respectively, obtained for the twelve subjects in the younger male and female groups. The results of the ANOVA on attenuation indicated that there were significant effects of the protector condition $[F(3,66)=46.48, p<0.0001]$, frequency $[F(7,154)=126.49, p<0.0001]$, protector by frequency $[F(21,462)=7.77, p<0.0001]$, and gender by frequency $[F(7,154)=2.17, p<0.04]$. Post hoc analyses using Fisher's LSD test[13] indicated that from 0.25-1 kHz, the attenuation provided by M was significantly greater than that for MG, MR, and MGR. There was no difference between MG and MR but both exceeded MGR. From 2-8 kHz, the attenuation provided by M was greater than that for MG and MGR. At 4 kHz and 6 kHz, M was also greater than MR. Generally, MR and MG provided more attenuation than MGR but were not consistently different from each other.

The ANOVA on the results of the FAAF test indicated that there were significant effects of the protector condition $[F(4,88)=4.00, p<0.005]$, background $[F(1,22)=544.38, p<0.0001]$, and protector by background $[F(4,88)=3.32, p<0.01]$. Post hoc comparisons showed that within each of the five protector conditions, the percentage of consonants correctly discriminated was significantly greater in quiet than in noise $(p<0.05)$. In quiet, there was no difference to the protector condition. In noise, listening with M, MR or MG resulted in significantly higher scores that did unoccluded listening.. There was no difference due to the various combinations of devices.

The results demonstrated that for young listeners the wearing of other safety gear (glasses and half mask respirator) alone or in combination significantly decreased the attenuation provided by Class A muffs attached to a hard hat. The results for males and females did not differ. Mean attenuation values achieved by both groups were within 7 dB of the manufacturer's specification, indicating that a good fit had been achieved. The results observed for the consonant discrimination task were similar to those reported previously.[6] The use of the muffs in noise proved beneficial relative to unoccluded listening. The decrease in attenuation when other safety gear were worn was not sufficient to diminish this effect.

REFERENCES

1. CSA (1994). CSA Z94.2-94 "Hearing protectors" (Canad Standards Assoc., Rexdale, Ont. Canada).

2. Ribera, J.E., Mason, K.T., Mozo, B.T. and Murphy, B.A. (1996). "Communication survey of CH-47D crew-members," Mil Med. 161, 387-391.

3. Wagstaff, A.S., Tvete, O., and Ludvigsen B. (1996). "The effect of a headset leakage on speech intelligibility in helicopter noise," Aviat. Space & Environ. Med. 67, 1034-1038.

4. Abel, S.M., Alberti, P.W., Hathornthwaite, C., and Riko, K. (1982). "Speech intelligibility in noise: Effects of fluency and hearing protector type," J. Acoust. Soc. Am. 71, 708-715.

5. Abel, S.M., Alberti, P.W., and Rokas, D. (1988). "Gender differences in real-world hearing protector attenuation," J. Otolaryngol. 17, 86-92.

6. Abel, S.M., Armstrong, N.M., and Giguère, C. (1993). "Auditory perception with level-dependent hearing protectors," Scand. Audiol. 22, 71-85.

7. Abel, S.M., and Hay, V.H. (1996). "Sound localization: The interactive effects of aging, hearing loss and hearing protection," Scand. Audiol. 25, 3-12.

8. Abel, S.M., and Spencer, D.L. (1997). "Active noise reduction vs. conventional hearing protection: The relative benefits for normal-hearing and impaired listeners," Scand. Audiol. 26, 155-167.

9. Yantis, P.A (1985). "Puretone air-conduction testing," in Handbook of Clinical Audiology, 3rd ed., edited by J. Katz (Williams & Wilkins, Baltimore), pp. 153-169.

10. Giguère, C., and Abel, S.M. (1990). "A multi-purpose facility for research on hearing protection," Appl. Acoust. 31, 295-311.

11. ANSI (1984). ANSI S12.6-1984 "Method for the measurement of the real-ear attenuation of hearing protectors" (Am National Standards Ins, New York).

12. Foster, J.R., and Haggard, M.P. (1979). "FAAF—An efficient analytical test of speech perception," in Proc. of the Inst. of Acoustics, MRC Institute of Hearing Research, Nottingham, England, pp. 9-12.

13. Daniel, W.W. (1983). Biostatistics: A Foundation for Analysis in the Health Sciences (Wiley,New York).

HYDRODYNAMICS OF OTOACOUSTIC EMISSIONS

Taha Jaffer[1,2] and Hans Kunov[1,2]

1. Institute of Biomaterial and Biomedical Engineering, University of Toronto, Toronto, Ontario, Canada. M5S 3G9.
2. Department of Electrical and Computer Engineering, University of Toronto, Toronto, Ontario, Canada. M5S 3G4.

1. Introduction

The discovery of Otoacoustic Emissions (OAE's) by David Kemp in 1978 has greatly aided the study of the mammalian auditory system. OAE's are sounds that are emitted from the cochlea and have been related to hearing function. OAE diagnosis is objective and non-invasive, however, the diagnostic value of OAE's can only be appreciated if the underlying physiology of the cochlea is properly understood.

Classical cochlear models suffer from an inability to realistically simulate OAE's because of the simplified treatment of the hydrodynamics at the interface between the oval window, stapes, and cochlear fluid. In the classical model, the cochlea is considered a tapered fluid-filled canal, split into two chambers by an elastic partition. There are two boundary conditions in this model. The first relates to a hole at the apex of the partition, known as the helicotrema, whose function is to null the trans-chamber pressure. The second describes the fluid displacement by the stapes at the base of the canal in response to sound entering the ear. However, when the sound is removed, the continued movement of the cochlear partition causes volume displacement in the cochlear canal, forcing fluid flow, and creating OAE's. The purpose of this present work is to mathematically describe this added hydrodynamic mechanism.

2. Classical Cochlear Hydrodynamics

The fluids within the cochlea are considered mechanically similar, acting in a linear, lossless, and incompressible fashion. The cochlear fluid flows in one direction, parallel to the Cochlear Partition (CP). Following the treatment given by Dallos (1973), the cochlear hydrodynamics are described by the following relation,

$$2\frac{\rho b(x)}{S(x)}\frac{\partial^2 z}{\partial t^2} = \frac{\partial^2 P}{\partial x^2} \qquad [1]$$

where $z(x,t)$ is the vertical displacement of the CP, $P(x,t)$ is the fluid pressure difference between the scala tympani and vestibuli, $b(x)$ is the width of the CP, and $S(x)$ is the cross sectional area of the canals.

One-dimensional cochlear models are constrained by two boundary conditions. The first describes the pressure variation at the helicotrema, a tiny opening at the apex of the CP. The second boundary condition describes the fluid displacement by the stapes at the base of the canal in response to sound entering the ear. Depending on the model of the middle ear used, this condition can vary. Generally, the boundary condition is taken to be

$$\frac{\partial P}{\partial x}(0,t) = G_{ME}(t)P_s(t) \qquad [2]$$

where $G_{ME}(t)$ describes the middle ear response and $P_s(t)$ describes the sound stimulus pressure.

The basal boundary condition [2] does not allow for reverse transmission after the presentation of sound stimuli. If the applied pressure in the ear canal is zero, that is, $P_s(t)=0$, then the fluid velocity at the oval window is also zero. Thus, the original boundary condition cannot reproduce this behavior and is incomplete and needs to be revised.

3. The Revised Basal Boundary Condition

The purpose of this derivation is to describe the boundary condition at the oval window with reference to the fluid flow in the entire cochlea. The CP is not perfectly compliant, it does not follow the applied sound pressure exactly because it has inertia and viscoelasticity. When the applied pressure is removed, the motion of the CP should continue, causing fluid volume displacements in the cochlear canal, thus, driving the oval and round windows. As the partition comes to rest after stimulation, only then will the reverse transmission cease. To incorporate the dynamics suggested, the original boundary condition at the base of the CP needs to be revised.

The actual fluid pressures seen in the base of the scala vestibuli is sum of the driving stapes and the pressure induced by the fluid flow in the scala vestibuli caused by CP motion. Using Newton's Second Law of Motion, and assuming that the cochlear fluids behave incompressibly, the fluid flow at the base of the CP can be described by,

$$\frac{\partial P}{\partial x}(0,t) = G_{ME}(t)P_s(t) - \frac{\partial P}{\partial x}(+0,t) \qquad [3]$$

where $+0$ is a point on the CP marginally apical to the base. It remains to determine the contribution of the CP motion to the fluid flow seen at its base. The classical model ignores this added contribution.

4. Basal Effect of CP Motion

The effect of CP movement without the sound stimulation can be deduced from [1]. Consider integrating [1] along x, from $+0$ to L_c, which amounts to summing the volume displacements induced by every portion of the CP. The result is

$$\frac{\partial P}{\partial x}(L_c,t) - \frac{\partial P}{\partial x}(+0,t) = 2\delta_{cp}(t) \qquad [4]$$

where

$$\delta_{cp}(t) = \int_{+0}^{L_c} \frac{\rho b(x)}{S(x)}\frac{\partial^2 z}{\partial t^2}dx \qquad [5]$$

With the knowledge that fluid flow through the helicotrema is negligible, the revised basal boundary condition can be obtained by substituting [4] into [3], and introducing a reverse inefficiency parameter $G_{rv}(x,t)$. The result is the revised CP basal boundary

condition,

$$\frac{\partial P}{\partial x}(0,t) = G_{ME}(t)P_s(t) + G_{rv}(x,t)\mathcal{S}_{cp}(t) \qquad [6]$$

Note, the derivation reduces to the well-known classical basal boundary condition [2], when the flows induced by the movement of the CP are not taken into account. In addition, after the stimulus pressure is turned off, the movement of the partition still influences the overall dynamics and sends acoustic energy back out into the ear canal to be recorded by the microphone as an OAE.

5. Simulation of TEOAE's

To test the efficacy of this revised basal boundary condition [6] a preliminary simulation was constructed. The simulations were carried out using a finite difference approach in a MATLAB computing environment.

Following Viergever (1980), cochlear parameters of mass, viscoelasticity, and stiffness were selected to best represent a traveling wave on the CP. A simple lossy lever model of the middle ear was employed based on a description given by de Boer (1980). The reverse transmission inefficiency was taken to be a constant and estimated based on the tone-burst response from the model cochlea. The simulation was run for 1 kHz, 1.5 kHz, and 3 kHz tone bursts of duration 50ms with amplitudes 44 dB (SPL), 44 dB (SPL), and 40 dB (SPL). After the presentation of the stimuli all stimulation was turned off and the resulting oval window movement computed. The results are shown in Figure 2 and corresponding live observations are shown in Figure 1. The results demonstrate that the responses obtained in simulation closely resemble that recorded in patients both in frequency content and time evolution as seen in Geisler (1998). The "echo" like behavior is apparent.

6. Summary

In this paper the basal boundary condition for the classical one-dimensional cochlear model was reconsidered. A revision of the basal boundary condition was derives by arguing that the movement of the CP introduces additional fluid volume displacements to the stapedial pumping of the oval window. Simulations incorporating this additional dynamic were successful in producing output very similar to current Transiently Evoked OAE's using tonal bursts. Future work will explore the applicability of this boundary condition to other classes of OAE's including the Spontaneous, Stimulus Frequency, and Distortion Product families.

8. Acknowledgments

7. References

Dallos, P. The Auditory Periphery: Biophysics and Physiology. New York: Academic Press, 1973.

de Boer, E. (1980) "Auditory Physics: Physical Principles in hearing theory I," Physics Reports, 62(2):88-174.

Geisler, C.D. From Sound to Synapse. New York: Oxford, University Press, 1998.

Jaffer, T. Longitudinal Elasticity of the Cochlear Partition and Distortion Product Otoacoustic Emissions. M.A.Sc Thesis, University of Toronto, 2000.

Viergever, M.A. Mechanics of the Inner Ear. Doctoral Dissertation, Delft University of Technology. Delft: Delft University Press, 1980
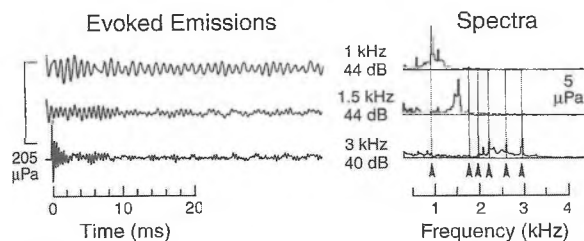

Figure 1. Time evolution and spectra of typical Transiently Evoked OAE from a normal human ear. Adapted from Geisler (1998), page 161, with permission from Elsevier.
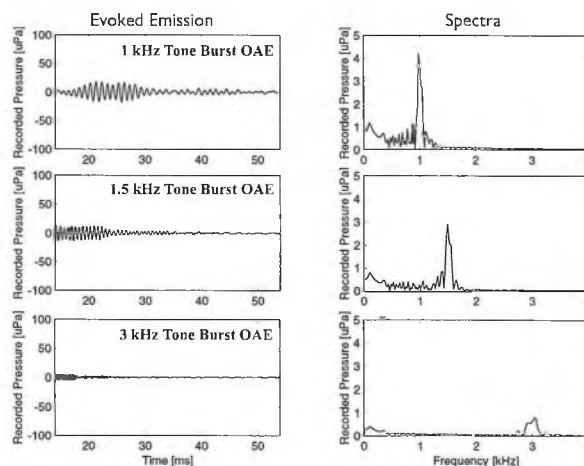

Figure 2. Simulated time evolution and spectra of Transiently Evoked OAE in a model of the human ear with the revised basal boundary condition. The similarity between Figure 1 and Figure 2 are striking.

Review Of Literature On Acoustic Warning Signals And Forklift Trucks

Chantal Laroche[1] and Stéphane Denis[2]

1. Audiology and Speech Pathology, Faculty of Health Sciences, University of Ottawa, Ottawa, ON K1N 6N5
2. Groupe d'Acoustique de l'université de Montréal, C.P. 6128, Succ. Centre-Ville, Montréal, QC, H3C 3J7

1. INTRODUCTION

A recent literary review (Laroche & Denis, 2000) of the norms, regulations and scientific articles related to acoustic signals on forklift trucks discerned this problem. This project brought forth 10 major conclusions :

1. A significant number of fatal accidents occur each year and many involve pedestrians travelling near forklift trucks. In the past 24 years, Quebec has had a serious or fatal accident involving contact between a pedestrian and a forklift truck every two years. Between 1994 and 1997, the CSST compensated 583 victims of forklift trucks, 54% of which were pedestrians hit by these vehicles. In the United States, OSHA counts, on average, 11 deaths and over 9500 injuries related to forklift trucks yearly.
2. Forklift trucks are used in all industrial settings to ensure material transportation or storage.
3. Most norms and regulations do not insist on the installation of reverse alarms on forklift trucks since the rear view is not considered obstructed on this type of vehicle. However, certain regulations (e.g. OSHA) forbid the disconnection of reverse alarms already installed on forklift trucks.
4. The reverse alarms currently available do not fulfill the auditory warning devices' conception criteria proposed by Tran Quoc and Hétu (1996).
5. Forklift operators' work is very complex and involves repetitive movements in order to ensure some safety behind the vehicle.
6. No security device (e.g. mirror, video camera, horn), taken in isolation, seems sufficient in ensuring the safety of pedestrians travelling near forklift trucks.
7. The devices available for obstacle detection (e.g. infrared system) are not yet sufficiently reliable to ensure safety behind forklift trucks.
8. In view of all the limits of the many security devices, many researchers recommend the use of reverse alarms while taking into account the environmental constraints and work execution constraints (e.g. ambient noise, number of vehicles simultaneously travelling in reverse).
9. Not one Quebec or Canadian manufacturer produces forklift trucks.Consequently, easily implemented short-term solutions must be found seeing that foreign manufacturers will unlikely apply solutions involving the design of forklift trucks, in the near future.
10. Prior to proposing the use of reverse alarms, it seems justifiable to proceed with the development of a questionnaire geared towards the forklift truck operators, the pedestrians and the interveners as well as an observation chart of the forklift truck's movements in different industrial settings, in order to determine the reverse alarm's relevance in these settings.

There seems to be situations in which the reverse alarm could be harmful and others where it could represent an indispensable security device. However, the characteristics of the current reverse alarms and horns do not ensure their audibility. The recent works of Laroche & al. (1995), Laroche & Lefebvre (1998), Guindon (1996) and Wilcox (1994) are sufficiently eloquent to support proceedings aiming at the improvement of this type of auditory warning signal.

2. ACOUSTIC SIGNALS AND FORKLIFT TRUCKS

Wilcox (1994) addressed the question of acoustic signals on forklift trucks by first presenting the most common causes of accidents involving a forklift truck striking a pedestrian. According to Wilcox, four major causes can explain the majority of accidents : 1) forklift trucks are relatively quiet, 2) forklift trucks are used in noisy environments, 3) pedestrians and forklift trucks cannot be completely isolated, and 4) there is restricted visibility on the forklifts. In Wilcox's opinion, many accidents would be prevented if the pedestrians were better informed of the forklift's presence. Visual and auditory modalities should therefore be solicited. Thus, the use of auditory and visual warning signals should be seriously considered.

This author finds it difficult to explain why reverse alarms are not mandatory on forklift trucks. He seems to attribute this fact to the manufacturers who claim, particularly in the context of legal pursuits, that their vehicles are safe and that security systems, such as reverse alarms, do not need to be added to them. Thereafter, Wilcox attempts to demonstrate that the manufacturers have every intention to improve the safety of their vehicles and discusses the 11 myths associated to this problem. Every one of these myths will be presented and briefly discussed for it allows the importance of the problem to be properly discerned.

1. Pedestrians get used to the alarms and these thereby lose their efficiency over time :

According to Wilcox, people get used to false alarms but do not get used to the useful information that inform them on the presence of forklift trucks.

2. The use of warning signals leads to more negligent operators :

Wilcox finds no evidence in the literature that having access to a security device, such as an auditory signal, influences the operators' degree of vigilance.

3. The presence of many forklift trucks, each equipped with a warning signal, would create confusion :

The main question is whether it is safer to be surrounded by forklifts that are seen and heard or that aren't. Wilcox presents the following analogy : is it safer to cross an intersection filled with noisy vehicles or silent vehicles?

4. Warning signals cause difficulties and are annoying :

Warning signals cause difficulties because reverse alarm manufacturers have not included a sound quality criterion in their design. According to Wilcox, modifying the alarms' acoustic characteristics could solve this problem. Moreover, Wilcox adds that even if it were difficult to completely eliminate all difficulties created by alarms, it would nonetheless be preferable to use them than to allow for more accidents to occur.

5. As opposed to work on the forklift's design, forklift truck operator training and a safe work environment represent better solutions for risk control :

Wilcox recalls the hierarchy that ergonomic professionals generally apply : 1) eliminate the risk, 2) protect only when the risk cannot be eliminated, 3) inform only when the risk cannot be eliminat-

ed nor controlled through protection, and 4) consider training only when the risk cannot be treated with any of the three alternatives. The reasoning behind this hierarchy is that nobody is perfect.

6. The accidents are caused by a task that demands too much of the victim's attention and not by faulty forklifts :

What surprises Wilcox in this myth is that the situation where an individual is too concentrated on his/her task and has not heard the forklift, is precisely the condition under which reverse alarms should be considered in order to draw the individual's attention.

7. Accidents can be avoided, for example, by driving in reverse or by looking around the load :

Wilcox notes that it is unreasonable to think that all forklift truck operators will continually "strain their necks" to optimize their visual field. Ergonomically, the forklift truck operator's position represents a risk for all sorts of chronic problems if the driving is done in reverse. Consequently, the manufacturers cannot blame the forklift truck operators for the accident when, in fact, the vehicle's design does not respect the ergonomic criteria.

8. The clients should decide what to install :

Wilcox specifies that the clients who purchase the forklift trucks are not experts in this field. They are thereby not qualified to evaluate the risks associated to these vehicles, or to know what should be done to improve the level of safety.

9. The use of warning signals for the forward and backward courses would create confusion and danger for the workers who are unaware of the direction in which the forklift truck is moving :

Wilcox easily objects to this myth by reporting that the idea is to inform the individuals of an approaching forklift, regardless of its direction.

10. Workers could disconnect the warning devices :

According to Wilcox, the risk of employees disconnecting the device is associated to the quality of the device's design and is not a valid argument against the installation of such a device.

11. The warning devices should be adjusted to the workplace's particularities :

There are many ways to adjust a warning signal to the reality of the environment. For example, the warning signal could be adjusted according to the ambient noise. Many adjustments are technically feasible.

All arguments enumerated by Wilcox argue in favor of the use of reverse alarms on forklift trucks. Another author also supports this view. Miller (1988) reports some examples of serious accidents that involved forklift trucks and insists on the importance of auditory warning signals, either a horn or a reverse alarm, due to the forklift truck operator's complex task.

Amongst other topics, Guindon's (1996) report addresses the analysis of certain situations involving the perception of the forklift truck's horn. No reverse alarms were studied in this project because, according to Hétu, who was responsible for the project, these alarms are often judged harmful and do not transmit useful information due to the cacophony often induced and the habituation phenomenon.

On this basis, we can contend that an unquestionable doubt seems to subsist as for the pertinence of reverse alarms. As for the results related to the horns, they are rather eloquent. Out of 235 situations where horns are used in 8 different establishments, only 30 condi-

tions were judged adequate when using the Detectsound software (Laroche & al., 1991) as an analysis tool. These results lead Hétu and Denis (1995) to conclude that we should have access to horns with multiple frequency components for which the intensity would be automatically adjustable as a function of ambient noise.

3. CONCLUSION

In summary, the relevance of reverse alarms on forklift trucks is not clearly established yet, especially in those situations where the forklifts often circulate in reverse and where the noise level is already relatively elevated. Moreover, the spectral and temporal characteristics should be defined with greater specificity in order to ensure the audibility of reverse alarms in the conditions where it would be pertinent. There does not seem to be any perfect short term, or medium term, solutions, whether it be in visual ergonomics (use of luminous signals, of video systems or of mirrors) or in the arrangement of the forklift truck operators' work position. On the basis of the above stated studies, the use of reverse alarms would consequently be recommended while taking into account the apprehensions also stated. Further studies should be realized in order to establish the conditions for which the reverse alarms would be recommended.

4. ACKNOWLEDGEMENT

5. REFERENCES

1 Guindon, J.C. (1996). Pour des avertisseurs sonores efficaces. Rapport de recherche R-145, IRSST, 40 pp.

2 Hétu,R. & Denis, S. (1995). Caractérisation des avertisseurs sonores à [l'établissement A et H], Rapport interne, GAUM, mars 1995.

3 Laroche, C. & Denis, S. (2000). Bilan des connaissances sur la signalisation acoustique et les chariots élévateurs. Subv. 99-029, IRSST, 64 p.

4 Laroche, C., Ross, M.-J., Lefebvre, L. & Larocque, R. (1995). Détermination des caractéristiques acoustiques optimales des alarmes de recul. Rapport de recherche IRSST R-117. 89 pp.

5 Laroche, C. and Lefebvre, L. (1998). Determination of optimal acoustic features for reverse alarms. Ergonomics, 41, 1203-1221.

6 Laroche, C., Tran Quoc, H., Hétu, R. & McDuff, S. (1991). « Detectsound » : A computerized model for predicting the detectability of warning signals in noisy workplaces. Applied Acoustics, 32, 193-214.

7 Miller, B.C. (1988). Forklift safety by design. Professional Safety, September 1988, 18-21.

8 Tran Quoc, H. & Hétu, R. (1996). La planification de la signalisation acoustique en milieu industriel : critères de conception des avertisseurs sonores de danger. Canadian Acoustics, 24(2), 3-17.

9 Wilcox, S.B. (1994). Why forklifts need signaling devices. Ergonomics in Design, October 1994, 17-20.

SPEAKER IDENTIFICATION BY COMPUTER AND HUMAN EVALUATED ON THE SPIDRE CORPUS

Hassan EZZAIDI and Jean ROUAT

ERMETIS, DSA, Université du Québec à Chicoutimi, Chicoutimi, Québec, Canada, G7H 2B1.

1. INTRODUCTION

Although many experiments on clean speech report high identification rates for computer systems, results on noisy telephone speech with different handsets are usually too poor for practical identification tasks (noise, limited bandwidth, effect of the channel, telephone handsets variability)[1].

What would be the identification rate of humans in the same conditions? A reference is necessary in order to evaluate the performance of computer systems. The comparison between computer and human has been already made. For a review one can refer for example to the work by Doddingtion [2]. As the performance of human has been chown to be dependent of the speech nature, we propose to examine the effect of telephone handset variability for text-independent speaker identification of telephone speech. We report human and computer speaker identification with the SPIDRE database.

Section 2 describes the experimental conditions while section 3 and 4 are the results and discussion. Section 5 is the conclusion.

2. EXPERIMENTAL CONDITIONS

2.1 SPIDRE database

Closed set Speaker Identification experiments were performed on a SPIDRE subset of the Swichboard corpus with *matched* and *mismatched* telephone handset conditions. We refer to the *matched* conditions, when (for a same speaker) the training and testing sessions were collected from the same telephone handset. In the *mismatched* conditions, different handsets were used for training and testing sessions.

Based on the pitch frequency (F_0) distribution, we first ran a speaker identification experiment on the 45 speakers of the SPIDRE corpus. We then extracted the most confusable speakers to create a subset of 10 women speakers (Female speakers with similar F_0 distribution). Each speaker has 4 conversations originating from 3 different handsets. The sampling rate is 8 Khz.

2.2 Listening conditions

Sixty pairs of sentences were randomly chosen and played through a Sennheiser HD250 linearII headphone. Ten naïve listeners (one woman and nine men) were asked to tell if the speaker was the same for both sentences. The listeners could not use sex as discrimination criteria. For each sentence, five seconds of speech were played. The listeners are French speaking and most of them could not understand spoken American English. For each pair, the listener had to make four choices:1. certainly the same speaker; 2. probably the same speaker; 3. probably different speakers; 4. certainly different speakers.

2.3 Computer experiments

Speech analysis

The speech is first preemphazised (0.97), then, a sliding Hamming window with a length of 32 ms and a shift of 10 ms is positioned on the signal. Twelve cepstral Mel coefficients, twelve delta Mel cepstral coefficients (computed according to the regression weighting), one log power and one delta log power are then extracted by using a liftering of 22 . Cepstral mean normalization is also performed. The final dimension of the MFCC vectors is 26.

Identification

We use two clustering technics. The first recognizer is based on a nonparametric pattern recognizer. For now, we use the LVQ-SLP as proposed by J. He and al. [3]. Each speaker is characterized by one codebook. The codebook size is the same for all speakers. We performed experiments with codebook sizes of 128, 256 and 512. The second recognizer is based on a parametric estimation of the probability distributions of the MFCC. A Gaussian Mixture Model (GMM) is associated to each speaker (one model for each speaker). For a given speaker, the GMM is supposed to model the statistical distribution of the MFCC. We used models with 32 Gaussian mixtures. We also assumed a diagonal variance matrix for each mixture component and parameters were estimated via the E.M algorithm.

Training and testing

The impact of mismatched and matched conditions is evaluated. In matched condition, the same telephone handset is used for training and testing. One conversation is used for training and the second one for testing. With mismatched handsets, training is performed on 3 conversations (pronounced through 2 handsets) and testing is made on the 4th Conversation coming from the 3rd handset.

Recognition criterion

The tested conversations were divided into fixed block lengths of 10 ms. With the GMM, the log likelihood of each block is computed, whereas, the nearest neighbour algorithm is used for the LVQ-SLP. A speaker is recognized if, for the entire test conversation (all blocks) it has the minimal distance (LVQ-SLP) or the maximum-likelihood (GMM).

3. EXPERIMENTS AND RESULTS

3.1 Listening tests

Table 1 reports rates for intra-speaker (columns 2 and 3) and inter-speaker (column 4) identification. Listeners are reported in column 1. In the matched conditions, one finds an averaged rate of 81%. The variance is significant and is mainly due to listeners L1 and L6. For the mismatched conditions, the recognition rate falls of 11%, with a weaker variance. In the case of the inter-speaker identification it is not possible to verify if the same telephone handset can yield confusions between speakers (speakers declared to be same speaker instead of declaring different) as the database labeling does not include the description of the handset characteristics. It is observed that the identification rates are coherent with those of

columns 2 and 3.

Analysis of the tests clearly shows that the handset has a predominant influence on the perception of listeners. In many situations with the same speaker and two handsets for the two sentences, listeners identified the two conversations as coming from different talkers.

Listeners	Identical speaker in test		Different speakers in test
	In Matched condition	In Mismatched condition	
L1	60 %	68 %	67 %
L2	90 %	74 %	77 %
L3	90 %	72 %	75 %
L4	70 %	72 %	72 %
L5	90 %	72 %	75 %
L6	50 %	64 %	65 %
L7	90 %	71 %	92 %
L8	83 %	62 %	75 %
L9	100 %	72 %	62 %
L10	90 %	72 %	75 %
Mean	81 %	70 %	73.5 %
σ	16	4	8.2

Table 1 : Averaged scores for 10 listeners . Last column, refers to conversation pairs involving two different speakers using unknown handsets.

3.2 Computer tests

Handsets condition	Codebook size (LVQ-SLP)			32 GMM
	512	256	128	
Matched	90 %	90 %	90 %	-
Mismatched	60 %	60 %	60 %	90 %

Table 2: Computer speaker recognition rates. *Matched* (One conversation in training, another in testing, identical handset); *Mismatched* (Three conversations in training, another in testing, different handset).

The LVQ-SLP recognizer yields an identification rate of 90% when talkers use the same telephone handset. With different handsets in training and testing (mismatched) the scores drop to 60%. It is interesting to note that the LVQ-SLP rates are independent of the codebook sizes.

The GMM recognizer outperforms the LVQ-SLP recognizer when mismatched handsets are used (90% in comparison to 60%). With the same handset we would expect better results.

4 DISCUSSION

It is observed that the confusion between speakers is mainly due to the strong telephone handset influence. Thus, the speaker acoustical characteristics are found to be largely degraded by the telephone handsets.

Except for L1 and L6, all listeners presented the same faculty to distinguish between the 10 women. In matched conditions, if one does not consider L1 and L6 in the statistics, the average identification rate can increase around 90%.

Interestingly, the difference in performance when changing from matched to mismatched condition is smaller for listeners than for computers.

Although the task presented to listeners and computers is not comparable – the listeners task is easier with a comparison of two speech segments and the computer has to carry out the classification between 10 speakers presented simultaneously - it is observed that the mismatched conditions degrade the performance for human and computer.

It is possible to infer that the success of the computer is related to the efficiency of the models and to the quality of the parameters (reduction of the channel and handset effects) for the subset of 10 women.

5 CONCLUSION

Even if the task was easy in comparison to the identification of forty speakers, the relatively low performance of the listeners gives an idea of the complexity of the SPIDRE corpus.

The selection of ten females has been based on pitch frequency distribution. They have a similar distribution of pitch. We already found that based on the pitch, the task was tedious for computers when using exclusively cues derived from the pitch distribution [4]. Manipulation of the pitch frequency confuses listeners when identifying speakers [5]. This suggests that pitch frequency is in fact a fundamental cue which can not be fully exploited by listeners on our test set because of the pitch distribution similarity. Furthermore, Itoh and Saito [6] found that the spectrum envelope is more important in speaker identification than excitation. The MFCC recognizers rely mainly on the spectrum envelope and formants and are probably more accurate than listeners to identify speakers based on spectral characteristics only.

For a subset of 10 female speakers with high confusable pitch distribution the recognizer based on the MFCC and GMM outperforms the listeners.

ACKNOWLEDGEMENT

REFERENCES

[1] C.R Jankowski Jr., T.F. Quatieri, and D.A. Reynolds. Measuring fine structure in speech: Application to speaker In *IEEE-ICASSP*, pages 325-328, 1995.

[2] G. Doddington: Speaker recognition-identifying people by their voices In *Proc. IEEE* Vol 73, pp1651-1664.

[3] Jialong He, Li Liu, and Günther Palm. Speaker identification using hybrid LVQ-SLP networks. In Proc. *IEEE ICNN'95*, volume 4, pages 2051—2055, 1995.

[4] J. Rouat, H. Ezzaidi et M. Lapointe. Nouveaux algorithmes d'extraction en vue de caractériser le locuteur. *Technical report*, ERMETIS, Université du Québec à Chicoutimi, March 1999. Contrat W2213-9-2234/SL, rapport final, 67 pages.

[5] S. V. Bemis and S. W. Nunn. Acoustic features and human perception of speaker identity In Proc. AVIOS, pages 85-96, 1998.

[6] Itoh K. and Saito S. Effects of Acoustical Feature Parameters on Perceptual Speaker Identity *In Review of the Electrical Communications Laboratories*, vol. 35, N0.1.

Wavelet Noise Reduction: Application To Speech Enhancement

Mohammed BAHOURA and Jean ROUAT

ERMETIS, DSA, Université du Québec à Chicoutimi, Chicoutimi, Québec, Canada, G7H 2B

1. Introduction

During the past decade, the Wavelet Transforms (WT) have been applied to various research areas. Their applications include signal and image denoising, compression, detection, and pattern recognition.

To our knowledge, denoising methods based on the wavelet thresholding have not been successfully applied to speech enhancement. However, wavelet transform combined with other signal processing tools has been proposed.

In this paper, we pass in review the principal wavelet denoising methods published in the literature. Then, we expose the speech enhancement techniques using wavelet transform. Next, we point out the difficulties encountered in the wavelet thresholding methods and finely we propose some solutions.

2. Noise reduction by wavelets

2.1 Principe

Two basic approaches are proposed to remove noise by wavelet transform. The first is based on the singularity information analysis [1], whereas the second is based on the thresholding of the wavelet coefficients [2].

Mallat et al. [1] proved that modulus maxima of the wavelet coefficients give the complete representation of the signal and they proposed an iterative algorithm to remove noise. In the singularity analysis context, Xu et al. [3] developed a noise filtration method based on the spatial correlation between the wavelet coefficients over adjacent scales. An improved version is proposed by Pan et al. [4]. The thresholding method will be described in the next section.

2.2 Wavelet shrinkage

Donoho [2] proposed a powerful approach for noise reduction. It is based on the thresholding of the wavelet coefficients:

- Transform the noisy signal y into wavelet coefficients w,
- Apply a soft or hard threshold λ at each scale,
- Transform back the resulting coefficients, and get the estimated signal.

Donoho and Johnstone [5,6] define the soft threshold by

$$T_\lambda(w) = \begin{cases} sgn(w)(w-\lambda) & \text{if } |w| \geq \lambda \\ 0 & \text{if } |w| < \lambda \end{cases} \quad (1)$$

The authors proposed a universal threshold λ for the WT

$$\lambda = \sigma\sqrt{2\log(N)} \quad (2)$$

with $\sigma = MAD/0.6745$, where N is the length of y and σ is the noise level. MAD represent the absolute median estimated on the first scale. In the Wavelet Packets Transform (WPT) case, the threshold becomes:

$$\lambda = \sigma\sqrt{2\log(N\log_2 N)} \quad (3)$$

Johnstone and Silverman [7] studied the correlated noise situation and proposed a "level-dependent" threshold

$$\lambda_j = \sigma_j\sqrt{2\log(N_j)} \quad (4)$$

with $\sigma_j = MAD_j/0.6745$, and N_j is the number of samples in scale j.

The discriminatory threshold is also defined using other criterion like Minimax and SURE (Stain's Unbiased Risk Estimate) [6,7].

The time-adaptation of the threshold that takes into consideration the time behaviour of the noisy signal constitutes an interesting approach [10].

3. Application to speech enhancement

The wavelet transforms are successfully applied to improve the performance of speech enhancement methods. Unfortunately, the wavelet thresholding technique can not be applied directly because the simple threshold can not discriminate very efficiently the speech components from the noise ones. In this section we summarize the principal speech enhancement technique's using wavelet.

3.1 Wavelet thresholding

An algorithm based on the wavelet thresholding is proposed for speech enhancement algorithm [11]. To prevent the speech quality deterioration during the thresholding process, the unvoiced regions are classified first and then thresholding is applied in different ways.

The problem is not completely resolved, but this approach constitutes an interesting step to avoid the speech degradation.

3.2 Wiener filtering in the wavelet domain

The wavelet transform based Wiener filtering is a special application of the Wiener filtering. This idea arises from the fact that wavelet transforms tend to decorrelate data.

A multi-microphone system is proposed for speech enhancement [12]. The Wiener filtering performances in the wavelet domain are better than those obtained in the Fourier domain. Another version that combines Wiener and coherence in the wavelet domain is also proposed [13].

3.3 Wavelet filter bank

Most of the speech enhancement systems are conceived around filter banks. This tendency is justified by the behavior of the cochlea, which operates like a filter bank. In addition, it is recognized that the frequency-bands of the cochlear filters are not uniformly distributed. Several transformations (scales) are proposed to take into account the perceptive aspect of hearing (Mel, Bark, etc...). The wavelet transform is used as a bank of filters (not uniformly distributed) to improve performance of the speech enhancement method based on the spectral subtraction [14].

A modified version of the speech enhancement method based on the coherence function is proposed [15]. The wavelet transform is also used as a filter bank.
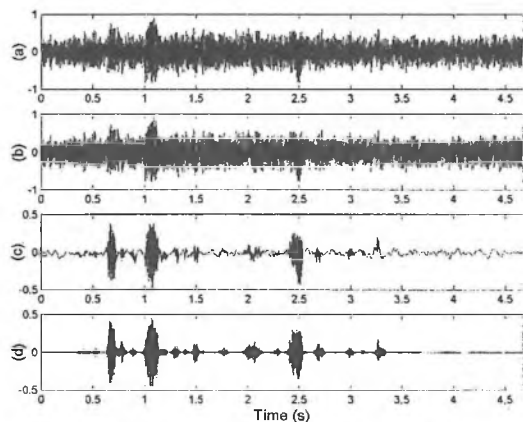
Fig. 1. Speech enhancement results: a) noisy speech recorded in a aircraft plane, b) enhancement using WT with an universal threshold, c) enhancement using WT with level-dependent threshold, and d) enhancement using WPT with level-dependent threshold.
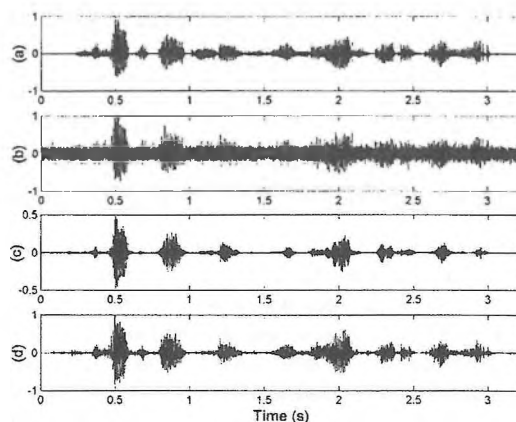

Fig. 2. Speech enhancement results: a) clean signal, b) noisy version (SNR=0dB), c) enhancement using WPT with level-dependent threshold, d) enhancement using WPT with level-dependent and *time-adapted* threshold.

4. Proposed approach

The wavelet thresholding technique is a simple method to remove noise from corrupted signal. As pointed out previously, it was not successfully applied in speech enhancement. These difficulties are simultaneously associated to the speech signal complexity and to the nature of the noise.

To improve the wavelet thresholding enhancement, we then propose:

* The use of the WPT instead of the WT,
* To extend the concept of the level-dependent threshold (Equation4) to the WPT,
* The use of *time-adapted* threshold based on the speech waveform energy.

5. Results

The proposed approach is tested using speech sound corrupted by white noise and speech recorded in real environments (in a sawmill, in a car, and aircraft cockpit).

The speech signal of Fig. 1-a is corrupted by a narrow-band noise. The standard threshold (the same value for all scales) of the WT (Fig. 1-b) is inefficient to remove noise (the same result is obtained by the standard threshold of the WPT). However, the filtered results using the level-dependent thresholding of the WPT are better when obtained by using the WT (respectively represented on Fig. 1-d and 1-c).

The *time-adapting* effect is carried out using speech from the TIMIT database (Fig. 2-a) that is corrupted by white noise (Fig. 2-b). It can be seen that the enhanced speech using the *time-adapted* threshold becomes very close to the original clean speech (Fig. 2-d).

5. Conclusion

The proposed method constitutes a successful application of the wavelet thresholding for speech enhancement. The level-dependent threshold using WPT permits to remove various environmental noises (narrow or large frequency-band). Whereas, the *time-adapting* of the threshold avoids the speech degradation quality during the thresholding process.

References

[1] S. Mallat and W.L. Hwang: Singularity Detection and Processing with Wavelets, IEEE Trans Inform Theory, 38 617-643, 1992.

[2] D.L. Donoho. Nonlinear wavelet methods for recovering signals, images, and densities from indirect and noisy data. Proceedings of Synposia in Applied Mathematics. 47 :173-205, 1993.

[3] Y. Xu, J.B. Weaver, D.M Healy, and J. Lu. Wavelet transform domain filters: A spatially selective noise filtration technique. IEEE Trans. Image Processing, 3(6) :747-758, Nov. 1994.

[4] Q. Pan, L. Zhang, G. Dai, and H. Zhang, Two denoising methods by wavelet transform, IEEE Trans. Signal Processing, vol. 47, no. 12, pp. 3401-3406, December 1999.

[5] D.L. Donoho and I.M. Johnstone. Ideal spatial adaptation by wavelet shrinkage. Biometrika, 81(3) :425-455, 1994.

[6] D.L. Donoho. De-noising by soft-thresholding. IEEE Trans. Inform. Theory, 41(3) :613-627, May 1995.

[7] I.M. Johnstone and B.W. Silverman. Wavelet threshold estimators for data with correlated noise. J. Roy. Statist. Soc. B, 59 :319-351, 1997.

[8] D.L. Donoho and I.M. Johnstone. Adapting to unknow smoothness via wavelet shrinkage. J. Amer. Stat. Assoc., 1200-1224, 1995.

[9] X.P. Zhang and M.T. Desai. Adaptative denoising based on SURE risk. IEEE Signal Processing Letters, 5(10) :265-267, October 1998.

[10] B. Vidakovic and C.B. Lozoya. On time-dependant wavelet denoising. IEEE Trans. Signal Processing, 46(9) :2549-2554, September 1998.

[11] J.W. Seok and K.S. Bae. Speech enhancement with reduction of noise components in the wavelet domain. In ICASSP 1997, pages 1223-1326, Munich, Germany, April 1997.

[12] D. Mahmoudi. A microphone array for speech enhancement using multiresolution wavelet transform. In Proc. Of Eurospeech'97, pages 339-342, Rhodes, Greece, Sept. 1997.

[13] D. Mahmoudi and A. Drygajlo. Combined wiener and coherence filtering in wavelet domain for microphone array speech enhancement. In ICASSP98, pages 385-388, 1998.

[14] T. Gulzow, A. Engelsberg, and U. Heute. Comparison of a discrete wavelet transformation and nonuniform polyphase filterbank applied to spectral-subtraction speech enhancement. Signal Processing, 64 :5-19, 1998.

[15] J. Sika and V. Davidek. Multi-channel noise reduction using wavelet filter bank. In EuroSpeech'97, pages 2591-2594, Rhodes, Greece, Sept. 1997.

AN OVERVIEW OF COMET® SOFTWARE

S. T. Raveendra
Automated Analysis Corporation, Ann Arbor, MI 48104, USA

1.0 INTRODUCTION

Increased customer demands for quieter products as well as government restrictions and environmental concerns have created a need for cost effective noise prediction methods. While analytical methods are mostly applicable for simple problems and experimental methods require the need to build costly and time consuming prototypes, numerical (or computational) methods not only permits the simulation of complex problems but they also allow the evaluation of the acoustical performance at the early stage of design process. Further, numerical methods allow the evaluation of many and major design iterations rapidly as well as permit the evaluation of optimal solution satisfying many design criteria. As a result a product's time to market is minimized and the cost is reduced.

In a broader sense, numerical methods can be grouped into two categories: differential or domain methods and integral or surface methods. Among the differential methods, finite element method is the most popular and versatile method and among the integral methods, boundary element is the widely used technique. The method that is most suitable for a given situation is based on the problem type. For example, modal analysis and modeling of inhomogeneous and thin structures are easily handled by the finite element method. On the other hand, boundary element method is well suited for the analysis of radiation problems as well as the modeling of half-plane and acoustic sources.

COMET is a computational simulation tool based on finite element and boundary element methods that models sound propagation in fluid, structural and elastic porous domains. COMET software consists of a graphical user interface called COMET/Vision® and a family of solvers grouped under COMET/Acoustics®. The modules of COMET are schematically depicted in figure 1.
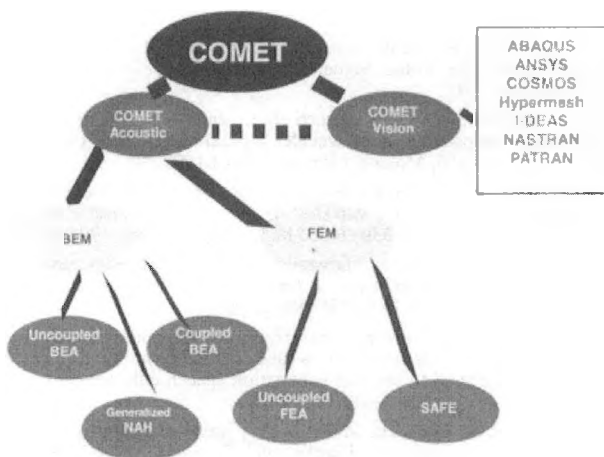
Fig 1. Schematic representation of COMET modules

A typical analysis in COMET involves the creation of a mesh that represents the geometry of the problem and the imposition of loading (boundary condition). Both of these informations are generated by using third party software. This information is imported into COMET using the COMET/Vision.

2.0 COMET Modules

2.1 Graphical User Interface – COMET/Vision

COMET/Vision is an easy to use pre- and post-processor that is designed to work the way engineers intuitively think about acoustic problems. It is tightly integrated with CAD/CAM packages such as I-DEAS®, Hypermesh® and PATRAN® as well as with structural vibration CAE software programs such as ABAQUS™, ANSYS®, COSMOS® and NASTRAN®.

2.2 Uncoupled BEA

This module is used to solve uncoupled acoustic problems. In a vibration induced noise analysis, this implies that the analysis considers the effect of vibration on the sound field and assumes that the effect of the sound field on the vibration is negligible. The solution is based on the boundary element method. Boundary element method requires the modeling of the surface of the acoustic domain and as a result the modeling (mesh generation) effort is minimal. Additionally the method satisfies the radiation condition of exterior problems, hence does not require any additional tedious modeling techniques. Analyses available in the module are frequency response, transient response and normal mode response. In addition to predicting sound field the module is effective for the treatment of a wide class of problems:

- Sensitivity analysis: Provides the effect on the sound field due to change in surface velocity. Together with structural sensitivity it provides information as to how structural changes affect the acoustical performance.
- Panel Acoustic Contribution Analysis (PACA): Provides a systematic process for the identification of areas of noise contribution and associated design modification.
- Multi-fluid Analysis: Allows the accurate modeling of piecewise homogeneous acoustic domains. This includes the modeling of bulk complex material properties.
- Mean-Flow analysis: Incorporates the effect of mean flow on wave propagation.
- Enhanced Rayleigh Integral analysis: Allows the evaluation of radiated sound field rapidly during design iteration.

These solutions are further enhanced by the use of nonlinear matrix interpolation technique for multi-frequency acoustic analysis and procedures that eliminate the irregular, non-unique behavior of exterior solutions.

2.3 Coupled BEA

In situations where the effect of the acoustics on structural vibration is not negligible one needs to use this module in which the struc-

tural response based on finite element method is coupled with the boundary element method based acoustic response. This module is also used to perform reverberant field analysis. Further, the analyses described in the previous sub-section are all available in this module.

2.4 Uncoupled FEA

Finite element method requires the modeling of the acoustic domain and thus the modeling effort is substantial compared to the boundary element method modeling requirement. On the other hand the method is well suited for the analysis of thin and inhomogeneous domains. This module can be used to perform both frequency response and normal mode analyses.

2.5 SAFE – Structural Acoustic Foam Engineering

SAFE module can be used to analyze and optimize sound in elastic-porous (e.g. foam), solid and fluid domains. Unlike approximate solution tools that have been used for the modeling of foam type materials, SAFE is based on rigorous physical and mathematical principles. SAFE is a powerful tool for the analysis of noise controls treatments such as glass fiber, mineral wool and thinsulate. Typical applications include, vehicle sound insulation, mufflers and ducts, headliners, seats, carpets, trim lining and enclosure liners. The development of SAFE module was partially funded by NASA.

2.6 Generalized NAH (Nearfield Acoustical Holography)

Noise prediction analysis requires knowledge of the noise sources. However, evaluation of noise sources is difficult when there are multiple sources and the interaction among them is complex. Holography is an inverse solution technology in which one can identify and rank sources using near field sound measurement. Conventional holography is applicable for simple geometry such as planar, cylindrical or spherical surfaces. COMET/NAH allows source identification in complex structures based on measurements taken using flexible non-planar layout. This module can be used to identify noise sources that are coherent, incoherent or partially coherent. The development of COMET/NAH is partially supported by an ongoing research program funded by NASA.

3.0 APPLICATION AREAS

COMET has been used to solve a wide class of acoustic problems in many industries [1-11]. Application areas of COMET include:

Automotive: Prediction of vehicle passby noise, component (e.g. manifold, air cleaner, engine, engine cover) sound radiation analysis, analysis of sound transfer through porous seat design, engine sound quality analysis, interior noise analysis, analysis of silencer performance, optimization of material properties, noise source identification in power plant.

Aerospace: Reverberant (diffuse) field analysis, determination of structural response of payloads during launch, prediction and optimization of interior aircraft noise, noise source identification in the interior of aircraft.

Consumer Products: Characterization of acoustical absorption properties of multi-layer material, prediction of noise transmitted through foam barriers, noise performance analysis of computer disk drive.

Construction Equipment: Analysis of the effect of sound absorbing material on engine noise, prediction of noise contribution from systems components, optimization of engine cover to minimize noise emission, interior cab acoustics, mount optimization.

REFERENCES

G. F. Dargush, S. T. Raveendra and P. K. Banerjee. Boundary Element Formulation for Structural Acoustics Including Mean Flow Effects. AMD-Vol. 178, ASME, 1993.

A. Selamet, P. M. Radavich and N. S. Dickey. Multi-Dimensional Effects on Silencer Performance, National Congress on Noise Control Engineering, 1994.

N. Vlahopoulos, S. T. Raveendra and C. Mollo. Development of BEM for Structural Acoustic Sensitivity Analysis Using Boundary Elements and Dynamic Response, MSC World User's Conference Proceedings, 1994.

K. Zhang, J. Yang and M. Lee, A New Approach for Noise Reduction of Thin-Shell Structures, Inter-Noise 95, Newport Beach, CA, 1995.

S. R. Sorenson. Investigation of Different Techniques for Quantifying Automotive Panel Noise Radiation, SAE 951267, 1995.

N. Basavanhalli, R. Sommers, L. Brookes, F. Zweng and W. Kargus. Reduction of Passenger Car Road Noise Using Computational Analysis. SAE 951092, 1995.

K. Cunefare, S. P. Crane, S. P. Englestad and E. A. Powell. A Tool for Design Minimization of Aircraft Interior Noise, AIAA 96-1702, 1996.

N. Vlahopoulos, S. T. Raveendra, B. Gardner, S. Messer. Numerical Computation of Noise Transmitted Inside a Payload Fairing due to External Reverberant Field Excitation, Noise-Con96, 1996.

S. Y. Jee, C. Birkett and B. Tsoi. Passenger Care Interior Noise Reduction, Noise-Con96, 1996.

E.-J. Ni, D. S. Snyder, G. F. Walton, N. E. Mallard, G. E. Barron, J. T. Browell, B. N, Aljundi. Radiated Noise from Tire/Wheel Vibration. ASA Tire Conference, 1996.

S. T. Raveendra, B. Gardner and R. Stark. An Indirect Boundary Technique for Exterior Periodic Acoustic Analysis, *SAE Transactions – Journal of Passenger Cars*, 1998.

Noise Optimization of Air-Intake Manifolds. Automotive Engineering International, 1998.

S. T. Raveendra. A Technique for Extracting Natural Frequencies, Noise-Con98, 1998.

B. K. Gardner and M. K. Tandon, Y. J. Kang, J. S. Bolton. Design of foam materials to maximize acoustical absorption by using FEA, Noise-Con98, 1998.

S. T. Raveendra, B. K. Gardner, P. Kondapalli and R. Stark. Transient Noise Analysis Using an Indirect Boundary Element Formulation, Proceedings of Noise-Con98, 1998.

S. T. Raveendra, Keeping Truck Cabs Quiet, Machine Design, S18-S21, 1999.

S. T. Raveendra, S. Sureshkumar, E. Williams, Noise Source Identification in An Aircraft Using Nearfield Acoustical Holography, AIAA-2000-2097, 2000.

I-DEAS VIBRO-ACOUSTICS AND RAYON SOLVERS: FEATURES AND CAPABILITIES

S. ASSAF and M.A HAMDI

Straco, SA, 60200 Compiegne Cedex, France

Introduction

I-DEAS Vibro-Acoustics is a Computer Aided Analysis (CAA) software product resulting from the integration of STRACO's RAYON Solvers family in the general graphical environment of I-DEAS Master Series of SDRC and IDEAS-TEST of MTS. This CAA engineering tool is developed by STRACO company (France), and is dedicated to numerical modeling and analysis of vibro-acoustics problems. It is composed by an intuitive and easy-to-use graphical user interface, which integrates RAYON solvers family dedicated to the analysis of complex three-dimensional vibrating structures coupled to one or several acoustic fluids and subjected to deterministic or random mechanical and/or acoustic excitations.

Numerical Methods

RAYON solver is based on an unified variational formulation coupling Boundary, Finite and Infinite Element Methods. Those methods can be mixed to solve internal, external or internal-external acoustic problems.

RAYON Boundary Element (BEM) solver address uncoupled acoustic problems as well as coupling structural-acoustic problems. It simplifies model generation because only the boundary of the acoustic domain has to be discretized. This method yields stable and accurate solutions for internal/external problems. Both direct and indirect methods are implemented and managed automatically depending on the number of acoustic domains (single or multi-acoustic domains).

RAYON Finite Element (FEM) solver is well adapted to solve internal acoustic problems. It is used to compute acoustic modes, elasto-acoustic modes, and frequency responses for coupled and uncoupled internal acoustic cavities.

RAYON Infinite Element (IEM) solver is an alternative to BEM for external problems. It is based on unique technology from AT&T Bell Labs and dedicated to model scattered and/or radiated acoustic field in external domain surrounding a radiating structure.

All these solvers share the same graphical user environment and can be mixed to perform efficiently a vibro-acoustic analysis. Typically, BEM/FEM solvers combination is used to solve internal acoustic cavity coupled to an external domain through an elastic structure. IDEAS-Vibro-Acoustics can be used as an integrated task within I-DEAS general environment exploiting transparently other I-DEAS modules (geometry, mesh, test, structure analysis ...) or as a stand alone package interfaced with other pre/post or Structural Analysis software(ABAQUS, ANSYS or NASTRAN).

Analysis Types

Several types of analysis can be performed by I-DEAS Vibro-Acoustics:

- Pure acoustic computation for diffraction and radiation acoustic problems without considering fluid structure coupling effects. This kind of problems usually refer to bodies excited by pure acoustic sources and external problems involving a vibrating structure.

- Modal analysis for internal acoustic problems, which consists in computing pure acoustic or elasto-acoustic modes.

- Coupled analysis for problems involving the interaction between one or several acoustic domains. They can be internal, external or mixed internal-external problems. The structure and fluid meshes may not to be compatibles.

Different Boundary Conditions can be applied in I-DEAS Vibro-Acoustics such as:

Prescribed acoustic pressure.

Prescribed acoustic acceleration, velocity or displacement.

Elastic surfaces (surfaces which in contact with an elastic structure)

Acoustic impedance (sound absorbing material modeling).

Fluid/Fluid interface.

Excitation Types

Multiple deterministic or random excitations can be applied simultaneously in the same problem and managed in a single solver run. The type of acoustic sources available in Vibro-Acoustics are:

Monopole.

Plane Wave.

Diffuse Sound field.

The mechanical loads are defined as part of the structure model.

Computation Results

A broad of physical quantities are computed and post-processed by I-DEAS Vibro-Acoustics:

Vibro-acoustic surface results, which include structural acceleration, mean squared velocity, acoustic pressure, acceleration and intensity.

Vibro-acoustic field results including panel participation factors, modal contributions, transmission loss factor, noise reduction, acoustic pressure, acceleration, and intensity.

Secondary results include acoustic energies radiated in the external domain or absorbed by acoustic materials, kinetic and deformation energy of the structure, injected power by mechanical excitation, radiation efficiency, ...etc.

New Features

2 modules are implemented in the new version of I-DEAS Vibro-Acoustics:

Poro-elastic material module (RAYON-PEM), which is based on a new mixed displacement-pressure formulation fully compatible with the implemented formulation. It allows the automatic integration of porous absorbing components in the passenger and engine compartments of vehicles.

Inverse Boundary Element Method (RAYON-IBEM) module, allowing the identification and the characterization of complex noise sources (engine, exhaust line, tires). This advanced module uses near field acoustic measurements, combined with an innovative Inverse Boundary Element technique based on a generalized wave envelope reciprocity principle for computing acoustic transfer functions.

Application fields

Vibro-Acoustics has been validated in many real life applications such as:

Aerospace applications covering a wide range of vehicles from aircraft to rocket launchers and satellites. They also cover various flight phases, from lift-off to atmospheric cruise flight. In particular STRACO used I-DEAS Vibro-acoustics to perform numerical studies of the European launchers (Ariane family) in cooperation with Aerospatiale (France), European Space Agency (ESA, Holland), "Centre National d'Etude Spatiale (CNES, France), Dornier (Germany) and Contraves (Switzerland). These studies focus on the prediction at the design stage of the Fairing Acoustic Protection (FAP) of payloads from reflected jet noise during take off, (see figure 1 and reference [1]).

Automotive applications covering the vibro-acoustic analysis of separate vehicle components (engine, air conditioning system, exhaust line, tires,…etc) or of the global vehicle by predicting interior noise and exterior performances (see figures2 and 3 and references [2,3]).

I-DEAS Vibro-acoustics can also be used to improve the acoustic characteristics of a wide range of other industrial products, from building applications (windows noise transmission, ...) to factory equipments and electronic devices.

References:

[1] H. DEFOSSE, M.A. HAMDI. "Vibro-acoustic study of ARIANE V launcher during lift-off", Inter-noise 2000; Nice.

[2] M.A Hamdi, H. Defosse, F Damagnes , T. Beauvilain and P. Varet. "Use of Reciprocity Principle in a Hybrid Modelling Technique (HMT) based on Inverse Boundary Element Method (IBEM) for the determination of the optimal spectral characteristics of a complex radiating noise source", Inter-noise 2000; Nice.

[3] J.M. Auger, M.A. Hamdi, G. Amadasi 1E. Girimondi, "Pass By Noise Modelling with Boundary Elements",SAE Noise &Vibration Conf., Traverse City, May 20-22, 1997

Fig. 1:Firing test
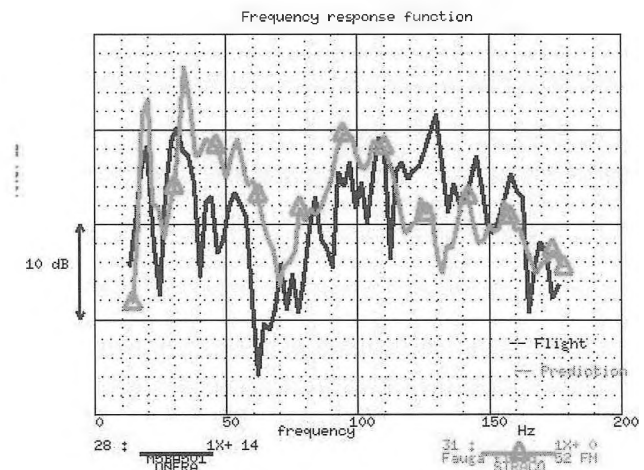
Fig. 2 : Flight/Analysis comparison of V501

Microphone Array

External Acoustic Domain Ω_a

n

S
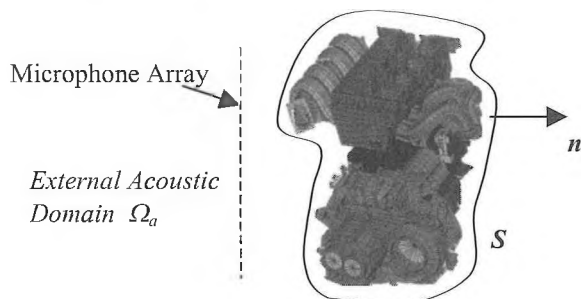
Fig. 2-a: Noise Source enveloped

Figure 2-b: Experimental set up of a car engine
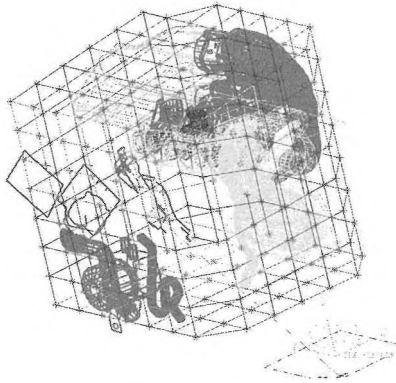
Figure 3-a. Engine IBEM Model
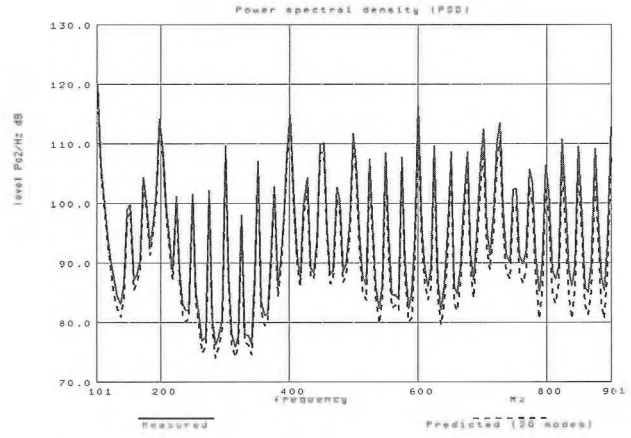
Figure 3-b. Averaged Sound Pressure Level
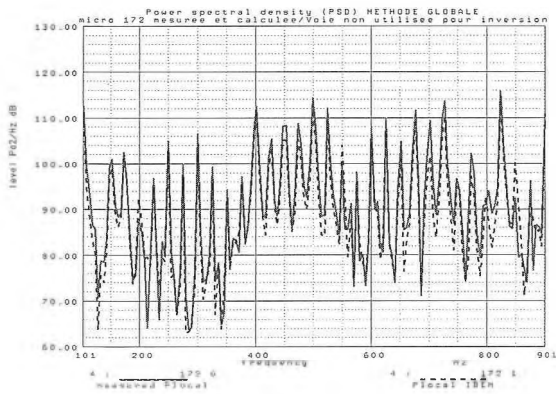
Figure 3-c. Local Sound Pressure Level
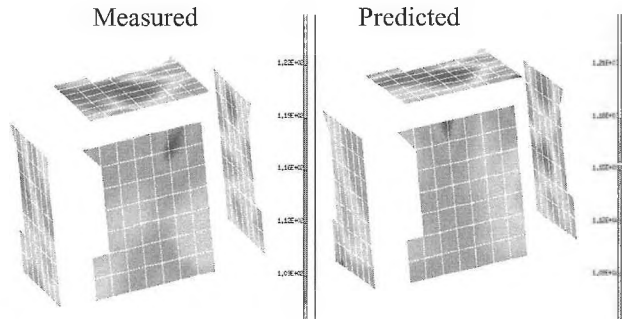
Figure 3-d. Radiated Acoustic Pressure at 600Hz

AN OVERVIEW OF AUTOSEA2

Paul Bremner, Hugues Nelisse, Phil Shorter
Vibro-Acoustic Sciences, 12555 High Bluff Drive, Suite 310 , San Diego, CA 92130, USA.

1. Overview

This paper provides an overview of the AutoSEA2 statistical energy analysis (SEA) code and discusses various analysis capabilities and applications.

2. Statistical Energy Analysis

The statistical energy analysis (SEA) method [1] was introduced in 1960's as a means with which to predict the vibro-acoustic response of rocket payloads subjected to broadband excitation during launch. Since then its use has become widespread and it is currently used in a multitude of different applications ranging from shipboard noise [2] to automobile acoustics [3]. SEA is well suited to predicting the response of complex structural-acoustic systems over a large frequency range (typically 50 – 20,000 hz), and it can be used to model both random and tonal sources.

As a computer-based simulation method, SEA at first appears to offer the same time-saving and cost-saving relief from prototype build & test methods as other computer-aided engineering (CAE) tools such as finite element (FE) analysis. However, FE methods often have serious limitations when applied to the design process [4]. Typically, FE models need a great deal of detail which is not available in the early design process; the models take a long time to build and the output information is often so complex that only the analyst - not the designer - can understand it. The product designer today needs faster design feedback earlier in the design process and in terms of the physical design parameters over which he or she has some control [5].

An additional problem, that becomes apparent at higher frequencies, is the misconception that a detailed deterministic analysis of a statistically uncertain dynamical system can yield meaningful response information. Ongoing research work on probabilistic approaches to FE are an acknowledgement of this important issue [6]. By contrast, SEA is based on a probabilistic formulation which requires much simpler - but still physically meaningful – models. The underlying theory of SEA is based on the principles of statistical mechanics and conservation of energy and there are many parallels between an SEA analysis and a thermal analysis.

SEA is essentially a sub-structuring analysis method, where noise and vibration levels are estimated from the space, frequency and ensemble average energy contained within various mode groups in each sub-structure region. The transmission problem is represented as a "diffusion" or flow of energy from regions of higher modal energy to regions of lower modal energy. The underlying behavior of the physical system can then be characterized without the need for a detailed description of the response of individual modes (which is advantageous for complex structural-acoustic systems which can contain millions of modes). The equivalent thermal analogy is that, when looking at the thermodynamic response of a system, one is not usually interested in the response of individual particles at a molecular level but rather the space and

time averaged energy of a group of particles (their temperature). Relaxing the noise and vibration response estimate to the spatial average response within a given frequency band – as for room acoustics – allows a simple but powerful statistical reduction in the description of each local region's modal parameters and for the dynamics of each junction's energy transmission characteristics [1].

As such, SEA can be classified as a "node-connector" type of modeling, similar to network analysis in thermal, electrical and fluid flow problems. In this case, the SEA "nodes" represent the reverberant energy level of resonant mode groups in each sub-structure region and the "connectors" represent the energy flow paths between nodes. Most older generation SEA codes use this network paradigm extensively as the basis for modeling.

The network approach is attractive for simple problems in one or two dimensions with only a few sub-structure regions. However, for larger problems and general 3 dimensional structures, the network approach soon becomes unworkable - except by a few very devoted SEA analysts. This is partially illustrated by the pictorial comparison in Figure 1, which shows one of the simplest 3-dimensional SEA problems – predicting the noise level in a room bounded by a floor, a roof and four wall panels.
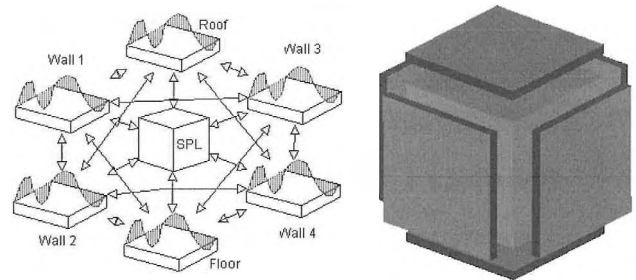

Figure 1. Comparison of model representations for a simple SEA room acoustics application; Network model (left) and more intuitive 3D model (right)

The development of AutoSEA2 now enables analysts and designers to create SEA models using a 3D modeling interface rather than the older network paradigm.

3. AutoSEA2

As shown in Figure 2, each member of the AutoSEA2 family of subsystems essentially provides a mapping between the actual (typically non-uniform) shape of a region of the real system being modeled and the library of "ideal" SEA subsystems, for which the statistical dynamic formulations are known. This mapping essentially consists of computing the characteristic lengths, areas and volume using regression to obtain the best-fit SEA parameters for a given subsystem. Figure 3 shows a typical AutoSEA2 automobile model constructed from the various generic subsystems.
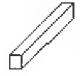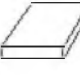
Subsystem	Wavefields	SEA Idealisation	Nodal Geometry	Faceted 3D Solid
BEAM	Bending Ixx Bending Iyy Torsion Extension			
FLAT PLATE	Transverse Bending In-plane Extension In-plane Shear			
SINGLY - CURVED SHELL	Transverse Bending In-plane Extension In-plane Shear			
CYLINDER	Transverse Bending In-plane Extension In-plane Shear			
DOUBLY - CURVED SHELL	Transverse Bending In-plane Extension In-plane Shear			
ACOUSTIC DUCT	1D Acoustic wave			
ACOUSTIC CAVITY	3D Acoustic wave			

Figure 2. Summary of the AutoSEA2 family of 3 dimensional SEA subsystems

The physical sub-structures in AutoSEA2 are called subsystems - consistent with SEA convention – because they encompass both structural and acoustic regions. However, each physical subsystem typically supports multiple mode groups, each with its own unique dynamic properties (eg. wavespeed, modal density and damping loss factor) and its own unique reverberant energy level. In AutoSEA2, these different mode groups are denoted "wavefields". The full SEA solution matrix [7] is formulated to correctly account for the coupling of the wavefield components and resultant energies, even though the user defines only a single physical subsystem.

Considerable new development in AutoSEA2 has been devoted to the modeling of energy transmission junctions. This includes automatic junction creation directly from 3D geometry; general "multi-port" junction configurations; correct statistical treatment of junction properties and modeling of local junction detail. A direct consequence and major advantage of modeling all AutoSEA2 subsystems explicitly with 3D node points is that the energy transmission junctions can be automatically detected and computed uniquely from the connected subsystem properties and the global junction geometry. The creation of logical point-, line- and area-junctions is implemented as an "auto-connect" algorithm. Subsystems with common node numbers are considered connected – common contiguous node numbers define a line junction and common non-contiguous node numbers define a point junction.
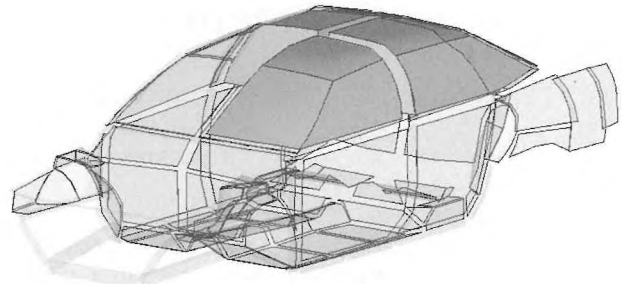

Figure 3. AutoSEA2 model of an automobile containing beam, shell and acoustic cavity subsystems.

4. Summary

AutoSEA2 contains many new-advances which assist in the creation, management and solution of complex SEA models. The 3D subsystem formulation makes the SEA modeling process more intuitive and minimizes cumulative "guestimation" errors. The auto-connect function greatly reduces modeling time and avoids manual data input errors. The implementation of full wave transmission theory improves accuracy and minimizes the need for user expertise in modeling junctions. The fast solution times and thermogram diagnostic plots encourage the engineer to understand the model better; and empower the engineer to find more globally-optimal noise and vibration solutions and to provide more practical feedback to product designers.

While AutoSEA2 still requires the engineer to build a 3D geometry-based model, the "super-element" nature of the SEA sub-systems make this process at least an order of magnitude faster that FE model building. In summary, the latest advances in SEA software development have demonstrated the power of AutoSEA2 as a general purpose computer-aided engineering tool. It delivers a new "design evaluation" solution which may mean that designers can now address noise and vibration performance issues even before the structural and thermal FE analysts have completed their first analysis cycle.

5. References

[1] Lyon, R.H. and DeJong, R.G. "Theory and Application of Statistical Energy Analysis" Butterworth-Heinemann, 1995

[2] Plunt, J. "Methods for Predicting Noise levels in Ships. Part II: Prediction of Structure-borne Sound Transmission in Complex Structures with the SEA Method" PhD Thesis, Dept. Building Acoustics, Chalmers University of Technology, Gothenburg, Sweden, April 1980.

[3] Onsay, T., Akanda, A. and Goetchius, G.M. "Transmission of Structure-borne Tire/Road Noise in a Mid-size Car: Statistical Energy Analysis (SEA)", Proc. Noise-Con 98, Ypsilanti MI, April 1998

[4] Housner, J.M. and Pinson, L.D. "NASA CST Aids U.S. Industry", Focus '93: Computational Structures Technology, Aerospace America, February 1993

[5] Waterman, P. "First-Pass FEA: Automated, But Not Out of Control" Desktop Engineering, Vol. 3, Issue 12, August 1998

[6] Contreras, H. "The Stochastic Finite Element method", Computers & Structures, Vol. 12, No. 3, 1980

[7] Vibro-Acoustic Sciences, "AutoSEA2 Theory and Quality Assurance Manual"

APPLICATION OF SEA IN VEHICLE SOUND PACKAGE DESIGN

H. Nelisse[1], J. Pan[2] and J. Van Buskirk[2]
Vibro-Acoustic Sciences, Inc. Troy, Michigan, USA.
Rieter Automotive, Farmington Hills, Michigan, USA.

INTRODUCTION

Statistical Energy Analysis (SEA) was first applied in the automotive industry to study vehicle interior noise over a decade ago [1-2] and has been developed as a tool for design and development of sound package in automobiles [3-6].

Application of SEA in a vehicle program starts in the early design stage. SEA models are used to negotiate and determine real estates (size and thickness) of sound package components such as dash insulator and carpet to ensure that vehicle acoustical performance targets are met. The SEA models are continuously updated throughout the vehicle program to reflect the latest design and are used to guide the design of sound package components. In this paper, the construction, organization and validation of a trimmed-body vehicle SEA model and component SEA models are described. Example problems are presented to illustrate the application of the SEA models.

OVERVIEW OF THE SEA MODEL

A trimmed body SEA model was built for a mid-size car using AutoSEA2. While the model contains all the major structural and acoustic components, the primary objective of the study was to handle airborne-noise problems. Thus, focus has been made on the validation for airborne noise only. With the node-based approach implemented in AutoSEA2, the structural subsystems have been defined using a finite element model of an existing vehicle.

The SEA model contains all major structural components (panels, rails, pillars and glass) as well as acoustic spaces (interior, exterior, engine compartment and trunk. The model contains almost 300 structural subsystems, 80 exterior acoustic subsystems and 30 interior cavities (including engine compartment, door and trunk cavities). The model contained enough geometric information so that the coupling loss factors (CLF) were obtained automatically using the "Autoconnect" feature of AutoSEA2. Then, the majority of CLF and modal densities were defined analytically [7]. Damping loss factors and absorption coefficients were obtained either from existing Rieter acoustical database or directly from in-situ decay-rate tests. The main components of the sound package included in the model are shown in Figure 1.

Three major components of the sound package, the dash, floor and package tray, were defined using a component-level approach. The component-level approach consisted of creating, in parallel, detailed transmission loss models of the components while keeping the level of details for these components to a minimum in the full-vehicle model. These TL models were used to evaluate the insertion loss of noise control treatments. The insertion loss results were then imported in the full-vehicle model. It is to be noted that details such as leaks, pass-thru, speaker, percentage of coverage, holes, etc. were included only in the component models, the full-vehicle model using subsystems made of bare sheet metal. The advantages of using the component-level approach are: (i) allows defining almost completely the sound package under only one AutoSEA2 database (the "User-Defined Treatment" database). Thus, quick design changes on the sound package can be made with very few

manipulations of the model; (ii) since the sound package is defined using insertion loss and absorption coefficient spectra, it becomes easy to create a library or database of different sound packages; (iii) it gives the flexibility to perform both component and full-vehicle level analysis.

VALIDATION

Two load-cases have been considered for the validation of the model: 35 mph chassis roll and 3000 rpm engine noise.

During chassis-roll operation, sound pressure level (SPL) measurements have been done in different locations: wheelhouse cavities (front and rear), near the glasses (exterior, front and rear), driver's ear, rear passenger ear, leg space (front and rear), dash/toe-pan area (interior), etc. SPL's inside the wheelhouse cavities have been used as sources in the model and SEA predictions have been compared to the test results. For engine noise, SPL measurements were performed, while the engine was running at 3000 rpm, in the engine compartment and in some cavities in the interior cabin. The predicted transfer functions between the engine cavities and the interior cavities SPL were then compared to test data.

As an example, Figure 2 shows of the SEA predictions compared to the test results for the SPL at two locations for the chassis-roll load-case: exterior SPL near the front glass and interior SPL at driver's ear. For each location (cavities) the SEA predictions were compared to measurements at two different microphone locations. Good agreements are obtained for frequencies above 250 Hz. For lower frequencies it was not expected to obtain good correlation since structure-borne excitations were not included in the model. Similar type of results and accuracy has been obtained for other locations in the interior of the vehicle.

SOUND PACKAGE ANALYSIS

The model has been used extensively to perform and evaluate various design changes on the sound package of the vehicle. The objective was to reduce the contribution of the main power flow paths thus optimize and propose a better sound package. The majority of the analysis was done on the full-vehicle model to evaluate the impact and the performance of the sound package at the vehicle level. However, part of the analysis was also performed at the component-level using the component models.

As an example of design change evaluation, figure 3 presents a design alternative where the package tray absorption has been changed from the standard material to the Rieter Ultra Light (RUL) material (higher absorption). In that particular case, a relatively small improvement (up to 0.6 dB) has been predicted at driver's ear. Although it might seem to be a small improvement, it contributes to the overall performance of the vehicle when combined with other design changes.

Another use of the model was the study of percentage of coverage for acoustic treatments. AutoSEA2 include a feature that allows to easily define the percentage of coverage for an acoustic treatment on a subsystem. It automatically updates all coupling and

damping loss factors as well as areas for absorption calculations. That feature has been used for several components to evaluate the effect of partial coverage in some areas of the vehicle. To illustrate the use of the feature in AutoSEA2, a simple transmission loss (TL) model has been built and predictions have been compared to tests. The tested structure was a flat 0,8 mm thick steel plate that was non-perfectly covered by a 2-layer treatment made of a 15 mm thick pad and a 3-psf barrier. SEA predictions compared to test results are presented in figure 4. It is shown that 97% of coverage correlated very well with the test data. While 3% might seem a small percentage of uncovered area, it is shown that it can have a significant impact on the transmission loss (more than 20 dB at high frequencies).

Finally, it is to be noted that the model was built based on existing vehicle geometry (production vehicle) with the intent to use it later for new design of the vehicle. The model has then been modified ("morphed") using a FE model of the new design. Sound package analysis can now be performed using the updated model.

ACKNOWLEDGMENTS

REFERENCES

1. R. G. DeJong, "A Study of Vehicle Interior Noise Using Statistical Energy Analysis," SAE Paper 850960, 1985.
2. S. Shaw, "Analysis and Prediction of the Acoustical Characteristics of Automobile Bodies Using Statistical Energy Analysis," Unikeller Conference 1987.
3. M. Moeller, J. Pan, and R. G. DeJong, "A Novel Approach to Statistical Energy Analysis Model Validation," SAE paper 951328, 1995.
4. B. Dong, M.G. Green, M. Voutyras, P. Bremner, and P Kasper., "Road Noise Modeling Using Statistical Energy Analysis Method," SAE Paper 951327, 1995.
5. A.V. Parrett, J.K. Hicks, T.E. Burton, and L. Hermans, "Statistical Energy Analysis of Airborne and Structure-Borne Automobile Interior Noise," SAE Paper 971970, 1997.
6. T. Onsay, *et al*, "Transmission of structure-borne tire/road noise in a mid-size car: Statistical Energy Analysis (SEA)", *Proceedings of* Noise-Con 98, Ypsilanti, April 1998.
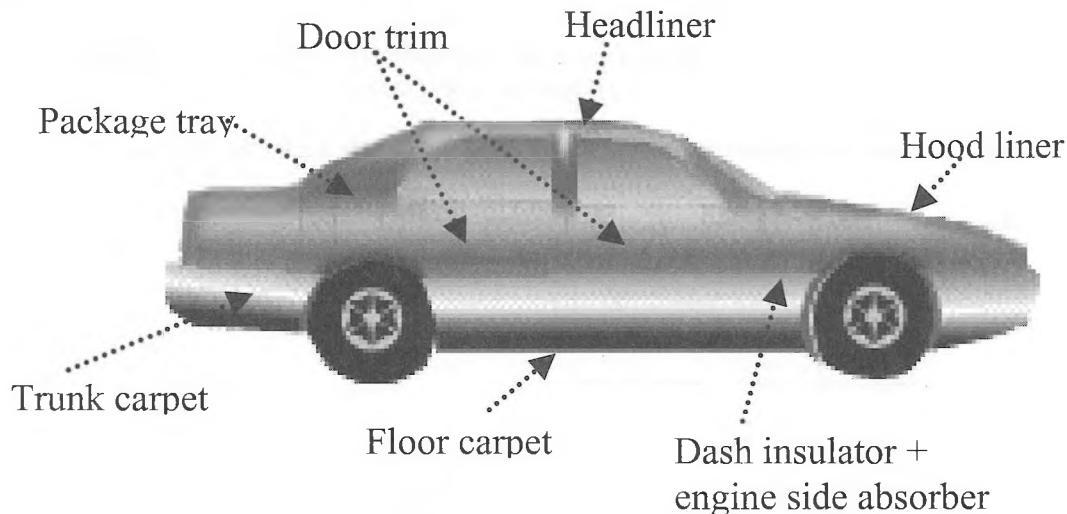7. *AutoSEA2 Theory manual*, Vibro-Acoustic Sciences, San-Diego, 2000.

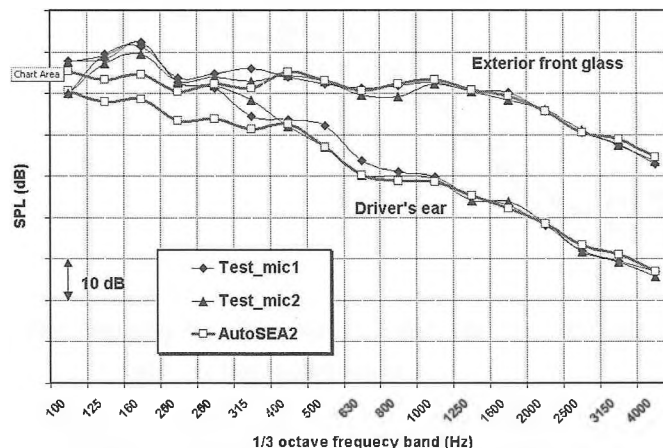**Figure 1: Major components of the sound package**

1/3 octave frequecy band (Hz)

Figure 2: Chassis roll 35 mph: AutoSEA2 predictions vs test results.
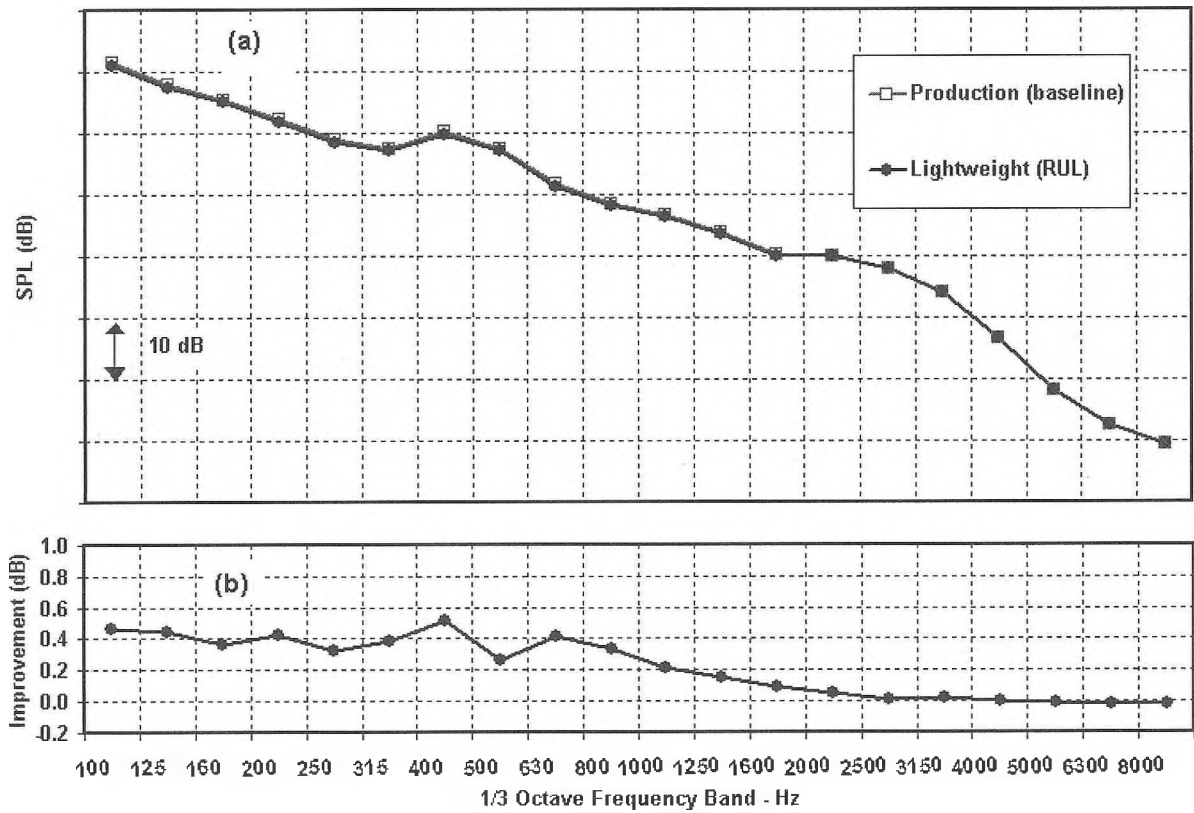
Figure 3: Design alternative evaluation for tire/road noise reduction: change in the package tray absorption.
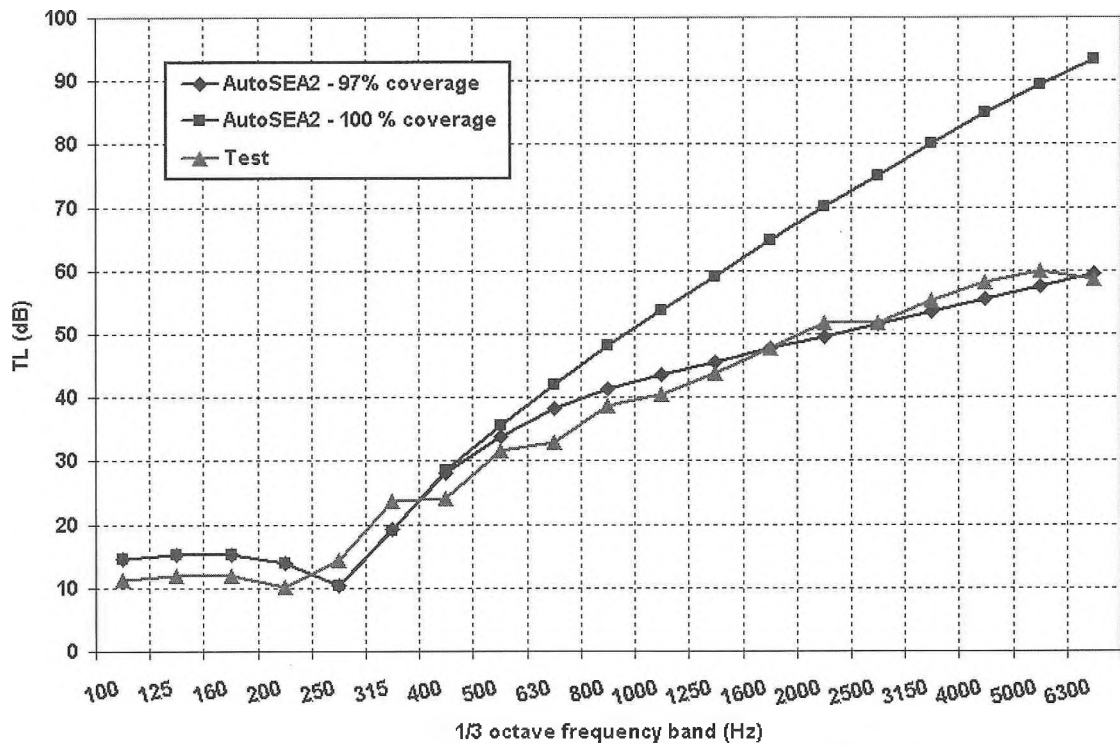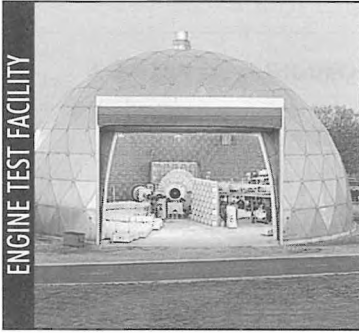

Figure 4: Transmission Loss of a simple panel covered by a 2-layer treatment: SEA predictions with 100% and 97% coverage compared to test data with imperfect coverage.
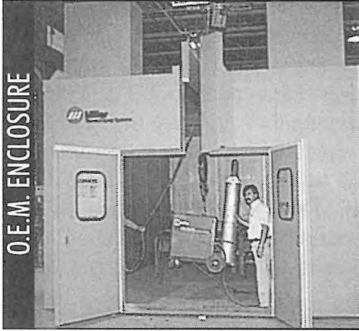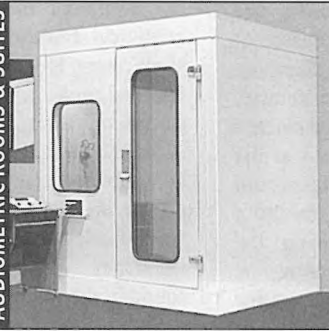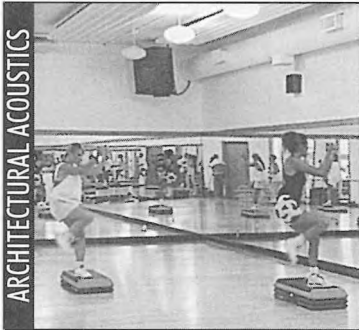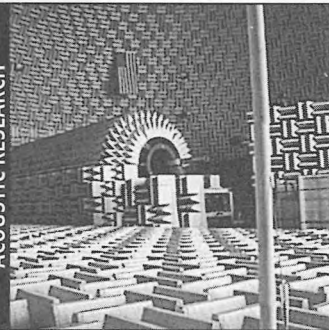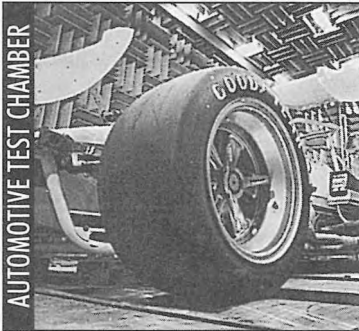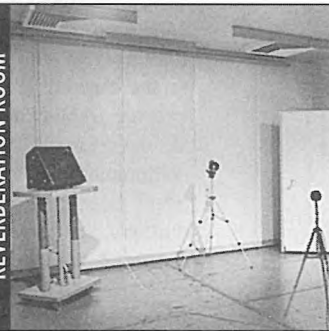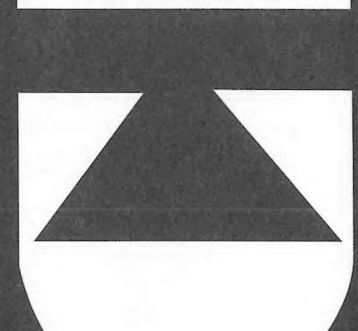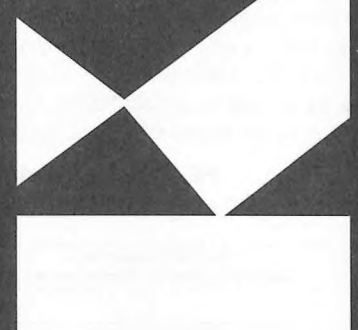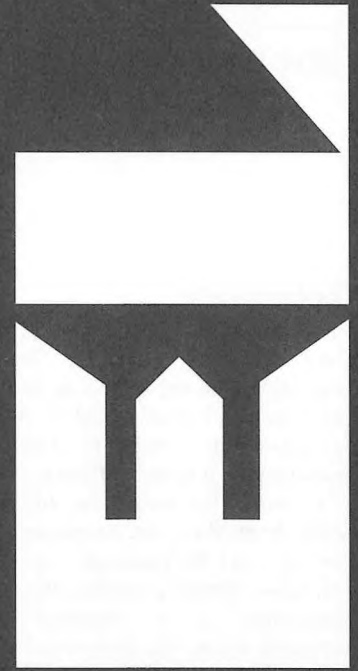
BIW Damping Package Evaluation/Optimization Using FEA/SEA Combined Approach

Denis Blanchet[1], Anab Akanda[2], Taner Onsay[1] andGregory M. Goetchius[2]

[1] Vibro-Acoustic Sciences and [2] DaimlerChrysler

INTRODUCTION

Following styling and surface definitions, FEA models for structural subsystems, such as floor and wheelhouse, are constructed early in the vehicle design/development process. At this early stage, there is a need to define appropriate damping treatment and their coverage for different panels in the vehicle. Computationally, it is more efficient to calculate average surface velocities from FEA models for different configurations at the subsystem level. However, comparison of these velocities would not directly yield the passenger's perception of SPLs resulting from different damping configurations. In the following, the implementation of a combined FEA/SEA method is demonstrated during the evaluation of damping treatments for an automobile.

As shown in Figure 1, the process starts by extraction of physical properties of visco-elastic material. In the next step, the classical RKU analysis is employed to calculate the equivalent properties of composite damping treated vehicle panels. Later, a subsystem FEA model with the derived damping and coverage information is used to calculate the surface averaged velocity response. Finally, the panel velocities are used in a SEA model to predict SPL at the driver's ear location.
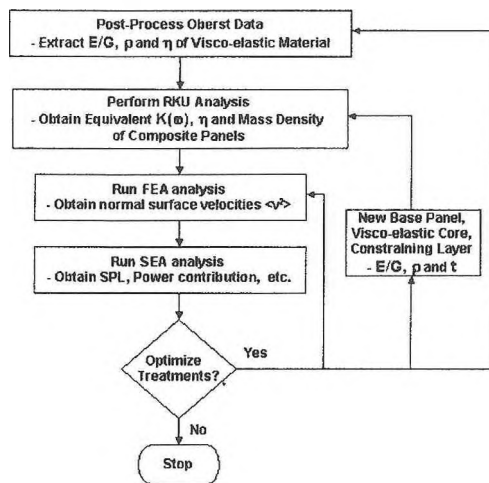
FEA/SEA Modeling & Design Iteration Process

Figure 1 – FEA/SEA Modeling & Design Iteration Process.

MODELING DAMPING MATERIAL

During a typical design evaluation process, different damping treatments are considered, such as SOM (Sprayed On Mastic), BOM (Baked On Mastic), MPM (Metal Polymer Metal) and PCL (Patched-on Constrained Layer). As shown in Figure 2, these treatments are applied to floor panels, toe-board, wheelhouses and dash panels.

Different modeling approaches can be used to create an analytical representation of these damping treatments. In this study, Ross-Kerwin-Ungar (RKU) method was used. This method is based on an equivalent single layer representation of a damping treatment. Because of its accuracy, simplicity and ease of use, this is the most widely used method to represent the equivalent bending stiffness and loss factor of a panel treated with simple single or double layered damping treatments. The RKU method provides a way of calculating equivalent properties of a panel as a function of frequency. A complete description of the RKU method can be found in the reference [1].
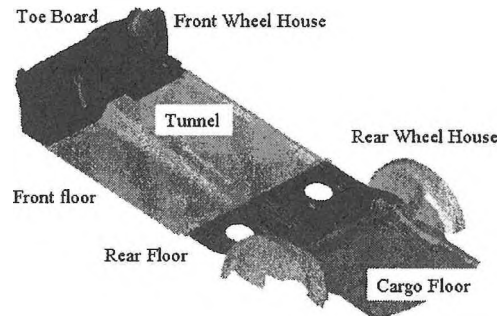
Figure 2 - Areas where damping treatments are applied.

FEA MODEL

Once the equivalent properties of damping treated panels are computed, they are applied to all corresponding elements in the FEA model. The source of excitation can be a force that is applied to the desired location(s) with defined spectrum. In return, the average squared velocities $<v^2>$ over treated/untreated floor areas are determined for each configuration of damping treatment. The component of velocity that is oriented normal to the surface of the panel is considered for the calculation of $<v^2>$. In this study, multiple unit force spectra were applied at the attachment points to excite all structure-borne paths. The lower panels of the vehicle Body-In-White (BIW) were represented in the FEA model, as shown in Figure 2. The objective was to predict the trends (dB) rather than absolute response levels. Surface-averaged velocities for different damping configurations are compared in Figure 3.

These results are then used in the SEA model to predict the driver's ear SPL. During this analysis, all interior sound package components, such as seats, carpet, and headliner, are represented in the coarse SEA model. As a result, this method gives a quick and efficient way of evaluating the effects of damping treatments at the driver's ear location.

Figure 3 – Typical surface-average mean-squared velocity from FEA model.

SEA MODEL

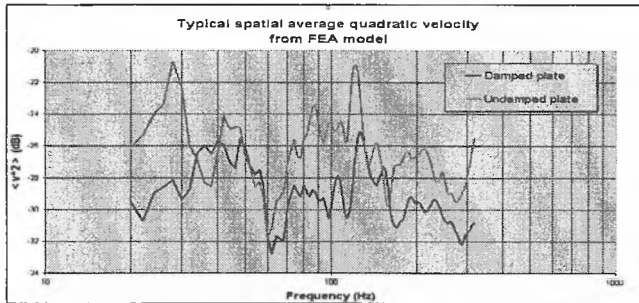In order to convert surface-averaged mean-squared velocity $\langle v^2 \rangle$ obtained from FEA model to SPL at driver's ear, a coarse SEA model is built. Diffuse field acoustic characteristics of all interior components are represented in the SEA model. The model is made up of SEA subsystems, which represents the geometry of the vehicle, SEA junctions, material database and load cases.

In the SEA model, the interior cavities were defined by subdividing the total volume into partitioned-cavities, which matched the floor partitions in the FEA model. There were less than 50 subsystems in this coarse SEA model of the automobile. Due to its coarse nature, the model was built significantly faster and was different from a fully detailed SEA model [2]. As an airborne model, no structural elements were defined, structural behavior being captured by the FEA model and accounted for in the average velocity levels. Seats were also considered since they replaced a large amount of volume that needed to be taken out from the interior space. The engine compartment, exterior and under floor acoustic spaces were not included in the model.

In this study, seven acoustic cavities were defined to describe interior air space. The sum of the volumes, areas and perimeters of these seven cavities represent the acoustic behavior of the complete interior cavity. For this reason geometric properties (perimeter and surface) of each of these cavities have to be overridden in AutoSEA2 to avoid artificial effects on mode count.

The equivalent damping loss factor resulting from the RKU representation of each treated panel is supplied to the AutoSEA2 model as a damping loss factor (DLF) spectrum. The data is brought into AutoSEA2 in a narrowband format and later converted automatically by band-averaging to 3rd-Octave frequency representation. Equivalent bending rigidity is provided as the mean value across the whole spectrum, since AutoSEA2 does not allow frequency dependent bending stiffness.

Equivalent bending stiffness and damping loss factor of the panels treated with damping material are set according to RKU results. In addition, the non-structural mass (NSM) due to the damping material is added to treated panels. This is done by computing a new equivalent density and applying it to each corresponding panel.

In the SEA model, a high damping loss factor is assigned to represent the heavy air in the seat cavities. Other interior acoustic cavities are assigned damping loss factors (DLF) based on typical experimental data (decay rate with trimmed interior)

from similar vehicle constructions. Acoustic treatments relevant to the current problem were also included in the SEA model, such as the transmission loss of the floor carpet.

In the SEA model, the targeted panel velocities are constrained by using average velocity supplied from the FEA model. These constraints are based on the RMS velocities obtained from the FEA model. Since these velocities are normal to the surface of the panels, the constraints are imposed only on the flexural wave fields.

In AutoSEA2, the effect of each damping treatment can be compared to others by using either graphs or thermogram [3]. An example of thermogram for a bare, baseline and full coverage configuration is presented in **Error! Reference source not found.**. Histogram shows that adding damping treatment reduces SPL at ear level in front and cargo area of vehicle while rear section remains almost constant.

In Figure 4, a gain of 2-3 dB at driver's ear location is observed when bare panel is treated with full coverage BOM. These results are expected to still over-predict the damping effect of each configuration because no flanking paths, such as through windows, are considered. Also, since no exterior cavities were considered, the energy is transmitted and accumulated only in the interior of the vehicle. Adding exterior cavities would improve the representation of the physical vehicle configuration in the model.
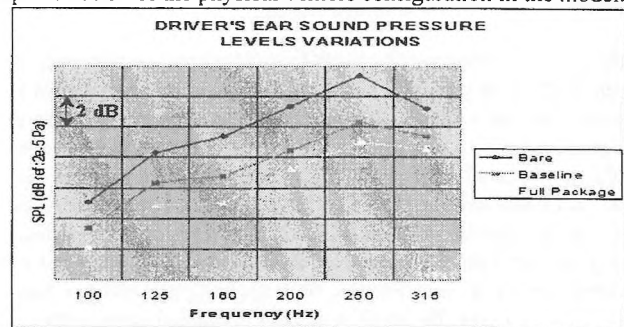
Figure 4 – Effect of each damping treatments on driver's ear SPL

CONCLUSION

The combined FEA/SEA methodology outlined in this study provides a fast and effective way of evaluating different damping treatment configurations at the early stages of design process. Since typically the performance criteria is based on the response of the system in terms of SPL at the driver's ear, this methodology gives a direct comparison between design alternatives. The efficiency of the methodology is due to employment of subsystem FEA and coarse SEA models.

REFERENCES

1. Akanda, A. and Goetchius, G.M., "Representation of Constrained/Unconstrained Layer Damping Treatments in FEA/SEA Vehicle System Models: A Simplified Approach," SAE Paper 99NV-153, 1999.

2. T. Onsay, A. Akanda, and G.M. Goetchius, "Transmission of Structure-borne Tire/road Noise in a Mid-size Car: Statistical Energy Analysis (SEA)," Proceedings of Noise-Con 98, Ypsilanti, 543-548, Apr.1998.

3. M.J. Moeller, M. J., Pan, J. and R.G. DeJong, "A Novel Approach to Statistical energy Analysis Model Validation," SAE Paper 951328, 1995.

Comparison Of Sea And Pffea Predictions Of In-Air And Underwater Radiated Noise From A Ring-Stiffened Cylinder

Layton E. Gilroy

Defence Research Establishment Atlantic, P.O. Box 1012, Dartmouth, Nova Scotia, B2Y 3Z7

INTRODUCTION

Both Statistical Energy Analysis (SEA) and Power Flow Finite Element Analysis (PFFEA) have been under investigation at Defence Research Establishment Atlantic (DREA) as methods of predicting high frequency vibrations and radiated noise. PFFEA [1-7] is an analysis method that is based on a conductivity approach in which the flow of vibrational energy is modelled in a similar fashion to heat conduction with convective losses. SEA [8-9] is a more mature method that is based on an energy balance between substructures. DREA has recently performed investigations [10] to both validate the PFFEA software and to compare it against a commercially available SEA code, SEAM [11]. This paper discusses both in-air and underwater experiments performed with a ring-stiffened cylinder with an internal deck. In these experiments, the input mobility to the test model and its response were measured under broadband excitation along with the resulting radiated noise both in-air and submerged in seawater. These data were then compared with both PFFEA and SEA predictions.

PFFEA uses a conductivity model of structural components in which the flow of vibration energy is examined by applying time-averaged and local space-averaged expressions for energy density and power flow to a unit volume of a structural component. This results in a second-order conductivity equation governing the distribution of vibration energy. The basic equations for PFFEA are obtained by spatial discretisation of the differential equation. Energy in each vibration type (e.g. flexural, torsional, etc.) can be modelled separately with PFFEA, with coupling occurring at junctions of components. The PFFEA system, embodied as the software suite SNAP [7], consists of a translator program, which converts a finite element model to a PFFEA model, and a field equation solver, which performs the PFFEA analysis.

Cambridge Collaborative's SEAM software provides a method of analysis that is particularly well suited for studying the dynamic response of complex structures at high frequencies. SEAM includes a complete implementation of SEA. The complex dynamic system being analysed is divided into a set of substructures and acoustic elements. The modes of each substructure and acoustic element form the SEA subsystems. The flow of energy between the different subsystems is proportional to the modal energies of the subsystems and the coupling factors. SEAM calculates all required coupling factors and performs a power balance for each subsystem. The resulting equations are solved for the modal energy and response of each subsystem.

EXPERIMENTAL PROCEDURE

DREA's ring-stiffened right cylinder is a 9.5mm thick tube, 3m in length, with a nominal diameter of 762mm. It has five internal ring stiffeners welded into the tube at equal intervals of 0.5m each having a square cross-section (38.1mm). The cylinder has 76.2mm thick endcaps with central "hatches" for access. A stiffened deck was welded into the cylinder to simulate a non-symmetric and more complex structure. Figure 1 shows the cylinder on its transport carriage (the painted lines mark the stiffener locations).
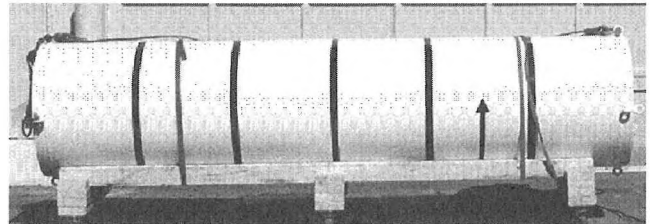A Wilcoxon F4/F7 shaker was used to excite the cylinder over a

Figure 1: DREA Ring-Stiffened Cylinder

frequency range from 0 Hz to 12.8 kHz. The shaker was mounted on the second rib from one end (at the 1/3 point of the cylinder) driving radially (see Figure 2). For the in-air tests, the cylinder rested horizontally on a wooden carriage with contact only at the thick endcaps. For the underwater testing, the cylinder was submerged with the cylinder axis normal to the water surface.
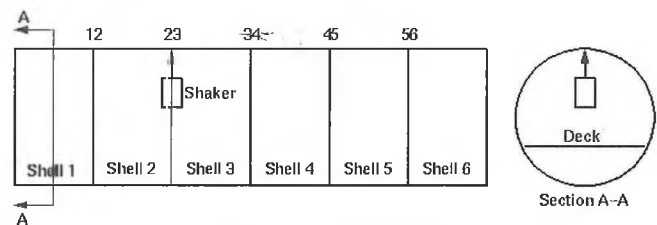
Figure 2: Schematic of Cylinder with Shaker

The cylinder was configured with approximately 50 internal mounting blocks for accelerometers located on both the stiffeners and the shell plating as well as several deck locations. For both the in-air and submerged trials, the accelerometer signals, along with a signal from the impedance head (force and acceleration) on the shaker, were fed to a signal analyser. From these signals, narrow band input mobility and transfer mobility were determined. For the radiated noise testing, the signal from either a microphone or a hydrophone was fed to the analyser to determine the sound pressure levels.

NUMERICAL MODELS

The numerical model used in the PFFEM analysis consisted of 13 structural elements with or without fluid loading, as required. Radiated noise predictions were made with a boundary element based post-processing software. The material properties used are those of mild steel (Young's modulus of 200~GPa, Poisson's ratio of 0.3, density of 7600 kg/m^3, and a loss factor of 0.005).
The SEAM model consisted of 16 structural elements (also with fluid loading as required), 2 acoustic elements and 27 structural and structural-acoustic connections and used similar material properties

to the PFFEA model. As the software does not explicitly support radiated noise predictions that vary with distance from the source, corrections were made to the acoustic space element at each distance to predict an appropriate sound pressure level.

RESULTS

Figure 3 shows the in-air input mobility measurements and predictions. Experimentally there was virtually no difference between the submerged and in-air input mobilities and this was also reflected in both the SEAM prediction, which was reasonably accurate, and the SNAP prediction, which, while roughly correct in level, did not correctly reflect the trend of the experimental data.

A typical response measurement and prediction is shown in Figure 4. This figure shows the underwater response of the shell adjacent to the input location (shell 3). As can be seen SEAM and SNAP accurately predicted the response. This was typical of the underwater shell and stiffener responses in general. The structural response predictions in the in-air case were typically slightly less accurate than the submerged responses.

Figure 5 shows the in-air radiated noise measurement and predictions. As can be seen, the predictions were fairly accurate, with SEAM underpredicting the exterior noise and SNAP underpredicting the interior noise (not shown) by about 10 dB. Finally Figure 6 shows a typical underwater radiated noise comparison in which SNAP gives a more accurate prediction and better represents the general trend of the data.

CONCLUSIONS

Both SEAM and SNAP accurately predicted the input mobility to the ring-stiffened cylinder and gave reasonable predictions for structural response. SEAM typically underpredicted exterior radiat-

ed noise while SNAP underpredicted interior noise. This may be due in part to the lack of free-field radiated noise prediction capabilities in SEAM and the lack of a true reverberent acoustical space element in SNAP.

REFERENCES

[1] Burrell, S.C., Chernuka, M.W., "Extension of Power Flow Finite Element Analysis to Ship Structures - Final Report Part I", Martec Ltd., DREA Contractor Report 91/410 (1990)

[2] Burrell, S.C., Orisamolu, I.R, Chernuka, M.W., "Extension of Power Flow Finite Element Analysis to Ship Structures - Final Report Part II", DREA Contractor Report, CR/93/424, Martec Ltd. (1993)

[3] Burrell, Lieu, Q., S.C., Chernuka, M.W., "Extension of Power Flow Finite Element Analysis to Ship Structures - Final Report Part III", DREA Contractor Report 92/450 (1990)

[4] Smith, M.J., Chernuka, M.W., "Extension of Power Flow Finite Element Analysis to Ship Structures," DREA Contractor Report 96/406 (1996)

[5] Smith, M.J., "Enhancement of Software for PFFEA Modelling and Analysis of Ship Structures," Martec, Ltd., DREA Contractor Report 97/410 (1997)

[6] Smith, M.J., "Advanced Modelling Capabilities for Power Flow Finite Element Analysis (PFFEA)," DREA Contractor Report 97/447 (1997)

[7] Smith, M.J., "Structural Noise Analysis Program (SNAP) Version1 User's Manual", DREA CR 1999-142 (1999)

[8] Lyon, R.H., *Statistical Energy Analysis of Dynamical Systems*, MIT Press, Cambridge, Massachusetts (1975)

[9] Craik, R.J.M., *Sound Transmission Through Buildings Using Statistical Energy Analysis*, Gower, Vermont (1996)

[10] Gilroy, L.E., Smith, M.J., "Comparison of SEA and PFFEA Predictions of Radiated Noise from a Stiffened Box Structure," Proceedings of Internoise '99 (1999)

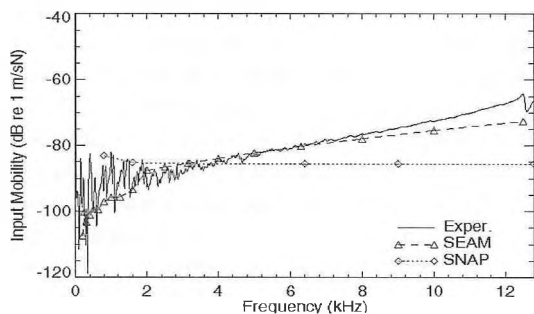[11] SEAM User's Manual, Cambridge Collaborative Inc, Massachusetts (1999)
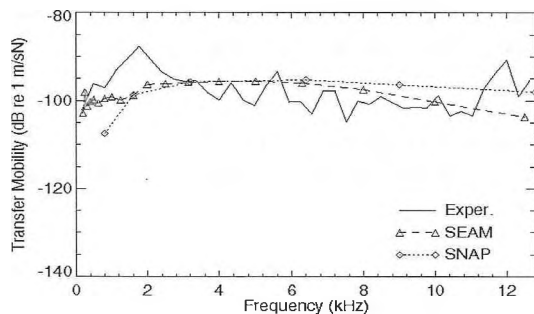
Figure 3: In-Air Input Mobility

Figure 5: Exterior Radiated Noise
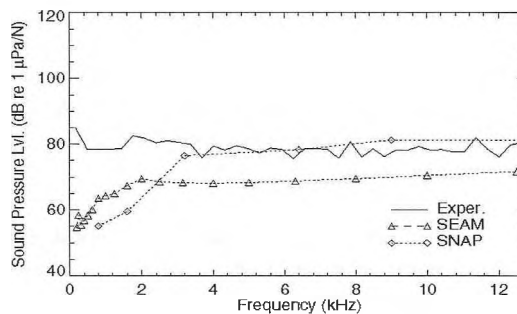

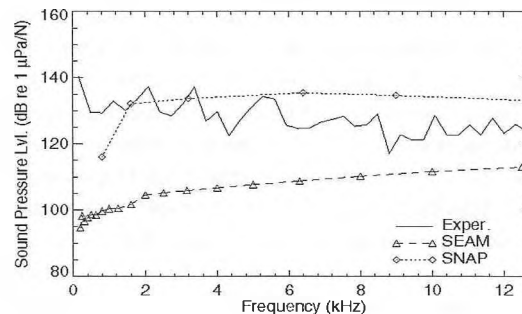**Figure 4: Underwater Response in Shell 3**

Figure 6: Underwater Radiated Noise

List Of Non-Available Summaries / Liste Des Sommaires Non-Disponibles

CAA at Pratt & Whitney Canada: Status and Future Research
Djaffar Ait-Ali-Yahia
Pratt & Whitney Canada

Designing modern turbofan engines with higher bypass ratios is significantly limited by increasingly restrictive airport noise regulations. Independent of takeoff, cruise or landing operations, the fan rotor-stator interactions remain as one of the major engine sources of noise. Therefore, interest in understanding, modeling and eventually reducing this noise has recently increased the need for advanced computational aeroacoustics (CAA) codes to serve as a primary tool in the fan design process. Pratt & Whitney Canada recently initiated a research effort in collaboration with Concordia University to develop axisymmetric linear and 3D nonlinear CAA tools for noise radiation from turbofan inlets. The linear fan-tone code is characterized by its low CPU time and memory requirements and therefore would be highly useful for aeroacoustic design. This code is however limited to axisymmetric nacelle geometries with zero angle of attack flight conditions and does not include nonlinear effects such as rotor leading-edge shocks or high levels of acoustic pressure. A 3D multidomain spectral code based on the nonlinear Euler equations was then developed to be used as an analysis tool for investigating new concepts, such as scarf inlets, for noise reduction. The linear and nonlinear fan-tone codes will be presented as well as several validations on generic and industrial relevant problems.

Dispositf pour l'évaluation et la certification de l'atténuation effective procurée par un des bouchons d'oreilles
J. Voix (ETS, Montréal)

Les normes actuellement en vigueur pour la certification de l'efficacité de protection des protecteurs individuels contre le bruit (P.I.B.) reposent toutes sur l'utilisation de mesures subjectives de détection du seuil d'audition (Real-Ear Attenuation at Threshold).(Normes ANSI S3.14 ou S12.6, CSA Z94.2 et ISO 4869-1). Bien que les résultats obtenus permettent actuellement de certifier les PIB, il importe de se rappeler qu'AUCUNE de ces mesures ne permet de s'assurer effectivement que le PIB protège efficacement un individu donné. Cette lacune a d'ailleurs conduit de nombreux organismes dont le NIOSH (National Institute for Occupationnal Safety and Health) à recommander l'utilisation de mesures in-situ (mesure de la pression tympanique) dans le cas d'exposition à des niveaux critiques de bruit. La méthode développée s'inscrit dans la série des mesures « semi-objectives » MIRE (Microphone In The Real Ear) et permet à par-tir d'une simple mesure -objective- de la réduction de bruit (Noise Reduction) sur un individu donné de prédire la perte par insertion (Insertion Loss) procurée par un protecteur de type « bouchon d'oreille ». Ce résultat permet d'une part de s'assurer de la protection adéquate du porteur et d'autre part de procurer un estimateur valable pour la comparaison avec les techniques de mesures objectives recourant à l'utilisation de têtes artificielles notamment. Un dispositif permettant cette mesure et compatible avec les contraintes d'utilisation industrielle a par ailleurs été développé.

Dry Scrubber Fan Noise Reduction Project at Alcan Laterrière Smelter by Installing Absorptive Baffle Silencers to Attenuate the Environmental Noise Emission from the Scrubber Stack Exit
O. Bouchard, J. Karivelil (Alcan, Jonquière)
G. Leroux (Decibel Consultants Inc.) T. Paige (Vibron Ltd.)

In 1998, Alcan Laterrière Plant had given a mandate do Decibel Consultants inc. to reduce the noise generated trough their four 150 feet high, 13 feet diameter wet scrubber exhaust fans chimneys. The mandate consisted of validation of the previous environmental noise data and the supply of four (4) absorptive silencers, in order to reduce the ambient noise level in the residential area located around the plant property limit. In order to achieve optimum noise reduction performance and to minimize pressure drop throughout the system, a mock-up prototype was built and pressure drop calculation were performed on computer program. A 30 feet long, 13 feet diameter prototype was build at Vibron Ltd, metal shop in Mississauga, Ontario. The first set of baffles were placed inside the mock-up to predict the insertion loss (T.L) using the actual chimney noise frequency recording. Based on the prototype noise reduction results, the silencers were installed on the existing stack, without stopping the wet scrubber fans. A continuous monitoring system was installed at the top of one of the stack to record the noise emission and to verify the performance of the silencer baffles. A successful noise reduction of 23 dBA with less than 0.75" pressure drop was achieved for this Alcan / Decibel Consultants inc. project.

Cogénération, bruit du délestage de vapeur
J.L. Allard, C. Chamberland, M. .Meunier (SNC Lavalin, Montréal)

A power plant was set up on the Montreal domestic waste landfill site (former Miron quarry) in 1996. This plant is powered by biogas given off during waste decomposition.

The biogas is composed chiefly of methane. Due to the location of the plant near residential zones, noise was given special consideration at the engineering phase in order to ensure compliance with the applicable regulations. At commissioning, the plant was found to be compliant in continuous operation mode. However, the steam shedding operations required during start-up and shutdown cycles as well as in emergency situations greatly exceeded the applicable standards, drawing complaints from the citizens. The noise was caused by the rapid release of steam into the atmosphere through a globe valve that discharged to the outside. The installation of a muffler on this valve brought the noise emissions within the applicable standards. However, the performance was less than anticipated based on the manufacturer's data. It should also be concluded that sound sources of a sporadic nature are just as important as those associated with continuous operations. All the operating conditions of a power plant must be considered in the detail engineering of a project in order to ensure its compliance with the applicable acoustic standards.

Effect of Resilient Rail Boots on Vibration Levels Produced by TTC Streetcars
M. Bracken (Aeroacoustics Engineering Ltd., Rexdale), P. Howse (Toronto Transit Commission)

The vibration produced by Toronto Transit Commission Streetcars results in high maintenance of the concrete beds that surround the rails and supporting structure. This vibration results in high maintenance costs. A study was undertaken to determine the effectiveness of resilient rail boots in reducing the vibration levels, and the resulting cost to maintain the track structure.

Ground Borne Vibration Propagation Patterns Measured in Toronto's Rail Transit System
M. Bracken (Aeroacoustics Engineering Ltd. Rexdale)

A major study was undertaken for which a large number of vibration propagation measurements were taken on different soil types, and soil layering geometries. The results of the study were compared to theoretical predictions of wave propagation in layered media to determine if it possible to predict ground borne vibration propagation.

Residential Development versus Railway Yards
D. Giusti (Jade Acoustics Inc., Concord)

With the reduction of available land for residential development within urban areas as well as the desire to rezone industrial lands for residential purposes, areas that were not previously considered suitable for residential development are now being re-evaluated. Rail yards are a particular source that are experiencing an attempt by residential proponents to build adjacent to their property lines. There have been several rail yards in Southern Ontario where residential applications have been made on lands adjacent to or in the vicinity of the rail yards. This paper will discuss the challenges associated with permitting residential development adjacent to rail yards. It will include a discussion of the sound sources in a rail yard, the possible mitigative measures and the decisions given by the Ontario Municipal Board on several applications for residential development adjacent to rail yards.

Application of the Finite Element Method in Active Control Analysis of Aerospace Structures Using Piezoelectric Materials
K. Mourad, A. Amir-Yazdani, A. Gakwaya, L. Cheng (Laval University, Québec)

Oberst Beam Excitation Using Piezo Electric Actuators
J.L. Wojtowicki (GAUS, Sherbrooke)

The «Oberst beam» is a classical method for the characterization of damping material based on a multilayer cantilever beam (base beam + one or two layers of other materials). As the base beam is made of a rigid and lightly damped material (steel, aluminum), the most critical aspect of this method is to properly excite the beam without adding weight or damping. This presentation deals with the use of two piezoelectric actuators glued near the clamping boundary limit on each side of the beam used to generate a bending force. As it is not possible to cover the actuator with the material under test, the effect of neglecting the energy loss near the clamping has been studied . It has been demonstrate that the actuator does not add damping to the base beam and that the uncovered section near the clamping by the damping material lightly underestimates the dissipated energy. A simple statistical algorithm for the estimation of modal parameters has been developed to increase accuracy compared to Df/f at n dB or other generic curve fitting methods. Some experimental results are given.

Noise and Vibration from Underground Trains
B. Howe (HGC Engineering, Mississauga)

HGC Engineering was involved with mitigating groundborne noise and vibration intrusions within Imperial Oil's Research Facility following the construction of CN's rail tunnel under the St. Clair River. A great deal of vibration and radiated noise measurements have been taken on an annual basis over the past ten years, revealing interesting trends in the noise and vibration impact. Special constructions were implemented to control the noise and vibration levels in the

Main Conference room, located in the basement immediately above the tunnel, and to control the vibration levels impacting a Scanning Electron Microscope and a Nuclear Mass Resonance Spectrometer. This presentation will outline the nature of the noise and vibration impact, trends experienced over time, and the mitigation measures undertaken and the performance achieved.

Implications of the GTAA Mitigation Measures for Aircraft Noise
D. Giusti (Jade Acoustics Inc., Concord)

In February 1997 when the MMA changed the aircraft policy to limit residential development to under NEF/NEP 30 many developments were already draft approved. The new Provincial Policy Statement recognized this and allowed these developments to proceed. The GTAA stipulated very specific requirements. The requirements are entrenched in Subdivision and Development Agreements and are non-negotiable. The implementation of these mitigative measures has caused some difficulties for the builders as well as for the acoustical consultants. This paper will discuss the required mitigation measures, the difficulties encountered during the implementation stage and the merits of this mitigation.

Practical Method for Active Control of Sounds with Large Dynamic Range
A.J. Brammer, G.J. Pan (NRC, Ottawa)

The performance of an adaptive active sound control system is influenced by the analogue signal amplitudes within the input and output analogue-digital (A/D) and D/A converters, and hence is sensitive to the sound pressure being controlled. While compensation is commonly provided within the algorithm for variations in input power, for example, by normalizing the adaptation step size, the full potential of the A/D and D/A subsystems is not realized. Solutions lie in surrounding the digital control system with a variable gain control system, together with discontinuing adaptation when the sound being controlled is indistinguishable from the background noise. An analogue gain control system has been developed consisting of linked, reciprocal variable gain amplifiers, so arranged that the changes in signal amplitude at the A/Ds and D/As are smaller than the changes in sound pressure of the acoustic system being controlled. The gain control system operates on the error and control signals so as to maintain the error path impulse response unchanged. In this way, the gain changes are transparent to the digital controller. The application of the method to an adaptive active control system for a headset will be described. [Work supported by the Defence and Civil Institute of Environmental Medicine]

Approche énergétique locale pour le transitoire : formalisme et applications
M.N. Ichchou, F. Sh. Sui, L. Jezequel (École Centrale de Lyon, France)

Probabilistic Methodology for Uncertainty Modelling in Computational Acoustics
D.P. Brennan, U. Akpan, X. Luo (Martec Ltd., Halifax)

Modal Analysis and Radiation Factor of a Toothed Wheel
L. Lefebvre (Bombardier Produits Récréatifs, Valcourt)

The probabilistic reliability approach is proving to be a very effective and rational way for accounting for the uncertainties in any engineering system. This approach has been successful in the characterization of uncertainties and the prediction of structural behavior in several sectors of the engineering industry. Notable examples of industrial applications include aerospace structures, ships, offshore structures, pipelines, automobiles, machinery, civil construction and nuclear structures. The technology has formed an important part of design, analysis, maintenance and inspection planning of engineering structures. In the field of computational acoustics, the relative complexity of fluid and structural material properties, as well as loading and boundary conditions, make it very difficult to represent radiated and scattered sound pressure fields using a traditional deterministic boundary/finite element modelling formulation. A representation using a probabilistic model, however, is possible, and in some cases more suitable. In this study, an advanced probabilistic reliability technique, which is based on first-order and second-order reliability methods, is presented within the framework of a coupled boundary element-finite element modelling strategy. The merit of the probabilistic approach is demonstrated via the solution of several example problems, where probabilistic sensitivity studies are used to identify the most important model parameters. In addition, it is shown that the methodology presented would prove valuable in the practical design of acoustic systems.

Isolation acoustique de la décharge du compresseur de gaz naturel
J.L. Allard, C. Chamberland, M. Meunier (SNC Lavalin, Montréal)

Etude pratique et les solutions adaptées pour le bruit routier dans la ville d'Alger
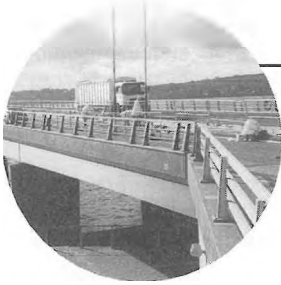Rabah IDDIR & Nadir LARADI

Vibration Insulation
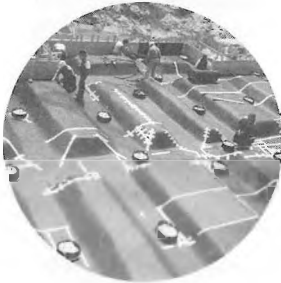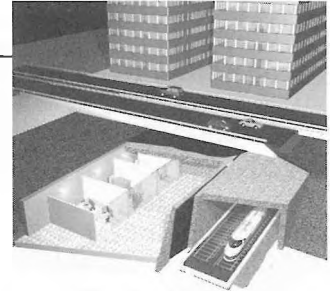
2 ways — Regupol · Regufoam

1 goal — Optimal vibration absorption and insulation of __structure-borne sound__ using recycled rubber and foam materials.

Road Construction

For rail and tunnel construction, as well as for road and bridge construction, Regupol and Regufoam are used for vibration insulation and shockproofing.

Foundations

To protect against ground vibration, Regupol and Regufoam insulate large buildings with appropriate load distribution slabs.
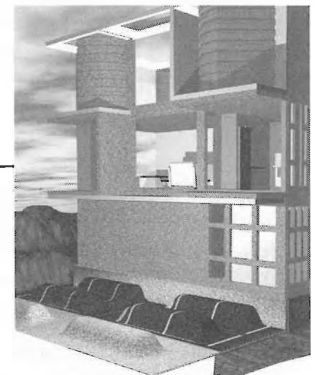
High-Rise Building

Whether for elevator motors, pumps, ventilation systems or block-type thermal power stations, structure-borne sound insulation and vibration absorption with Regupol and Regufoam are simple and permanent.
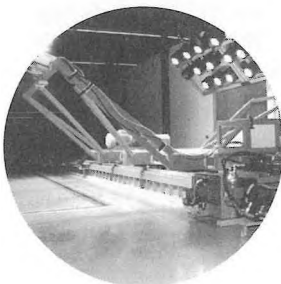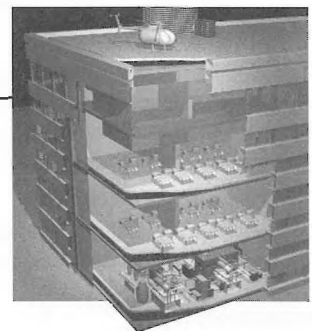
Industry

Here Regupol and Regufoam are used for the active insulation of machines and passive insulation of floor slabs for precision measuring instruments, laboratory facilities or measuring chambers. Both sub-critical and supercritical bearings are possible.
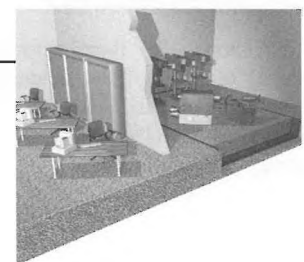
NEWS / INFORMATIONS

CONFERENCES

The following list of conferences was mainly provided by the Acoustical Society of America. If you have any news to share with us, send them by mail or fax to the News Editor (see address on the inside cover), or via electronic mail to desharnais@drea.dnd.ca

2000

31 August – 2 September: International Conference on Noise and Vibration Pre-Design and Characterization Using Energy Methods (NOVEM), Lyon, France. Contact: LVA, INSA de Lyon, Bldg. 303, 20 avenue Albert Einstein, 69621 Villeurbane, France; Fax: +33 4 7243 8712; Web: www.insa-lyon.fr/Laboratoires/lva.html

3-6 September: 5th French Congress on Acoustics — Joint meeting of the Swiss and French Acoustical Societies, Lausanne, Switzerland. Contact: M.-N. Rossi, Ecole Polytechnique Fédérale, 1015 Lausanne, Switzerland; Fax: +41 21693 26 73.

13-15 September: International Conference on Noise and Vibration Engineering (ISMA 25), Leuven, Belgium. Contact: Mrs. L. Notré, K. U. Leuven, PMA Division, Celestijnenlaan 300B, 3001 Leuven, Belgium; Fax: +32 16 32 24 82; Email: lieve.notre@mech.kuleuven.ac.be

17-21 September: Acoustical Society of Lithuania First International Conference, Vilnius, Lithuania. Contact: Acoustical Society of Lithuania, Kriviu 15-2, 2007 Vilnius, Lithuania; Fax: +370 2 223 451; Email: daumantas.ciblys@ff.vu.lt

18-22 September: 47th Seminar on Acoustics (OSA2000), Zalem Solinski, Poland. Email: osa@atena.univ.rzeszow.pl

29 September – 1 October: Tone Wood Forum, Quesnel, BC, Canada. Contact: J. Griffin, Island Mountain Arts, P.O. Box 65, Wells, BC, V0K 2R0, Canada; Fax: 250-994-3433; Web: www.imarts.com

3-5 October: WESPRAC VII, Kumamoto, Japan. Contact: Computer Science Dept., Kumamoto Univ., 2-39-1 Kurokami, Kumamoto, Japan 860-0862; Fax: +81 96 342 3630; Email: wesprac7@cogni.eecs.kumamoto-u.ac.jp

3-6 October: EUROMECH Colloquium on Elastic Waves in Nondestructive Testing, Prague, Czech Republic. Contact: Z. Prevorovsky, Institute of Thermomechanics, Dolejskova 4, 182 00 Prague 8, Czech Republic; Fax: +420 2 858 4695; Email: ok@bivoj.it.cas.cz

12-14 October: International Conference on Newborn Hearing Screening, Milan. Fax: +39 2 23993360; Web: www.biomed.polimi.it/diphtm/WorkShops.html

16-18 October: 2nd Iberoamerican Congress on Acoustics, 31st National Meeting of the Spanish Acoustical Society, and EAA Symposium, Madrid, Spain. Contact: Spanish Acoustical Society, c/Serrano 144, 28006 Madrid, Spain; Fax: +34 91 411 7651; email: ssantiago@fresno.csic.es

CONFÉRENCES

La liste de conférences ci-jointe a été offerte en majeure partie par l'Acoustical Society of America. Si vous avez des nouvelles à nous communiquer, envoyez-les par courrier ou fax (coordonnées incluses à l'envers de la page couverture), ou par courrier électronique à desharnais@drea.dnd.ca

2000

31 août – 2 septembre: Conférence internationale sur l'utilisation des méthodes d'énergie pour la prévision vibroacoustique (NOVEM), Lyon, France. Info: LVA, INSA de Lyon, Bldg. 303, 20 avenue Albert Einstein, 69621 Villeurbane, France; Fax: +33 4 7243 8712; Web: www.insa-lyon.fr/Laboratoires/lva.html

3-6 septembre: 5e Congrès français d'acoustique — Rencontre conjointe des Sociétés suisse et française d'acoustique, Lausanne, Suisse. Info: M.-N. Rossi, Ecole Polytechnique Fédérale, 1015 Lausanne, Suisse; Fax: +41 21693 26 73.

13-15 septembre: Conférence internationale d'ingénierie sur le bruit et les vibrations (ISMA 25), Leuven, Belgique. Info: Mrs. L. Notré, K. U. Leuven, PMA Division, Celestijnenlaan 300B, 3001 Leuven, Belgium; Fax: +32 16 32 24 82; Email: lieve.notre@mech.kuleuven.ac.be

17-21 septembre: 1e Conférence internationale de la Société d'acoustique de Lithuanie, Vilnius, Lithuanie. Info: Acoustical Society of Lithuania, Kriviu 15-2, 2007 Vilnius, Lithuania; Fax: +370 2 223 451; Email: daumantas.ciblys@ff.vu.lt

18-22 septembre: 47e Séminaire sur l'acoustique (OSA2000), Zalem Solinski, Pologne. Email: osa@atena.univ.rzeszow.pl

29 septembre – 1 octobre: Forum Tone Wood, Quesnel, CB, Canada. Info: J. Griffin, Island Mountain Arts, B.P. 65, Wells, CB, V0K 2R0, Canada; Fax: 250-994-3433; Web: www.imarts.com

3-5 octobre: WESPRAC VII, Kumamoto, Japon. Info: Computer Science Dept., Kumamoto Univ., 2-39-1 Kurokami, Kumamoto, Japan 860-0862; Fax: +81 96 342 3630; Email: wesprac7@cogni.eecs.kumamoto-u.ac.jp

3-6 octobre: Colloque EUROMECH sur les ondes élastiques pour les tests non-destructifs, Prague, République tchèque. Info: Z. Prevorovsky, Institute of Thermomechanics, Dolejskova 4, 182 00 Prague 8, Czech Republic; Fax: +420 2 858 4695; Email: ok@bivoj.it.cas.cz

12-14 octobre: Conférence internationale sur l'évaluation de l'audition des nouveau-nés, Milan. Fax: +39 2 23993360; Web: www.biomed.polimi.it/diphtm/WorkShops.html

16-18 octobre: 2e congrès ibéro-américain sur l'acoustique, 31e Rencontre nationale de la Société d'acoustique espagnole, et Symposium de l'EAA, Madrid, Espagne. Info: Spanish Acoustical Society, c/Serrano 144, 28006 Madrid, Spain; Fax: +34 91 411 7651; email: ssantiago@fresno .csic.es

16-20 October: 6th International Conference on Spoken Language Processing, Beijing, China. Contact: ICSLP 2000 Secretariat, Institute of Acoustics, PO Box 2712, 17 Zhong Guan Cun Road, 100 080 Beijing, China; Fax: +86 10 6256 9079; Email: mchu@plum.ioa.ac.cn

22-25 October: IEEE Ultrasonics Symposium, San Juan, Puerto Rico. Contact: R. Almar, 896 Buttonwood Ln., Altamonte Springs, FL 32714; Fax: 407-290-5181; Web: www.uffcsymp2000.org

28-29 October: 2000 Acoustics Week in Canada, Sherbrooke, QC, Canada. Contact: Alain Berry, Université de Sherbrooke, 2500, boul. Université, Sherbrooke, QC, J1K 2R1, Canada. Fax: 819-821-7163; Email: alain.berry@gme.usherb.ca; Web: www-gaus.gme.usherb.ca

24-27 November: 21st Tonmeistertagung (VDT International Audio Convention), Hannover, Germany. Contact: Convention Office VDT, Am Zaarshäuschen 9, 51427 Bergisch-Gladbach, Germany; Fax: +49 2204 21584; Web: www.tonmeister.de

4-8 December: 140th Meeting of the Acoustical Society of America, Newport Beach, CA. Contact: Acoustical Society of America, Suite 1NO1, 2 Huntington Quadrangle, Melville, NY 11747-4502; Tel: 516-576-2360; Fax: 516-576-2377; Email: asa@aip.org; Web: asa.aip.org

2001

30 April-3 May: 2001 Society of Automotive Engineers (SAE) Noise & Vibration Conference and Exposition, Traverse City, MI. Contact: Patti Kreh, SAE Int'l., 755 W. Big Beaver Rd., Suite 1600, Troy, MI 48084; Tel.: 248-273-2474; Fax: 248-273-2494; Email: pkreh@sae.org

4-8 June: 141st Meeting of the Acoustical Society of America, Chicago, IL. Contact: Acoustical Society of America, Suite 1NO1, 2 Huntington Quadrangle, Melville, NY 11747-4502; Tel: 516-576-2360; Fax: 516-576-2377; Email: asa@aip.org; Web: asa.aip.org

28-30 August: Inter-Noise 2001, The Hague, The Netherlands. Email: secretary@internoise2001.tudelft.nl; Web: internoise2001.tudelft.nl

2-7 September: 17th International Congress on Acoustics (ICA), Rome, Italy. Contact: A. Alippi, Dipartimento di Energetica, Universita di Roma "La Sapienza," Via A. Scarpa 14, 00161 Rome, Italy; Fax: +39 6 4424 0183; WWW: www.uniroma1.it/energ/ica.html

10-13 September: International Symposium on Musical Acoustics (ISMA 2001), Perugia, Italy. Contact: Perugia Classico, Comune di Perugia, Via Eburnea 9, 06100 Perugia, Italy; Fax: +39 75 577 2255; Email: perugia@classico.it

17-19 October: 32nd Meeting of the Spanish Acoustical Society, La Rioja, Spain. Contact: Serrano 144, Madrid 28006, Spain; Fax: +34 91 411 76 51; Web: www.ia.csic.es/sea/index.html

16-20 octobre: 6e conférence internationale sur le traitement de la langue parlée, Beijing, Chine. Info: ICSLP 2000 Secretariat, Institute of Acoustics, PO Box 2712, 17 Zhong Guan Cun Road, 100 080 Beijing, China; Fax: +86 10 6256 9079; Email: mchu@plum.ioa.ac.cn

22-25 octobre: Symposium Ultrasons de l'IEEE, San Juan, Porto Rico. Info: R. Almar, 896 Buttonwood Ln., Altamonte Springs, FL 32714; Fax: 407-290-5181; Web: www.uffcsymp2000.org

28-29 octobre: Semaine d'acoustique canadienne 2000, Sherbrooke, QC, Canada. Info: Alain Berry, Université de Sherbrooke, 2500, boul. Université, Sherbrooke, QC, J1K 2R1, Canada. Fax: 819-821-7163; Email: alain.berry@gme.usherb.ca; Web: www-gaus.gme.usherb.ca

24-27 novembre: 21e Tonmeistertagung (Convention Audio Internationale VDT), Hannover, Allemagne. Info: Convention Office VDT, Am Zaarshäuschen 9, 51427 Bergisch-Gladbach, Germany; Fax: +49 2204 21584; Web: www.tonmeister.de

4-8 décembre: 140e recontre de l'Acoustical Society of America, Newport Beach, CA. Info: Acoustical Society of America, Suite 1NO1, 2 Huntington Quadrangle, Melville, NY 11747-4502; Tél.: 516-576-2360; Fax: 516-576-2377; Email: asa@aip.org; Web: asa.aip.org

2001

30 avril-3 mai: Conférence et exposition 2001 de la Société des Ingénieurs d'autos (SAE) sur le bruit et les vibrations, Traverse City, MI. Info: Patti Kreh, SAE Int'l., 755 W. Big Beaver Rd., Suite 1600, Troy, MI 48084; Tél.: 248-273-2474; Fax: 248-273-2494; Email: pkreh@sae.org

4-8 juin: 141e rencontre de l'Acoustical Society of America, Chicago, IL. Info: Acoustical Society of America, Suite 1NO1, 2 Huntington Quadrangle, Melville, NY 11747-4502; Tel: 516-576-2360; Fax: 516-576-2377; Email: asa@aip.org; Web: asa.aip.org

28-30 août: Inter-Noise 2001, La Haye, Pays-Bas. Email: secretary@internoise2001.tudelft.nl; Web: internoise2001 .tudelft.nl

2-7 septembre: 17e Congrès international sur l'acoustique (ICA), Rome, Italie. Info: A. Alippi, Dipartimento di Energetica, Universita di Roma "La Sapienza," Via A. Scarpa 14, 00161 Rome, Italy; Fax: +39 6 4424 0183; WWW: www.uniroma1.it/energ/ica.html

10-13 septembre: Symposium international sur l'acoustique musicale (ISMA 2001), Perugia, Italie. Info: Perugia Classico, Comune di Perugia, Via Eburnea 9, 06100 Perugia, Italy; Fax: +39 75 577 2255; Email: perugia@classico.it

17-19 octobre: 32e rencontre de la Société espagnole d'acoustique, La Rioja, Espagne. Info: Serrano 144, Madrid 28006, Spain; Fax: +34 91 411 76 51; Web: www.ia.csic.es/sea/index.html

16-21 September: Forum Acusticum 2002 (Joint EAA-SEA-ASJ Meeting), Sevilla. Fax: +34 91 411 7651; Web: www.cica.es/aliens/forum2002

MORE NEWS...

Degree awarded.

In May 2000, Mr. Thomas Kelly, P. Eng., M. Sc., was awarded the degree of Master of Science with distinction in Environmental Engineering, from the University of Portsmouth, U.K. The title of Mr. Kelly's thesis is: *The Sociological Noise Impact of Aircraft Overflying a Canadian National Park: Formulation of a Preliminary Dose-Response Relationship.* Dr. John Bradley acted as Mr. Kelly's remote academic supervisor.

Mr. Kelly is the National Manager, Environmental Management with NAV CANADA. NAV CANADA is the country's provider of civil air navigation services and is a non-share capital corporation with operations coast to coast providing air traffic control, flight information, aviation weather information and electronic aids to navigation.

AUTRES NOUVELLES...

Diplôme décerné.

En mai 2000, M. Thomas Kelly, P. Eng., M. Sc., a obtenu une maîtrise en Sciences avec distinction en Génie environnemental à l'Université de Portsmouth, Royaume-Uni. La thèse de M. Kelly est intitulée: *The Sociological Noise Impact of Aircraft Overflying a Canadian National Park: Formulation of a Preliminary Dose-Response Relationship.* Dr John Bradley était le superviseur académique à distance de M. Kelly.

M. Kelly est le Directeur national, Gestion de l'environnement, NAV CANADA. NAV CANADA est une société sans capital-actions qui opère d'un océan à l'autre, et procure les services de navigation de l'aviation civile au Canada tels le contrôle de la circulation aérienne, l'information de vol, l'information météorologique pour l'aviation, et les aides électroniques à la navigation.

INSTRUCTIONS TO AUTHORS
FOR THE PREPARATION OF MANUSCRIPTS

Submissions: The original manuscript and two copies should be sent to the Editor-in-Chief.

General Presentation: Papers should be submitted in camera-ready format. Paper size 8.5" x 11". If you have access to a word processor, copy as closely as possible the format of the articles in Canadian Acoustics 18(4) 1990. All text in Times-Roman 10 pt font, with single (12 pt) spacing. Main body of text in two columns separated by 0.25". One line space between paragraphs.

Margins: Top - title page: 1.25"; other pages, 0.75"; bottom, 1" minimum; sides, 0.75".

Title: Bold, 14 pt with 14 pt spacing, upper case, centered.

Authors/addresses: Names and full mailing addresses, 10 pt with single (12 pt) spacing, upper and lower case, centered. Names in bold text.

Abstracts: English and French versions. Headings, 12 pt bold, upper case, centered. Indent text 0.5" on both sides.

Headings: Headings to be in 12 pt bold, Times-Roman font. Number at the left margin and indent text 0.5". Main headings, numbered as 1, 2, 3, ... to be in upper case. Sub-headings numbered as 1.1, 1.2, 1.3, ... in upper and lower case. Sub-sub-headings not numbered, in upper and lower case, underlined.

Equations: Minimize. Place in text if short. Numbered.

Figures/Tables: Keep small. Insert in text at top or bottom of page. Name as "Figure 1, 2, ..." Caption in 9 pt with single (12 pt) spacing. Leave 0.5" between text.

Line Widths: Line widths in techincal drawings, figures and tables should be a minimum of 0.5 pt.

Photographs: Submit original glossy, black and white photograph.

Scans: Should be between 225 dpi and 300 dpi. Scan: Line art as bitmap tiffs; Black and white as grayscale tiffs and colour as CMYK tiffs;

References: Cite in text and list at end in any consistent format, 9 pt with single (12 pt) spacing.

Page numbers: In light pencil at the bottom of each page.

Reprints: Can be ordered at time of acceptance of paper.

DIRECTIVES A L'INTENTION
DES AUTEURS PREPARATION DES MANUSCRITS

Soumissions: Le manuscrit original ainsi que deux copies doivent être soumis au rédacteur-en-chef.

Présentation générale: Le manuscrit doit comprendre le collage. Dimensions des pages, 8.5" x 11". Si vous avez accès à un système de traitement de texte, dans la mesure du possible, suivre le format des articles dans l'Acoustique Canadienne 18(4) 1990. Tout le texte doit être en caractères Times-Roman, 10 pt et à simple (12 pt) interligne. Le texte principal doit être en deux colonnes séparées d'un espace de 0.25". Les paragraphes sont séparés d'un espace d'une ligne.

Marges: Dans le haut - page titre, 1.25"; autres pages, 0.75"; dans le bas, 1" minimum; latérales, 0.75".

Titre du manuscrit: 14 pt à 14 pt interligne, lettres majuscules, caractères gras. Centré.

Auteurs/adresses: Noms et adresses postales. Lettres majuscules et minuscules, 10 pt à simple (12 pt) interligne. Centré. Les noms doivent être en caractères gras.

Sommaire: En versions anglaise et française. Titre en 12 pt, lettres majuscules, caractères gras, centré. Paragraphe 0.5" en alinéa de la marge, des 2 cotés.

Titres des sections: Tous en caractères gras, 12 pt, Times-Roman. Premiers titres: numéroter 1, 2, 3, ..., en lettres majuscules; sous-titres: numéroter 1.1, 1.2, 1.3, ..., en lettres majuscules et minuscules; sous-sous-titres: ne pas numéroter, en lettres majuscules et minuscules et soulignés.

Equations: Les minimiser. Les insérer dans le texte si elles sont courtes. Les numéroter.

Figures/Tableaux: De petites tailles. Les insérer dans le texte dans le haut ou dans le bas de la page. Les nommer "Figure 1, 2, 3,..." Légende en 9 pt à simple (12 pt) interligne. Laisser un espace de 0.5" entre le texte.

Largeur Des Traits: La largeur des traits sur les schémas technique doivent être au minimum de 0.5 pt pour permettre une bonne reproduction.

Photographies: Soumettre la photographie originale sur papier glacé, noir et blanc.

Figures Scanées: Doivent être au minimum de 225 dpi et au maximum de 300 dpi. Les schémas doivent être scannés en bitmaps tif format. Les photos noir et blanc doivent être scannées en échelle de gris tifs et toutes les phoots couleurs doivent être scannées en CMYK tifs.

Références: Les citer dans le texte et en faire la liste à la fin du document, en format uniforme, 9 pt à simple (12 pt) interligne.

Pagination: Au crayon pâle, au bas de chaque page.

Tirés-à-part: Ils peuvent être commandés au moment de l'acceptation du manuscrit.

The Canadian Acoustical Association	**l'Association Canadienne d'Acoustique**

SUBSCRIPTION INVOICE

Subscription for the current calendar year is due January 31. New subscriptions received before July 1 will be applied to the current year and include that year's back issues of Canadian Acoustics, if available. Subscriptions received from July 1 will be applied to the next year.

FACTURE D'ABONNEMENT

L'abonnement pour la présente année est dû le 31 janvier. Les nouveaux abonnements reçus avant le 1 juillet s'appliquent à l'année courante et incluent les anciens numéros (non-épuisés) de l'Acoustique Canadienne de cette année. Les abonnements reçus après le 1 juillet s'appliquent à l'année suivante.

Check ONE Item Only:

			Cocher la case appropriée:
CAA Membership	_____	$50	_____ Membre individuel
CAA Student membership	_____	$10	_____ Membre étudiant(e)
Institutional Subscription	_____	$50	_____ Membre institutionnel
Sustaining Subscription	_____	$150	_____ Abonnement de soutien
Total Remitted		$_____	Versement total

INFORMATION FOR MEMBERSHIP DIRECTORY
Check areas of interest (max 3):

RENSEIGNEMENT POUR L'ANNUAIRE DES MEMBRES
Cocher vos champs d'intérêt (max. 3):

Architectural Acoustics	1.	_____	1. Acoustique architecturale
Engineering Acoustics / Noise Control	2.	_____	2. Génie acoustique / Contrôle du bruit
Physical Acoustics / Ultrasound	3.	_____	3. Acoustique physique / Ultrasons
Musical Acoustics / Electroacoustics	4.	_____	4. Acoustique musicale / Electroacoustique
Psychological / Physiological Acoustics	5.	_____	5. Physio/psycho-acoustique
Shock and Vibration	6.	_____	6. Chocs et vibrations
Hearing Sciences	7.	_____	7. Audition
Speech Sciences	8.	_____	8. Parole
Underwater Acoustics	9.	_____	9. Acoustique sous-marine
Signal Processing / Numerical Methods	10.	_____	10. Traitement des signaux / Méthodes numériques
Other	11.	_____	11. Autre

Business telephone number (_____) _____ Numéro de téléphone au bureau
Business facsimile number (_____) _____ Numéro de télécopieur au bureau
Business E-Mail number _____ Numéro de courier électronique au bureau

PLEASE TYPE NAME AND ADDRESS BELOW:

VEUILLEZ ECRIRE VOTRE NOM ET VOTRE ADRESSE CI-DESSOUS:

Faites parvenir ce formulaire à l'adresse suivante en prenant soin d'y joindre un chèque fait au nom de
L'ASSOCIATION CANADIENNE D'ACOUSTIQUE:

Make cheques payable to
THE CANADIAN ACOUSTICAL ASSOCIATION. Mail this form with payment to:

Trevor Nightingale
Secretary, Canadian Acoustical Association
P. O. Box 74068
Ottawa, Ontario K1M 2H9

The Canadian Acoustical Association
l'Association Canadienne d'Acoustique

PRESIDENT **PRÉSIDENT**	**John Bradley** IRC, NRCC Ottawa, Ontario K1A 0R6	(613) 993-9747 john.bradley@nrc.ca
PAST PRESIDENT **PRÉSIDENT SORTANT**	**John Hemingway** 2410 Old Pheasant Road Mississauga, Ontario L5A 2S1	(416) 798-0522 jrh@mail.globalserve.net
SECRETARY **SECRÉTAIRE**	**Trevor Nightingale** P. O. Box 74068 Ottawa, Ontario K1M 2H9	(613) 993-0102 trevor.nightingale@nrc.ca
TREASURER **TRÉSORIER**	**Dalila Giusti** Jade Acoustics 545 North Rivermede Road, Suite 203 Concord, Ontario L4K 4H1	(905) 660-2444 dalila@jadeacoustics.com
MEMBERSHIP **RECRUTEMENT**	**Don Jamieson** Hearing Health Care Res. Unit Elborn College University of Western Ontario London, Ontario N6G 1H1	(519) 661-3901 jamieson@audio.hhcru.uwo.ca
EDITOR-IN-CHIEF **RÉDACTEUR EN CHEF**	**Ramani Ramakrishnan** Aiolos Engineering 51 Constellation Court Suite 200 Toronto, Ontariol M9W 1K4	(416) 674-3017 ramani@aiolos.com

DIRECTORS **DIRECTEURS**	**Noureddine Atalla** **Meg Cheesman** **David DeGagne** **Karen Fraser** **M. K. (Kathy) Fuller** **Tim Kelsall** **Dave Stredulinsky** **Douglas J. Whicker**	(819) 821-7102 (519) 279-2111, #8283 (403) 297-3200 (416) 217-6466 (604) 822-4716 (905) 855-7600 (902) 426-3100 (604) 988-2508

WORLD WIDE WEB HOME PAGE: **http://www.uwo.ca/hhcru/caa/**

SUSTAINING SUBSCRIBERS / ABONNES DE SOUTIEN

The Canadian Acoustical Association gratefully acknowledges the financial assistance of the Sustaining Subscribers listed below. Annual donations (of $150.00 or more) enable the journal to be distributed to all at a reasonable cost. Sustaining Subscribers receive the journal free of charge. Please address donation (made payable to the Canadian Acoustical Association) to the Secretary of the Association.

L'Association Canadienne d'Acoustique tient à témoigner sa reconnaissance à l'égard de ses Abonnés de Soutien en publiant ci-dessous leur nom et leur adresse. En amortissant les coûts de publication et de distribution, les dons annuels (de $150.00 et plus) rendent le journal accessible à tous nos membres. Les Abonnés de Soutien reçoivent le journal gratuitement. Pour devenir un Abonné de Soutien, faites parvenir vos dons (chèque ou mandat-poste fait au nom de l'Association Canadienne d'Acoustique) au secrétaire de l'Association.

ACO Pacific
2604 Read Ave.
Belmont, CA, USA 94002
(650) 595-8588 FAX: (650) 591-2891

Acoustec Inc.
Attn: Dr. J.G. Migneron
1381 rue Galilée, Suite 103
Québec, Québec G1P 4G4
(418) 682-2331 FAX: (418) 682-1472

Aercoustics Engineering Limited
Barman & Associates
50 Ronson Drive, Suite 127
Rexdale, Ontario M9W 1B3
(416) 249-3361 FAX: (416) 249-3613

Atlantic Acoustical Associates
P.O. Box 96, Station M
Halifax, Nova Scotia B3J 2L4
(902) 425-3096

H. L. Blachford Ltd.
Attn: Mr. D.E. Watson
2323 Royal Windsor Dr.
Mississauga, Ontario L5J 1K5
(905) 823-3200 FAX: (905) 823-9290

Bruel & Kjaer Canada Ltd.
90 Leacock Road
Pointe Claire, Québec H9R 1H1
(514) 695-8225 FAX: (514) 695-4808

J. E. Coulter Associates Ltd.
Suite 507
1200 Sheppard Ave. E
Willowdale, Ontario M2K 2S5
(416) 502-8598 FAX: (416) 502-3473

Dalimar Instruments Inc.
193, Joseph Carrier
Vaudreuil-Dorion, Québec J7V 5V5
(514) 424-0033 FAX: (514) 424-0030

Eckel Industries of Canada Ltd.
Attn: Mr. Blake Noon
P.O. Box 776
Morrisburg, Ontario K0C 1X0
(613) 543-2967 FAX: (613) 543-4173

Dodge-Regupol Inc.
Atten: Paul Downey
33 Craighurst Ave.
Toronto, ON M4R-1J9
Tel: 416-440-1094
Fax: 416-440-0730
E-mail: pcd@regupol.com

Environmental Acoustics Inc.
Attn: Mr. H.J. Doedens
#13 - 5155 Spectrum Way
Mississauga, Ontario L4W 5A1
(905) 238-1077 FAX: (905) 238-9079

Hatch Associates Ltd.
Attn: Tim Kelsall
2800 Speakman Dr.
Mississauga, Ontario L5K 2R7
(905) 855-7600 FAX: (905) 855-8270

HGC Engineering
Plaza One, Suite 203
2000 Argentia Road
Mississauga, Ontario L5N 1P7
(905) 826-4044 FAX: (905) 826-4940

Hydro-Quebec
Vice-presidence Environnement
75 Rene Levesque ouest, 16e etage
Montreal, Québec H2Z 1A4

Industrial metal Fabricators (Chatham) Ltd.
Industrial Noise Control
Attn: Mr. Frank Van Oirschot
P.O. Box 834, 288 Inshes Ave.
Chatham, Ontario N7M 5L1
(519) 354-4270 FAX: (519) 354-4193

Integral DX Engineering Ltd.
907 Admiral Ave.
Ottawa, Ontario K1Z 6L6
(613) 761-1565 FAX: (613) 729-4337

Jade Acoustics Inc.
545 North Rivermede Road, Suite 203
Concord, Ontario L4K 4H1
(905) 660-2444 FAX: (905) 660-4110

John Swallow Associates
Attn: John C. Swallow
250 Galaxy Boulevard
Etobicoke, Ontario M9W 5R8
(416) 798-0522

Larson Davis Laboratories
1681 West 820 North
Provo, Utah, USA 84601
(801) 375-0177

MJM Conseillers en Acoustique Inc.
Attn: M. Michel Morin
6555 Cote des Neiges, Suite 400
Montréal, Québec H3S 2A6
(514) 737-9811 FAX: (514) 737-9816

Nelson Industries Inc.
Corporate Research Dept.
P.O. Box 600
Stoughton, WI, USA 53589-0600
(608) 873-4370

OZA Inspections Ltd.
P.O. Box 271
Grimsby, Ontario L3M 4G5
(905) 945-5471 FAX: (905) 945-3942

Peutz & Associés
Attn: Marc Asselineau
34 rue de Paradis
F-75010 Paris, France
+33 1 45230500 FAX: +33 1 45230504

J. L. Richards & Assoc. Ltd.
Attn: Fernando Ribas
864 Lady Ellen Place
Ottawa, Ontario K1Z 5M2
(613) 728-3571 FAX: (613) 728-6012

Scantek Inc.
916 Gist Ave.
Silver Spring, MD, USA 20910
(301) 495-7738 FAX: (301) 495-7739

SNC/Lavalin Environment Inc.
2 Felix Martin Place
Montréal, Québec H2Z 1Z3
(514) 393-1000

Spaarg Engineering Limited
Noise and Vibration Analysis
822 Lounsborough St.
Windsor, Ontario N9G 1G3
(519) 972-0677 FAX: (519) 972-0677

State of the Art Acoustik Inc.
Attn. Dr. C. Fortier
Unit 43, 1010 Polytek St.
Ottawa, Ontario, K1J 9J3

Tacet Engineering Ltd.
Attn: Dr. M.P. Sacks
111 Ava Road
Toronto, Ontario M6C 1W2
(416) 782-0298 FAX: (416) 785-9880

University of Alberta
MEANU, Dept. of Mech. Eng.
6720 - 30 St.
Edmonton, Alberta T6P 1J6
(403) 466-6465 FAX: (403) 466-6465

Valcoustics Canada Ltd.
30 Wertheim Court, Unit 25
Richmond Hill, Ontario L4B 1B9
(905) 764-5223 FAX: (905) 764-6813

West Caldwell Calibration Labs
5200 Dixie Road, Suite 118
Missauga, Ontario L4W 1E4
(905) 624-3919 FAX: (905) 624-3926

Wilrep Ltd.
1515 Matheson Blvd. E, Unit C 10
Mississauga, Ontario L4W 2P5
(905) 625-8944 FAX: (905) 625-7142